MODE INTERACTION IN LIPPED CHANNEL COLUMNS UNDER CONCENTRIC OR ECCENTRIC LOADING

by

Joseph Loughlan, B.Sc., M.Sc.

Thesis Presented for the Degree of

Doctor of Philosophy in Mechanical Engineering

Department of Mechanics of Materials

University of Strathclyde

1979

ABSTRACT

ABSTRACT

In this thesis an investigation into the behaviour of thin walled lipped channel columns under combined end compression and bending is reported.

The thesis begins with a short introduction, followed by a review of the relevant published literature. In the introduction an outline is given of the different buckling characteristics associated with Euler, local and coupled Euler-local modes of behaviour. The scope of the literature review spans from the early development work on coupled mode buckling through to the wide variety of interaction problems covered in present day studies. An introduction to the basic differential equations and elastic strain energy expressions used in the theoretical approach of the lipped channel problem is then briefly outlined.

Theoretical analyses of local instability and post-local buckling interaction behaviour are presented. The local buckling analysis is undertaken for the section using the Rayleigh-Ritz method. In this, the cross-sectional deflected shape is taken as a series of algebraic polynomials and each polynomial set in the series is arranged to satisfy all compatibility and equilibrium boundary conditions at the plate junctions and at the free edges of the lip. The analysis is carried out for various values of section length, to obtain that value for which the lowest buckling load is induced. From this multi-term buckling analysis a very accurate approximation is used as the first term in the subsequent semi-energy post-buckling

analysis, which incorporates also an additional set of algebraic polynomials to take account of changes in the deflected form in the post-buckling range. Thus, the deflection functions postulated are extremely accurate at the point of buckling and have a built-in facility to change in the post-buckling range. The numerical work involved in the analysis was carried out in the University's ICL 1904S computer for which a program was written using the FORTRAN IV programming language.

Details are given of an experimental investigation which was carried out to obtain information on the interactive buckling behaviour of lipped channel columns and to provide experimental results to authenticate the validity of the theoretical solutions. A description of the loading rig and its operation is presented in conjunction with a full set of assembly and component design drawings. In general, the procedure used in the investigation was to load columns of various section dimensions and with various loading eccentricities to collapse, recording strain measurements and overall deflections as loading progressed. A strain investigation was carried out to obtain knowledge of the stress variations at the centre of the column at various stages of loading.

A comparison of experimental results with theoretical predictions is given. The agreement between theory and experiment is good in general, and in particular for the comparisons of stress variations with progressive loading.

A summary of the investigation is included, together with conclusions and suggestions for further research and extension of the analysis.

The publications discussed in the literature review appear in a chronological bibliography list at the end of the text.

The thesis is concluded by six short appendices which supplement the main text and enlarge on some aspects of the investigation.

CONTENTS

CONTENTS

Contents cont.

Contents cont.

NOMENCLATURE

NOMENCLATURE

A_n	Coefficient in flange deflection function
a_n	Arbitrary integer used as exponent in flange deflection function
B_n	Coefficient in flange deflection function
b	Width of flange
b_f	Half width of flange
b_ℓ	Width of lip
b_n	Arbitrary integer used as exponent in flange deflection function
b_w	Width of web
D	Plate flexural rigidity $D = \frac{E\,t^3}{12\,(1-\nu^2)}$
D_n	Coefficient in the web deflection function
d	Distance of section neutral axis from lips prior to local buckling
d*	Distance of section neutral axis from lips after local buckling
E	Youngs modulus of elasticity
e	Eccentricity of applied load
$\overline{ec}$	Non dimensional eccentricity $\overline{ec} = \frac{e}{\bar{y}}$
F_i, F_{i1}, F_{i2}	Stress Function

G	Modulus of elasticity in shear
G_n	Coefficient in the web deflection function
G_{nm}	Lip potential energy integral
$g_{n1} \ldots g_{n4}$	Coefficients in the flange deflection function after local instability
$h_{n1} \ldots h_{n6}$	Coefficients in the web deflection function after local instability
I	Second moment of area
I^*	Reduced second moment of area
i	Suffix relating to particular plate element of section (flange: $i = 1$, web: $i = 2$, lip: $i = 3$)
K_f	Flange buckling coefficient
K_n	Coefficient in the web deflection function
k_n	Arbitrary integer used as exponent in web deflection function
L	Column length
M	Moment about section lips
M_x	Moment per unit width of plate perpendicular to the x direction
M_y	Moment per unit width of plate perpendicular to the y direction
M_{xy}	Twisting moment per unit width of plate perpendicular to the x direction

N_x	Mid-plane force per unit width of plate in x direction
N_x^*	Average compressive edge force on flange
$N_x^*{}_{crit}$	Critical average compressive edge force for local instability
N_y	Mid-plane force per unit width of plate in y direction
N_{xy}	Mid-plane shearing force per unit width of plate
P	Axial load on column
$\bar{P}$	Non-dimensional axial load $\bar{P} = \frac{Pb}{\pi^2 D}$
P_{crit}	Critical local buckling load
$\bar{P}_{crit}$	Non-dimensional critical local buckling load
P_E	Euler load
$\bar{P}_E$	Non-dimensional Euler load
P_E^*	Reduced Euler load
$p_{n1} \cdots p_{n6}$	Coefficients in the lip deflection function after local instability
Q_n	Coefficient in the lip deflection function
Q_x	Shearing force parallel to the z axis per unit width of plate perpendicular to the x axis
Q_y	Shearing force parallel to the z axis per unit width of plate perpendicular to the y axis
R_n	Coefficient in the lip deflection function

S	Half-wavelength of column central buckle
T_n	Coefficient in lip deflection function
T_{nm}	Web potential energy integral
t	Plate thickness
t_n	Arbitrary integer used as exponent in lip deflection function
u	Displacement of a point in the middle plane of a plate in the x direction
u*	Compressive end displacement of flange at node of a central buckle
V_B	Strain energy of bending and twisting
V_M	Strain energy of mid-plane forces
V_T	Total strain energy $V_T = V_B + V_M$
v	Displacement of a point in the middle plane of a plate in the y direction
W_n	Local deflection coefficient
w, w_i	Deflection of plate in z direction
x	Cartesian co-ordinate
Y_i, Y_{in}	Local deflection functions for plate i
y	Cartesian co-ordinate
y_i	Cartesian co-ordinate for plate i
$\bar{y}$	Distance of section neutral axis from flange prior to local buckling

Z_{nm} Lip bending strain energy integral

z Cartesian co-ordinate

α Compression eccentricity factor

β_n Coefficient in the web deflection function after satisfaction of the edge boundary conditions

Γ_{inmrp} Membrane strain energy integral for plate i

Γ_n Flange potential energy integral

γ_n Coefficient in the web deflection function after satisfaction of the edge boundary conditions

γ_{xy} Shear strain in xy plane

δ_c Central deflection of column

ε_x Direct strain in the x direction

ε_y Direct strain in the y direction

Θ_{inm} Membrane strain energy integral

Θ_{nm} Summation of potential energy integrals
$\Theta_{nm} = \Gamma_{nm} + T_{nm} + G_{nm}$

λ_{nm} Summation of the bending strain energy integrals
$\lambda_{nm} = \Psi_{nm} + \phi_{nm} + Z_{nm}$

μ_n Coefficient in the web deflection function after satisfaction of the edge boundary conditions

ν Poisson's ratio

ξ_n Coefficient in the flange deflection function after satisfaction of the edge boundary conditions

ρ_n — Coefficient in the lip deflection function after satisfaction of the edge boundary conditions

σ_x — Direct stress in the x direction

σ_x^* — Average compressive edge stress on flange

$$\sigma_x^* = \frac{N_x^*}{t}$$

σ_y — Direct stress in the y direction

τ_{xy} — Shear stress in xy plane

τ_n — Coefficient in the lip deflection function after satisfaction of the edge boundary conditions

Φ_{inmrp} — Membrane strain energy integral for plate i

ϕ_{nm} — Web bending strain energy integral

ψ_{nm} — Flange bending strain energy integral

Ω_n — Coefficient in the lip deflection function after satisfaction of the edge boundary conditions

Symbols not listed in the Nomenclature are defined throughout the text where they first appear.

CHAPTER ONE

INTRODUCTION AND REVIEW OF THE RELEVANT LITERATURE

1.0 INTRODUCTION AND REVIEW OF THE RELEVANT LITERATURE

1.1 INTRODUCTION

Column flexural buckling is characterised by a lateral movement of the column cross-section whereby the cross-sectional shape is substantially unaltered. This type of buckling occurs when the length of a structural element is much greater than its cross-sectional dimensions and is known as Euler, or sometimes overall, buckling.

when the length of column is of the same order as the cross-sectional dimensions, local buckling will occur. This type of buckling is characterised by out of plane deflections of the column walls, causing a substantial change in shape of the cross-section and a redistribution of the stress system across the widths of its component plate elements.

In Euler buckling the straight form of the column becomes unstable at the critical load and the column deflects laterally, perpendicular to the axis of least second moment of area of the section. While the magnitude of the column deflection tends to become very large, the maximum load the column can attain is its critical buckling load. This behaviour is classified as neutral buckling.

In local buckling the flat form of the plate elements of the cross-section become unstable at the critical load and the plates

develop out of plane deflections. Unlike Euler buckling, however, the column can sustain loads greater than the critical buckling load, i.e. the column has a post local buckling reserve of strength. This type of behaviour is classified as stable buckling.

Although these two modes of buckling have been described independently, there are certain combinations of dimensions and structural forms which provide coupled buckling or interaction behaviour between the two modes. It is this type of behaviour which is the subject of examination in this thesis.

The ratio of load carrying capacity to structural weight of a thin walled member is often denoted as a measure of its practical structural efficiency. Increasing the structural efficiency, however, tends to lead to geometrical configurations which, although they make efficient use of material, become increasingly liable to exhibit complicated buckling behaviour. Since structural forms which provide high strength to weight ratios are becoming more widely used in present day practical applications, a knowledge and understanding of buckling behaviour due to interaction between different buckling modes has become essential.

The work presented in this thesis describes the mechanics of the interaction between the local and overal flexural behaviour of a thin walled lipped channel column when subjected to end compression and bending. Although much of the published works on interaction buckling deal extensively with columns whose critical buckling loads

are relatively close and which are therefore highly susceptible to geometrical imperfections and unstable post interaction behaviour, the work in this thesis deals in the main with columns whose critical loads are sufficiently far apart that stable post interaction behaviour is experienced. Columns in this range are not as sensitive to geometrical imperfections regarding their ultimate loads as are those which have nearly simultaneous buckling loads.

The characteristic behaviour of a lipped channel column when loaded through its centroid and designed such that it lies in the stable interaction range is such that the column takes load with no column or local deflections up to the initial local buckling load. Further increase in load then leads to an elastic interaction phase whereby column and local deflections grow simultaneously and the load tends asymptotically towards a reduced Euler load based on the tangent bending stiffness of the locally buckled section. Since, however, the locally buckled form does not remain constant during loading, the reduced Euler load becomes continually smaller as the loading increases. Finally, the elastic interaction phase terminates when the stresses within the column reach the yield stress of the material. The column then enters an elasto-plastic phase of behaviour which, although short, results in further loss of section stiffness and eventual column collapse.

Apart from some isolated works in the early 1950's and early 1960's, knowledge of the problem of non-linear interactive buckling has come to light and received widespread attention in only the last ten years or so. This growing interest in non-linear buckling phenomena is the result of a quest by researchers to gain a full understanding of the possible catastrophic elastic buckling failures which can exist in a structure due to the coupling or interaction of buckling modes. Buckling of this type is characterised by a structure with close critical loads, which in themselves are essentially stable, but which interact to produce a highly unstable non-linear buckling behaviour.

1.2 REVIEW OF THE EARLY DEVELOPMENT WORK

The local instability and post buckling behaviour of plates in compression under a wide variety of loading and boundary conditions has been thoroughly investigated over the years by numerous researchers. The buckling and post-buckling behaviour of systems of plates forming a wide variety of cross-sectional shapes has also received a great deal of attention over the years and the findings are well documented in the literature. In view of this the author feels justified in referring the reader to the works of Timoshenko and Woinowsky-Krieger (1), Bleich (3), Walker (12), Bulson (13) and Rhodes (19) in which the main results of such investigations are

presented and to restrict his own attention to the review of literature pertaining to the interaction of local buckling with other buckling modes.

One of the earliest publications on interaction buckling was presented by Bijlaard and Fisher (4) in 1952. In this work Bijlaard considered theoretically the interaction at buckling of centroidally loaded box, I, H, T and angle section columns, while co-author Fisher carried out tests for a considerable range of slenderness ratios of two aluminium alloy box sections. For one of these the local buckling stress was in the plastic domain, and for the other in the elastic domain. In the introduction to their work the authors suggest that although buckling is supposed to occur at the lower of the two critical stresses, column or local for a given column, in reality there was an interaction of these two modes such that the real buckling stress σ_{CR} would be smaller than either of the buckling stresses corresponding to column or local modes of behaviour. By his method of split rigidities Bijlaard then developed simple formulae which expressed the actual buckling stress σ_{CR} directly in terms of the column and local buckling stresses. He found from his analysis that for the box, I and H sections considered, stress reduction due to interaction of the buckling modes was non-existent. He did find, however, that for sections which have a tendency to behave in a torsional manner, such as the T and angle sections analysed, significant interaction effects were predicted.

The results by Bijlaard yielding non-existent interaction effects are, of course, due to the fact that the sections considered have minimum buckling stresses for the individual modes of local and column buckling which require quite different buckle half wavelengths. For such cases the actual buckling stress is simply the lower of either the column or local buckling stresses. If, however, the buckling modes occur at the same stress, or nearly the same stress, the unstable nature of the post-buckling interaction behaviour of the column causes a high sensitivity to imperfections which can result in failure of the column at a much lower stress. This, however, is not particularly evident from the experimental results of Fisher since the columns he tested were manufactured from $2\frac{1}{2}$" square (outside dimensions) aluminium drawn tubing which exhibited extremely good accuracy regarding imperfections. The results, as shown in Figure 1.2.1, do indicate however that in the area of near simultaneous buckling stresses the ultimate stress of the column is in the region of the local buckling stress, which shows the unstable post-buckling interaction behaviour in this area.

Harvey (5) in 1952 studied the local instability of various structural sections when subjected to column and beam loading respectively. For a detailed description of the method used by Harvey to obtain the section buckling coefficients and corresponding local buckling loads of plain and lipped channel sections in

compression the reader is referred to reference (5). In his treatment of centroidally loaded plain and lipped channel columns Harvey, after obtaining the local buckling stress, considered failure of the column to occur when the edge membrane stress of the plate element initiating section buckling reached the yield stress of the material. Using an effective width equation which incorporated the section buckling coefficient he then obtained the average ultimate stress of this plate element and compared this with the experimental ultimate stress derived by dividing the ultimate load by the column cross-sectional area.

Of particular interest to the author is the experimental work by Harvey on centroidally loaded lipped channel columns whereby the slenderness ratio of the columns tested was varied with change in the web dimension b_w. The choice of dimensions by Harvey were such that both stable and unstable post-buckling interaction behaviour, as well as neutral column buckling, were exhibited during test. His results, in the form of an ultimate load-slenderness plot, are presented in Chapter 6 where comparison is made with the theoretical predictions obtained from the interaction analysis presented in Chapters 3 and 4 of this thesis.

In the light of their previous experimental work (4), Bijlaard and Fisher (6), in 1953, focussed their attention on the strength of columns whose component plate elements buckled locally before the

ultimate column load was reached. The first authors method of split rigidities was used in the theoretical part of this work to compute the column buckling stress for centroidally loaded box and H sections which, after buckling locally, remain straight up to the point of incipient column buckling. In the elastic range a simple formula was developed expressing the apparent bending stiffness of the locally buckled section in the form of an equivalent modulus of elasticity E_{eq}. The stiffness values obtained from this formula lay between the secant and tangent stiffnesses of the section and reduced to Young's modulus E at the local buckling stress. The ultimate column stress in the elastic range is then given by the formula $\sigma_u = \frac{\pi^2 E_{eq}}{(L/R)^2}$. In the plastic range Bijlaard accounted for the influence of plastic deformations by using an appropriate Johnson parabola depending partly for its location on the empirical crushing strength of short columns in which only plate buckling and no column buckling can occur. The ultimate stress curve, by Bijlaard, is therefore one of a double branched nature consisting of a Johnson parabola with its apex at the section crushing strength at $\frac{L}{r} = 0$ and which joins tangentially the elastic buckling stress curve, obtained by the method of split rigidities, at some intermediate slenderness ratio between zero and that at which the local and Euler buckling stresses are equal. This two-part curve is shown in Figure 1.2.2 in comparison with the experimental results obtained by Fisher on $2\frac{1}{2}$" x $2\frac{1}{2}$" aluminium box section tubing having a wall

thickness of 0.047". The results presented by Fisher, with the exception of that at $\frac{L}{r} = 58$, are those obtained in his earlier investigation (4) carried out in 1952 (see Figure 1.2.1). In comparing Figures 1.2.1 and 1.2.2, however, a difference in the theoretically computed local buckling stress is apparent and since the ultimate stress curve by Bijlaard depends partly for its location on the local buckling stress, this would tend to cast some doubt on the claimed accuracy shown in Figure 1.2.2. In the region of near simultaneous buckling stresses the theory of Bijlaard predicts ultimate stress values in excess of the local buckling stress, indicating that in this area initially stable post-buckling interaction behaviour is exhibited.

In 1954, Seidenfaden (7) attempted a theoretical analysis of the interaction behaviour of centroidally loaded, pin ended, plain channel columns. An energy method of solution was employed by Seidenfaden in which the energy expressions for bending and mid-surface stretch were utilised in terms of the derivatives of the displacements u, v and w. By postulating expressions for u, v and w in terms of both local and overall deflection coefficients and by subsequent minimisation of the strain energy with respect to these coefficients, Seidenfaden obtained the behaviour of the column in the interaction range. His treatment of the problem, however, can only be described as inadequate, and consequently his results as inaccurate. One of the main factors contributing to

the inadequacy of Seidenfaden's solution is that his analysis was applied to columns whose ends were constrained to remain straight and the resulting definitive equations were modified to account for pinned end conditions. The modifications, however, took absolutely no account of the quite different post local buckling behaviour which exists between uniformly compressed sections and those whose ends are allowed to rotate.

Cherry (8) in 1960 investigated the influence of local buckling on the lateral stability of thin walled beams. The beams investigated were of I and T section and of such dimensions that local buckling was confined to occur in the compression flange. The loading applied to the beams was that of equal end moments in the plane of the web. By means of an empirically based effective width equation for the compression flange, Cherry obtained modified flexural, torsional and warping stiffness values for the locally buckled section resulting in an elastic lateral buckling curve which showed good agreement with experiment. His experiments showed, however, that in the region of near simultaneous critical moments, the actual moment to cause failure was less than the theoretical local buckling moment. This is due, of course, to the sensitivity of the buckling in this region to initial imperfections. The reason that Cherry obtained good agreement in this area is due to the fact that his effective width equation was obtained by trial and development on the basis of the experimental evidence obtained from the beams tested.

From a compression test on a short aluminium alloy square tube, the result of which is shown in Figure 1.2.3, Jombock and Clark (9), in 1961, obtained the variation in section tangent stiffness from the onset of local buckling to final collapse or crippling of the section. Through a suitable choice of effective width expression which allowed an approximate simulation of this stiffness variation the authors then examined the effect of local buckling on longer lengths of section in which column buckling becomes an increasingly more influential factor. This was achieved quite simply by replacing Young's modulus in the Euler column formula with the section tangent stiffness corresponding to a particular average stress and obtaining the required slenderness value to initiate column buckling at this stress. The ultimate stress curve obtained in this way showed that in the region of nearly simultaneous local and column buckling loads, the capacity of the column was limited to its local buckling load. This result differed from that of Bijlaard (6) due to the fact that Jombock and Clark (9) did not consider the effect on section stiffness of a modification in local mode shape due to interaction with the overall bending mode.

The following year Koiter and Skaloud (10) contested the then generally accepted opinion that the optimum design of a compression member was one in which local buckling and overall buckling occurred at the same stress. Koiter pointed out, with

reference to a compressed integrally stiffened panel, that as soon as the plate buckles locally between the stiffeners its rigidity is reduced by about half, which means that the bending rigidity of the entire panel is also considerably reduced, resulting in a structure whose equilibrium at buckling is unstable and which is exceedingly sensitive to imperfections. Koiter showed qualitatively that, for structures with an unstable bifurcation point, the effect of initial imperfections was to considerably reduce the ultimate load. These remarks by Koiter on the questionable validity of the optimality of simultaneous mode designs were to be corroborated some years later by several investigators.

Using an exact determinantal method Bulson (13) in 1967 obtained the variation in buckling stress with change in flange width for uniform thickness T sections loaded in pure compression and having an imposed hinge support condition along the web-free edge. In his analysis Bulson considered the effect of mode coupling on the stability for such a problem and found that, in the area of close torsional and local modes of behaviour, a considerable reduction in buckling stress, due to interaction, was apparent. It should be pointed out, however, that Bulson's theory is limited to the evaluation of interaction in which the mode of local buckling is given by a single half wave. Figure 1.2.4 shows his results for T sections whose length to web ratio $\emptyset$ is equal to four. It is clearly indicated in this figure that interaction has its strongest

effect in the region of near simultaneous torsional and local buckling modes.

Bulson used the same method of analysis in his consideration of the interaction at buckling between the local and overall flexural modes of behaviour for a uniform thickness I section. For a section whose cross-sectional dimensions were of such proportions as to preclude the occurrence of torsional instability he showed that, for column lengths in which overall buckling was predominant, his interaction analysis gave values for the buckling stress which were marginally smaller than the Euler buckling stress.

In the same year a theory was presented by Graves Smith (14) for predicting the ultimate strengths in compression of locally buckled box section columns, the author giving due consideration to the effects of plasticity and to the interaction of column and plate behaviour. In his compression analysis of short columns free from bending he obtained, through the use of a relaxation process, an approximate solution to von Karman's equations whereby displacement functions for the locally deflected shape were realised in terms of unknown parameters. After satisfaction of the kinematic boundary conditions at the plate junctions the resulting deflected form obtained was constrained to retain its shape during post local buckling and could change in magnitude only by means of a single deflection parameter.

When considering plasticity Graves Smith assumed that the section material behaved in an elastic-perfectly plastic manner and that the extent of the plastic zones within the section were governed by the von Mises Criterion. By numerically integrating discrete expressions for the plastic and elastic components of strain energy he obtained the total strain energy stored in the section corresponding to any particular value of applied axial strain and by minimising this energy with respect to the unknown deflection parameter achieved an approximate equilibrium state corresponding to the applied strain considered.

Results from this analysis are shown in Figure 1.2.5 in the form of post buckling stiffness curves for various values of material yield stress, these curves pertaining to a square section with width to thickness ratio of the plates equal to 58.8. From this figure a considerable loss in section stiffness due to plasticity is apparent and the theory is seen to be able to describe the region of load shedding typically observed in actual tests. Cf. the work of Jombock and Clark (9), Figure 1.2.3.

In his interaction analysis, associated with longer columns which have the tendency to buckle Euler-wise under axial load, Graves Smith considered the application of an infinitesimal bending strain to the column for each value of axial strain considered in his compressional analysis. By solving modified von Karman equations

to describe this situation he evaluated the bending stiffness of the column during the application of this strain. The variation in bending stiffness with average column stress is shown in Figure 1.2.6 in the form of corresponding apparent Young's Modulus curves and the bending stiffness is seen to drop considerably as the ultimate load is approached, and in the purely elastic case is seen to level out at a reduced value as the average column stress is increased.

In support of his theory Graves Smith carried out a fairly extensive series of tests on model columns cut from thin walled steel and aluminium drawn tubing. This work is described in another paper (15). Figure 1.2.7 shows the comparison of his theory with tests carried out on 2 " square (outside dimensions), 0.04 " thick aluminium specimens and it will be seen that they compare well. It should be noted, however, that the interaction curve developed by Graves Smith is similar to that of Bijlaard (6) on the same problem in that it suggests that in the region of near simultaneous local and Euler buckling stresses the equilibrium at buckling is initially stable.

Although the analysis by Graves Smith has the facility of allowing for the effects of local imperfections, it is evident from his work that he did not fully realise the significance of such imperfections in the range of near simultaneous mode behaviour. This is indicated in the comparison of his theory, as presented in reference (15), with tests carried out on steel specimens in which

his results are generally poorer than those obtained from his aluminium tests. Graves Smith attributed the scatter in his results to the initial variation in material yield stress from column to column where in actual fact his results are poorest in the region of simultaneous buckling modes where the buckling is entirely elastic. The ultimate average stress for columns in this region were as much as 16% below the local buckling stress.

1.3 THE ONSET OF A GROWING INTEREST IN NON-LINEAR BUCKLING PHENOMENA

In 1968 van der Neut (17) used a simple two-flange column model to examine the equilibrium state at bifurcation for columns subject to the interaction of local and overall buckling. Figure 1.3.1 shows some typical structural forms and the representative model used by van der Neut to describe the phenomena under consideration. The model, as depicted, consists of two load carrying flanges of width b and thickness h connected at a distance 2c by fictitious webs, the webs having no longitudinal stiffness but being rigid laterally and considered to provide simple support conditions to the edges of the load carrying flange elements.

To aid in the solution of his column interaction buckling problem van der Neut (16) first examined the post local buckling behaviour of a simply supported imperfect plate in compression, the

plate having stress-free boundary conditions prevailing on the unloaded edges. For the perfect plate he obtained the deflected form at buckling by solving von Karman's equilibrium equation corresponding to a uniform longitudinal compressive stress and subsequently satisfying the relevant equilibrium and compatibility requirements at the plate boundaries. The post-buckling behaviour of the plate was then obtained by postulating deflections in this range tohave the same form as that attained at buckling and solving von Karman's compatibility equation exactly, subject to the relevant in-plane movement and stress boundary conditions, to obtain membrane stresses which were in compliance with the assumed deformations. The final relationships between compressive strain and out of plane deformations and hence between plate load and compressive strain were then realised by solving the equilibrium equation approximately using the Ritz-Galerkin technique. For the imperfect plate van der Neut assumed the imperfection to have the same form as the buckling mode for the perfect plate.

Using the relationships developed in his plate analysis (16), van der Neut established the elastic buckling capacity K_b of his two flange column model (17) by evaluating the bending stiffness of the column in terms of the local tangent stiffness of the material in the cross-section. Hence for the load carrying flanges in the locally buckled state he used the elastic tangent modulus ζE in place of the full material stiffness E, which from the bending

stiffness point of view can be interpreted as replacing the actual plate of width b by one having an effective width η b. The elastic tangent modulus η E is defined as the local slope of the curve relating the average strain along the length of the load carrying flanges to the average applied stress.

For the ideal model with perfectly straight axis and perfectly flat plate elements the buckling load K_b, for a column whose flanges have undergone local buckling, is given by $K_b = \eta K_E$ where K_E is the classical Euler load for the locally unbuckled column and η, as defined previously, is the ratio of the post to pre-local buckling tangent stiffness of the load carrying flanges. At the local buckling load $K = K_L$, however, the bending stiffness of the section on the application of an infinitesimal column deflection, is given not as η EI but as $\frac{2\eta}{1+\eta}$ EI due to the fact that as the column bends at this load one flange gets increased post local buckling strain whereas the other flange returns to the locally unbuckled condition. Using the value of 0.4083 for η from his plate analysis van der Neut found that column buckling occurred at the local buckling load for the perfect model when $1 < \frac{KE}{KL} < 2.45$ and that the character of the equilibrium at buckling was unstable, i.e. explosive collapse, when $1 < \frac{KE}{KL} < 1.725$.

To study the effects of local imperfections in the design region of near simultaneous buckling modes van der Neut

considered an equal imperfection parameter α applied to each flange of the column, α being the ratio of the imperfection amplitude to the flange thickness. Figure 1.3.2 shows the relationship obtained between $\frac{Kb}{KL}$ and $\frac{KE}{KL}$ for several values of α where it can be seen that the reduction in buckling strength due to α is more severe in the vicinity of $\frac{KE}{KL} = 1$, e.g. for $\alpha = 0.2$ the reduction in strength is 30%. By using a truncated Taylor-expansion to represent the relation between flange load and strain in the direct vicinity of the buckling load Kb van der Neut ascertained the character of the equilibrium at bifurcation for those columns with initial imperfections, finding that the equilibrium was unstable, i.e. explosive collapse, over a range of $\frac{KE}{KL}$ the extent of which depended on the degree of imperfection.

Although the work by van der Neut deals with a hypothetical structural form and is basically illustrative, the findings from his analysis were the first concrete step in confirming the suspicions of Koiter and Skaloud (10), regarding the imperfection sensitivity of structures with an unstable bifurcation point. His work can also be said to be responsible for creating the subsequent interest shown by a great many researchers in non-linear buckling behaviour.

Further contributions using the same model have been presented by Meijer and van der Neut (20) in 1970, Koiter and Kuiken (22) in 1971, Thompson and Lewis (26) in 1972, van der

Neut (31) in 1973, Gilbert and Calladine (33) in 1974 and in 1975 by Svensson and Croll (42).

Meijer and van der Neut (20) examined the effect of imposing unequal flange imperfections α_1 and α_2 in the load carrying elements of the model, considering the problem to be again one of bifurcation by choosing restrained boundary conditions at the column ends in conjunction with a column length twice that of a column having the same section and with simply supported ends. For this situation the point of application of the compressive force K moves such that the column remains straight during the process of loading up to the buckling load Kb. Figure 1.3.3 shows some results from this analysis for $\alpha_1 = 0.05$ and $0.4 \geqslant \alpha_2 \geqslant 10^{-7}$. It will be seen from this that $\frac{Kb}{KL} < 1$ when $\frac{KE}{KL} < 2$ for the values of α_1 and α_2 considered and that the unfavourable effect of reduction in buckling strength is maximal at $\frac{KE}{KL} = 1$. It is also interesting to note that when α_2 approaches zero the same kind of degeneration of the buckling curve appears as with the column without imperfections, i.e. over a certain range of $\frac{KE}{KL}$ the ratio $\frac{Kb}{KL}$ has almost constant value. Meijer and van der Neut also found that over a range of $\frac{KE}{KL}$ explosive collapse was induced due to the unstable nature of the equilibrium at bifurcation and that the instability was more severe with smaller imperfections.

Koiter and Kuiken (22) presented a somewhat more mathematically elegant treatment of the two flange column problem

with equal flange imperfections. Their energy approach, based on Koiter's general non-linear theory of elastic stability, provided almost identical numerical solutions with those of van der Neut (17), as well as useful asymptotic formulae. Although their analysis does not yield significant new results the authors point out that it requires far less numerical work than other available methods and that the simple and new asymptotic formulae developed enable the effect of equal imperfections to be readily assessed in individual cases.

Thompson and Lewis (26) investigated the optimality of the two flange column model with the view to obtaining the highest possible buckling load subject to the constraint that the structural weight of the column be held constant. Using the results of van der Neut (17) the authors showed that a local optimum existed when the buckling load $Kb = KE = KL$ but due to imperfection sensitivity in this region the optimum shifts to some value $\frac{KE}{KL} < 1$ depending on the imperfection value α while the buckling magnitude diminishes with increasing α. The optimisation scheme was such that the column had a prescribed length L, the web width $2C$ connecting the load carrying flange elements was set equal to the flange width b so that the section under consideration would be square at all times and the structural weight held constant by maintaining constant cross-sectional area, i.e. the area of the flange elements bh = constant. Using this scheme higher values

of Kb can be obtained for the perfect model, for the same structural weight, by making $\frac{KE}{KL}$ large. It should be noted, however, that in this region local deformation of the flanges will be increasingly severe before the onset of column buckling. In such a case the post buckling stiffness of the flanges will change with load, due to changes in the locally deflected form, thus leading to a considerable reduction in Kb from that which would be obtained by approximating the post buckling stiffness of the flanges to be constant. By postulating this elastic deterioration in stiffness to be represented by a relaxed linear relationship with load, Thompson and Lewis found that the local optimum of the perfect model at Kb = KE = KL resulted in the complete optimum, while allowing for the possible erosion of this by initial imperfections. The authors concluded that it pays to make $KE < KL$. This is contrary to the simple argument that, since local buckling does not exhaust the load carrying capacity, it would be best to make $KE > KL$.

Although van der Neut, in his earlier reconnaissance work (17), considered imperfection sensitivity to both local and column axis imperfections, the effect of the latter was studied only in brief. As a result, some uncertainty in respect of his numerical evaluations was apparent and consequently only a qualitative picture of the response to imperfections in the overall mode was presented. To rectify this van der Neut carried out a more in depth investigation (31)

pertaining to a column with clamped ends in which the column axis imperfection was assumed to correspond to the Euler buckling mode. The required relationship between column strength and imperfection magnitude was attained by van der Neut through the satisfaction of the governing non linear differential equations, this being achieved by postulating column deflections under load to be simulated by a trigonometric cosine series.

The main findings from this more complete analysis are depicted in Figures 1.3.4 and 1.3.5. Figure 1.3.4 shows the column strength parameter $\lambda = \frac{K}{KL}$ plotted as a function of the imperfection parameter $\beta = \frac{e_o}{C}$ for various values of $R = \frac{KE}{KL}$ and a fixed value of the local imperfection parameter $\alpha = 0.025$ (e_o = half the imperfection magnitude at the column centre and C = half the web width). From this figure it is seen that for the smaller R values any imperfection β yields reduction of the failure load as compared to the buckling load $\frac{Kb}{KL}$ of the perfectly straight column. For larger R values it is seen that there is again reduction of strength provided β exceeds some critical value β_{CR}; however, for $\beta < \beta_{CR}$ the maximum load tends to $\lambda_b = \frac{Kb}{KL}$ as the column deflection tends to ∞. This is analogous, as pointed out by van der Neut, with the behaviour of rotating shafts whereby, due to initial deflection or eccentric masses, the shaft experiences a dynamic jump, when accelerated slowly, as it traverses the critical speed. Figure 1.3.5 shows λ

as a function of R for several values of β and two values of $\alpha \simeq 0.0125$ and 0.025. The upward sweep of the ultimate load curves, for constant β, towards the $\frac{Kb}{KL}$ curve ($\beta = 0$) occurs at the value of R for which $\beta = \beta_{CR}$. In comparing Figures 1.3.5 and 1.3.2 it can be said that by taking the practical limit of β to be in the region of 6 or 7 per cent, local (α) and overall (β) imperfections yield about equal strength reduction in the region of $\frac{KE}{KL} = 1$ whereas the reduction due to β is more important when $R > 1$.

Other work associated with the two flange column model was carried out by Gilbert and Calladine (33) and Svensson and Croll (42). The first authors used a graphical method, in conjunction with the stress-strain relations from the elastic plate analysis of van der Neut (16), to obtain the sensitivity response corresponding to arbitrary combinations of local and overall imperfections while the second authors used a combined perturbation/Newton-Raphson approach to test the reliability of the van der Neut model in constituting a valid basis for obtaining quantitative strength estimates of thin walled box columns. In considering ultimate column strength Svensson and Croll used the criteria, as is used in this thesis, that the strength is exceeded when the average flange stress in the concave flange at the middle of the column reaches a certain value σ_{ult}, this being attained when the value of the maximum edge

stress σ_e reaches the yield stress σ_y. To give a more complete presentation of their work they developed, on the basis of the van der Neut model and the strength criterion previously mentioned, a generalised version of the well known Perry-Robertson formula, using this to give a realistic estimate of the ultimate carrying capacity of square box columns. Figure 1.3.6 shows some results whereby the column strength P is plotted as a function of the plate width to thickness ratio λ such that the structural weight remains constant for a specific column length. From this figure it can be seen that the effect on carrying capacity of increasing length is considerable, especially for the smaller λ values encompassing the range which provides near simultaneous mode behaviour for each perfect structure. It will also be noticed that increasing length shifts the optimum geometrical design, in respect of strength, to cross-sectional configurations with higher values of λ. The theoretical curves presented by Svensson and Croll are seen to be comparable with those of the earlier work by Kloppel and Schubert mentioned in the same paper.

1.4 COUPLED BUCKLING BEHAVIOUR OF STIFFENED PANELS

Now that researchers were aware of the possible dangers associated with coupled mode buckling and the manner in which a conventional buckling analysis could overestimate structural strength,

concentrated efforts were made to investigate the interactive behaviour of more practical structural shapes.

One such configuration which received widespread attention was the stiffened plate panel with plain flat outstands. Panels of this nature are used essentially in situations where high strength to weight ratio is important, as for example in box girder bridges or the superstructures of off-shore oil platforms. Figure 1.4.1 shows a typical panel geometry and Figure 1.4.2 shows schematically the cross-section geometry of a box girder.

After the Second World War many of the road bridges built throughout Europe utilised the box girder in their construction. A series of failures, however, occurring in the late 1960's, raised some doubts about the ability of existing analytical methods to predict the carrying capacity of these bridges. Although there is no single criterion which can be used as an overriding factor in the design of box girders, it is not difficult, using present-day knowledge, to envisage some form of interactive buckling as being the initiating factor in causing failure.

Tvergaard (30), in 1973 investigated the initial post buckling behaviour of wide integrally stiffened panels loaded in compression. The panels investigated had the geometry and geometrical notation shown in Figure 1.4.1 and were simply supported along the edges on which the compressive load acts.

Although his analysis could account for the torsional behaviour of the stiffeners, Tvergaard found that this effect could be neglected for a large range of practical structures having small values of stiffener eccentricity. Special attention was directed to panel designs in which the Euler and local buckling modes occur simultaneously with a view to establishing the imperfection sensitivity that may be inherent in these designs.

Tvergaard determined the behaviour of the panels by using the general initial post buckling theory of elastic structures as developed by Koiter (11), this being essentially a perturbation technique which relies for its solution on the principle of stationary potential energy. The resulting asymptotic equilibrium expressions obtained from his analysis, relating the applied load to local and overall displacements and local and overall imperfections, demonstrated that the simultaneous mode design was very sensitive to geometrical imperfections and that the panel was more sensitive to imperfections in the shape of the local buckling mode than to imperfections in the shape of the Euler buckling mode. It should be emphasised, however, as mentioned by Tvergaard, that for panels with near simultaneous buckling modes the single mode initial post buckling analysis is only adequate in the immediate vicinity of the critical bifurcation point. This is due, of course, to the presence of the other buckling mode corresponding to a buckling stress only slightly above the critical stress, with a non-linear coupling between the two buckling modes.

Having established that in cases when Euler type buckling and local buckling occur at the same critical stress, the stiffened panel structure is particularly imperfection sensitive, Tvergaard (32) focussed his attention on the influence of post buckling behaviour on the optimal design of these panels. Since, however, the asymptotic results of his earlier work (30) are not applicable for this purpose, as the adequacy of the single mode initial post buckling analysis is limited to very small deflections, Tvergaard based his analysis on an approximate solution of the non-linear differential equations by application of the Galerkin method.

Some of the results obtained by Tvergaard are shown in Figures 1.4.3 and 1.4.4. From these figures it can be seen that the optimum design, from the point of view of post buckling behaviour, often differs significantly from the design with two simultaneous buckling stresses. Figure 1.4.3 indicates that for the panel geometry considered, the highest carrying capacities are predicted in the range where the local buckling stress has been exceeded, where in fact the ultimate load can be larger than the critical load of the perfect structure in the simultaneous buckling case. In this stable range, however, the limit load corresponds to quite large mode deflections and in practice plastic deformations may often reduce the maximum load as predicted by Tvergaard's elastic theory.

From the point of view of retaining a high section stiffness at the highest possible load level, Tvergaard points out that the best design is usually one in which the critical stress for Euler type buckling is smaller than that for local buckling and that in some cases the optimum design has a local buckling stress that is more than twice the Euler buckling stress. Figure 1.4.4 shows the ultimate loads attainable for designs in this region. It can be seen from this figure that local mode imperfections of a given amplitude have a more serious effect than Euler type imperfections of the same amplitude and it may be said that if imperfections can be kept small, the optimum design will correspond to values of the ratio of local buckling stress to Euler buckling stress slightly higher than unity, but for larger imperfections the ratio for optimum design increases considerably. Although Tvergaard uses a simplified structural model in his analysis, in that the stiffeners do not participate in local buckling but may buckle torsionally, his work must be regarded as a useful first reconnaissance in an attempt to establish the significance of mode interaction in stiffened panels.

It is not surprising that the work by Tvergaard caught the attention of several researchers already working in the field of non-linear buckling and induced them to apply some of their efforts to the stiffened panel problem. This was apparent from the number of papers (34, 35, 36, 37) presented to the IUTAM Symposium on Buckling

of Structures, held at Harvard University, Cambridge, USA, in June 1974. Van der Neut (34) examined the mode interaction of panels stiffened by top hat stringers and with rigidly restrained boundary conditions at the panel ends. Koiter and Pignataro (35) used an approach similar to that used in Koiter's earlier work (22) to examine the interactive behaviour of stiffened panels of the type investigated by Tvergaard (30, 32). Thompson, Tulk and Walker (36) made use of small scale epoxy plastic models in their experimental investigation of the imperfection sensitivity of stiffened panels, while Tvergaard and Needleman (37) studied the effect of mode interaction on the plastic bifurcation of stiffened panels.

Although Van der Neut (34) included the participation of local buckling of the stiffeners in his analysis, the structural model employed for the panel overestimates the adverse effect of interaction. This is due to the fact that the webs of the top hat stiffeners are neglected in the post buckling range and serve only to maintain the structural integrity of the assembly. The model employed is essentially a two flange column with unequal flanges and with rotational edge restraints obtained from a linear buckling analysis of the full panel cross-section. The coefficients of edge restraint of the flanges are assumed to be constant through the whole range of applied edge strains and equal to their values obtained at buckling. On the other hand, the analysis by Koiter and Pignataro (35) underestimates the adverse interaction behaviour of panels with solid

integral stiffeners, due to its assumption that the local mode shape of the cross-section remains unaltered in the post buckling domain.

Of particular interest in the work by Thompson, Tulk and Walker (36) was the use of an epoxy plastic in the manufacture of small scale test models. The low modulus of elasticity of this material allowed the models to be tested on a simple hand-operated rig, while the material had the added advantage of remaining elastic up to large strains so that yielding was avoided and the models could be tested repeatedly. Another advantageous property of the epoxy plastic is that the material suffers from a considerable amount of creep at elevated temperatures. Thus, if a panel was loaded to its local buckling load and then heated, it was possible to induce local imperfections having a geometric form corresponding precisely to the local buckling mode.

Tvergaard and Needleman (37) investigated the plastic buckling of wide integrally stiffened panels of the type investigated in Tvergaard's earlier work (30,32). In order to make the panels bifurcate at plastic strains, these had been given a relatively larger plate thickness and stiffener eccentricity than those in (32). The initial post bifurcation behaviour in the plastic range was determined using an asymptotic analysis to obtain approximate results for the ultimate panel load and for the corresponding buckling mode deflections. An interesting feature of the work by Tvergaard and Needleman is that in the plastic range the propagation of elastic

unloading zones into the material play an important role in the subsequent panel behaviour after bifurcation. In a further paper, Tvergaard and Needleman (43) presented a more detailed description of their bifurcation and post bifurcation analyses together with details of their numerical procedure. Some results for the effect of plastic yielding on imperfect panels designed so that bifurcation of the perfect structure occurs in the elastic range were also presented.

Further work on the elastic buckling of panels with heavy stiffener outstands was carried out by Walker (40) and Walker and Davies (41) in 1975 and by Tulk and Walker (45) in 1976.

In the analysis by Walker (40), the behaviour of the plate between the stiffeners was described by two simple expressions relating the local deflection amplitude w and the corresponding end shortening displacement δ to the applied stress σ on the plate. From these relationships, however, the resulting reduction in section flexural rigidity, which is responsible for the adverse non-linear interaction between local and overall buckling, is found to remain constant for all values of load in the post critical range of local buckling. This is due, of course, to the implied assumption in the simple plate expressions used that the locally deflected form remains constant during loading, as has also been the case in the work of previous researchers. For perfect panels, Walker (40) shows all load-overall deflection curves tending asymptotically towards a constant reduced Euler load based on the tangent bending

rigidity of the section after the occurrence of local buckling. The ultimate elastic load that a panel, designed in the stable range, can therefore attain is the reduced Euler load and theoretically its post interaction behaviour will always be stable. If, however, his analysis had the facility of allowing the locally deflected form to change during loading then the initially stable behaviour of the panels would eventually become unstable. Walker's analysis included the effect on ultimate load of overall imperfections and he compared his theoretical findings with previous experimental work (36) on small scale models. The models, however, had imposed local mode imperfections and the effect of these is clearly indicated in his comparison.

Walker and Davies (41) used a similar approach to that of Walker (40) in their elastic buckling analysis of stiffened panels. This time, however, the simple parametric relationships employed included terms which took into account the effect of local imperfections. The local imperfection parameters in the relationships were based on the assumption that the initial local deflections had the same form as the critical mode shape and the complete expressions implied that the locally deflected form altered with increasing load. The inclusion of local imperfections in their analysis provided good agreement between theory and experiment (36). Walker and Davies (41) considered, experimentally, the behaviour of panels

having torsionally flexible stiffeners (see also reference (36)) and of panels under combined longitudinal and shear displacements. From this, it was found that the interaction of the stiffener torsion mode and the panel overall mode gives rise to a very violent type of buckling and a high degree of imperfection sensitivity and that shear displacements also considerably reduce the panel ultimate load.

The work presented by Tulk and Walker (45) on the model elastic studies of stiffened panels gives more details of the experimental work of reference (36).

Up to this point, studies of the interaction of local buckling and Euler buckling in stiffened panels have in the main considered panels which have relatively stocky compact stiffeners, thereby causing local buckling effects to occur solely in the plate between the stiffeners which lies parallel to the axis about which the panel bends. In the case of thinner and deeper stiffening members, however, local buckling may have its predominant effects in the stiffeners which are perpendicular to the bending axis of the panel, resulting in a substantially different post-buckling interaction behaviour. A consequence of designs with thinner and deeper stiffening members is, of course, the introduction of a third mode of buckling associated with the local-torsional behaviour of the stiffeners. The effect of this mode on the overall behaviour of stiffened panels was investigated in 1976 by Fok, Rhodes and

Walker (44). A simplified mathematical model, based on a semi-energy post local buckling analysis of the stiffener in which the stiffener was considered to be fully rotationally fixed to the plate, was used to describe the buckling process of the panel. Fok, Rhodes and Walker (44) considered the effect of overall imperfections in their analysis and the comparison of their theoretical results with experiment was shown to be good for load deflection behaviour but less accurate regarding imperfection sensitivity. Although the mathematical model retains only certain of the physical attributes of the real structure, their analysis led to a sufficiently accurate description of the buckling process and provided a basis for further investigation. In 1977 Fok, Walker and Rhodes (53) extended their previous work (44) to include the effect of local imperfections in the stiffener outstands. From this, more accurate panel sensitivity curves could be obtained.

Having examined the behaviour of stiffened panels with solid stiffeners (35), Koiter and Pignataro (47), in 1977, turned their attention to those with thin walled stringers. To evaluate the reduction in panel flexural rigidity due to local buckling, Koiter and Pignataro used a lower bound approach in which the strain energy due to transverse normal stresses and shear stresses is neglected. Although the approach used gives an overestimate of the effects of interaction, their results show that for top hat stiffened panels interaction is much less severe than that predicted by van der

Neut (34). The exaggeration of the adverse interaction behaviour in the work of van der Neut (34) is due to the fact (as previously implied) that the flanges of his representative two flange model are elastically uncoupled and therefore behave independently in local buckling.

Van der Neut (52) in 1977 and, more recently, Koiter and van der Neut (57) in 1979 have investigated the effect of allowing changes in the local mode shape after the occurrence of local instability. To account for the interdependence in local buckling of the plate elements in real structural forms, van der Neut (52) and Koiter and van der Neut (57) used a two flange model in which the flanges were coupled by an elastic medium having a constant stiffness per unit area. The model allowed a rather simple analytical treatment, however, in that the flanges were treated as being simply supported on their unloaded edges with either stress-free or straight edge boundary conditions.

From these works (52,57) it followed that changes in the local mode pattern were insignificant for the panel with top hat stiffeners (52), but quite significant for the square tube section (57) in which a modification of the local mode shape due to interaction with the overall bending mode was apparent. In the region of near simultaneous local and overall buckling modes, the model predicts initially stable post-buckling interaction behaviour, indicating that

in this region the local buckling load is not the ultimate load. The eventual column buckling load is, however, unstable in this region and continues to be so over a range of Euler to local buckling stress up to about two. The results from the model for square tubes (57) are indicative of those obtained from the much earlier work of Bijlaard and Fisher (6) and from the later work of Graves Smith (14) - see Figures 1.2.2 and 1.2.7.

1.5 LOCAL AND OVERALL BUCKLING OF BEAMS AND COLUMNS

As has been shown in the previous section, a considerable amount of work on interactive buckling has been associated with the stiffened panel structural configuration. In parallel with this, however, the interactive buckling behaviour of beams and columns having various cross-sectional shapes and under several loading conditions, have been examined.

Using a unified matrix approach, Ghobarah and Tso (18), in 1969, investigated the stability of uniformly compressed plain channel columns, their analysis including the interaction of overall flexural and local buckling modes of behaviour but precluding overall torsional behaviour. The matrix formulation used by these authors, however, which expresses the state vector at any particular point (in terms of deflection, slope, moment and shear) as a linear combination of the same quantities at another point, was applied, not

to the channel section, but to a rather crude intuitive structural model, the critical load of which was assumed to give a realistic estimate of the buckling stress of the channel. The theoretical results obtained from their analysis therefore can only be regarded as approximate.

Skaloud and Zornerova (21), in 1970, carried out an extensive experimental investigation to study the interaction of the buckling of compressed columns with the buckling of their plate elements. The columns tested were fabricated from top hat sections having very small lips and joined together at the lips to form closed tubes, as shown in Figure 1.5.1. Due to this method of manufacture local buckling was initiated by the flange plates, since the small lips give added buckling strength to the webs. From the results of their investigation the authors confirmed that, due to initial irregularities of column axis and plate flatness as found in real structures, the ultimate column stress was lower than either the plate stress or the Euler stress for columns with nearly simultaneous buckling modes.

The stability behaviour of plain channels in compression was examined by Wittrick and Williams (24) in 1971. The authors used a matrix approach, treating each individual flat wall of the section as a single element. In their analysis the buckling stress was ascertained from the determinant of the overall stiffness matrix of the structure, this single equation containing all the possible buckling

modes whether local, Euler or torsional. Due to the exact nature of their theory Wittrick and Williams accounted fully for the possibility of mode interaction. They found, however, that all buckling modes obtained contained mixtures of local and overall deformations although one mode may only have been present in negligible proportion. Figure 1.5.2 shows the results of their exact solution compared with those of Ghobarah and Tso (18) on the same problem and although Ghobarah and Tso did not account for torsional behaviour in their analysis, appreciable differences in the other two modes are evident.

As an extension of his earlier work (14,15), Graves Smith (25), in 1971, examined the effect of residual stresses, as well as geometrical imperfections, on the strengths of thin walled welded box columns. Using a variational approach in conjunction with modified elastic stress-strain relations, which took account of the residual stresses caused by welding, he found that column strength reduction due to the welding stresses was of the same order of magnitude as the residual compressive stress in the plates.

In 1973 contributions to the knowledge of interactive beam and column behaviour were made by Rajasekaran and Murry (27) using a finite element method, Hill (28) using the semi energy method of analysis as is essentially employed in this thesis, and Wang and Tien (29) using the concept of effective width in conjunction with a numerical iteration procedure.

Rajasekaran and Murry (27) studied the interaction of local plate buckling with overall member buckling for axially loaded columns and transversely loaded beams of I-shaped cross-section. Their analysis precluded post local-buckling interaction behaviour and consideration was given to the interaction of local and Euler buckling and of local and lateral buckling at the initial instability stress only. The inability of their finite element model, however, to predict the uncoupled critical local buckling stress of sections with small flange to web ratios, restricted the authors in their interaction analysis to sections having wide flanges only. The reason for this rather unfortunate feature of their work lies in the fact that the assumed local displacement shape functions used by them were not general enough to describe the fundamental local buckling mode for sections whose buckling is initiated by the web.

Hill (28) examined the local-Euler interactive buckling behaviour of lipped channel columns by selecting displacement functions in the post local buckling range to describe the local form of the column cross-section in terms of one unknown coefficient and by assuming the form of the column lateral deflection to be sinusoidal. In his analysis, however, he neglects the complementary function solution of von Karman's compatibility equation and, due to the fact that local deflections are controlled by a single coefficient, he constrains the buckled form to remain constant throughout all stages of loading in the post local buckling range. Although the application

of the semi-energy method yields, in general, an upper bound solution for stiffness, the use of a single "guessed" term by Hill in the post-buckling solution, i.e. the deflected form used, was not obtained from a Rayleigh-Ritz local buckling analysis or the like, along with the disregard of the complementary function solution of von Karman's equation and the assumed form for column lateral deflection, renders his solution to be of only an approximate upper bound nature.

Wang and Tien (29) determined the elastic column instability stress of locally buckled centroidally loaded rectangular columns using Winter's effective width expression to account for the post local buckling strength of the plate elements of the section and a numerical iteration procedure to predict the critical column stress. By careful selection of the geometrical parameters, however, solutions were obtained for columns in which local buckling was confined to occur theoretically in the wider plate elements of the cross-section only, the other plate elements remaining flat. As confirmatory evidence of the reliability of their method it would perhaps have been better if they could have obtained results for centroidally loaded square box sections in which all plate elements buckle simultaneously and compared these with the well established experimental work of Bijlaard and Fisher (4) and Graves Smith (15) whose theoretical work they mention in the introduction of their paper.

A brief state-of-the-art review of interactive buckling behaviour in plate structures was presented in 1974 by Maquoi and Massonnet (38), this being a consequence of a commitment by one of the authors in the drafting of structural codes at Belgian and European level. The main aim of their paper was to examine the validity of the academic criticisms presented in the literature against the classical naive simultaneous mode approach in design. The authors concluded that although imperfections reduce considerably the ultimate strength in this area and in many cases result in an optimum shift to designs in which the ratio of overall mode to local mode is less than one, in the case of box columns the so-called naive approach still constitutes an acceptable tool for selecting plate thickness. This conclusion, however, is not surprising since academic arguments against simultaneous mode design, on the basis of optimum shift caused by imperfections, were set up from either the consideration of an idealised two flange model which disregards the presence of webs and their interaction with the other plate elements of the cross-section, or on the stiffened panel type of configuration in which local mode deflections are largely confined to one side of the cross-section leading to substantially different behaviour than that of the box section in which the primary local mode in compression displays significant deflections on both sides of the neutral axis.

In the same year De Wolf, Peokoz and Winter (39) tackled the problem of columns subject to local buckling by means of a semi-empirical approach utilising the concept of effective width. Test columns were manufactured from plain channels connected to form rectangular and I-shaped cross-sections and due to this local buckling was confined to occur in the wider plate elements for rectangular sections and in the unstiffened plate elements for the I-shaped sections. The analytical approach used by De Wolf et al was based on the Engesser-Shanley tangent modulus equation for the bifurcation stress of a column, this equation being suitably modified to account for the effects of non-uniform material properties and local buckling, the latter being included by means of the effective width expressions developed by the third writer in the 1940's. The authors found that the effective width approach used gave reasonably good predictions of the ultimate strengths of the columns tested.

An interesting comparison was made by Rhodes and Harvey (46) in 1976, in their analysis of the local and post local buckling behaviour of plain channel struts in compression. Although no account was taken of other forms of buckling in their analysis, a reasonable estimate of the effects of Euler buckling was obtained by evaluating the Euler stresses from simple theory and superposing these on the local buckling stresses from their energy analysis. Figure 1.5.3 compares the results from this simple method with those

of the more rigorous interaction approach used by Wittrick and Williams (24). For the strut length to flange ratios of 7.5 and 15 it can be seen that the Euler, torsional and local buckling modes act separately with no stress reduction occurring due to mode interaction. On the other hand, for the length to flange ratio of 2 stress reduction due to interaction of local and Euler buckling is clearly indicated, this being due to the buckle half wavelengths of the two modes being of the same order. The comparison of results shown is very good and would tend to highlight the approximate nature of the work by Ghobarah and Tso (18) as shown in the comparison by Wittrick and Williams (24). The slight differences in the local buckling curves are due to the different values of Poisson's ratio used in each analysis.

Continued interest in non-linear coupled buckling behaviour was apparent from the papers (48,49,50) presented at the Second International Colloquium on the Stability of Steel Structures held in Liege in 1977. Skaloud and Naprstek (48), working at the Czechoslovak Academy of Sciences in Prague, used the concept of effective width and a numerical technique combining the methods of successive approximation and Runge-Kutta to determine the equilibrium state of rectangular box section columns, the authors terminating the elastic solution at the onset of yielding to obtain an estimate of column capacity. Figure 1.5.4 shows some results from this simple

approach, the ultimate load $\overline{N}$ being plotted as a function of the column length for columns loaded centroidally and having pinned ends. The curve N_{CR}^{e} (el) is the classical Euler value and the curve N_{CR}^{e} (pl) indicates the onset of yielding, both these curves being depicted for locally buckled columns without imperfections. The curve $\overline{N}$ is the limiting load caused by yielding for columns having an overall imperfection in the form $y_o = f_o \sin \frac{\pi x}{L}$ and whose amplitude f_o is realistically based on statistical observations. As is shown in Figure 1.5.4, the method used by these authors predicts substantial strength reductions due to this type of imperfection; some comparison with experimental work would, however, determine its reliability.

Reis and Roorda (49) examined the sensitivity of the buckling load to changes in design and imperfection parameters in their study concerning the interaction of lateral torsional and local plate buckling in thin walled beams. As a special case of the relevant governing differential equilibrium equations they obtained the uncoupled non-linear equilibrium path for a simply supported T-section beam subjected to increasing applied end moments in the plane of the web and having overall lateral torsional imperfections. Along this uncoupled path the compound bifurcation moment Λ_b was determined by means of a generalised Rayleigh-Ritz analysis which obtained the local plate stability of a beam element at mid-span of the beam.

Figure 1.5.5 shows qualitatively the equilibrium behaviour obtained by Reis and Roorda of a thin walled T-section beam subject to mode interaction. In this figure the parameter Λ_I is the critical load parameter associated with torsional buckling of the perfect or ideal beam, Λ_{II} the critical local parameter, Λ_b the compound parameter and Λ_r the reduced parameter towards which all equilibrium paths are asymptotic. The parameters ϵ and β are imperfection and design parameters respectively. Figure 1.5.6 shows the local co-ordinate system of the beam element considered by Reis and Roorda and the assumed local form at instability along the uncoupled equilibrium path. Comparison of theoretical buckling moments with experimental results are shown in Figure 1.5.7, where it is seen that simultaneous mode designs are highly imperfection sensitive.

The work by Rhodes and Harvey (50) examined the interactive behaviour of plain channel columns under eccentric loading, their approach taking into consideration local buckling in all elements of the section and also allowing for variation in the locally deflected form after buckling. In their approach the buckling load and shape of the local buckles were obtained very accurately using a multi-term energy analysis and the deflected form so obtained then used in a semi-energy post buckling analysis. Although the load-deflection equilibrium equation developed by Rhodes and Harvey for the locally

buckled column was derived on the basis that only the magnitudes of the local buckles changed after buckling, the authors, while still retaining the simple form of this equation, took into account changes in local form by setting up a large number of such equations corresponding to the initial compression eccentricity applied and also for a range of other eccentricities. The authors then chose the lowest envelope of all such curves as being the most accurate solution based on the premise that due to the relationship between load point displacement and column deflection it prescribes approximately the least value of the potential energy of the system. Figure 1.5.8 shows some interesting points highlighted from their results. Figures (a) and (b) indicate the geometrical notation and positive sense for overall deflections employed in their analysis while figures (c) and (d) show the reduction in Euler load and neutral axis shift at buckling. N_{CR} is the Euler load for locally unbuckled columns while N_{CR}^{*} and e^{*} are the reduced Euler loads and new neutral axis position respectively at buckling. In figure (c) the full line indicates the immediate reduction in N_{CR} at buckling and the dotted line the asymptotic value well into the post buckling range. For columns with narrow flanges, $h/h_w < 0.325$, overall deflections will develop in the negative direction at the point of local buckling as is indicated in figure (d) by the neutral axis moving further away from the web. For columns with wide flanges,

$h/h_w > 0.325$, the neutral axis approaches the web after local buckling and the column buckles in the positive direction. Figure (c) shows greater reduction in Euler load for columns which deflect in the positive direction than those for negative direction buckling.

The finite element method was used by Wang and Wright (51) in 1977 to determine the torsional flexural behaviour of locally buckled beams. In their analysis, the resulting determinantal equation, in which the coefficients of the elastic stiffness matrix were computed on the basis of the effective cross-section corresponding to the current moment distribution in the beam, was solved iteratively to obtain the lateral buckling strength of the beams. Figure 1.5.9 shows some results for simply supported continuous beams loaded uniformly along the centre span. A reduction in lateral buckling strength due to local buckling is indicated.

Several of the experimental results of this thesis were published in 1978 in the work by Thomasson (54) for the Swedish Council for Building Research in Stockholm. Thomasson carried out many tests on lipped channel columns with single and double vee stiffener grooves running along the flange and also without stiffeners. His test rig, however, was limited to the application of concentric loads only and to supplement his results the test

work of this thesis was made available. Thomasson found that increasing the section stiffness through the provision of one or two stiffeners in the flange was not entirely favourable. The consequence of the higher stiffness was that the column remained straight up to a load level which was higher than that for a similar column without stiffeners but which resulted in higher stresses in the webs and the subsequent introduction of a local torsional buckling mode. Thomasson found that this type of buckling caused collapse and in several cases the collapse was of a violent character.

The columns tested without stiffeners were found to have large local flange imperfections of the order of 2 to $3\frac{1}{2}$ times the flange thickness and this, coupled with the high flange width to thickness ratios tested (as high as 475), resulted in very pronounced local buckling effects in the flange at relatively low loads. In his conclusions Thomasson states that for all the columns tested without stiffeners collapse occurred as a result of loss of stability and that a dynamic jump occurred when the stability limit was reached. He did not state, however, the nature of the instability. Preliminary calculations have shown that even if the whole flange was ineffective insofar as carrying load is concerned, then the reduced Euler load would still be in excess of the actual collapse loads occurring experimentally and therefore some other type of instability must have taken place. Figure 1.5.10 shows the distribution of axial

membrane stresses obtained from strain readings for two of the columns tested by Thomasson from the onset of loading to final collapse. It can be seen that the highest membrane stresses occur at the flange web junction and that the magnitude at collapse is of the order of half the yield stress. It would appear from these stress distributions that due to the high ineffectiveness of the flange, coupled with overall column deflections, loading on the cross-sections is concentrated in the main at the flange-web junctions and it would seem reasonable therefore that some sort of corner instability could have caused collapse of the columns. In fact, Thomasson mentions that at collapse the load decreased by 50% in some cases and at the same time a mechanism was formed at the point of failure, this being due to the increased column deflections during load reduction. From several of the photographic plates in his report the failure point would appear to be indicated by buckled corners of the "crinkly" collapse mode as recently examined by Graves Smith and Sridharan (60) whose work will be discussed later.

The work of this thesis has been presented in two papers (55,56), one in 1978 to the Annual Conference of the Stress Analysis Group of the Institute of Physics, held at University College in Cardiff (55), and one in 1979 to the International Conference on Thin Walled Structures, held at the University of

Strathclyde (56), and organised in association with Constrado and the Institution of Structural Engineers. Both these papers are to be published in the conference proceedings. The first paper (55) outlines the theoretical approach used in the thesis and pays special attention to the study of columns with coincident or nearly coincident local and Euler buckling loads, while in the second paper (56) a more deteailed development of the approximate governing differential equation is presented and results are shown for columns which retain post-local buckling stiffness.

The International Conference at Strathclyde received several other contributions (58,59,60,61) on non-linear coupled buckling behaviour. Wang and Pao (58) examined the stability of locally buckled plain channel columns, Reis and Branco (59) studied the lateral-local stability of plain channel section beams eccentrically loaded with respect to the shear centre, Graves Smith and Sridharan (60) analysed the elastic collapse of thin walled box columns in which failure is initiated through instability of the corners in the post local buckling range while Konig and Thomasson (61) reviewed some of the earlier results by Thomasson (54) on lipped channels subject to axial compression and also some results for pure bending.

Perhaps the most interesting contribution was that of Graves Smith and Sridharan (60), the authors using the finite strip method to determine the elastic collapse loads of thin walled box

columns giving due consideration to the geometrical instability of the section corners associated with their waviness in the post local buckling range prior to failure. In order to account for the instability of the corners, Graves Smith and Sridharan enforced compatibility between the in plane and out of plane displacements at the junctions and included second order terms of the in plane local displacements in the large deflection strain-displacement relations since these terms become important when considering the effect of the waviness of the corners of the columns, i.e. the destabilising effects of the transverse in plane displacements. In their analysis the authors specified series solutions for the in plane and out of plane local displacements and used these in conjunction with the more complete form of the large deflection strain-displacement relations to evaluate the internal strain energy for a prescribed end compression. The equilibrium paths of the columns were then found by the usual procedure of differentiating the strain energy with respect to the global degrees of freedom and equating the resulting derivatives to zero. It should be noted, however, that in order to satisfy in plane equilibrium at the boundaries many higher harmonics were needed for the transverse in plane displacement series than for the out of plane series and due to this the analysis contains some approximation in the form of minor incompatibilities at the corners due to unmatched harmonics. The post critical behaviour of square

box section columns with various b/t ratios are shown in Figure 1.5.11. The effects of corner waviness along the post local buckling paths is clearly indicated and the ability of the theory to predict the maxima on these paths clearly demonstrated. Although Graves Smith and Sridharan use these maxima as the theoretical prediction of the failure loads of the columns, their experimental work on columns manufactured from a commercially available curing silicone rubber suggests that the actual failure is associated with a further bifurcation involving collapse of the corners in the so-called "crinkly" mode. The authors, however, have not yet been able to model this behaviour theoretically. It is the writer's opinion that corner instability of this nature was responsible for the elastic-dynamic collapse behaviour of the columns tested by Thomasson (54) in which, due to the pronounced local buckling effects in the compression flanges coupled with overall deflections, stresses on the cross-sections, as discussed previously and shown in Figure 1.5.10, were concentrated at the section corners.

1.6 CONCLUDING REMARKS

The literature review has shown that over the last decade a wide variety of interaction problems have been studied and the effects of various design and imperfection parameters on the buckling behaviour investigated. A considerable amount of work has been

published on the interactive buckling behaviour of structural designs with close critical loads, most of these using simplified structural models to highlight the susceptibility of such designs to geometrical imperfections and unstable post buckling behaviour. In this thesis the interactive behaviour of pin ended lipped channel columns is studied, consideration being given to the interaction of local plate buckling with overall column flexural behaviour. The work deals in the main with column designs whose critical loads are far apart in order that stable post-local interactive behaviour is exhibited. The ultimate loads of columns in this range are far less sensitive to geometrical imperfections than those with close critical loads which lie in the unstable domain. Local buckling in all elements of the section are taken into consideration and changes in the locally deflected form after buckling also considered. The analysis describes the mechanics of the interaction of the modes and examines the growth of deflections and stress variations with applied loading. The work precludes the effects of column torsional buckling and of web-lip local torsional buckling.

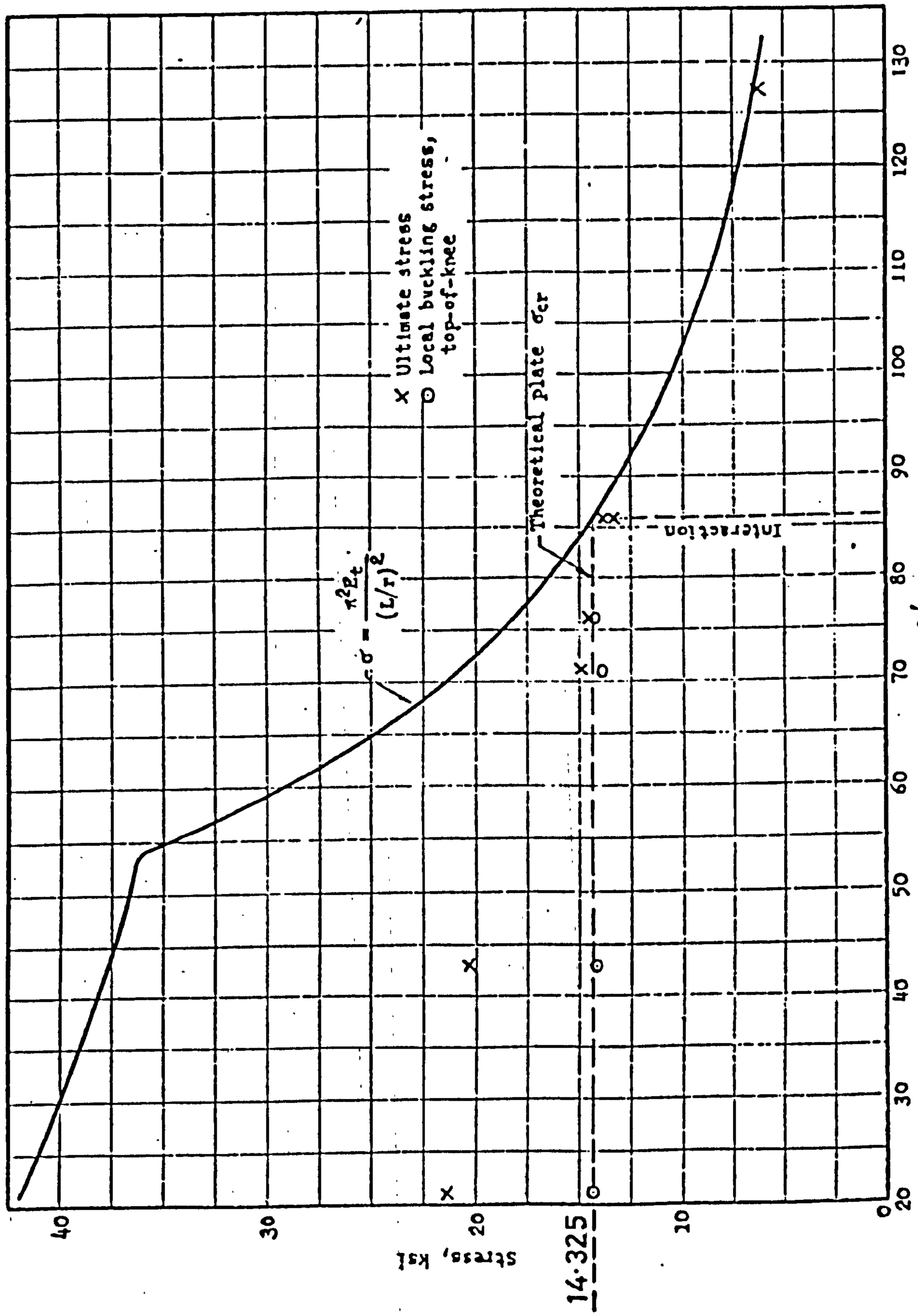

FIG. 1.2.1 EXPERIMENTAL LOCAL INSTABILITY AND ULTIMATE STRESSES FOR SQUARE ALUMINIUM BOX SECTION COLUMNS BY BIJLAARD AND FISHER (4)

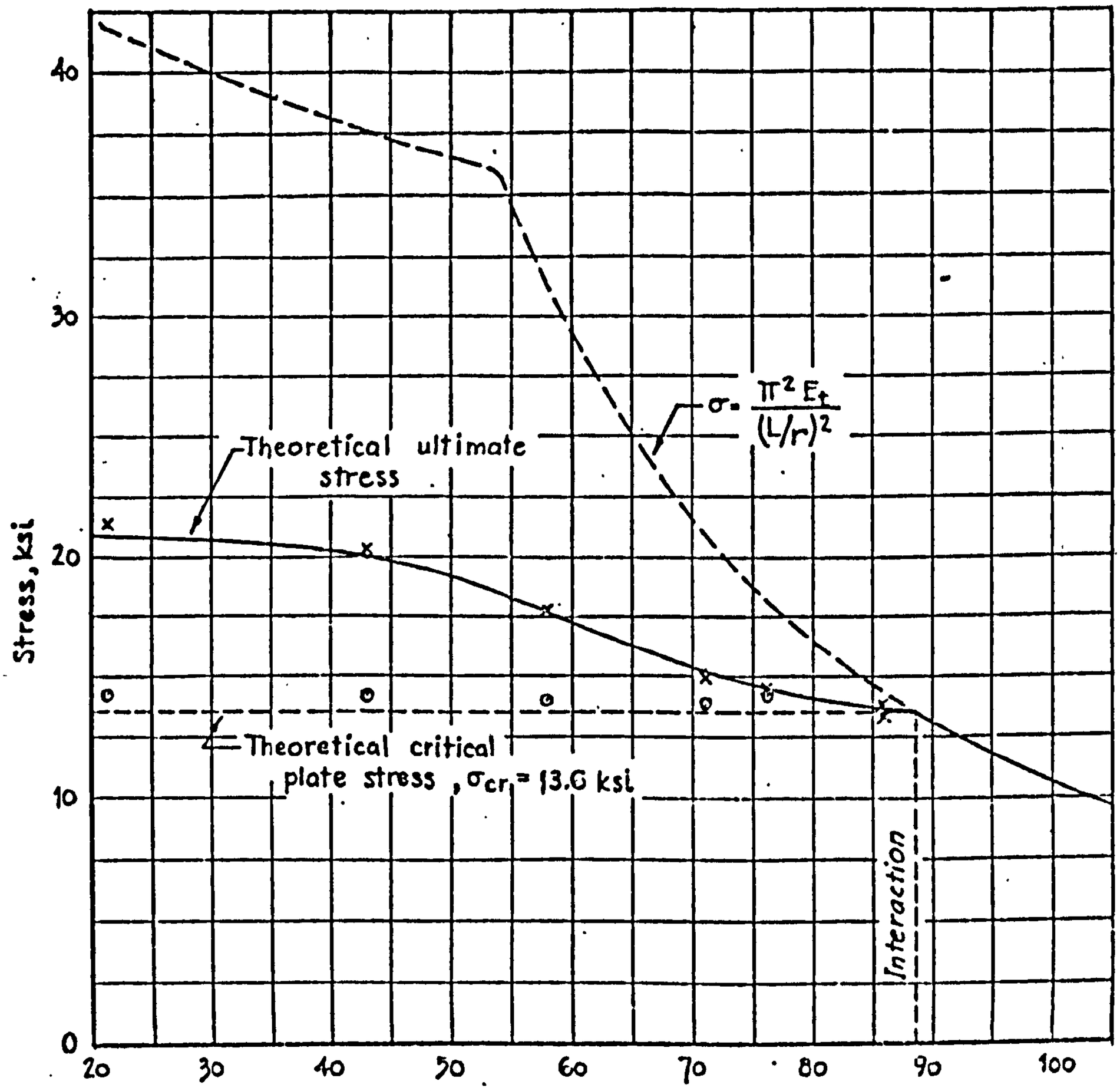

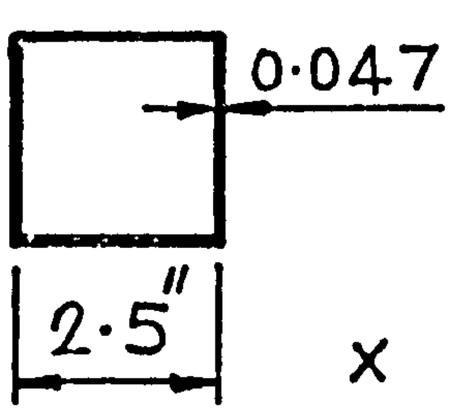

square tube section.

x ultimate stress
⊙ critical plate stress
} experimental.

FIG. 1.2.2 COMPARISON OF THEORETICAL AND EXPERIMENTAL RESULTS BY BIJLAARD AND FISHER (6)

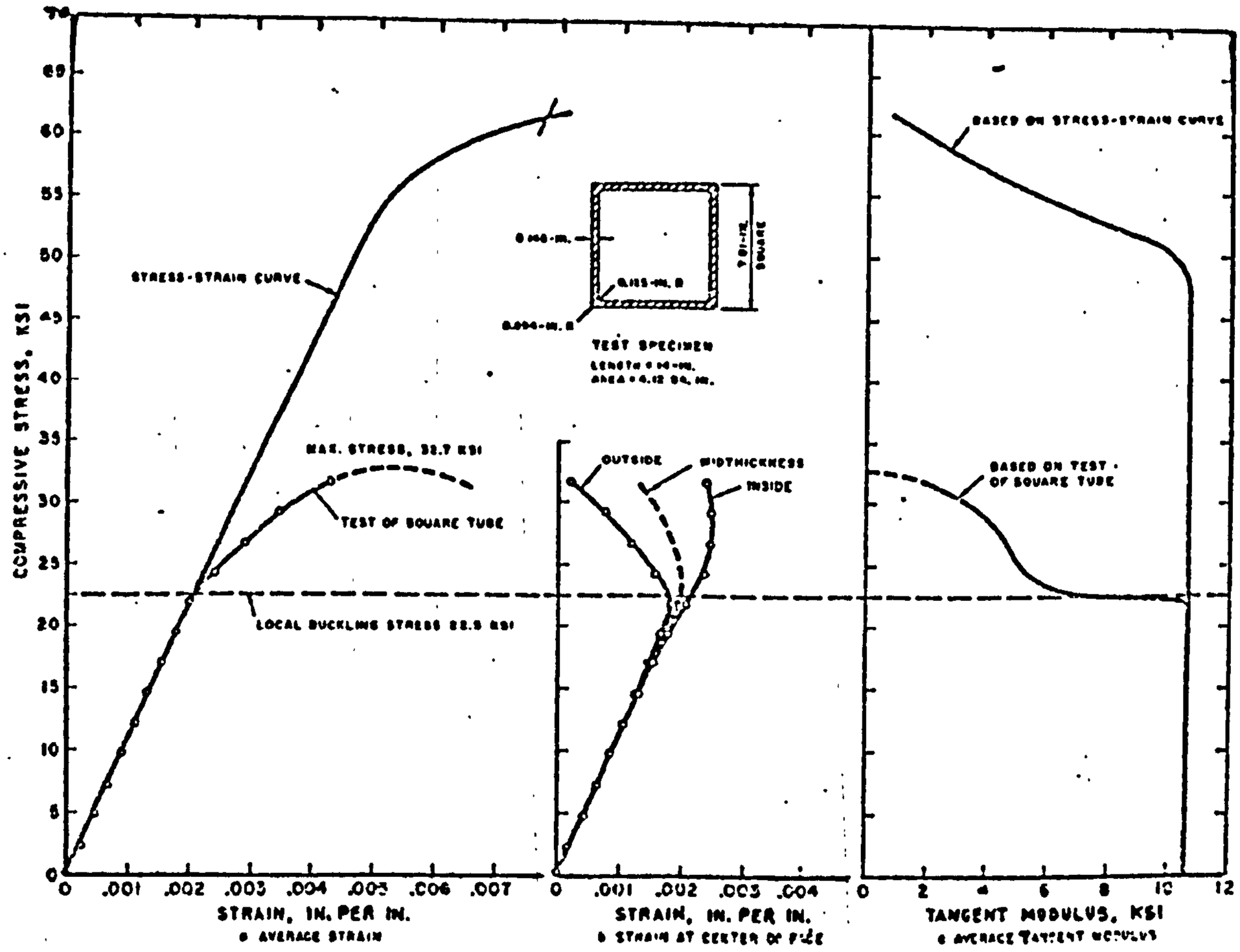

FIG. 1.2.3 BOX SECTION TANGENT STIFFNESS IN COMPRESSION FROM EXPERIMENTAL WORK OF JOMBOCK AND CLARK(9)

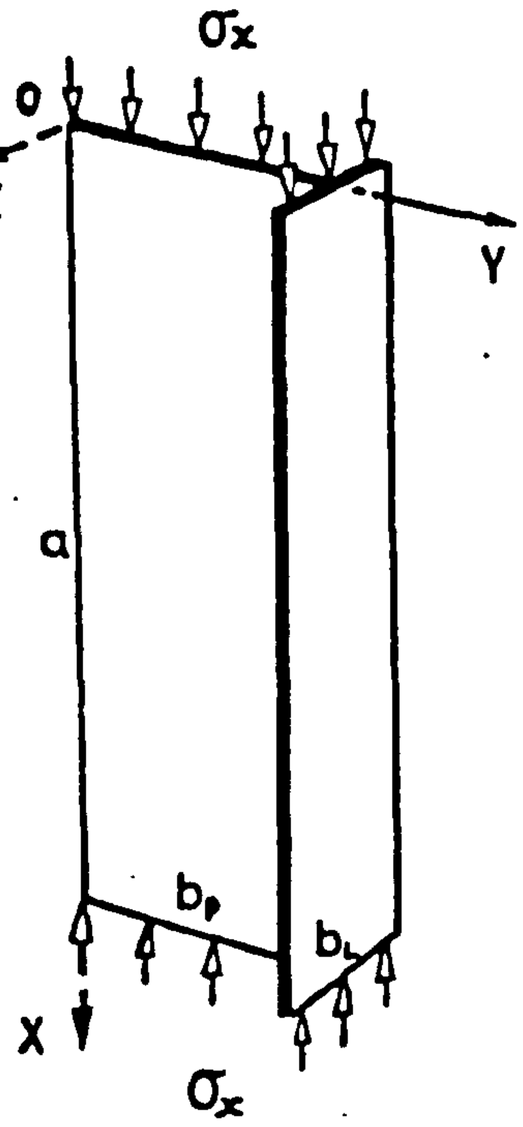

Mode (i) — Torsional

Mode (ii) — Local

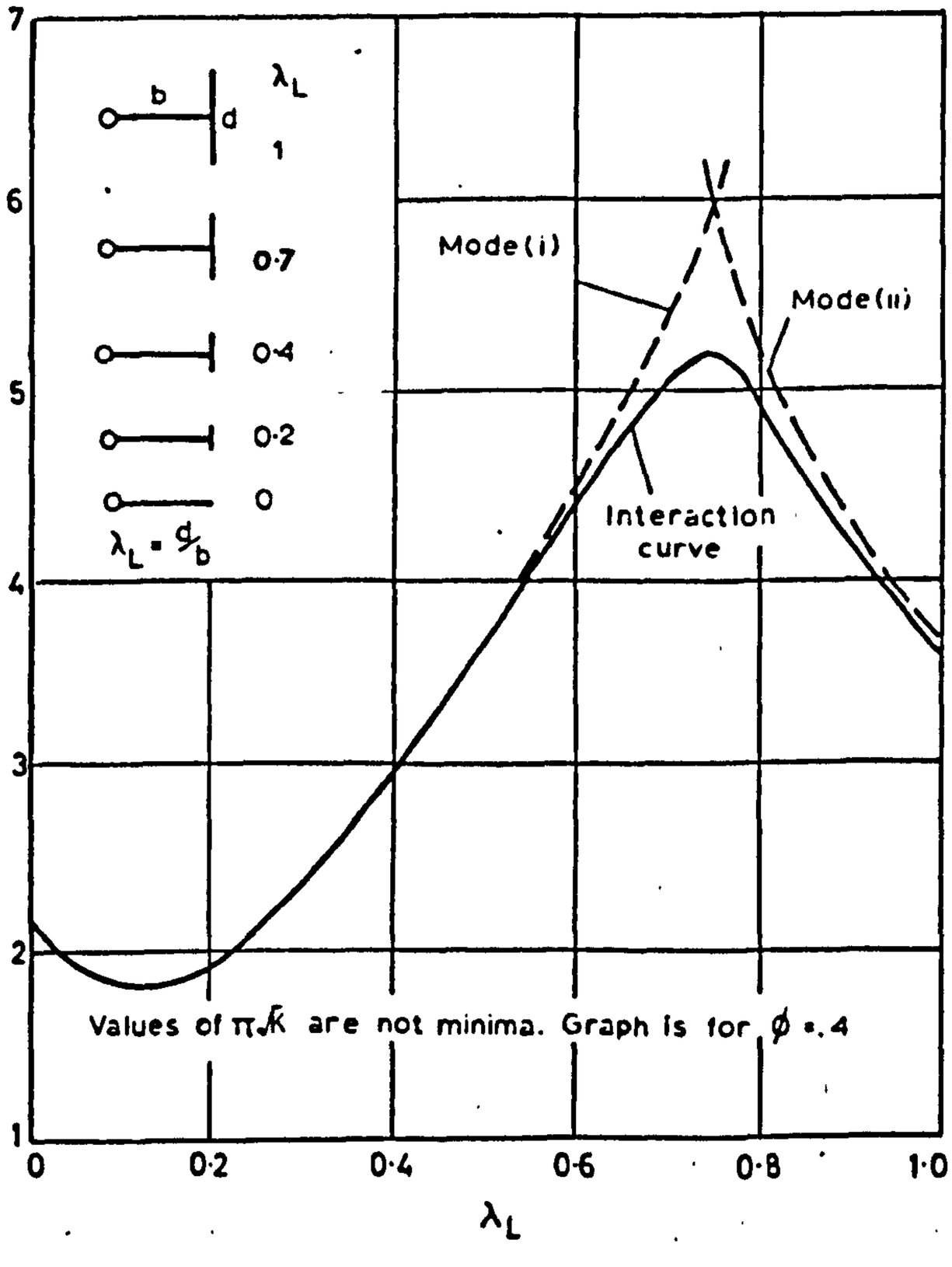

FIG. 1.2.4 MODE COUPLING AT INSTABILITY

BY BULSON (13)

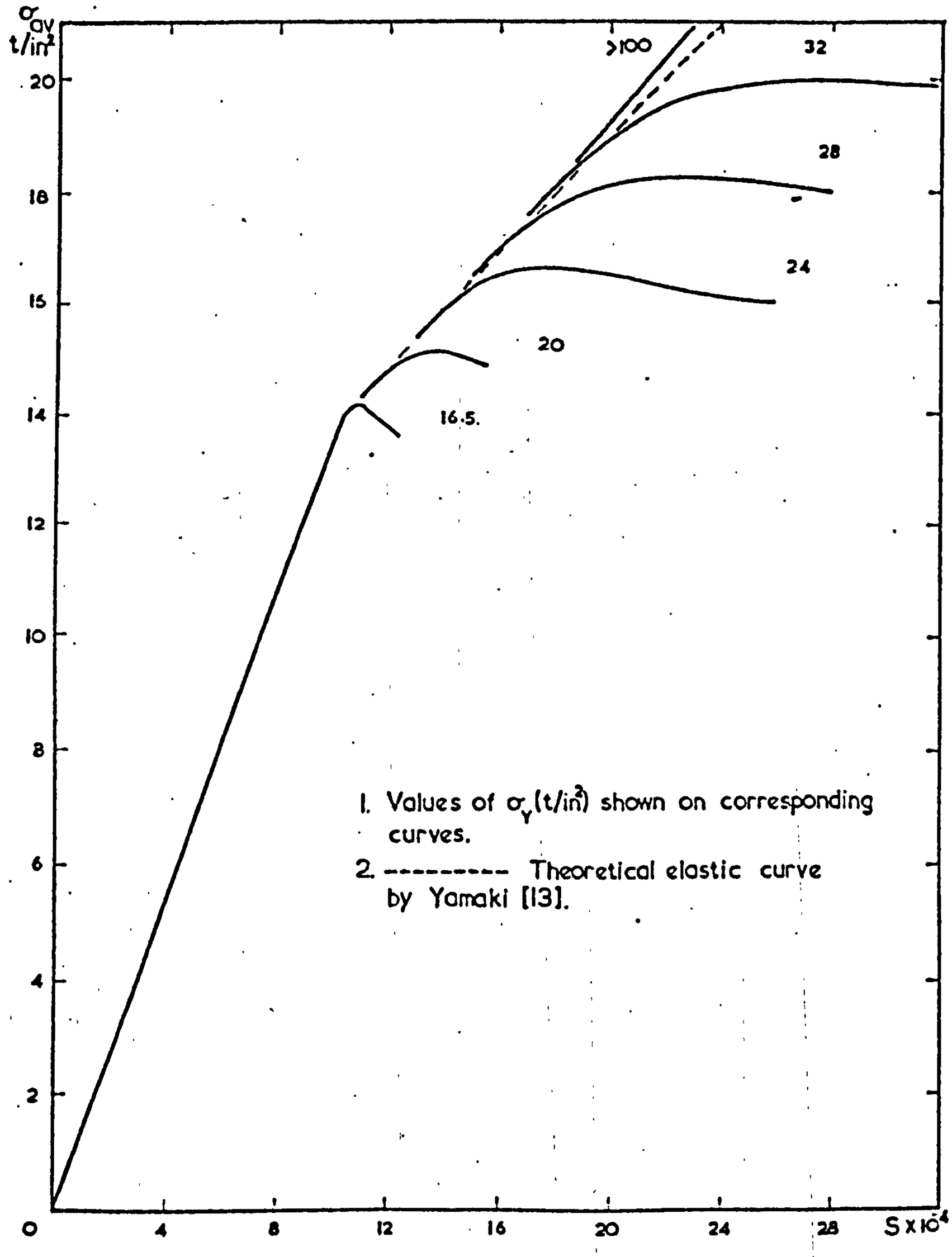

FIG. 1.2.5 THEORETICAL POST-BUCKLING STIFFNESS CURVES OF GRAVES SMITH(14) SHOWING THE EFFECTS OF PLASTICITY

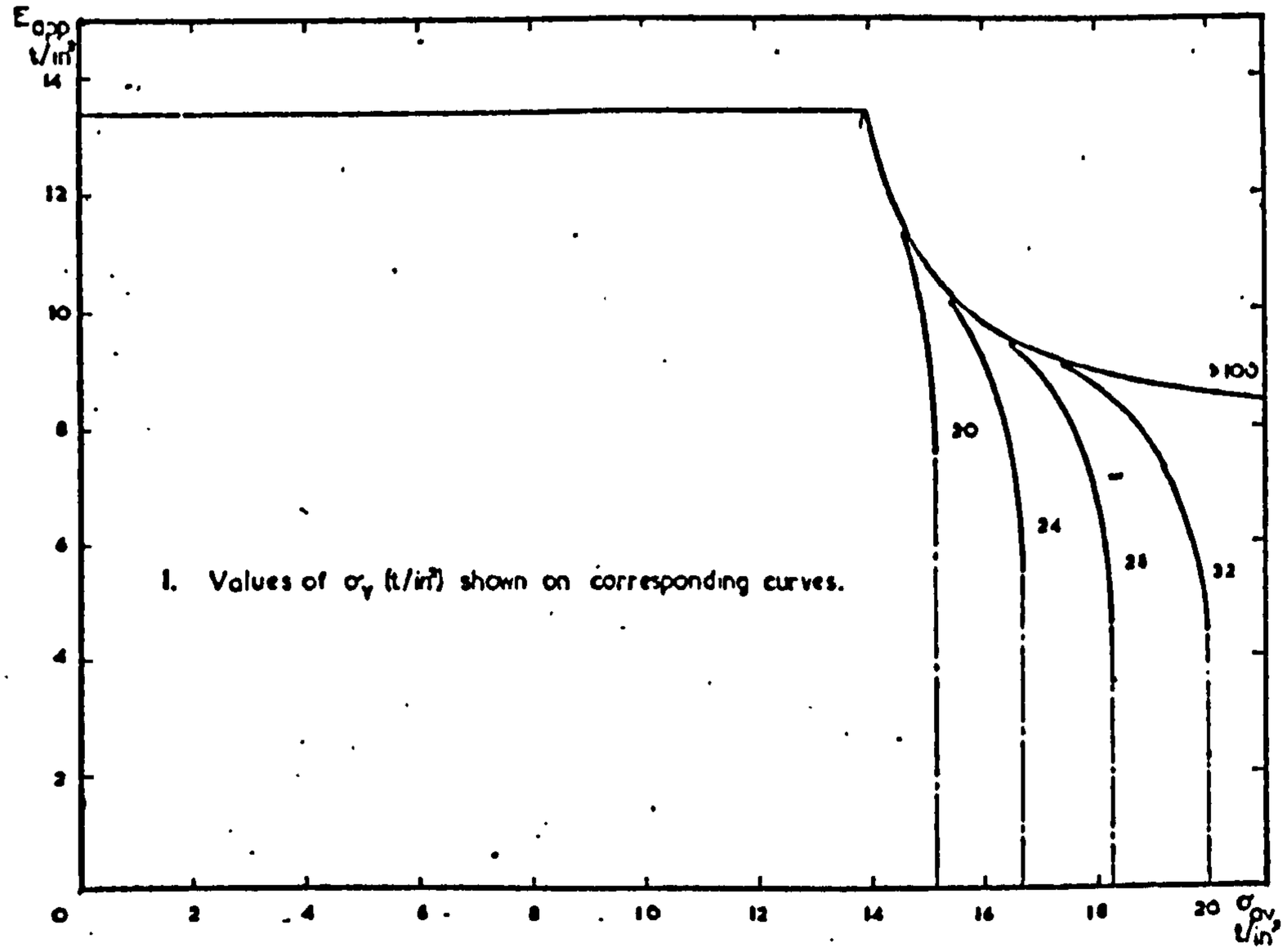

FIG. 1.2.6 THEORETICAL APPARENT COMPRESSIONAL STIFFNESS CURVES OF GRAVES SMITH(14)

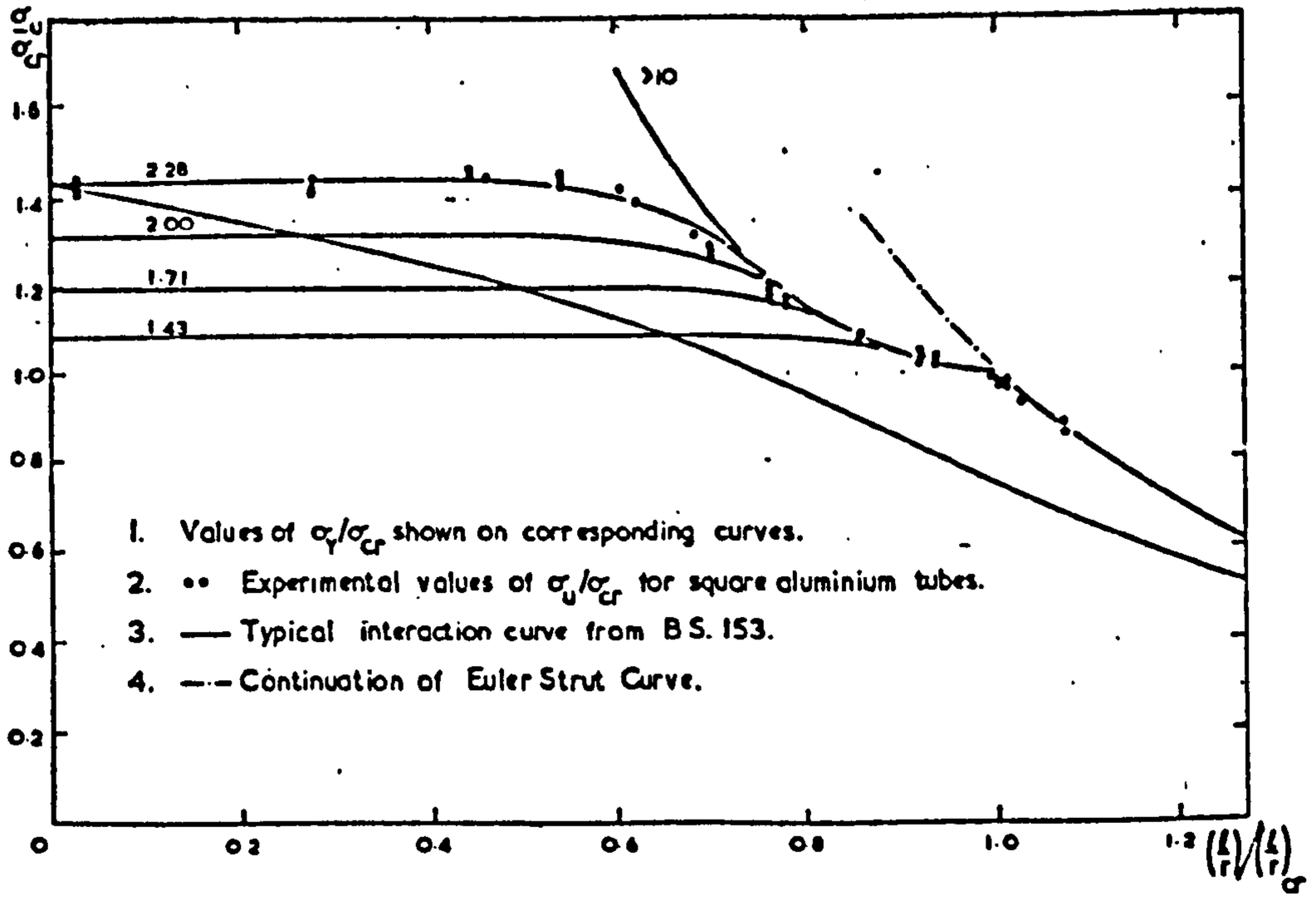

FIG. 1.2.7 COMPARISON OF THEORETICAL AND EXPERIMENTAL RESULTS OF GRAVES SMITH(14)

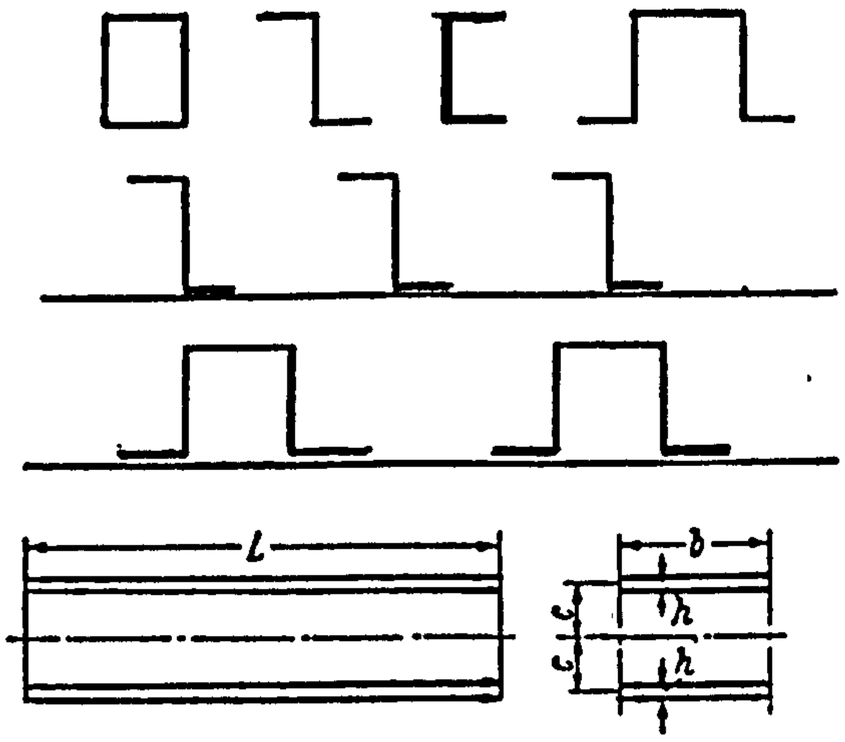

FIG.1.3.1 TYPICAL STRUCTURAL FORMS AND THE REPRESENTATIVE MODEL OF VAN DER NEUT(17)

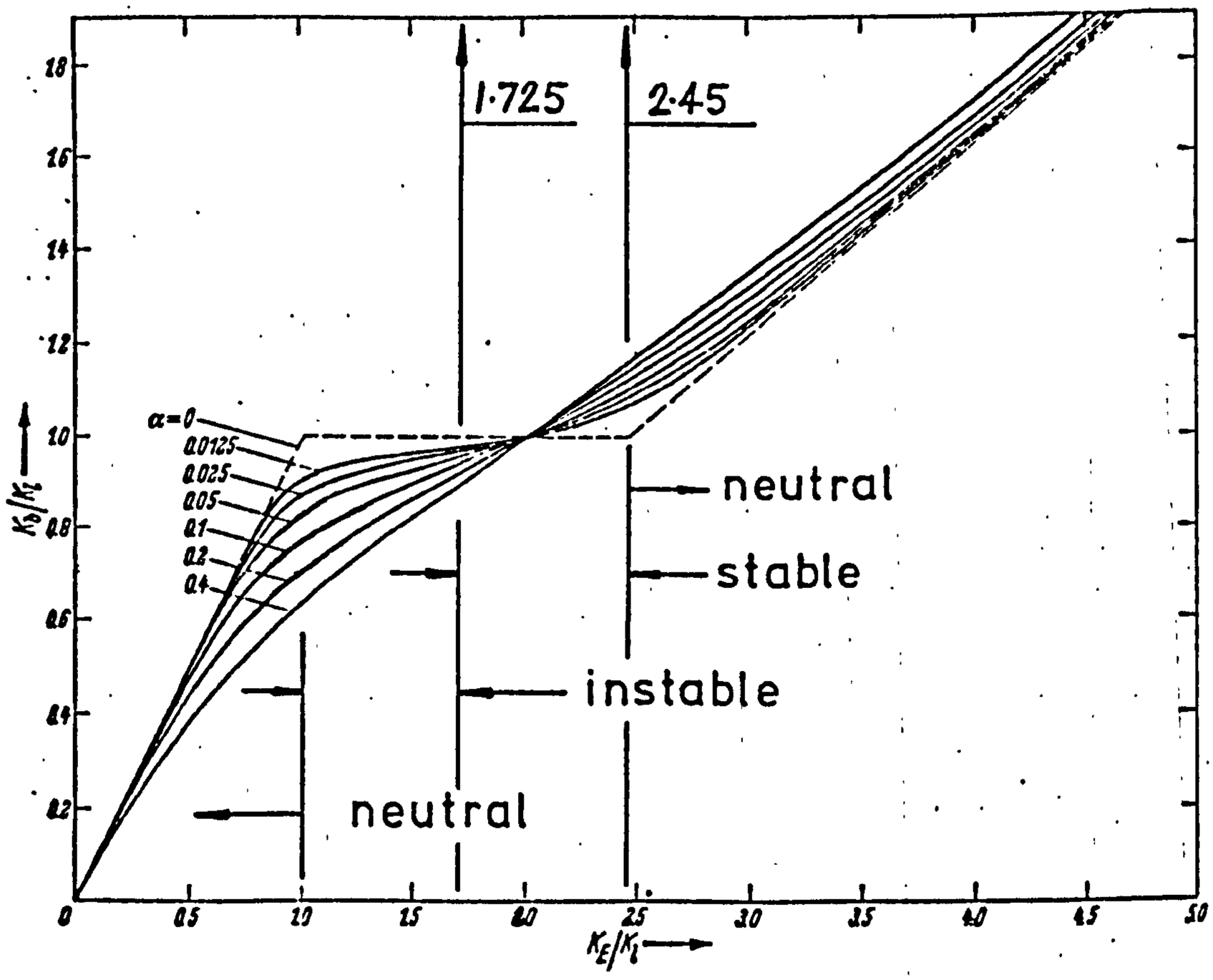

FIG. 1.3.2 CHARACTER OF THE EQUILIBRIUM AT BUCKLING AND THE EFFECTS OF IMPERFECTIONS FROM THE MODEL OF VAN DER NEUT(17)

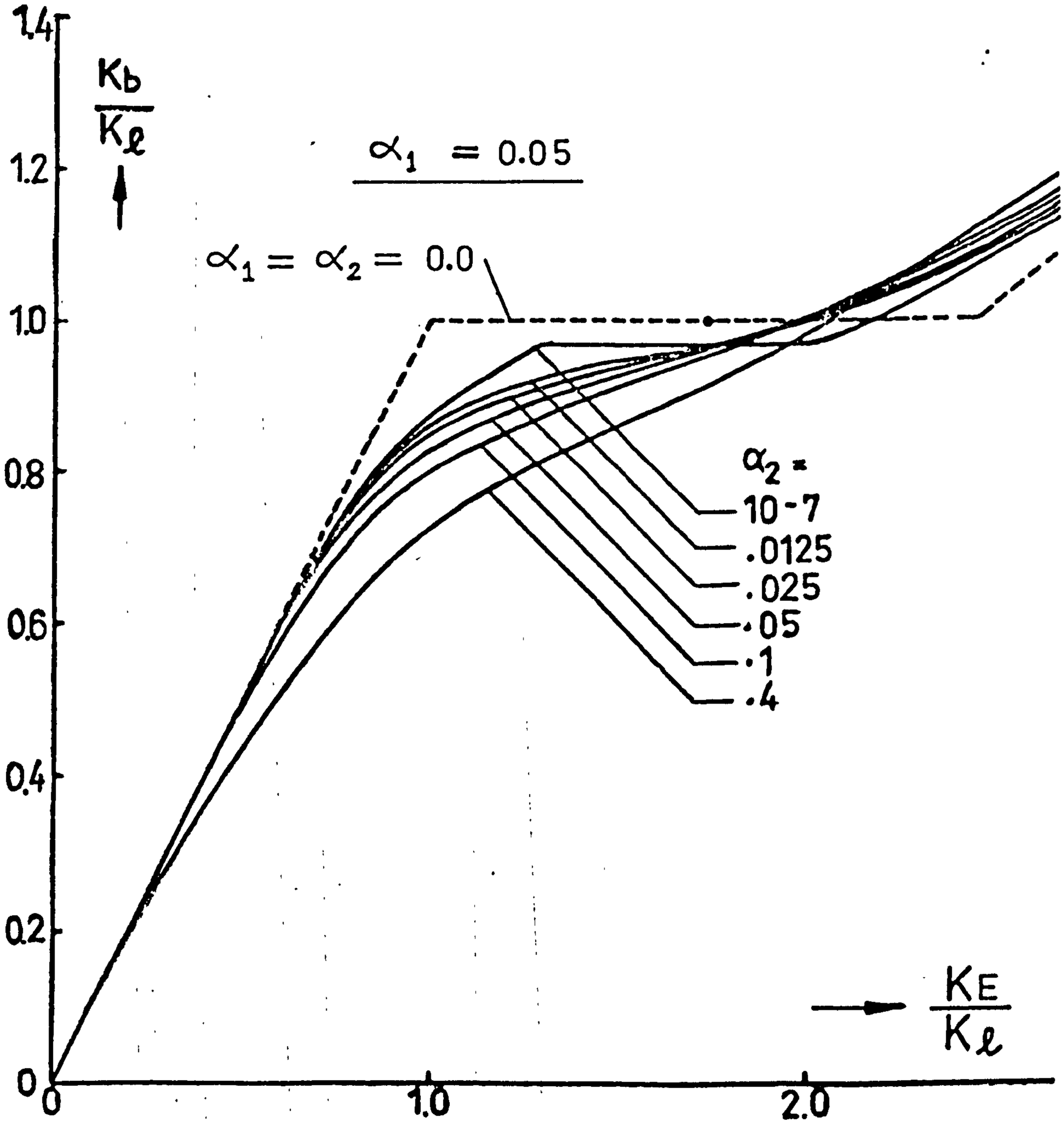

FIG. 1.3.3 COLUMN BUCKLING CURVES OF MEIJER AND VAN DER NEUT(20) SHOWING THE REDUCTION IN LOAD DUE TO UNEQUAL FLANGE IMPERFECTIONS

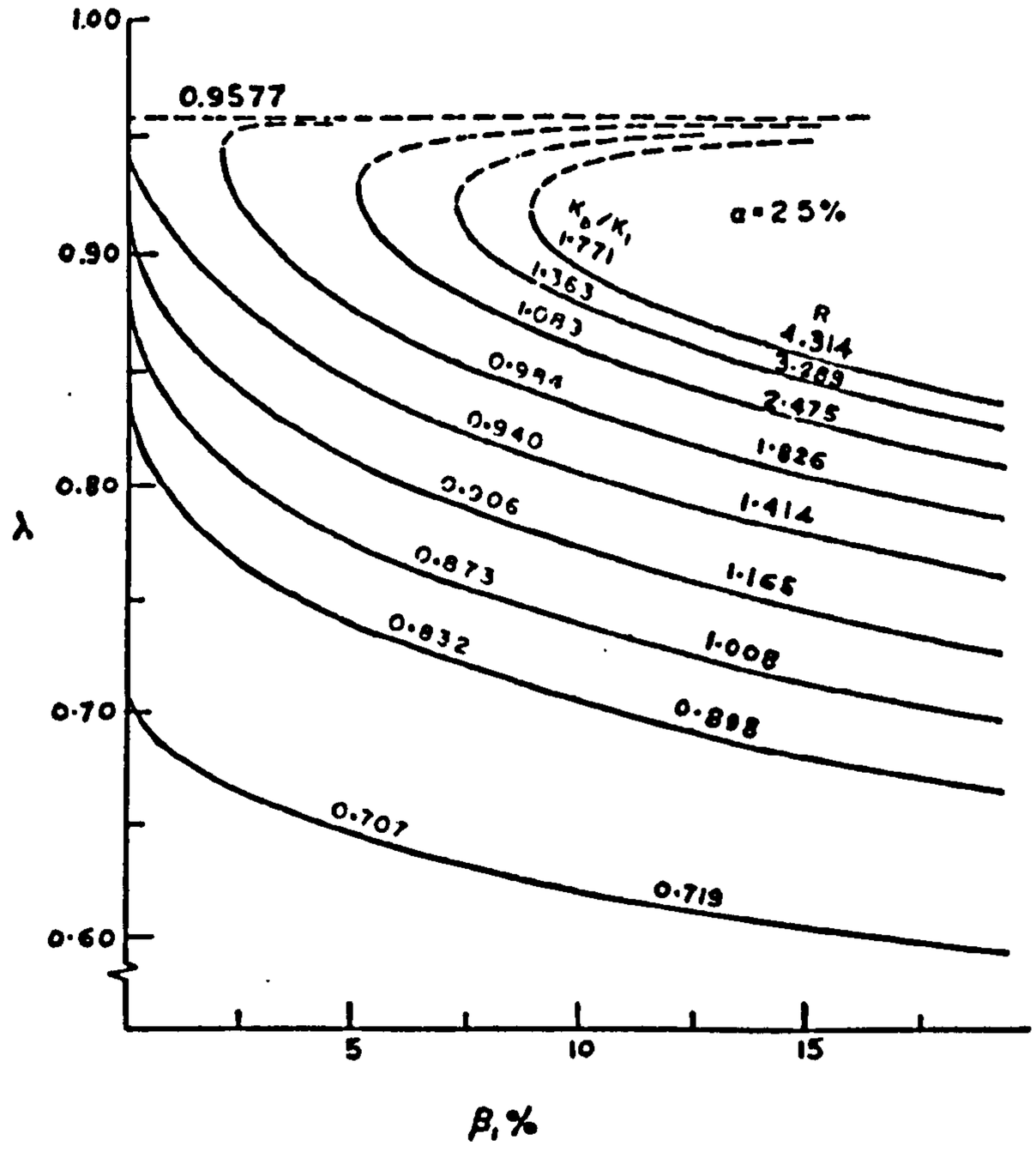

FIG. 1.3.4 COLUMN STRENGTH PARAMETER λ OF VAN DER NEUT(31) PLOTTED AS A FUNCTION OF THE OVERALL IMPERFECTION PARAMETER β.

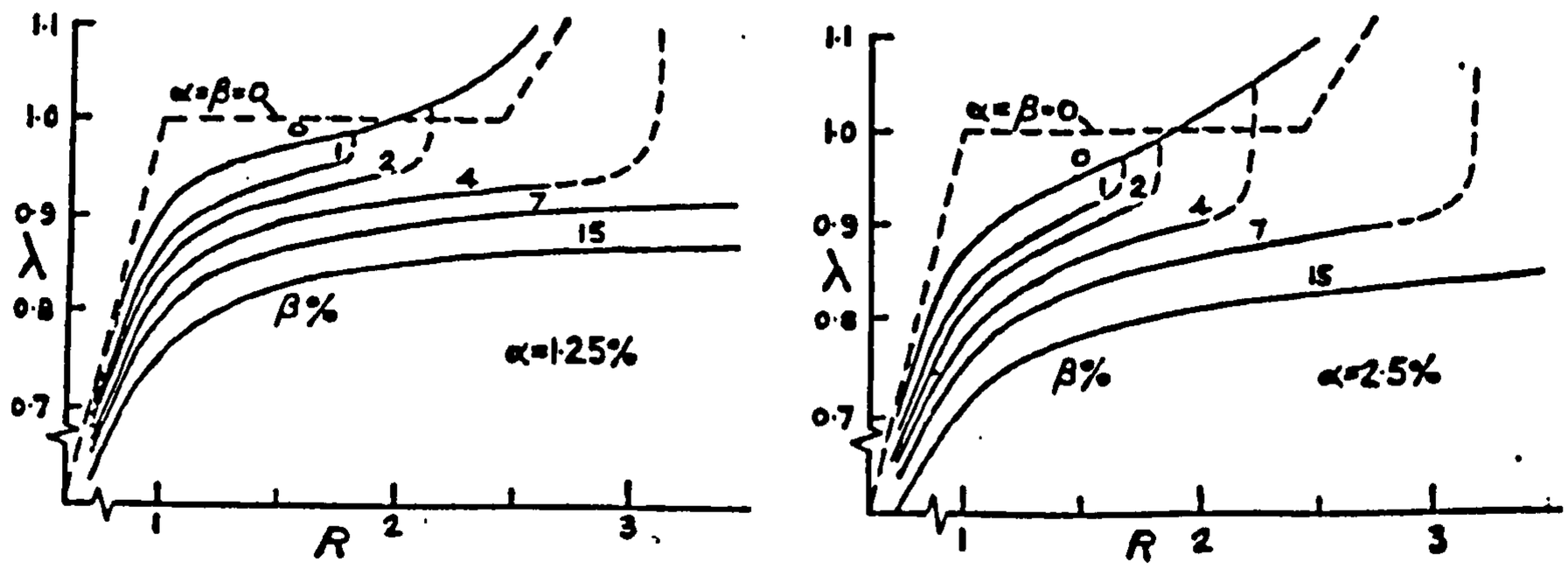

FIG. 1.3.5 COLUMN STRENGTH PARAMETER λ OF VAN DER NEUT(31) PLOTTED AS A FUNCTION OF THE RATIO $R=K_E/K_L$

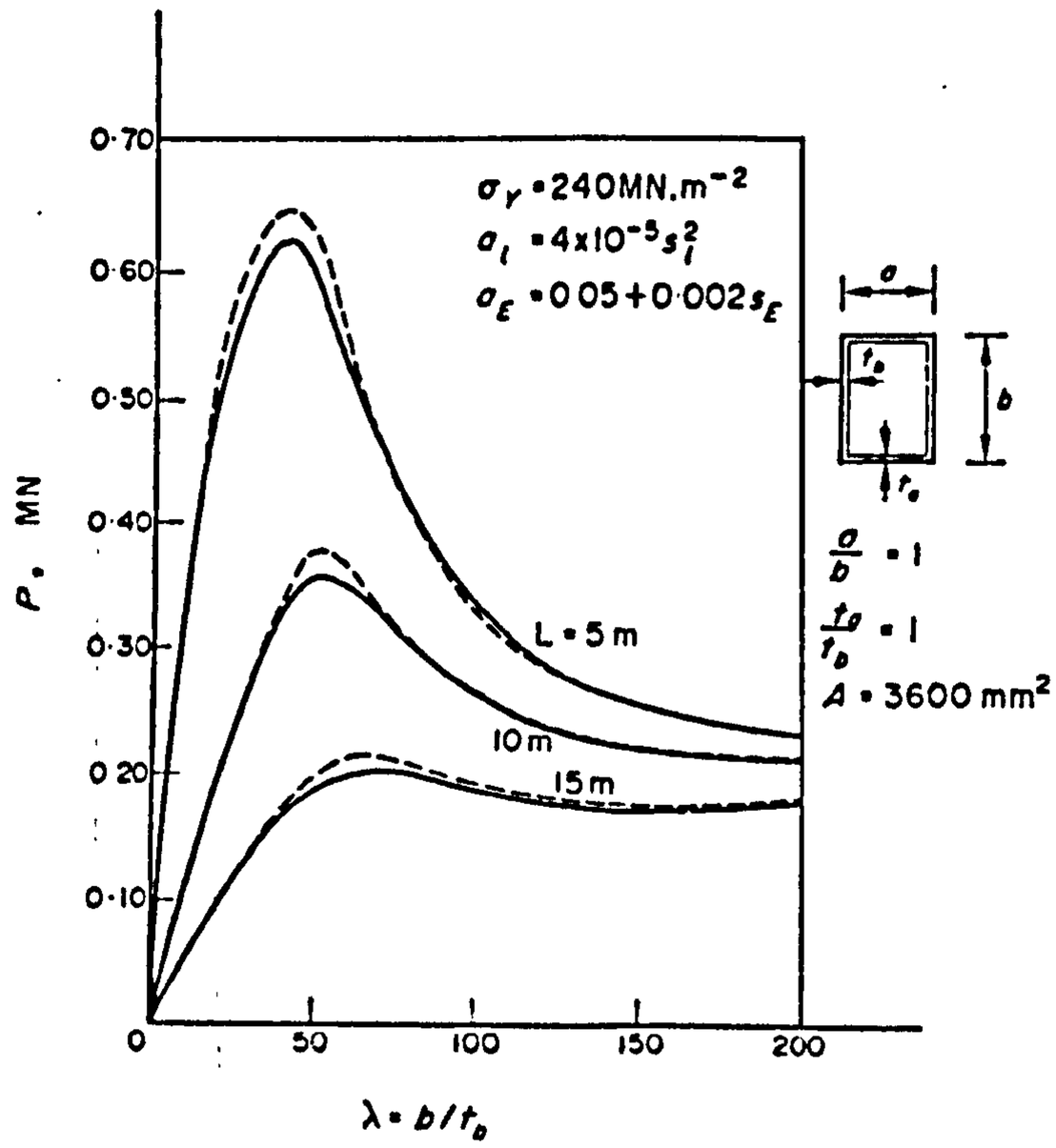

——— Kloppel and Schubert.

-----Svensson and Croll.

a_l = Local imperfection parameter

a_E = Overall imperfection parameter

$s_l = \lambda = b/t$, $s_E = L/r$.

FIG. 1.3.6 STRENGTH CURVES OF SQUARE BOX COLUMNS BY SVENSSON AND CROLL(42)

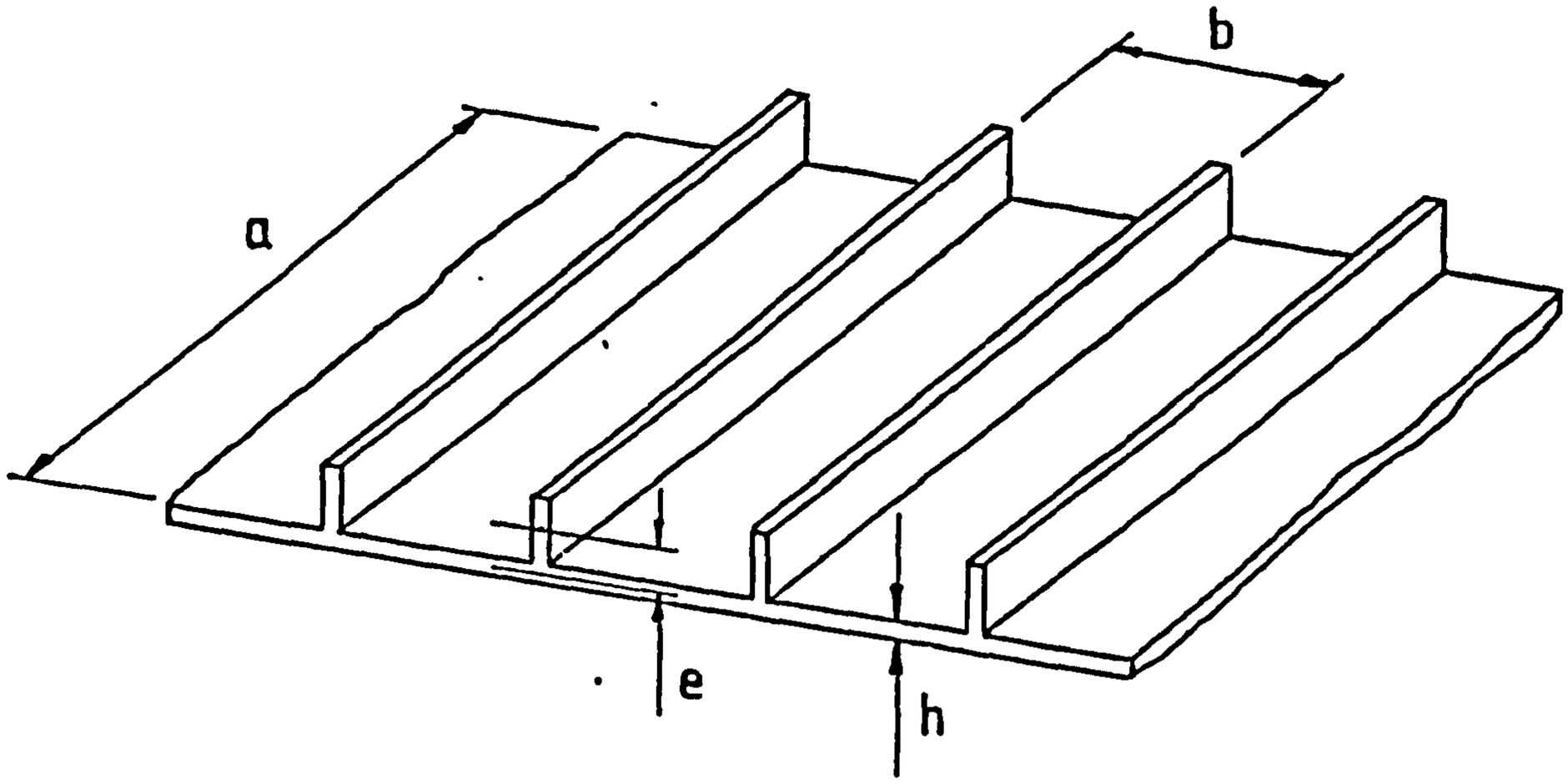

FIG. 1.4.1 INTEGRALLY STIFFENED PANEL SHOWING TYPICAL GEOMETRICAL NOTATION.

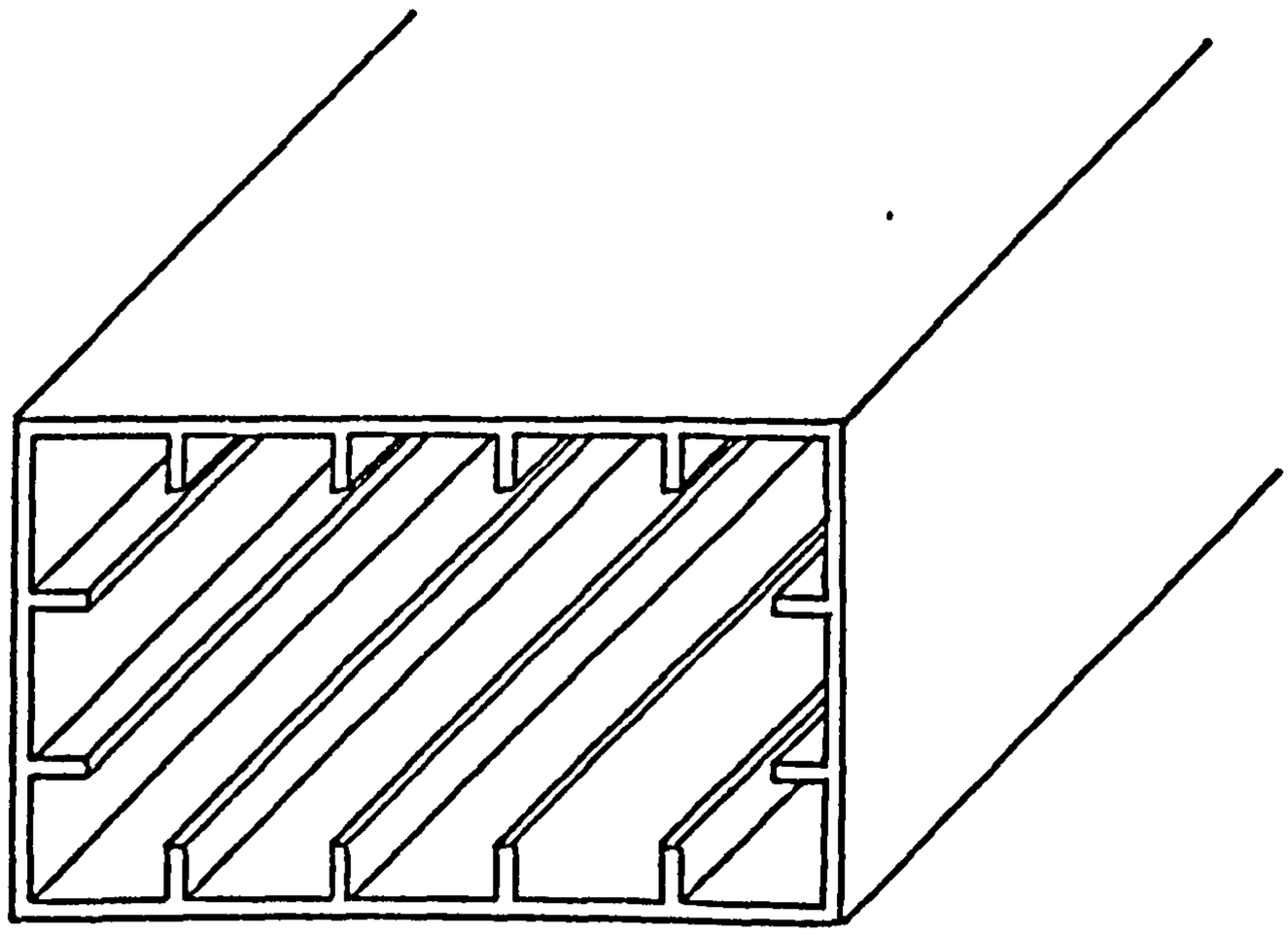

FIG. 1.4.2 SCHEMATIC CROSS SECTION OF A BOX GIRDER.

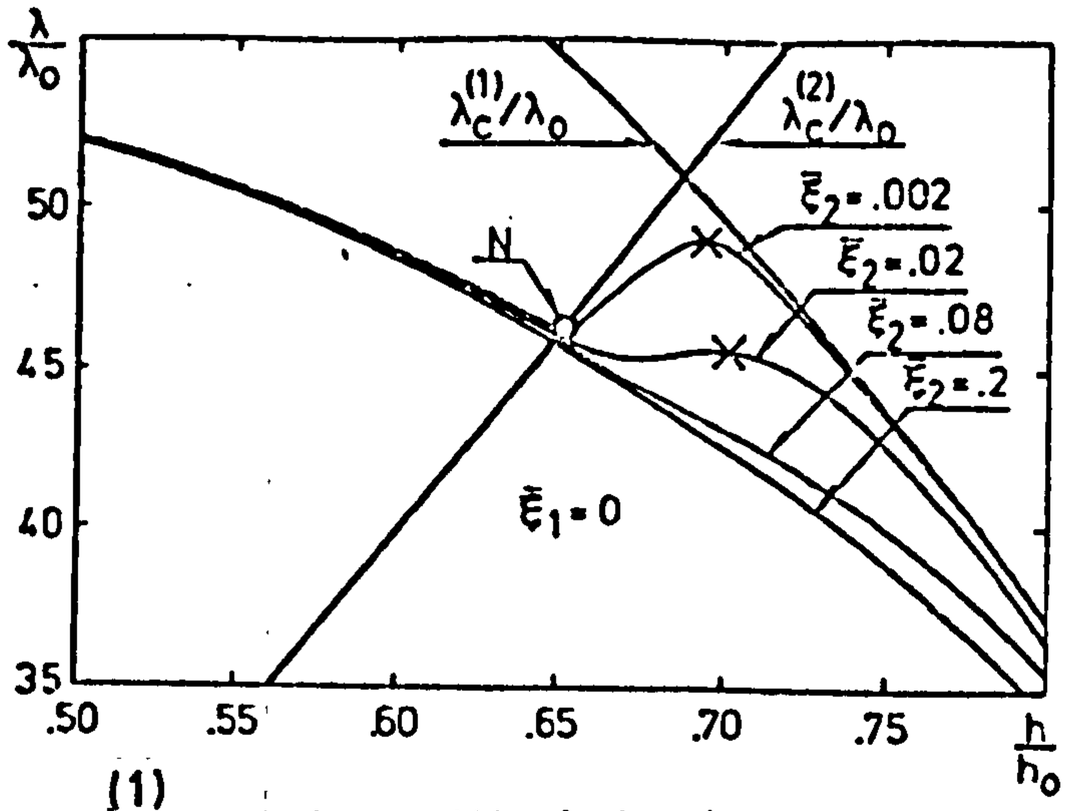

$\lambda_c^{(1)}$ = Euler critical load parameter.

$\lambda_c^{(2)}$ = Local critical load parameter.

λ_0 = Critical load parameter when $h/h_0 = 1$

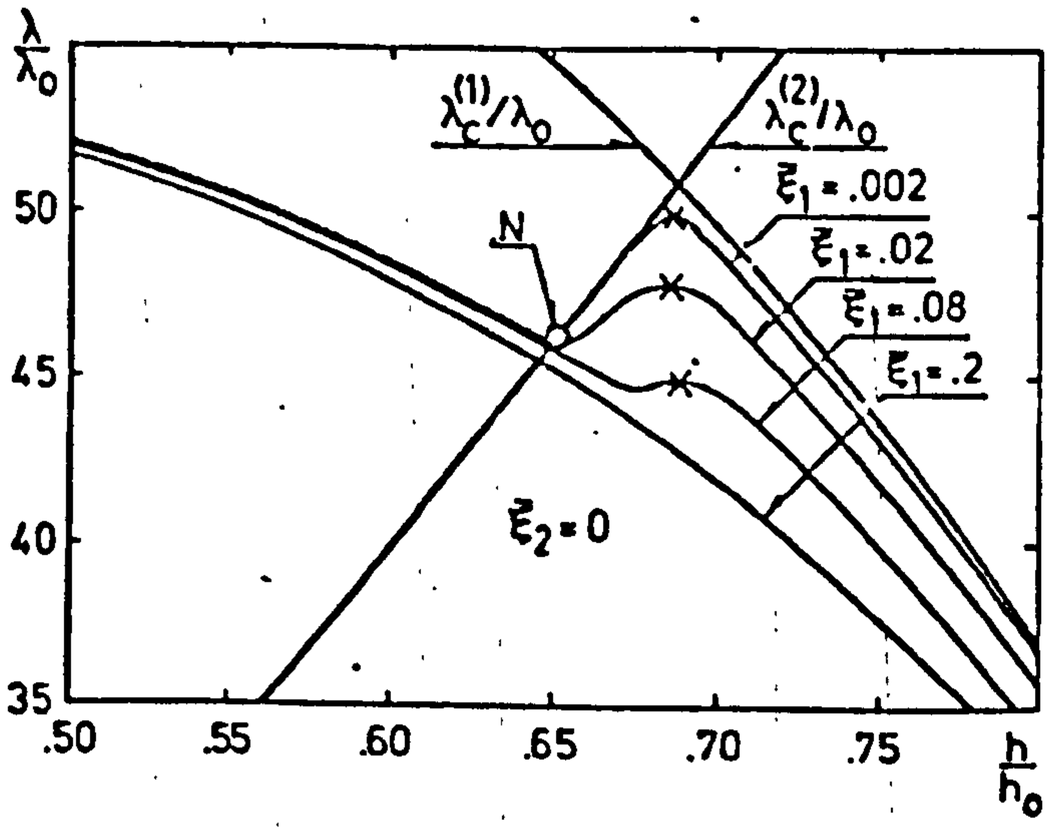

$\bar{\xi}_1$ = Euler imperfection parameter

$\bar{\xi}_{12}$ = Local imperfection parameter

N = Point at which behaviour of perfect structure changes from stable to unstable.

h/h_0 = Ratio between the amount of material in the plate and that in the whole panel.

FIG. 1.4.3. RESULTS OF TVERGAARD (32) FOR A PANEL SPECIFIED BY :- $a/b = 4$ $e/b = 0,05$ and $h_0/b = 0,0128$

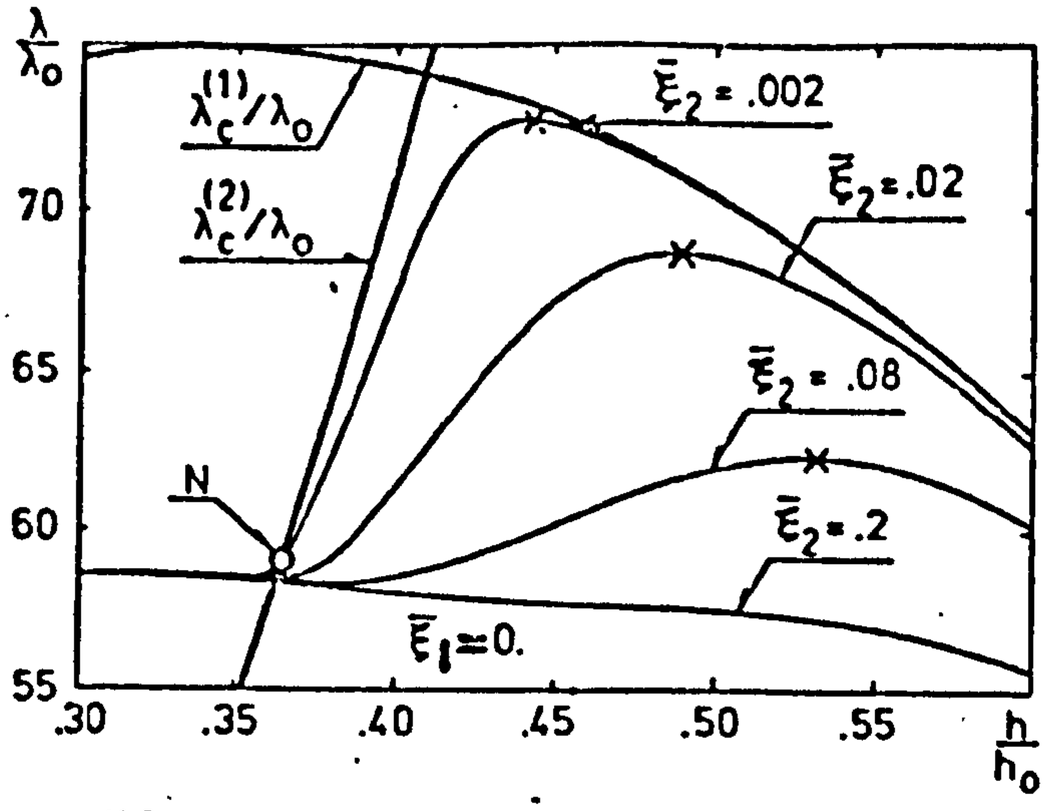

$\lambda_c^{(1)}$ = Euler critical load parameter.

$\lambda_c^{(2)}$ = Local critical load parameter.

λ_o = Critical load parameter when $h/h_o = 1$

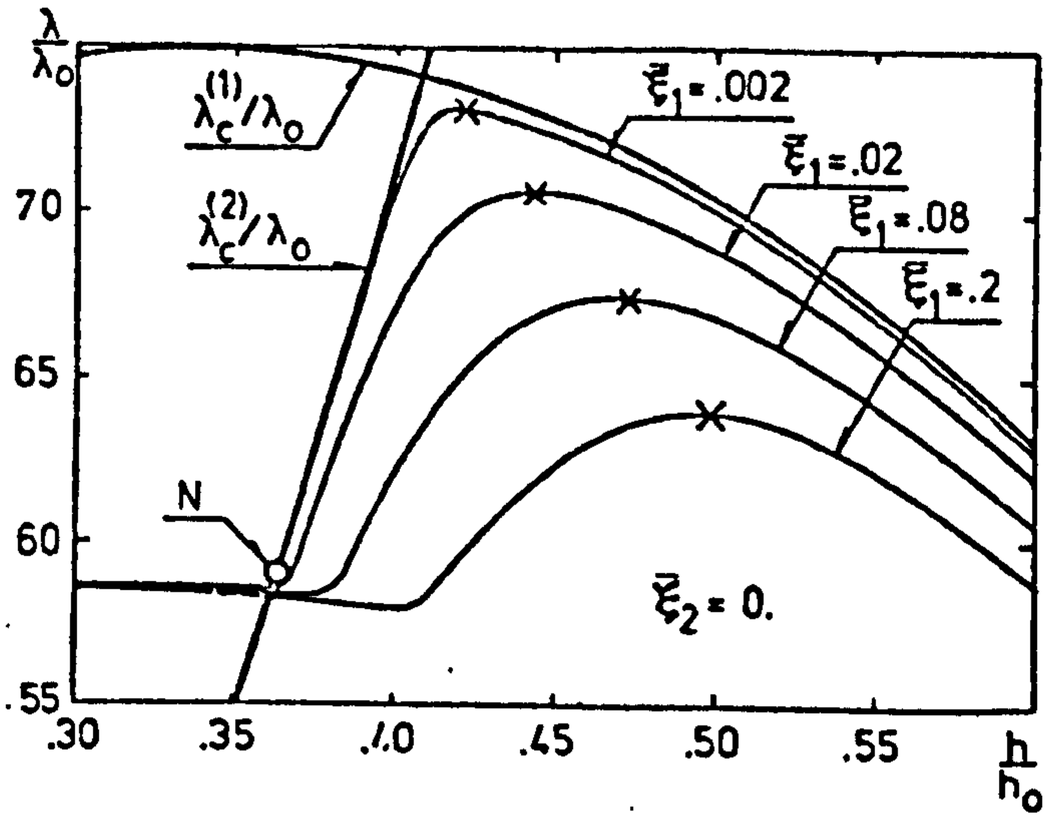

$\bar{\xi}_1$ = Euler imperfection parameter.

$\bar{\xi}_2$ = Local imperfection parameter.

N = Point at which behaviour of perfect structure changes from stable to unstable.

h/h_o = Ratio between the amount of material in the plate and that in the whole panel.

FIG. 1.4.4. RESULTS OF TVERGAARD (32) FOR A PANEL SPECIFIED BY :-

$a/b = 8$, $e/b = 0{,}1$ and $h_o/b = 0{,}0256$.

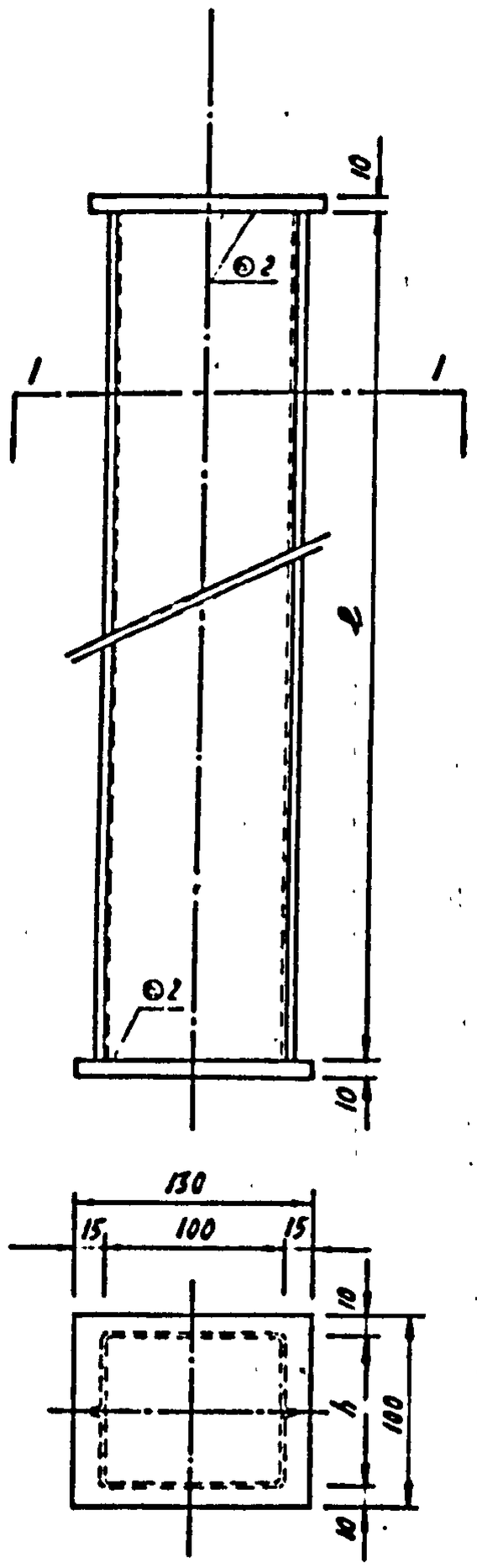

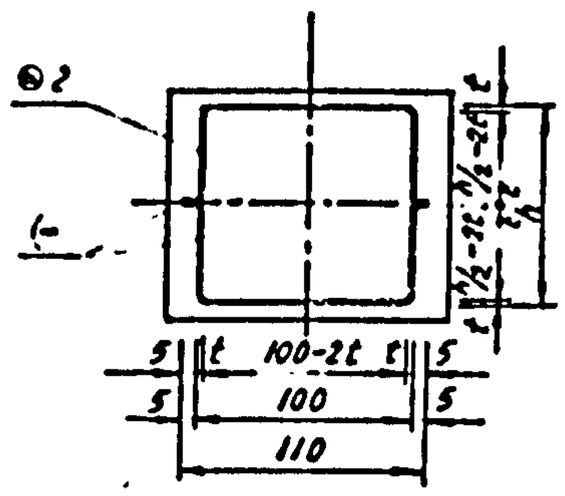

FIG. 1.5.1 FABRICATION OF RECTANGULAR BOX COLUMNS TESTED BY SKALOUD AND ZÖRNEROVÁ (21)

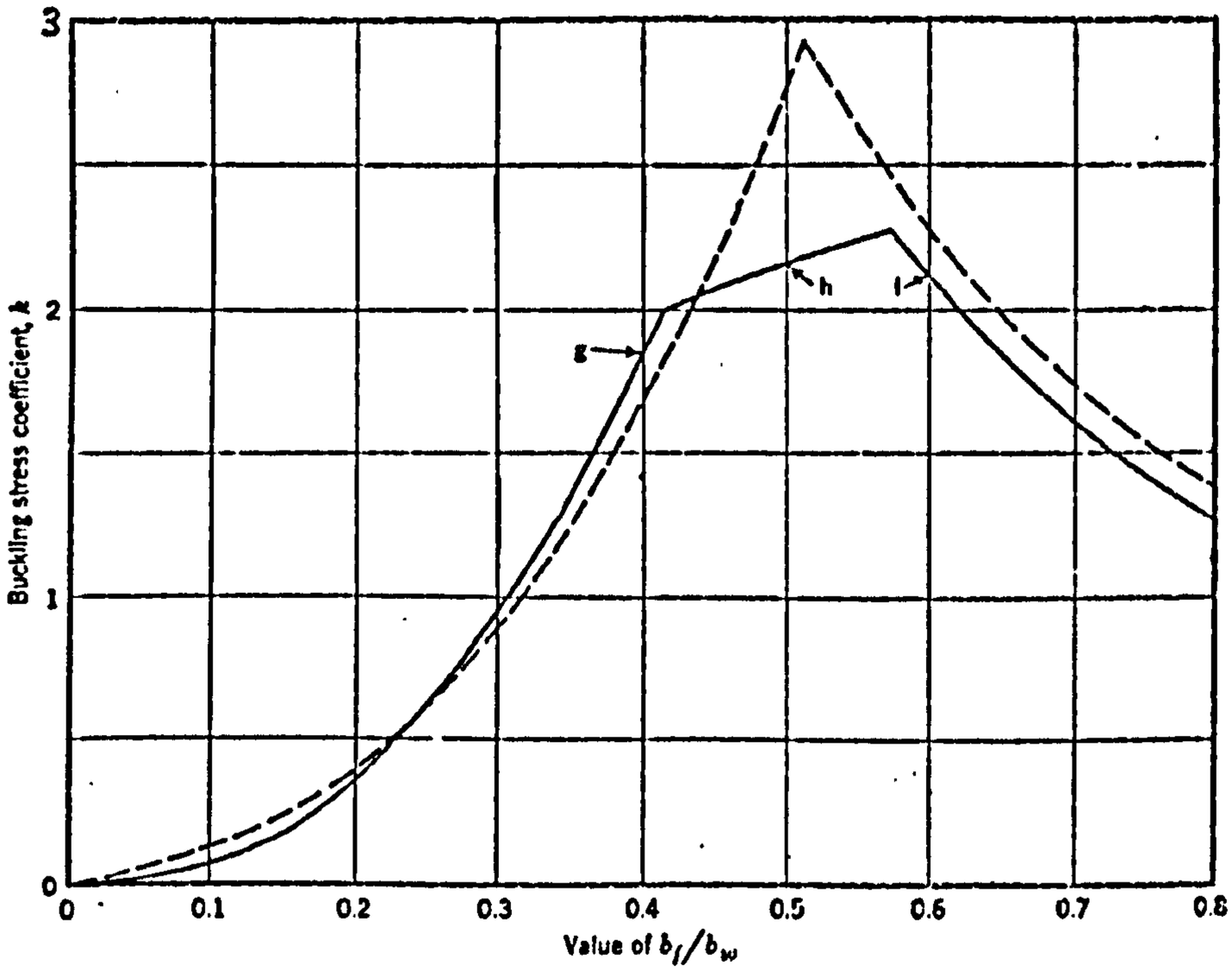

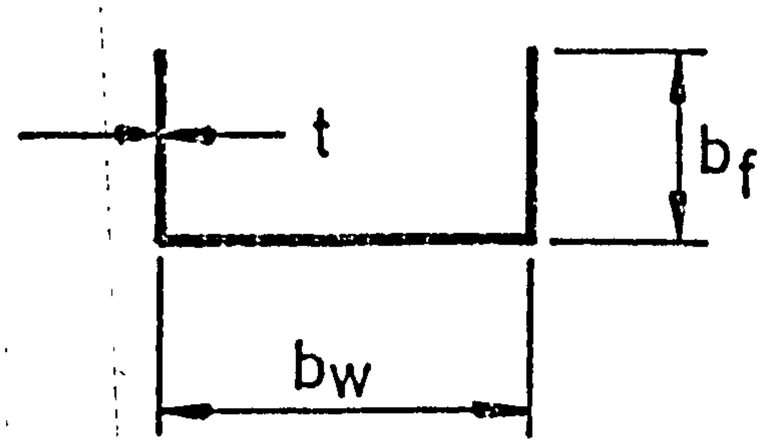

plain channel section.

$\frac{L}{b_w} = 15, \quad \frac{b_w}{t} = 50, \quad \nu = 0{\cdot}36$

——— Wittrick and Williams.

–––– Ghobarah and Tso.

g— Euler buckling.

h— Torsional buckling.

i— Local buckling.

FIG. 1.5.2 COMPARISON OF THE INITIAL BUCKLING STRESSES OF WITTRICK AND WILLIAMS (24) WITH THOSE OF GHOBARAH AND TSO (18)

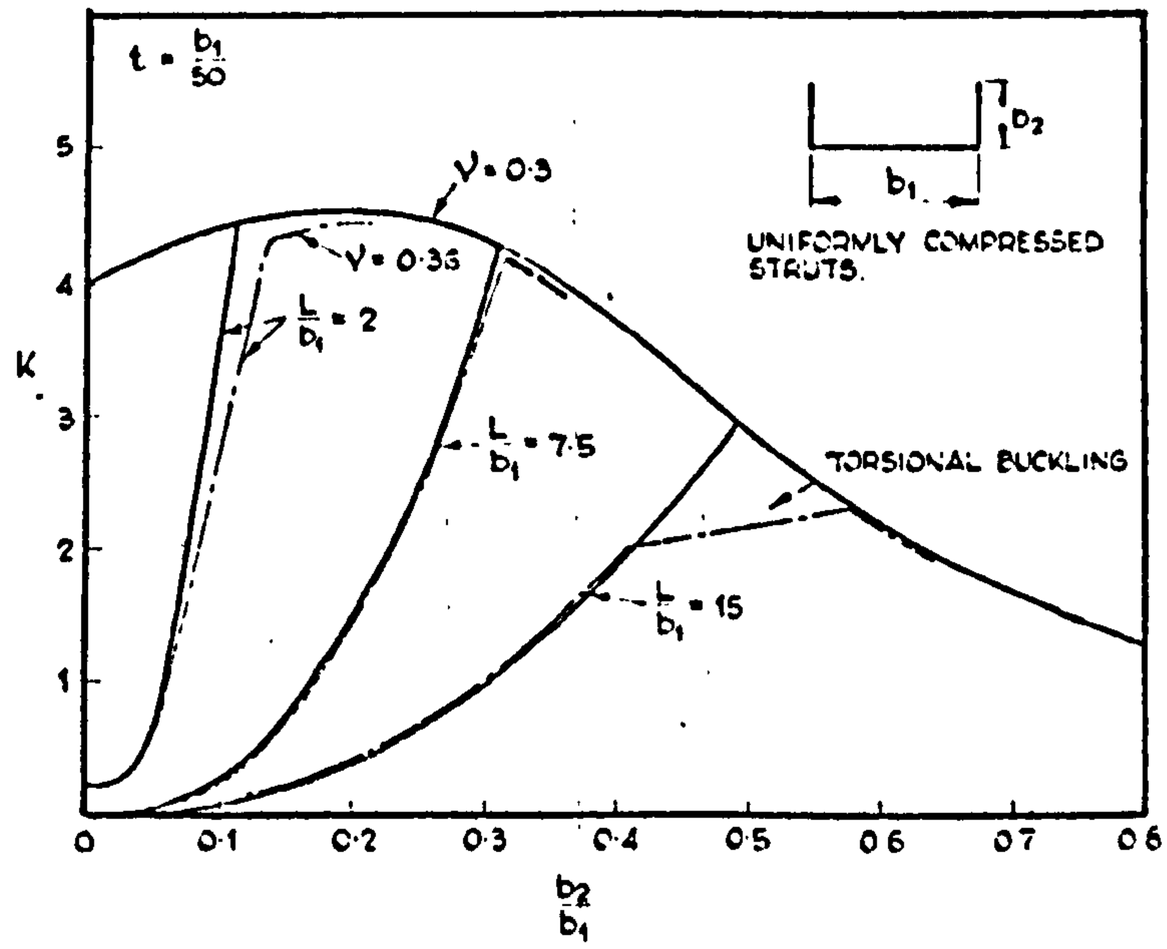

——— Rhodes and Harvey

– – – – Wittrick and Williams

FIG. 1.5.3 COMPARISON OF THE INITIAL BUCKLING STRESSES OF RHODES AND HARVEY(46) WITH THOSE OF WITTRICK AND WILLIAMS(24)

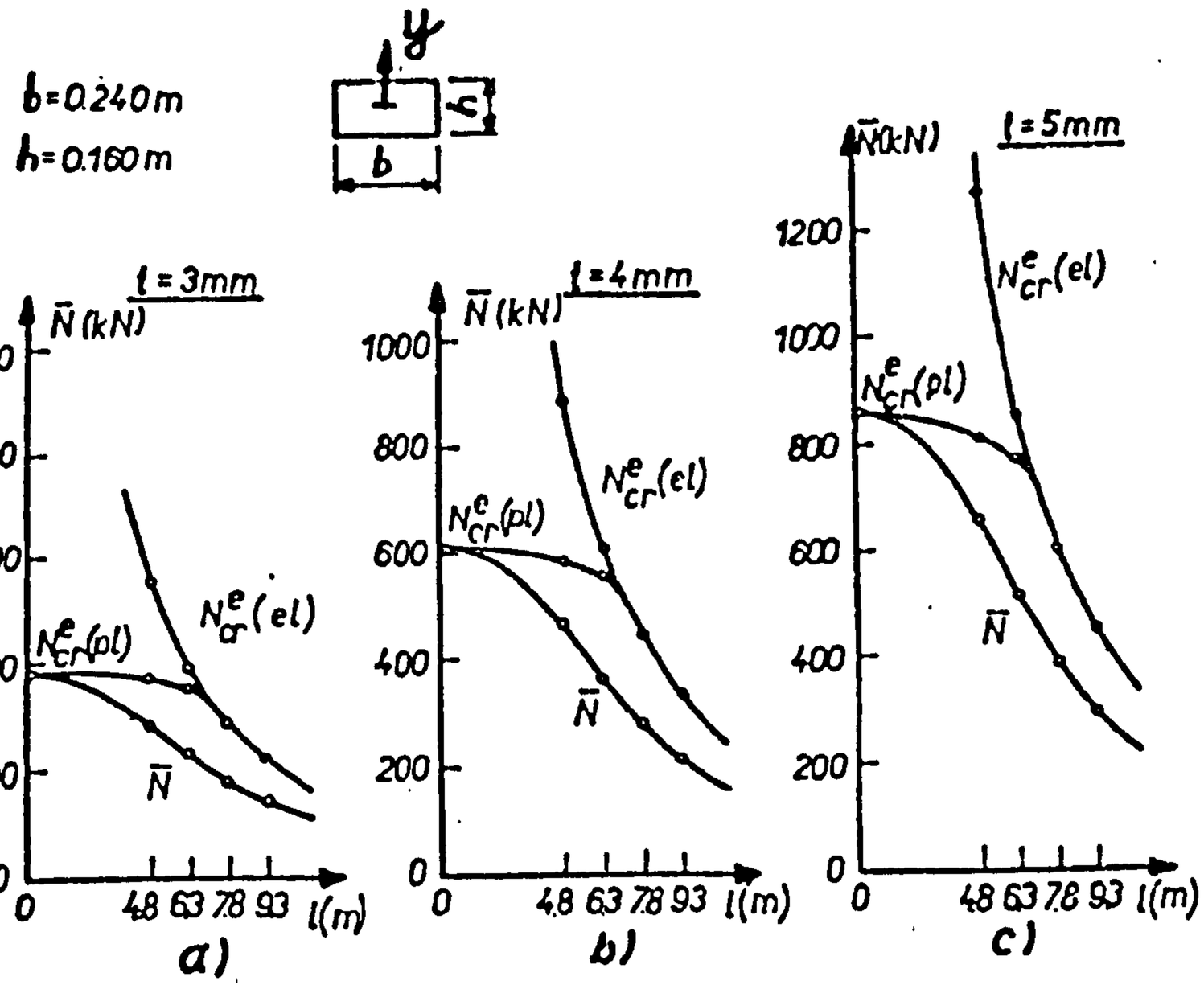

FIG. 1.5.4 ULTIMATE LOAD CURVES OF SKALOUD AND NAPRSTEK(48) FOR RECTANGULAR BOX COLUMNS

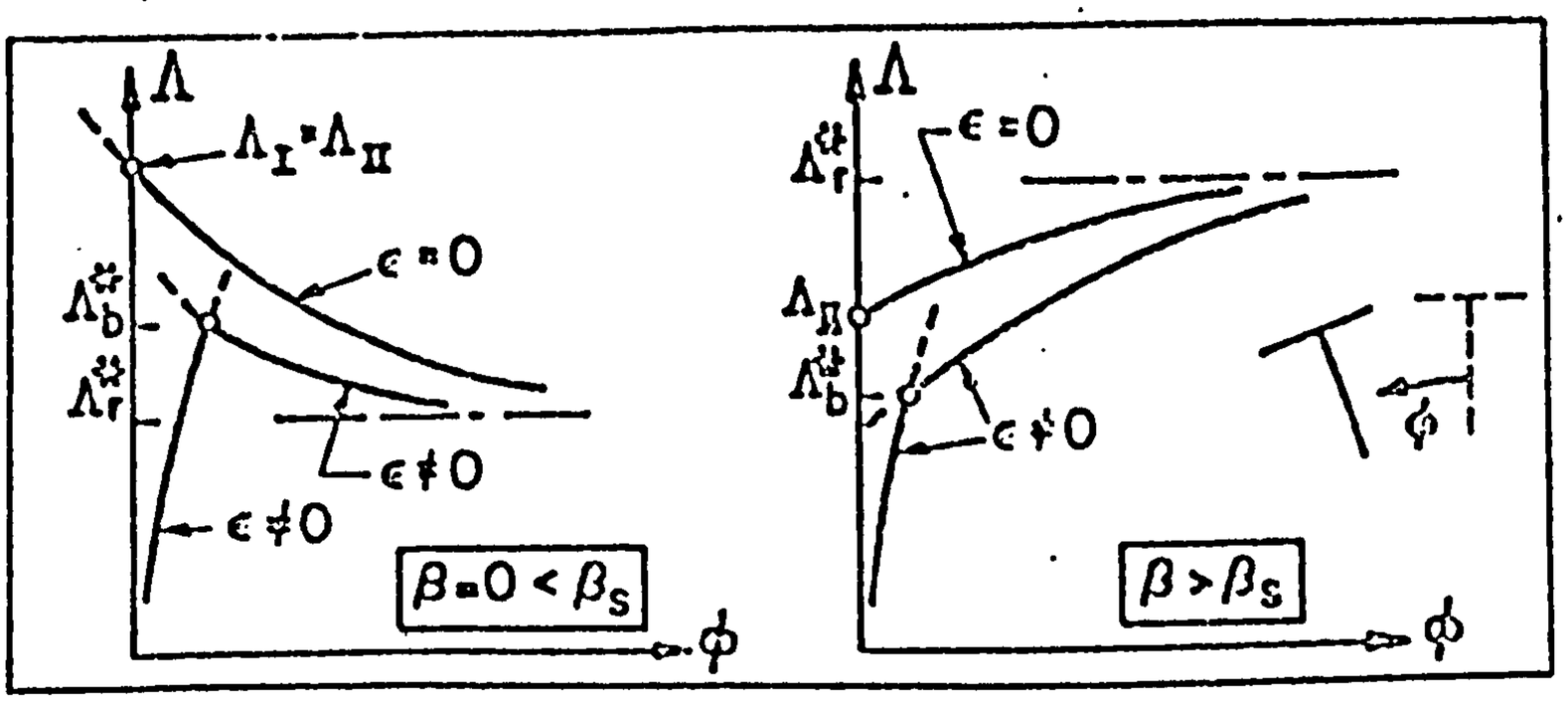

POST BUCKLING PATHS OF THIN WALLED BEAMS SUBJECT TO MODE INTERACTION

FIG. 1.5.5 QUALITATIVE EQUILIBRIUM PATHS OBTAINED BY REIS AND ROORDA (49)

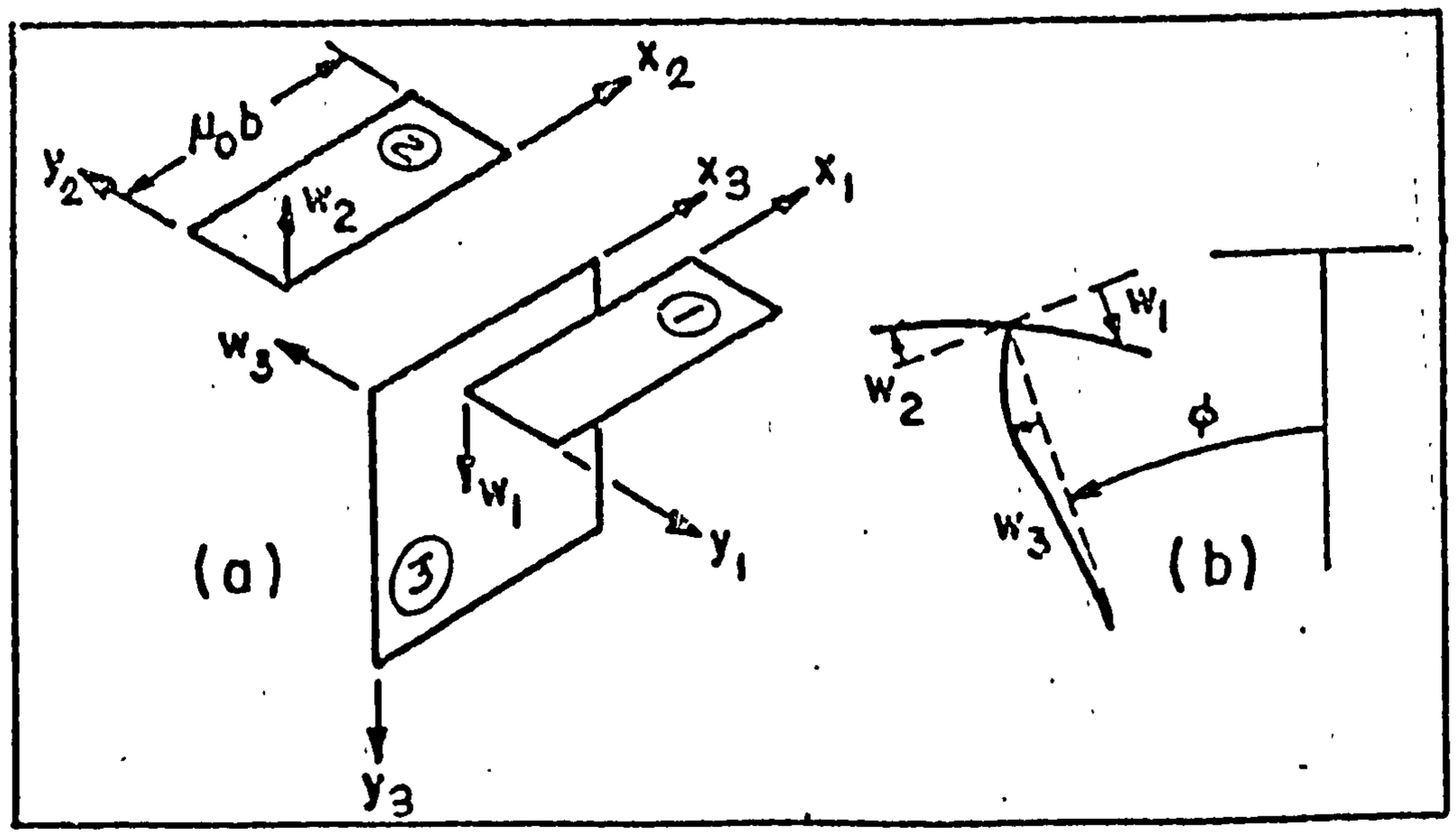

LOCAL BUCKLING COORDINATES

FIG. 1.5.6 CO-ORDINATE SYSTEM USED BY REIS AND ROORDA (49)

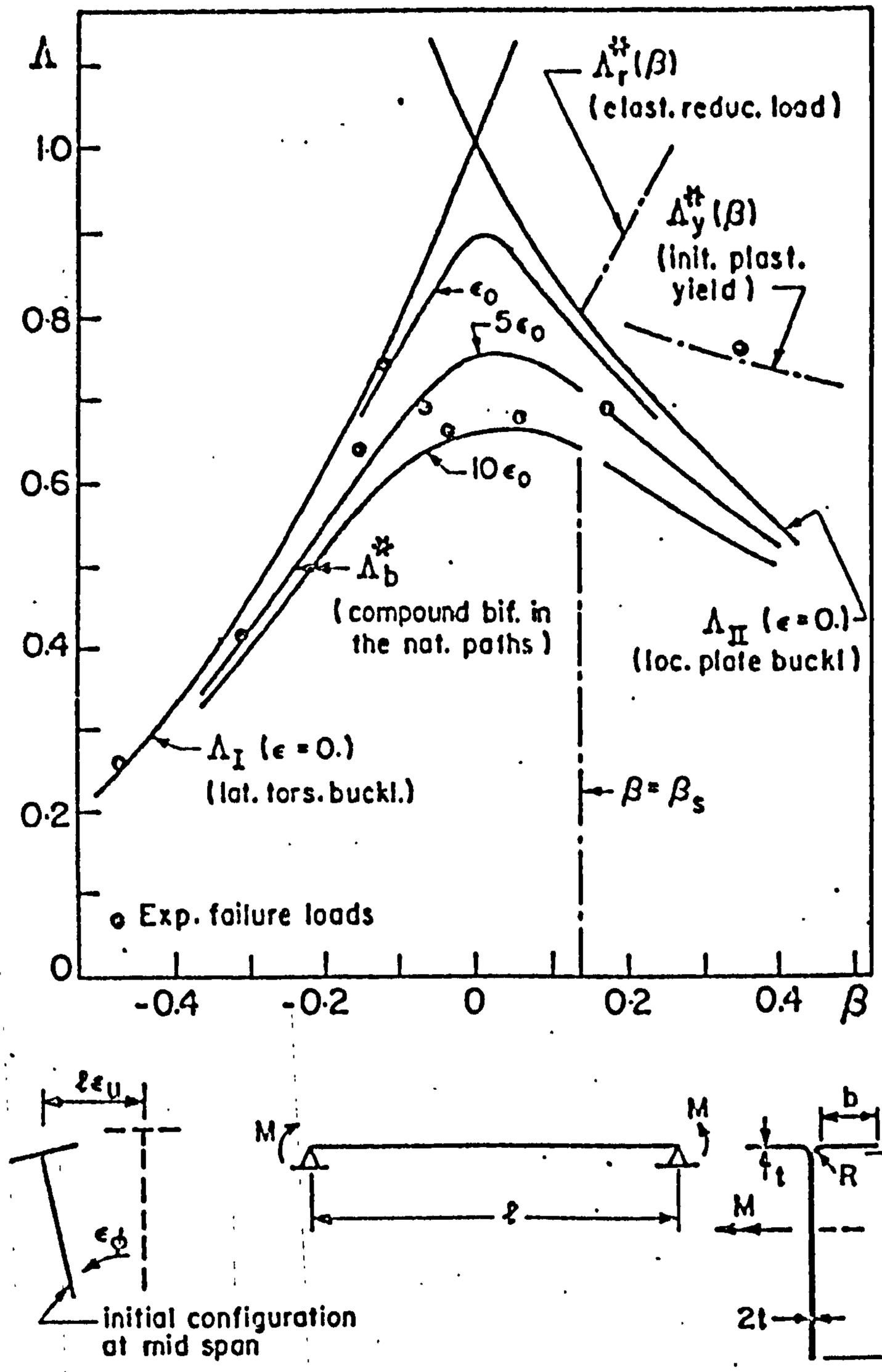

THEORETICAL AND EXPERIMENTAL RESULTS FOR THIN WALLED T BEAMS. ($\Lambda = M/M_o$; $b = (1+\beta)b_o$; $d = d_o - 3b_o$; $b_o = 24.22$ mm; $d_o = 101.09$ mm; $M_o = 521$ KN mm; $t = 0.62$ mm; $\ell = 1654$ mm; $R = 1.9$ mm; $\epsilon = \epsilon_o = \{\epsilon_u; \epsilon_\phi\} = \{0.0001; 0.005\}$)

FIG. 1.5.7 COMPOUND BIFURCATION MOMENTS BY REIS AND ROORDA (49)

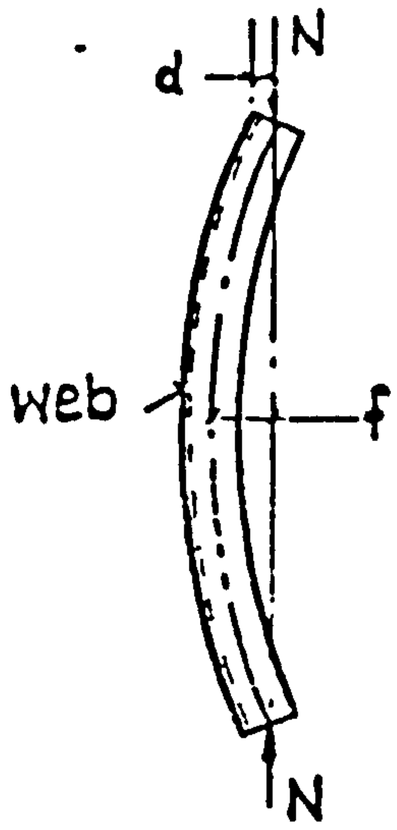

(a) Column under Load

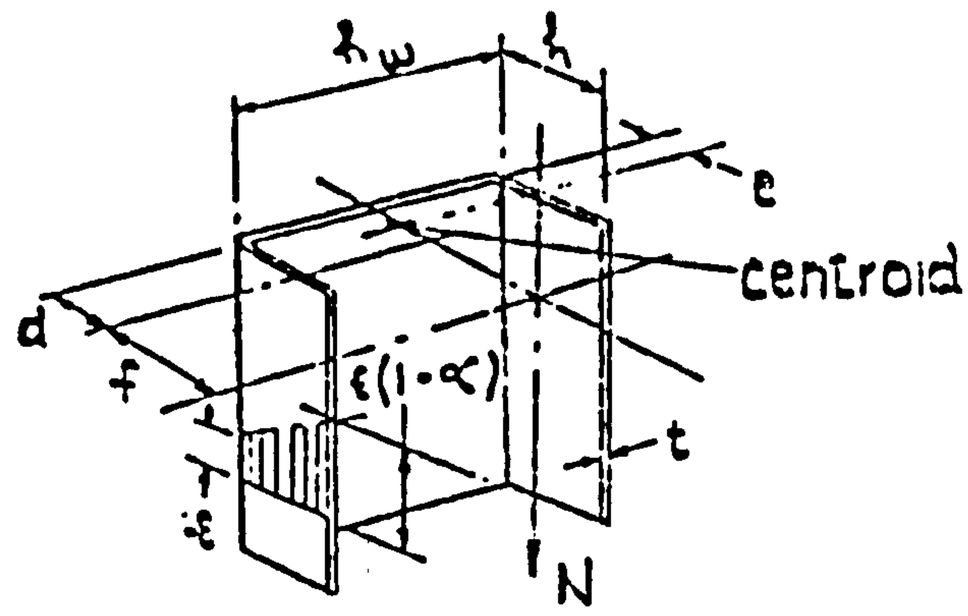

(b) Short Section of Column

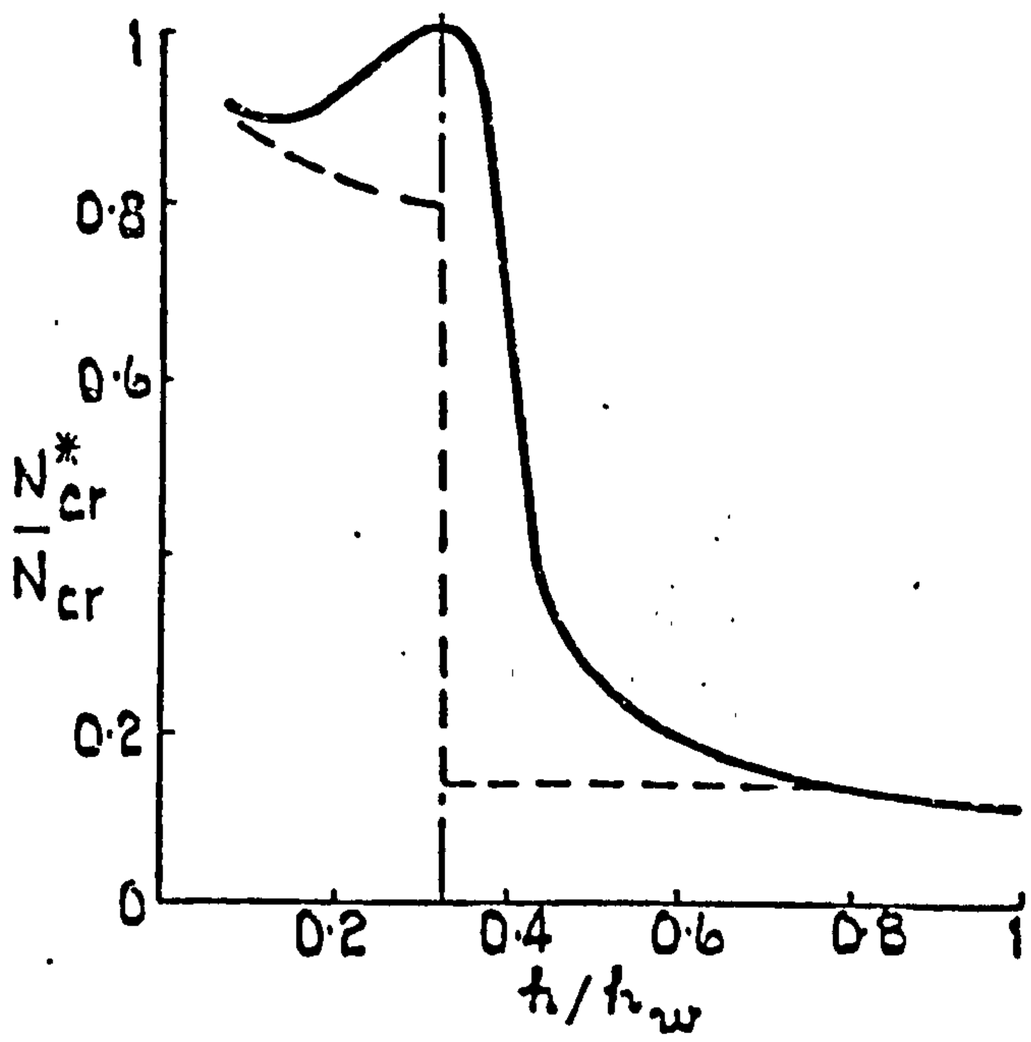

(c) Reduced Euler Loads

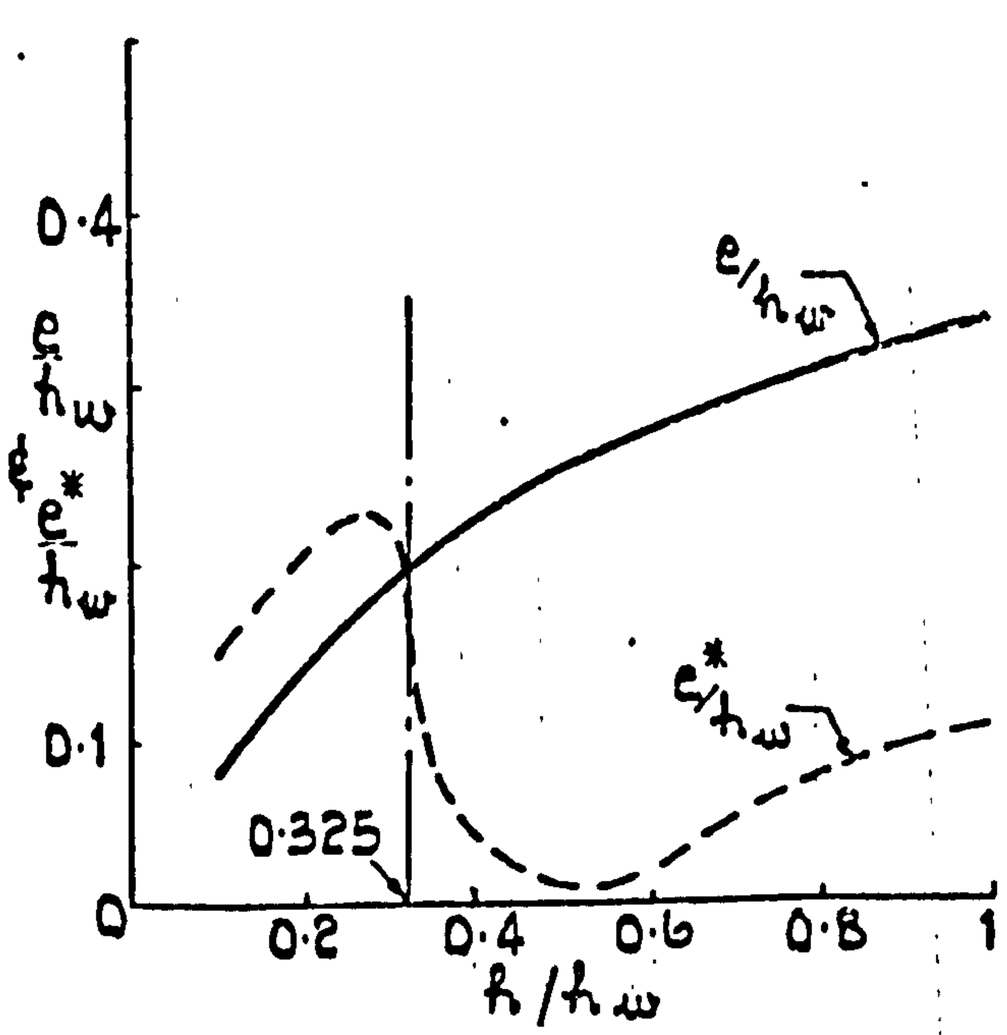

(d) Change in Neutral Axis

FIG 1.5.8 REDUCTION IN EULER LOAD AND SHIFT IN NEUTRAL AXIS AT BUCKLING BY RHODES AND HARVEY (50)

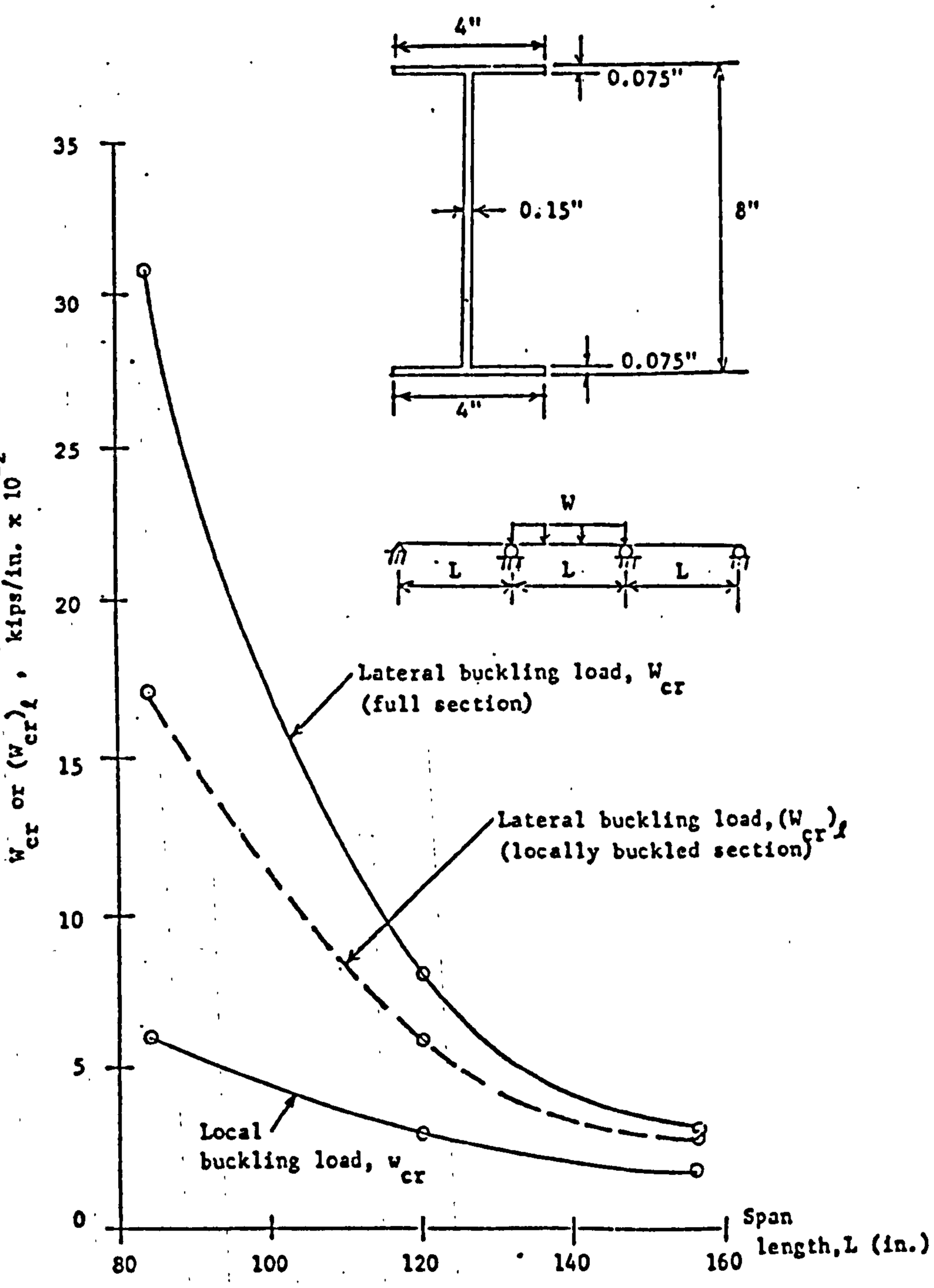

Lateral Buckling Strength of Locally Buckled Continuous Beams

FIG 1.5.9 THEORETICAL RESULTS OF WANG AND WRIGHT(51)

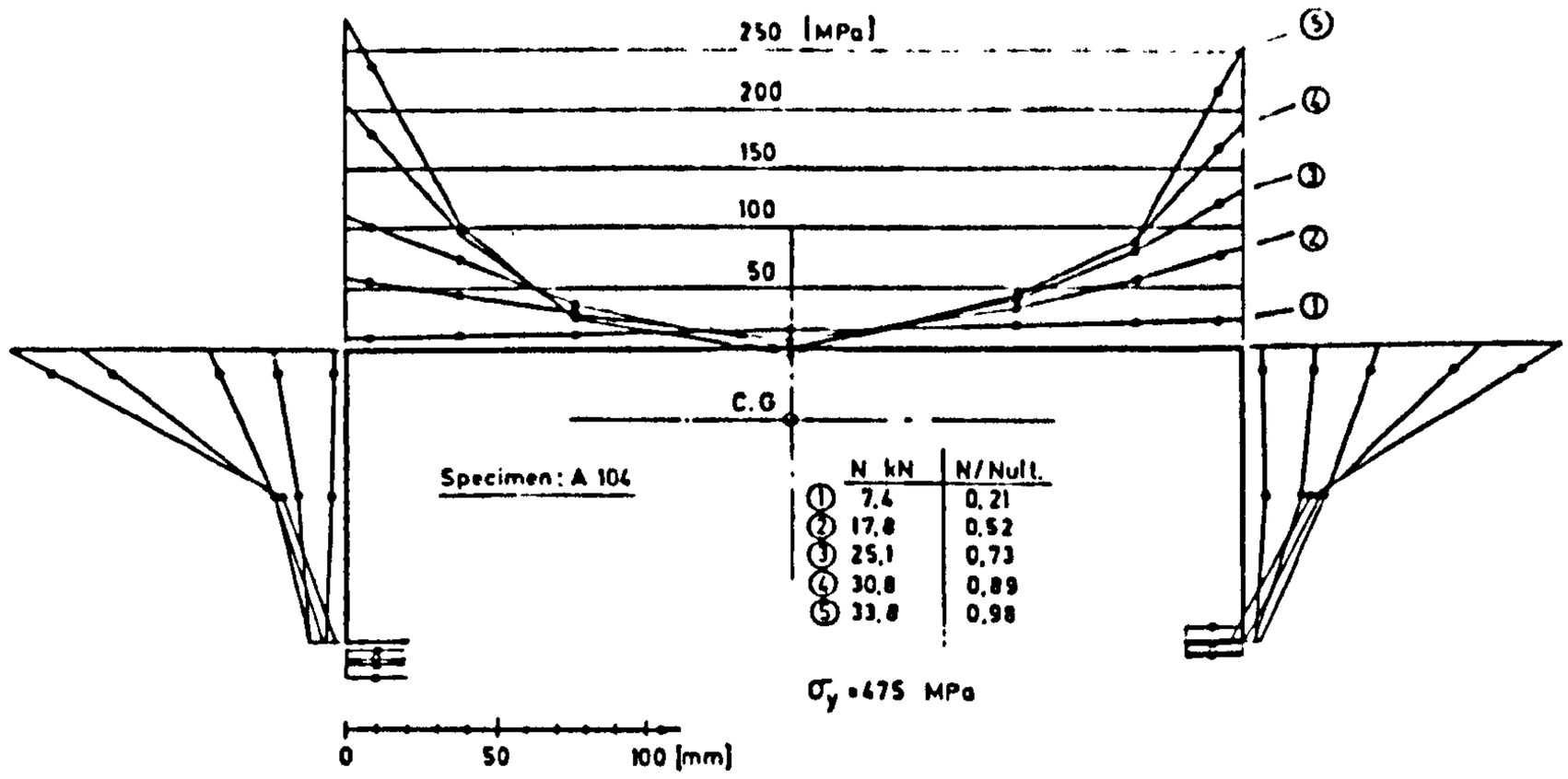

flange = 298.3 mm, web = 99.6 mm, lip = 19.5 mm,

thickness = 0.96 mm, N = axial load.

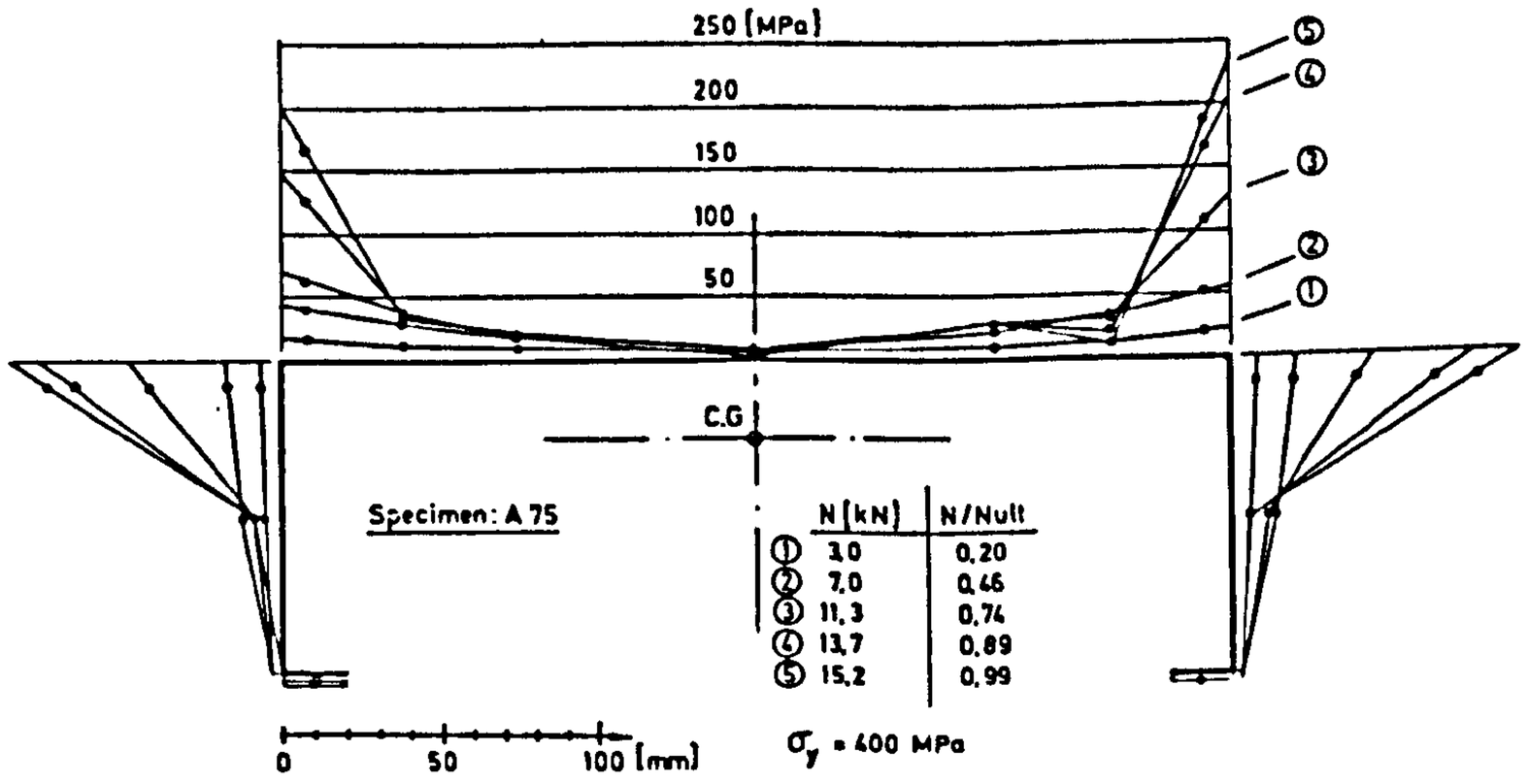

flange = 299.2 mm, web = 100.5 mm, lip = 20.0 mm,

thickness = 0.64 mm, N = axial load.

FIG 1.5.10 DISTRIBUTION OF AXIAL MEMBRANE STRESSES FROM EXPERIMENTAL STRAIN READINGS BY THOMASSON (54)

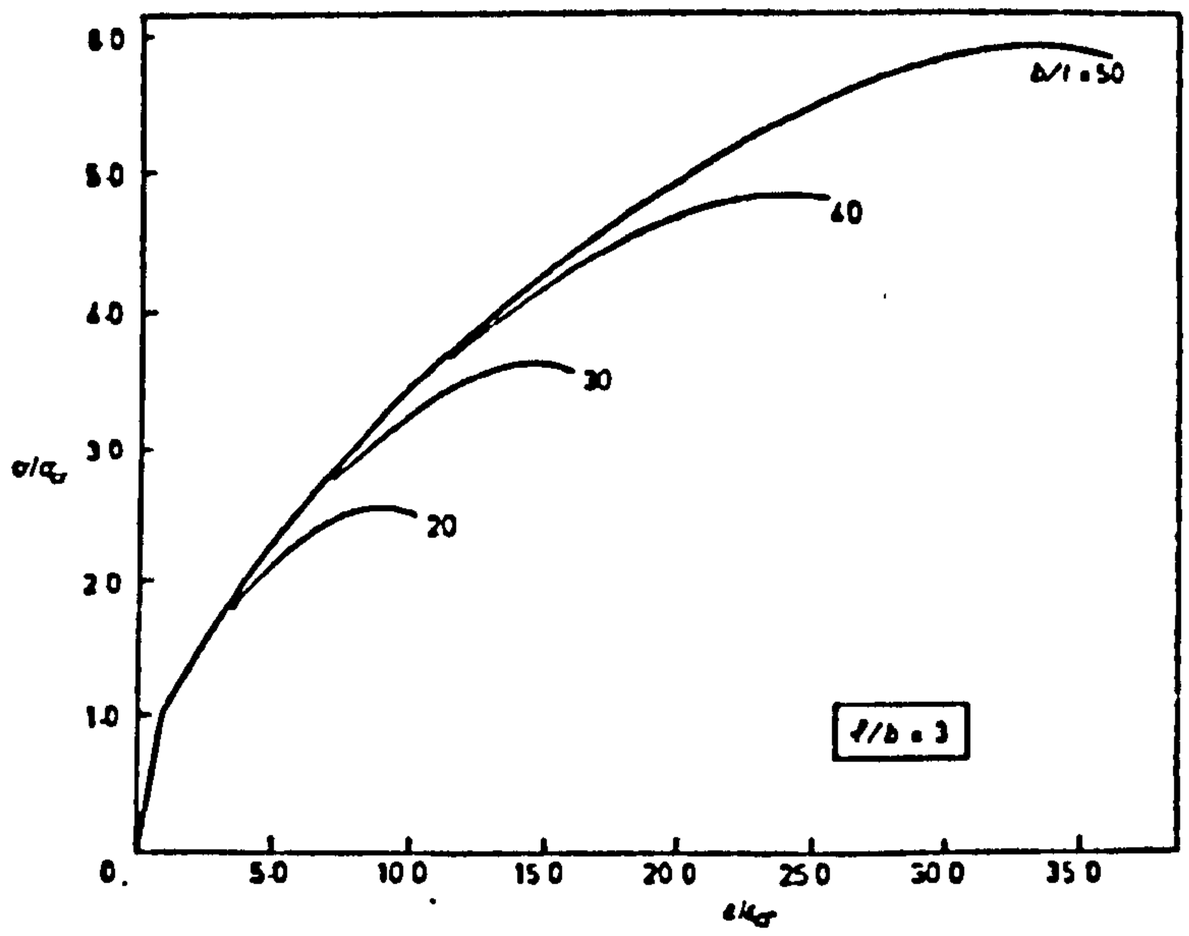

σ, ε = average stress and strain in column

σ_{CR}, ε_{CR} = critical stress and strain of column

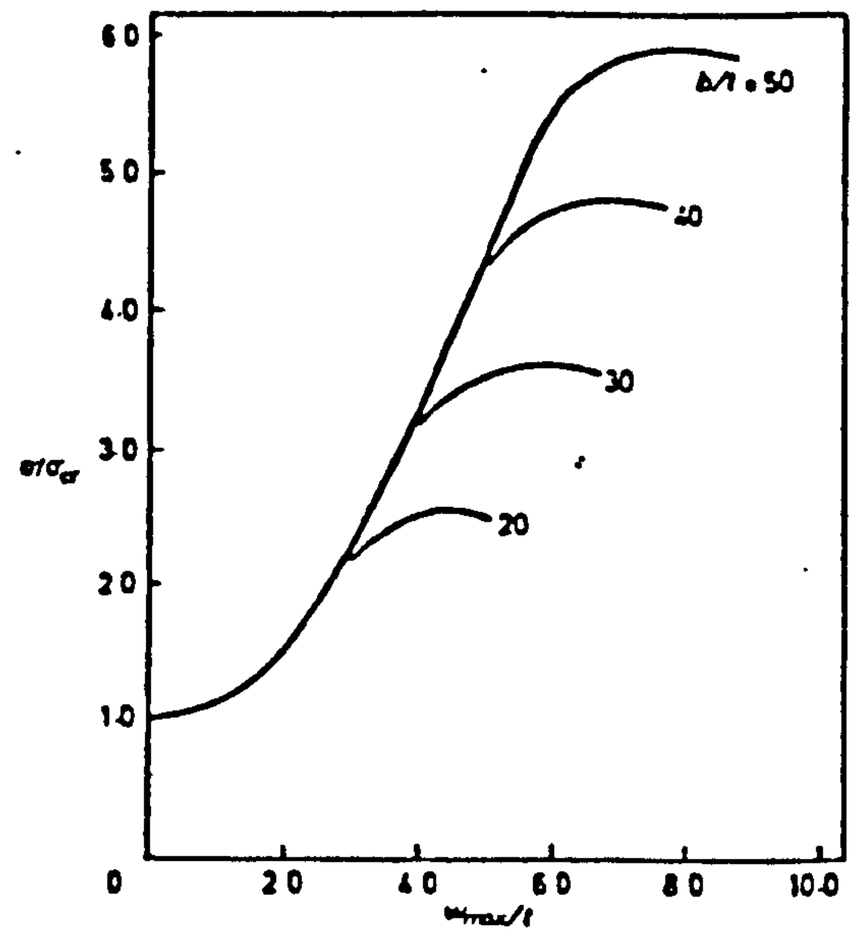

ℓ = column length, b = width of wall, t = wall thickness

W_{max} = maximum out of plane displacement of column wall.

FIG. 1.5.11 THE EFFECT OF CORNER WAVINESS ON THE OVERALL BEHAVIOUR OF THIN WALLED SQUARE BOX COLUMNS BY GRAVES SMITH AND SRIDHARAN (60)

CHAPTER TWO

INTRODUCTION TO THE BASIC THEORY

2.0 INTRODUCTION TO THE BASIC THEORY

2.1 VON KARMAN'S EQUILIBRIUM AND COMPATIBILITY EQUATIONS

Consider an element cut out of a plate by two pairs of planes parallel to the xz and yz planes, as shown in Figure 2.1.1. The element is acted upon by moments and vertical shearing forces, the positive directions of these moments and forces being as indicated. The element also has a distributed load over its upper surface, the intensity of this loading being denoted by q, so that the load acting on the element is q dx dy.

From consideration of the equilibrium of the element in the z direction, moment equilibrium with respect to the x axis and moment equilibrium with respect to the y axis, the following three equations are obtained.

$$\frac{\partial Q_x}{\partial x} + \frac{\partial Q_y}{\partial y} + q = 0 \qquad (2.1.1)(a)$$

$$\frac{\partial M_{xy}}{\partial x} - \frac{\partial M_y}{\partial y} + Q_y = 0 \qquad (2.1.1)(b)$$

$$\frac{\partial M_{yx}}{\partial y} + \frac{\partial M_x}{\partial x} - Q_x = 0 \qquad (2.1.1)(c)$$

Expressions for the moments M_x, M_y, M_{xy} and M_{yx} can be obtained (see Timoshenko and Woinowsky-Krieger (1)) in terms of the plate deflections in the z direction as follows.

$$M_x = -D\left(\frac{\partial^2 w}{\partial x^2} + \nu \frac{\partial^2 w}{\partial y^2}\right) \qquad (2.1.2)(a)$$

$$M_y = -D\left(\frac{\partial^2 w}{\partial y^2} + \nu \frac{\partial^2 w}{\partial x^2}\right) \qquad (2.1.2)(b)$$

$$M_{xy} = -M_{yx} = D(1-\nu)\frac{\partial^2 w}{\partial x \partial y} \qquad (2.1.2)(c)(d)$$

Determination of the shearing forces Q_x and Q_y from equations (2.1.1)(b)(c) and substituting into equation (2.1.1)(a) gives the equation of lateral equilibrium in the z direction in the following form.

$$\frac{\partial^2 M_x}{\partial x^2} + \frac{\partial^2 M_y}{\partial y^2} - 2\frac{\partial^2 M_{xy}}{\partial x \partial y} = -q \qquad (2.1.3)$$

Up to this point the bending of a plate due to lateral loads only has been contemplated. If in addition to these loads there are forces acting in the middle plane of the plate, then these forces must be taken into account when deriving the differential equation of lateral equilibrium.

Consider then a plate element acted on by middle surface forces as shown in Figure 2.1.2. Equilibrium of the element in the x and y

directions gives rise to the following two equations

$$\frac{\partial Nx}{\partial x} + \frac{\partial Nxy}{\partial y} = 0 \qquad (2.1.4)(a)$$

$$\frac{\partial Nxy}{\partial x} + \frac{\partial Ny}{\partial y} = 0 \qquad (2.1.4)(b)$$

It should be noted that these equations are completely independent of the three equations of equilibrium (2.1.1) considered earlier and due to this independence may be treated separately. Considering the projection of the forces shown in Figure 2.1.2 on the z axis and taking into account the bending of the plate, the following three expressions, which describe the projection of the normal forces N_x and N_y and the shearing forces N_{xy} and N_{yx} on the z axis, are obtained.

$$N_x \frac{\partial^2 w}{\partial x^2} dx dy + \frac{\partial Nx}{\partial x} \frac{\partial w}{\partial x} dx dy \qquad (2.1.5)(a)$$

$$N_y \frac{\partial^2 w}{\partial y^2} dx dy + \frac{\partial Ny}{\partial y} \frac{\partial w}{\partial y} dx dy \qquad (2.1.5)(b)$$

$$2N_{xy} \frac{\partial^2 w}{\partial x \partial y} dx dy + \frac{\partial Nxy}{\partial x} \frac{\partial w}{\partial y} dx dy + \frac{\partial Nxy}{\partial y} \frac{\partial w}{\partial x} dx dy \qquad (2.1.5)(c)$$

Adding expressions (2.1.5) and utilising equations (2.1.4) gives an expression for the projection of all mid-surface normal and shearing forces in the z direction. This expression is now added to the load q dx dy acting on the element to obtain, instead of equation (2.1.3), the following equation of lateral equilibrium.

$$\frac{\partial^2 M_x}{\partial x^2} - 2\frac{\partial^2 M_{xy}}{\partial x \partial y} + \frac{\partial^2 M_y}{\partial y^2} = -\left(q + N_x\frac{\partial^2 w}{\partial x^2} + N_y\frac{\partial^2 w}{\partial y^2} + 2N_{xy}\frac{\partial^2 w}{\partial x \partial y}\right) \quad (2.1.6)$$

Substitution of equations (2.1.2) for the moments M_x, M_y and M_{xy} enables the left hand side of equation (2.1.6) to be written purely in terms of the deflections w. The stress resultants N_x, N_y and N_{xy} can be replaced by a stress function F such that

$$\sigma_x = \frac{N_x}{t} = \frac{\partial^2 F}{\partial y^2}, \quad \sigma_y = \frac{N_y}{t} = \frac{\partial^2 F}{\partial x^2}, \quad \tau_{xy} = \frac{N_{xy}}{t} = -\frac{\partial^2 F}{\partial x \partial y} \quad (2.1.7)$$

This form of stress function automatically satisfies the equations of equilibrium (2.1.4).

Assuming now that q is zero, the following equilibrium equation, initially derived by Von Karman, describing the deflection of a plate subjected to mid-plane forces only is obtained.

$$\frac{\partial^4 w}{\partial x^4} + 2\frac{\partial^4 w}{\partial x^2 \partial y^2} + \frac{\partial^4 w}{\partial y^4} = \frac{t}{D}\left[\frac{\partial^2 F}{\partial y^2}\frac{\partial^2 w}{\partial x^2} + \frac{\partial^2 F}{\partial x^2}\frac{\partial^2 w}{\partial y^2} - 2\frac{\partial^2 F}{\partial x \partial y}\cdot\frac{\partial^2 w}{\partial x \partial y}\right] \quad (2.1.8)$$

This is known as Von Karman's equilibrium equation.

Considering now the x, y and z components of displacement that a point in the middle plane of the plate experiences during

buckling, expressions may be stated for the strains in terms of these displacements (Timoskenko and Woinowsky-Krieger (1))

$$\varepsilon_x = \frac{\partial u}{\partial x} + \frac{1}{2}\left(\frac{\partial w}{\partial x}\right)^2 \qquad (2.1.9)(a)$$

$$\varepsilon_y = \frac{\partial v}{\partial y} + \frac{1}{2}\left(\frac{\partial w}{\partial y}\right)^2 \qquad (2.1.9)(b)$$

$$\gamma_{xy} = \frac{\partial u}{\partial y} + \frac{\partial v}{\partial x} + \frac{\partial w}{\partial x}.\frac{\partial w}{\partial y} \qquad (2.1.9)(c)$$

Taking the second derivatives of (a) w.r.t. y, (b) w.r.t. x and (c) w.r.t. x and y and adding, gives a single differential equation linking the mid-surface strains to the lateral displacements.

$$\frac{\partial^2 \varepsilon_x}{\partial y^2} + \frac{\partial^2 \varepsilon_y}{\partial x^2} - \frac{\partial^2 \gamma_{xy}}{\partial x \partial y} = \left(\frac{\partial^2 w}{\partial x \partial y}\right)^2 - \left(\frac{\partial^2 w}{\partial x^2}\right)\left(\frac{\partial^2 w}{\partial y^2}\right) \qquad (2.1.10)$$

The two dimensional stress strain relationships for a linear elastic material are now used to describe the strains in terms of the stresses

$$\varepsilon_x = \frac{1}{E}\left(\sigma_x - \nu \sigma_y\right) \qquad (2.1.11)(a)$$

$$\varepsilon_y = \frac{1}{E}\left(\sigma_y - \nu \sigma_x\right) \qquad (2.1.11)(b)$$

$$\gamma_{xy} = \frac{1}{G}\tau_{xy} = \frac{2(1+\nu)}{E}\tau_{xy} \qquad (2.1.11)(c)$$

Substitution of equations (2.1.11) and (2.1.7) into (2.1.10) yields the final equation

$$\frac{\partial^4 F}{\partial x^4} + 2\frac{\partial^4 F}{\partial x^2 \partial y^2} + \frac{\partial^4 F}{\partial y^4} = E\left[\left(\frac{\partial^2 w}{\partial x \partial y}\right)^2 - \frac{\partial^2 w}{\partial x^2}\cdot\frac{\partial^2 w}{\partial y^2}\right] \qquad (2.1.12)$$

This equation was first derived by Von Karman and since it is derived from compatibility considerations is known as Von Karman's compatibility equation.

2.2 ELASTIC STRAIN ENERGY STORED IN A SYSTEM OF PLATES DUE TO BENDING AND TWISTING

Consider an element under the action of moments M_x and M_y as shown in Figure 2.2.1. The elastic strain energy stored due to M_x is given by $\frac{1}{2} M_x \theta_x$ per unit volume, where $\theta_x = -\frac{\partial^2 w}{\partial x^2}\,dx$ as shown in Figure 2.2.2. Similarly the strain energy stored per unit volume due to M_y is $\frac{1}{2} M_y \theta_y$ where $\theta_y = -\frac{\partial^2 w}{\partial y^2}\,dy$, the negative sign for θ_x and θ_y being due to the sign convention chosen for w.

The strain energy contained in the element due to M_x and M_y is therefore

$$dV_1 = -\frac{1}{2}\left[M_x\frac{\partial^2 w}{\partial x^2} + M_y\frac{\partial^2 w}{\partial y^2}\right]dx\,dy$$

substituting for the moments from equations (2.1.2) gives

$$dV_1 = \frac{D}{2}\left[\left(\frac{\partial^2 w}{\partial x^2}+\frac{\partial^2 w}{\partial y^2}\right)^2 - 2(1-\nu)\,\frac{\partial^2 w}{\partial x^2}\cdot\frac{\partial^2 w}{\partial y^2}\right] dx\,dy \qquad (2.2.1)$$

Consider now the same element loaded by twisting moments M_{xy} and M_{yx} as shown in Figure 2.2.3, the strain energy due to M_{yx} is given by $\frac{1}{2} M_{yx}\frac{\partial \phi}{\partial x}$ dx dy where $\frac{\partial \phi}{\partial x} = \frac{\partial}{\partial x}\left(\frac{\partial w}{\partial y}\right) = \frac{\partial^2 w}{\partial x \partial y}$. Similarly the strain energy due to M_{xy} is given by $\frac{1}{2} M_{xy}\frac{\partial \gamma}{\partial y}$ dx dy where $\frac{\partial \gamma}{\partial y} = \frac{\partial}{\partial y}\left(\frac{\partial w}{\partial x}\right) = \frac{\partial^2 w}{\partial y \partial x} = \frac{\partial^2 w}{\partial x \partial y}$. The strain energy due to M_{xy} is the same as the strain energy due to M_{yx} hence the total strain energy due to twisting is therefore

$$dV_2 = M_{xy}\,\frac{\partial^2 w}{\partial x\,\partial y}\,dx\,dy$$

Substituting for M_{xy} from equation (2.1.2) gives

$$dV_2 = D(1-\nu)\left(\frac{\partial^2 w}{\partial x\,\partial y}\right)^2 dx\,dy \qquad (2.2.2)$$

The strain energy due to both bending and twisting is obtained from the sum of (2.2.1) and (2.2.2) to give

$$dV_B = dV_1 + dV_2$$

$$dV_B = \frac{D}{2}\left[\left(\frac{\partial^2 w}{\partial x^2}+\frac{\partial^2 w}{\partial y^2}\right)^2 - 2(1-\nu)\left(\frac{\partial^2 w}{\partial x^2}\cdot\frac{\partial^2 w}{\partial y^2} - \left(\frac{\partial^2 w}{\partial x \partial y}\right)^2\right)\right] dx\,dy \qquad (2.2.3)$$

For a system of plates connected at their edges to form a section, used perhaps as a column or beam, expression (2.2.3) is integrated over each plate and summed for all plates to give the total strain energy in the section due to plate bending and twisting. This expression takes the form:

$$V_B = \frac{D}{2}\sum_{i=1}^{i=h}\iint\left\{\left[\frac{\partial^2 w_i}{\partial x^2}+\frac{\partial^2 w_i}{\partial y_i^2}\right]^2 - 2(1-\nu)\left[\frac{\partial^2 w_i}{\partial x^2}\frac{\partial^2 w_i}{\partial y_i^2}-\left(\frac{\partial^2 w_i}{\partial x \partial y_i}\right)^2\right]\right\} dx\, dy_i \quad (2.2.4)$$

h being the number of plates in the system, and the limits of integration being the boundaries of each plate.

2.3 ELASTIC STRAIN ENERGY STORED IN A SYSTEM OF PLATES DUE TO FORCES ACTING IN THE MIDDLE SURFACE

Consideration is now given to the strain energy stored in an element of linear elastic material subjected to stresses σ_x, σ_y and τ_{xy} as shown in Figure 2.3.1. The strain energy in the small element due to these mid-surface stresses is given by the following expression.

$$dV_M = \frac{t}{2}\left(\sigma_x \epsilon_x + \sigma_y \epsilon_y + \tau_{xy}\gamma_{xy}\right) dx\, dy \quad (2.3.1)$$

Integrating over the plate gives the total strain energy due to mid-surface stresses as

$$V_M = \frac{t}{2}\iint\left(\sigma_x \epsilon_x + \sigma_y \epsilon_y + \tau_{xy}\gamma_{xy}\right) dx\, dy \quad (2.3.2)$$

Substitution of equations (2.1.11) and (2.1.7) into (2.3.2) yields the strain energy in terms of the stress function F in the following form.

$$V_M=\frac{t}{2E}\iint\left\{\frac{\partial^2F}{\partial y^2}\left(\frac{\partial^2F}{\partial y^2}-\nu\frac{\partial^2F}{\partial x^2}\right)+\frac{\partial^2F}{\partial x^2}\left(\frac{\partial^2F}{\partial x^2}-\nu\frac{\partial^2F}{\partial y^2}\right)+2(1+\nu)\frac{\partial^2F}{\partial x\partial y}\cdot\frac{\partial^2F}{\partial x\partial y}\right\}dxdy \quad (2.3.3)$$

Rearranging equation (2.3.3) and considering a system of plates gives the final expression for the total strain energy in a section due to mid-surface stresses in the component plates.

$$V_M=\frac{t}{2E}\sum_{i=1}^{i=k}\iint\left\{\left[\frac{\partial^2F_i}{\partial x^2}+\frac{\partial^2F_i}{\partial y_i^2}\right]^2-2(1+\nu)\left[\frac{\partial^2F_i}{\partial x^2}\frac{\partial^2F_i}{\partial y_i^2}-\left(\frac{\partial^2F_i}{\partial x\partial y_i}\right)^2\right]\right\}dxdy_i \quad (2.3.4)$$

The total strain energy stored in the section is given by the sum of expressions (2.2.4) and (2.3.4), the stress function F having satisfied Von Karman's compatibility equation. Consider now a system of plates used as a column under an eccentrically applied axial load. It is required to find the critical load at which initial plate instability of the section occurs. To do this consider the section to be under an end displacement system such that the section is just on the point of buckling locally but is still in the plane undeflected state. At this point the force system acting on the ends of the plates is known, since it is directly related to the displacement system. The loss in potential of the applied end force system at the instant of section local buckling is;

$$-\frac{1}{2}\sum_{i=1}^{i=n}\iint [N_x]_i \left(\frac{\partial w_i}{\partial x}\right)^2 dx\,dy_i \qquad (2.3.5)$$

the negative sign indicating a potential loss. The total potential change in the system at the instant of local buckling is now given by the sum of expressions (2.2.4) and (2.3.5).

$$V=\sum_{i=1}^{i=n}\iint\left[\frac{D}{2}\left[\left(\frac{\partial^2 w_i}{\partial x^2}+\frac{\partial^2 w_i}{\partial y_i^2}\right)^2-2(1-\nu)\left(\frac{\partial^2 w_i}{\partial x^2}\frac{\partial^2 w_i}{\partial y_i^2}-\left(\frac{\partial^2 w_i}{\partial x\,\partial y_i}\right)^2\right)\right]-\frac{[N_x]_i}{2}\left(\frac{\partial w_i}{\partial x}\right)^2\right]dx\,dy_i \qquad (2.3.6)$$

In order to find the critical local buckling load for the column the deflections w_i are represented by a series of functions which satisfy the boundary conditions of displacement and moment equilibrium at the plate junctions, each function being associated with an unknown deflection coefficient. The deflection functions w_i are substituted into (2.3.6) and the total potential is minimised by differentiating (2.3.6) with respect to each deflection coefficient in turn. This results in a series of N simultaneous equations known as an eigenproblem, which in matrix notation takes the form $(A - \lambda B)X = O$ where A is a real symmetric matrix, B a real symmetric positive definite matrix, λ is the eigenvalues of the problem and X the corresponding eigenvectors. The lowest eigenvalue, corresponding to the lowest buckling stress, is required to evaluate the column local instability load, the corresponding eigenvector specifying the buckled form of the section at this load. In the post local buckling analysis

the buckled form from the eigen solution is used, multiplied by an unknown coefficient, as the first term in the deflection functions w_i. Subsequent terms and corresponding coefficients are added to this in order to obtain the best buckled form using the principle of minimum strain energy.

The method used in the post local buckling analysis is to obtain the stress functions F_i in terms of the deflection coefficients in w_i by solving equation (2.1.12) (Von Karman's compatibility equation) and satisfying the relevant stress conditions at the plate boundaries. The deflection functions w_i and the stress functions F_i are now substituted into equations (2.2.4) and (2.3.4) respectively in order to evaluate the total strain energy V_T in terms of the unknown deflection coefficients. The determination of these coefficients follows from the minimisation of the total strain energy expression with respect to each coefficient in turn. Knowledge of the values of the deflection coefficients permits the evaluation of the lateral deflections of all plates (buckled form) and the stresses within the section. The applied load on the column can be evaluated by integration of the in-plane stresses in the axial direction around the section.

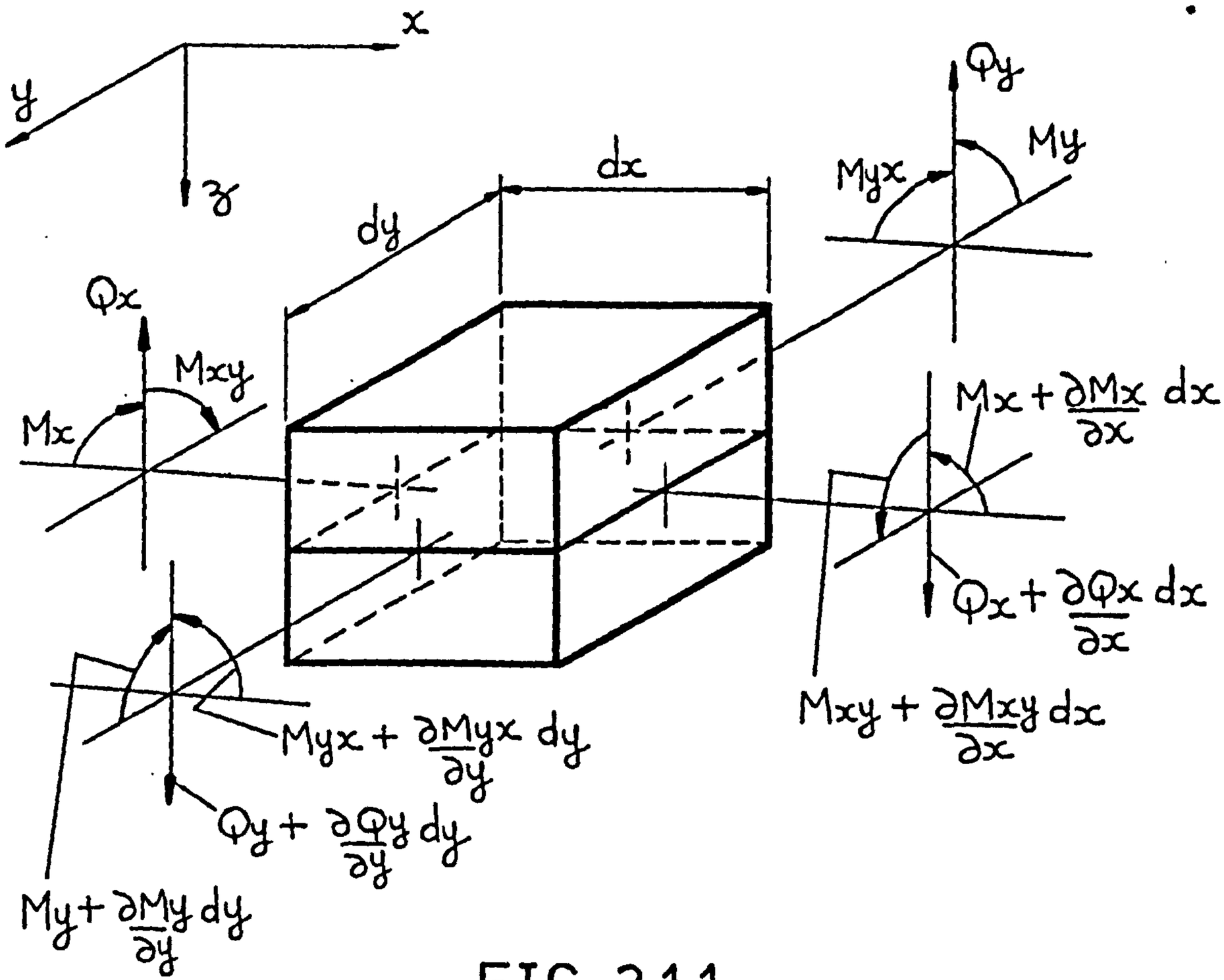

FIG. 2.1.1

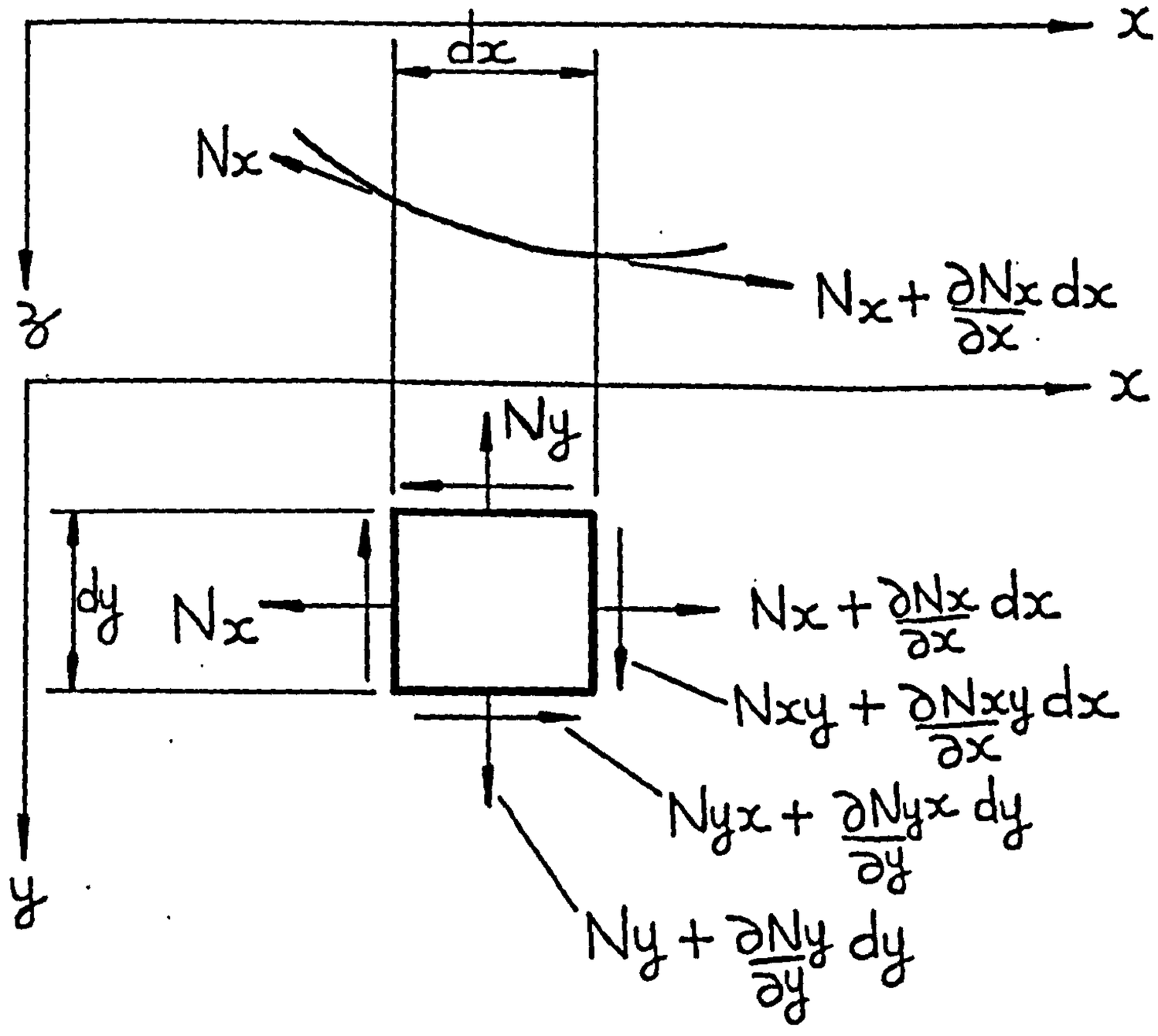

FIG. 2.1.2

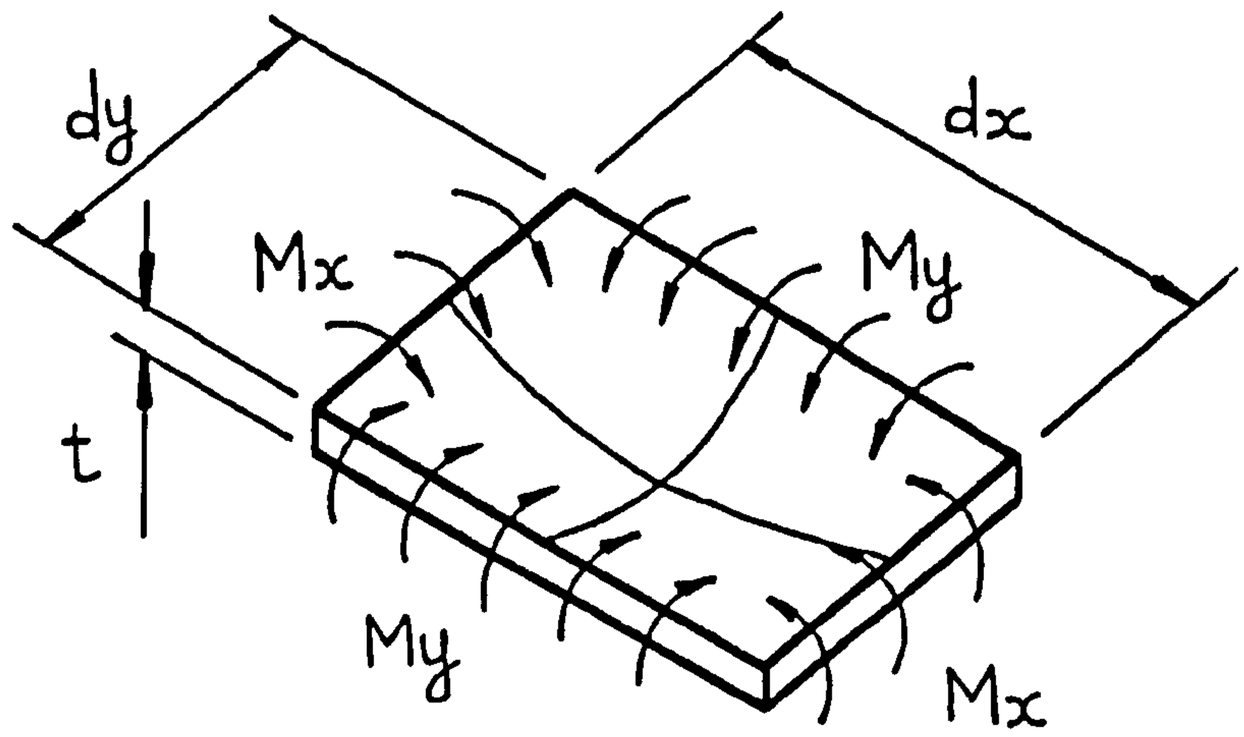

FIG. 2.2.1

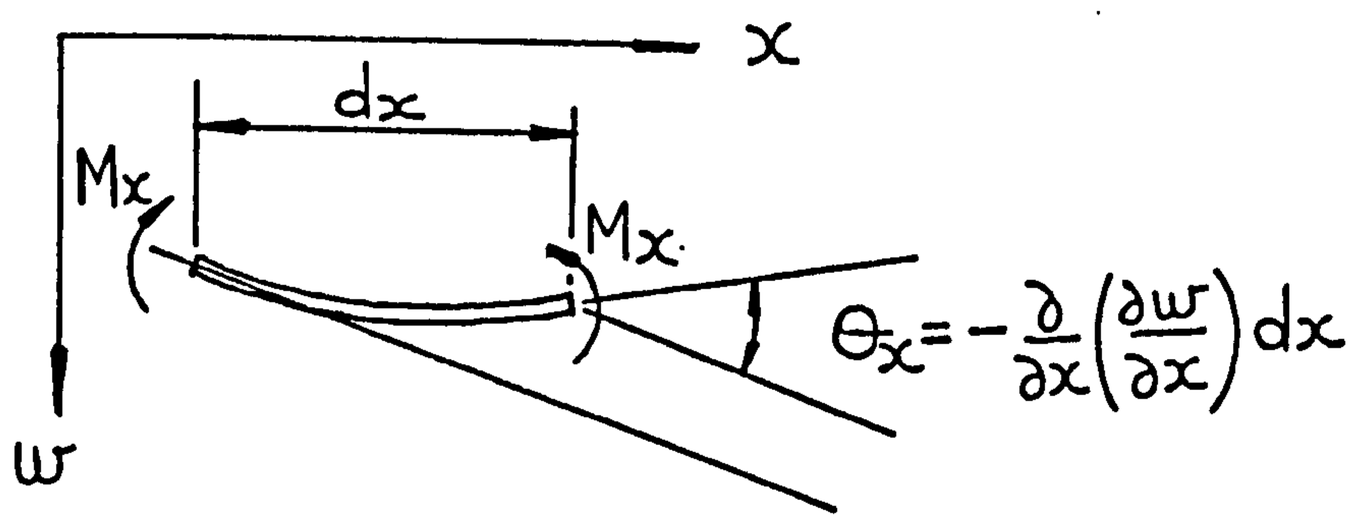

FIG. 2.2.2

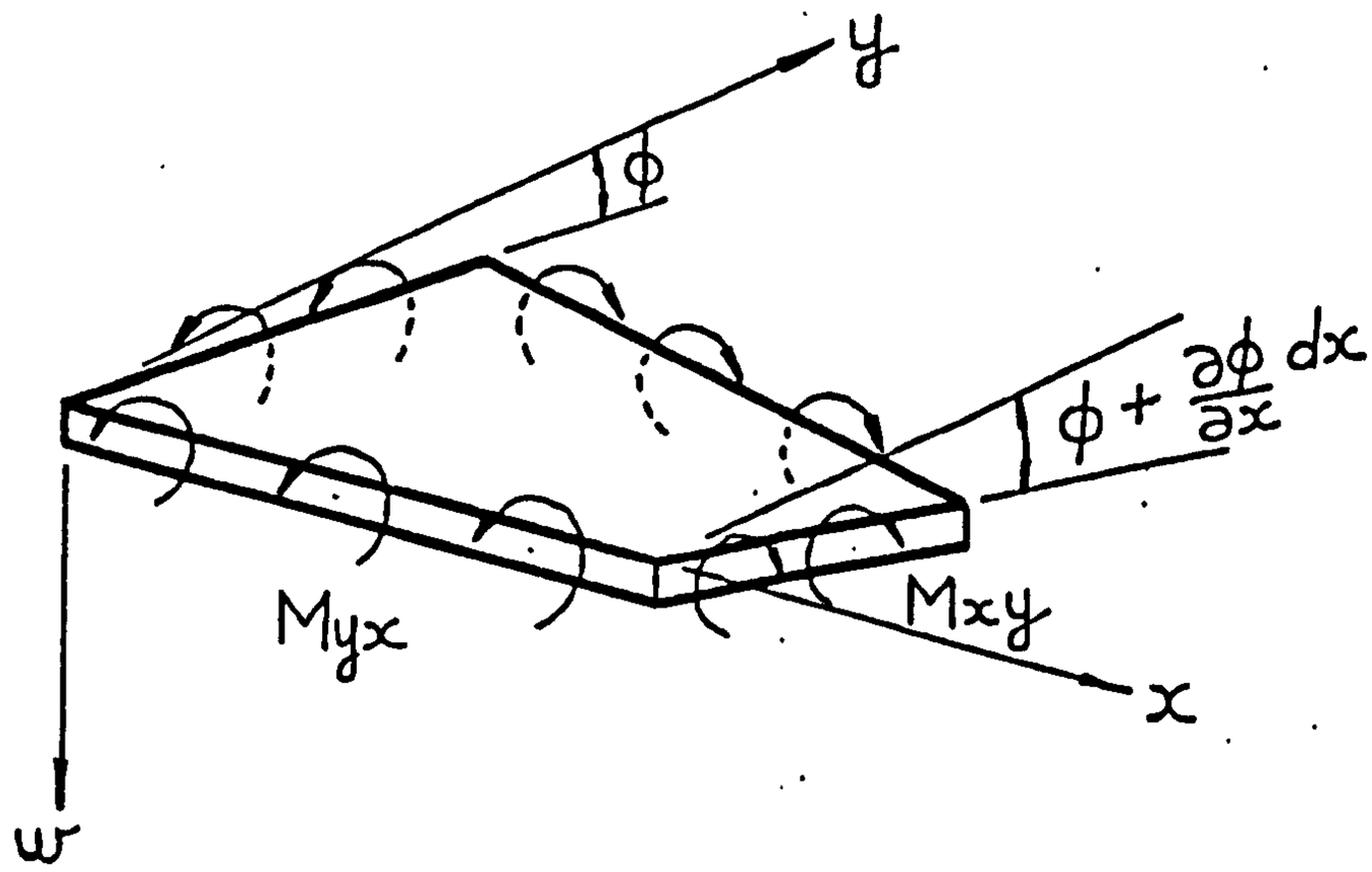

FIG. 2.2.3

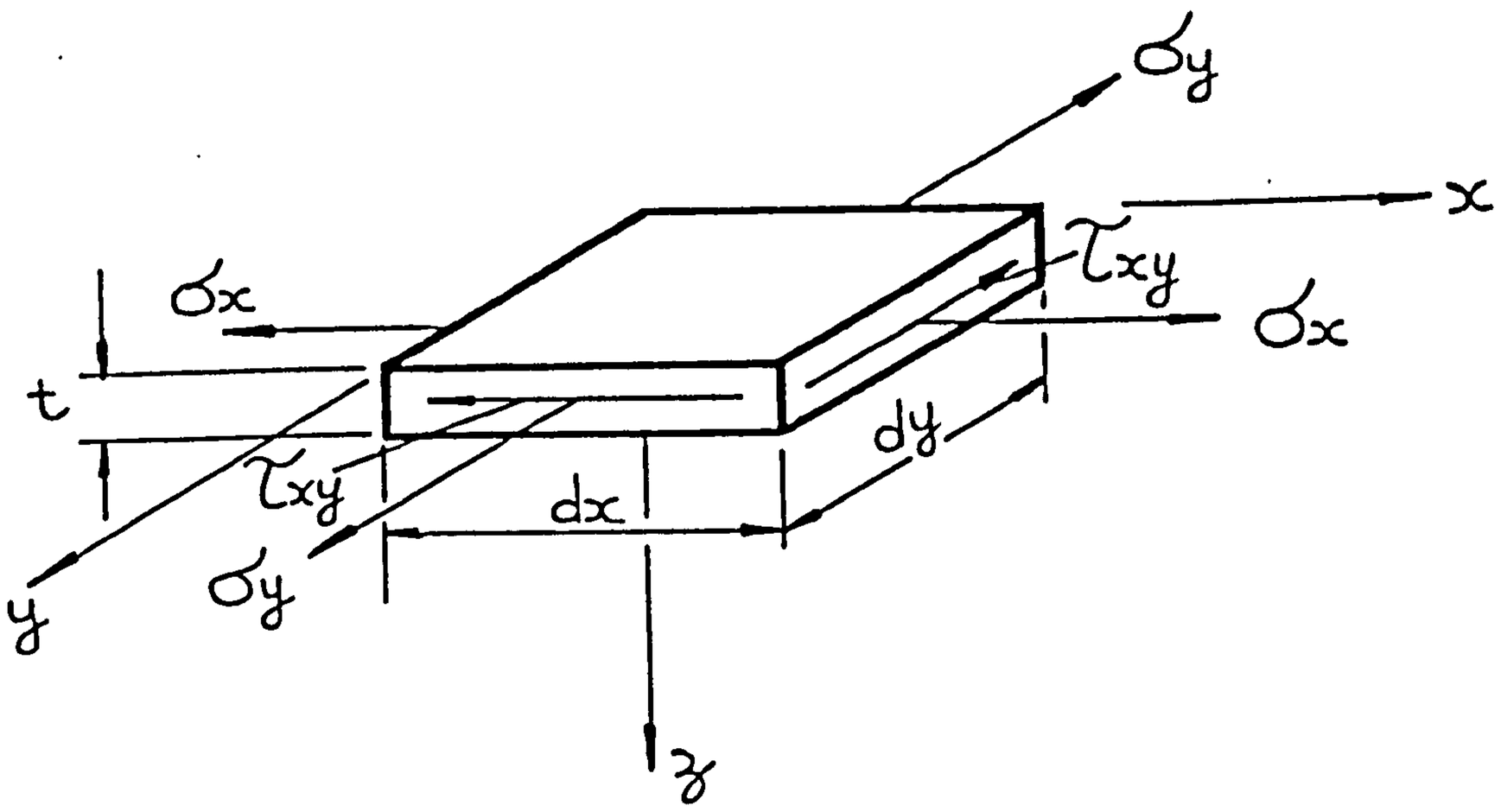

FIG. 2.3.1

CHAPTER THREE

ANALYSIS OF THE INITIAL INSTABILITY LOAD FOR AN ECCENTRICALLY LOADED COLUMN

3.0 ANALYSIS OF THE INITIAL INSTABILITY LOAD FOR AN ECCENTRICALLY LOADED COLUMN

3.1 INSIGHT TO THE PROBLEM

It is required to evaluate the initial local instability load for a thin walled column under the action of an eccentrically applied axial load. The boundary conditions at the ends of the column are taken as those of pin joints. The theoretical analysis is described with reference to a lipped channel section, Figure 3.1.1, this being treated as a system of thin plates joined at the edges and acted upon by an in plane axial stress system.

Consider a lipped channel column loaded eccentrically towards the flange by an amount e which has just developed local buckles along its length, Figure 3.1.2. It is assumed that a local buckle at the centre of the column has a sinusoidal form in the x direction, with half-wavelength S. Just at the point of initial instability the stress system along the column at the nodes of the central buckle will be as depicted in Figure 3.1.3, α being a compression eccentricity factor. The method of analysis is to consider the total potential content of the central buckle of the column as distinct from the column as a whole. To do this it is necessary to think of the centre buckle as a short strut of length S acted on externally by the force system shown in Figure 3.1.3. The deflection functions

w_i are now prescribed in terms of unknown deflection coefficients, and equation (2.3.6) (Chapter 2) used to evaluate the total potential of the system in terms of these coefficients. Minimisation of this potential with respect to each coefficient results in the eigenproblem mentioned in Chapter 2, the lowest eigenvalue yielding the critical flange stress σ^*_{crit} to cause local buckling. It should be noted at this point that values of S and α must be prescribed before evaluation of σ^*_{crit} is possible.

As a first approximation to the correct value of S, the length of the column L is divided by the flange width b, the nearest integer below the value obtained being taken as a first approximation to the number of buckles along the column. Using this number of buckles a first value of S is obtained from which σ^*_{crit} is found when using a specific value of α. The number of buckles is now increased by one and a new value of σ^*_{crit} found for the same value of α. This process is repeated by adding more buckles to the column and determining new values of σ^*_{crit} corresponding to the number of buckles postulated. The column will naturally assume the number of buckles which yields the lowest value of σ^*_{crit}, hence when the minimum value of σ^*_{crit} is reached this gives the correct number of buckles and the correct value of S.

At this point the critical flange stress and hence the critical load are evaluated for a specific value of α. It is now necessary to establish whether this value of α provides equilibrium of the

internal stress system at σ^*_{crit} with the externally applied load P on the column. With reference to Figures 3.1.2 and 3.1.3, axial equilibrium produces the following equation

$$P = N^*_{x_{CRIT}}\left[b+2b_w\left(1-\frac{\alpha}{2}\right)+2b_\ell\left(1-\alpha\right)\right] \qquad (3.1.1)$$

while moment equilibrium about the lips of the section gives

$$M=N^*_{x_{CRIT}}b_w\left[b+b_w\left(1-\frac{\alpha}{3}\right)\right] = P\left[e+d+\delta_c\right] \qquad (3.1.2)$$

The equation for the central deflection δ_c of an eccentrically loaded column is given from the simple "Engineers Theory of Bending" as

$$\delta_c = e\left[\sec\frac{\pi}{2}\sqrt{\frac{P}{P_E}} - 1\right] \qquad (3.1.3)$$

where P_E is Euler's critical column load.

Substituting equation (3.1.3) into equation (3.1.2) and then substituting equation (3.1.1) into the result, allows equation (3.1.2) to be written for a specified column geometry and eccentricity of applied axial load, as a function of α and $N^*_{x\,crit}$ as follows.

$$N^*_{x_{CRIT}}\left[b_w\left(b+b_w\right)-\alpha\frac{b_w^2}{3}-\left[\left(b+2b_w+2b_\ell\right)-\alpha\left(b_w+2b_\ell\right)\right]\left[d+\right.\right.$$

$$\left.\left.+ e\,\mathrm{sec}\frac{\pi}{2}\sqrt{\frac{N^*_{x_{CRIT}}\left[\left(b+2b_w+2b_\ell\right)-\alpha\left(b_w+2b_\ell\right)\right]}{P_E}}\right]\right] = 0 \qquad (3.1.4)$$

Equation (3.1.4) is solved numerically to obtain the value of $\propto$ and hence the value of $N^*_{x\,crit}$ which produces both axial and moment equilibrium of the column. The technique used in the solution is known as the so-called "regula falsi" or the method of false position which approximates the given curve by a chord in the vicinity of the required root.

Knowing the equilibrium values of $\propto$ and $N^*_{x\,crit}$ the initial local buckling load and central deflection for the column are obtained from equations (3.1.1) and (3.1.3) respectively.

3.2 DEFLECTION FUNCTIONS AND BOUNDARY CONDITIONS

The buckled shape of the column central cross section at the instability load will be of the form shown in Figure 3.2.1, the positive directions for the plate deflections being as indicated.

The local out of plane displacements of the plate components of the section as shown in Figure 3.2.1 may be described by

$$w_i = Y_i(y_i)\cos\left(\frac{\pi x}{s}\right) \qquad (3.2.1)$$

where $$Y_i(y_i) = \sum_{n=1}^{n=N} Y_{in}(y_i) \qquad (3.2.2)$$

N being the number of terms used in the solution and i a particular plate element in the section.

The deflection functions Y_{in} are given the following form

$$Y_{in} = A_n\left[1 - \left(\frac{y_i}{b_f}\right)^{a_n}\right] + B_n\left[1 - \left(\frac{y_i}{b_f}\right)^{b_n}\right] \qquad (3.2.3)(a)$$

$$Y_{2n} = D_n\left(\frac{y_2}{b_w}\right) + G_n\left(\frac{y_2}{b_w}\right)^2 + K_n\left(\frac{y_2}{b_w}\right)^{k_n} \qquad (3.2.3)(b)$$

$$Y_{3n} = Q_n\left(\frac{y_3}{b_\ell}\right) + R_n\left(\frac{y_3}{b_\ell}\right)^2 + T_n\left(\frac{y_3}{b_\ell}\right)^{t_n} \qquad (3.2.3)(c)$$

The coefficients B_n, D_n, G_n, K_n, Q_n, R_n and T_n are evaluated in terms of the coefficient A_n through satisfaction of the boundary conditions at the plate junctions and the lip free edge. The indices a_n, b_n, k_n, t_n are arbitrary integers subject to certain restrictions which will be mentioned later.

With reference to Figure 3.2.1 the boundary conditions to be satisfied at the flange-web junction are

(a) the local deflections of both flange and web are zero

(b) the slopes are equal at the junction

(c) there is moment equilibrium about the junction.

These conditions are met by satisfaction of the following equations at $y_1 = b_f$, $y_2 = b_w$

$$w_1 = w_2 = 0 \qquad (3.2.4)(a)(b)$$

$$\frac{\partial w_1}{\partial y_1} = \frac{\partial w_2}{\partial y_2} \qquad (3.2.4)(c)$$

$$\left[\frac{\partial^2 w_1}{\partial y_1^2} + \nu\frac{\partial^2 w_1}{\partial x^2}\right] = -\left[\frac{\partial^2 w_2}{\partial y_2^2} + \nu\frac{\partial^2 w_2}{\partial x^2}\right] \qquad (3.2.4)(d)$$

Using equations (3.2.1) and (3.2.2), equations (3.2.4) take the following form

$$Y_{1n} = Y_{2n} = 0 \qquad (3.2.5)(a)(b)$$

$$Y_{1n}' = Y_{2n}' \qquad (3.2.5)(c)$$

$$Y_{1n}'' = - Y_{2n}'' \qquad (3.2.5)(d)$$

The primes denote differentiation with respect to y_1.

Satisfaction of equations (3.2.5)(a) and (b) results in the simplified form of equation (3.2.5)(d) as shown.

Similar conditions exist at the junction of the web and lip $y_2 = 0$, $y_3 = 0$. The equations to be satisfied at this junction are as follows

$$Y_{2n} = Y_{3n} = 0 \qquad (3.2.6)(a)(b)$$

$$Y_{2n}' = Y_{3n}' \qquad (3.2.6)(c)$$

$$Y_{2n}'' = - Y_{3n}'' \qquad (3.2.6)(d)$$

The boundary conditions at the free edge of the lip $y_3 = b_\ell$ are zero moment and zero shear stress. These are written in the form

$$\left[\frac{\partial^2 w_3}{\partial y_3^2} + \nu \frac{\partial^2 w_3}{\partial x^2}\right] = 0 \qquad (3.2.7)(a)$$

$$\left[\frac{\partial^3 w_3}{\partial y_3^3} + (2-\nu)\frac{\partial^3 w_3}{\partial y_3 \partial x^2}\right] = 0 \qquad (3.2.7)(b)$$

using equations (3.2.1) and (3.2.2), equations (3.2.7) are simplified

as follows

$$Y_{3n}'' - \nu \frac{\pi^2}{S^2} Y_{3n} = 0 \qquad (3.2.8)(a)$$

$$Y_{3n}''' - (2-\nu) \frac{\pi^2}{S^2} Y_{3n}' = 0 \qquad (3.2.8)(b)$$

All the boundary conditions at the plate edges have now been stated and the relevant equations necessary to satisfy these conditions have been developed. A series of compatible deflected forms Y_n for the section will be obtained on satisfaction of the above conditions, and the most accurate buckled shape for the section is then realised from the minimisation of the total potential.

So far the conditions at the plate edges only, have been considered. Consider now the end displacements of the plates at the nodes of the central buckle of the column, Figure 3.2.2, the flange is compressed by an amount u^*, the web compression varying from u^* at the flange to $u^*(1 - \alpha)$ at the lips, and the lips compressed by this same amount. The displacements of the plate ends at the nodes of the central buckle are as follows.

$$\text{flange compression} = u^* \qquad (3.2.9)(a)$$

$$\text{web compression} = u^*\left(1 - \alpha + \alpha \frac{y_2}{b_w}\right) \qquad (3.2.9)(b)$$

$$\text{lip compression} = u^*(1-\alpha) \qquad (3.2.9)(c)$$

This compression being measured over one half of the length of the central buckle.

3.3 SATISFACTION OF THE BOUNDARY CONDITIONS

All the boundary conditions have now been stated and the deflection functions for each plate prescribed. These functions are now used with their derivatives to satisfy equations (3.2.5), (3.2.6) and (3.2.8). Equation (3.2.5)(a) is satisfied automatically by the choice of equation (3.2.3)(a) for Y_{1n}, since this equation has the value zero at $y_1 = b_f$. The remaining three equations of (3.2.5) take the following form on substitution of the relevant Y_{in}, Y_{in}' and Y_{in}''

$$D_n + G_n + K_n = 0 \qquad (3.3.1)(a)$$

$$\frac{b_w}{b_f}\left[A_n a_n + B_n b_n\right] = -\left[D_n + 2G_n + K_n k_n\right] \qquad (3.3.1)(b)$$

$$\frac{b_w^2}{b_f^2}\left[A_n a_n(a_n-1) + B_n b_n(b_n-1)\right] = \left[2G_n + K_n k_n(k_n-1)\right] \qquad (3.3.1)(c)$$

Equations (3.2.6)(a) and (b) are automatically satisfied at the lip-web junction by the choice of equations (3.2.3)(b) and (c) for Y_{2n} and Y_{3n}, provided the values for k_n and $t_n \neq 0$. The remaining two equations of (3.2.6) are written in the following form after substitution of Y_{in}' and Y_{in}''

$$\frac{D_n}{b_w} = \frac{Q_n}{b_\ell} \qquad (3.3.2)(a)$$

$$\frac{G_n}{b_w^2} = -\frac{R_n}{b_\ell^2} \qquad (3.3.2)(b)$$

the previous expressions being true provided k_n and $t_n \neq 1,2$.

Substitution of Y_{3n}, Y_{3n}', Y_{3n}'' and Y_{3n}''' in equations (3.2.8) yields the following two expressions representing the conditions at the lip free edge

$$\frac{1}{b_\ell^2}\left[2R_n+T_n t_n(t_n-1)\right]-\nu\frac{\pi^2}{S^2}\left[Q_n+R_n+T_n\right]=0 \qquad (3.3.3)(a)$$

$$\frac{1}{b_\ell^3}\left[T_n t_n(t_n-1)(t_n-2)\right]-(2-\nu)\frac{\pi^2}{b_\ell S^2}\left[Q_n+2R_n+T_n t_n\right]=0 \qquad (3.3.3)(b)$$

After some manipulation of equations (3.3.1), (3.3.2) and (3.3.3) expressions are obtained for B_n, D_n, G_n, K_n, Q_n, R_n and T_n in terms of A_n. These are described as follows.

$$B_n = -\xi_n A_n \qquad (3.3.4)$$

where

$$\xi_n=\frac{\left[\left[1-\lambda_n\frac{b_\ell}{b_w}\right](k_n-1)(k_n-2)-\left[2+\frac{b_w}{b_f}(a_n-1)\right]\left[(k_n-1)\lambda_n\frac{b_\ell}{b_w}-(k_n-2)\right]\right]\left(\frac{a_n}{b_n}\right)}{\left[\left[1-\lambda_n\frac{b_\ell}{b_w}\right](k_n-1)(k_n-2)-\left[2+\frac{b_w}{b_f}(b_n-1)\right]\left[(k_n-1)\lambda_n\frac{b_\ell}{b_w}-(k_n-2)\right]\right]} \qquad (3.3.5)$$

and

$$\lambda_n=\frac{\left[2\left(\frac{\pi b_\ell}{S}\right)^2(2-\nu)\left[t_n(t_n-1)-\nu\left(\frac{\pi b_\ell}{S}\right)^2\right]+\left[2-\nu\left(\frac{\pi b_\ell}{S}\right)^2\right]\left[(t_n-1)(t_n-2)-(2-\nu)\left(\frac{\pi b_\ell}{S}\right)^2\right]t_n\right]}{\left[\nu\left(\frac{\pi b_\ell}{S}\right)^2\left[(t_n-1)(t_n-2)-(2-\nu)\left(\frac{\pi b_\ell}{S}\right)^2\right]t_n-\left(\frac{\pi b_\ell}{S}\right)^2(2-\nu)\left[t_n(t_n-1)-\nu\left(\frac{\pi b_\ell}{S}\right)^2\right]\right]} \qquad (3.3.6)$$

$$K_n = \beta_n A_n \qquad (3.3.7)$$

where

$$\beta_n = \left[\frac{\left(\frac{bw}{bf}\right)^2\left[a_n(a_n-1)-\varphi_n b_n(b_n-1)\right]+\frac{2bw}{bf}\left[a_n-\varphi_n b_n\right]}{(k_n-1)(k_n-2)}\right] \quad (3.3.8)$$

$$G_n = -\gamma_n A_n \quad (3.3.9)$$

where

$$\gamma_n = \left[\frac{bw}{bf}\left[a_n-\varphi_n b_n\right]+\beta_n(k_n-1)\right] \quad (3.3.10)$$

$$D_n = \mu_n A_n \quad (3.3.11)$$

where

$$\mu_n = \gamma_n-\beta_n \quad (3.3.12)$$

$$Q_n = \rho_n A_n \quad (3.3.13)$$

where

$$\rho_n = \frac{b\ell}{bw}\mu_n \quad (3.3.14)$$

$$R_n = \Omega_n A_n \quad (3.3.15)$$

where

$$\Omega_n = \left(\frac{b\ell}{bw}\right)^2 \gamma_n \quad (3.3.16)$$

$$T_n = \tau_n A_n \quad (3.3.17)$$

where

$$\tau_n = \left[\frac{\nu\left(\frac{\pi b\ell}{s}\right)^2\left[\rho_n+\Omega_n\right]-2\Omega_n}{t_n(t_n-1)-\nu\left(\frac{\pi b\ell}{s}\right)^2}\right] \quad (3.3.18)$$

Substitution of equations (3.3.4), (3.3.7), (3.3.9), (3.3.11), (3.3.13), (3.3.15) and (3.3.17) into equations (3.2.3) gives a buckled shape for the section in terms of one unknown deflection coefficient A_n, this buckled shape satisfies compatibility and equilibrium at the plate junctions and also the lip free edge conditions of zero moment and zero shear stress. The deflection functions for the plate elements are now written in the following manner.

$$Y_{1n} = \left\{\left[1 - \left(\frac{y_1}{bf}\right)^{a_n}\right] - \varrho_n\left[1 - \left(\frac{y_1}{bf}\right)^{b_n}\right]\right\} A_n \qquad (3.3.19)(a)$$

$$Y_{2n} = \left\{\mu_n\left(\frac{y_2}{bw}\right) - \gamma_n\left(\frac{y_2}{bw}\right)^2 + \beta_n\left(\frac{y_2}{bw}\right)^{k_n}\right\} A_n \qquad (3.3.19)(b)$$

$$Y_{3n} = \left\{\varrho_n\left(\frac{y_3}{b\ell}\right) + \Omega_n\left(\frac{y_3}{b\ell}\right)^2 + \tau_n\left(\frac{y_3}{b\ell}\right)^{t_n}\right\} A_n \qquad (3.3.19)(c)$$

As stated earlier the indices used in the deflection functions are arbitrary with the values of k_n and t_n being subject to certain restrictions, the only restriction imposed on the values of a_n and b_n is that they are even integers to ensure symmetry of the buckled form. Since the indices are arbitrary a variety of deflected forms can be specified for the section simply by choosing different values for the indices.

3.4 MINIMISATION OF THE TOTAL POTENTIAL

Equation (2.3.6)(Chapter 2) is now used to evaluate the total potential change at buckling in terms of the deflection coefficients A_n.

Substituting (3.2.1) into (2.3.6) and integrating in the x direction between the limits $\pm S/2$ gives

$$V=\sum_{i=1}^{i=3}\int_{bo}^{b_1}\left[\frac{SD}{4}\left[\left[Y_i''-\left(\frac{\pi}{S}\right)^2 Y_i\right]^2+2(1-\nu)\left(\frac{\pi}{S}\right)^2\left[Y_iY_i''+(Y_i')^2\right]\right]-\frac{\pi^2}{4S}(N_x)_i\,Y_i^2\right]dy_i \quad (3.4.1)$$

where b_o and b_1 are the plate boundaries in the y direction. For the flange and web the integral $\int_{bo}^{b_1}(Y_i\ Y_i''+(Y_i')^2)\,dy_i$ is equal to $\left[Y_i'\,Y_i\right]_{bo}^{b_1}$ and is therefore zero for both these plates since Y_i is zero at their boundaries. The expressions to be used for $(N_x)_i$ take the following form for the flange, web and lip respectively.

$$\text{flange}\quad (N_x)_1 = N_x^* \quad (3.4.2)(a)$$

$$\text{web}\quad (N_x)_2 = N_x^*\left(1-\alpha+\alpha\frac{y_2}{bw}\right) \quad (3.4.2)(b)$$

$$\text{lip}\quad (N_x)_3 = N_x^*\left(1-\alpha\right) \quad (3.4.2)(c)$$

Using equations (3.2.2), (3.3.19), (3.4.1) and (3.4.2) expressions are obtained for the change in potential of each plate as follows

$$V_{FLANGE}=2\sum_{n=1}^{n=N}\sum_{m=1}^{m=N}A_nA_m\left\{\frac{SD}{4}\psi_{nm}-\frac{\pi^2}{4S}N_x^*\Gamma_{nm}\right\} \quad (3.4.3)$$

where

$$\psi_{nm}=\int_0^{bf}\left\{\left[\left[\frac{e_n b_n(b_n-1)}{bf^2}\left(\frac{y_1}{bf}\right)^{b_n-2}-\frac{a_n(a_n-1)}{bf^2}\left(\frac{y_1}{bf}\right)^{a_n-2}\right]\right.\right.$$

$$\left.\left.-\left(\frac{\pi}{S}\right)^2\left[1-e_n-\left(\frac{y_1}{bf}\right)^{a_n}+e_n\left(\frac{y_1}{bf}\right)^{b_n}\right]\right]X\right.$$

$$X\left[\left[\frac{\varepsilon_m b_m(b_m-1)}{bf^2}\left(\frac{y_1}{bf}\right)^{bm-2}-\frac{a_m(a_m-1)}{bf^2}\left(\frac{y_1}{bf}\right)^{am-2}\right]\right.$$

$$\left.-\left(\frac{\pi}{S}\right)^2\left[1-\varepsilon_m-\left(\frac{y_1}{bf}\right)^{am}+\varepsilon_m\left(\frac{y_1}{bf}\right)^{bm}\right]\right\}dy_1 \quad (3.4.4)$$

and

$$\Gamma_{nm}=\int_0^{bf}\left[1-\varepsilon_n-\left(\frac{y_1}{bf}\right)^{an}+\varepsilon_n\left(\frac{y_1}{bf}\right)^{bn}\right]\left[1-\varepsilon_m-\left(\frac{y_1}{bf}\right)^{am}+\varepsilon_m\left(\frac{y_1}{bf}\right)^{bm}\right]dy_1 \quad (3.4.5)$$

Similarly for the change in potential of the two webs the expressions

are

$$V_{WEB}=2\sum_{n=1}^{n=N}\sum_{m=1}^{m=N}A_nA_m\left\{\frac{SD}{4}\phi_{nm}-\frac{\pi^2}{4S}N_x^*T_{nm}\right\} \quad (3.4.6)$$

where

$$\phi_{nm}=\int_0^{bw}\left[\left[\frac{\beta_n k_n(k_n-1)}{bw^2}\left(\frac{y_2}{bw}\right)^{kn-2}-\frac{2\gamma_n}{bw^2}\right]-\left(\frac{\pi}{S}\right)^2\left[\mu_n\left(\frac{y_2}{bw}\right)-\gamma_n\left(\frac{y_2}{bw}\right)^2+\beta_n\left(\frac{y_2}{bw}\right)^{kn}\right]\right]X$$

$$\left[\left[\frac{\beta_m k_m(k_m-1)}{bw^2}\left(\frac{y_2}{bw}\right)^{km-2}-\frac{2\gamma_m}{bw^2}\right]-\left(\frac{\pi}{S}\right)^2\left[\mu_m\left(\frac{y_2}{bw}\right)-\gamma_m\left(\frac{y_2}{bw}\right)^2+\beta_m\left(\frac{y_2}{bw}\right)^{km}\right]\right]dy_2 \quad (3.4.7)$$

and

$$T_{nm}=\int_0^{bw}\left[1-\alpha+\alpha\left(\frac{y_2}{bw}\right)\right]\left[\mu_n\left(\frac{y_2}{bw}\right)-\gamma_n\left(\frac{y_2}{bw}\right)^2+\beta_n\left(\frac{y_2}{bw}\right)^{kn}\right]\left[\mu_m\left(\frac{y_2}{bw}\right)-\gamma_m\left(\frac{y_2}{bw}\right)^2+\beta_m\left(\frac{y_2}{bw}\right)^{km}\right]dy_2 \quad (3.4.8)$$

The expressions for the two lips being

$$V_{LIP} = 2\sum_{n=1}^{n=N}\sum_{m=1}^{m=N} A_n A_m \left\{ \frac{SD}{4} Z_{nm} - \frac{\pi^2}{4S} N_x^* G_{nm} \right\} \quad (3.4.9)$$

where

$$Z_{nm} = \int_0^{b\ell} \left[\left[\frac{2\Omega_n}{b\ell^2} + \frac{\tau_n t_n (t_n-1)}{b\ell^2} \left(\frac{y_3}{b\ell}\right)^{t_n-2} \right] \left[\frac{2\Omega_m}{b\ell^2} + \frac{\tau_m t_m (t_m-1)}{b\ell^2} \left(\frac{y_3}{b\ell}\right)^{t_m-2} \right] \right.$$

$$-2\nu\left(\frac{\pi}{S}\right)^2 \left[\rho_n \left(\frac{y_3}{b\ell}\right) + \Omega_n \left(\frac{y_3}{b\ell}\right)^2 + \tau_n \left(\frac{y_3}{b\ell}\right)^{t_n} \right] \left[\frac{2\Omega_m}{b\ell^2} + \frac{\tau_m t_m (t_m-1)}{b\ell^2} \left(\frac{y_3}{b\ell}\right)^{t_m-2} \right]$$

$$+\left(\frac{\pi}{S}\right)^4 \left[\rho_n \left(\frac{y_3}{b\ell}\right) + \Omega_n \left(\frac{y_3}{b\ell}\right)^2 + \tau_n \left(\frac{y_3}{b\ell}\right)^{t_n} \right] \left[\rho_m \left(\frac{y_3}{b\ell}\right) + \Omega_m \left(\frac{y_3}{b\ell}\right)^2 + \tau_m \left(\frac{y_3}{b\ell}\right)^{t_m} \right] + 2(1-\nu)\left(\frac{\pi}{b\ell S}\right)^2$$

$$\left. \times \left[\rho_n + 2\Omega_n \left(\frac{y_3}{b\ell}\right) + \tau_n t_n \left(\frac{y_3}{b\ell}\right)^{t_n-1} \right] \left[\rho_m + 2\Omega_m \left(\frac{y_3}{b\ell}\right) + \tau_m t_m \left(\frac{y_3}{b\ell}\right)^{t_m-1} \right] \right] dy_3 \quad (3.4.10)$$

and $$G_{nm} = \int_0^{b\ell} (1-\alpha) \left[\rho_n \left(\frac{y_3}{b\ell}\right) + \Omega_n \left(\frac{y_3}{b\ell}\right)^2 + \tau_n \left(\frac{y_3}{b\ell}\right)^{t_n} \right] \left[\rho_m \left(\frac{y_3}{b\ell}\right) + \Omega_m \left(\frac{y_3}{b\ell}\right)^2 + \tau_m \left(\frac{y_3}{b\ell}\right)^{t_m} \right] dy_3 \quad (3.4.11)$$

Adding equations (3.4.3), (3.4.6) and (3.4.9) gives the total potential change at the instant of local buckling as

$$V = \frac{SD}{2} \sum_{n=1}^{n=N}\sum_{m=1}^{m=N} A_n A_m \left\{ \lambda_{nm} - \frac{\pi^2}{DS^2} N_x^* \Theta_{nm} \right\} \quad (3.4.12)$$

where $$\lambda_{nm} = \Psi_{nm} + \phi_{nm} + Z_{nm} \quad (3.4.13)(a)$$

and $$\Theta_{nm} = \Gamma_{nm} + T_{nm} + G_{nm} \quad (3.4.13)(b)$$

using now a flange buckling coefficient, defined by the relationship

$$K_f = \frac{N^*_{x_{CRIT}}\, b^2}{\pi^2 D} \qquad (3.4.14)$$

equation (3.4.12) can be written

$$V = \frac{SD}{2} \sum_{n=1}^{n=N} \sum_{m=1}^{m=N} A_n A_m \left\{ \lambda_{nm} - K_f \frac{\pi^4}{b^2 S^2} \theta_{nm} \right\} \qquad (3.4.15)$$

Minimisation of the above equation with respect to A_n gives

$$\frac{\partial V}{\partial A_n} = SD \sum_{m=1}^{m=N} A_m \left\{ \bar{\lambda}_{nm} - K_f \frac{\pi^4}{b^2 S^2} \theta_{nm} \right\} = 0 \qquad (3.4.16)$$

where $\bar{\lambda}_{nm} = \frac{\lambda_{nm} + \lambda_{mn}}{2}$

Equation (3.4.16) gives a series of N simultaneous equations

which can be expressed in the following matrix form

$$\begin{bmatrix} (\bar{\lambda}_{11} - K_f \frac{\pi^4}{b^2 S^2} \theta_{11}) + \cdots\cdots\cdots (\bar{\lambda}_{1N} - K_f \frac{\pi^4}{b^2 S^2} \theta_{1N}) \\ \vdots \\ (\bar{\lambda}_{N1} - K_f \frac{\pi^4}{b^2 S^2} \theta_{N1}) + \cdots\cdots\cdots (\bar{\lambda}_{NN} - K_f \frac{\pi^4}{b^2 S^2} \theta_{NN}) \end{bmatrix} \begin{bmatrix} A_1 \\ A_2 \\ \vdots \\ A_N \end{bmatrix} = 0 \qquad (3.4.17)$$

To obtain the initial local instability load for the column it is necessary to find the lowest eigenvalue of the system of equations (3.4.17), the corresponding eigenvector giving the buckled shape of the section.

The method used to find the required eigenvalue is the same as that employed in the solution of equation (3.1.4), whereby an

iterative approach to the evaluation of the flange buckling coefficient K_f is employed using the following equation.

$$K_{f_{n+2}} = K_{f_{n+1}} + \frac{\lambda_{n+1}}{\lambda_{n+1} - \lambda_n}\left(K_{f_n} - K_{f_{n+1}}\right) \qquad (3.4.18)$$

λ_n and λ_{n+1} being the values of the determinant of equation (3.4.17) on substitution of the approximations K_{f_n} and $K_{f_{n+1}}$ respectively.

To start the iterative scheme (3.4.18) two approximations K_{f_1} and K_{f_2} are required, the closer these approximations are to the exact value the faster will be the convergence of the scheme.

The first approximation K_{f_1} is found by considering only two terms in the buckling solution, the determinant of equation (3.4.17) when equated to zero reducing to a quadratic equation in K_f. The lower root of this equation being assigned to K_{f_1} as a first approximation to the required buckling coefficient. Knowing that this approximation will be higher than the exact value due to the upper bound nature of the energy method used, a second approximation is made in the form $K_{f_2} = 0.9\ K_{f_1}$.

The iterative scheme (3.4.18) is now used until the difference between two consecutive approximations is within a specified accuracy, i.e. when $K_{f_{n+2}} - K_{f_{n+1}} \approx 0$, the accuracy of the buckling coefficient K_f depending on the suitability of the functions Y_n used and the number of terms in the solution.

Knowing the value of K_f, the local instability load P_{crit} can be evaluated using equations (3.4.14) and (3.1.1) in the following

non-dimensionalised form

$$\frac{P_{CRIT}\, b}{\pi^2 D} = 2K_f\left[\frac{1}{2} + \frac{bw}{b}\left(1-\frac{\alpha}{2}\right) + \frac{b\ell}{b}\left(1-\alpha\right)\right] = \overline{P}_{CRIT} \quad (3.4.19)$$

The initial buckling solution was programmed in the FORTRAN language for the University's ICL 1904S computer: the use of four terms in the solution proving to give highly accurate values for the buckling coefficient K_f.

To test the accuracy of this solution, different integers were used for the arbitrarily imposed indices in the deflection functions (3.2.3). It was found that changing the values of these indices had no effect on the subsequent solution for K_f, this being evaluated to six decimal places.

For a given section geometry and length of column the time taken by the computer to evaluate the buckling load was approximately four seconds.

3.5 THEORETICAL CURVES

The following theoretical curves show the effect on the buckling load of varying independently the geometrical parameters involved in the column problem.

Figure 3.5.1 shows the variation in the non dimensional load parameter $\overline{P}_{crit}$ with variation in slenderness ratio $\left(\frac{L}{r}\right)$ for various values of eccentricity factor $\overline{ec}$.

The variation in $\frac{P_{crit}}{P_E}$ with $\overline{ec}$ is shown in Figure 3.5.2 for various values of $\frac{t}{b}$, while Figures 3.5.3 and 3.5.4 show the variation in $\overline{P}_{crit}$ with $\overline{ec}$ for various $\left(\frac{L}{b}\right)$ and $\left(\frac{b\omega}{b}\right)$ values respectively.

The effect of changing $\left(\frac{b\ell}{b}\right)$ is shown in Figure 3.5.5 where $\overline{P}_{crit}$ is plotted against $\left(\frac{b\omega}{b}\right)$.

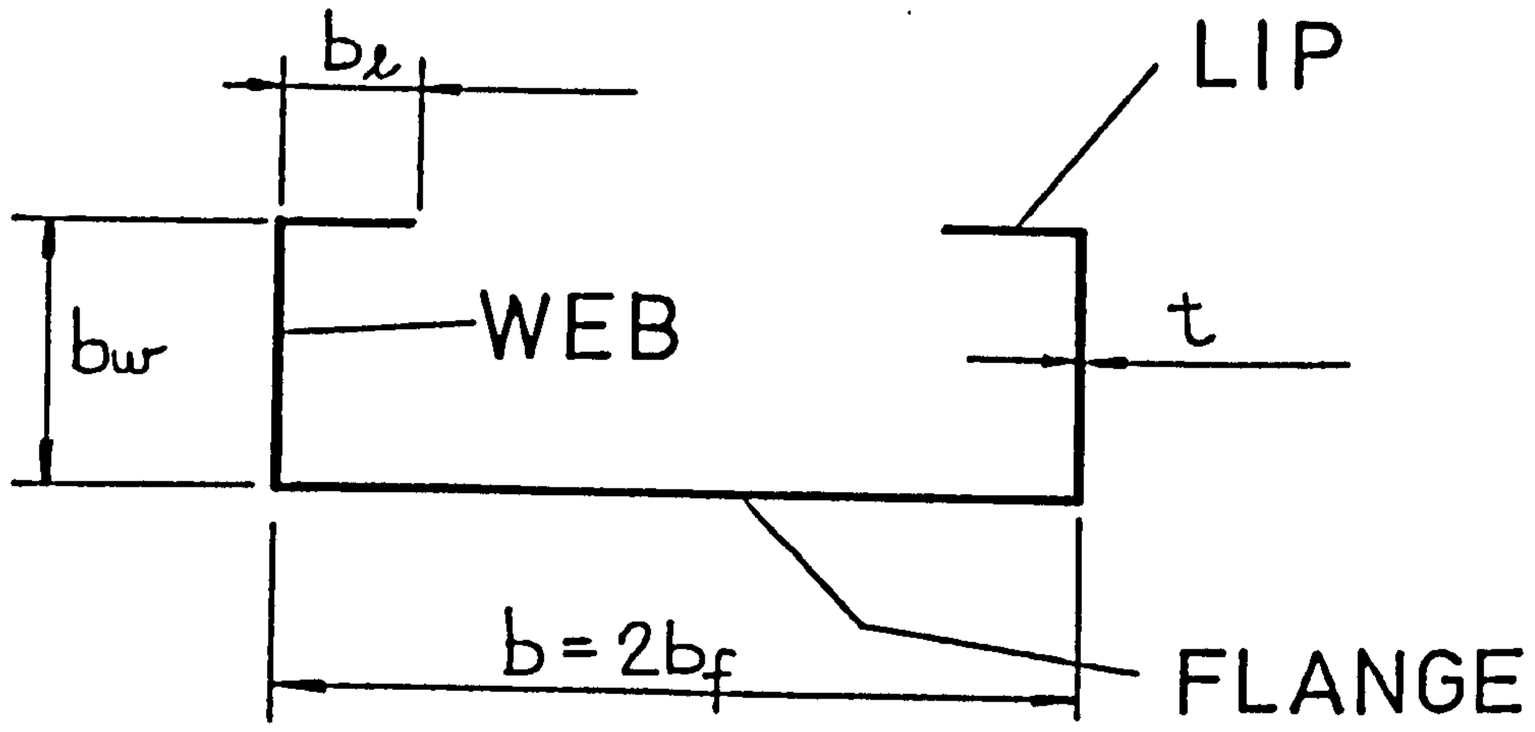

FIG. 3.1.1 CROSS SECTIONAL NOTATION OF LIPPED CHANNEL.

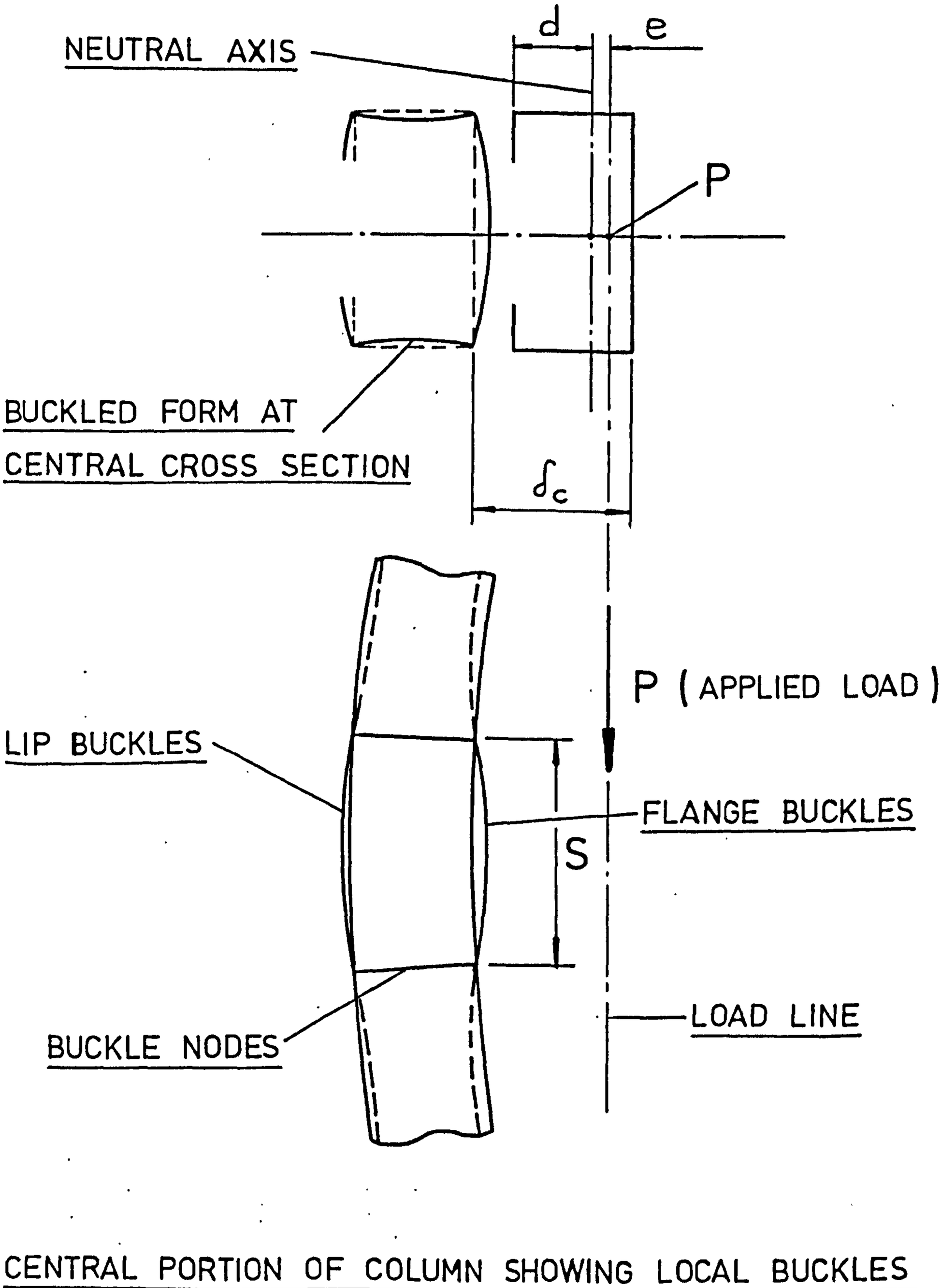

CENTRAL PORTION OF COLUMN SHOWING LOCAL BUCKLES

FIG 3.1.2

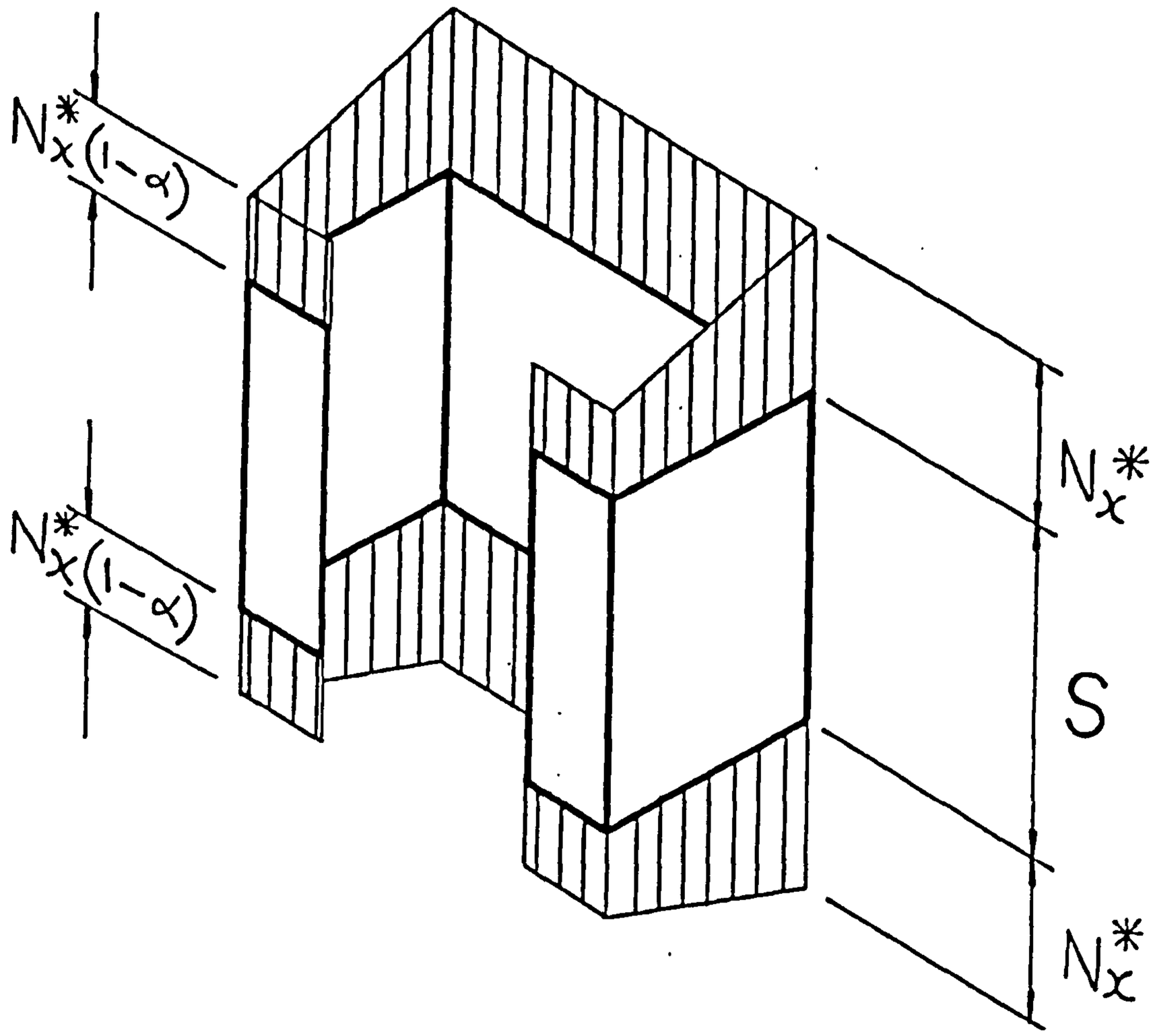

FIG. 3.1.3 STRESS SYSTEM PRIOR TO LOCAL BUCKLING.

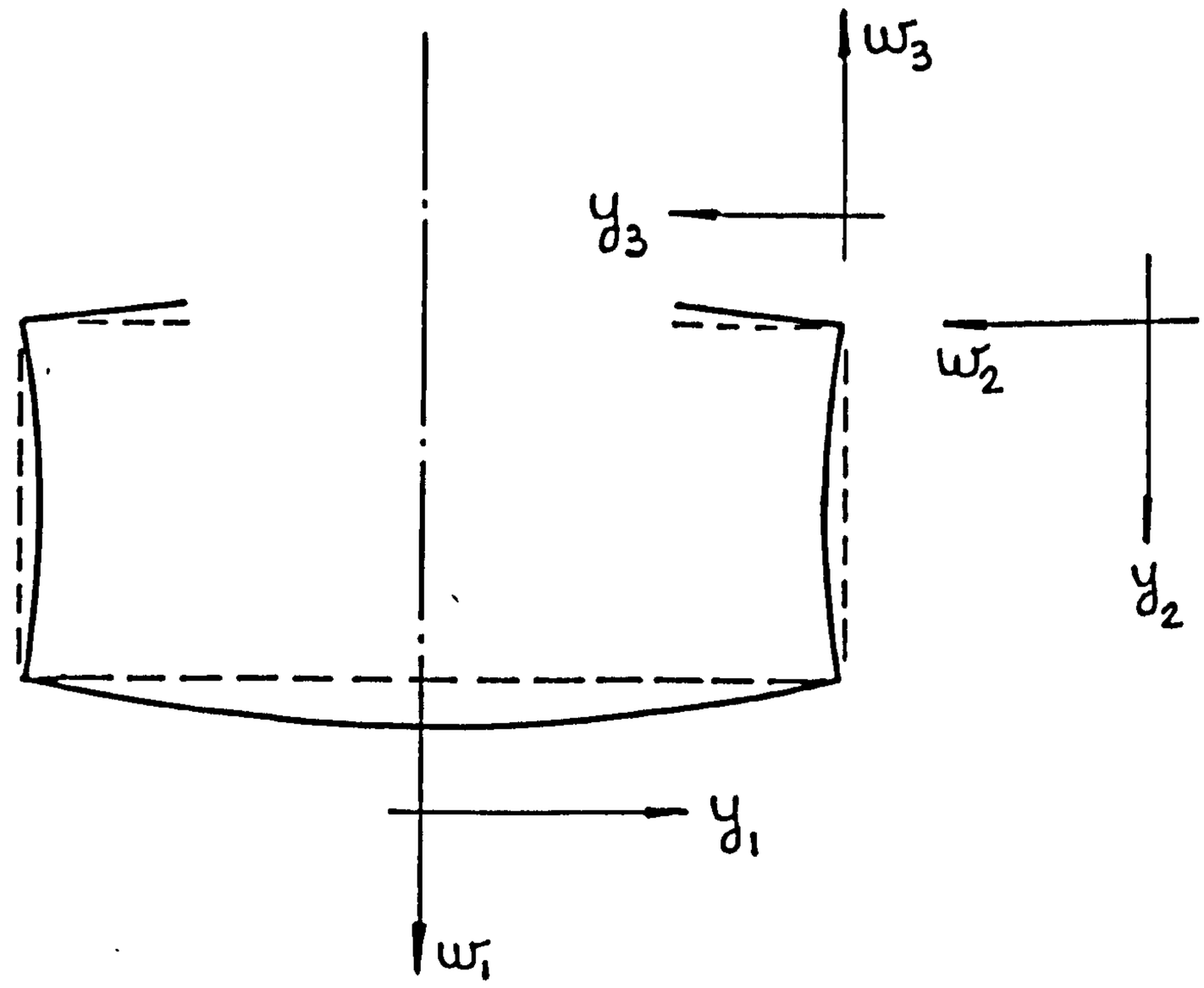

FIG. 3.2.1 CO-ORDINATE SYSTEM FOR LOCAL DEFLECTIONS. BUCKLED FORM SHOWN SCHEMATICALLY.

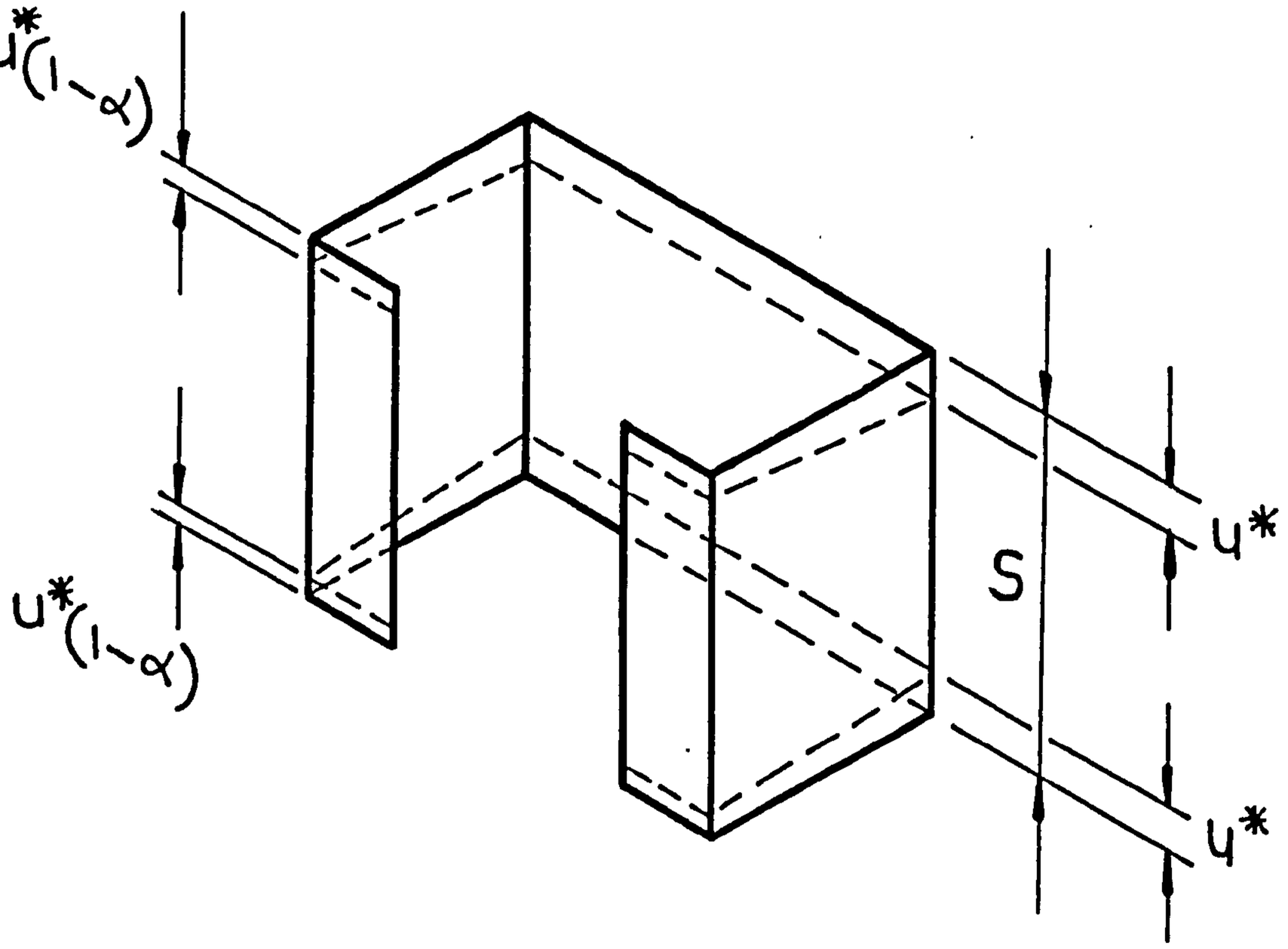

FIG. 3.2.2 COMPRESSION SYSTEM AT NODES OF CENTRAL BUCKLE.

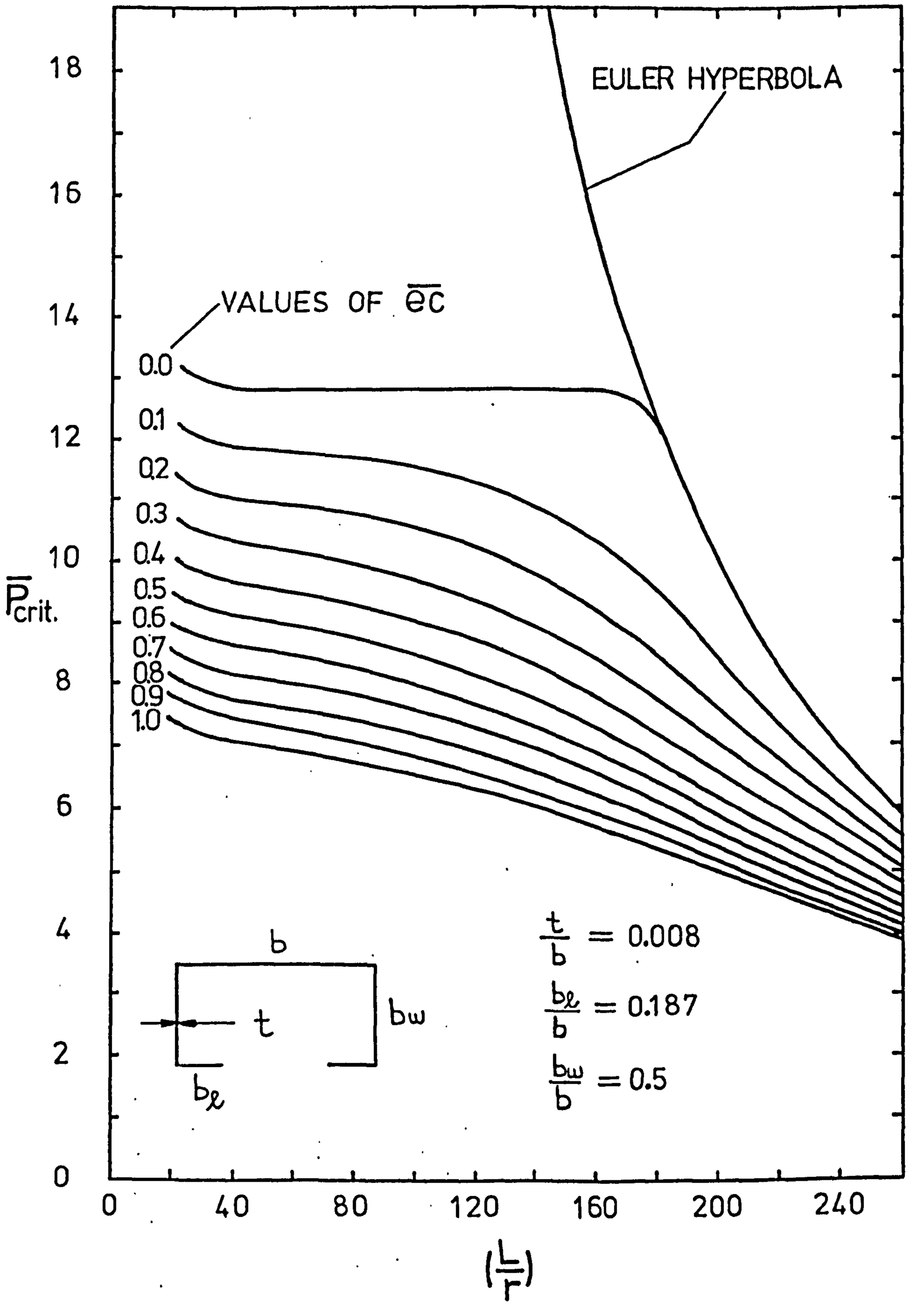

FIG. 3.5.1 VARIATION IN CRITICAL LOCAL BUCKLING LOAD WITH SLENDERNESS RATIO FOR VARIOUS VALUES OF ECCENTRICITY.

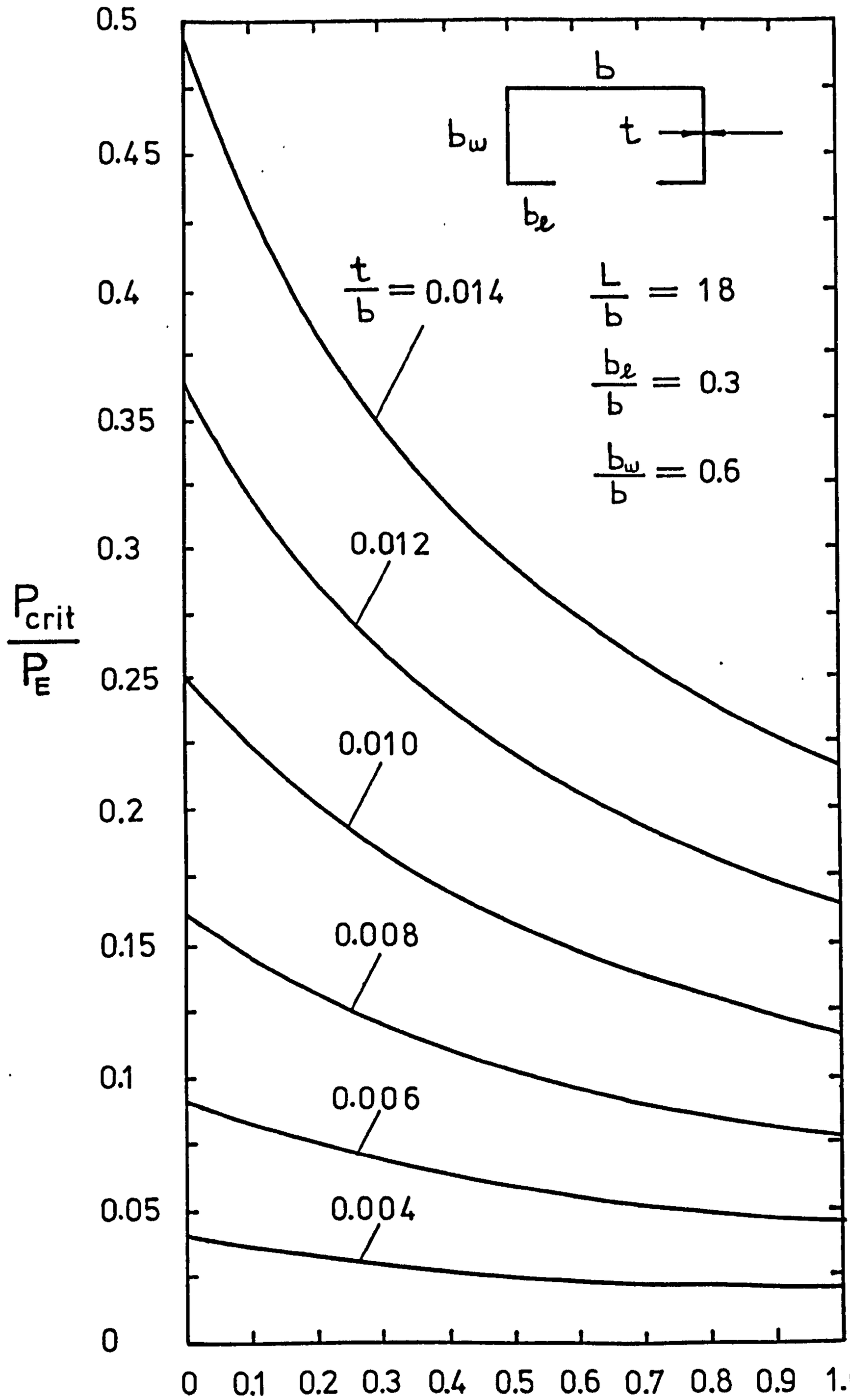

FIG. 3.5.2 VARIATION IN THE RATIO OF CRITICAL LOCAL BUCKLING LOAD TO EULER LOAD WITH LOADING ECCENTRICITY FOR VARIOUS VALUES OF t/b.

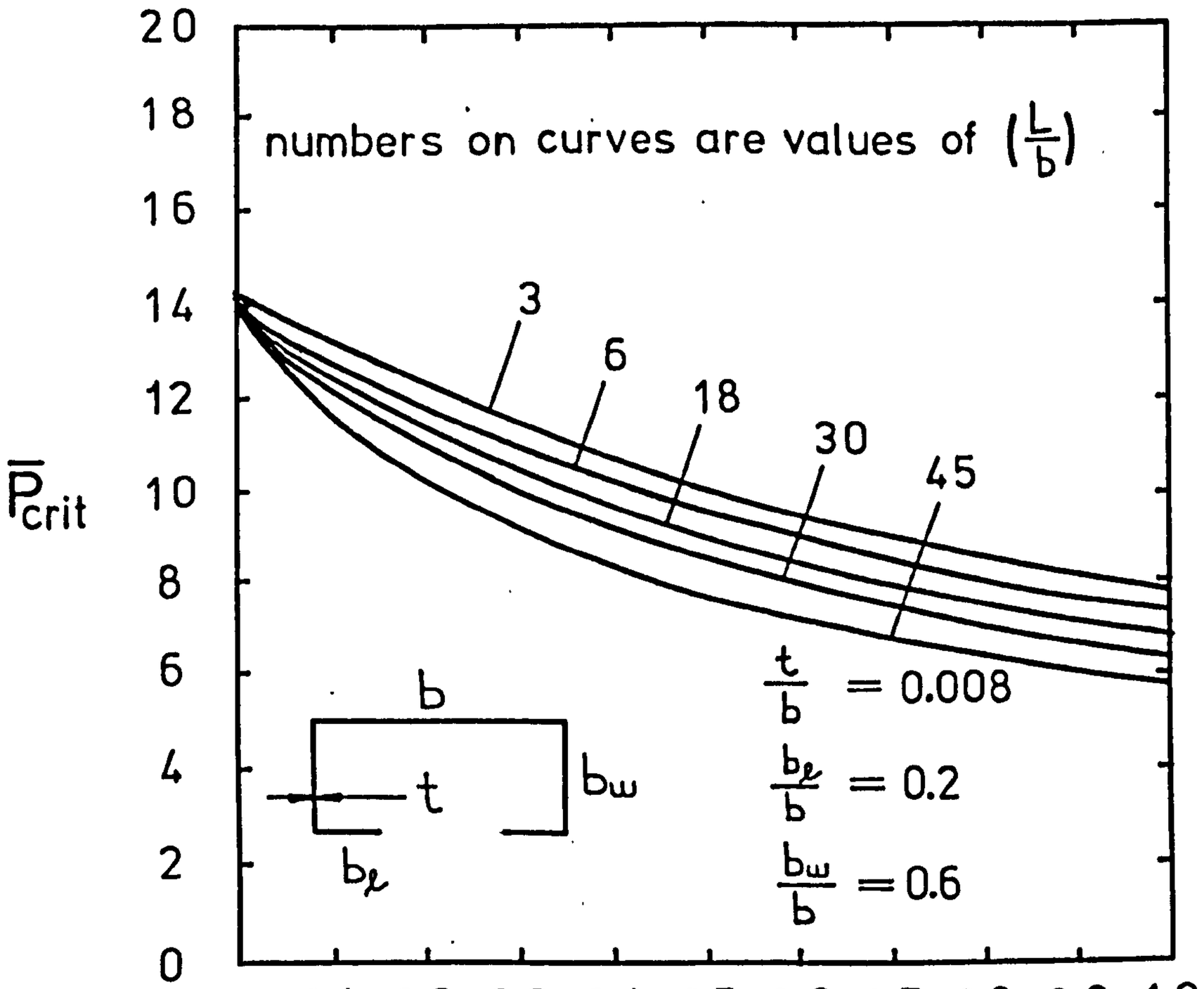

FIG. 3.5.3 VARIATION IN CRITICAL LOCAL BUCKLING LOAD WITH LOADING ECCENTRICITY FOR VARIOUS VALUES OF L/b.

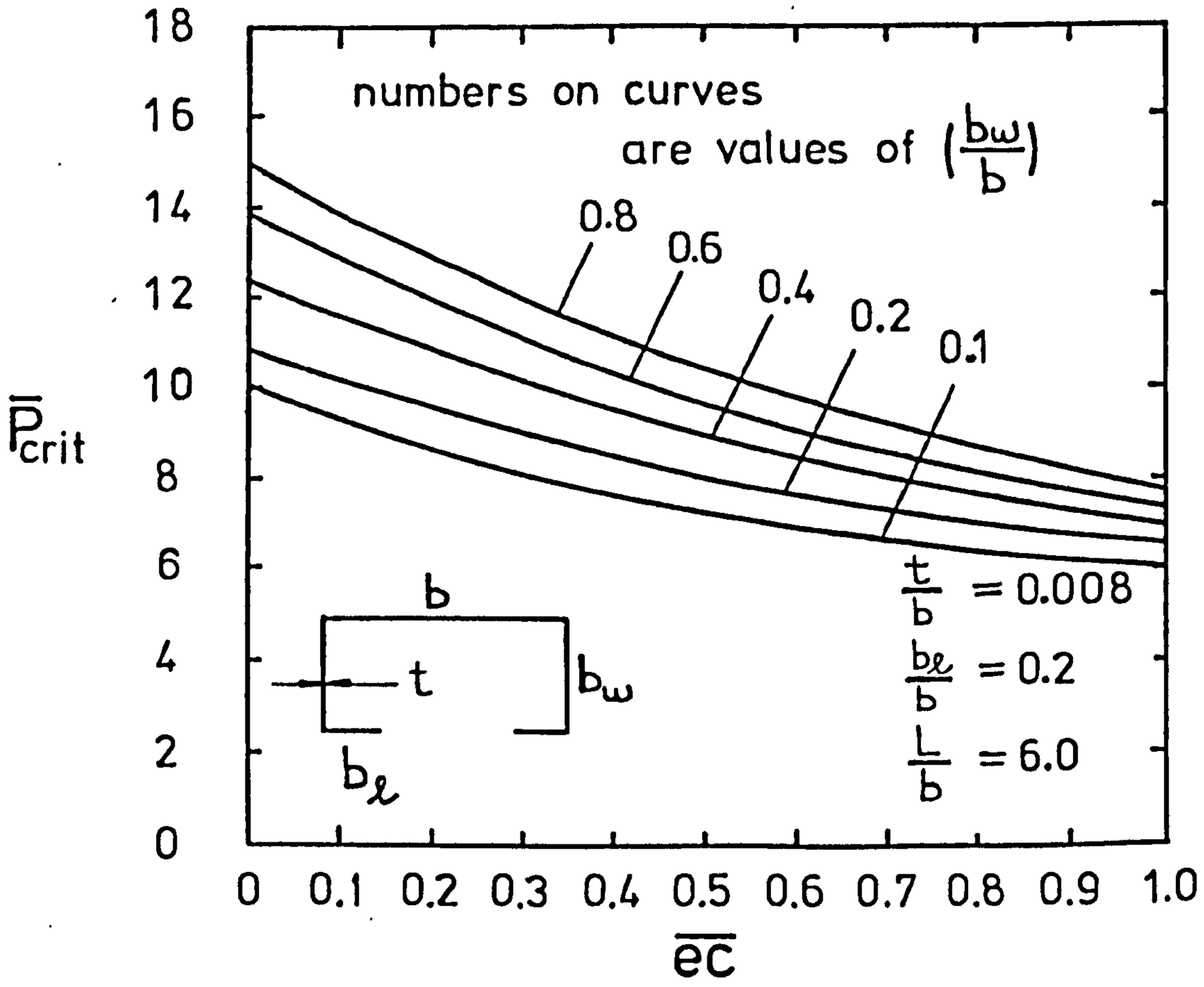

FIG. 3.5.4 VARIATION IN CRITICAL LOCAL BUCKLING LOAD WITH LOADING ECCENTRICITY FOR VARIOUS VALUES OF bw/b.

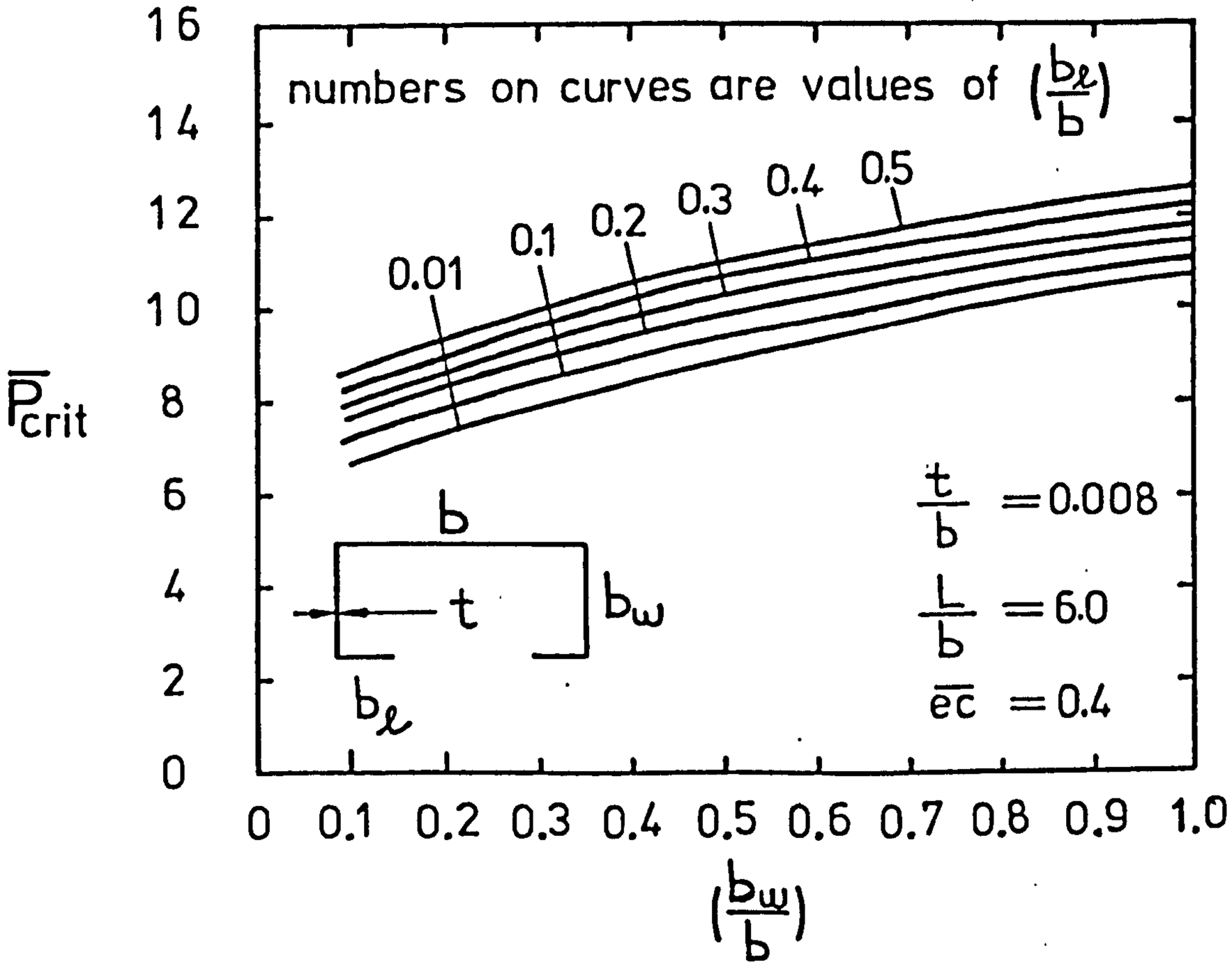

FIG. 3.5.5 VARIATION IN CRITICAL LOCAL BUCKLING LOAD WITH b_w/b FOR VARIOUS VALUES OF b_e/b.

CHAPTER FOUR

POST LOCAL BUCKLING ANALYSIS

4.0 POST LOCAL BUCKLING ANALYSIS

4.1 INTRODUCTION

After the initiation of the local instability load the column can continue to carry increased loads causing out of plane deflections in the column walls and stress distributions which are non-linear.

These out of plane deflections weaken both the compressional and bending stiffness of the column and reduce considerably its ultimate load carrying capacity. The theoretical work presented in this chapter is aimed at predicting the elastic post buckling behaviour for the lipped channel column. Characteristics such as the local stresses and deformations occurring within the column, and the change in overall lateral column deflection with increased load are presented. These characteristics give an understanding of the mechanics of the columns elastic post buckling behaviour.

In the post local buckling analysis, equation (2.2.4) is still used for the strain energy due to plate bending, but due to the non-linear stress distributions set up after local buckling, the strain energy due to in plane forces is now described by equation (2.3.4). This equation is rewritten as follows.

$$V_M = \frac{t}{2E} \sum_{-s/2}^{+s/2} \int_{b_o}^{b_1} \left\{ \left[\frac{\partial^2 F_i}{\partial x^2} + \frac{\partial^2 F_i}{\partial y_i^2} \right]^2 - 2(1+\nu) \left[\frac{\partial^2 F_i}{\partial x^2} \cdot \frac{\partial^2 F_i}{\partial y_i^2} - \left(\frac{\partial^2 F_i}{\partial x \, \partial y_i} \right)^2 \right] \right\} dx \, dy_i \quad (4.1.1)$$

The stress functions F_i are found in terms of the coefficients in the deflection functions w_i by solving Von Karman's compatibility

equation (2.1.12) and satisfying the boundary conditions for the stresses and in plane deformations. Von Karman's equation is rewritten here for convenience.

$$\frac{\partial^4 F_i}{\partial x^4}+2\frac{\partial^4 F_i}{\partial x^2 \partial y_i^2}+\frac{\partial^4 F_i}{\partial y_i^4}=\nabla^4(F_i)=E\left\{\left(\frac{\partial^2 w_i}{\partial x \partial y_i}\right)^2-\frac{\partial^2 w_i}{\partial x^2}\cdot\frac{\partial^2 w_i}{\partial y_i^2}\right\} \quad (4.1.2)$$

Taking the general expression for the out of plane deflections w_i in the form $w_i = Y_i\ (y_i)\cos\frac{\pi x}{s}$ and substituting in equation (4.1.2), the following relationship is obtained.

$$\frac{\partial^4 F_i}{\partial x^4}+2\frac{\partial^4 F_i}{\partial x^2 \partial y_i^2}+\frac{\partial^4 F_i}{\partial y_i^4}=\frac{E\pi^2}{2s^2}\left\{\left[Y_i Y_i''+(Y_i')^2\right]+\left[Y_i Y_i''-(Y_i')^2\right]\cos\frac{2\pi x}{s}\right\} \quad (4.1.3)$$

The solution of the above equation may be written in the following form

$$F_i = F_{i1}+F_{i2}\cos\frac{2\pi x}{s} \quad (4.1.4)$$

where F_{i1} and F_{i2} are functions of y_i only. Substitution of equation (4.1.4) into equation (4.1.3) and separating the final equation into its component parts gives the following two equations from which the solutions of F_{i1} and F_{i2} are obtained.

$$F_{i1}^{IV}=\frac{E\pi^2}{2s^2}\left[Y_i Y_i''+(Y_i')^2\right] \quad (4.1.5)$$

$$F_{i2}^{IV}-2\left(\frac{2\pi}{s}\right)^2 F_{i2}''+\left(\frac{2\pi}{s}\right)^4 F_{i2}=\frac{E\pi^2}{2s^2}\left[Y_i Y_i''-(Y_i')^2\right] \quad (4.1.6)$$

The solutions of the two previous equations yield the final solution F_i of Von Karman's equation. In order to solve Von Karman's equation it is necessary to postulate compatible deflection functions Y_i, these functions containing unknown deflection coefficients whose magnitude will be obtained from the minimisation of the total strain energy.

4.2 DEFLECTION FUNCTIONS

The general expression chosen for the deflection functions Y_i in the post buckling analysis is as follows.

$$Y_i = \sum_{n=1}^{n=N} W_n Y_{in} \qquad (4.2.1)$$

N being the number of terms in the post buckling solution and W_n the deflection coefficient associated with the n^{th} term.

The first term in the deflection series (4.2.1) is taken as the actual shape obtained from the relevant eigenvector of the buckling solution in equation (3.4.17), this shape being multiplied by the deflection coefficient W_1. Subsequent terms in the series are made effective by choosing arbitrary values for the A_n n = 1, 2, 3, 4 in equations (3.3.19). This produces a completely compatible deflected form satisfying the necessary boundary conditions at the plate junctions and at the lip free edge, while also providing the facility of allowing the buckled form to change as the local deflections increase.

Expanding equations (3.3.19) to four terms and using the following values for the indices a_n, b_n, k_n, t_n, $n = 1, 2, 3, 4$.

n	a_n	b_n	k_n	t_n
1	2	4	3	3
2	4	6	4	4
3	2	4	5	5
4	4	6	6	6

provides the deflection functions Y_1 in the post buckling range for the flange, web and lip respectively, these are

$$Y_1 = \sum_{n=1}^{n=N} W_n \left[g_{n1} + g_{n2}\left(\frac{y_1}{bf}\right)^2 + g_{n3}\left(\frac{y_1}{bf}\right)^4 + g_{n4}\left(\frac{y_1}{bf}\right)^6 \right] \qquad (4.2.2)(a)$$

$$Y_2 = \sum_{n=1}^{n=N} W_n \left[h_{n1}\left(\frac{y_2}{bw}\right) + h_{n2}\left(\frac{y_2}{bw}\right)^2 + h_{n3}\left(\frac{y_2}{bw}\right)^3 + h_{n4}\left(\frac{y_2}{bw}\right)^4 + h_{n5}\left(\frac{y_2}{bw}\right)^5 + h_{n6}\left(\frac{y_2}{bw}\right)^6 \right] \qquad (4.2.2)(b)$$

$$Y_3 = \sum_{n=1}^{n=N} W_n \left[h_{n1}\left(\frac{y_3}{b\ell}\right) + h_{n2}\left(\frac{y_3}{b\ell}\right)^2 + h_{n3}\left(\frac{y_3}{b\ell}\right)^3 + h_{n4}\left(\frac{y_3}{b\ell}\right)^4 + h_{n5}\left(\frac{y_3}{b\ell}\right)^5 + h_{n6}\left(\frac{y_3}{b\ell}\right)^6 \right] \qquad (4.2.2)(c)$$

In order that the initial buckled form be incorporated in the first term of the post buckled deflection series, the following must be true

$$g_{11} = A_1(1-\xi_1) + A_2(1-\xi_2) + A_3(1-\xi_3) + A_4(1-\xi_4)$$

$$g_{12} = -(A_1 + A_3)$$

$$g_{13} = (A_1\xi_1 - A_2 + A_3\xi_3 - A_4)$$

$$g_{14} = (A_2\xi_2 + A_4\xi_4) \qquad (4.2.3)$$

$$h_{11} = (A_1\mu_1 + A_2\mu_2 + A_3\mu_3 + A_4\mu_4)$$

$$h_{12} = -(A_1\gamma_1 + A_2\gamma_2 + A_3\gamma_3 + A_4\gamma_4)$$

$$h_{13} = A_1\beta_1$$

$$h_{14} = A_2\beta_2$$

$$h_{15} = A_3\beta_3$$

$$h_{16} = A_4\beta_4 \qquad (4.2.4)$$

$$f_{11} = (A_1\ell_1 + A_2\ell_2 + A_3\ell_3 + A_4\ell_4)$$

$$f_{12} = (A_1\Omega_1 + A_2\Omega_2 + A_3\Omega_3 + A_4\Omega_4)$$

$$f_{13} = A_1\tau_1$$

$$f_{14} = A_2\tau_2$$

$$f_{15} = A_3\tau_3$$

$$f_{16} = A_4\tau_4 \qquad (4.2.5)$$

where the coefficients A_n n = 1, 2, 3, 4 are the values obtained from the eigenvector of the buckling solution. As stated earlier subsequent terms in the series are generated by choosing arbitrary values for the A_n in equations (3.3.19).

Now that the deflection functions have been developed and described in detail, equations (4.1.5) and (4.1.6) may now be solved for F_{i1} and F_{i2} respectively in terms of the deflection coefficients W_n.

4.3 SOLUTION OF VON KARMAN'S EQUATION

Using the relationships between the stresses and the stress function as described in equation (2.1.7) it should be noted that since F_{i1} is a function of y_i only, then $\frac{\partial^2 F_{i1}}{\partial x \partial y_i} = \frac{\partial^2 F_{i1}}{\partial x^2} = 0$, F_{i1} producing a stress in the x direction only, this being $\frac{\partial^2 F_{i1}}{\partial y_i^2}$ or F_{i1}".

Since the function of interest for this part of F_i is F_{i1}" then the function F_{i1} need not be evaluated.

The function F_{i1}" is found by integrating equation (4.1.5) twice, utilizing the standard procedure for integration by parts. Integrating once gives

$$F_{i1}''' = \frac{E\pi^2}{2S^2} Y_i Y_i' + C_1$$

Integrating again gives

$$F_{i1}'' = \frac{E\pi^2}{4S^2} Y_i^2 + C_1 y_i + C_2 \qquad (4.3.1)$$

The constants of integration C_1 and C_2 are used to satisfy the boundary conditions regarding in-plane movements at the nodes of the centre buckle of the column. Knowing the function Y_i in terms of y_i, F_{i1}" is obtained directly from equation (4.3.1).

Equation (4.1.6) can now be solved for the flange, web and lip respectively. The solutions are obtained in the following manner:

Flange Solution

Substitution of equation (4.2.2)(a) into equation (4.1.6) produces the following relationship

$$F_{12}^{IV} - 2\left(\frac{2\pi}{s}\right)^2 F_{12}^{II} + \left(\frac{2\pi}{s}\right)^4 F_{12} = \frac{E\pi^2}{2s^2 b_f^2} \sum_{n=1}^{n=N} \sum_{m=1}^{m=N}$$

$$W_n W_m \left[G_{1nm} + G_{2nm}\left(\frac{y_1}{bf}\right)^2 + G_{3nm}\left(\frac{y_1}{bf}\right)^4 + G_{4nm}\left(\frac{y_1}{bf}\right)^6 + \right.$$

$$\left. + \quad G_{5nm}\left(\frac{y_1}{bf}\right)^8 + G_{6nm}\left(\frac{y_1}{bf}\right)^{10} \right] \qquad (4.3.2)$$

where

$$G_{1nm} = 2 g_{n1} g_{m1}$$

$$G_{2nm} = (12 g_{n1} g_{m3} - 2 g_{n2} g_{m2})$$

$$G_{3nm} = (30 g_{n1} g_{m4} + 4 g_{n2} g_{m3} - 6 g_{n3} g_{m2})$$

$$G_{4nm} = (18 g_{n2} g_{m4} - 4 g_{n3} g_{m3} - 10 g_{n4} g_{m2})$$

$$G_{5nm} = (6 g_{n3} g_{m4} - 12 g_{n4} g_{m3})$$

$$G_{6nm} = -6 g_{n4} g_{m4} \qquad (4.3.3)$$

putting $$F_{12} = \frac{E\pi^2}{2s^2 b_f^2} \sum_{n=1}^{n=N} \sum_{m=1}^{m=N} W_n W_m \psi_{1nm}(y_1)$$

and substituting in equation (4.3.2) gives the following expression

$$\psi_{1nm}^{IV} - 2\left(\frac{2\pi}{s}\right)^2 \psi_{1nm}^{II} + \left(\frac{2\pi}{s}\right)^4 \psi_{1nm} = G_{1nm} + G_{2nm}\left(\frac{y_1}{bf}\right)^2$$

$$+ G_{3nm}\left(\frac{y_1}{bf}\right)^4 + G_{4nm}\left(\frac{y_1}{bf}\right)^6 + G_{5nm}\left(\frac{y_1}{bf}\right)^8 + G_{6nm}\left(\frac{y_1}{bf}\right)^{10} \qquad (4.3.4)$$

Putting $\psi_{1nm} = d_{1nm} + d_{2nm}\left(\frac{y_1}{bf}\right)^2 + d_{3nm}\left(\frac{y_1}{bf}\right)^4 + d_{4nm}\left(\frac{y_1}{bf}\right)^6 + d_{5nm}\left(\frac{y_1}{bf}\right)^8 + d_{6nm}\left(\frac{y_1}{bf}\right)^{10}$,

substituting in equation (4.3.4) and equating the coefficients of the resulting equation gives the particular integral solution of equation

(4.3.2) in the form

$$F_{12_{P.I.}} = \frac{E\pi^2}{2S^2 b_f^2} \sum_{n=1}^{n=N} \sum_{m=1}^{m=N} W_n W_m \left[d_{1nm} + d_{2nm}\left(\frac{y_1}{b_f}\right)^2 + d_{3nm}\left(\frac{y_1}{b_f}\right)^4 + d_{4nm}\left(\frac{y_1}{b_f}\right)^6 + d_{5nm}\left(\frac{y_1}{b_f}\right)^8 + d_{6nm}\left(\frac{y_1}{b_f}\right)^{10} \right] \quad (4.3.5)$$

where

$$d_{6nm} = \left(\frac{S}{2\pi}\right)^4 G_{6nm}$$

$$d_{5nm} = \left(\frac{S}{2\pi}\right)^4 \left[G_{5nm} + \frac{180\, d_{6nm}}{b_f^2} \left(\frac{2\pi}{S}\right)^2 \right]$$

$$d_{4nm} = \left(\frac{S}{2\pi}\right)^4 \left[G_{4nm} + \frac{112\, d_{5nm}}{b_f^2} \left(\frac{2\pi}{S}\right)^2 - \frac{5040}{b_f^4} d_{6nm} \right]$$

$$d_{3nm} = \left(\frac{S}{2\pi}\right)^4 \left[G_{3nm} + \frac{60 d_{4nm}}{b_f^2} \left(\frac{2\pi}{S}\right)^2 - \frac{1680}{b_f^4} d_{5nm} \right]$$

$$d_{2nm} = \left(\frac{S}{2\pi}\right)^4 \left[G_{2nm} + \frac{24\, d_{3nm}}{b_f^2} \left(\frac{2\pi}{S}\right)^2 - \frac{360}{b_f^4} d_{4nm} \right]$$

$$d_{1nm} = \left(\frac{S}{2\pi}\right)^4 \left[G_{1nm} + \frac{4\, d_{2nm}}{b_f^2} \left(\frac{2\pi}{S}\right)^2 - \frac{24}{b_f^4} d_{3nm} \right] \quad (4.3.6)$$

The complementary function solution of equation (4.3.2) is

$$F_{12_{C.F.}} = \frac{E\pi^2}{2S^2 b_f^2} \sum_{n=1}^{n=N} \sum_{m=1}^{m=N} W_n W_m \left[t_{1nm} \cosh\frac{2\pi y_1}{S} + t_{2nm}\left(\frac{y_1}{b_f}\right) \sinh\frac{2\pi y_1}{S} + t_{3nm} \sinh\frac{2\pi y_1}{S} + t_{4nm}\left(\frac{y_1}{b_f}\right) \cosh\frac{2\pi y_1}{S} \right] \quad (4.3.7)$$

The general solution F_{12} is given by the sum of the particular integral and complementary function solutions,

i.e. $F_{12} = F_{12_{P.I.}} + F_{12_{C.F.}}$

$$F_{12} = \frac{E\pi^2}{2S^2 b_f^2} \sum_{n=1}^{n=N} \sum_{m=1}^{m=N} W_n W_m \left[\left[d_{1nm} + d_{2nm}\left(\frac{y_1}{b_f}\right)^2 + d_{3nm}\left(\frac{y_1}{b_f}\right)^4 \right.\right.$$

$$+ d_{4nm}\left(\frac{y_1}{b_f}\right)^6 + d_{5nm}\left(\frac{y_1}{b_f}\right)^8 + d_{6nm}\left(\frac{y_1}{b_f}\right)^{10} \Big] + \Big[t_{1nm} \cosh \frac{2\pi y_1}{S}$$

$$+ t_{2nm}\left(\frac{y_1}{b_f}\right) \sinh \frac{2\pi y_1}{S} + t_{3nm} \sinh \frac{2\pi y_1}{S}$$

$$\left. \left. + t_{4nm}\left(\frac{y_1}{b_f}\right) \cosh \frac{2\pi y_1}{S} \Big] \right] \qquad (4.3.8)$$

The constants $t_{1nm} - t_{4nm}$ are evaluated from the stress boundary conditions, and will be considered later.

The solutions of equation (4.1.6) for the web and the lip are obtained by exactly the same method as that used for the flange, substitution of the functions Y_2 and Y_3 from equations (4.2.2) produces the solutions F_{22} and F_{32} in the following form.

Web Solution

$$F_{22} = \frac{E\Pi^2}{2S^2 b_w^2} \sum_{n=1}^{n=N} \sum_{m=1}^{m=N} W_n W_m \left[\left[b_{1nm} + b_{2nm}\left(\frac{y_2}{b_w}\right) + b_{3nm}\left(\frac{y_2}{b_w}\right)^2 \right.\right.$$

$$+ b_{4nm}\left(\frac{y_2}{b_w}\right)^3 + b_{5nm}\left(\frac{y_2}{b_w}\right)^4 + b_{6nm}\left(\frac{y_2}{b_w}\right)^5 + b_{7nm}\left(\frac{y_2}{b_w}\right)^6 + b_{8nm}\left(\frac{y_2}{b_w}\right)^7$$

$$\left. + b_{9nm}\left(\frac{y_2}{b_w}\right)^8 + b_{10nm}\left(\frac{y_2}{b_w}\right)^9 + b_{11nm}\left(\frac{y_2}{b_w}\right)^{10} \right] +$$

$$+ \left[C_{1nm} \cosh \frac{2\pi y_2}{S} + C_{2nm} \sinh \frac{2\pi y_2}{S} \right.$$

$$\left. \left. + C_{3nm}\left(\frac{y_2}{b_w}\right) \cosh \frac{2\pi y_2}{S} + C_{4nm}\left(\frac{y_2}{b_w}\right) \sinh \frac{2\pi y_2}{S} \right] \right] \qquad (4.3.9)$$

The coefficients $C_{1nm} - C_{4nm}$ are obtained from the stress boundary conditions at the web-flange junction and at the web-lip junction.

The coefficients $b_{1nm} - b_{11nm}$ are as follows.

$$b_{11nm} = \left(\frac{S}{2\pi}\right)^4 R_{11nm}$$

$$b_{10nm} = \left(\frac{S}{2\pi}\right)^4 R_{10nm}$$

$$b_{9nm} = \left(\frac{S}{2\pi}\right)^4 \left[R_{9nm} + \frac{180}{b_w^2} b_{11nm} \left(\frac{2\pi}{S}\right)^2 \right]$$

$$b_{8nm} = \left(\frac{S}{2\pi}\right)^4 \left[R_{8nm} + \frac{144}{b_w^2} b_{10nm} \left(\frac{2\pi}{S}\right)^2 \right]$$

$$b_{7nm} = \left(\frac{s}{2\pi}\right)^4 \left[R_{7nm} + \frac{112}{bw^2} b_{9nm}\left(\frac{2\pi}{s}\right)^2 - \frac{5040}{bw^4} b_{11nm}\right]$$

$$b_{6nm} = \left(\frac{s}{2\pi}\right)^4 \left[R_{6nm} + \frac{84}{bw^2} b_{8nm}\left(\frac{2\pi}{s}\right)^2 - \frac{3024}{bw^4} b_{10nm}\right]$$

$$b_{5nm} = \left(\frac{s}{2\pi}\right)^4 \left[R_{5nm} + \frac{60}{bw^2} b_{7nm}\left(\frac{2\pi}{s}\right)^2 - \frac{1680}{bw^4} b_{9nm}\right]$$

$$b_{4nm} = \left(\frac{s}{2\pi}\right)^4 \left[R_{4nm} + \frac{40}{bw^2} b_{6nm}\left(\frac{2\pi}{s}\right)^2 - \frac{840}{bw^4} b_{8nm}\right]$$

$$b_{3nm} = \left(\frac{s}{2\pi}\right)^4 \left[R_{3nm} + \frac{24}{bw^2} b_{5nm}\left(\frac{2\pi}{s}\right)^2 - \frac{360}{bw^4} b_{7nm}\right]$$

$$b_{2nm} = \left(\frac{s}{2\pi}\right)^4 \left[R_{2nm} + \frac{12}{bw^2} b_{4nm}\left(\frac{2\pi}{s}\right)^2 - \frac{120}{bw^4} b_{6nm}\right]$$

$$b_{1nm} = \left(\frac{s}{2\pi}\right)^4 \left[R_{1nm} + \frac{4}{bw^2} b_{3nm}\left(\frac{2\pi}{s}\right)^2 - \frac{24}{bw^4} b_{5nm}\right] \quad (4.3.10)$$

where R_{1nm} - R_{11nm} are related to the coefficients h_{n1} - h_{n6} in the deflection function Y_2 by the following expressions

$$R_{11nm} = -6 h_{n6} h_{m6}$$

$$R_{10nm} = -10 h_{n6} h_{m5}$$

$$R_{9nm} = (6 h_{n4} h_{m6} - 5 h_{n5} h_{m5} - 12 h_{n6} h_{m4})$$

$$R_{8nm} = (12 h_{n3} h_{m6} - 8 h_{n5} h_{m4} - 12 h_{n6} h_{m3})$$

$$R_{7nm} = (18 h_{n2} h_{m6} + 5 h_{n3} h_{m5} - 4 h_{n4} h_{m4} - 9 h_{n5} h_{m3} - 10 h_{n6} h_{m2})$$

$$R_{6nm} = (24 h_{n1} h_{m6} + 10 h_{n2} h_{m5} - 6 h_{n4} h_{m3} - 8 h_{n5} h_{m2} - 6 h_{n6} h_{m1})$$

$$R_{5nm} = \left(15k_{n1}k_{m5} + 4k_{n2}k_{m4} - 3k_{n3}k_{m3} - 6k_{n4}k_{m2} - 5k_{n5}k_{m1}\right)$$

$$R_{4nm} = \left(8k_{n1}k_{m4} - 4k_{n3}k_{m2} - 4k_{n4}k_{m1}\right)$$

$$R_{3nm} = \left(3k_{n1}k_{m3} - 2k_{n2}k_{m2} - 3k_{n3}k_{m1}\right)$$

$$R_{2nm} = -2k_{n2}k_{m1}$$

$$R_{1nm} = -k_{n1}k_{m1} \qquad (4.3.11)$$

Lip Solution

The solution of equation (4.1.6) for the lip is of the same form as that for the web since the deflection functions Y_2 and Y_3 have the same form.

$$F_{32} = \frac{E\pi^2}{2S^2b\ell^2}\sum_{n=1}^{n=N}\sum_{m=1}^{m=N} W_nW_m\left[\left[M_{1nm} + M_{2nm}\left(\frac{y_3}{b\ell}\right) + M_{3nm}\left(\frac{y_3}{b\ell}\right)^2 + M_{4nm}\left(\frac{y_3}{b\ell}\right)^3 + M_{5nm}\left(\frac{y_3}{b\ell}\right)^4 + M_{6nm}\left(\frac{y_3}{b\ell}\right)^5 + M_{7nm}\left(\frac{y_3}{b\ell}\right)^6 + M_{8nm}\left(\frac{y_3}{b\ell}\right)^7 + M_{9nm}\left(\frac{y_3}{b\ell}\right)^8 + M_{10nm}\left(\frac{y_3}{b\ell}\right)^9 + M_{11nm}\left(\frac{y_3}{b\ell}\right)^{10}\right] + \left[N_{1nm}\cosh\frac{2\pi y_3}{S} + N_{2nm}\sinh\frac{2\pi y_3}{S} + N_{3nm}\left(\frac{y_3}{b\ell}\right)\cosh\frac{2\pi y_3}{S} + N_{4nm}\left(\frac{y_3}{b\ell}\right)\sinh\frac{2\pi y_3}{S}\right]\right] \qquad (4.3.12)$$

The coefficients N_{1nm} - N_{4nm} are obtained from the stress boundary conditions at the web-lip junction and at the lip free edge.

Since the solutions F_{22} and F_{32} are of exactly the same form, equations (4.3.10) and (4.3.11) are used to evaluate the coefficients M_{1nm} - M_{11nm}. This is achieved simply by replacing b_{1nm} with M_{1nm} and b_w with b_ℓ in equations (4.3.10), while in equations (4.3.11) $hn_i\ hm_j$ is replaced with $pn_i\ pm_j$.

To fully specify the form of F_{12}, F_{22} and F_{32} in equations (4.3.8), (4.3.9) and (4.3.12) respectively, it remains only to evaluate the constants t_{1nm} - t_{4nm}, C_{1nm} - C_{4nm} and N_{1nm} - N_{4nm}. These constants are obtained by satisfaction of the stress conditions at the boundaries of each plate element.

4.4 CONDITIONS AT THE NODES OF THE CENTRE BUCKLE

The in-plane movements at the nodes of the centre buckle are as specified by equations (3.2.9) of Chapter 3 (see also Figure 3.2.2).

In order to obtain the stress conditions which comply with these movements, equation (2.1.9)(a) is utilized in the following form.

$$u_{x=\pm\frac{s}{2}} = \int_0^{\frac{s}{2}} \left[\varepsilon_x - \frac{1}{2}\left(\frac{\partial w_i}{\partial x}\right)^2\right] dx \qquad (4.4.1)$$

Substituting the strain ε_x in terms of the stresses gives

$$u_{x=\pm\frac{s}{2}} = \int_0^{\frac{s}{2}} \left[\frac{1}{E}\left[\frac{\partial^2 F_i}{\partial y_i^2} - \nu\frac{\partial^2 F_i}{\partial x^2}\right] - \frac{1}{2}\left(\frac{\partial w_i}{\partial x}\right)^2\right] dx \qquad (4.4.2)$$

Using equation (4.1.4) for F_i and the general expression for w_i in the form $w_i = Y_i(y_i)\cos\frac{\pi x}{s}$, the integral of equation (4.4.2) gives the following relationship for the in-plane movements at the nodes of the centre buckle.

$$u_{x=\pm\frac{s}{2}} = \frac{1}{E}\cdot\frac{s}{2}F_{i1}'' - \frac{\pi^2}{8s}Y_i^2 \qquad (4.4.3)$$

Equation (4.3.1) gives F_{i1}'' in terms of Y_i and the unknown constants C_1 and C_2, substitution into equation (4.4.3) gives

$$u_{x=\pm\frac{s}{2}} = \frac{s}{2E}\left[C_1 y_i + C_2\right] \qquad (4.4.4)$$

To obtain the constants C_1 and C_2, expression (4.4.4) is equated to the applied displacements as described by equations (3.2.9). Noting that the flange displacement or compression U* is negative the following relationships for the flange, web and lip are obtained.

$$\underline{\text{Flange}} \quad -u^* = \frac{s}{2E}\left[C_1 y_1 + C_2\right]$$

$$\underline{\text{Web}} \quad -u^*\left(1-\alpha+\alpha\frac{y_2}{bw}\right) = \frac{s}{2E}\left[C_1 y_2 + C_2\right]$$

$$\underline{\text{Lip}} \quad -u^*(1-\alpha) = \frac{s}{2E}\left[C_1 y_3 + C_2\right] \qquad (4.4.5)$$

The constants C_1 and C_2 can now be evaluated for each plate by manipulation of equations (4.4.5), these are

$$\underline{\text{Flange}} \quad C_1 = 0, \quad C_2 = -\frac{2E}{S}u^*$$

$$\underline{\text{Web}} \quad C_1 = -\frac{2E}{S}\frac{\alpha}{bw}u^*, \quad C_2 = -\frac{2E}{S}(1-\alpha)u^*$$

$$\underline{\text{Lip}} \quad C_1 = 0, \quad C_2 = -\frac{2E}{S}(1-\alpha)u^* \qquad (4.4.6)$$

The stress conditions necessary to comply with the specified in-plane movement system at the nodes of the centre buckle have now been satisfied.

4.5 CONDITIONS AT THE PLATE EDGES

It is assumed that there is no normal stress on the edges at all plate junctions, i.e. $\frac{\partial^2 Fi}{\partial x^2} = \sigma y = 0$, using equation (4.I.4) this is written as

$$\frac{\partial^2 F_i}{\partial x^2} = -\left(\frac{2\pi}{S}\right)^2 \cos\frac{2\pi x}{S} F_{i2} = 0$$

and since this must be true for all x, then F_{12} must equal zero at all edges, this gives

$$F_{12} = 0 \quad \text{at} \quad y_1 = b_f$$

$$F_{22} = 0 \quad \text{at} \quad y_2 = 0, bw$$

$$F_{32} = 0 \quad \text{at} \quad y_3 = 0, b\ell \qquad (4.5.1)$$

The shear flow and longitudinal direct stress at the junctions must be equal for adjacent plates. This gives the following equations

for the flange-web junction.

$$\frac{\partial^2 F_1}{\partial x\, \partial y_1} = \mp \frac{\partial^2 F_2}{\partial x\, \partial y_2} \quad \text{at } y_2 = bw,\ y_1 = \mp bf$$

$$\frac{\partial^2 F_1}{\partial y_1^2} = \frac{\partial^2 F_2}{\partial y_2^2} \quad \text{at } y_2 = bw,\ y_1 = \mp bf \qquad (4.5.2)$$

Since $F_{11}'' = F_{21}''$ automatically by the use of equations (4.4.6), the satisfaction of equations (4.5.2) is simplified to the following

$$F_{12}' = -F_{22}' \quad \text{at} \quad y_1 = bf,\ y_2 = bw$$

$$F_{12}'' = F_{22}'' \quad \text{at} \quad y_1 = bf,\ y_2 = bw \qquad (4.5.3)$$

The same conditions of shear flow and longitudinal direct stress exist at the web-lip junction as did those at the web-flange junction. These conditions result in the following.

$$\frac{\partial^2 F_2}{\partial x\, \partial y_2} = -\frac{\partial^2 F_3}{\partial x\, \partial y_3} \quad \text{at} \quad y_2 = 0,\ y_3 = 0$$

$$\frac{\partial^2 F_2}{\partial y_2^2} = \frac{\partial^2 F_3}{\partial y_3^2} \quad \text{at} \quad y_2 = 0,\ y_3 = 0 \qquad (4.5.4)$$

Using equations (4.4.6) sets $F_{21}'' = F_{31}''$ automatically at the web-lip junction and reduces equations (4.5.4) to the following form

$$F_{22}' = -F_{32}' \quad \text{at} \quad y_2 = 0,\ y_3 = 0$$

$$F_{22}'' = F_{32}'' \quad \text{at} \quad y_2 = 0,\ y_3 = 0 \qquad (4.5.5)$$

The last boundary condition to be satisfied is that of zero shear stress at the lip free edge, this gives

$$\tau_{xy_3} = -\frac{\partial^2 F_3}{\partial x \partial y_3} = F_{32}'\left(\frac{2\pi}{S}\right)\sin\frac{2\pi x}{S} = 0 \qquad (4.5.6)$$

Since equation (4.5.6) has to be true for all x, the shear stress boundary condition at the lip free edge simplifies to

$$F_{32}' = 0 \quad \text{at} \quad y_3 = b\ell \qquad (4.5.7)$$

All the boundary conditions have now been stated and the relevant equations to satisfy these conditions have been developed, it remains now to solve these equations by utilizing the unknown constants contained in F_{12}.

4.6 SATISFACTION OF THE STRESS CONDITIONS AT THE PLATE EDGES

Due to the symmetry of the flange out of plane deflections and stress distributions about the axis $y_1 = 0$, the constants t_{3nm} and t_{4nm} in equation (4.3.8) must be zero, since they are associated with anti-symmetrical functions. This leaves ten undetermined constants t_{1nm}, t_{2nm}, $C_{1nm} - C_{4nm}$, $N_{1nm} - N_{4nm}$ with which to satisfy the boundary equations (4.5.1), (4.5.3), (4.5.5) and (4.5.7).

The conditions of zero normal stress in the y_i direction as described by equations (4.5.1) result in the development of the following five equations, these equations being obtained after

substitution of the relevant y_i boundaries in equations (4.3.8), (4.3.9) and (4.3.12).

$$t_{1nm}\cosh\frac{2\pi bf}{s} + t_{2nm}\sinh\frac{2\pi bf}{s} = -\left[d_{1nm}+d_{2nm}+d_{3nm}+d_{4nm}+d_{5nm}\right]$$

$$C_{1nm} = -\,b_{1nm}$$

$$\left[C_{1nm}\cosh\frac{2\pi bw}{s} + C_{2nm}\sinh\frac{2\pi bw}{s} + C_{3nm}\cosh\frac{2\pi bw}{s} + C_{4nm}\sinh\frac{2\pi bw}{s}\right] = -\left[b_{1nm}+b_{2nm}+b_{3nm}+b_{4nm}+b_{5nm}+b_{6nm}+b_{7nm}+b_{8nm}+b_{9nm}+b_{10nm}+b_{11nm}\right]$$

$$N_{1nm} = -\,M_{1nm}$$

$$\left[N_{1nm}\cosh\frac{2\pi b\ell}{s} + N_{2nm}\sinh\frac{2\pi b\ell}{s} + N_{3nm}\cosh\frac{2\pi b\ell}{s} + N_{4nm}\sinh\frac{2\pi b\ell}{s}\right] = -\left[M_{1nm}+M_{2nm}+M_{3nm}+M_{4nm}+M_{5nm}+M_{6nm}+M_{7nm}+M_{8nm}+M_{9nm}+M_{10nm}+M_{11nm}\right]$$

(4.6.1)

The equality of shear flow and longitudinal direct stress at the flange-web junction, produces the following two equations on

substitution of the relevant F_{12}', F_{12}'' in equations (4.5.3) at

$y_1 = b_f$, $y_2 = b\omega$.

$$\frac{1}{b_f^2}\left[t_{1nm}\left(\frac{2\pi}{s}\right)\sinh\frac{2\pi b_f}{s} + t_{2nm}\left[\frac{2\pi}{s}\cosh\frac{2\pi b_f}{s} + \frac{1}{b_f}\sinh\frac{2\pi b_f}{s}\right]\right]$$

$$+\frac{1}{b\omega^2}\left[C_{1nm}\left(\frac{2\pi}{s}\right)\sinh\frac{2\pi b\omega}{s} + C_{2nm}\left(\frac{2\pi}{s}\right)\cosh\frac{2\pi b\omega}{s} + C_{3nm}\left[\right.\right.$$

$$\left.\frac{1}{b\omega}\cosh\frac{2\pi b\omega}{s} + \left(\frac{2\pi}{s}\right)\sinh\frac{2\pi b\omega}{s}\right] + C_{4nm}\left[\frac{1}{b\omega}\sinh\frac{2\pi b\omega}{s} +$$

$$\left.\left.\left(\frac{2\pi}{s}\right)\cosh\frac{2\pi b\omega}{s}\right]\right] = -\frac{1}{b\omega^3}\left[b_{2nm} + 2b_{3nm} + 3b_{4nm} +\right.$$

$$\left. 4b_{5nm} + 5b_{6nm} + 6b_{7nm} + 7b_{8nm} + 8b_{9nm} + 9b_{10nm} + 10b_{11nm}\right]$$

$$-\frac{1}{b_f^3}\left[2d_{3nm} + 4d_{5nm} + 6d_{7nm} + 8d_{9nm} + 10d_{11nm}\right].$$

$$\frac{1}{b_f^2}\left[t_{1nm}\left(\frac{2\pi}{s}\right)^2\cosh\frac{2\pi b_f}{s} + t_{2nm}\left[\left(\frac{2\pi}{s}\right)^2\sinh\frac{2\pi b_f}{s} + \frac{2}{b_f}\left(\frac{2\pi}{s}\right)\cosh\frac{2\pi b_f}{s}\right]\right]$$

$$-\frac{1}{b\omega^2}\left[C_{1nm}\left(\frac{2\pi}{s}\right)^2\cosh\frac{2\pi b\omega}{s} + C_{2nm}\left(\frac{2\pi}{s}\right)^2\sinh\frac{2\pi b\omega}{s} + C_{3nm}\left[\right.\right.$$

$$\left.\frac{2}{b\omega}\left(\frac{2\pi}{s}\right)\sinh\frac{2\pi b\omega}{s} + \left(\frac{2\pi}{s}\right)^2\cosh\frac{2\pi b\omega}{s}\right] + C_{4nm}\left[\frac{2}{b\omega}\left(\frac{2\pi}{s}\right)\cosh\frac{2\pi b\omega}{s}\right.$$

$$\left.\left.+\left(\frac{2\pi}{s}\right)^2\sinh\frac{2\pi b\omega}{s}\right]\right] = \frac{1}{b\omega^4}\left[2b_{3nm} + 6b_{4nm} + 12b_{5nm} +\right.$$

$$\left. 20b_{6nm} + 30b_{7nm} + 42b_{8nm} + 56b_{9nm} + 72b_{10nm} + 90b_{11nm}\right]$$

$$-\frac{1}{b_f^4}\left[2d_{3nm} + 12d_{5nm} + 30d_{7nm} + 56d_{9nm} + 90d_{11nm}\right]. \quad (4.6.2)$$

Using equations (4.5.5) and substituting the relevant F_{12}', F_{12}'' at $y_2 = 0$, $y_3 = 0$ gives the following two equations for the shear flow and direct stress conditions at the web-lip junction.

$$\frac{1}{bw^2}\left[C_{2nm}\left(\frac{2\pi}{S}\right)+C_{3nm}\frac{1}{bw}\right]+\frac{1}{b\ell^2}\left[N_{2nm}\left(\frac{2\pi}{S}\right)+N_{3nm}\frac{1}{b\ell}\right]$$

$$= -\frac{1}{b\ell^3}M_{2nm} - \frac{1}{bw^3}b_{2nm}$$

$$\frac{1}{bw^2}\left[C_{1nm}\left(\frac{2\pi}{S}\right)^2+\frac{2C_{4nm}}{bw}\left(\frac{2\pi}{S}\right)\right]-\frac{1}{b\ell^2}\left[N_{1nm}\left(\frac{2\pi}{S}\right)^2+\frac{2N_{4nm}}{b\ell}\left(\frac{2\pi}{S}\right)\right]$$

$$= 2\left[\frac{1}{b\ell^4}M_{3nm} - \frac{1}{bw^4}b_{3nm}\right] \qquad (4.6.3)$$

Substitution of F_{32}' at $y_3 = b\ell$ in equation (4.5.7) gives the equation to be satisfied for the condition of zero shear stress at the lip free edge, this is

$$N_{1nm}\left(\frac{2\pi}{S}\right)\sinh\frac{2\pi b\ell}{S}+N_{2nm}\left(\frac{2\pi}{S}\right)\cosh\frac{2\pi b\ell}{S}+N_{3nm}\left[\left(\frac{2\pi}{S}\right)\sinh\frac{2\pi b\ell}{S}\right.$$

$$\left.+\frac{1}{b\ell}\cosh\frac{2\pi b\ell}{S}\right]+N_{4nm}\left[\left(\frac{2\pi}{S}\right)\cosh\frac{2\pi b\ell}{S}+\frac{1}{b\ell}\sinh\frac{2\pi b\ell}{S}\right]$$

$$= -\frac{1}{b\ell}\left[M_{2nm}+2M_{3nm}+3M_{4nm}+4M_{5nm}+5M_{6nm}\right.$$

$$\left.+6M_{7nm}+7M_{8nm}+8M_{9nm}+9M_{10nm}+10M_{11nm}\right] \qquad (4.6.4)$$

The ten constants t_{1nm}, t_{2nm}, $C_{1nm} - C_{4nm}$, $N_{1nm} - N_{4nm}$ contained in equations (4.6.1), (4.6.2), (4.6.3) and (4.6.4) are evaluated numerically on the University's I.C.L. 1904S computer, use being made of a standard subroutine which gives the solution of a set of real linear equations with multiple right hand sides. The method of solution used by the subroutine is as follows:

Equations (4.6.1), (4.6.2), (4.6.3) and (4.6.4) are written in the matrix form AX = B, where B represents the known right hand sides given in these equations, A represents the coefficients of the unknown constants and X is the vector of unknown constants.

The matrix A is decomposed into triangles, A = LU, where L is lower triangular and U is unit upper triangular.

An approximation to X is found by back substitution and the residual matrix R = B - AX evaluated. A correction D to X is then found by back substitution in LUD = R, the vector X is now replaced by (X + D) and the process repeated until D becomes negligible.

The stress function F_{12} is now completely known and the strain energy for the section can be evaluated in terms of the unknown coefficients W_n.

4.7 MINIMISATION OF THE TOTAL STRAIN ENERGY

Substitution of equation (4.1.4) in equation (4.1.1) gives, upon expansion and integration in the x-direction, the following equation for the strain energy due to mid-plane stresses

$$V_M = \frac{tS}{4E}\sum_{i=1}^{i=3}\int_{bo}^{b_1}\left[\left[\left(\frac{2\pi}{S}\right)^4\left(F_{i2}\right)^2 - 2F_{i2}F_{i2}''\left(\frac{2\pi}{S}\right)^2 + 2F_{i1}''\right.\right.$$

$$\left.\left.+\left(F_{i2}''\right)^2\right] + 2(1+\nu)\left[F_{i2}F_{i2}''\left(\frac{2\pi}{S}\right)^2 + \right.\right.$$

$$\left.\left.\left(F_{i2}'\right)^2\left(\frac{2\pi}{S}\right)^2\right]\right] dy_i \qquad (4.7.1)$$

The second part of the integral (4.7.1) reduces to $\left[F_{12}\,F_{12}'\right]_{b_o}^{b_1}$ and since F_{12} is zero at all boundaries then this part is zero for all plate elements.

The strain energy due to mid-plane stresses is now given by the following expression

$$V_M = \frac{tS}{4E}\sum_{i=1}^{i=3}\int_{bo}^{b_1}\left[\left[F_{i2}'' - \left(\frac{2\pi}{S}\right)^2 F_{i2}\right]^2 + 2\left(F_{i1}''\right)^2\right] dy_i \qquad (4.7.2)$$

Substitution for F_{12}, F_{12}'' and F_{11}'' in equation (4.7.2) and using F_{12} in the general form $F_{i2} = \frac{E\pi^2}{2S^2 b_i^2}\sum\sum W_n W_m \psi_{inm}$, where b_1 and ψ_{inm} are obtained from equations (4.3.8), (4.3.9) and (4.3.12) respectively, gives the total strain energy in the centre buckle of the column due to in plane stresses as

$$V_M = \sum_{i=1}^{i=3} \left\{ \frac{tS}{2E} \left[\left(\frac{E\pi^2}{2S^2 b_i^2} \right)^2 \sum_{n=1}^{n=N} \sum_{m=1}^{m=N} \sum_{r=1}^{r=N} \sum_{h=1}^{h=N} W_n W_m W_r W_h \Gamma_{inmrh} \right.\right.$$

$$+ 2\left(\frac{E\pi^2}{4S^2}\right)^2 \sum_{n=1}^{n=N} \sum_{m=1}^{m=N} \sum_{r=1}^{r=N} \sum_{h=1}^{h=N} W_n W_m W_r W_h \Phi_{inmrh}$$

$$- \frac{2E^2\pi^2 u^*}{S^3} \sum_{n=1}^{n=N} \sum_{m=1}^{m=N} W_n W_m \Theta_{inm}$$

$$\left.\left. + K_i \right] \right\} \qquad (4.7.3)$$

where

$$\Gamma_{inmrh} = \int_0^{b_i} \left[\psi''_{inm} \psi''_{irh} - \left(\frac{2\pi}{S}\right)^2 \psi''_{inm} \psi_{irh} - \left(\frac{2\pi}{S}\right)^2 \psi_{inm} \psi''_{irh} + \left(\frac{2\pi}{S}\right)^4 \psi_{inm} \psi_{irh} \right] dy_i$$

$$\Phi_{inmrh} = \int_0^{b_i} Y_{in} Y_{im} Y_{ir} Y_{ih} \, dy_i$$

$$\Theta_{1nm} = \int_0^{b_f} Y_{1n} Y_{1m} \, dy_1$$

$$\Theta_{2nm} = (1-\alpha) \int_0^{b_w} Y_{2n} Y_{2m} \, dy_2 + \frac{\alpha}{b_w} \int_0^{b_w} y_2 Y_{2n} Y_{2m} \, dy_2$$

$$\Theta_{3nm} = (1-\alpha) \int_0^{b_\ell} Y_{3n} Y_{3m} \, dy_3$$

$$K_1 = 2\int_0^{b_f}\left(\frac{2EU^*}{S}\right)^2 dy_1$$

$$K_2 = 2\left(\frac{2EU^*}{S}\right)^2\int_0^{bw}\left(\frac{\alpha}{bw}\right)^2 y_2^2+\frac{2\alpha}{bw}(1-\alpha)y_2+(1-\alpha)^2\,dy_2$$

$$K_3 = 2\left(\frac{2EU^*}{S}\right)^2\int_0^{b\ell}(1-\alpha)^2\,dy_3 \qquad (4.7.4)$$

The total strain energy in the centre buckle due to plate bending is obtained, as in the initial buckling solution by the use of equation (2.2.4), Chapter 2.

This produces the following expression.

$$V_B = \frac{SD}{2}\sum_{i=1}^{i=3}\sum_{n=1}^{n=N}\sum_{m=1}^{m=N} W_n W_m Q_{inm} \qquad (4.7.5)$$

where

$$Q_{inm} = \int_0^{bi}\left[Y_{in}''-\frac{\pi^2}{S^2}Y_{in}\right]^2 dy_i+\frac{2\pi^2}{S^2}(1-\nu)\left[Y_{in}'Y_{in}\right]_0^{bi} \qquad (4.7.6)$$

The total strain energy V_T is now given by the summation of equations (4.7.3) and (4.7.5), i.e.

$$V_T = V_M + V_B \qquad (4.7.7)$$

By applying the principle of minimum strain energy to the centre buckle of the column the coefficients W_n in the deflection functions can be evaluated. This is achieved by differentiating equation (4.7.7) with respect to each coefficient in turn and equating to zero to give N simultaneous equations in the unknown W_n.

At this stage it is necessary to decide on the number of terms to be used in the post buckling solution. Since care has been taken to specify suitable compatible deflection functions, good accuracy can be obtained from the use of a small number of terms. The complexity of the energy expressions show also that the labour and computation time involved will increase rapidly with the increase in the number of terms used.

From consideration of the above points, it is thought that the use of two terms W_n will describe sufficiently accurately the column's post buckling behaviour. Differentiation of equation (4.7.7) with respect to the coefficients W_1 and W_2 respectively, and equating to zero gives the following two equations in W_1 and W_2.

$$4W_1^3\Theta_1 + 3W_1^2W_2\Theta_2 + 2W_1W_2^2\Theta_3 + W_2^3\Theta_4 + 2W_1\Theta_5 + W_2\Theta_6 = 0$$

$$W_1^3\Theta_2 + 2W_1^2W_2\Theta_3 + 3W_1W_2^2\Theta_4 + 4W_2^3\Theta_7 + W_1\Theta_6 + 2W_2\Theta_8 = 0 \qquad (4.7.8)$$

where

$$\Theta_1 = \sum_{i=1}^{i=3} \frac{\pi^4 E t}{16 S^3}\left[\frac{2\,\Gamma_{i1111}}{b i^4} + \Phi_{i1111}\right]$$

$$\Theta_2 = \sum_{i=1}^{i=3} \frac{\pi^4 E t}{16 S^3}\left[\frac{2}{b i^4}\left(\Gamma_{i1112} + \Gamma_{i11121} + \Gamma_{i12111} + \Gamma_{i21111}\right)\right.$$

$$\left. + \left(\Phi_{i1112} + \Phi_{i11121} + \Phi_{i12111} + \Phi_{i21111}\right)\right]$$

$$\Theta_3 = \sum_{i=1}^{i=3} \frac{\pi^4 E t}{16 S^3} \left[\frac{2}{b_i^4} \left(\Gamma_{i1122} + \Gamma_{i1212} + \Gamma_{i1221} + \Gamma_{i2112} + \Gamma_{i2121} + \Gamma_{i2211} \right) \right.$$

$$\left. + \left(\Phi_{i1122} + \Phi_{i1212} + \Phi_{i1221} + \Phi_{i2112} + \Phi_{i2121} + \Phi_{i2211} \right) \right]$$

$$\Theta_4 = \sum_{i=1}^{i=3} \frac{\pi^4 E t}{16 S^3} \left[\frac{2}{b_i^4} \left(\Gamma_{i1222} + \Gamma_{i2122} + \Gamma_{i2212} + \Gamma_{i2221} \right) \right.$$

$$\left. + \left(\Phi_{i1222} + \Phi_{i2122} + \Phi_{i2212} + \Phi_{i2221} \right) \right]$$

$$\Theta_5 = \sum_{i=1}^{i=3} \left[\frac{SD}{2} Q_{i11} - \frac{\pi^2 E t u^*}{S^2} \Theta_{i11} \right]$$

$$\Theta_6 = \sum_{i=1}^{i=3} \left[\frac{SD}{2} \left(Q_{i12} + Q_{i21} \right) - \frac{\pi^2 E t u^*}{S^2} \left(\Theta_{i12} + \Theta_{i21} \right) \right]$$

$$\Theta_7 = \sum_{i=1}^{i=3} \frac{\pi^4 E t}{16 S^3} \left[\frac{2 \Gamma_{i2222}}{b_i^4} + \Phi_{i2222} \right]$$

$$\Theta_8 = \sum_{i=1}^{i=3} \left[\frac{SD}{2} Q_{i22} - \frac{\pi^2 E t u^*}{S^2} \Theta_{i22} \right] \qquad (4.7.9)$$

Dividing equations (4.7.8) throughout by W_1^3, and putting $\Delta = \frac{W_2}{W_1}$, yields the following equations

$$\left[4\Theta_1 + 3\Delta\Theta_2 + 2\Delta^2\Theta_3 + \Delta^3\Theta_4 \right] = -\frac{1}{W_1^2} \left[2\Theta_5 + \Delta\Theta_6 \right]$$

$$\left[\Theta_2+2\Delta\Theta_3+3\Delta^2\Theta_4+4\Delta^3\Theta_7\right]=-\frac{1}{W_1^2}\left[\Theta_6+2\Delta\Theta_8\right] \qquad (4.7.10)$$

Cross multiplication of these equations eliminates W_1 and produces a quartic in Δ , i.e.

$$f(\Delta) = \varepsilon_1\Delta^4+\varepsilon_2\Delta^3+\varepsilon_3\Delta^2+\varepsilon_4\Delta+\varepsilon_5=0 \qquad (4.7.11)$$

where

$$\varepsilon_1 = \left[2\Theta_4\Theta_8-4\Theta_7\Theta_6\right]$$

$$\varepsilon_2 = \left[4\Theta_3\Theta_5-8\Theta_7\Theta_5-2\Theta_4\Theta_6\right]$$

$$\varepsilon_3 = \left[6\left(\Theta_2\Theta_8-\Theta_4\Theta_5\right)\right]$$

$$\varepsilon_4 = \left[2\Theta_2\Theta_6+8\Theta_1\Theta_8-4\Theta_3\Theta_5\right]$$

$$\varepsilon_5 = \left[4\Theta_1\Theta_6-2\Theta_2\Theta_5\right] \qquad (4.7.12)$$

Equation (4.7.11) is solved for a value of U* just above that required to initiate instability. The required root is known from the buckling solution to be approximately equal to zero since at buckling $W_1 = 1.0$ and $W_2 = 0$. The solution is thus obtained very quickly using a starting value $\Delta_n = 0$ in conjunction with Newtons Method of Successive Approximations, i.e. $\Delta_{n+1} = \frac{\Delta_n f'(\Delta_n)-f(\Delta_n)}{f'(\Delta_n)}$. Subsequent solutions of equation (4.7.11) for further increments of U* are obtained by setting the starting value Δ_n equal to the

solution from the previous increment.

Knowing the solution for Δ , the value of W_1 can be found by substitution in either of equations (4.7.10). W_2 is then obtained from $W_2 = \Delta\ W_1$.

Using these values of W_1 and W_2, the local deflections, membrane stresses, and bending stresses can be evaluated at any point within the centre buckle of the column.

4.8 SATISFACTION OF OVERALL EQUILIBRIUM

At this stage a solution has been obtained for a particular end movement system at the nodes of the central buckle. It is now necessary to examine the stress system caused by this end movement system to determine, as in the buckling solution, whether the internal stresses provide equilibrium with the externally applied load P on the column.

The membrane stresses in the x-direction, along the column length, only need be considered in establishing this equilibrium, these stresses taking the following form for any plate element i in the section.

$$\left[\sigma_x\right]_i = \frac{\partial^2 F_i}{\partial y_i^2} = F_{i1}'' + F_{i2}'' \cos\frac{2\pi x}{S} \qquad (4.8.1)$$

The total load P on the column is given by the integration of the σ_x stresses around the section as

$$P = 2t \sum_{i=1}^{i=3} \int_0^{b_i} \left[\sigma_x\right]_i \, dy_i \qquad (4.8.2)$$

where $b_1 = b_f$, $b_2 = bw$, $b_3 = b\ell$.

Substitution of equation (4.8.1) into equation (4.8.2) and summing gives

$$P = 2t\left[\int_0^{bf} F_{11}''\,dy_1 + \int_0^{bw} F_{21}''\,dy_2 + \int_0^{b\ell} F_{31}''\,dy_3 + \left[F_{12}'\right]_0^{bf} + \left[F_{22}'\right]_0^{bw} + \left[F_{32}'\right]_0^{b\ell}\right]\cos\frac{2\pi x}{s} \quad (4.8.3)$$

since $F_{12}' = -F_{22}'$ at $y_1 = b_f$, $y_2 = b_w$

$F_{22}' = -F_{32}'$ at $y_2 = 0$, $y_3 = 0$

$F_{12}' = 0$ at $y_1 = 0$

$F_{32}' = 0$ at $y_3 = b\ell$

then the term in equation (4.8.3) which varies with x reduces to zero to give the following equation for the column axial load

$$P = 2t\sum_{i=1}^{i=3}\int_0^{bi} F_{i1}''\,dy_i \quad (4.8.4)$$

To develop an expression for the moment on the section caused by the membrane stresses σ_x, moments are taken about an axis through the lips to give

$$M = 2t\left[b_w\int_0^{bf} F_{11}''\,dy_1 + b_w\left[F_{12}'\cos\frac{2\pi x}{s}\right]_0^{bf} + \int_0^{bw} F_{21}''\,y_2\,dy_2 + \left[y_2 F_{22}'\cos\frac{2\pi x}{s}\right]_0^{bw} - \left[F_{22}\cos\frac{2\pi x}{s}\right]_0^{bw}\right] \quad (4.8.5)$$

Using the boundary conditions for F_{12}', F_{22}' and F_{22} equation (4.8.5) simplifies to give the final expression for the moment M as

$$M = 2t\left[b_w\int_0^{bf} F_{11}''\,dy_1 + \int_0^{bw} y_2 F_{21}''\,dy_2\right] \quad (4.8.6)$$

It can be seen from this analysis of the σ_x membrane stresses that the load P and the moment M on the column cross section are completely independent of the second part of the stress function $F_{i2} \cos \frac{2\pi x}{s}$ in F_i, the only stresses contributing to the load and the moment being those obtained from F_{i1}".

Figure 4.8.1 shows the stress distribution around the section due to F_{i1}" on the crest of a local buckle at the columns central cross section. Substitution of equation (4.3.1) for F_{i1}" using the constants C_1 and C_2 from equations (4.4.6) into equation (4.8.4) and integrating gives the equation for the total axial load as

$$P = N_x^* \left[2b_f + 2b_w\left(1-\frac{\alpha}{2}\right) + 2b_\ell(1-\alpha) \right] - B_1 - 2B_2 - 2B_3 \quad (4.8.7)$$

where
$$B_i = \frac{E\pi^2 t}{4s^2} \int_{b_o}^{b_1} Y_i^2 \, dy_i \quad (4.8.8)$$

the limits of integration being the boundaries of each plate. The B_i are as depicted in Figure 4.8.1 and represent the loss in load of each plate element due to local buckling.

Substitution of the relevant F_{i1}" in equation (4.8.6) and integrating gives a more simplified expression for the moment M about the lips of the section as

$$M = N_x^* b_w \left[b + b_w\left(1-\frac{\alpha}{3}\right) \right] - \overline{B_1} - 2\overline{B_2} \quad (4.8.9)$$

where $\overline{B_1}$ and $\overline{B_2}$ are the moments about the lips caused by B_1 and B_2 respectively, and are obtained from

$$\overline{B_i} = \int_{b_o}^{b_1} \frac{E\pi^2 t}{4s^2} Y_i^2 \, y_i \, dy_i \quad (4.8.10)$$

To obtain equilibrium of the internal stress system with the externally applied load P, an expression for the column's lateral deflection δ must be known, this expression being given by the solution of the differential equation of equilibrium for the locally buckled column.

Due to the rather lengthy nature of the work required in the development and solution of the differential equation of equilibrium, the lateral deflection δ_c is simply stated at this point, and its derivation given in Appendix 1. This is

$$\delta_c = \left[e + (d - d^*) + \frac{M^*}{P}\right]\left[\sec\frac{\pi}{2}\sqrt{\frac{P}{P_E^*}} - 1\right] \qquad (4.8.11)$$

where $P_E^* = \dfrac{\pi^2 E I^*}{L^2}$

The physical significance of the terms d*, M*, I* and P_E* in equation (4.8.11) are given as follows:

(a) d* is the position of the neutral axis, from the section lips, in the post local buckling range.

(b) M* is an internal moment caused by the effects of local buckling. ++

(c) I* is the reduced second moment of area of the section in the post local buckling range.

(d) P_E* is denoted as the reduced Euler load of the column, the load-deflection equilibrium path being asymtotic towards this value after local buckling takes place.

++ see Appendix II for a more detailed explanation of the physical meaning of M*

If the effects of local buckling were not present then d* is equal to d, the neutral axis position of the unbuckled section, I* is equal to I, the second moment of area of the unbuckled section, M* is equal to zero and equation (4.8.11) reduces to equation (3.1.3) (Chapter 3) which describes the pre-local buckling load-deflection equilibrium path of the column.

The equilibrium of the internal stress system caused by a given compression U* and a given eccentricity of compression α, is obtained by equating the internal moment due to the σ_x stresses to the external moment. This gives

$$N_x^*\left[b_w(b+b_w)-\alpha\frac{b_w^2}{3}\right]-\bar{B}_1-2\bar{B}_2-P\left[e+d+\delta_c\right]=0 \qquad (4.8.12)$$

Substituting now equation (4.8.11) for the central deflection δ_c in equation (4.8.12) and then substituting equation (4.8.7) for the load P in the result, gives the equilibrium equation as a function of α in the following form

$$N_x^*\left[b_w(b+b_w)-\alpha\frac{b_w^2}{3}\right]-\bar{B}_1-2\bar{B}_2$$
$$-M^*\left[\sec\frac{\pi}{2}\sqrt{\frac{N_x^*\left[(b+2b_w+2b_\ell)-\alpha(b_w+2b_\ell)\right]-B_1-2B_2-2B_3}{P_E^*}}-1\right]$$
$$-\left[N_x^*\left[(b+2b_w+2b_\ell)-\alpha(b_w+2b_\ell)\right]-B_1-2B_2-2B_3\right]\times\left[d^*+\left[e+(d-d^*)\right]\sec\frac{\pi}{2}\sqrt{\frac{N_x^*\left[(b+2b_w+2b_\ell)-\alpha(b_w+2b_\ell)\right]-B_1-2B_2-2B_3}{P_E^*}}\right]$$
$$=f(\alpha)=0 \qquad (4.8.13)$$

Equation (4.8.13) is solved numerically to obtain the equilibrium value of α for any given flange compression U*, the technique used being the same as that employed in the solution of equation (3.1.4) (Chapter 3).

Consider a discrete value of U* just above that obtained at the initiation of local buckling, i.e. $U^* = U^*_{crit} + \delta U^*$. As a first approximation to the equilibrium value of α for this U* the critical local buckling solution is used, i.e. $\alpha = \alpha_1 = \alpha_{crit}$. Using this U* and α_1 equations (4.7.10) and (4.7.11) are generated and solved simultaneously to provide the deflection coefficients W_1 and W_2. Knowing the coefficients W_1 and W_2 the parameters d*, M*, P_E*, B_i and $\overline{B_i}$ are evaluated and the function $f(\alpha)$ as described by equation (4.8.13) takes the value $f_1(\alpha_1) \neq 0$.

A second approximation to the equilibrium value of α for the same U* is now used in the form $\alpha_2 = \alpha_1 + 0.5$ say, and the process previously described is repeated to obtain $f_2(\alpha_2) \neq 0$. The values of α_1, α_2, f_1 and f_2 are now used as the starting points in the iteration scheme

$$\alpha_{n+2} = \alpha_{n+1} + \frac{f_{n+1}}{f_{n+1} - f_n}\left(\alpha_n - \alpha_{n+1}\right) \qquad (4.8.14)$$

and the correct value of α for the given U* is very quickly obtained

by terminating equation (4.8.14) when the difference between two consecutive values of α is approximately equal to zero.

i.e. when $\alpha_{n+2} - \alpha_{n+1} = 0.00001$.

The solution is now complete for this particular value of U*, the column's axial load, central deflection, buckled form and stress distributions being obtained from the relevant equations developed in this chapter. To obtain the complete post-buckling equilibrium path for the column the procedure outlined is repeated for a number of discrete increments of compression U* applied to the flange.

As well as the facility of the theoretical solution to provide a continually changing buckled form throughout the post local buckling range, change in buckle half-wavelength S may also be taken into account. This can be achieved by obtaining several solutions of the column's complete load-deflection equilibrium path for various values of half-wavelength S, and choosing the lowest envelope of all such curves as being the most accurate. i.e. For any given column deflection δ_c the solution which gives the lowest axial load P is the most accurate.

It has been shown by several investigators (17), (32), (40) that the post local buckling equilibrium path is very dependent on the ratio of the critical local buckling load to the Euler load of the column. If the critical load is equal to or near the Euler load then the maximum load the column can take is the critical local buckling load and the subsequent equilibrium path is unstable. These types

of columns are very imperfection sensitive and their maximum loads are very quickly eroded by the effects of both local and overall imperfections. Alternatively, if the critical load is considerably less than the Euler load, the column will buckle locally and subsequently follow a stable equilibrium path which will culminate in an ultimate load caused by the effects of plasticity. These columns are not as imperfection sensitive regarding their ultimate loads as those described previously with unstable equilibrium paths.

Since a rigorous elasto-plastic analysis to describe the column's behaviour when parts of the material are undergoing plastic deformations, would be very time consuming, a simple collapse criterion is used to signify the ultimate load of the column. The ultimate load is taken as that load which makes the maximum total membrane stress, along the column's length, reach the yield stress of the material at the web-flange junction or the web-lip junction, whichever is applicable. This criterion does not, of course, take account of the loss in section stiffness due to plasticity, but provides a reasonable estimate of the ultimate load carrying capacity for such columns.

The theoretical work in this chapter is presented for the "ideal" or "perfect" column, i.e. the column whose axis is perfectly straight and whose constituent plate elements are perfectly flat. In the practical case however, the "perfect" structure is never realised: imperfections of a local or overall nature being inherent probably in

the manufacturing process. The effects of such imperfections on the lipped channel column are not covered in this thesis but will be studied by the author at a later date. Appendices III and IV supplement the theoretical work by giving the solutions of the energy integrals developed in the instability analysis of Chapter Three and the post local buckling analysis of this chapter respectively.

4.9 TYPICAL INTERACTION CURVES

To enable the reader to visualise the behaviour of the column during loading, the results of the foregoing analysis are presented in graphical form at the end of this chapter. The numerical work involved in the analysis was carried out in the University's ICL-1904S computer for which a program was written using the "high level" Fortran IV language. The various equations derived throughout the analysis were arranged in the computer program as they appear in the theory. Due to its rather lengthy nature however, the program is not listed in the thesis. A detailed flow chart showing the logic paths contained within the program is given in Appendix V.

Although an extensive amount of data is available from the computer, the author has restricted his presentation to a selection of results which he considers will be of most interest to the reader.

The majority of the curves are presented in non-dimensional form and are intended to provide the reader with an understanding of the complicated behaviour which exists in the presence of both local and Euler buckling modes. Such interaction behaviour is depicted in Figures 4.9.1 to 4.9.27, where the effect of changing such factors as column load position, material yield stress, and the various geometrical parameters, on column behaviour is shown. Each figure will now be discussed separately and the salient points noted.

Figure 4.9.1 shows several column load-deflection curves corresponding to various values of the eccentricity parameter $\overline{ec} = \frac{ec}{y}$. Of particular interest is the centroidally loaded column where it can be seen that the column deflections remain zero until the local buckling load is reached. For the section under consideration local buckling occurs mainly in the flange b and the section neutral axis position moves effectively towards the lips. Due to this the concentrically loaded column becomes effectively an eccentrically loaded one and for loads greater than the local buckling load the column begins to deflect in an overall manner. From the local buckling load onwards the curve is known as an interaction curve since both local and overall deflections occur simultaneously during loading.

For eccentricity values other than zero the column starts to deflect from the onset of loading. This is shown in Figure 4.9.1

where it can be seen that load eccentricity towards the lips results in increased local buckling strengths whereas load eccentricity towards the flange gives substantially reduced initial buckling loads. The increased buckling strength for eccentricity values less than zero is, of course, for this particular case, due to the flange plate initiating the section's instability. This factor is further indicated by the change in direction of the column's deflection δ_c after local buckling takes place.

If the yield stress of the column material had an infinite value then the various curves of Figure 4.9.1 would tend towards the reduced Euler load of the column $P_E^* = \frac{\pi^2 E I^*}{L^2}$, and since this quantity is continually reducing due to changes in the locally deflected form during loading, the stable load-deflection equilibrium paths of Figure 4.9.1 would eventually become unstable and the column load would begin to fall with increasing deflection. This behaviour has been shown by Rhodes and Harvey (50) in their investigation of plain channel columns and is covered later in more detail in the authors work. In the practical case however, the material will have a finite value of yield stress and the ultimate load of the column of Figure 4.9.1, with its stable load-deflection behaviour after local buckling, will result from an elasto-plastic mechanism of failure.

As previously mentioned in Section 4.8, an analysis of the column's plastic behaviour is not attempted in this thesis.

Instead, the ultimate load of the column is assumed to be reached when the maximum membrane stress at the flange-web junction along the columns length reaches the yield stress of the material. This simple collapse criterion will be shown later, in Chapter Six to give a reasonable estimate of the ultimate loads of the columns tested in the authors experimental work.

Figure 4.9.2 shows column load-deflection curves for various values of the parameter $\frac{L}{b}$. The column cross sectional dimensions are the same as those of Figure 4.9.1 and the load is applied eccentrically towards the lips by an amount $0.1\,\bar{y}$. Four cases of the ratio $\frac{L}{b}$ are considered, viz $\frac{L}{b} = 12.0,\ 14.4,\ 16.8$ and 19.2. In all four cases the deflection of the column is seen to change direction after local buckling and the post local buckling equilibrium paths are of a stable nature. The curve for $\frac{L}{b} = 19.2$ is seen to give the highest ratio of critical local buckling load to column Euler load, this being $\frac{P_{CR}}{P_E} = 0.535$. This curve has an initially steep equilibrium path after local buckling and is seen to "flatten out" thereafter for increasing column deflections. This is due to the column load P closely approaching the reduced Euler load P_E^*, i.e. $\frac{P}{P_E^*} = 0.94$ for a column deflection of $\delta c/bw = 0.2$. Although it is not apparent from Figure 4.9.2, due to the column load being plotted in the form $\frac{P}{P_E}$, increasing the column length results in increased local

buckling strength for the particular geometry considered in this case, but the ultimate load of the column reduces with increasing length.

Figures 4.9.3 and 4.9.4 show the effects of column length when the load is positioned on the centroid of the section and at $0.1\,\bar{y}$ towards the flange respectively. In these figures the curves for high $\frac{L}{b}$ lie above those for lower $\frac{L}{b}$. This is of course, due to the non-dimensional form chosen for the loading, i.e. $\frac{P}{P_E}$ and does not imply higher absolute load values for longer columns.

From the information given on Figure 4.9.3 for the centroidally loaded case the local buckling load is seen to be independent of the column length whereas the ultimate load reduces with increasing $\frac{L}{b}$. From the data supplied on Figure 4.9.4 for the eccentrically loaded case towards the flange both the local buckling load and the ultimate load may be seen to reduce with increasing $\frac{L}{b}$. In both these cases the $\frac{L}{b}$ values considered provide stable equilibrium behaviour after the occurrence of local buckling. The effect of increasing $\frac{L}{b}$ still further would be to eventually induce unstable behaviour, this will be shown later in Figure 4.9.24.

Figures 4.9.5, 4.9.6 and 4.9.7 show the effect on column behaviour of changing the lip dimension b_ℓ Three

different load positions are considered $\overline{ec}$ = -0.1, 0.0 and 0.1 and the load is plotted in the non dimensional form of $\overline{P} = \frac{Pb}{\pi^2 D}$. The $\frac{b\ell}{b}$ values shown in Figures 4.9.5 to 4.9.7 are of such proportions that the critical stress for the flange is less than the critical value for the lips and for the load cases considered the flange initiates the local instability of the section. This obviously means, as is seen from the figures, that increased local buckling strength will be experienced with increase in $\frac{b\ell}{b}$. After local buckling the load deflection equilibirum paths and the ultimate loads for all three cases of loading are seen to be lower for smaller values of $\frac{b\ell}{b}$. It should be pointed out however, that for certain cross sectional geometries and load positions the lips of the section will govern the local buckling strength of the column. In such cases column deflections will proceed in the negative direction and the loads will tend towards the reduced Euler loads pertaining to locally buckled forms dominated by lip deflection. Rhodes and Harvey (50) in their analysis of the plain channel column showed the positive and negative equilibrium paths taken after bifurcation depending on whether the flanges or the web of the section initiates local instability.

The effect on column behaviour of changing the web width b_w is shown in Figures 4.9.8 to 4.9.10 where column load-

deflection curves for a range of web width to flange width ratios are presented. The load positions previously used for changes in $\frac{L}{b}$ and $\frac{b\ell}{b}$ are again used for changes in $\frac{bw}{b}$ and the column load is plotted in terms of the parameter $\overline{P}$. For all three load cases considered lower local buckling loads, equilibrium paths after local buckling and subsequently lower ultimate loads are seen to result from reducing values of $\frac{bw}{b}$.

Figures 4.9.11 to 4.9.13 show column load-deflection behaviour for various values of flange width to thickness ratios $\frac{b}{t}$. As in previous results loading towards the lips, on the centroid and towards the flange of the section are considered and in the figures the load is plotted in the form of $\frac{P}{P_E}$. In all three loading cases and for all values of $\frac{b}{t}$ considered the ratio of critical local buckling load to Euler load is seen to be very small and subsequently the equilibrium paths after local buckling are stable. Reducing values of $\frac{b}{t}$ are seen to result in increased local buckling and ultimate strength values.

Up to this point results have been presented in the form of load-deflection curves describing the stable behaviour of columns for given ranges of the various geometrical parameters. Attention is now focussed on local deflections and stresses, unstable column behaviour and ultimate carrying capacity.

Figure 4.9.14 shows the local deflections of a centroidally loaded column of given dimensions for various values of axial load P. The deformations shown are those occurring at the crest of the central buckle of the column and for the sake of clarity the web and lip deflections are depicted for the maximum load case considered only. The column has cross sectional dimensions of such proportions that section instability is initiated by the flange and after buckling local deflections are seen to be predominant in the flange. The maximum deflections in the web and the lip under an axial load of 38.16 kN are seen to be of the same magnitude, whereas the maximum deflection of the flange is about 7.6 times that of the web for the same load. Compatibility of rotations is seen to exist at the flange-web junction and the web-lip junction for the axial load case of 38.16 kN and change in local buckled form during loading is also indicated.

Figures 4.9.15, 4.9.16 and 4.9.17 show the distribution of surface and membrane stresses, at the crest of the central buckle, corresponding to the five axial loads and buckled forms of the column of Figure 4.9.14. For clarity stress distributions across the lip are shown for the first two or three axial load cases only. The axial load value of 19.32 kN, which is approximately 2.2% greater than the critical local buckling load, is seen from Figure 4.9.17 to produce membrane stresses along the column

which are fairly constant across the section, slight reductions in stress being noticeable over the central portion of the flange and along part of the web nearest the flange. The surface stresses however, as shown in Figures 4.9.15 and 4.9.16, are seen to be more compressive on the inside of the section, over the central portion of the flange, than corresponding values on the outside surface. The surface stresses across the web are seen to be more compressive on the outside of the section than on the inside whereas those across the lip are seen to have practically the same value as the membrane stress, indicating that the lips have hardly buckled under the applied axial load of 19.32 kN. The higher compressive stresses at the inside surface of the flange, and those on the outside surface of the web, are the result of the flange plate buckling outwards and the web plate buckling inwards, as shown in Figure 4.9.14, causing compressive bending stresses to occur on the inside of the flange and outside of the web respectively.

Further increase in load through stages 2, 3, 4 and 5 results, not only in the growth of local deflections as shown in Figure 4.9.14, but also in the growth of overall column deflections as can be seen from the lower curve of Figure 4.9.3. These two modes of buckling acting together result in the increased stress distributions represented by curves 2, 3, 4 and 5 in Figures 4.9.15, 4.9.16 and 4.9.17. Due to the positive direction of column deflection, stresses in the flange are seen to be very much higher than those

in the lips, and increased local buckling is seen to produce high tensile stresses on the outside surface of the flange over the central portion where a considerable reduction in membrane stress is also indicated.

Figures 4.9.18, 4.9.19 and 4.9.20 show the surface and membrane stress distributions occurring at a cross section of the column mid-way between the crest and node of the central buckle. Since the locally buckled form at this cross section is less pronounced than that at the centre of the column, the surface stresses are seen to be similar in form to those of the central cross section but generally smaller in magnitude. Of particular interest are the membrane stress distributions at this cross section as shown on Figure 4.9.20: these stresses being the average axial membrane stresses of those occurring at the crest of the buckle and those occurring at the node. The average membrane stresses across the flange are seen to result in zero slope at the flange-web junction and a considerable reduction in stress is indicated over the central portion. The average membrane stresses across the web and lip however, show a negligible stress reduction due to local buckling, and are practically linear. Integration of the average axial membrane stresses of Figure 4.9.20 across the section gives the applied load P acting on the column.

At the cross section of the column containing the central buckle node, local out-of-plane deflections are absent, resulting

in longitudinal stress distributions which are constant across the plate thickness of the column. Figure 4.9.21 shows the growth of membrane stresses during loading at the node of the central buckle, the inside and outside surface stresses having the same values as those shown.

The change in position of the section neutral axis after local buckling is shown for a typical column in Figure 4.9.22. The column considered is loaded eccentrially towards the flange by an amount $0.2\ \bar{y}$ and has cross sectional dimensions such that local deflections are predominant in the flange. For the initially unbuckled section, $P < P_{cr}$, the distance of the neutral axis from the section lips is d, but as soon as the section begins to buckle, $P = P_{cr}$, the neutral axis position reduces to about 82% of this value, that is $d^* = 0.82\ d$. Further increase in load, $P > P_{cr}$, is seen to result in continual and more gradual movement of the neutral axis towards the lips.

Figure 4.9.23 shows the variation in theoretical ultimate load with slenderness ratio for centroidally loaded columns with the same cross sectional dimensions. It is seen from this figure that the ultimate load can occur in one of three different ways depending on the slenderness value of the column. If $\frac{L}{r}$ is less than 150, the ultimate load is assumed to be that load which makes the maximum membrane stress at the flange-web junction reach the yield stress of the material, this is represented by the

yield criterion curve on Figure 4.9.23 and it is seen that for small values of slenderness ratio a considerable amount of post local buckling takes place before the ultimate load is reached. If, however, the slenderness ratio lies between 150 and 176 the ultimate load of the column is the critical local buckling load, and for slenderness values greater than 176 the ultimate load is the Euler buckling load. These three ranges of slenderness ratio result in three different types of column load-deflection behaviour. For $\frac{L}{r}$ values less than 150, the column load-deflection curves after local buckling are of a stable nature whereas for $\frac{L}{r}$ values between 150 and 176 the load deflection paths are unstable. Slenderness values greater than 176 result in load-deflection curves whose equilibrium paths are neutral until such times as column deflections initiate local buckling and the equilibrium becomes unstable.

Figure 4.9.24 shows a selection of load deflection curves for columns whose slenderness ratios are within the three ranges previously discussed in Figure 4.9.23. The shaded area shown in Figure 4.9.24 represents the band width of the reduced Euler load curves for the range of slenderness ratios considered. The top and bottom limits of the band width are the reduced Euler loads for the columns with slenderness values of 186 and 101 respectively, and from these, a continual reduction in reduced

Euler load with increasing deflection is clearly indicated. Columns with slenderness values less than 150 are seen to buckle locally and tend towards their reduced Euler loads in a stable equilibrium path, the steepness of the curves becoming less pronounced with increasing deflection. Slenderness values within the range 150 to 176 are seen to have unstable load deflection paths after buckling, these curves tending downwards towards their reduced Euler loads, requiring load reduction with increasing deflection to maintain equilibrium. The slenderness value of 176 is seen to result in simultaneous local and Euler buckling. Columns with slenderness values greater than 176 are seen to buckle in an Euler fashion and deflect at constant load: this deflection continues until the stress in the flange reaches its instability value and the section buckles locally. At this stage the state of equilibrium of the load deflection curve changes from being neutral to unstable.

Figure 4.9.25 shows the ultimate loads attainable for centroidally loaded columns whose slenderness ratios change with web dimensions bw. For this situation the local buckling curve naturally reduces with increasing slenderness values or alternatively with reducing web dimension bw. For slenderness values in the range 147 to 173 the ultimate load the column can attain is its local buckling load and the subsequent load-deflection path

after buckling is unstable. For slenderness values less than 147 stable load-deflection behaviour exists after local buckling whereas neutral behaviour occurs after Euler buckling for $\frac{L}{r}$ values grater than 173.

Figure 4.9.26 shows column load-deflection curves for several values of the parameter $\frac{bw}{b}$ such that column slenderness ratios cover the three ranges previously mentioned in Figure 4.9.25. Stable behaviour after local buckling is clearly indicated for the $\frac{L}{r}$ values less than 147 whereas unstable behaviour is seen to occur for those in the range 147 to 173. Slenderness values greater than 173 are seen to result in neutral behaviour after Euler buckling with subsequent unstable behaviour after the occurrence of local buckling.

So far, theoretical results have been presented showing the effect on column behaviour, of changing the various geometrical parameters and the applied axial load position. Attention is now focussed however, on the effect that changing the material yield stress has on the ultimate carrying capacity of the column. Figure 4.9.27 shows the ultimate load curves corresponding to various values of yield stress σ_y. It is seen from this figure that for the lower slenderness ratios, where a considerable amount of post local buckling exists, higher yield stresses result in substantially increased ultimate loads. As the slenderness values

increase, the effect of yield stress becomes less and less until eventually all the ultimate load curves converge at a common point. This point occurs of course, at the slenderness ratio corresponding to the equality of the local buckling load and the reduced Euler load of the column. Here the ultimate load of the column is the local buckling load with subsequent unstable load-deflection behaviour after buckling, and due to this is independent of the value of material yield stress.

The theoretical curves presented in this Chapter have been chosen by the author as those exhibiting the most interesting and varied behaviour. In Chapter Six comparisons of the authors theory and experimental work are presented and discussed.

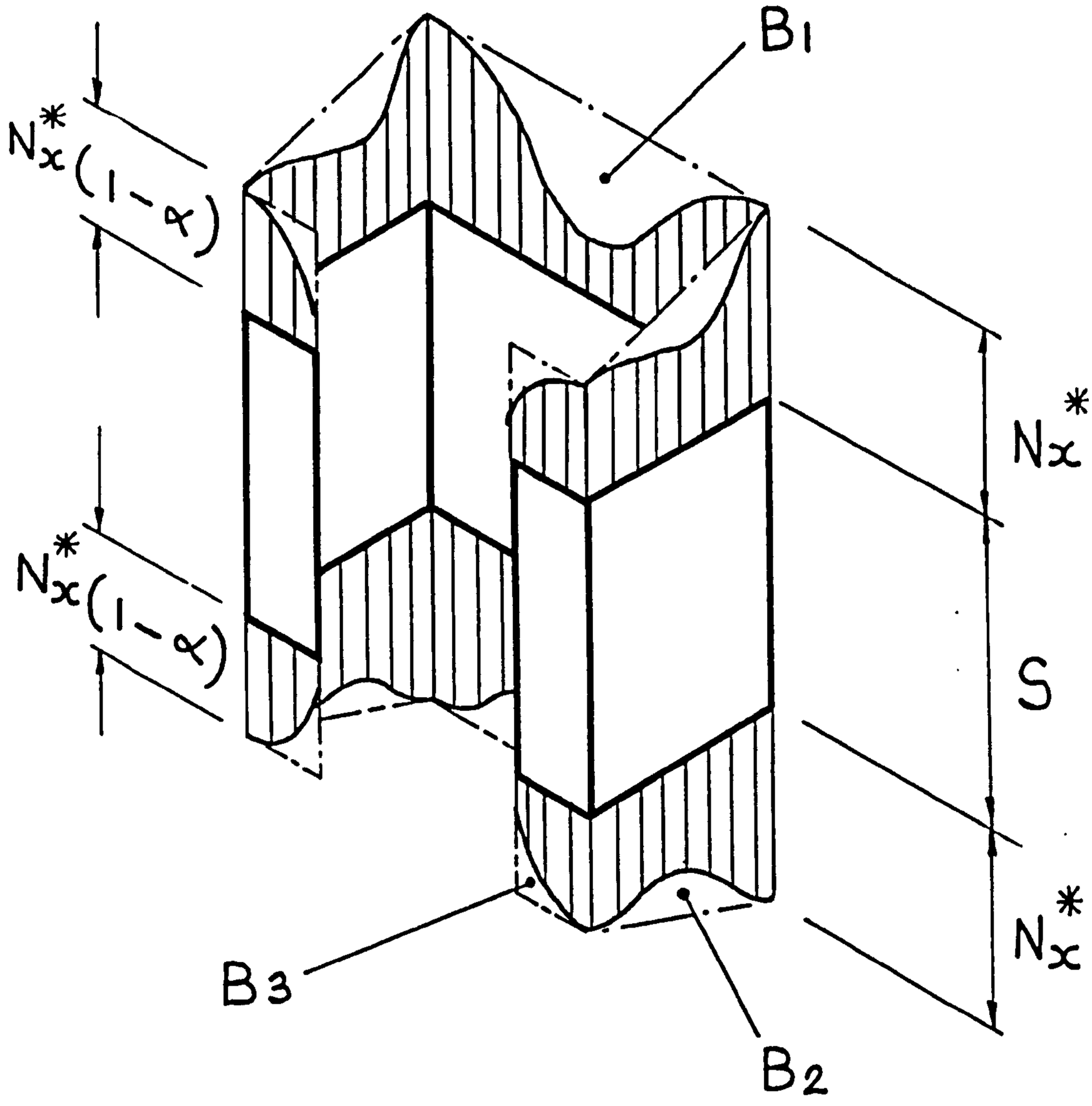

FIG. 4.8.1 AVERAGE STRESS SYSTEM AFTER THE OCCURRENCE OF LOCAL BUCKLING.

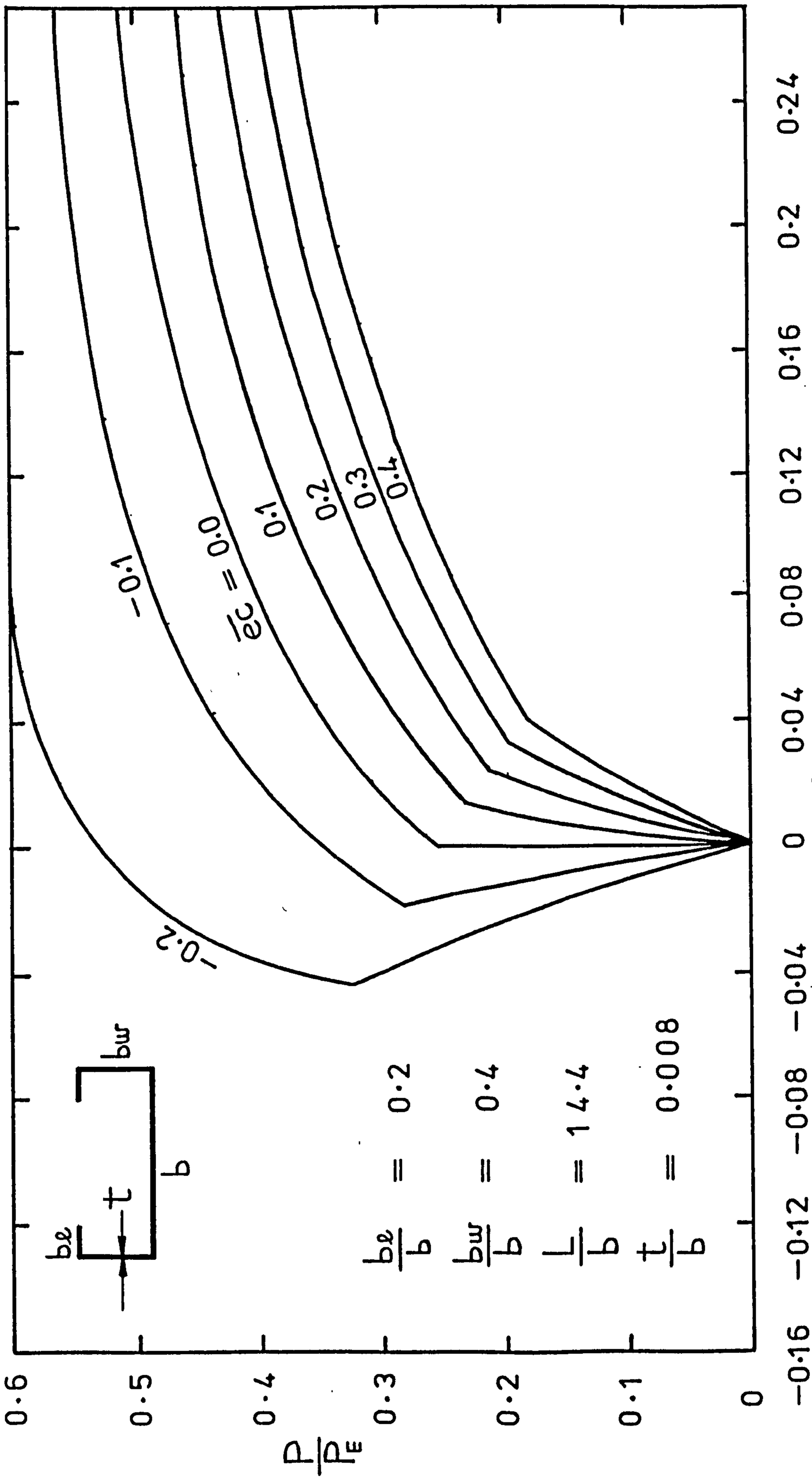

FIG. 4.9.1. LOAD – DEFLECTION CURVES FOR VARIOUS ECCENTRICITY VALUES.

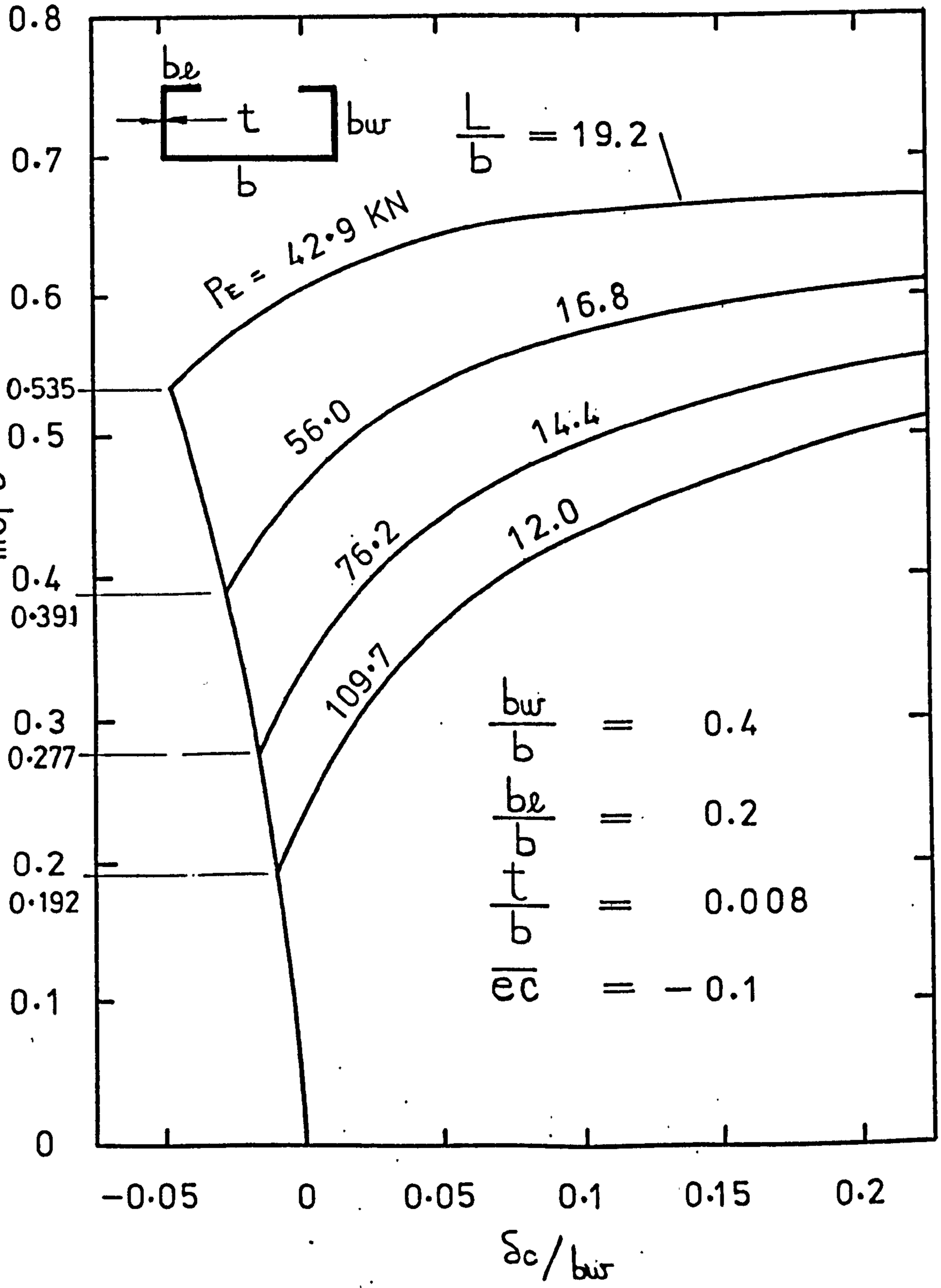

FIG. 4.9.2. LOAD — DEFLECTION CURVE FOR VARIOUS VALUES OF COLUMN LENGTH.

(ECCENTRICITY TOWARDS LIPS)

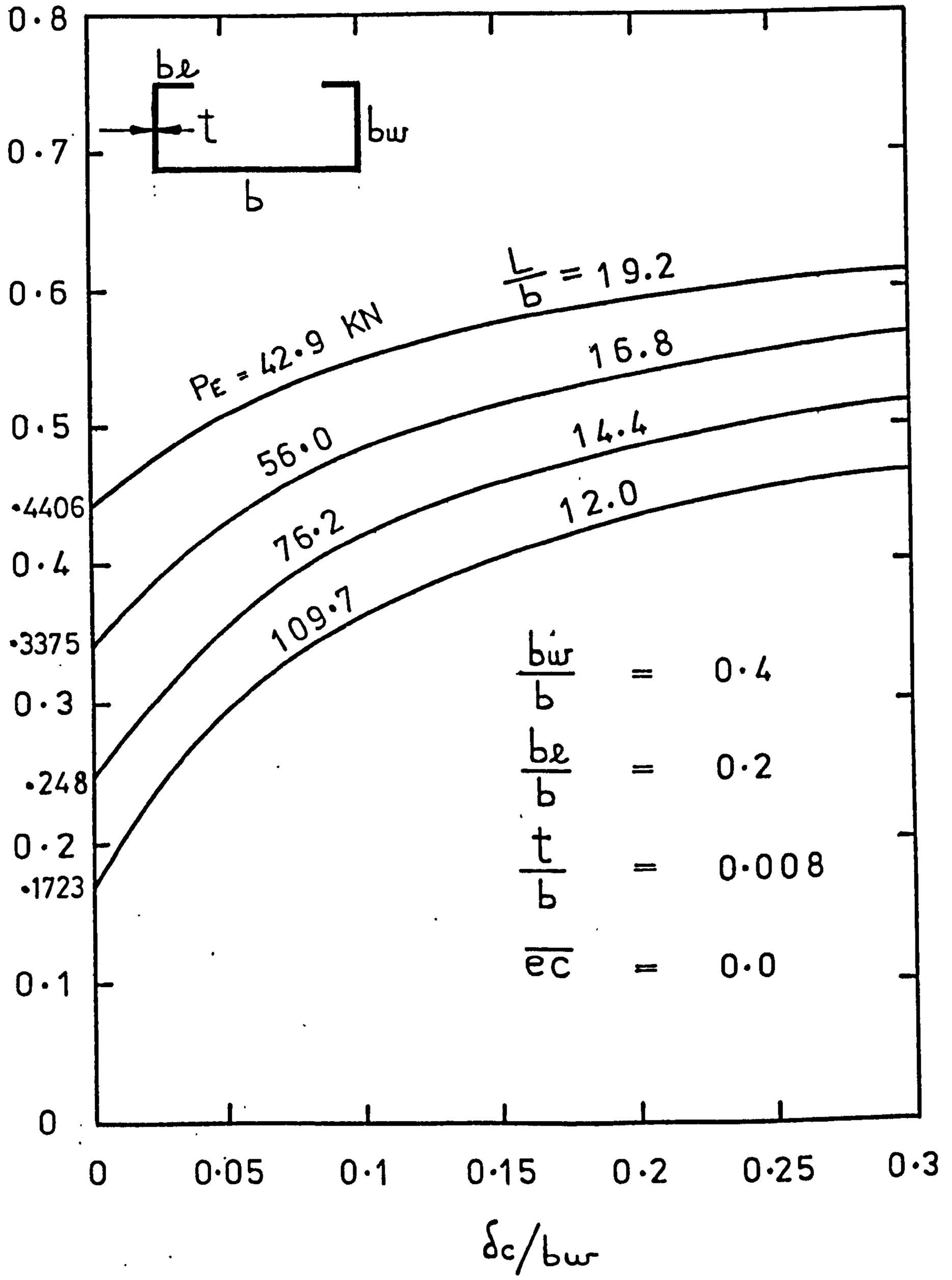

FIG. 4.9.3. LOAD — DEFLECTION CURVES FOR VARIOUS VALUES OF COLUMN LENGTH.

(COLUMN LOADED CENTROIDALLY)

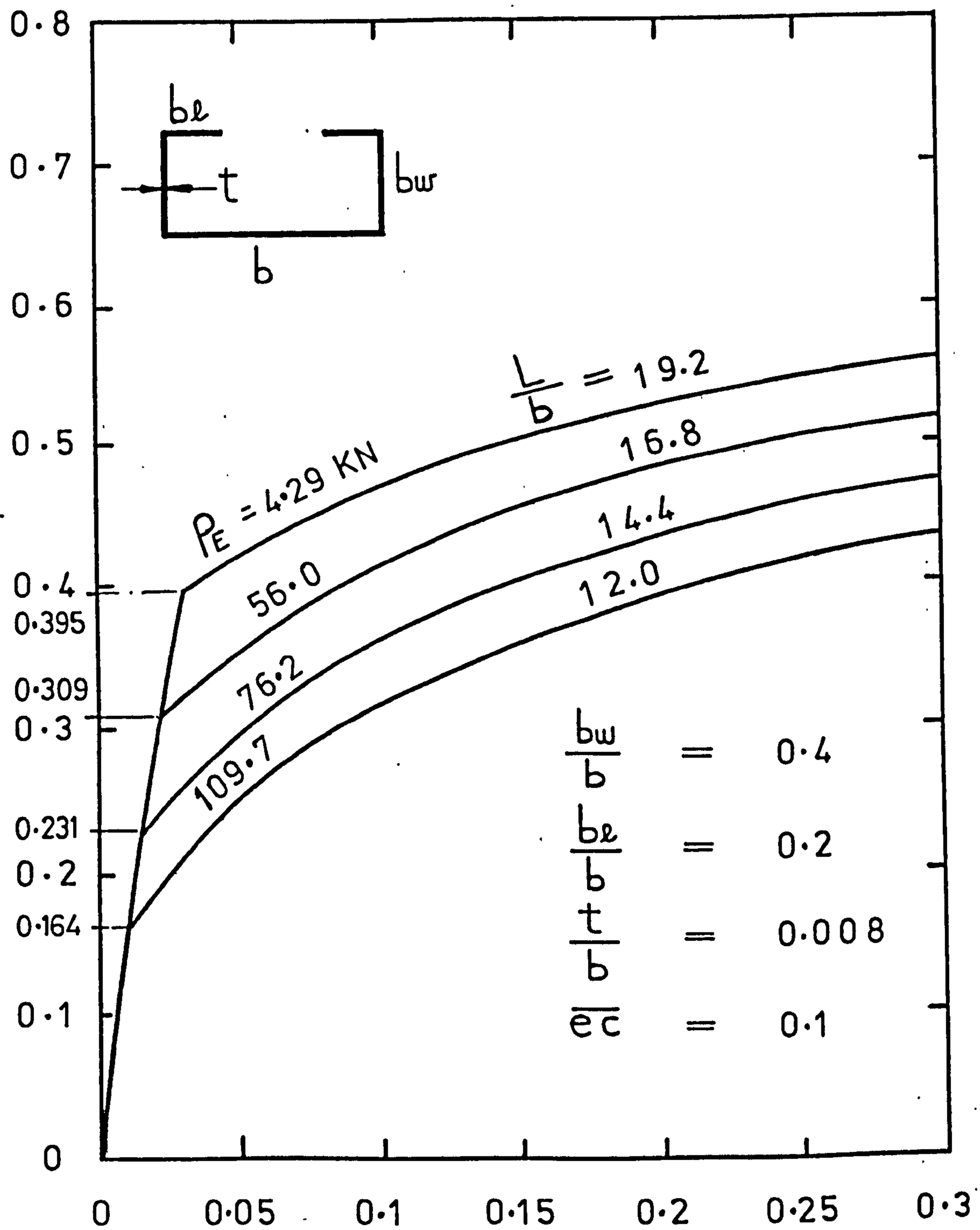

FIG. 4.9.4. LOAD – DEFLECTION CURVES FOR VARIOUS VALUES OF COLUMN LENGTH.

(ECCENTRICITY TOWARDS FLANGE)

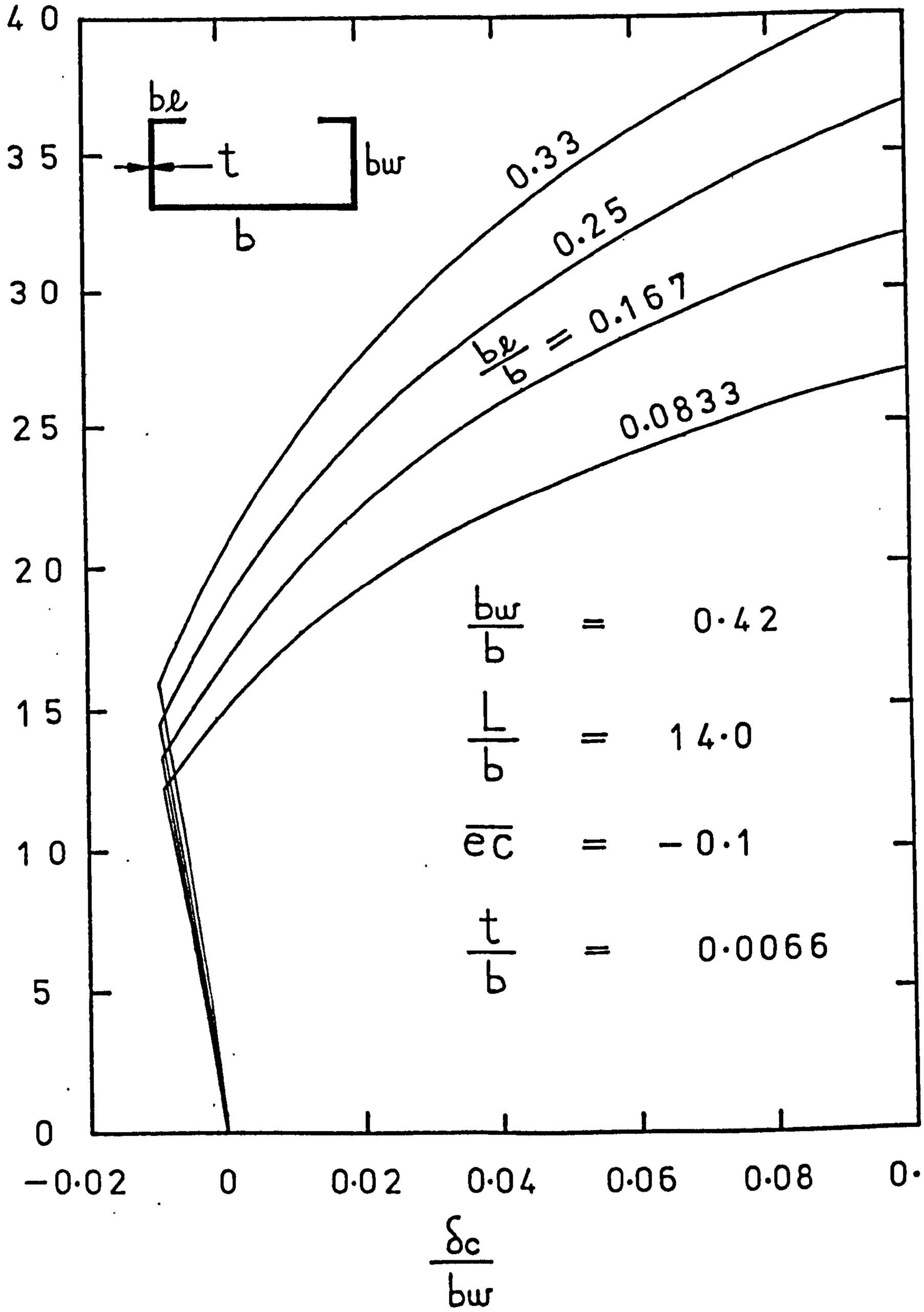

FIG. 4.9.5.

LOAD – DEFLECTION CURVES FOR VARIOUS VALUES OF bℓ. (ECCENTRICITY TOWARDS LIPS)

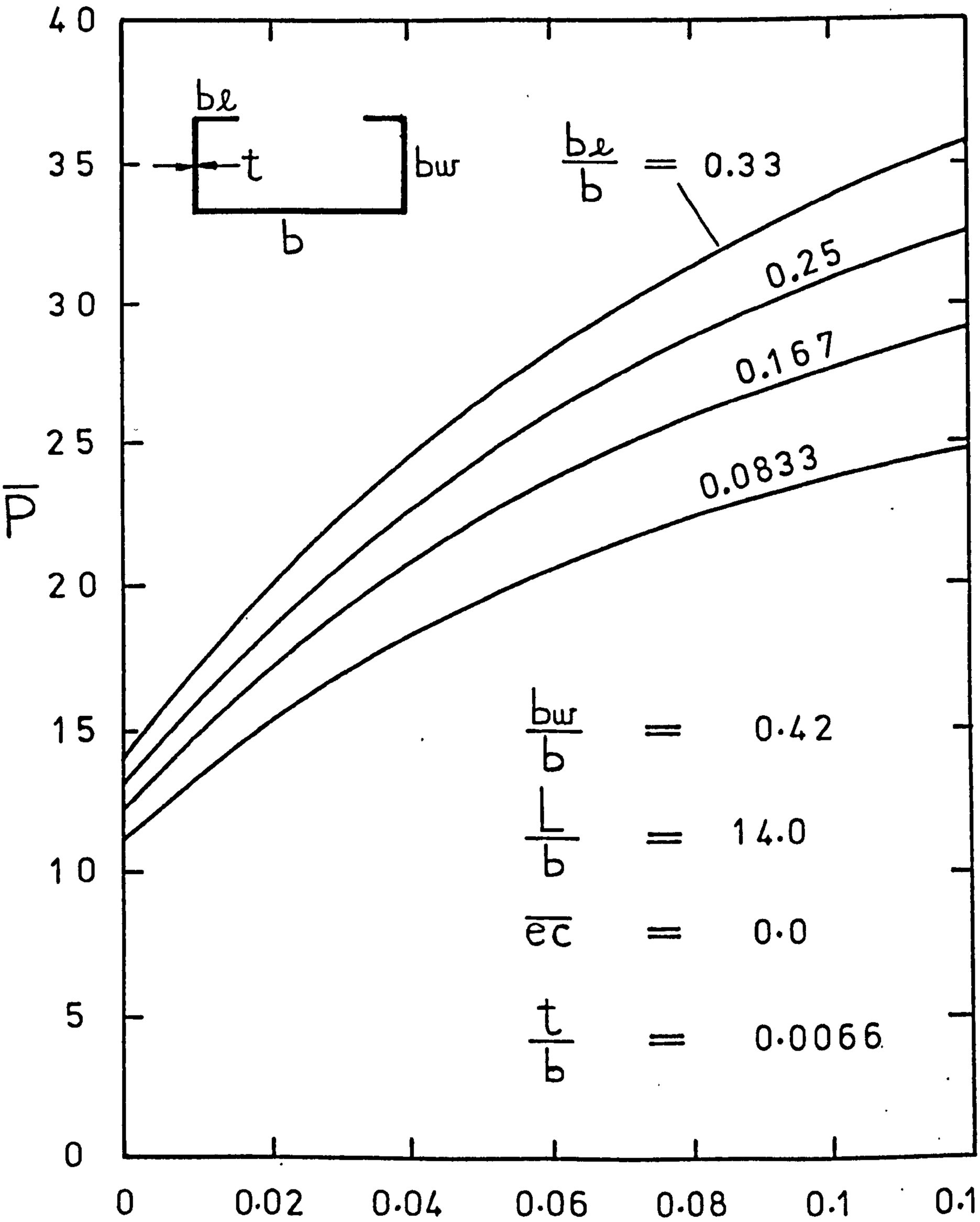

FIG. 4.9.6. LOAD – DEFLECTION CURVES FOR VARIOUS VALUES OF b_ℓ. (COLUMN LOADED CENTROIDALLY)

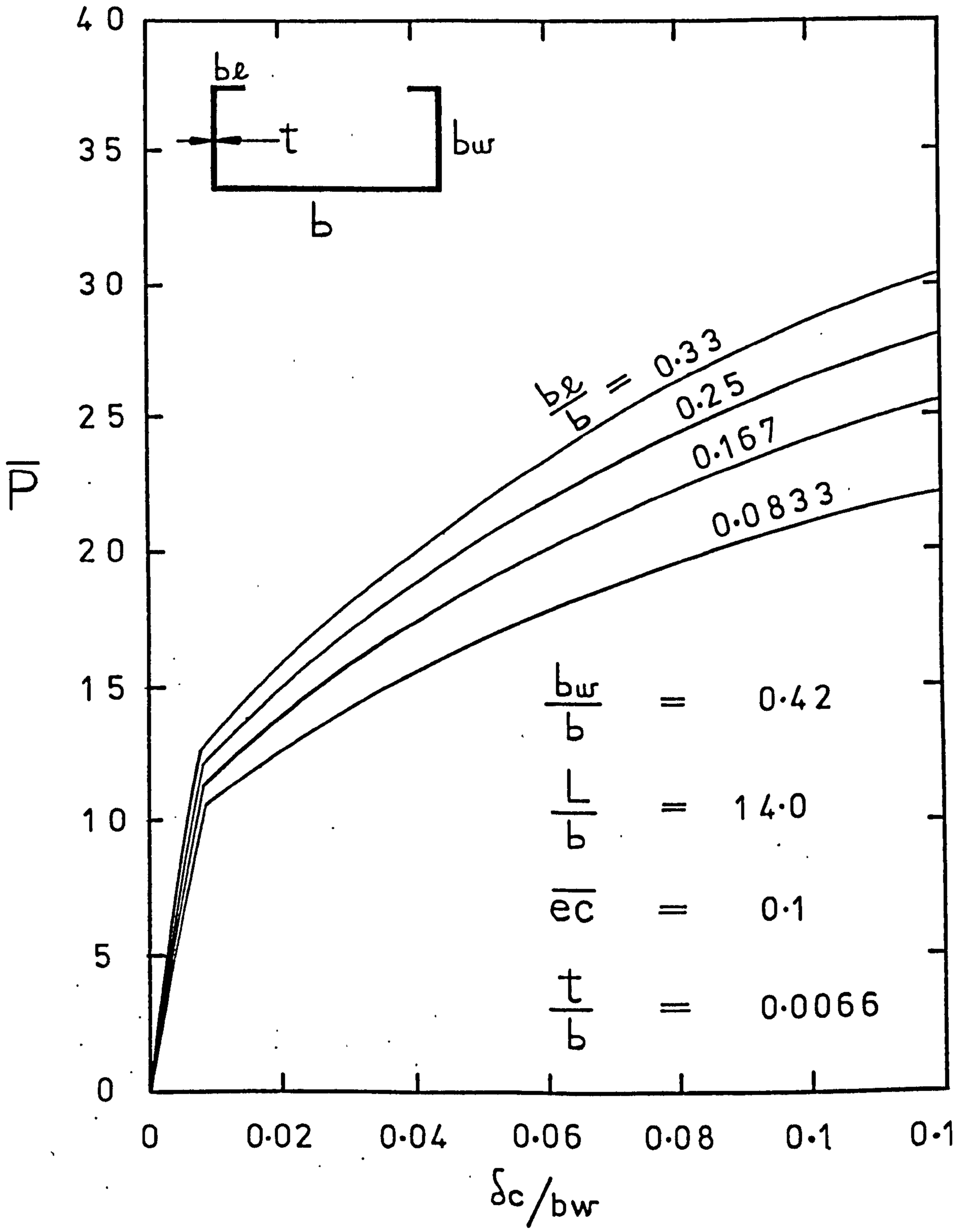

FIG. 4.9.7. LOAD – DEFLECTION CURVES FOR VARIOUS VALUES OF b_ℓ. (ECCENTRICITY TOWARDS FLANGE)

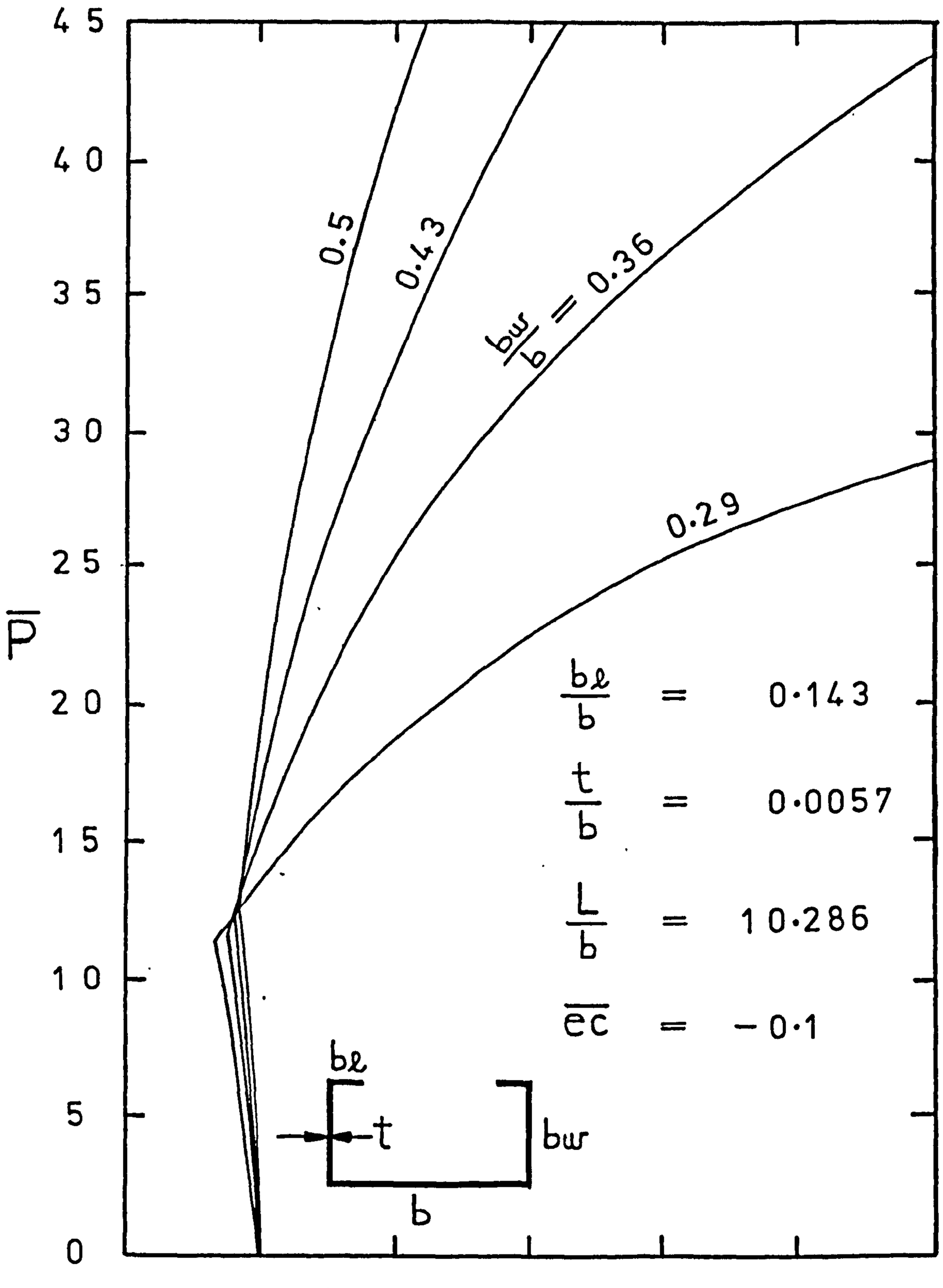

FIG. 4.9.8. LOAD-DEFLECTION CURVES FOR VARIOUS VALUES OF bw. (ECCENTRICITY TOWARDS LIPS)

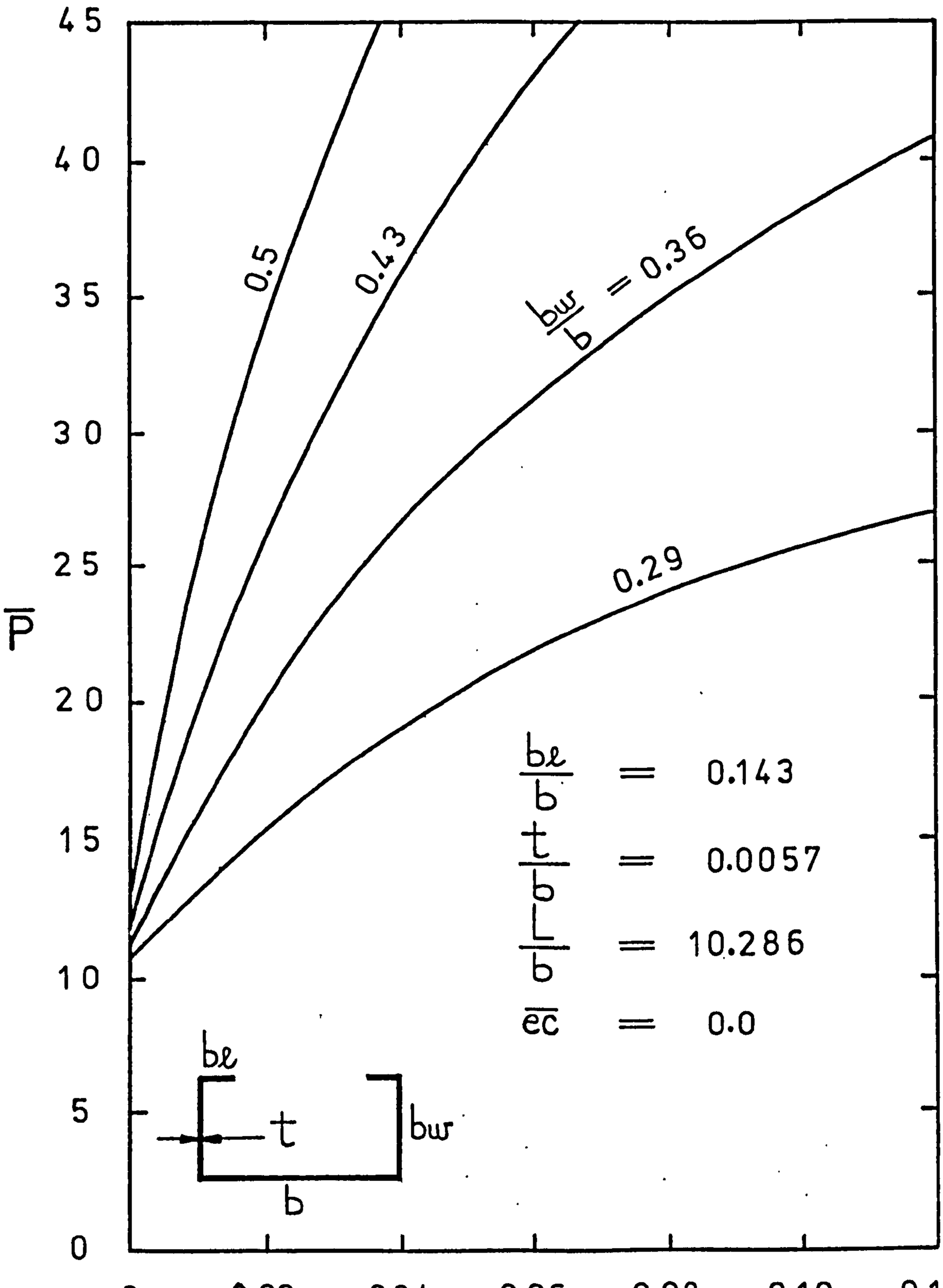

FIG. 4.9.9. LOAD – DEFLECTION CURVES FOR VARIOUS VALUES OF bw. (COLUMN LOADED CENTROIDALLY)

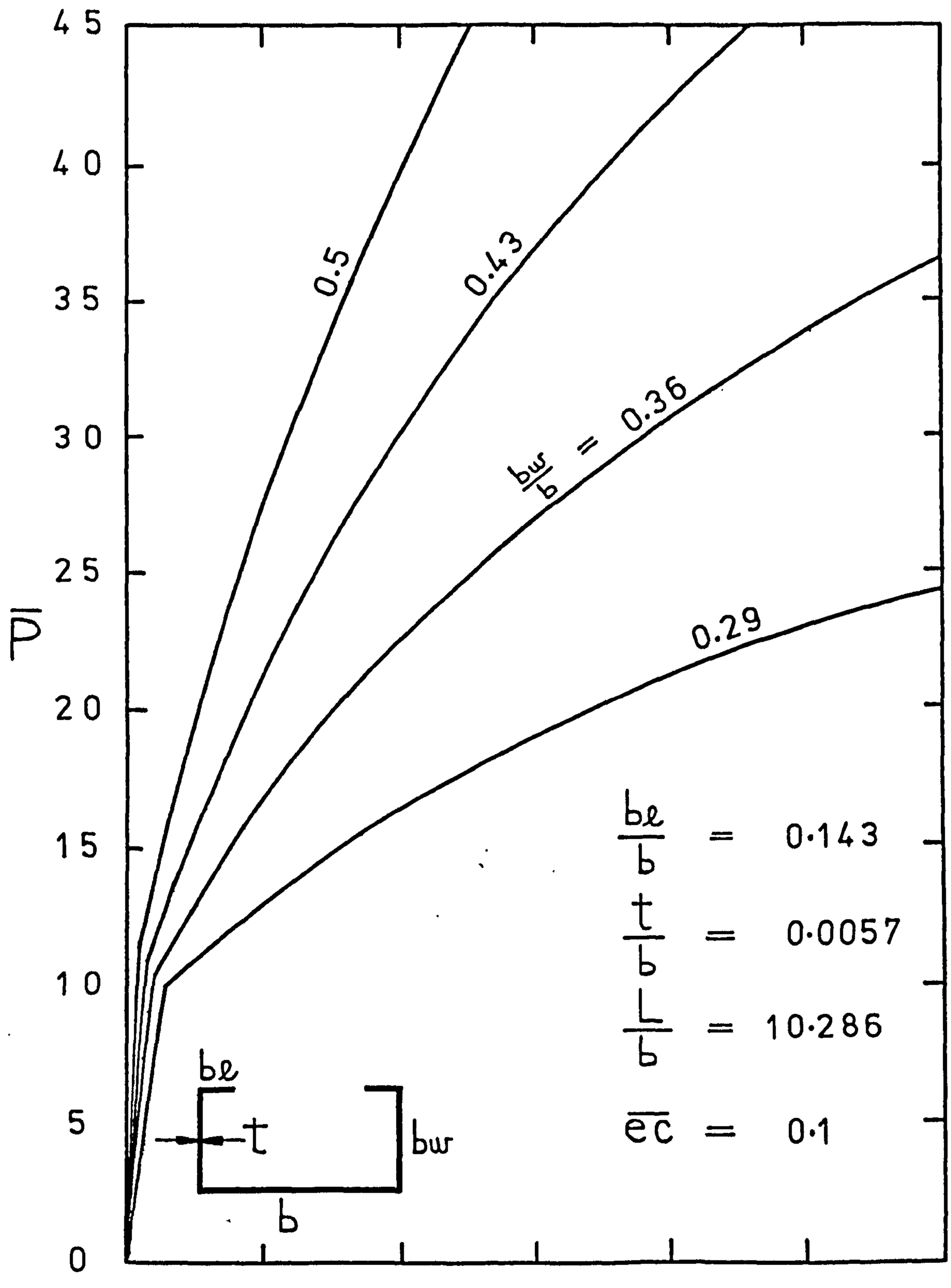

FIG. 4.9.10. LOAD ÷ DEFLECTION CURVES FOR VARIOUS VALUES OF bw. (ECCENTRICITY TOWARDS FLANGE)

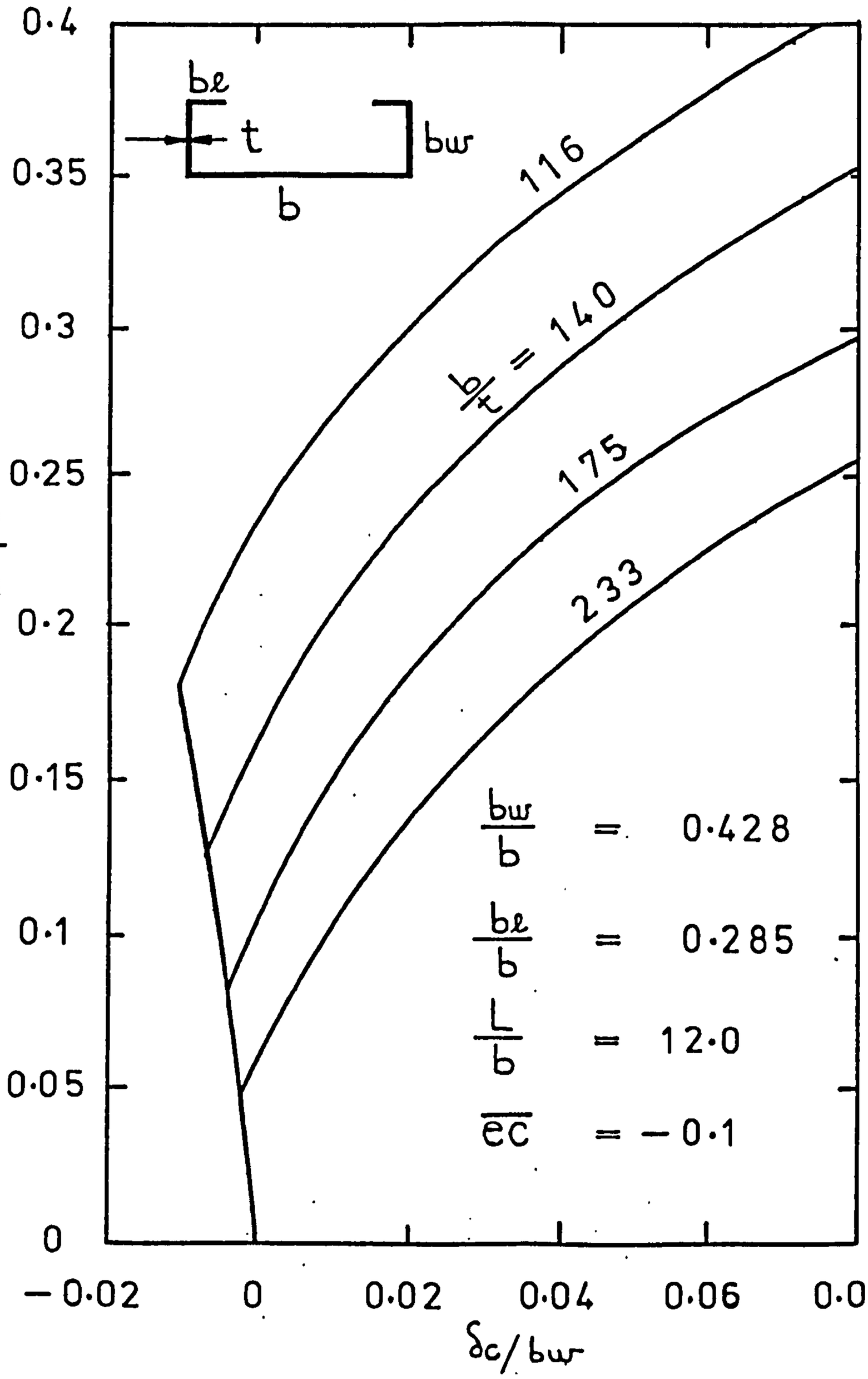

FIG. 4.9.11. LOAD – DEFLECTION CURVES FOR VARIOUS VALUES OF PLATE THICKNESS. (ECCENTRICITY TOWARDS LIPS)

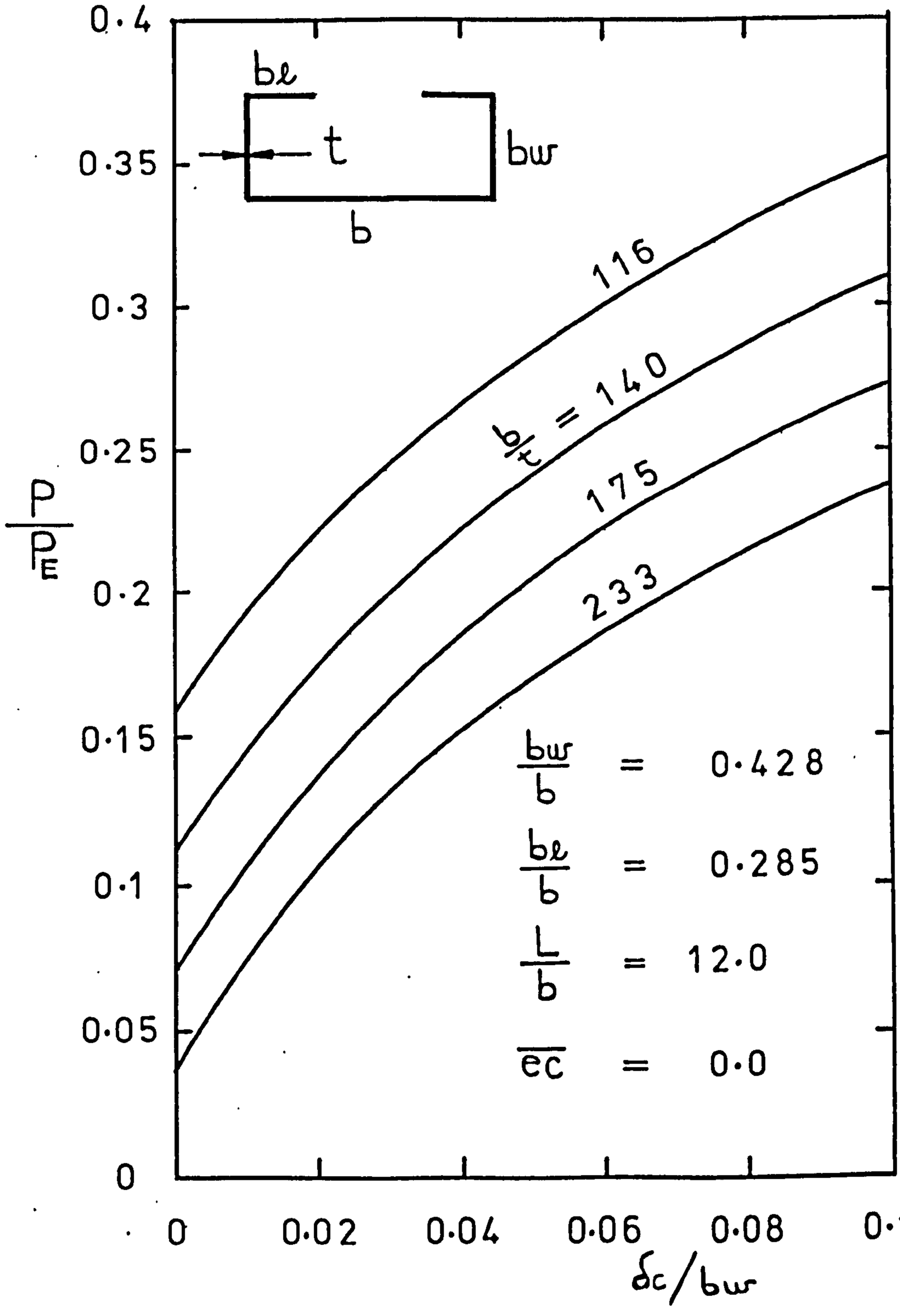

FIG. 4.9.12. LOAD-DEFLECTION CURVES FOR VARIOUS VALUES OF PLATE THICKNESS.
(COLUMN LOADED CENTROIDALLY)

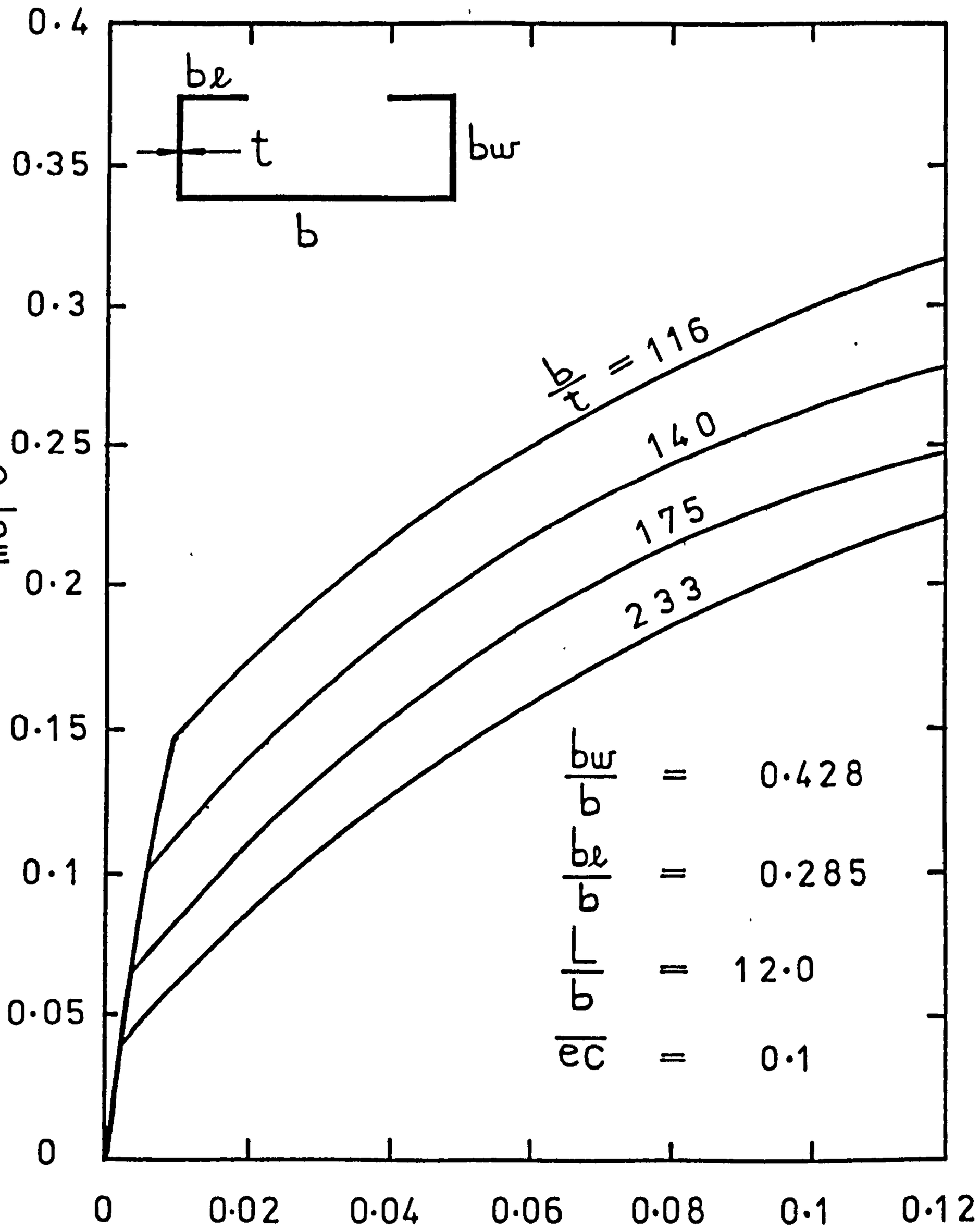

FIG. 4.9.13. LOAD - DEFLECTION CURVES FOR VARIOUS VALUES OF PLATE THICKNESS.

(ECCENTRICITY TOWARDS FLANGE)

1. AXIAL LOAD = 19·32 kN
2. AXIAL LOAD = 25·01 kN
3. AXIAL LOAD = 29·65 kN
4. AXIAL LOAD = 34·15 kN
5. AXIAL LOAD = 38·16 kN

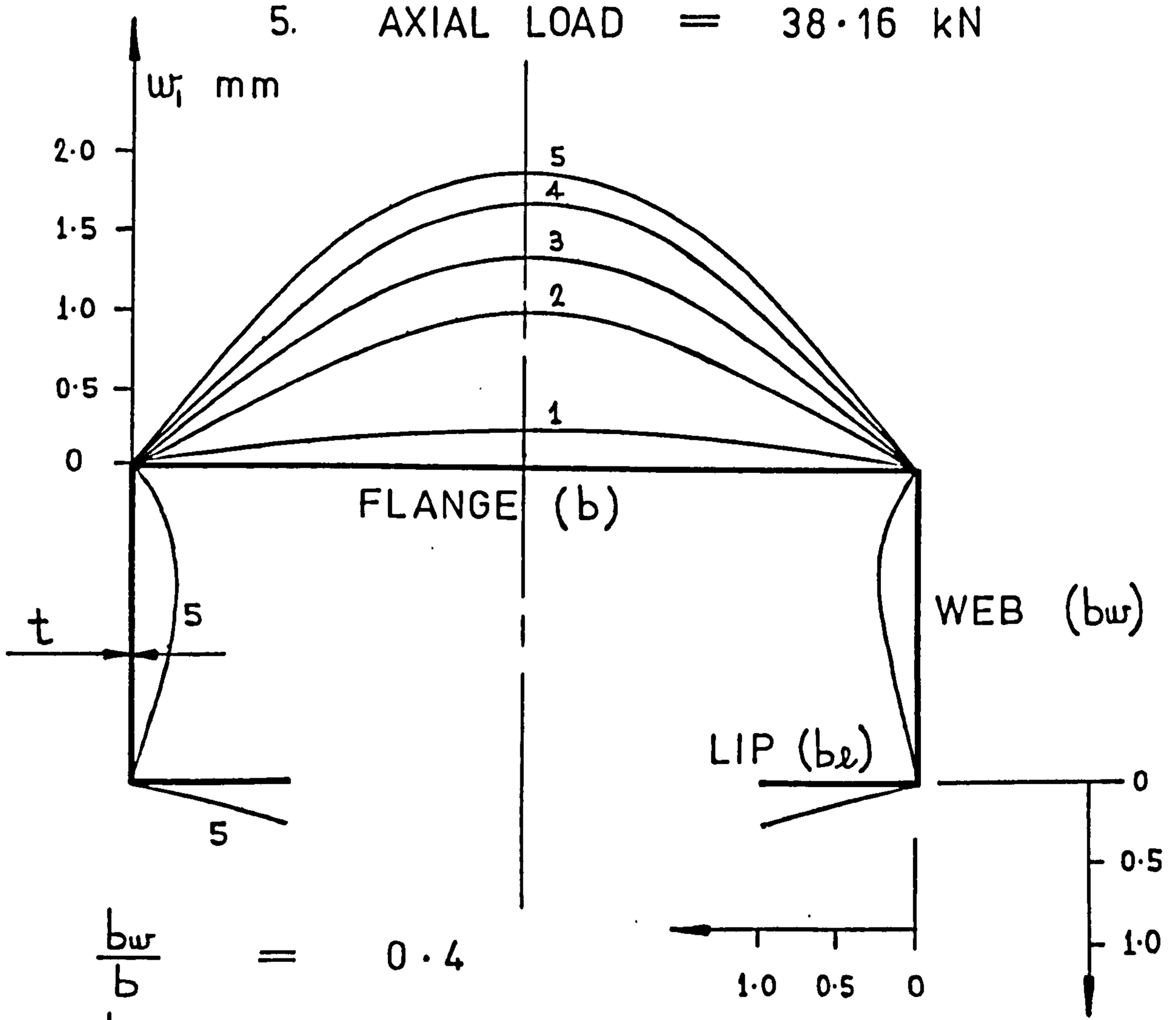

$\frac{b_w}{b}$ = 0·4

$\frac{b_e}{b}$ = 0·2

$\frac{t}{b}$ = 0·008

$\frac{L}{b}$ = 12·0

$\frac{e}{c}$ = 0·0

FIG. 4.9.14.

GROWTH OF BUCKLED FORM AT CREST OF CENTRAL BUCKLE.

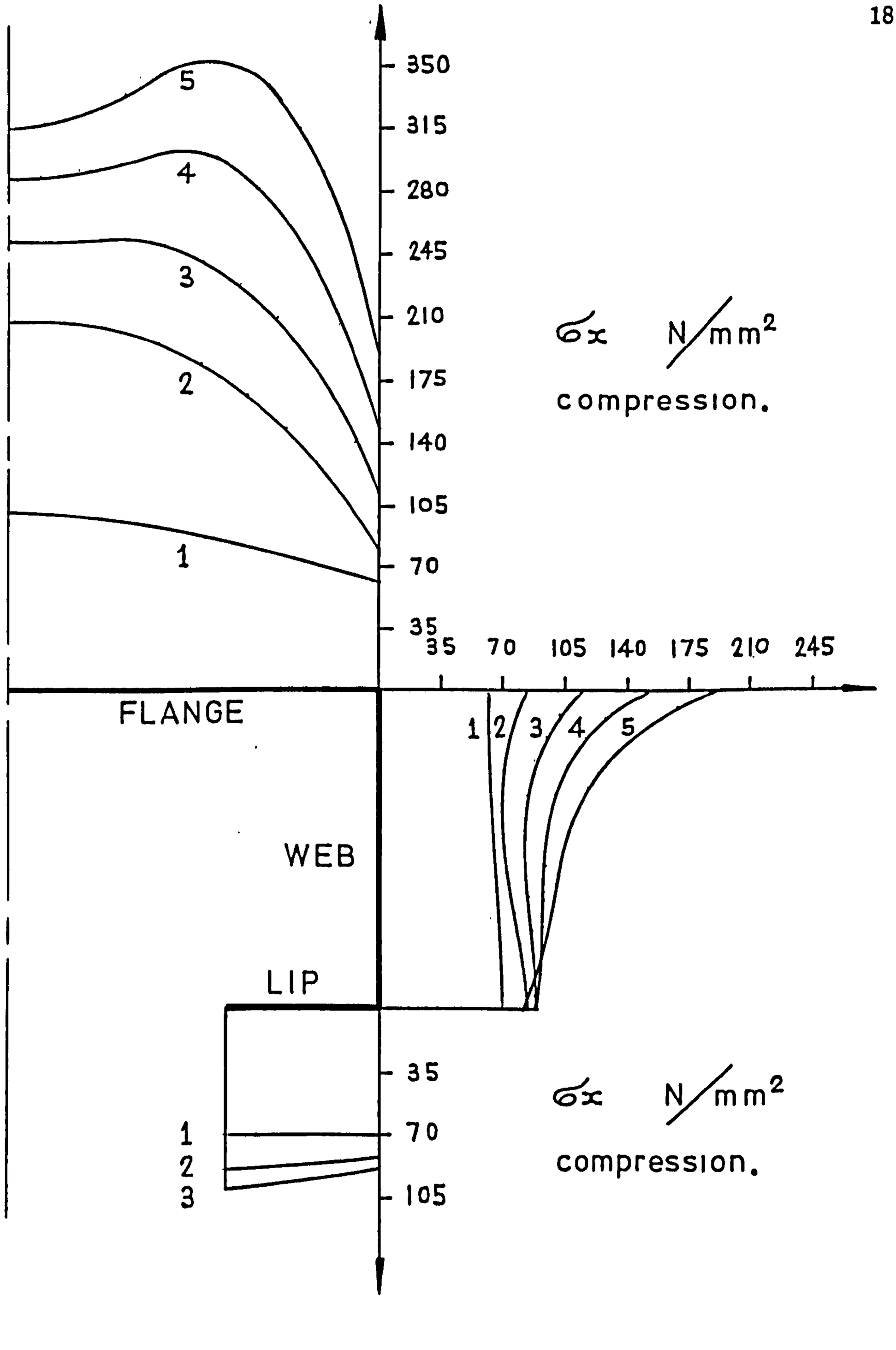

FIG. 4.9.15.

GROWTH OF INSIDE SURFACE STRESS DISTRIBUTION AT CREST OF CENTRAL BUCKLE.

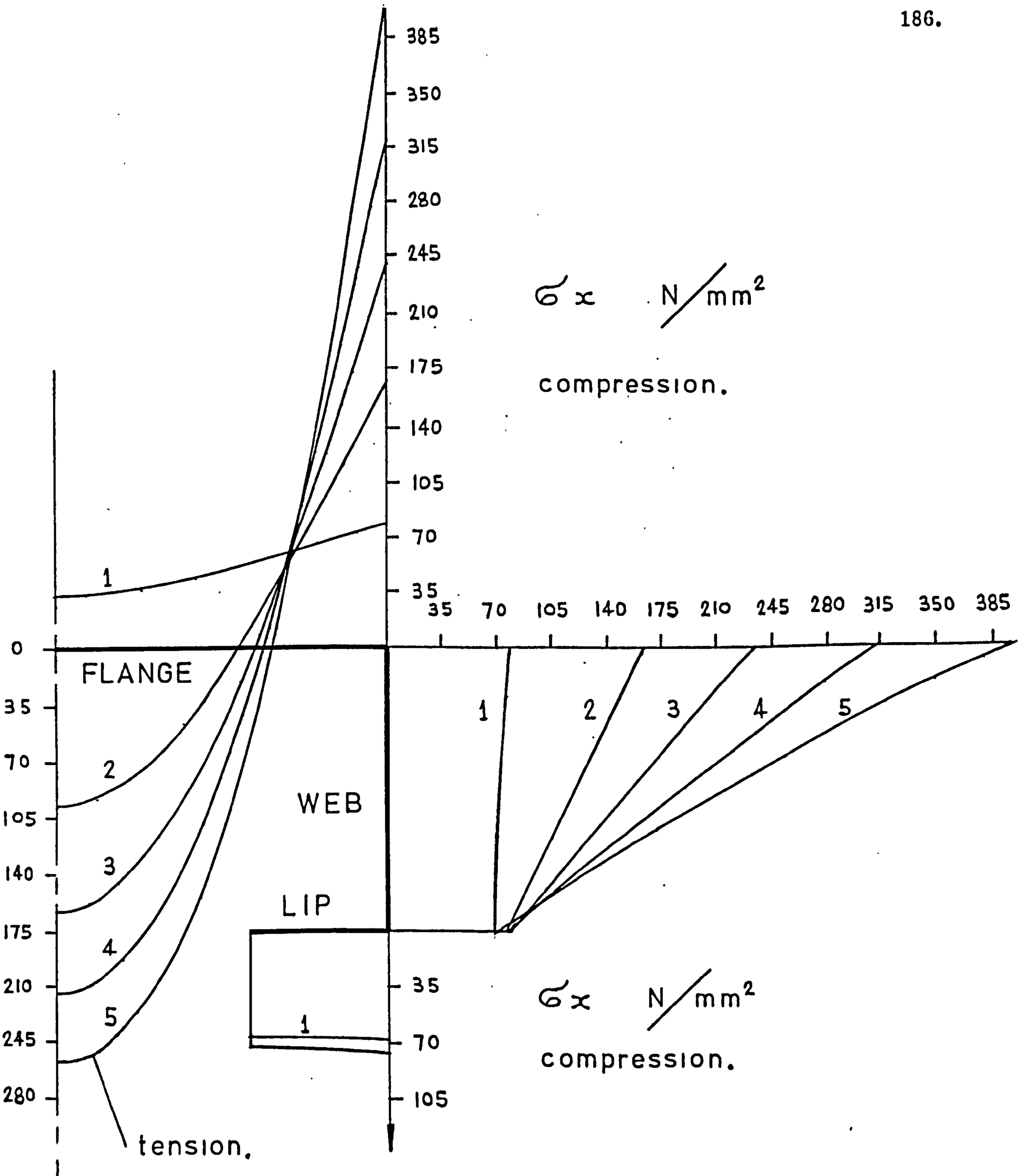

FIG. 4.9.16.

GROWTH OF OUTSIDE SURFACE STRESS DISTRIBUTION AT CREST OF CENTRAL BUCKLE.

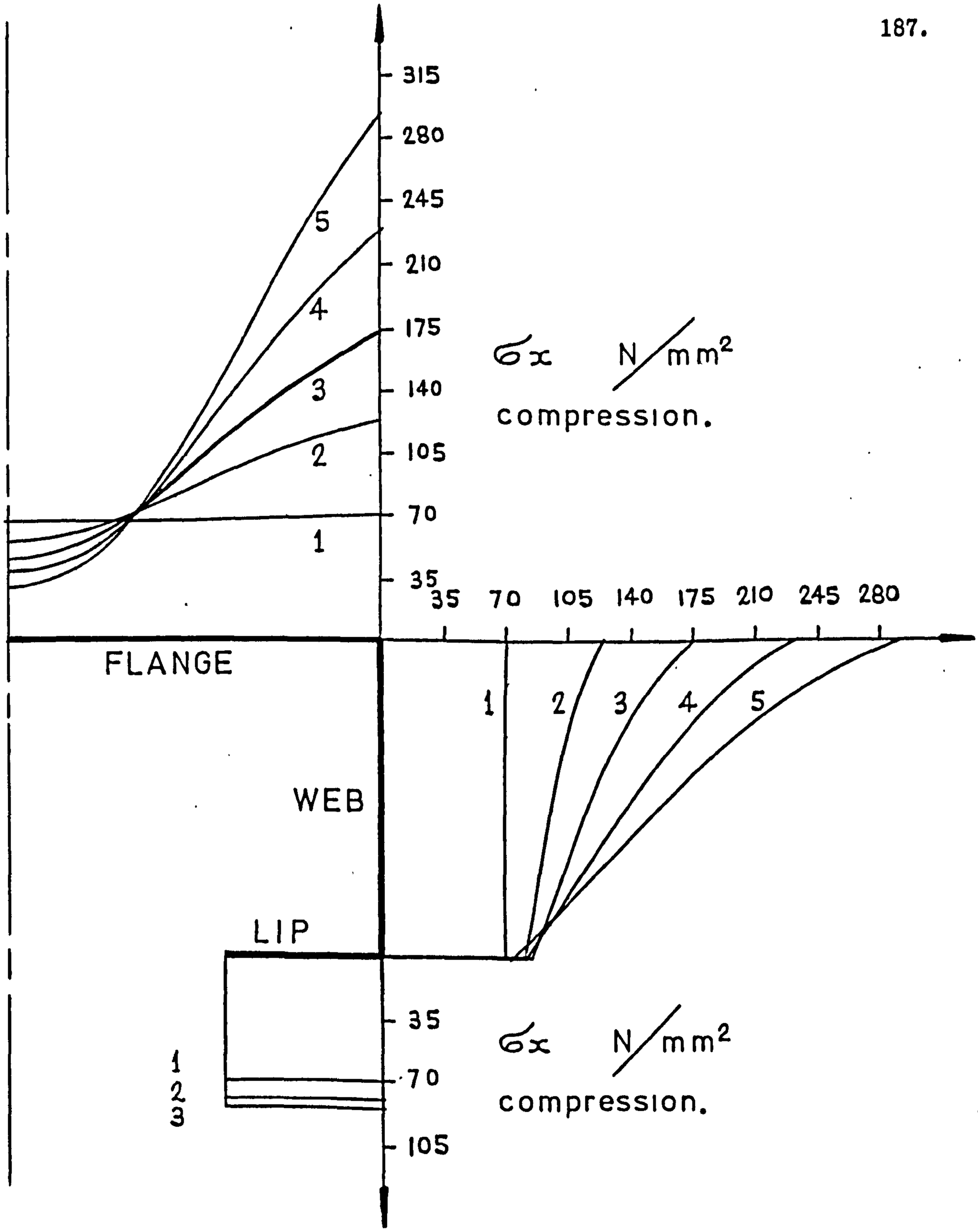

FIG. 4.9.17.

GROWTH OF MEMBRANE STRESS DISTRIBUTION AT CREST OF CENTRAL BUCKLE.

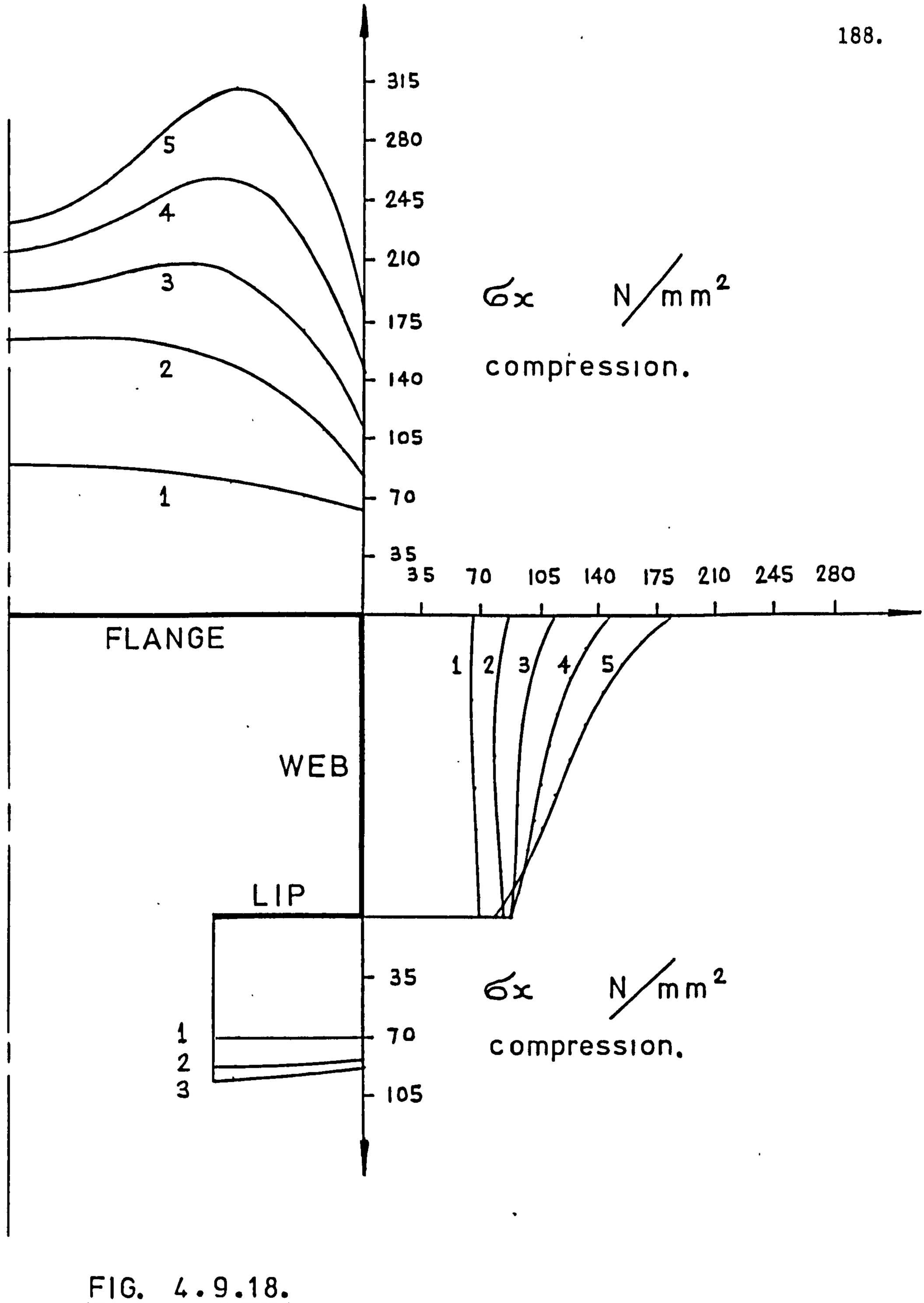

FIG. 4.9.18.

GROWTH OF INSIDE SURFACE STRESS DISTRIBUTION MID-WAY BETWEEN CREST AND NODE OF CENTRAL BUCKLE.

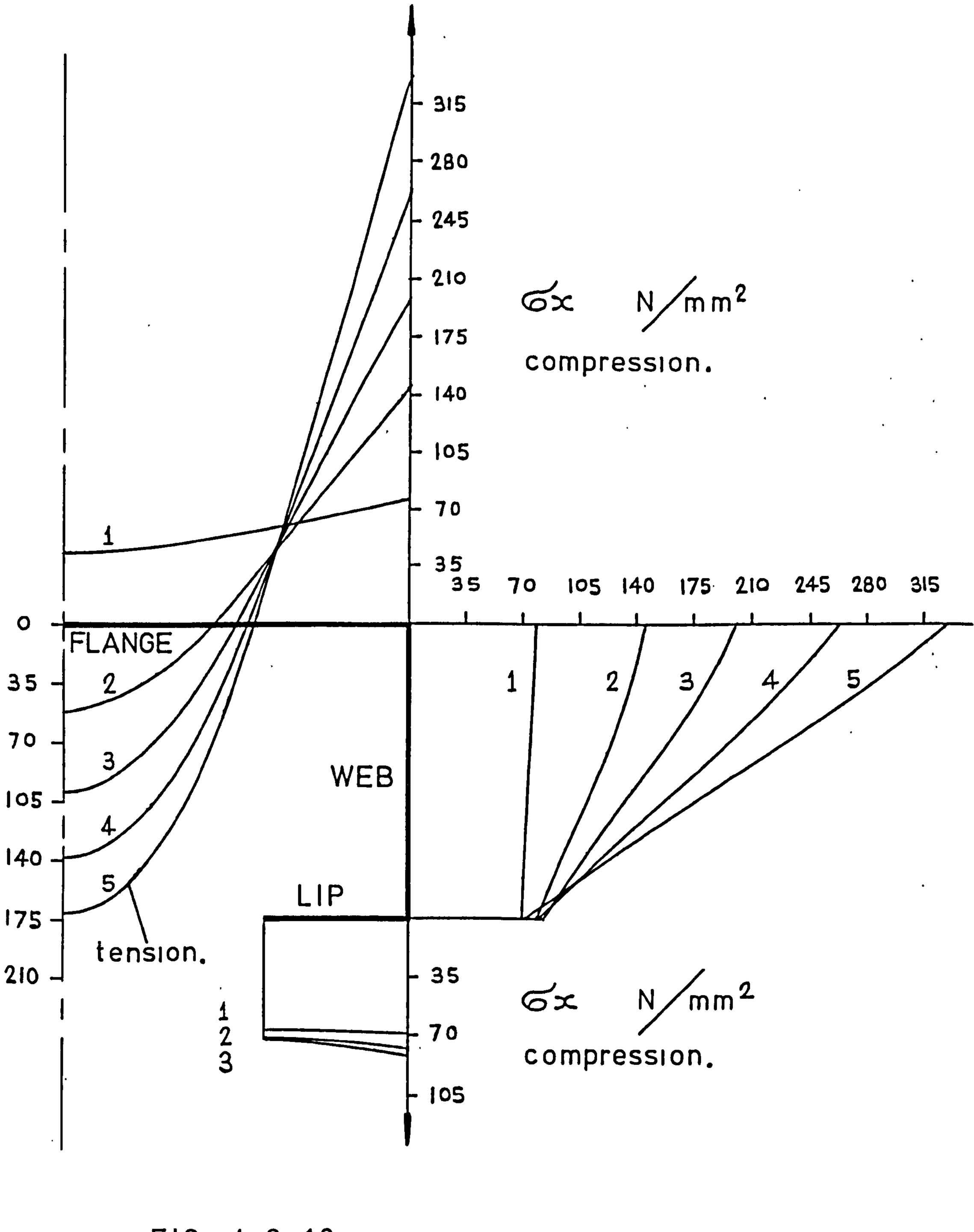

FIG. 4.9.19.

GROWTH OF OUTSIDE SURFACE STRESS DISTRIBUTION MID-WAY BETWEEN CREST AND NODE OF CENTRAL BUCKLE.

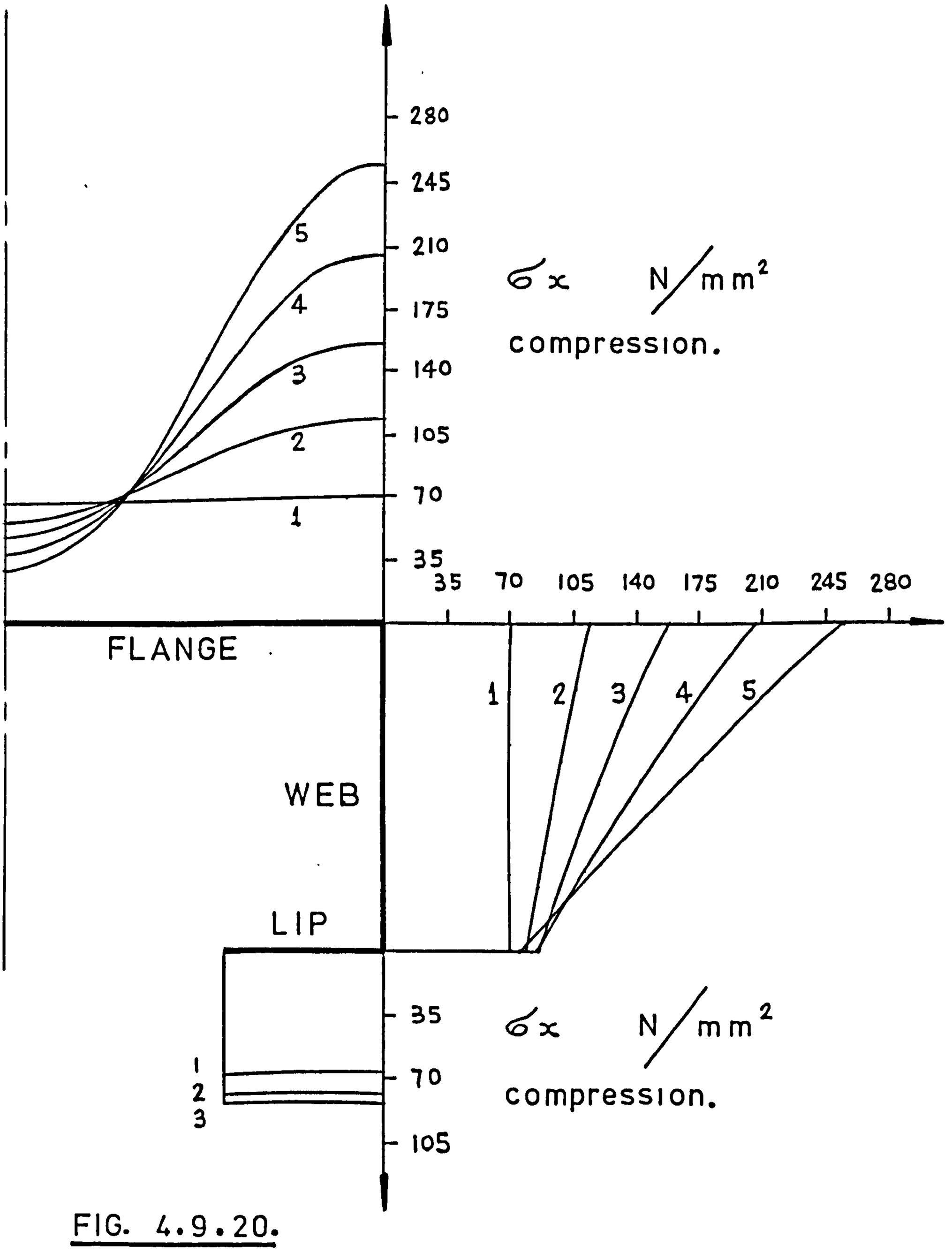

FIG. 4.9.20.

GROWTH OF MEMBRANE (AVERAGE) STRESS DISTRIBUTION MID-WAY BETWEEN CREST AND NODE OF CENTRAL BUCKLE.

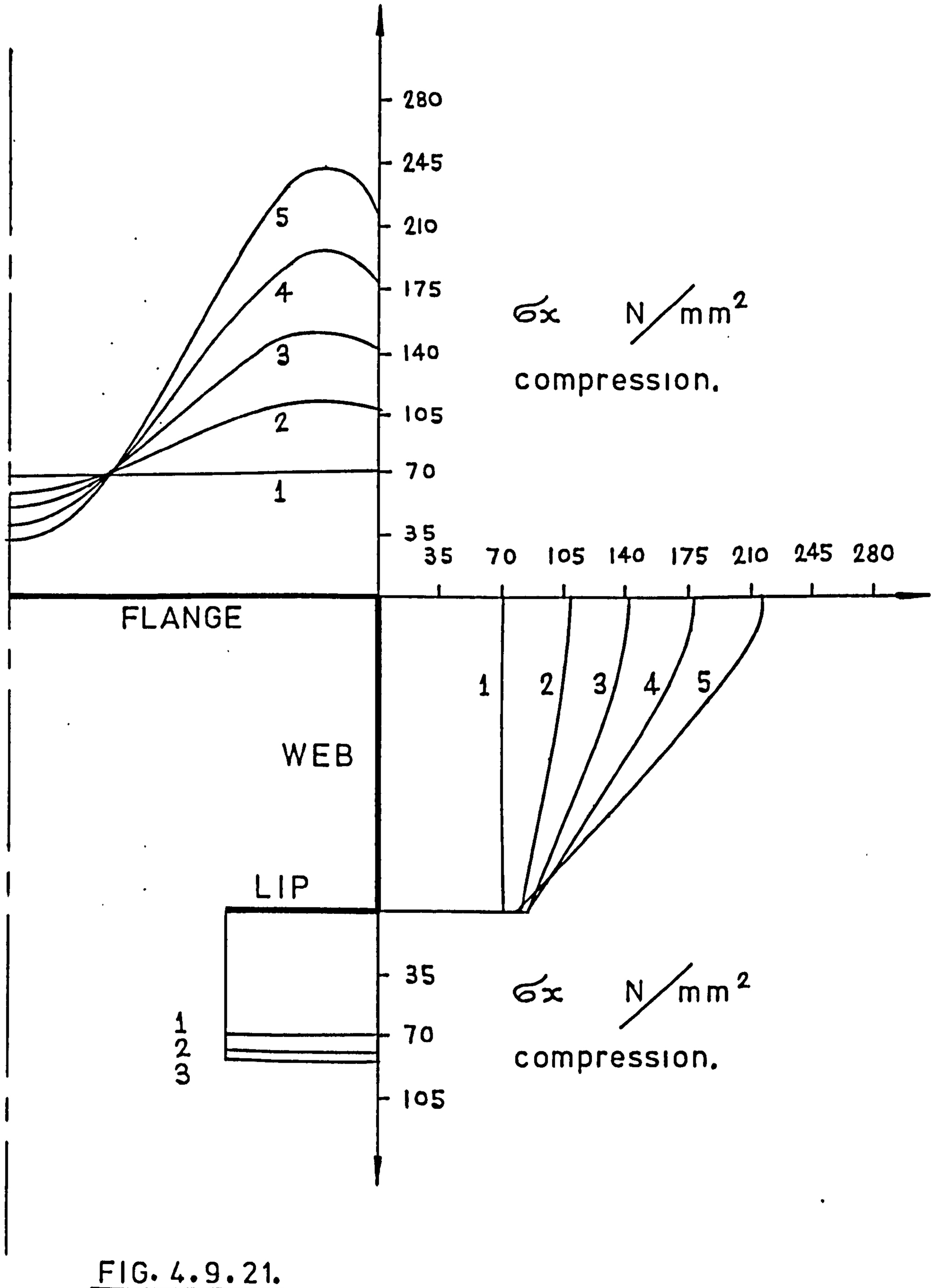

FIG. 4.9.21.

GROWTH OF MEMBRANE STRESS DISTRIBUTION AT NODE OF CENTRAL BUCKLE.

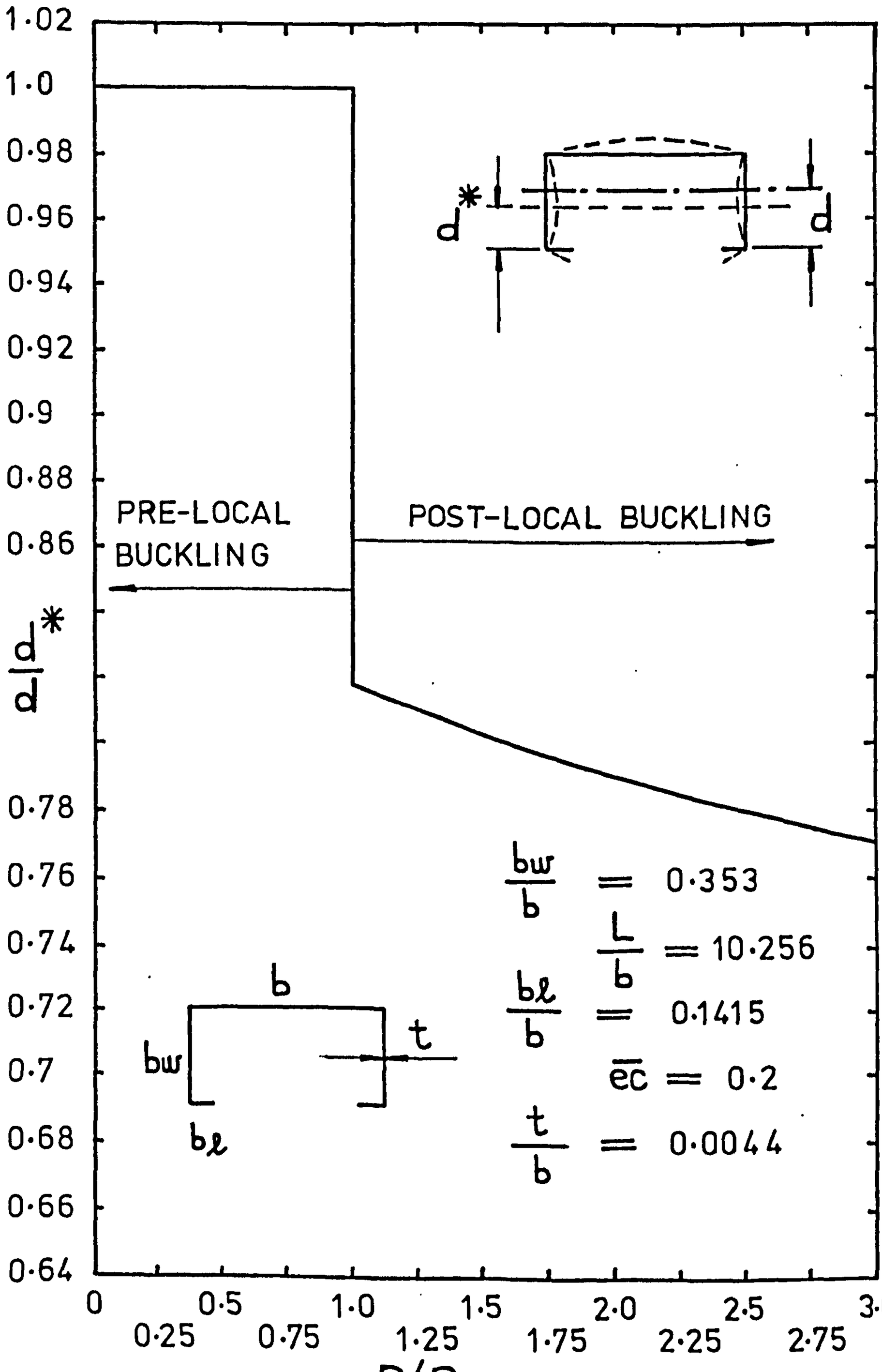

NEUTRAL AXIS SHIFT IN THE POST-BUCKLING RANGE.

FIG 4.9.22.

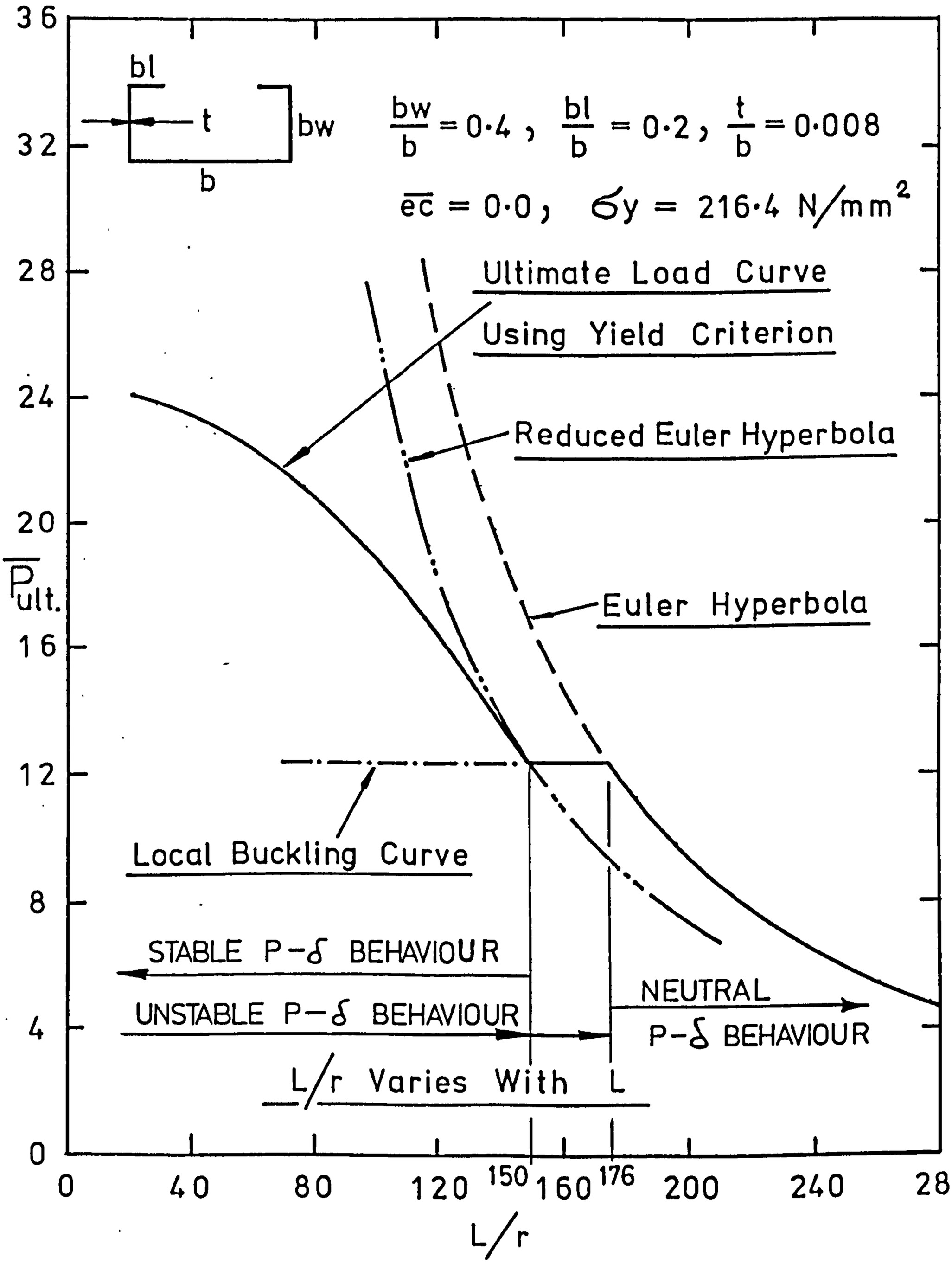

FIG.4.9.23.ULTIMATE LOAD VERSUS SLENDERNESS — RATIO FOR CONCENTRICALLY LOADED COLUMNS. SLENDERNESS RATIO VARYING WITH L.

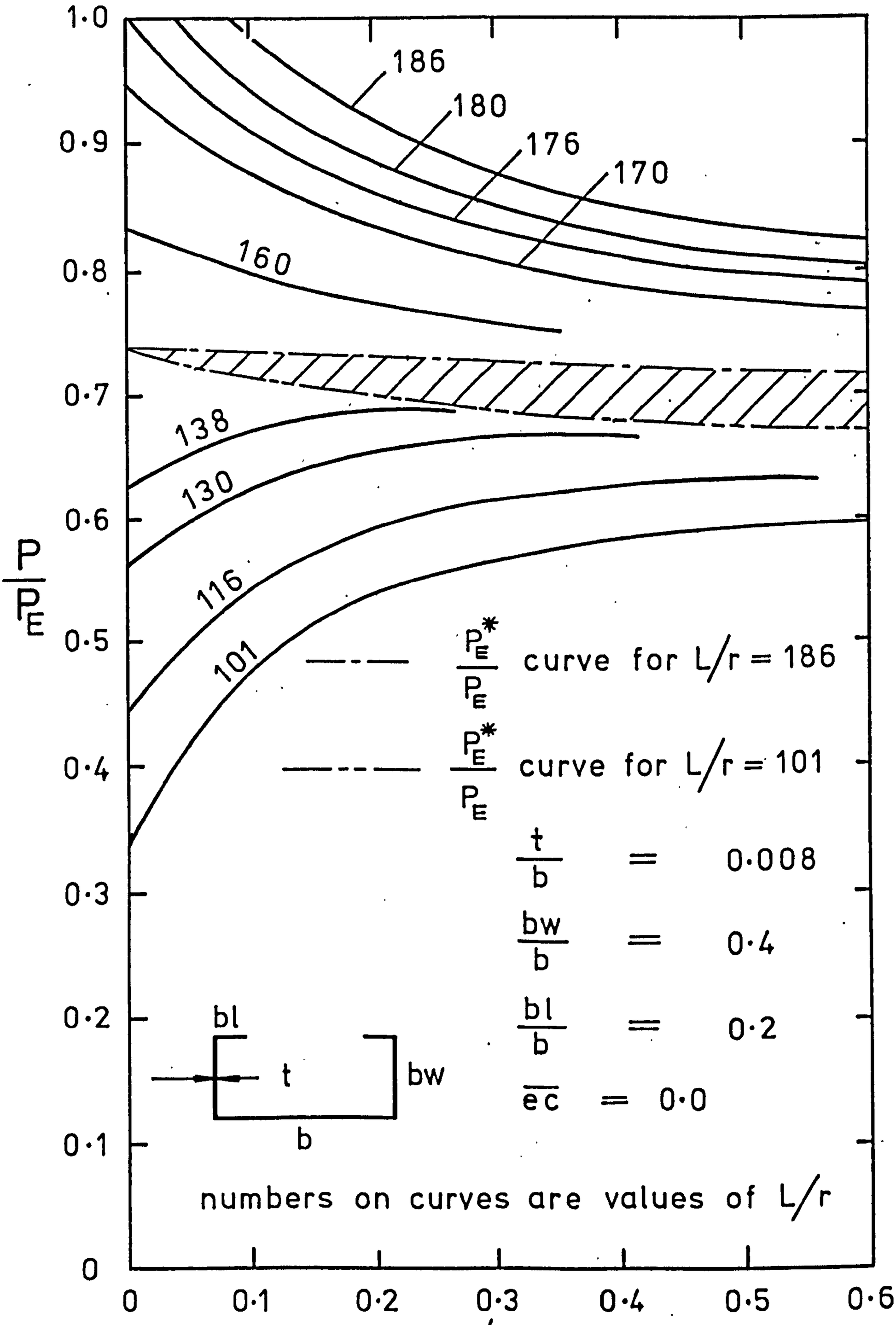

FIG. 4.9.24. STABLE AND UNSTABLE LOAD–DEFLECTION EQUILIBRIUM PATHS.

SLENDERNESS-RATIO VARYING WITH L.

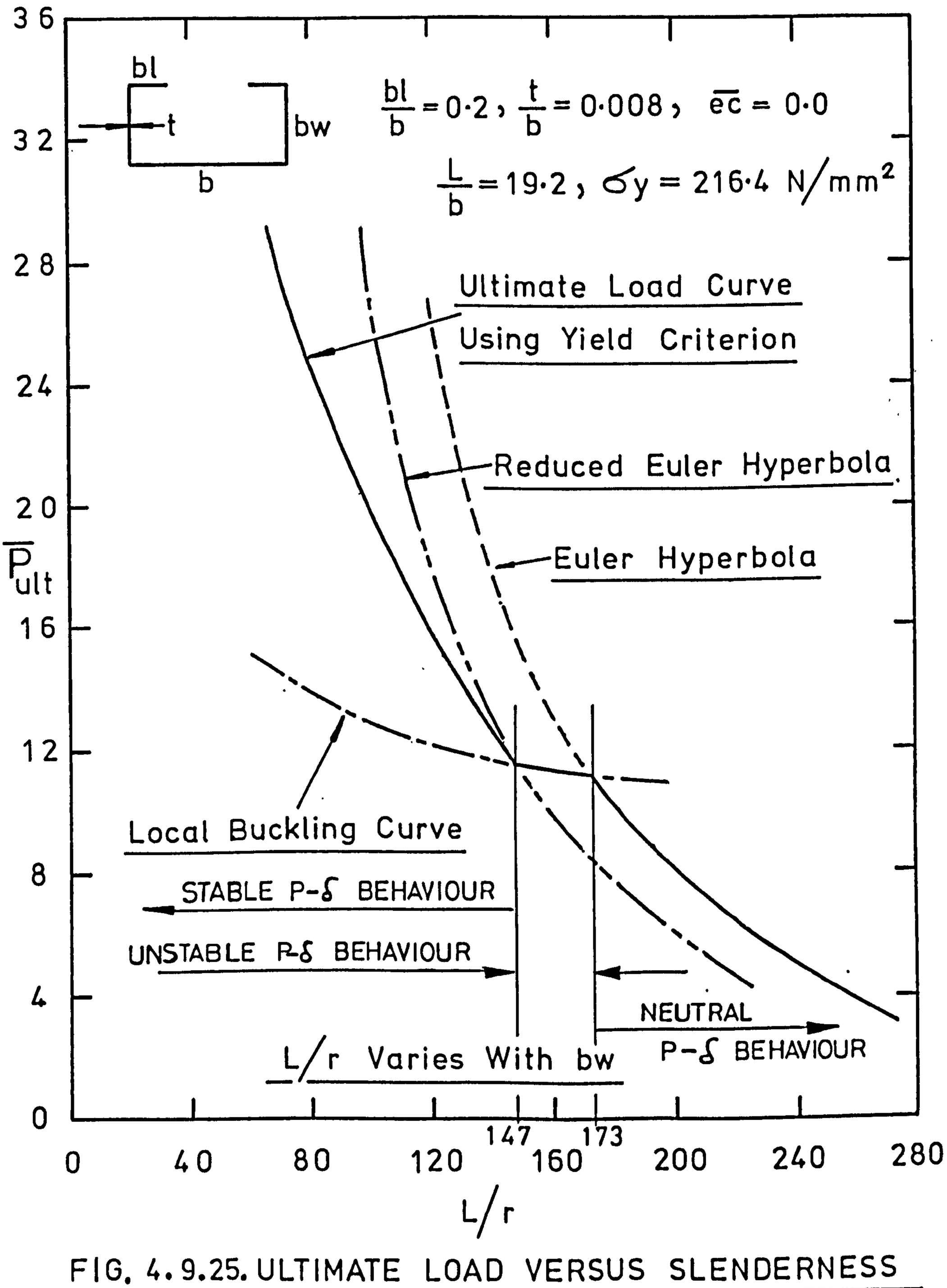

FIG. 4.9.25. ULTIMATE LOAD VERSUS SLENDERNESS — RATIO FOR CONCENTRICALLY LOADED COLUMNS. SLENDERNESS-RATIO VARYING WITH bw.

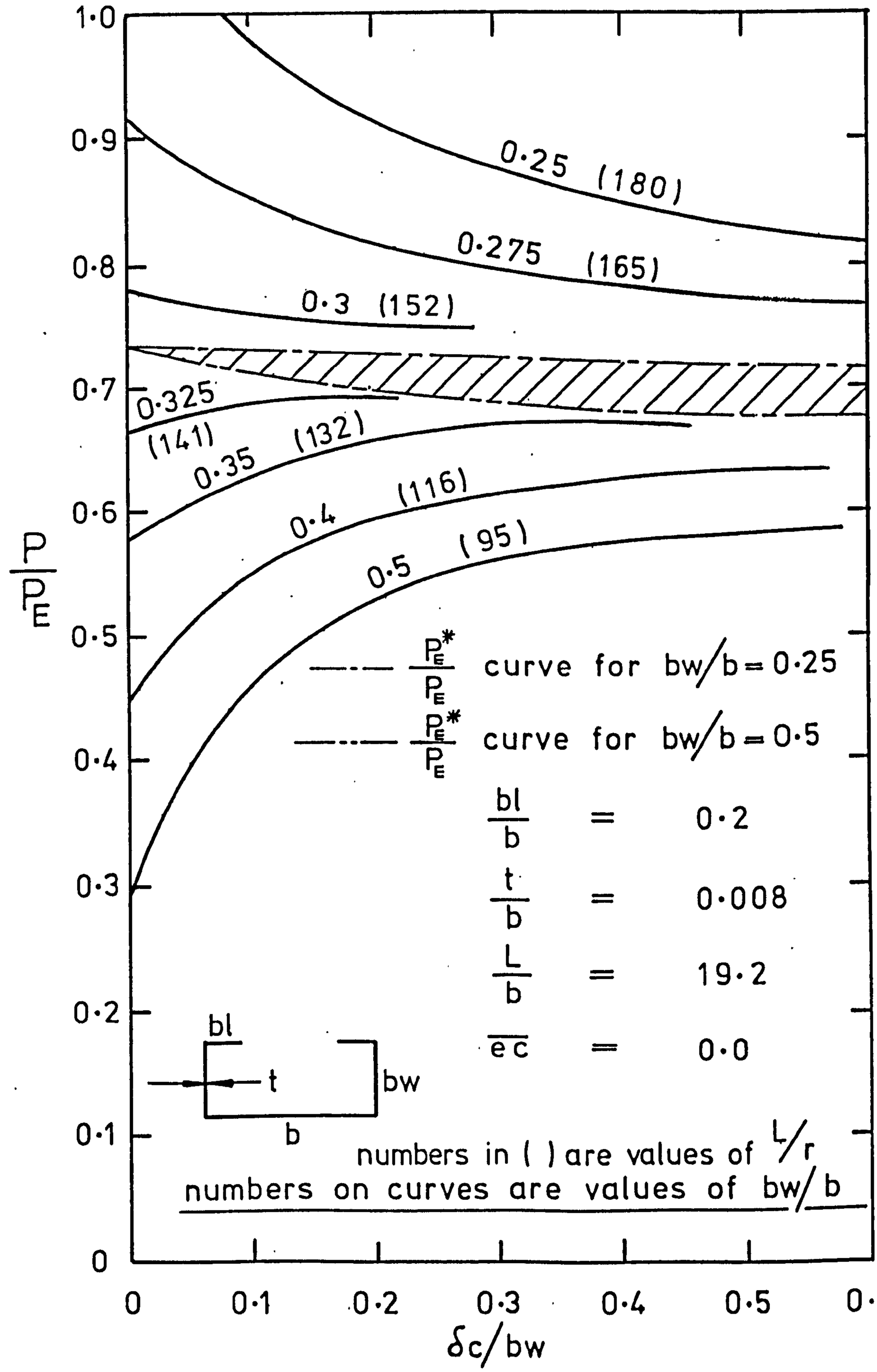

FIG.4.9.26. STABLE AND UNSTABLE LOAD—DEFLECTION EQUILIBRIUM PATHS. SLENDERNESS-RATIO VARYING WITH bw.

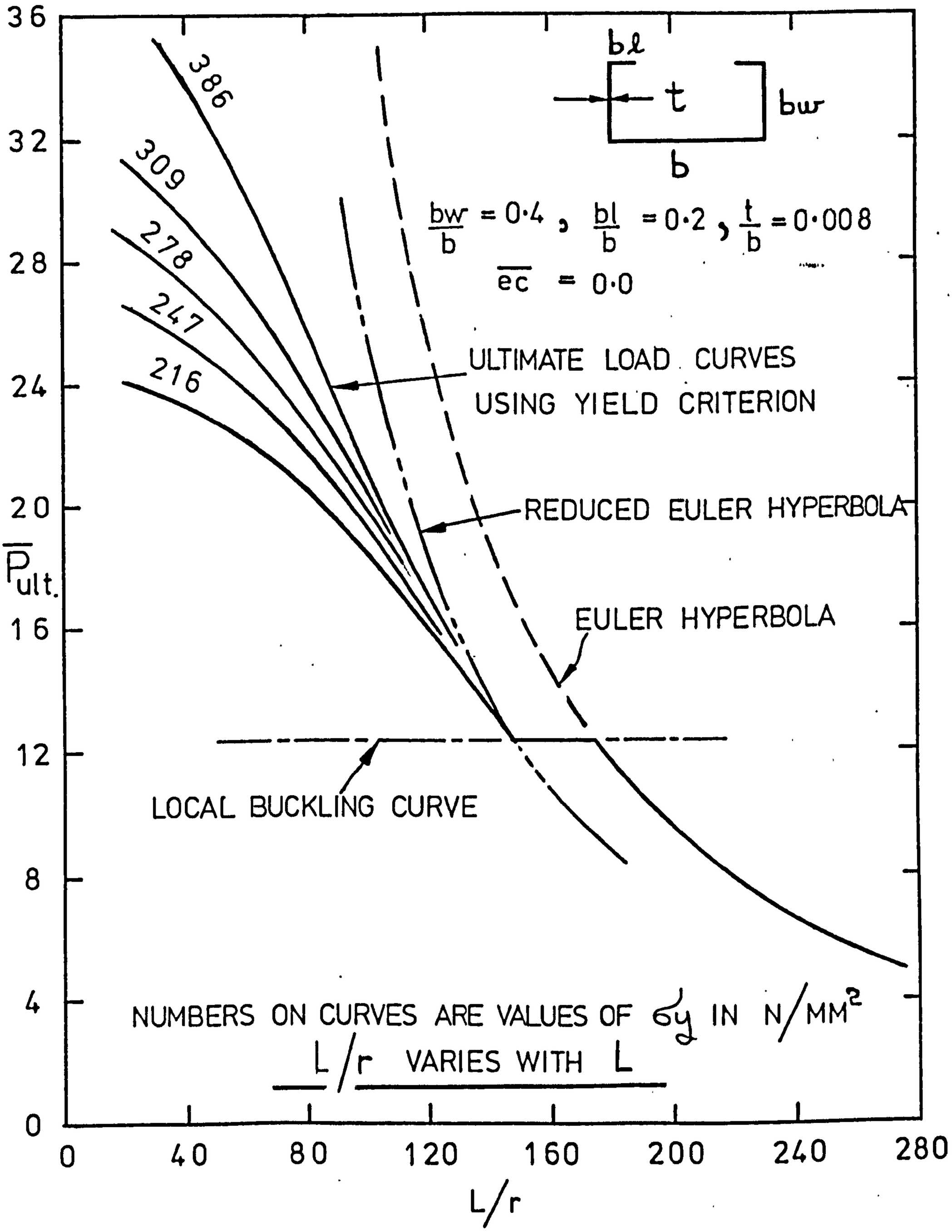

FIG. 4.9.27. ULTIMATE LOAD – SLENDERNESS CURVES FOR VARIOUS VALUES OF MATERIAL YIELD STRESS.

CHAPTER FIVE

EXPERIMENTAL INVESTIGATION

5.0 EXPERIMENTAL INVESTIGATION

5.1 OBJECTS OF THE INVESTIGATION

An experimental investigation was carried out to obtain information on the interactive buckling behaviour of thin walled lipped channel columns under concentric or eccentric loading.

To carry out the tests in the investigation a rig was designed by the author and manufactured in the University's laboratories. The rig was capable of providing pinned conditions at the column ends and of applying accurate uni-axial eccentricities about the axis of least second moment of area of the section. The dimensions of the columns tested were such that the local buckling loads were much smaller than the Euler buckling loads thus providing stable interaction behaviour after initial instability.

The general aim of the investigation was to observe the behaviour of the columns during their entire loading history and to provide experimental results to authenticate the validity of the theoretical solutions developed in Chapters Three and Four. The main objectives within this general aim are listed as follows.

1. To determine the values of the loads to initiate local instability in the columns.
2. To observe the column load-deflection behaviour throughout all stages of loading.

3. To determine the variation of the stress distributions throughout loading by means of strain gauges.

4. To obtain the values of the loads required to collapse the columns.

5.2 TEST SPECIMENS

The lipped channel columns were manufactured by cold pressing from mild steel sheet, thirty three columns in all being tested to collapse.

A check was made for "springback" of the right angle bends between the flange and web and between the web and lip at various positions along the lengths of several columns. The accuracy of the bends was found to be good. To eliminate any torsional effects during loading, the ends of the columns were filed accurately square with the column axis.

The sheet thickness and the outside dimensions of the flange, web and lip were measured at twelve different cross sections along the length of each column and the average of the values obtained taken as the cross sectional dimensions for the particular column considered. In this way the average centre line dimensions were obtained for each cross section for use as data in the computer solution.

The columns were manufactured in three different lengths 1219 mm, 1524 mm and 1829 mm and four different flange widths 102 mm, 127 mm, 152 mm and 178 mm. Two thicknesses of sheet were considered, 0.79 mm and 1.6 mm, two values of the web dimension, 51 mm and 64 mm, and two values of lip dimension 19 mm and 25 mm. These variations in dimensions were chosen so that stable column behaviour would be exhibited after the initiation of local buckling, since such columns are more likely to be used practically than those exhibiting unstable behaviour.

Values of yield stress and Young's Modulus were obtained from a number of standard tensile tests carried out on specimens cut from the flanges and webs of the columns tested. A Tinius Olsen testing machine was used to apply the loads while elongation of the specimens was measured by an electronic extensometer fitted over a 50 mm gauge length of the specimens.

Movements of the extensometer during loading were automatically plotted in the form of load-strain curves on the pen-recorder drum of the Tinius Olsen's loading system. From these curves the values of Young's Modulus and material yield stress were obtained.

A total of 16 specimens in all were tested, 8 specimens for each thickness of sheet considered. The average values of each parameter for use in the theoretical computer solutions were

as follows.

Material Thickness	Young's Modulus	Yield Stress
0.79 mm	201 kN/mm^2	242 N/mm^2
1.6 mm	208 kN/mm^2	233 N/mm^2

Poisson's Ratio was obtained from a number of tensile tests using strain gauges to measure the longitudinal and transverse surface strains at the centre of each specimen gauge length. The average value of ν obtained from these tests and the value used in the theoretical calculations was $\nu = 0.3$.

5.3 TEST RIG AND LOADING MACHINE

The test rig consists basically of two identical locating units which transmit the applied loading from the loading machine to the ends of the constituent plate elements of the column. Figure 5.3.1 shows the two locating units with a column in position while Figure 5.3.2 shows the plan and elevation of one of the units indicating the various component parts.

The basic principle of operation of the test rig is the movement of an end plate assembly unit, which locates and clamps the column ends, within a main base assembly unit, which has the load applied through its centroid. The end plate assembly can therefore be positioned such that the column centroid is coincident with the load centroid or at any desired eccentricity.

With reference to the general assembly of Figure 5.3.2, the main base assembly consists of the base plate of Figure 5.3.3, the guide bars of Figure 5.3.6, the datum block of Figure 5.3.9 and the loading block of Figure 5.3.13. To ensure good alignment with the end plate assembly the surfaces of the base plate and guide bars were accurately ground to size, the guide bars being positioned on the base plate with two 10 mm diameter dowels and held in position with three 10 mm diameter screws.

The loading block is fitted to the underside of the base plate with four 12 mm diameter screws and is positioned such that the load from the loading pin, Figure 5.3.12, is applied through the centroid of the base plate.

The datum block which, in conjunction with the calibrated positioning handle of Figure 5.3.10, measures the relative movement between the two assemblies, is fitted to the front side of the base plate with two 6 mm diameter screws as shown in Figure 5.3.2.

Due to the high bearing pressures between the loading pin and loading block, the spherical nose of the pin and the spherical recess of the block were hardened and polished. The spherical connection between the loading pin and block satisfying the theoretical requirement of pinned conditions at the column ends.

Again with reference to Figure 5.3.2, the end plate assembly consists of the end plate of Figure 5.3.4, the web and flange locating bars of Figure 5.3.5, the clamping plate of Figure 5.3.7; the wedge clamping pads of Figure 5.3.8 and the calibrated positioning handle of Figure 5.3.10.

The surfaces of the end plate were accurately ground to size to produce an easy sliding fit between the guide bars of the main base assembly. Fitted to the end plate, by means of 6 mm diameter screws, are the web and flange locating bars which locate the outside surfaces of the webs and flange along a line contact as can be seen from the detail of Figure 5.3.5. The webs and flange of the column are clamped against the web and flange locating bars by means of the clamping plate and wedge clamping pads of Figures 5.3.7 and 5.3.8 respectively. The clamping plate is fixed to the end plate by means of a 10 mm diameter screw and washer assembly; the screw fitting in a clearance slot in the clamping plate which allows perpendicular movement of the plate to the axis of the column.

When the clamping plate is pushed forward against the inside of the flange, it clamps the flange against the flange locating bar. In this position the screw and washer assembly are tightened and the wedge clamping pads are forced outwards to clamp the webs against the web locating bars. Due to the line contact on the inside and outside surfaces of the flange and webs,

this system of clamping the column ends provides simple support conditions to the flange and web plate elements of the section. The system however, does not clamp the lip plate element of the section.

Once the column has been located and clamped in the end plate assembly it is then positioned relative to the load centre of the main base assembly with the desired eccentricity by means of the calibrated positioning handle and datum block. The column is then locked in this position by means of the clamping screws of Figure 5.3.11 which are screwed into the end plate assembly through slots in the main base plate.

By manufacturing different sizes of clamping plates and wedge clamping pads as indicated in Figures 5.3.7 and 5.3.8, and by being able to fix the web locating bars in several positions on the end plate as shown by the various sets of tapped holes in Figure 5.3.4, the test rig was made capable of accommodating the variations in column cross sectional dimensions considered in the experimental investigation.

Figures 5.3.14 and 5.3.15 show pictorially the top and bottom connections respectively of a column under test in the loading machine. The figures show each locating unit in three dimensions and clearly indicate the end plate assembly unit, complete with its clamping system, housed in the main base assembly unit.

The machine used to apply the loads in the experimental investigation was a Tinius Olsen electro-mechanical testing machine. This machine is equipped with four load ranges and has a maximum capacity of 890 kN. The crosshead of the machine is raised and lowered by means of four pulling screws; these screws rotating in opposite directions which virtually eliminates the possibility of torsional stresses being applied to test specimens.

Figure 5.3.16 shows the Tinius Olsen indicating and control unit. The range selector switch changes the capacity range of the indicating system and the dial automatically shows the maximum value of the chosen range and the value of each scale division. Having chosen the load range the scales on the indicating dial are adjusted by means of the zero indicating knobs.

Testing speeds are electrically selected by means of the speed control dial and are infinitely variable within the speed range of the machine. Speeds in excess of 50 mm per minute are normally employed for simply raising or lowering the machine crosshead to accommodate specimens of varying length.

The high magnification recorder unit as shown in Figure 5.3.16 was used to plot load-strain curves of the several tensile tests carried out in the experimental investigation. This instrument has six magnifications ranging from 5:1 to 200:1, the

magnification used in the series of tensile tests being 5 : 1 which permitted a plot of the entire deformation to failure to be recorded. The rotation of the recorder drum is in direct proportion to the elongation of the specimen while the recorder pen moves across the drum in direct proportion to the increasing load applied to the specimen. This dual motion, the rotation of the recorder drum and the pen movement, produces a highly magnified and extremely accurate load-strain diagram.

5.4 EVALUATION OF EXPERIMENTAL BUCKLING LOAD

Although the theoretical solution of the column's load-deflection behaviour depicts a distinct discontinuity at the initial instability load, this point cannot be realised experimentally. Due to the slightest deviation from flatness of the plate elements of the section and to the incremental nature of the applied loading, a gradual transition between the pre and post local buckling curves replaces the bifurcation point obtained from the ideal theoretical solution. As a result of this gradual transition the accuracy and reliability with which the buckling loads can be obtained from the experimental load-deflection curves is considerably affected.

To obtain accurate estimates of the buckling loads it was necessary to measure the strains at the inside and outside surfaces of the flange at the central cross section of the column.

During loading the strains on both these surfaces would be reasonably similar before the occurrence of local buckling, but would vary to a large extent after buckling due to the high bending stresses caused by local out of plane deflections.

From the measured longitudinal surface strains at the centre of the flange, a plot of axial load against membrane strain can be constructed. In such a plot the membrane strain increases gradually in compression until the onset of local buckling, after which it becomes more tensile due to the stretching of mid-surface fibres.

The method used in the determination of the buckling loads was to consider that buckling takes place at the load corresponding to the intersection of the tangents to the pre and post local buckling paths of the membrane strain curve. This method, among others, is described by Coan (2) in his consideration of the buckling of flat plates, and was found by Rhodes (19) to give accurate results when applied to the local buckling of thin walled beams. It was on the basis of the work by these authors that the method was adopted for use in the present column work.

The strains were measured by using small electrical resistance strain gauges fixed to each surface of the flange and connected to an 'Elcomatic' strain recording unit. A description of the strain gauges and the strain recording equipment is given

in Section 5.6. Plots showing the variation in membrane and surface strains with increase in applied loading are shown and discussed in Chapter Six.

5.5 TEST PROCEDURE

The specimen under investigation was fitted horizontally in the locating units of the test rig and the required eccentricity of loading set at each end of the column. The complete assembly was then lifted into the testing machine and located on the bottom loading pin situated centrally on the machine base. With the column held in this position, the top loading pin, fixed centrally in the machine crosshead, was gradually lowered until the load-indicating dial was just beginning to register. At this point all axial play between the loading pins is eliminated. It is possible however, since the column is under zero load, for rotation of the complete assembly to occur about the loading axis.

To facilitate in the measurement of column deflections, care was taken at the beginning of loading to ensure that the principal axes of the test rig and the principal axes of the testing machine were coincident, i.e. to ensure that rotation of the assembly is zero and that the column is placed squarely in the testing machine. This was achieved by marking centre lines on the top and bottom locating units of the test rig and aligning them with those marked on the base and crosshead of the testing machine.

Overall deflections were measured by means of two 50 mm travel dial gauges, one placed at each flange-web junction at the central cross-section of the column. In this way the readings obtained were simply column deflection values and were not falsified by local deformations. For any particular value of load considered the average of the two gauge readings was taken as the column central deflection.

With the aid of a rigid upright stand and by the use of magnetic bases, the dial gauge spindles were set parallel to the principal axis plane of the testing machine and perpendicular to the axis of the column. By doing this the effect of cosine errors occurring in the deflection readings is eliminated.

Once the column was squarely positioned in the testing machine, the strain gauges were connected to the Elcomatic strain recording unit and all strain and dial gauges were set to zero. Loading to the column was then effected by setting the speed control dial on the Tinius Olsen's control unit to the required loading speed. The movement of this dial initiating rotation of the machines four pulling screws which in turn lower the machine crosshead at the selected speed. At the beginning of loading, the column was loaded in equal increments and at a steady loading speed, the increments being equivalent to about 8% of the theoretically estimated collapse load and the crosshead speed being 0.8 mm per minute. As the loading increased

however, and the bending stiffness of the section steadily reduced, the increments of loading and the loading speed were made progressively smaller. In this way an accurate measurement of the collapse load of the column could be obtained. At each load increment the column was allowed to settle and readings from the dial gauges and strain recording unit were noted along with the corresponding load value. The readings obtained in this way furnished the required information for predicting the local buckling load of the column and providing the load-deflection behaviour of the column throughout loading.

5.6 STRAIN INVESTIGATION AND STRAIN RECORDING EQUIPMENT

To determine the variation of the stress distributions during loading and to compare them with those predicted theoretically, a column was strain gauged at its central cross-section and loaded incrementally under various values of the eccentricity parameter $\overline{ec}$. To ensure that the stresses within the column remained elastic, loading was limited to approximately 2 to $2\frac{1}{2}$ times the theoretically estimated local buckling load for each eccentricity value considered.

The column tested was 1066.8 mm long and had nominal flange, web, lip and thickness dimensions of 177.8 mm, 63.5 mm, 25.4 mm and 0.79 mm respectively. The gauges used in the

investigation were manufactured by the Showa Measuring Instruments Company Limited and were of the two-gauge, 90° rosette type having a gauge length of 5mm, a resistance of 120 ohms and a gauge factor of 2.12. Figure 5.6.1 shows the layout of the strain rosettes round the central cross-section, 25 rosettes being fixed on the inside surface and 25 on the outside, a total of 100 gauge readings in all. Figure 5.6.2 depicts the column under test showing the strain gauges at the column centre and the necessary wiring leading to the strain recording unit.

The strain gauge recorder used was manufactured by Elcomatic Limited and was capable of accommodating up to 100 gauges. Figure 5.6.3 shows the recorder depicting its various component parts. At any particular load value, output of the gauge readings was obtainable from the tape output unit which provided a printed record of all 100 strain values corresponding to the selected load. In order to obtain mid-surface values of the strain pattern, the strain gauge rosettes were used in pairs such that, for a given load, each reading from the outside surface gauges had a corresponding reading from the same position on the inside surface.

The column under investigation was loaded firstly through its centroid and at each load increment up to approximately $2\frac{1}{2}$ times the theoretically estimated local buckling load; the strain readings from the Elcomatic were recorded. The column was then

unloaded, a new value of eccentricity applied to its ends, and the process repeated. The eccentricity values considered in the investigation were $\overline{ec}$ = 0.0, 0.1, 0.2, 0.3 and 0.4.

By dividing the readings from the Elcomatic at each load increment by the gauge factor to obtain the strains, evaluation of the experimental stresses could then be obtained from the stress strain relationships, that is

$$\sigma_x = \frac{E}{1-\nu^2}\left[\varepsilon_x + \nu\varepsilon_y\right]$$

The experimental stresses obtained in this way are presented and discussed in Chapter Six where comparison with the theoretically predicted stresses is also presented.

The strain gauges used in the general investigation to aid in the prediction of the experimental local buckling loads, were also manufactured by the Showa Measuring Instruments Company Limited. Two gauges were used for this purpose, one fixed to each surface at the centre of the flange on the columns central cross-section. The gauges measured the longitudinal surface strains at the centre of the flange, from which a plot of the growth in membrane strain could be obtained and hence a prediction of the columns local buckling load. The gauges had a 5 mm gauge length, a resistance of 119.7 ohms and a gauge factor of 2.10.

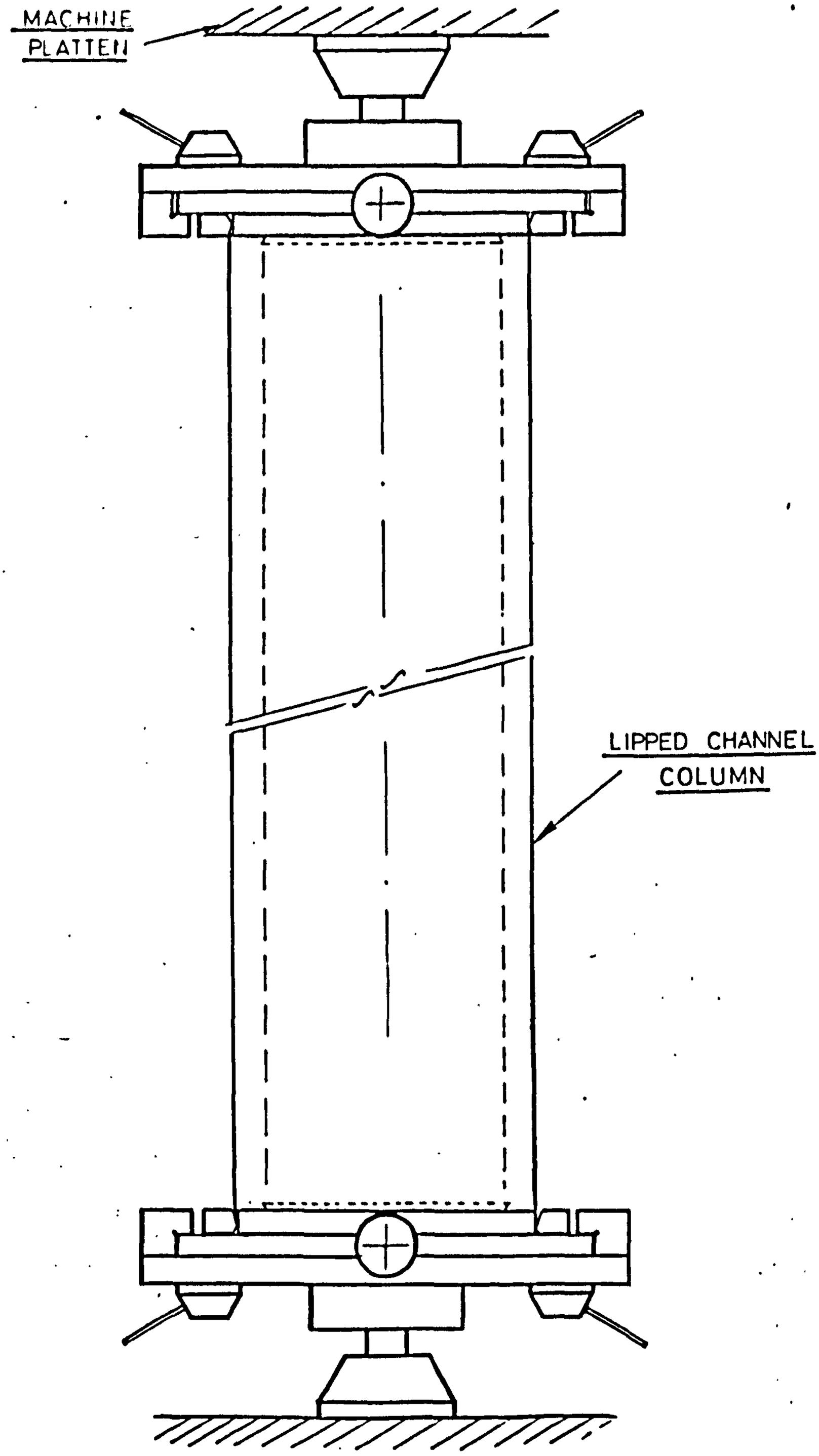

FIG 5.3.1 GENERAL ASSEMBLY OF LOADING RIG
SHOWING COLUMN IN POSITION

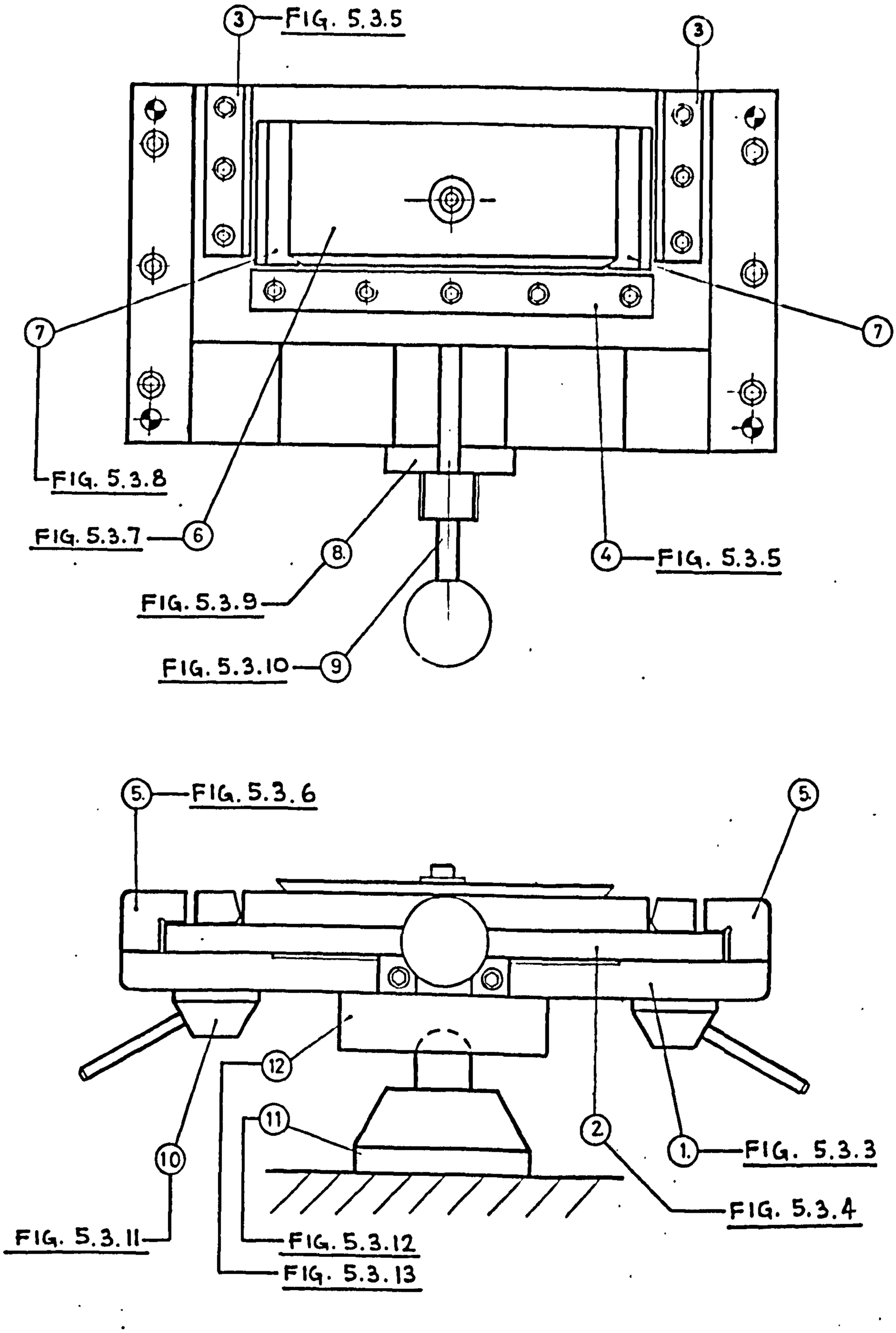

FIG 5.3.2 GENERAL ASSEMBLY OF LOADING RIG

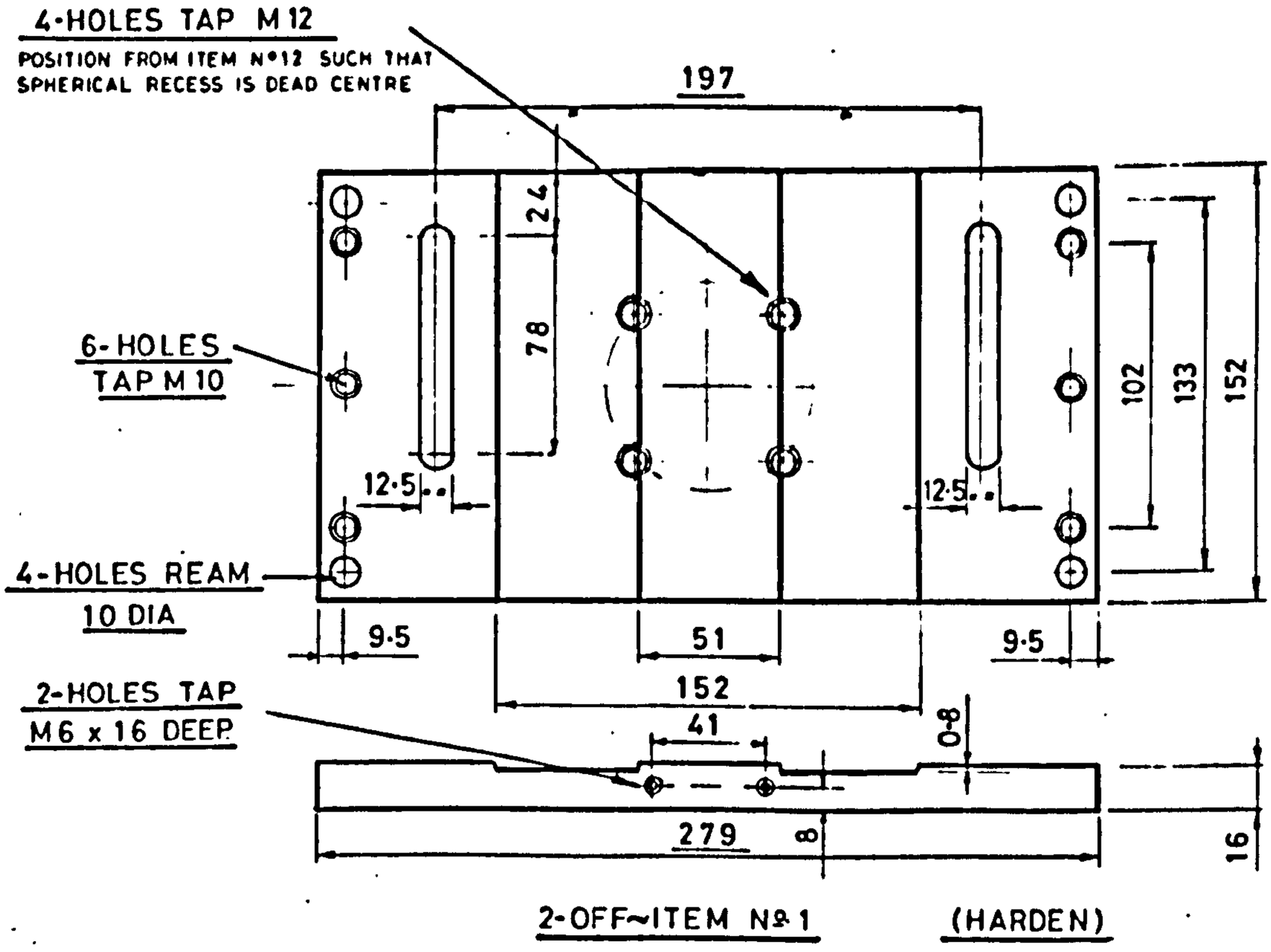

2-OFF~ITEM Nº 1 (HARDEN)

FIG 5.3.3 BASE PLATE

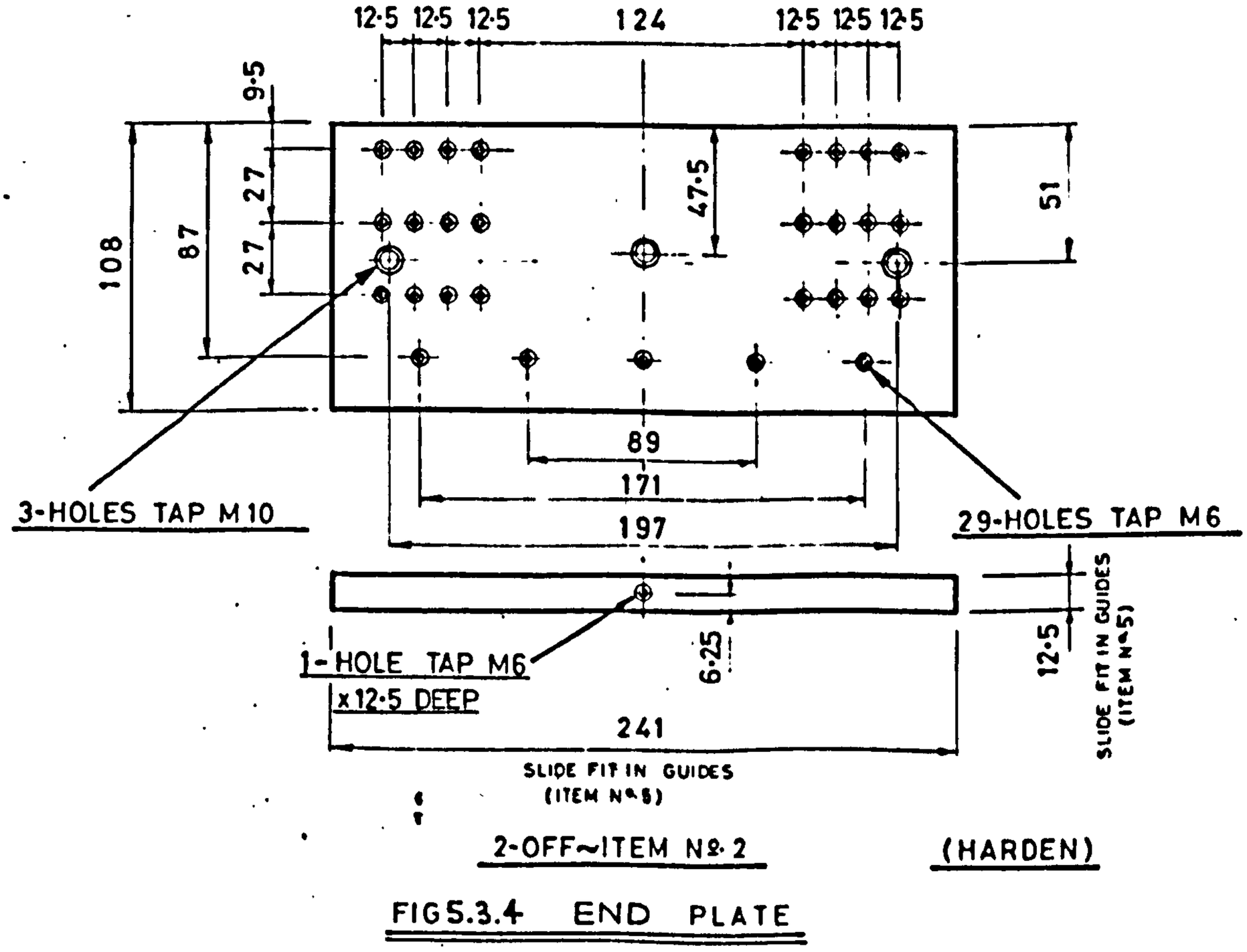

2-OFF~ITEM Nº 2 (HARDEN)

FIG 5.3.4 END PLATE

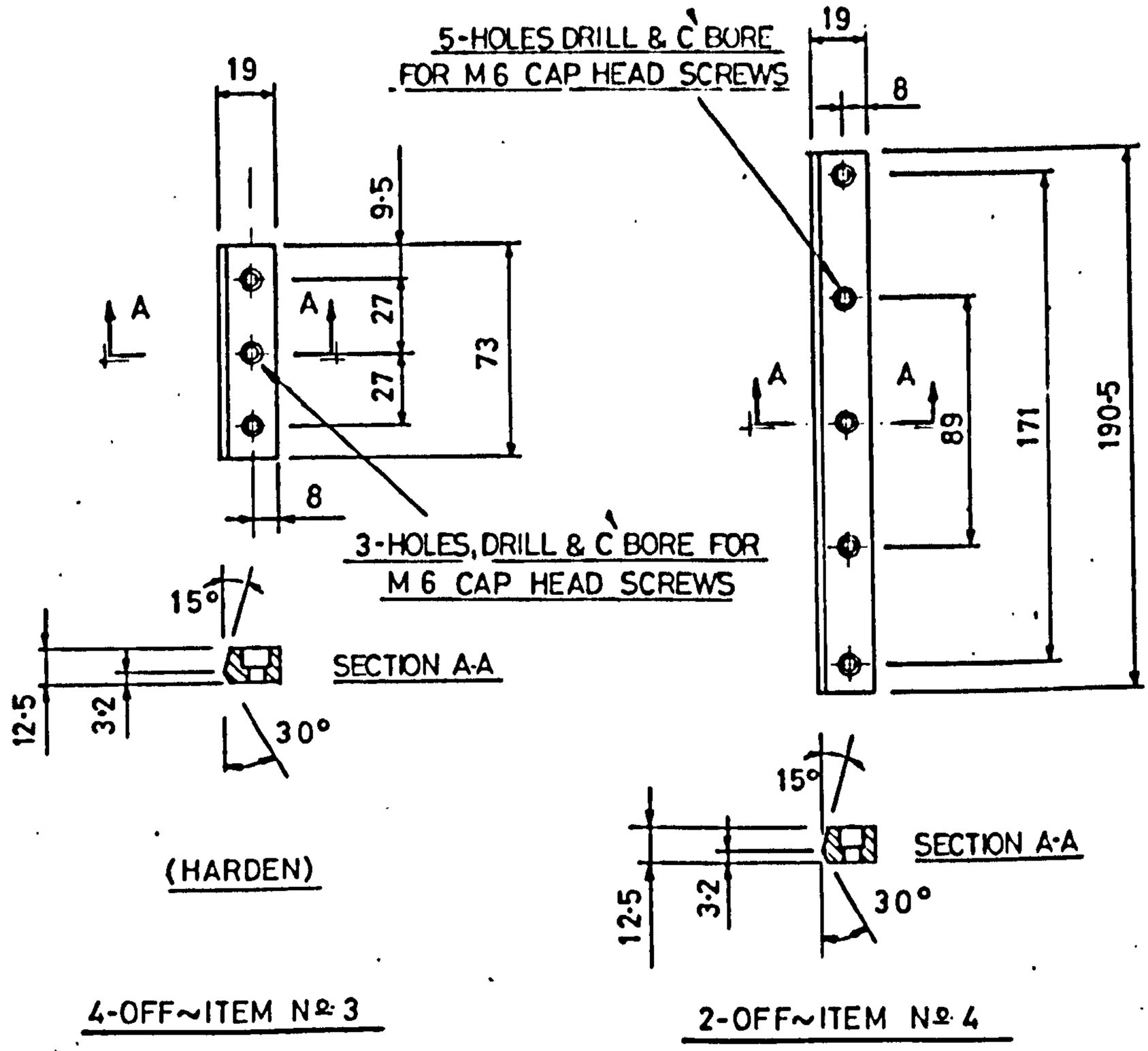

FIG 5.3.5 WEB AND FLANGE LOCATING BARS

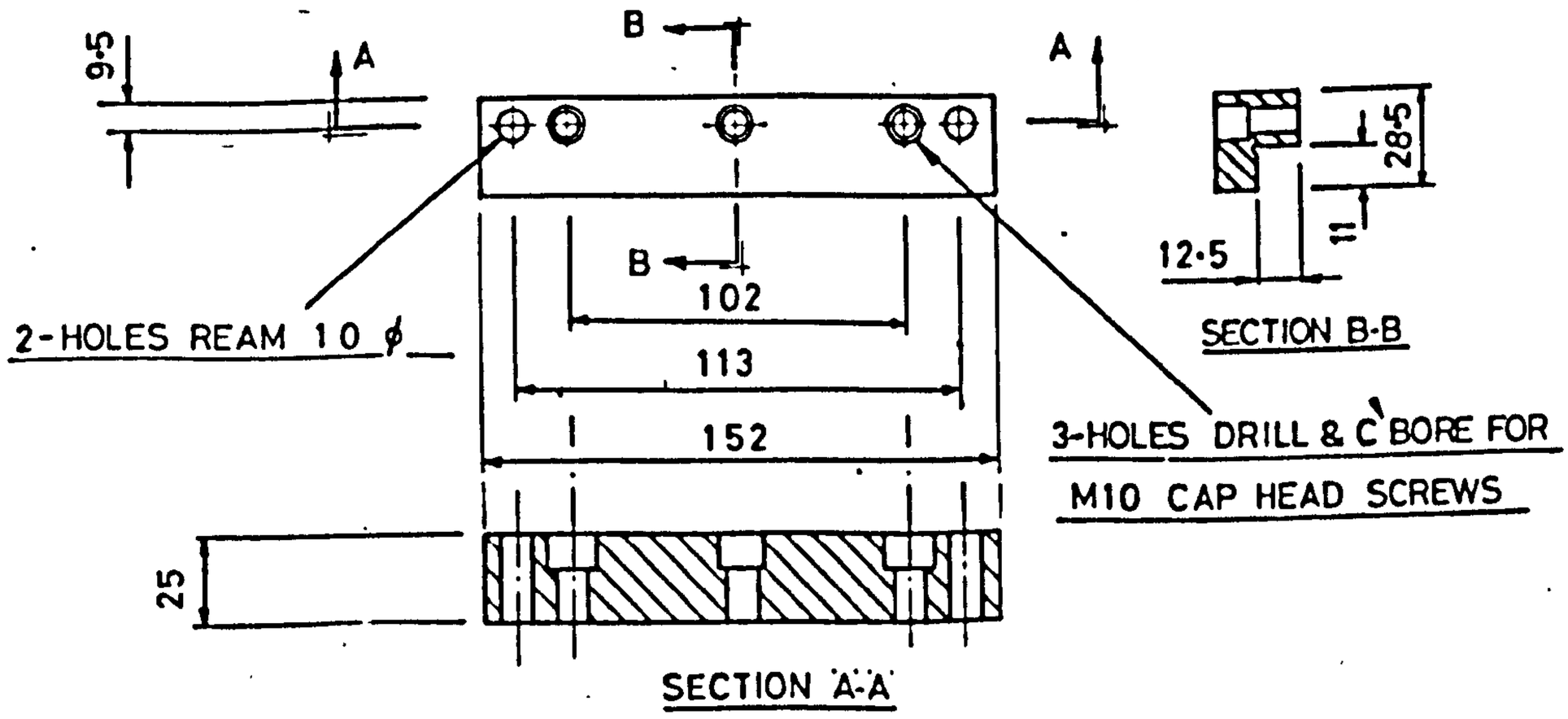

4-OFF~ITEM Nº 5 (HARDEN)

FIG 5.3.6 GUIDE BAR

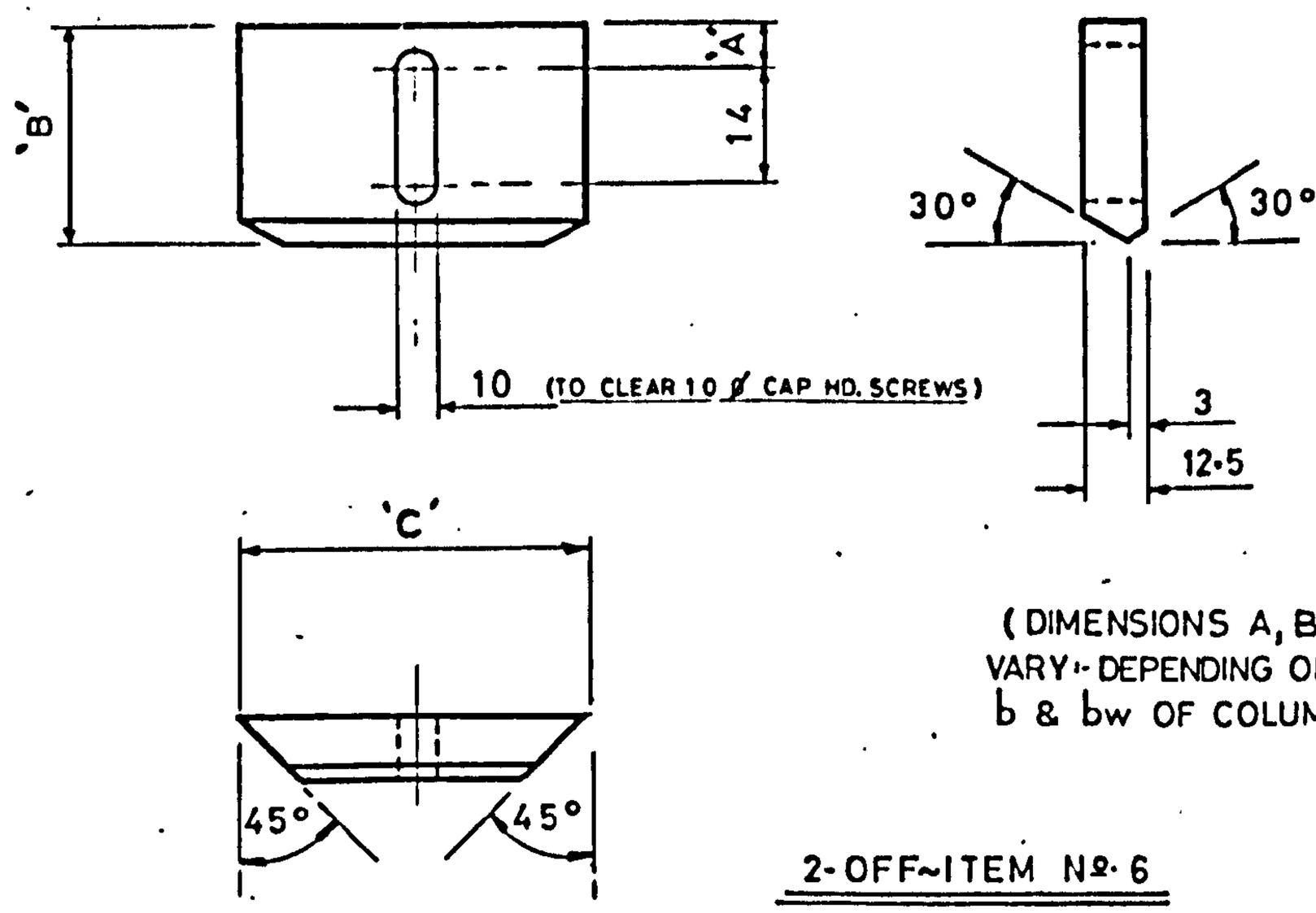

(DIMENSIONS A, B & C
VARY:- DEPENDING ON LENGTHS
b & bw OF COLUMN.)

2-OFF~ITEM Nº. 6

(HARDEN)

FIG 5.3.7 CLAMPING PLATE

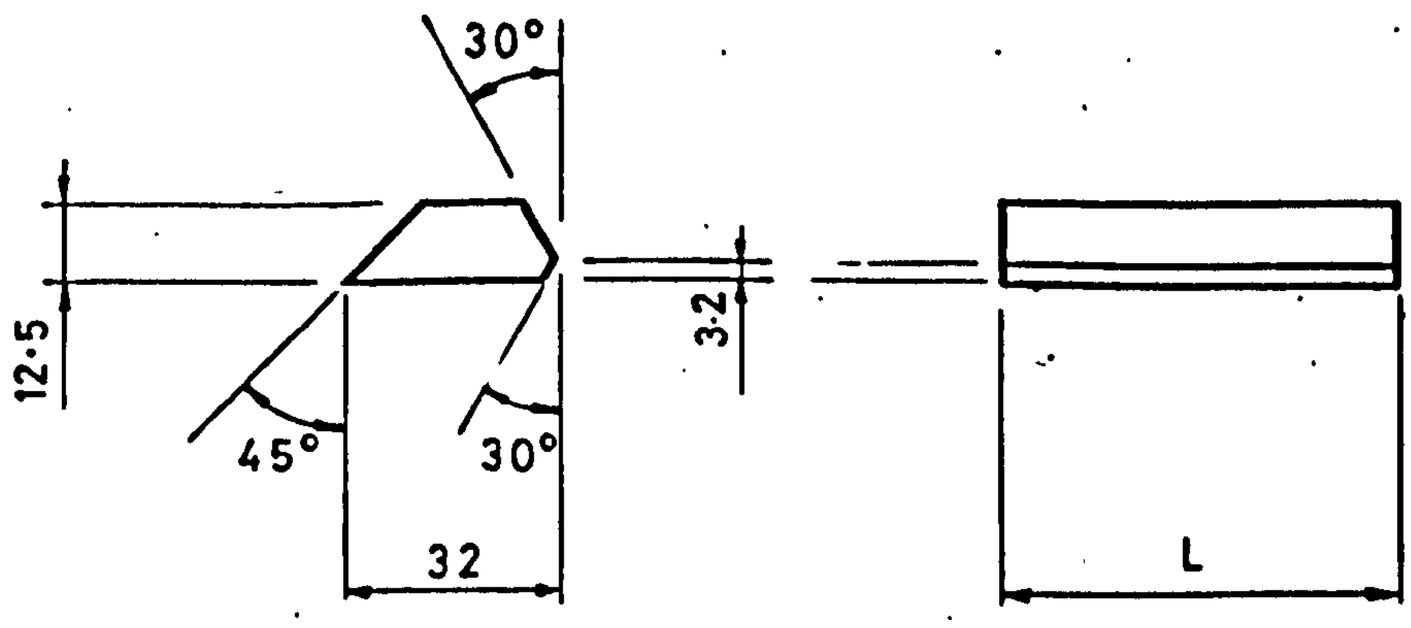

('L' DEPENDS ON DIMENSION
bw OF COLUMN)

4-OFF~ITEM Nº 7

(HARDEN)

FIG 5.3.8 WEDGE CLAMPING PAD

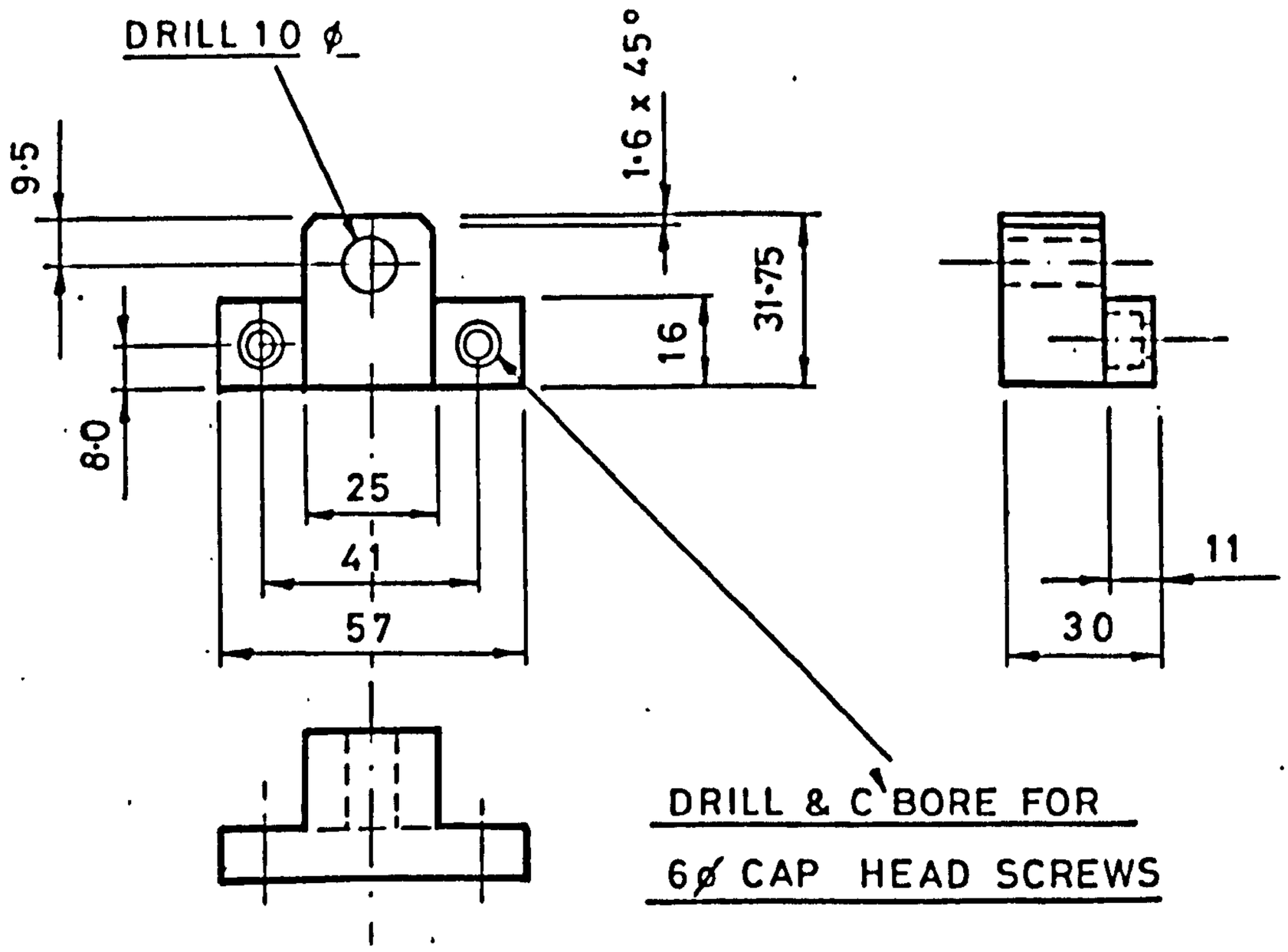

2-OFF~ITEM Nº 8

FIG 5.3.9 DATUM BLOCK

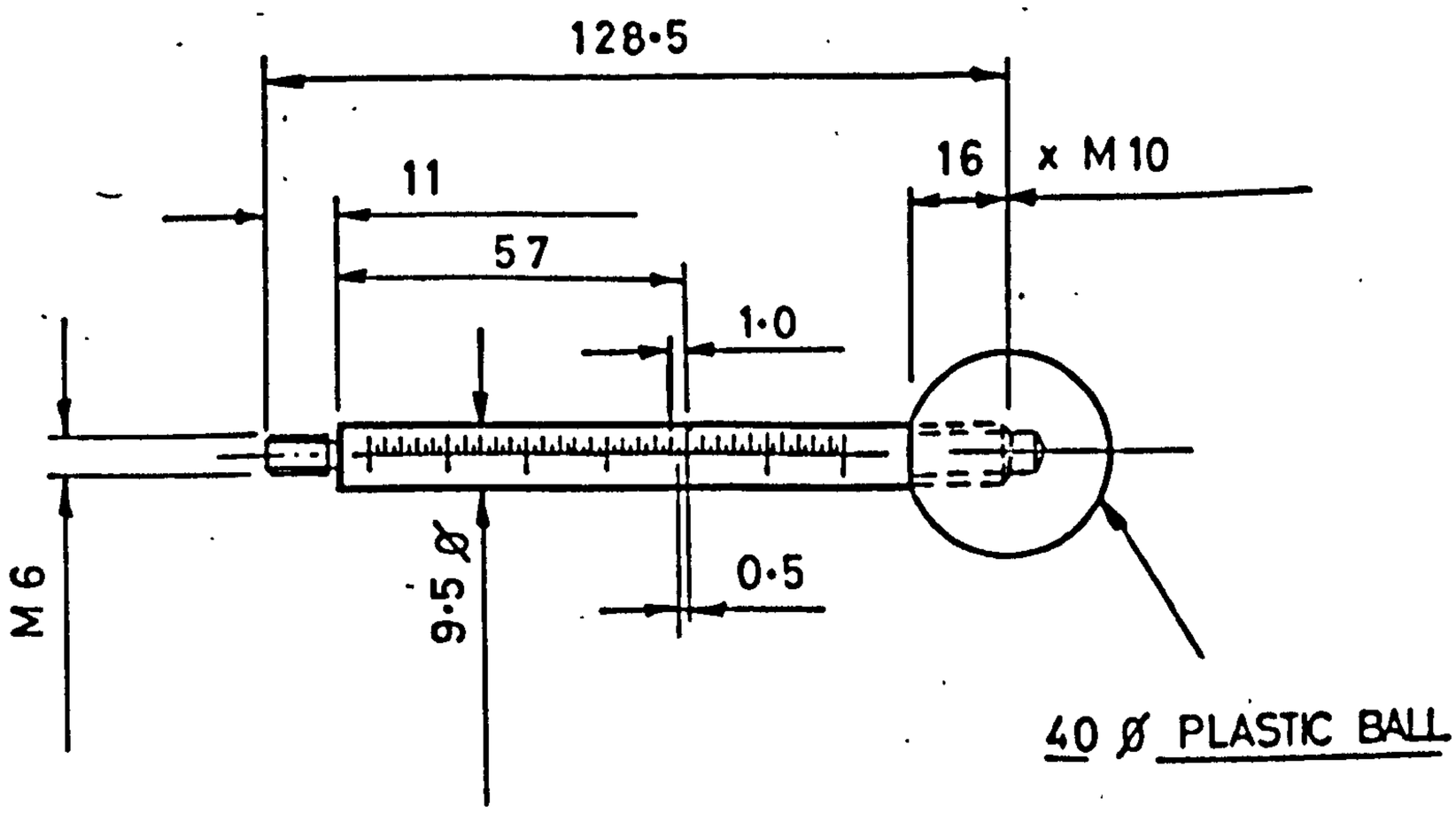

2-OFF~ITEM Nº 9

FIG 5.3.10 CALIBRATED POSITIONING HANDLE

SCREW HANDLE M6 x 12·5 LONG

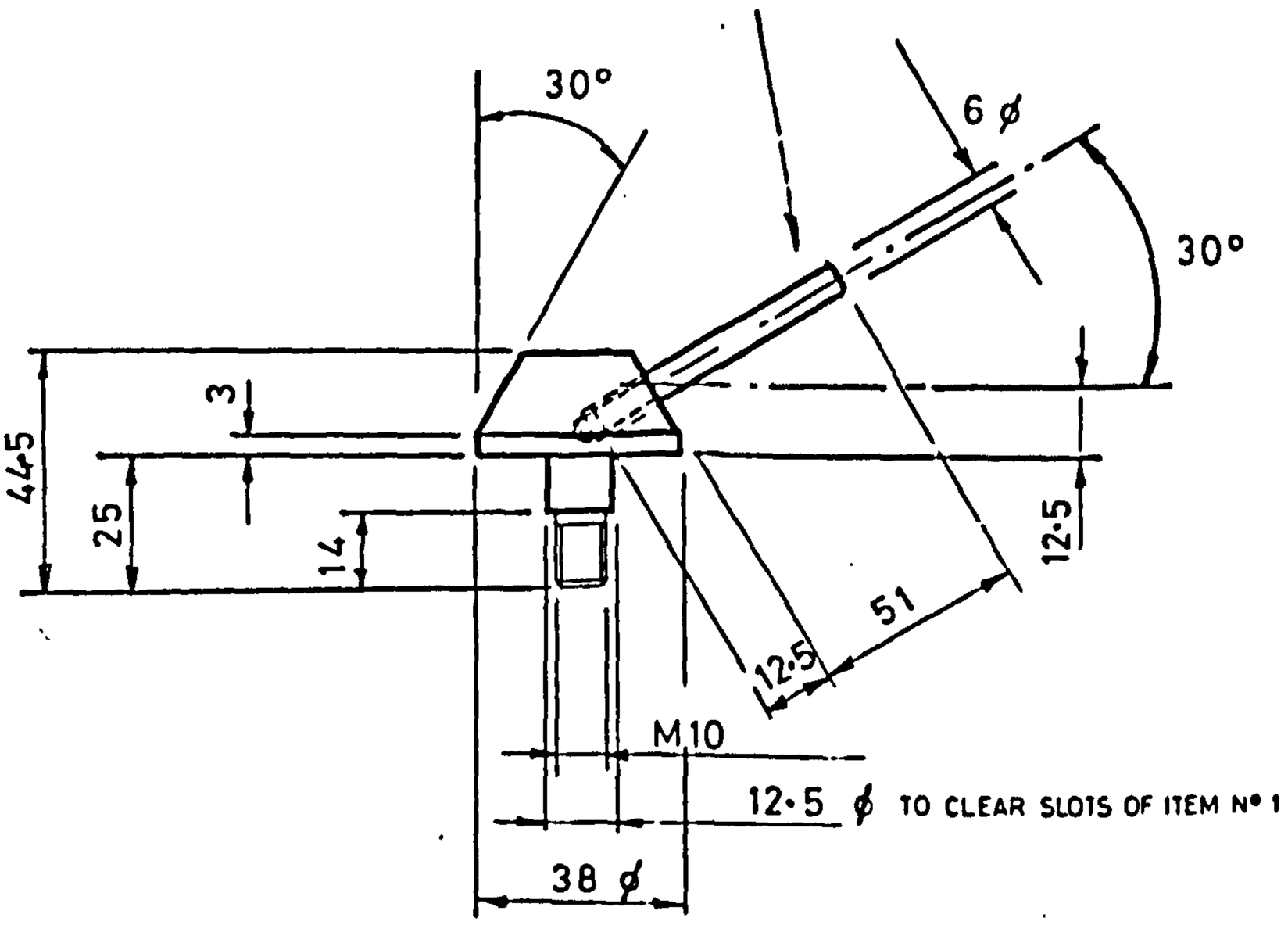

4-OFF~ITEM N♎10

FIG 5.3.11 CLAMPING SCREW

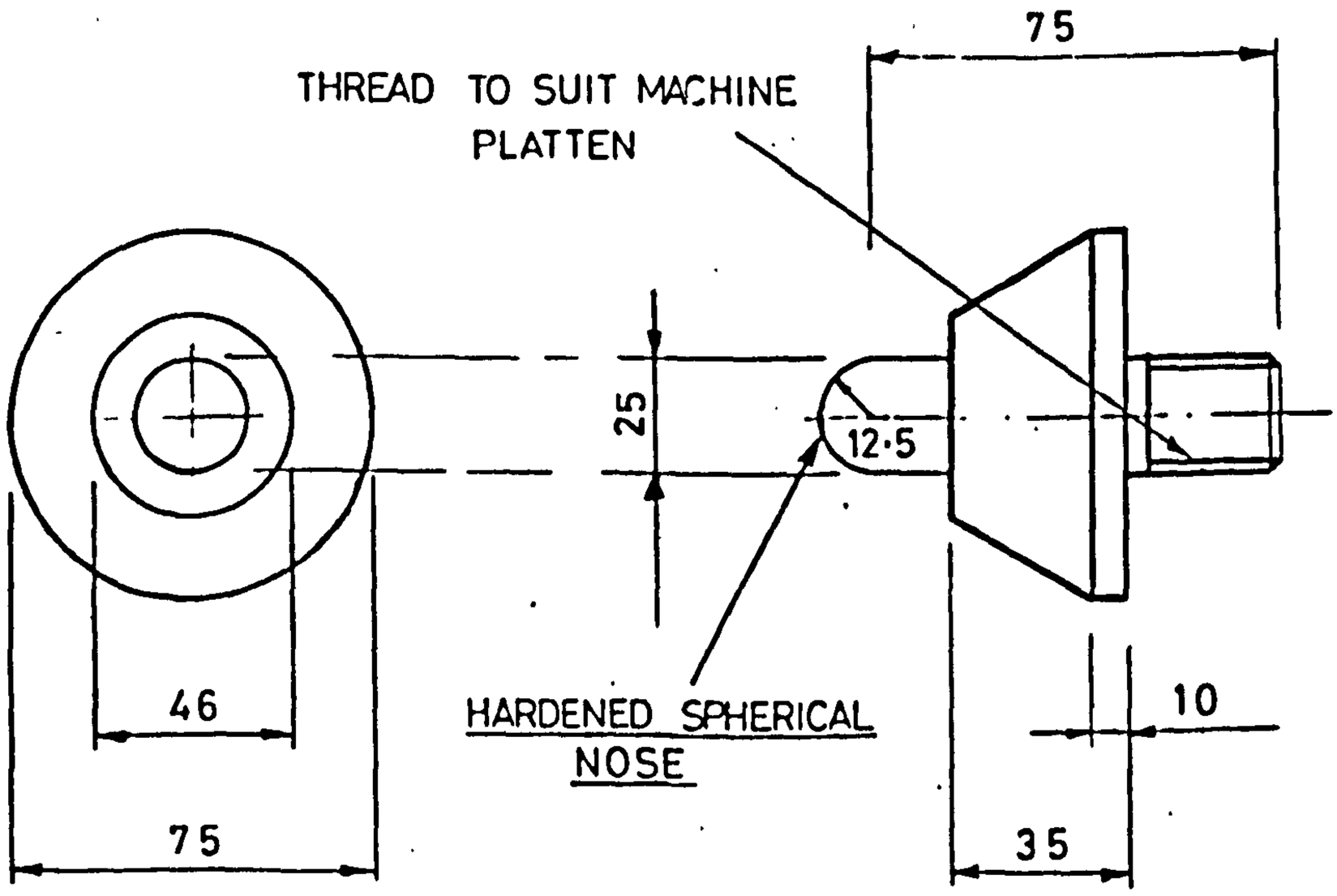

2-OFF~ ITEM N♎ 11

FIG 5.3.12 LOADING PIN

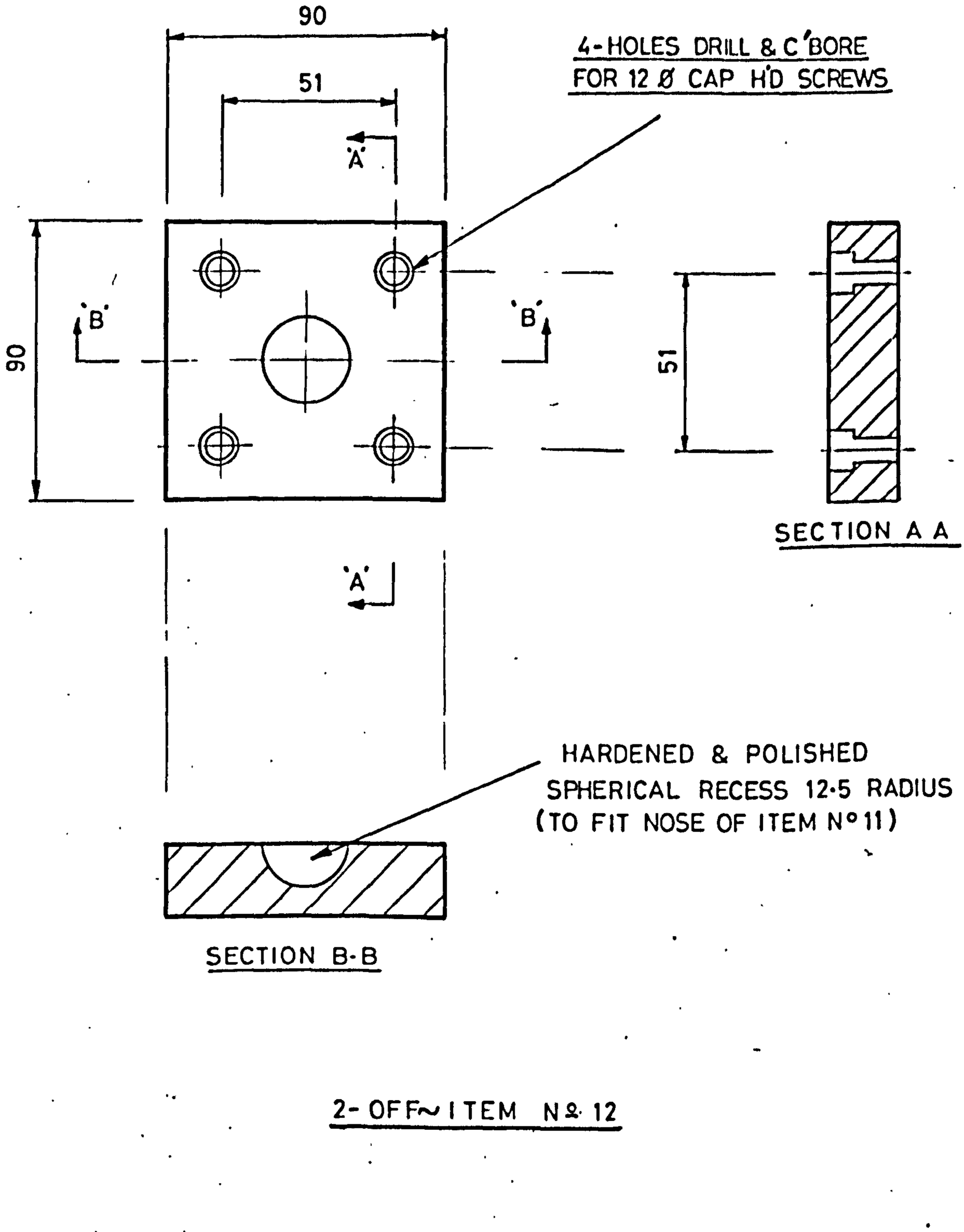

2- OFF~ ITEM N& 12

FIG. 5.3.13 LOADING BLOCK

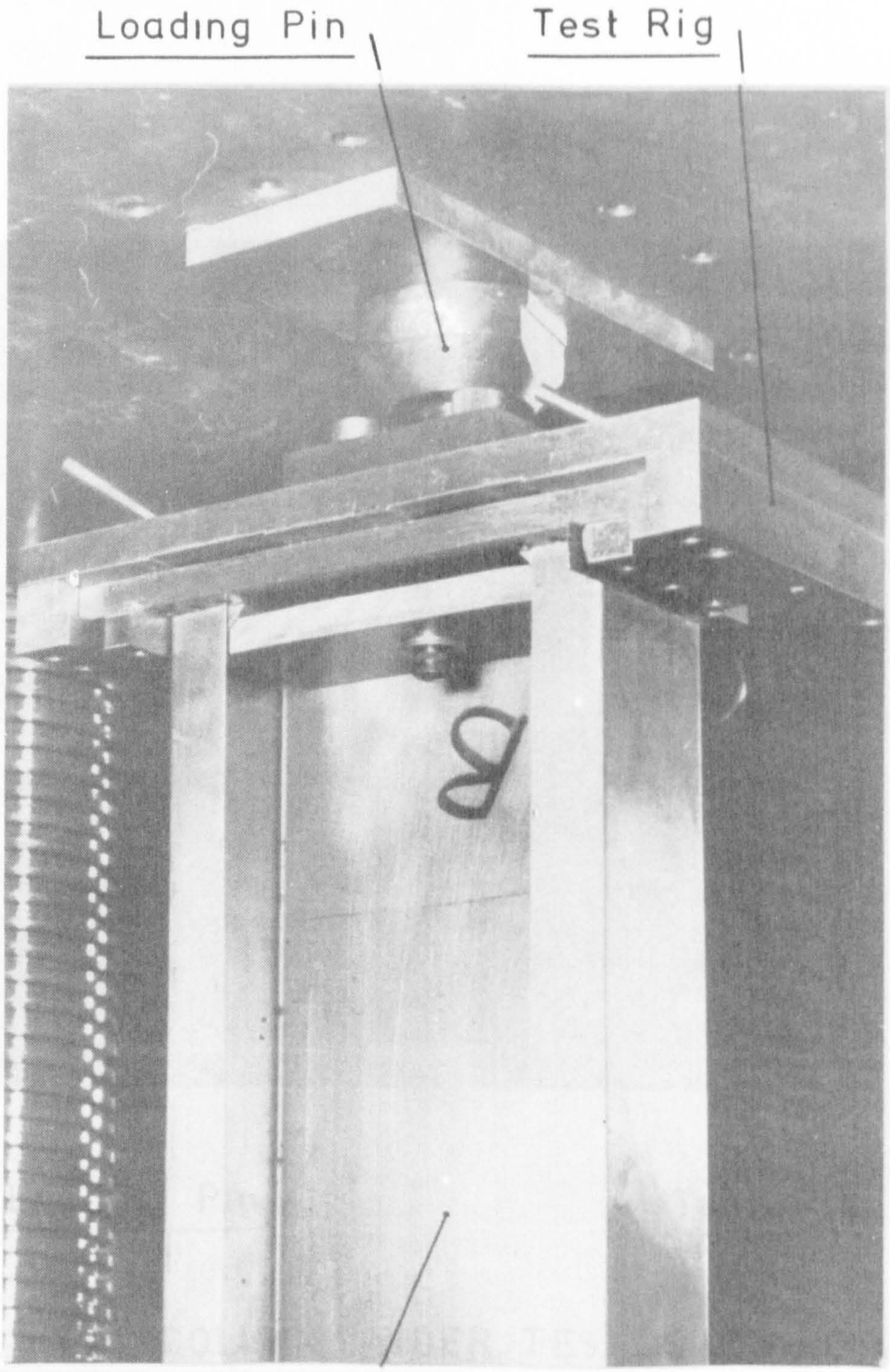

FIG. 5.3.14 COLUMN UNDER TEST SHOWING TOP CONNECTION AND LOADING PIN.

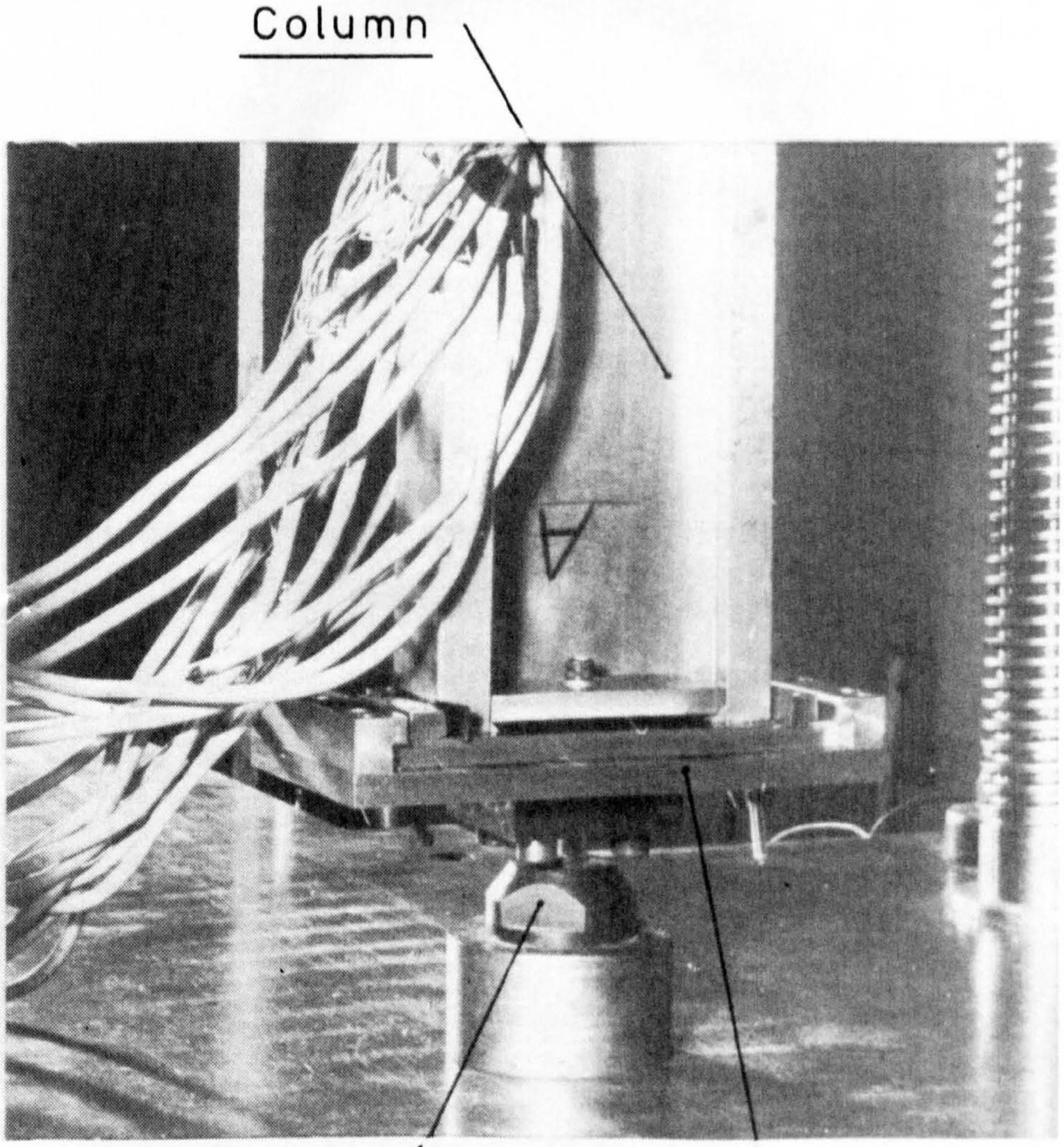

FIG. 5.3.15 COLUMN UNDER TEST SHOWING BOTTOM CONNECTION AND LOADING PIN.

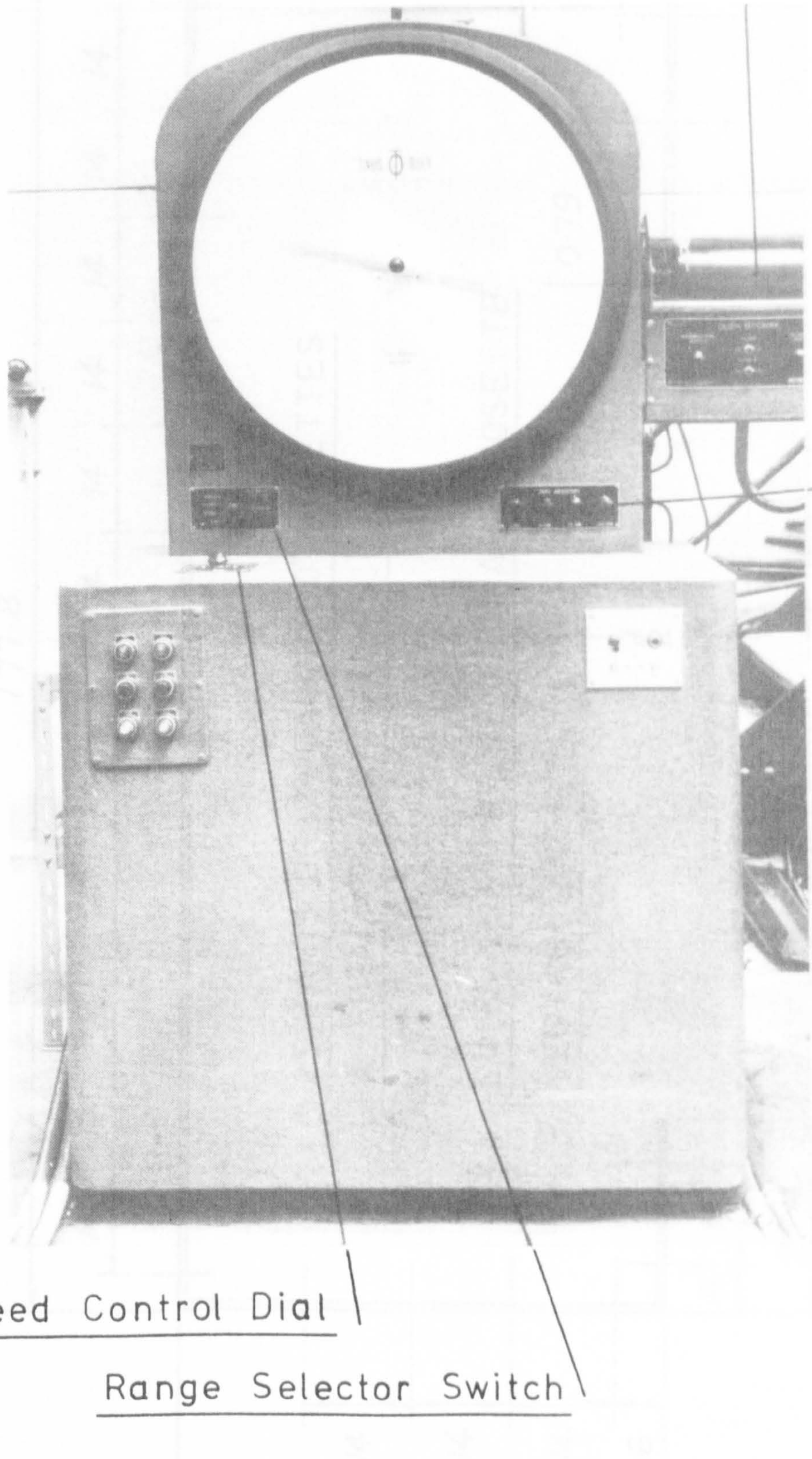

FIG. 5.3.16 TINIUS OLSEN LOAD INDICATING AND CONTROL UNIT.

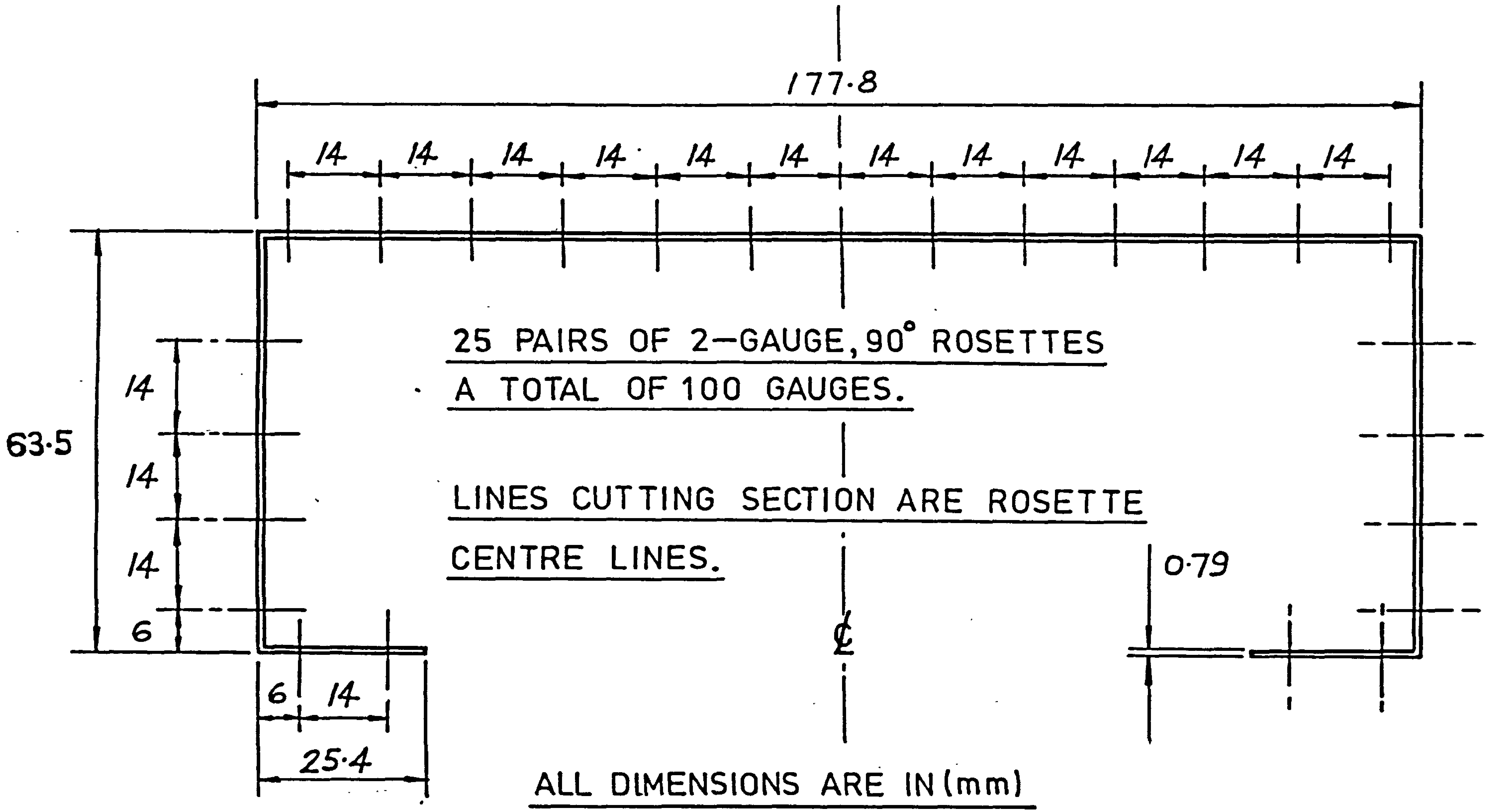

FIG. 5.6.1 STRAIN GAUGE POSITIONS ON CENTRAL CROSS SECTION OF COLUMN

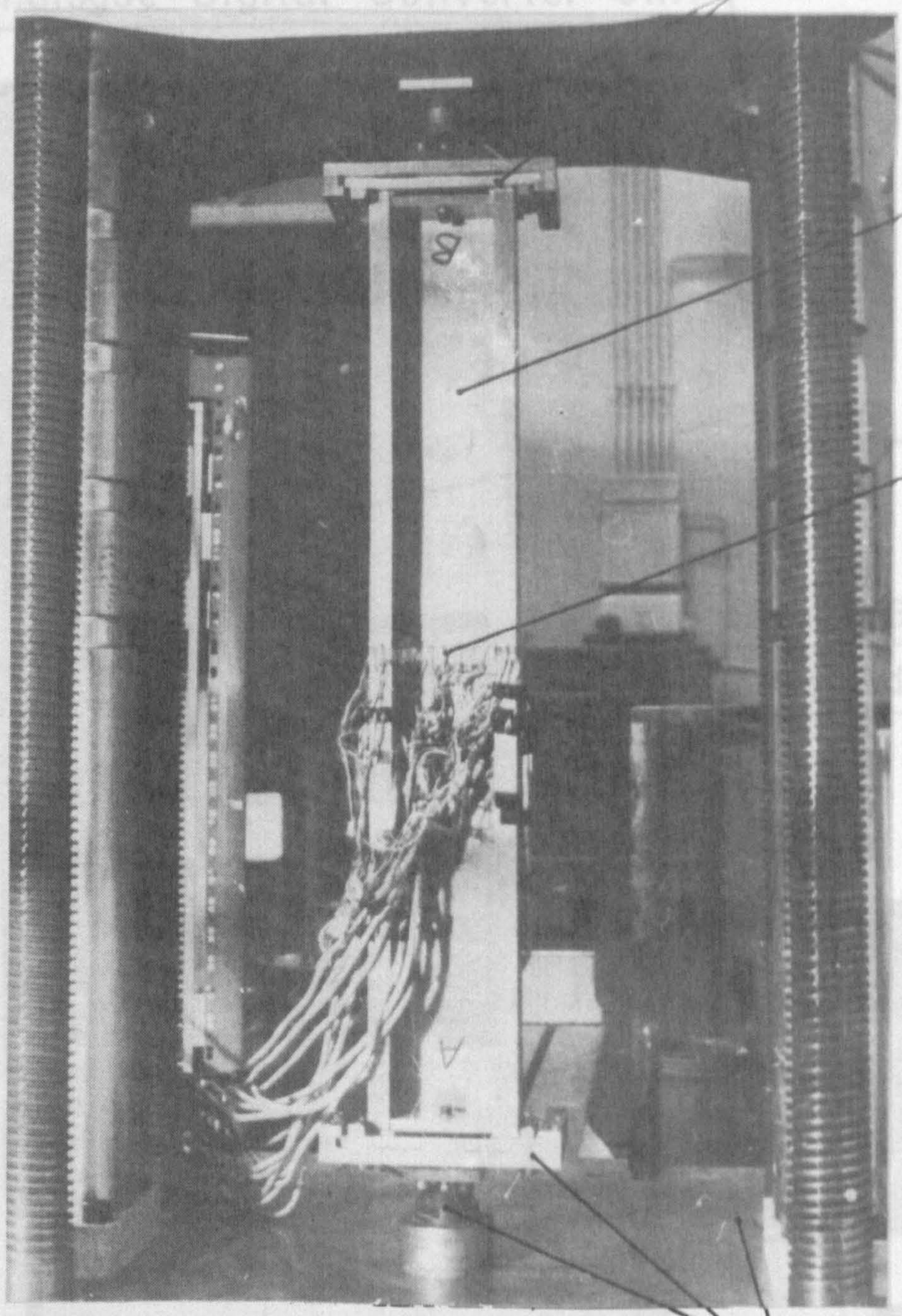

FIG. 5.6.2 COLUMN UNDER TEST SHOWING STRAIN GAUGES ON CENTRAL CROSS SECTION.

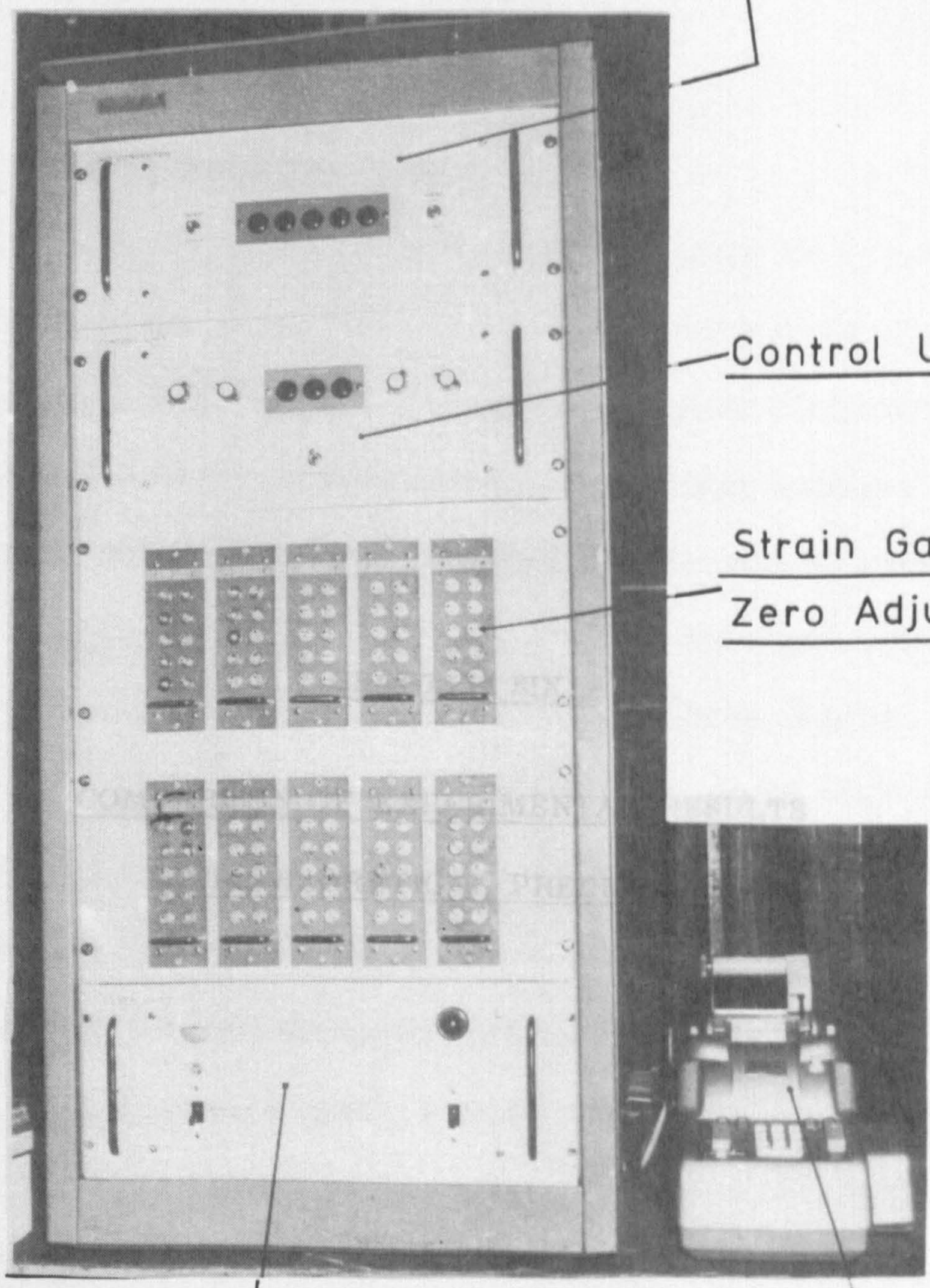

FIG. 5.6.3 ELCOMATIC STRAIN RECORDING EQUIPMENT

CHAPTER SIX

COMPARISON OF EXPERIMENTAL RESULTS WITH THEORETICAL PREDICTIONS

6.0 COMPARISON OF EXPERIMENTAL RESULTS WITH THEORETICAL PREDICTIONS

6.1 LOCAL BUCKLING LOADS

As previously mentioned, estimates of the local buckling loads in the experimental investigation were obtained from longitudinal surface strain measurements taken at the centre of the flange at the central cross-section of the column. Using these strains it was considered that the local buckling load was that which corresponded to the intersection of the tangents to the pre- and post- local buckling paths of the membrane strain curve in a load-strain diagram. Of the 33 columns tested in the experimental program, strain results from 8 were chosen to depict the membrane-tangent method of predicting local buckling loads, the strain curves from the 8 selected being typical of those of all the columns tested.

Figures 6.1.1 to 6.1.8 show the load-strain curves, ε_1 indicating strain values measured on the inside surface of the flange and ε_2 those measured on the outside surface. The membrane strain is the average of the two surface strains. With the exception of Figure 6.1.7, all the curves show that the outside surface strain continually increases in compression with increase in load, whereas the inside surface strain, after initial compression, becomes tensile. This indicates that, at the centre of the column, the flange has buckled inwardly towards the lips of the section whereas the curves

of Figure 6.1.7 show that the flange has buckled outwardly.

It will be realised that the membrane-tangent approach is merely a definition of the local buckling load and the results obtained from the method serve only as an approximate guess to the true buckling load. There are, however, other definitions of the local buckling load. Thomasson (54) used the membrane strain reversal method, according to which the local buckling load is approximately equal to the load which coincides with the maximum compressive membrane strain. The accuracy of this approach, however, diminishes with imperfections since these tend to result in a gradual change of slope of the membrane strain curve. The abrupt change of slope that would be experienced from the perfect plate or flange is therefore replaced by a gradual change of slope which tends to flatten out the membrane strain curve in the vicinity of slope change. It is this flattening out effect which adds to the difficulty in picking the load which corresponds to the maximum compressive membrane strain. The method, in general, gives results which are higher than those obtained from the membrane-tangent approach. Another definition of the local buckling load is the load at which the strain in one of the faces shows a maximum, i.e. the surface strain reversal approach. This method tends to give results which are lower than those obtained from the membrane-tangent approach, especially in the presence of imperfections.

Figures 6.1.1/2/3/4/7/8 show that the membrane strain reversal method would yield buckling loads higher than those obtained from the membrane-tangent approach. Figure 6.1.5 indicates that the membrane strain reversal method would yield a buckling load smaller than that obtained from the membrane-tangent method while Figure 6.1.6 shows that both methods would yield practically the same result. In the case of the surface strain reversal approach Figures 6.1.1 to 6.1.8 show that in all cases this method would yield buckling loads smaller, to varying degrees, than those obtained from the tangent method. The membrane-tangent method was described by Coan (2) as being accurate but consistently under-estimating the buckling loads in his investigation of plate buckling, while Rhodes (19) obtained very accurate results when applying the method to the buckling of thin walled beams under pure moment loading. It appears that the membrane-tangent method is less sensitive to local imperfections than the membrane and surface strain reversal approaches previously discussed. The method has, however, the disadvantage of requiring accurate determination of the correct points of tangency to the pre- and post-buckling parts of the membrane strain curve. In view of the points discussed it can be said that, although in general the results obtained from the different methods agree reasonably well, it is clear that the various definitions of the experimental buckling load are not free from some arbitrariness.

Due to the high flexibility in the choice of locally deflected forms at buckling, it will be realised that the theoretical buckling loads obtained from the Rayleigh-Ritz analysis of Chapter 3 will

indeed be very accurate approximations to the true buckling loads. In view of this and also the arbitrariness of the experimental approaches discussed, it would appear that any comparison between theory and experiment would serve only to illustrate the reliability of the experimental method rather than the accuracy of the theoretical approach. Such a comparison has been made, however, and the results are shown in Table 6.1.1. Although the theoretical buckling loads are output from the computer to six decimal places, these are rounded to two places and compared with the values from the membrane-tangent method. The dimensions and eccentricity of loading of each column tested are given in Appendix VI. Table 6.1.1 indicates good agreement between theory and experiment and also that no consistent pattern exists, as was found by Coan (2), for plates in compression. The experimental buckling loads are seen to be sometimes above and sometimes below the theoretical values, and in two cases are almost identical to the theoretical values.

6.2 COLUMN LOAD-DEFLECTION BEHAVIOUR

Comparisons between theoretical and experimental load-deflection behaviour give an indication of the accuracy with which the theoretical solution can predict changes in section bending stiffness and neutral axis shift during local buckling, these of course depending on how well the solution is able to represent the locally deflected form at

all stages of loading. This is fairly evident from equation 4.8.11, derived in Appendix I, for the central lateral deflection of the column in the post-local buckling domain. From this equation it can be seen that for a given load the lateral deflection at the centre of the column is clearly dependent on the values of section neutral axis position and tangent bending stiffness in the post-local buckling range. These in turn, along with the term M^* in the solution, are shown in Appendix I to be related to the current locally deflected shape and are therefore variable throughout the analysis. The accuracy of column load-deflection behaviour is therefore seen to be highly dependent on the accuracy of the deflection functions in approximating the actual local form during loading.

Although an energy type of solution could be expected to yield an upper estimate of the column's flexural stiffness, i.e. theoretically predicted deflections for a given load would be less than those obtained experimentally, approximations introduced in the analysis to aid in the satisfaction of overall equilibrium add further complications and the theoretical deflections may or may not exceed those from experiment. The approximations introduced stem from the use of equation I.15 of Appendix I for section curvature along the column. For a locally buckled column this relationship is really only true at the buckle nodes and due to this the requirement of the theoretical solution to give an upper bound to the column's stiffness does not hold.

To save repetition, the load-deflection results of only 16 of the 33 columns tested have been selected for comparison. These are shown in Figures 6.2.1 to 6.2.16, where good agreement between theory and experiment is indicated. In all cases the load-deflection comparison prior to local buckling is extremely good, showing the accuracy with which the eccentricities of loading were applied by the experimental loading rig. After local buckling the initial comparison between theory and experiment is seen to be good in all cases, although in some the theory is seen to overestimate column stiffness and in others the stiffness is underestimated. In each figure the load value at failure is shown and the final experimental point indicated was the last to be taken before failure. As the ultimate load of each column is approached the experimental points show a further reduction in section stiffness than that shown in the earlier part of the post-buckling curve. This is caused by the effects of plasticity and is depicted in the various figures by the greater inaccuracy of the elastic solution to predict column deflections in the region approaching collapse, i.e. the elastic solution overestimates column stiffness in this region. The theoretical curves of Figures 6.2.1 to 6.2.16 are terminated when the maximum membrane stress at the flange-web junction on the central buckle reaches the yield stress obtained from tensile tests of the column material.

Figures 6.2.10 and 6.2.11 show the results of two centroidally loaded columns. Deflection values obtained from experiment are seen to remain zero, or nearly so, up to the point of local buckling and thereafter to follow the theoretical curve fairly closely in each case throughout the post-local buckling phase. The theory is seen to underestimate column flexural stiffness in the initial post-buckling range and, due to this, deflection comparison in the region just before collapse is enhanced and the weakening effects of plasticity masked. Typical comparisons in which the theory overestimates column flexural stiffness are shown in Figures 6.2.1 and 6.2.8. In these the comparison prior to local buckling is excellent. From the onset of local buckling, however, theoretical deflections are seen to be less than those from experiment and due to this the effects of plasticity appear magnified in the region just before collapse. As mentioned earlier, the approximations introduced by using equation I.15 for curvature nullify the approximate upper bound requirement on flexural stiffness that would be expected from an energy type of solution. This has been substantiated by the comparisons shown in Figures 6.2.1 to 6.2.16. In some cases the theoretical predictions of column deflections are greater than those obtained from experiment, and in others less. This indicates that the solution is not bounded.

6.3 STRESS VARIATIONS

To further substantiate the theory, comparisons were made between the actual stresses under load at the centre of a column with those derived theoretically at the local buckle crest. Experimental stresses were obtained from the measured strain variations during loading of the column tested in the strain investigation of the experimental program. The dimensions of the column tested are given in Chapter 5. To provide a wide range for comparison and to test the consistency of agreement, stress variations were obtained for various degrees of loading eccentricity. In each case the column was loaded to about 2 to $2\frac{1}{2}$ times the theoretical local buckling load, with strain measurements being recorded at regular intervals. Careful checks were made to ensure that the maximum loads in each case did not cause yield at any point on the column. Figures 6.3.1 to 6.3.15 show the comparison of the growth in surface and membrane stresses corresponding to the various loading eccentricities considered. Due to the symmetry of stresses about the flange centre line, only one half of the section has been depicted in the figures. For each eccentricity value considered stress comparisons have been made at three load levels. One comparison is made slightly above the local buckling load, one at approximately 2 to $2\frac{1}{2}$ times the local buckling load and one intermediate to these.

Figures 6.3.1, 6.3.2 and 6.3.3 show the growth in stresses for the centroidal loading case. In Figure 6.3.1 the stress comparison

is at a load level just 8% above that to cause local buckling. From this the theoretical membrane stress is seen to be fairly constant around the section, although some loss in linearity is indicated over the central portion of the flange and very slightly across the web. It would appear from the comparison in Figure 6.3.1 that a slight local imperfection was present in the flange. This is substantiated by the comparisons shown at the higher load levels in Figures 6.3.2 and 6.3.3 from which it is evident that, while the magnitudes of the stresses are significantly affected around the local buckling load, they are less affected at the higher loads. The inside surface stress comparison over the central portion of the flange, however, is seen from the figures to be less accurate at the higher loads. Although the theory has the same general form as the experimental pattern in this region, the stress values are noted to be higher by some 12 to 20%. This dipping of the compressive surface stress pattern across the central portion of the flange is the consequence of the centre of the flange becoming less effective at higher loads and shedding load towards the flange edges. It would appear from Figure 6.3.3 that the theory has the tendency to slightly underestimate this ineffectiveness for the column considered, indicating that although the two term post-buckling solution allows for change in buckled form, perhaps the flexibility is not quite high enough to accurately predict the actual form. The effect of overall column deflections after local buckling is clearly indicated in

Figures 6.3.2 and 6.3.3 where it can be seen that, due to overall bending, stress variations across the web are more compressive at the flange-web junction than those at the web-lip junction. It will also be noted that local buckling effects occur predominantly in the flange. The stress predictions across the webs and lips are seen to be fairly accurate at all load levels and the comparisons shown for the centroidally loaded column can be said, in general, to support the theory.

Figures 6.3.4 to 6.3.15 show the consistency of agreement between theory and experiment of the results obtained for eccentric loading of the strain gauged column. The eccentricities of loading considered were $\overline{ec}$ = 0.1, 0.2, 0.3 and 0.4. In all loading cases the agreement is seen to be good except for that of the compressive inside surface stress over the central portion of the flange. Regarding this, the same comments apply as those made in relation to the centroidal case. Figures 6.3.13 to 6.3.15 show the comparisons of the growth in stress variations corresponding to the highest loading eccentricity considered. From these the eccentricity of compression across the section web is seen to be more susceptible to change than that corresponding to the centroidally loaded case depicted in Figures 6.3.1 to 6.3.3. This more rapidly changing compression eccentricity across the web is a characteristic associated with load eccentricity, as are the higher local bending stresses depicted across the flange. The effect of

load eccentricity is illustrated by comparing directly Figures 6.3.3 and 6.3.15, which show stress comparisons for the highest load level considered in the centroidal loading case and the highest eccentricity case respectively. It will be noted that the load on the column is approximately the same in each case, 11.125 kN for the centroidal loading and 11.57 kN for the eccentrically loaded case. The stress variations, however, are seen to be quite different. The membrane stress variation across the flange is seen to be slightly more reduced over the central portion and substantially increased towards the edges in the eccentric loading case. The magnitudes of the bending stresses are seen to be significantly higher in the eccentric loading case, in particular over the central portion of the flange. The eccentricity of compression across the web is seen to be much greater in the eccentric loading case, producing a high membrane stress at the flange-web junction and a low value at the web-lip junction. From this and the comparison shown in Figure 6.3.15 it can be said that although quite different stress variations are obtained for the eccentric loading case, the reliability of the theory to predict these is good. The comparison between theory and experiment for the other loading eccentricities considered is seen from the various figures to be fairly accurate and consistent, which, along with the load-deflection comparisons of the previous section, may be regarded as due corroboration of the theoretical approach.

6.4 COLLAPSE LOADS

As mentioned in section 6.2, the theoretical solution is terminated when the maximum membrane stress on the central buckle reaches the yield stress obtained from tensile tests of the column material. By postulating that failure ensues when this occurs it was found that a relatively close estimate of the failure load could be obtained from the elastic analysis. Table 6.4.1 shows the comparison between theory and experiment for the 33 columns tested in the experimental program. Although no account is taken of the weakening effects of plasticity it can be said, from the results shown, that failure is predicted with engineering accuracy on the assumption that collapse ensues when the maximum membrane stress reaches yield.

Figure 6.4.1 shows the comparison between the theoretical ultimate load prediction using the yield criterion for collapse, and the experimental work by Harvey (5) on centroidally loaded columns. The slenderness values of the volumns tested were varied with change in the web dimension b_w and due to this the theoretical local buckling loads are seen to reduce with increased slenderness. The web dimensions of the nine columns tested were 0.63, 0.83, 1.01, 1.17, 1.39, 1.74, 1.83, 2.08 and 2.51 inches. The experimental work by Harvey covered both stable and unstable post buckling behaviour as well as neutral column buckling and (with the exception of three results which seem to deviate to some extent from the general

trend) the comparison can be said to be good.

Figures 6.4.2 and 6.4.3 show comparisons of theoretical ultimate load predictions using the yield criterion, with collapse values obtained by McCall (23) from tests on centroidally and eccentrically loaded columns. The slenderness values of the columns tested were varied with change in column length and due to this the theoretical local buckling loads are seen from the figures to be unaltered with change in slenderness for the centroidal loading case and reduced with increase in slenderness for the eccentric loading case. The lengths of the columns tested in each case were 24.0, 36.0, 48.0, 60.0 and 72.0 inches. The experimental work by McCall covered stable post buckling behaviour only and, with the exception of two points in the centroidal loading case and one in the eccentric loading case the theory may be said to be able to predict ultimate loads with engineering accuracy.

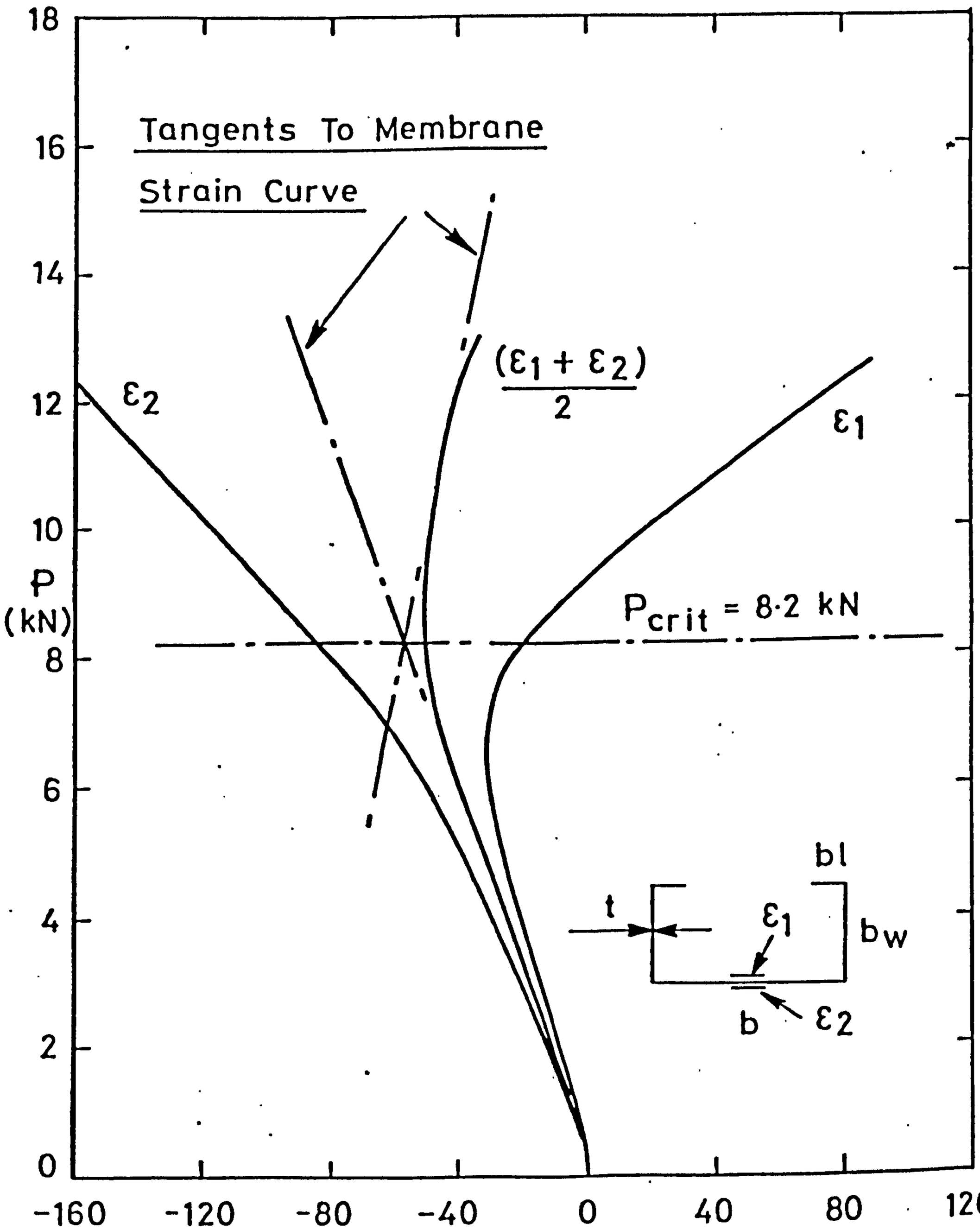

FIG. 6.1.1 DETERMINATION OF LOCAL BUCKLING LOAD FROM MEASURED STRAIN READINGS OF TEST COLUMN Nº 1.

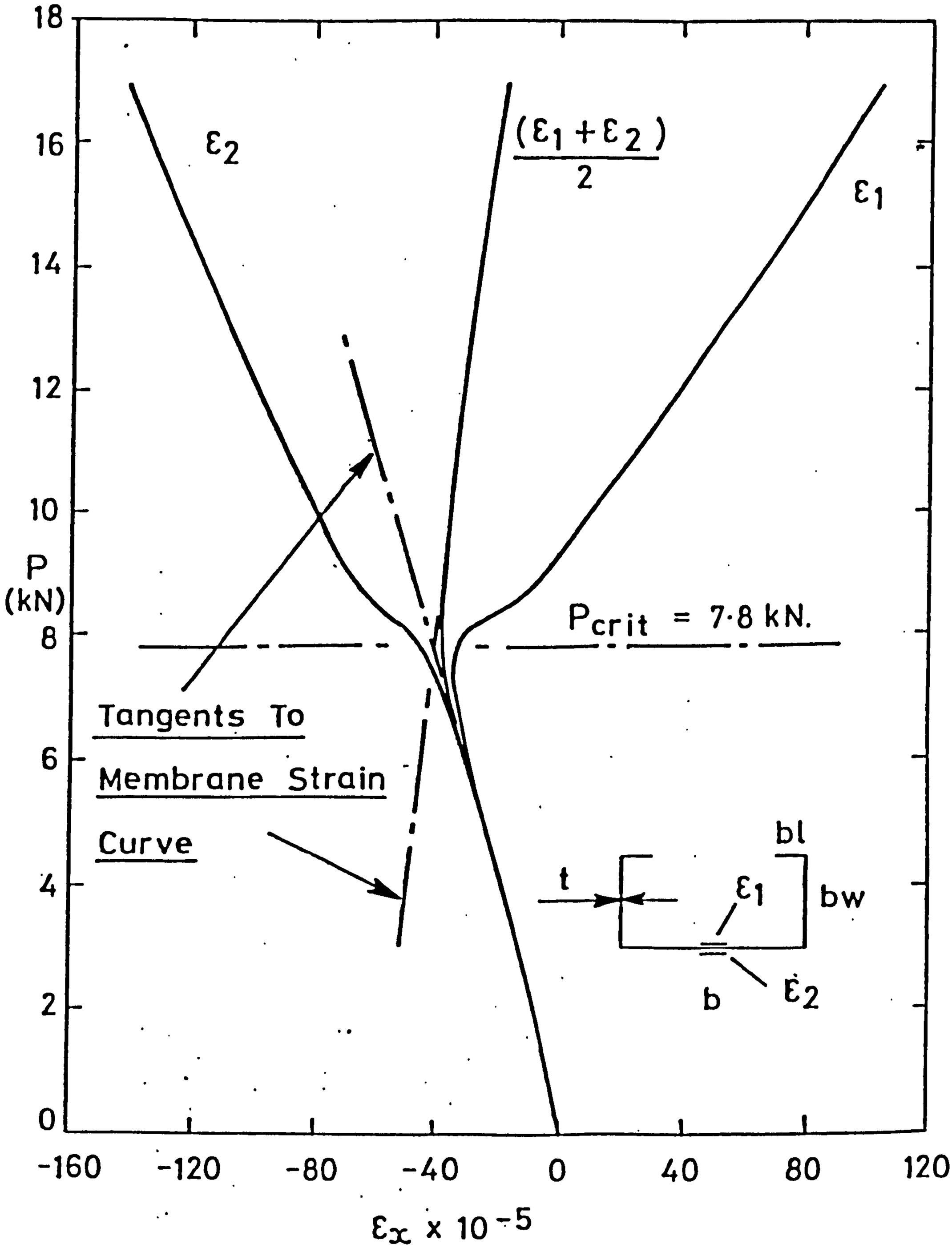

FIG. 6.1.2 DETERMINATION OF LOCAL BUCKLING LOAD. FROM MEASURED STRAIN READINGS OF TEST COLUMN Nº 7.

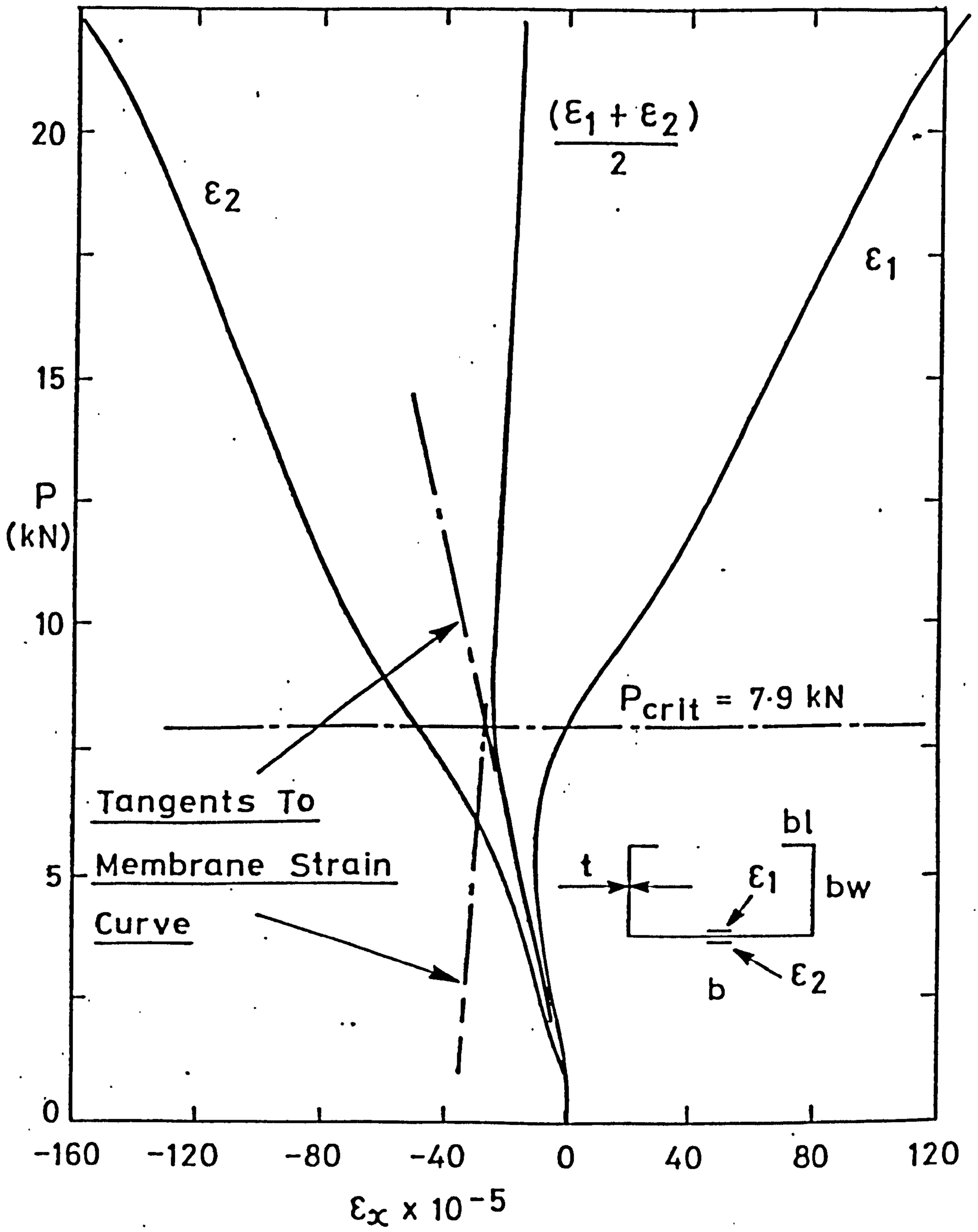

FIG. 6.1.3 DETERMINATION OF LOCAL BUCKLING LOAD FROM MEASURED STRAIN READINGS OF TEST COLUMN Nº 16.

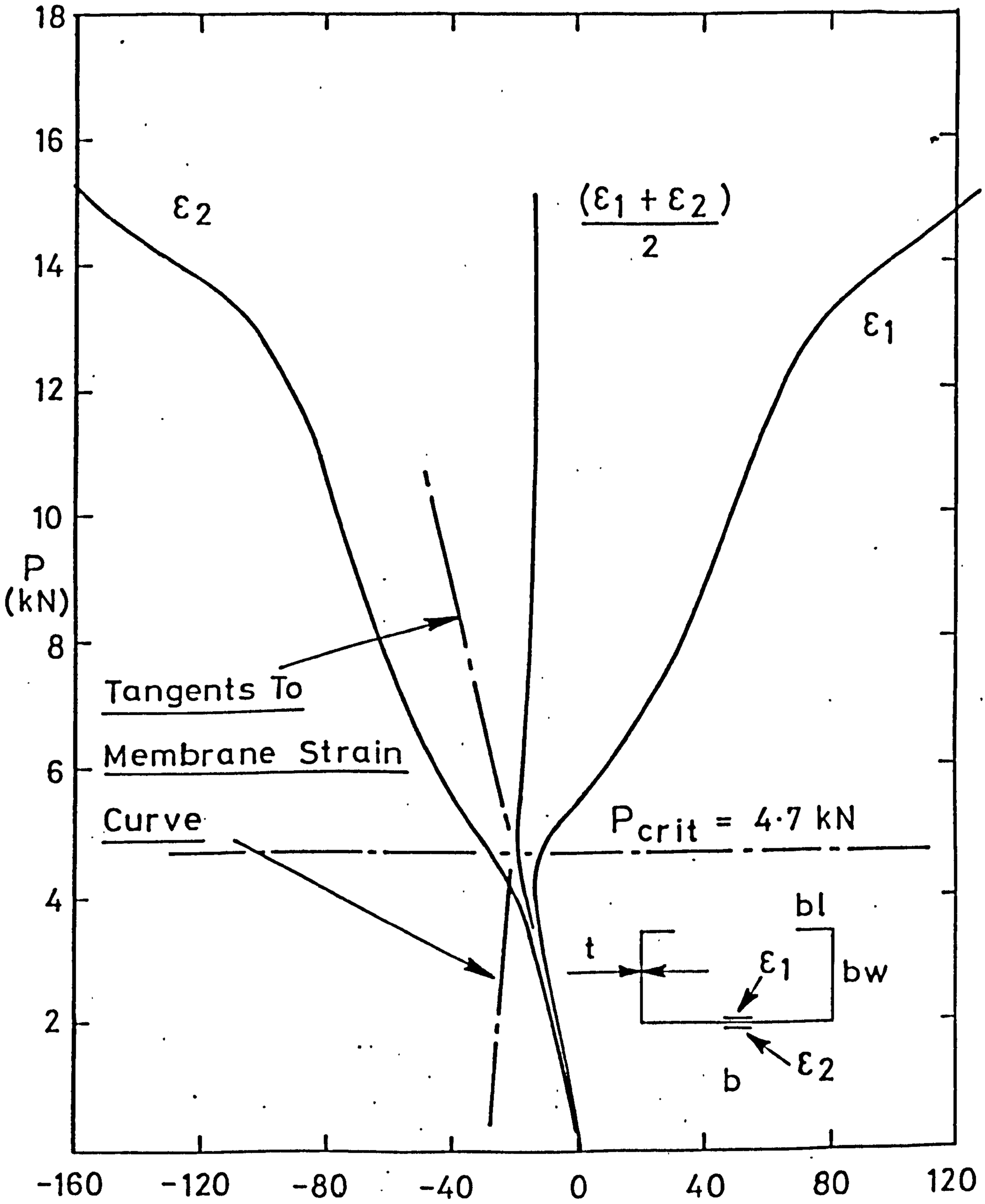

FIG. 6.1.4 DETERMINATION OF LOCAL BUCKLING LOAD FROM MEASURED STRAIN READINGS OF TEST COLUMN Nº 20.

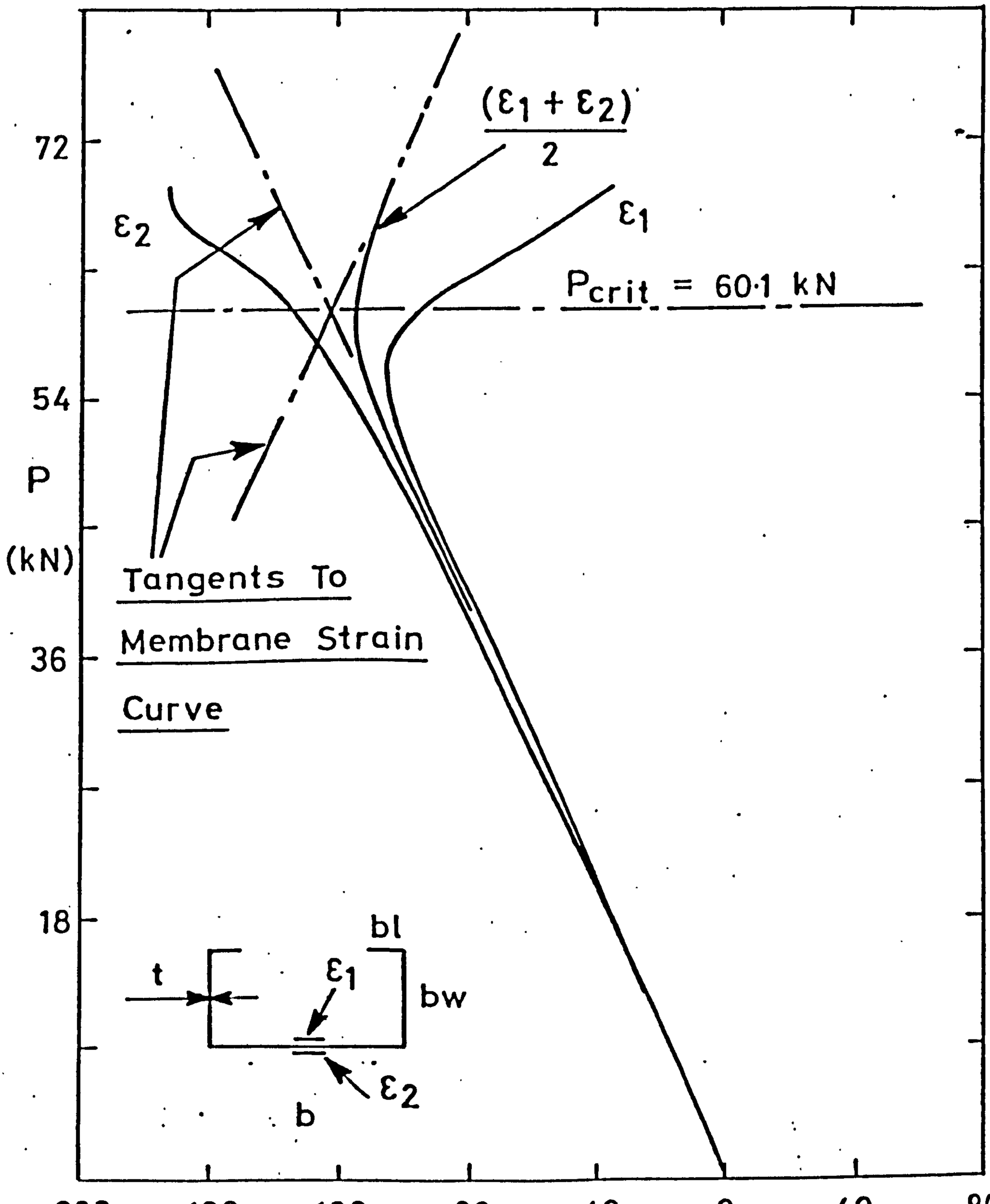

FIG. 6.1.5 DETERMINATION OF LOCAL BUCKLING LOAD FROM MEASURED STRAIN READINGS OF TEST COLUMN Nº 25

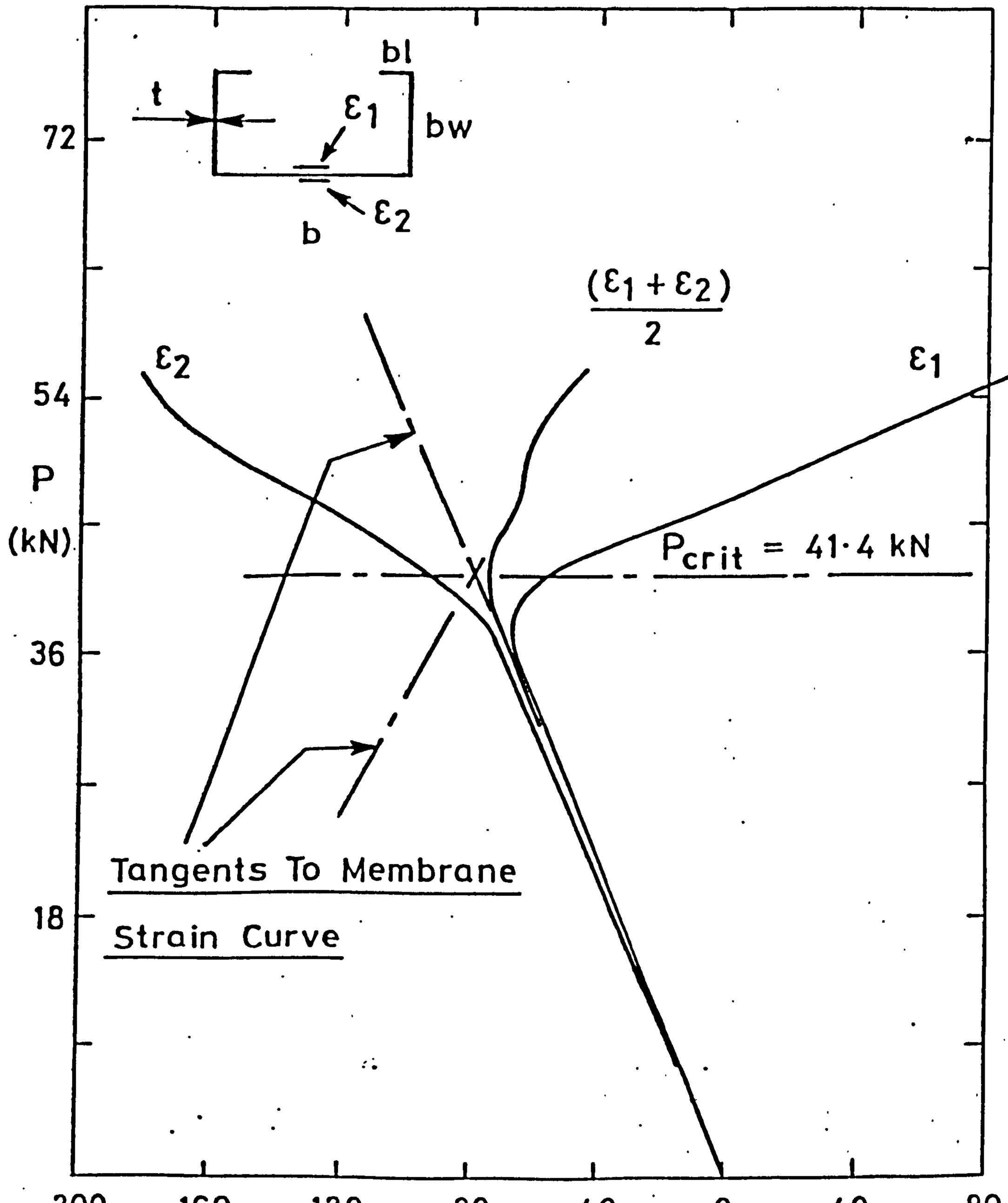

FIG. 6.1.6 DETERMINATION OF LOCAL BUCKLING LOAD. FROM MEASURED STRAIN READINGS OF TEST COLUMN Nº 29.

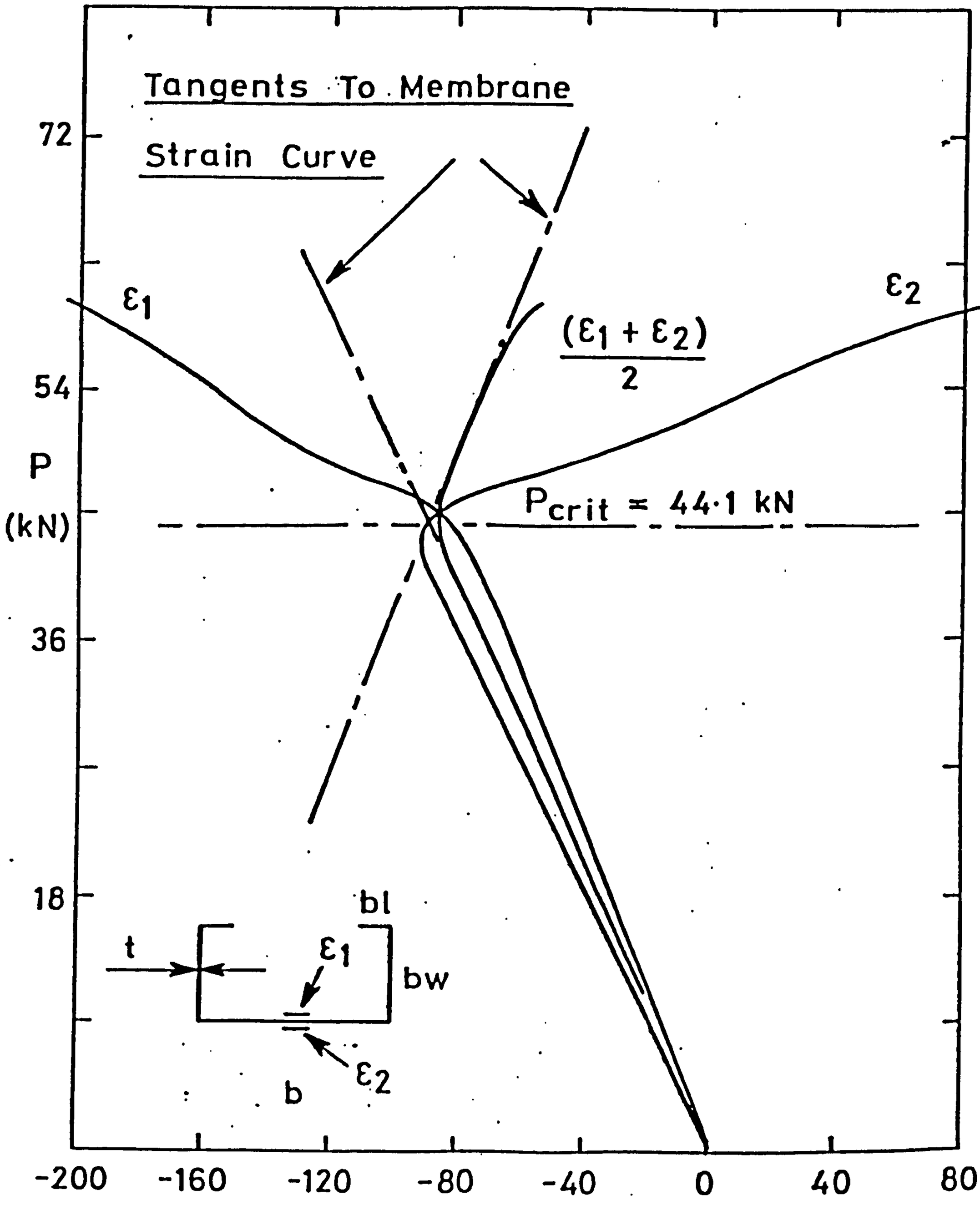

FIG. 6.1.7. DETERMINATION OF LOCAL BUCKLING LOAD FROM MEASURED STRAIN READINGS OF TEST COLUMN Nº 30.

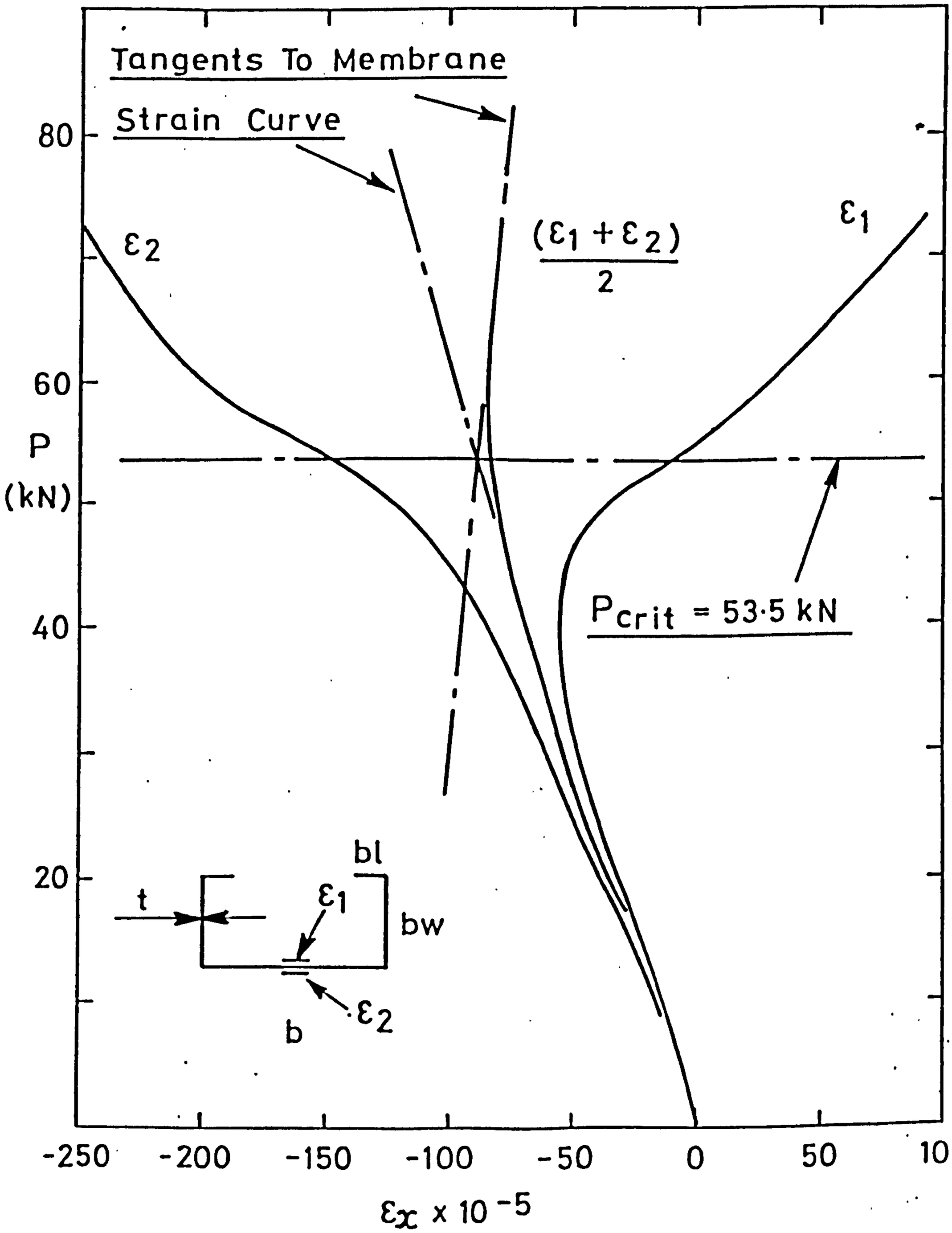

FIG. 6.1.8 DETERMINATION OF LOCAL BUCKLING LOAD FROM MEASURED STRAIN READINGS OF TEST COLUMN Nº 33

COLUMN Nº	$P_{crit\ exp}$ (kN)	$P_{crit_{theo}}$ (kN)	$\frac{P_{crit_{theo}}}{P_{crit\ exp}}$	COLUMN Nº	$P_{crit\ exp}$ (kN)	$P_{crit_{theo}}$ (kN)	$\frac{P_{crit_{theo}}}{P_{crit\ exp}}$	COLUMN Nº	$P_{crit\ exp}$ (kN)	$P_{crit_{theo}}$ (kN)	$\frac{P_{crit_{theo}}}{P_{crit\ exp}}$
1	8·2	8·53	1·04	12	5·4	5·63	1·04	23	5·25	5·11	0·97
2	8·3	8·13	0·98	13	5·2	5·57	1·07	24	56·9	58·36	1·03
3	8·8	8·46	0·96	14	5·36	5·72	1·07	25	60·1	61·05	1·02
4	9·2	9·49	1·03	15	7·4	7·01	0·95	26	60·15	63·89	1·06
5	8·9	8·78	0·99	16	7·9	7·23	0·92	27	62·7	62·74	1·00
6	7·6	7·25	0·95	17	7·7	7·14	0·93	28	40·0	40·16	1·00
7	7·8	7·40	0·95	18	3·9	4·15	1·06	29	41·4	42·23	1·02
8	7·5	7·66	1·02	19	4·7	4·29	0·91	30	44·1	43·15	0·98
9	7·1	7·62	1·07	20	4·7	4·49	0·96	31	48·5	51·03	1·05
10	8·0	7·86	0·98	21	4·36	4·78	1·10	32	49·15	51·58	1·05
11	8·1	8·33	1·03	22	5·1	5·27	1·03	33	53·5	52·41	0·98

TABLE 6.1.1 COMPARISON OF THEORETICAL AND EXPERIMENTAL LOCAL BUCKLING LOADS.

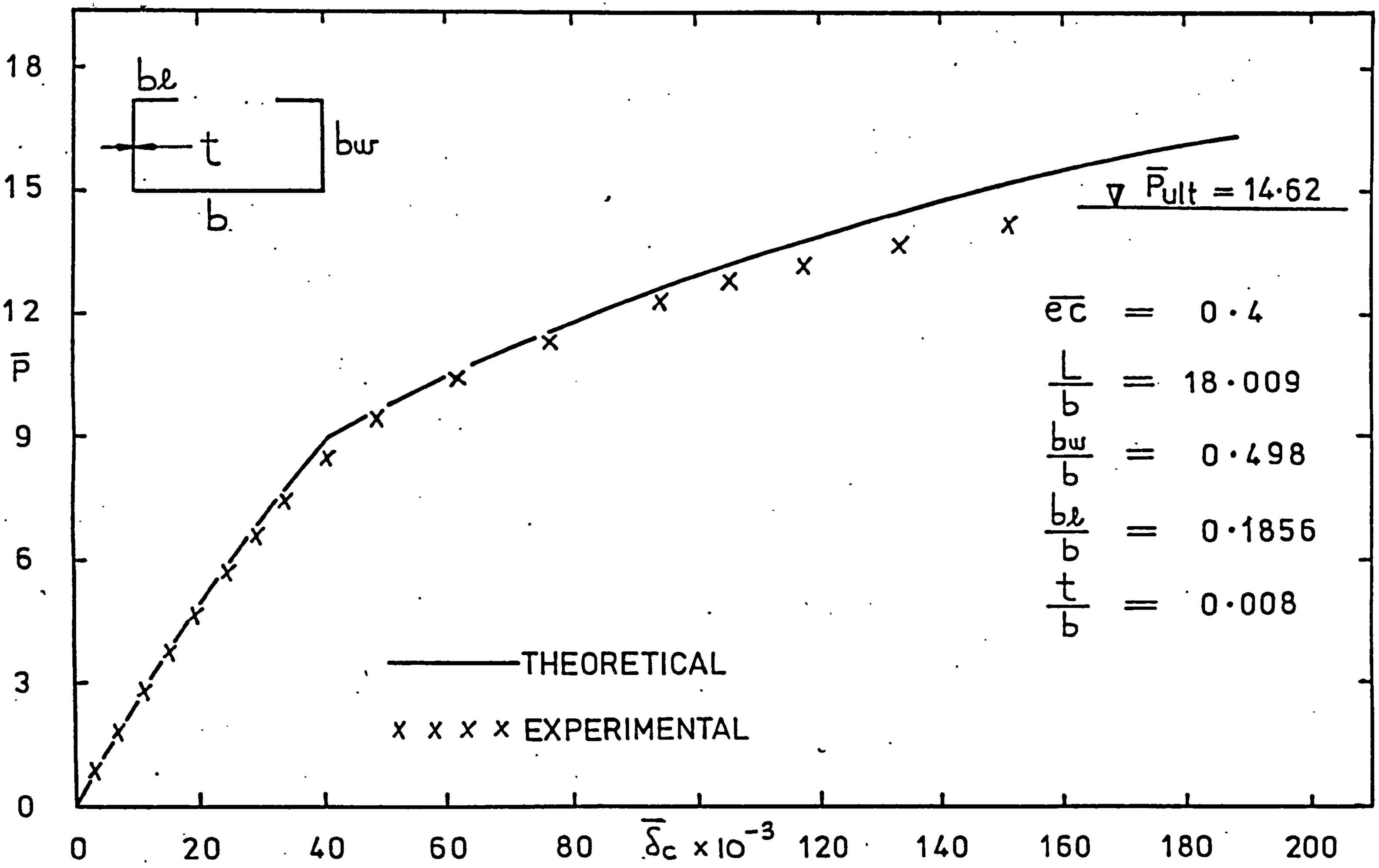

FIG. 6.2.1 LOAD–DEFLECTION COMPARISON FOR TEST COLUMN Nº 1.

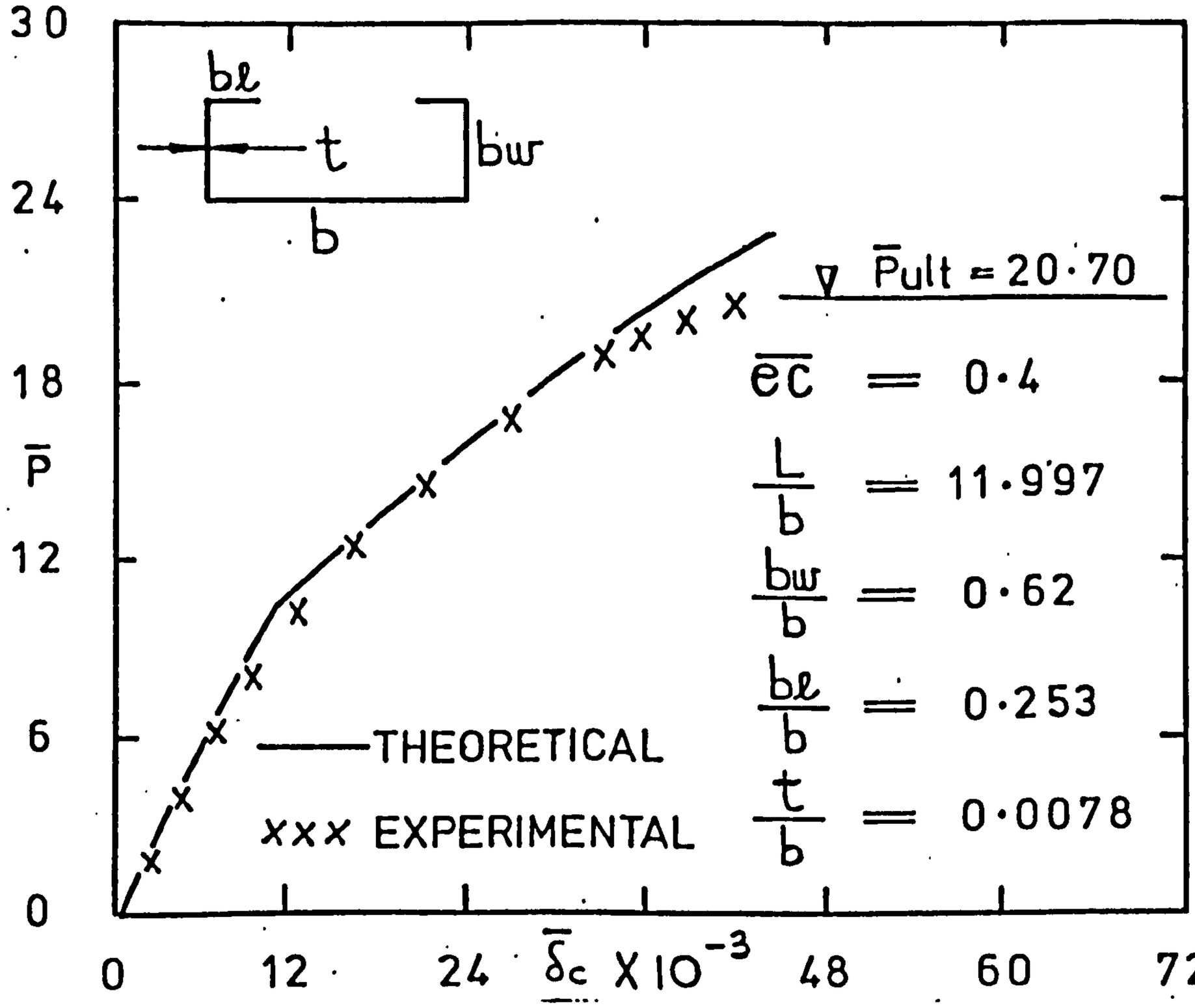

FIG. 6.2.2 LOAD-DEFLECTION COMPARISON FOR TEST COLUMN Nº 5.

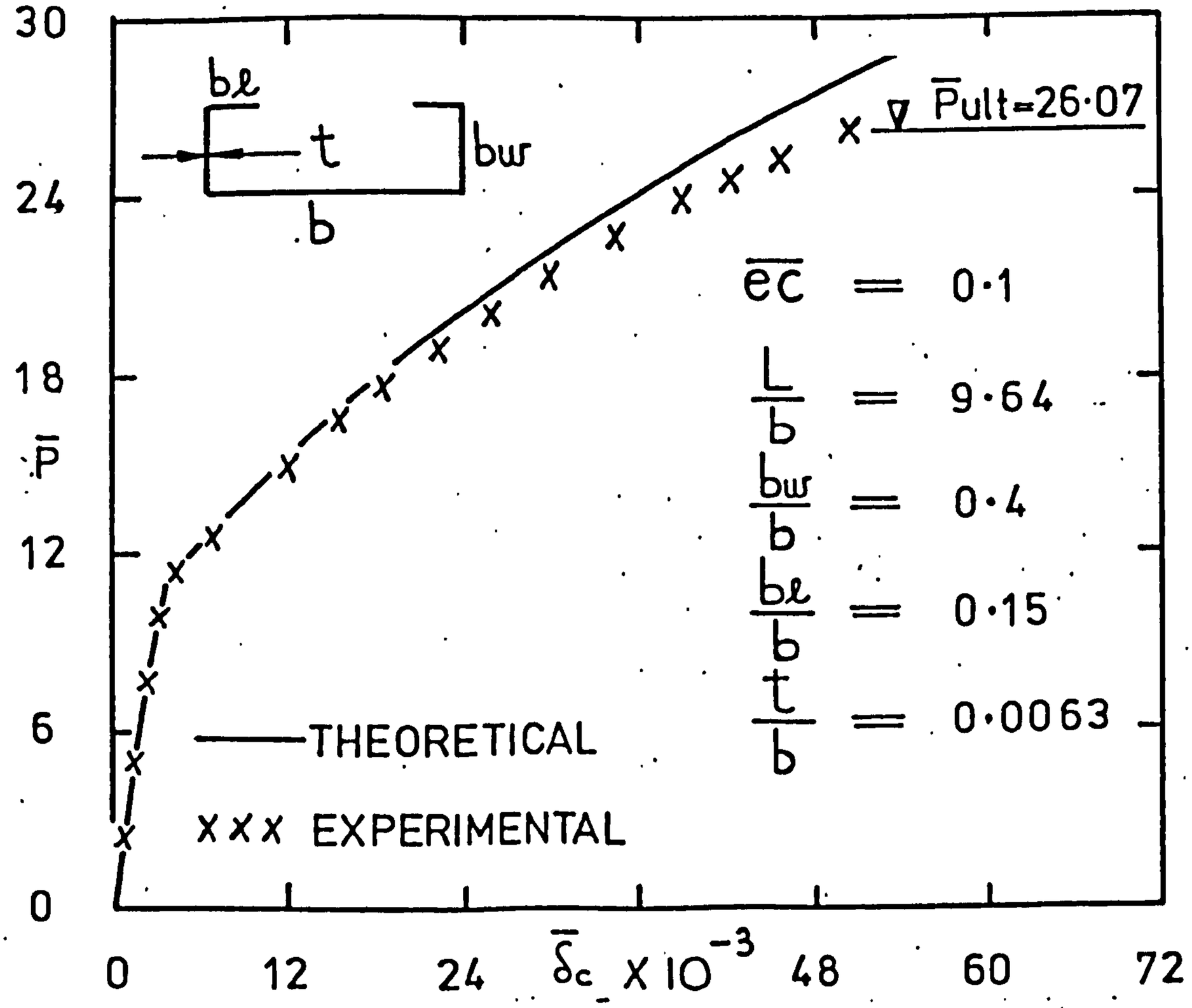

FIG. 6.2.3 LOAD-DEFLECTION COMPARISON FOR TEST COLUMN Nº 8.

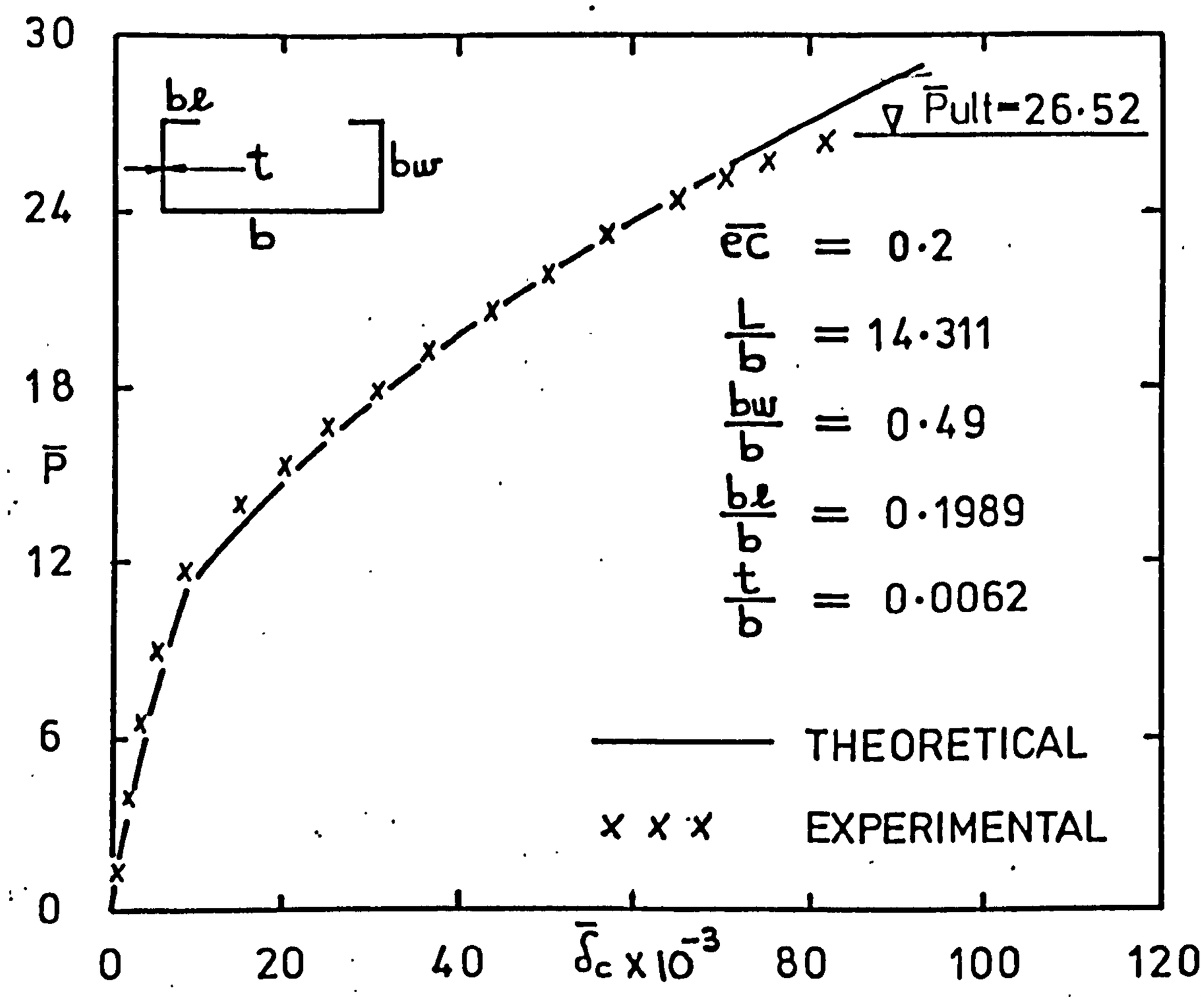

FIG. 6.2.4 LOAD-DEFLECTION COMPARISON FOR TEST COLUMN Nº 9.

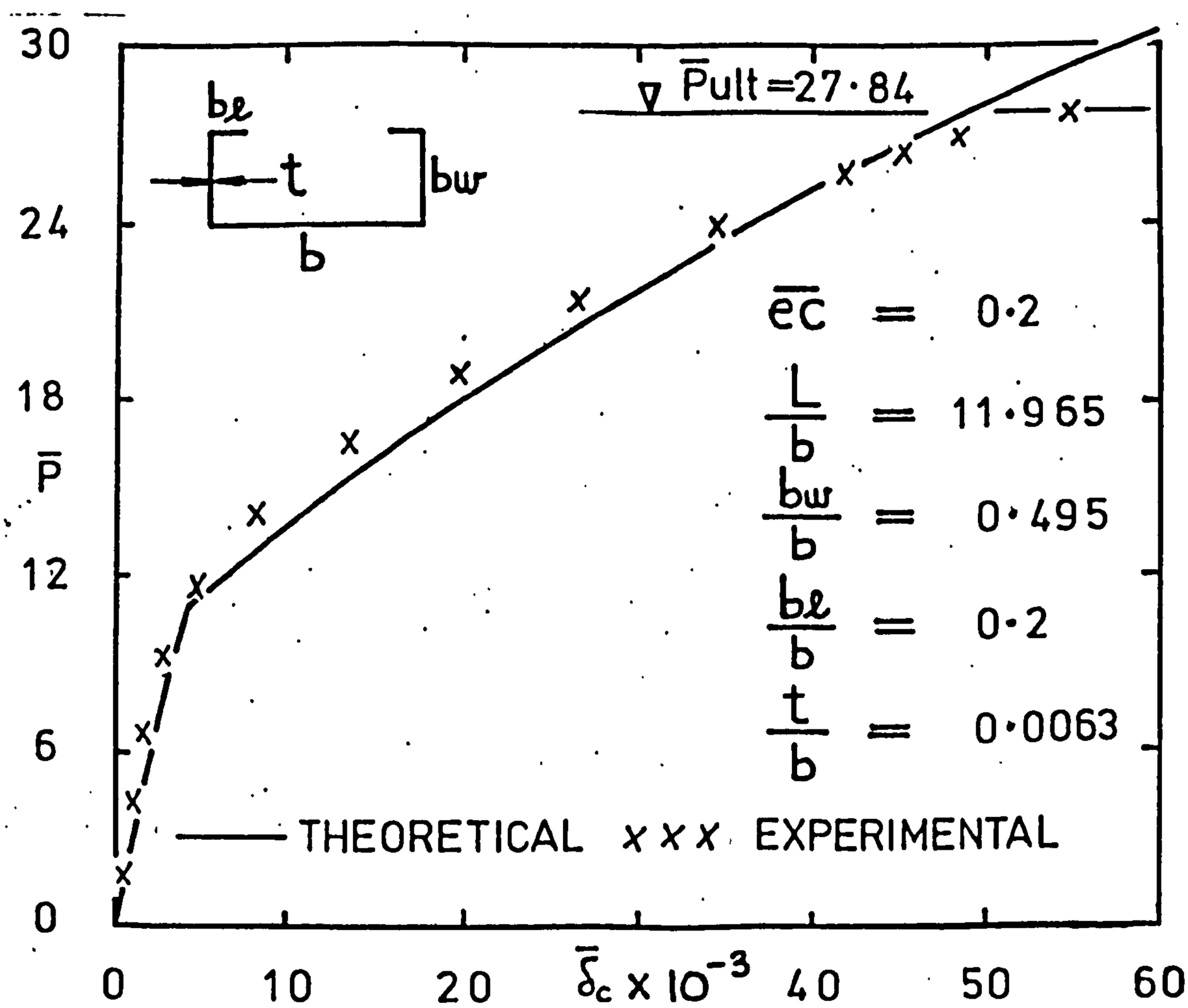

FIG. 6.2.5 LOAD-DEFLECTION COMPARISON FOR TEST COLUMN Nº 10.

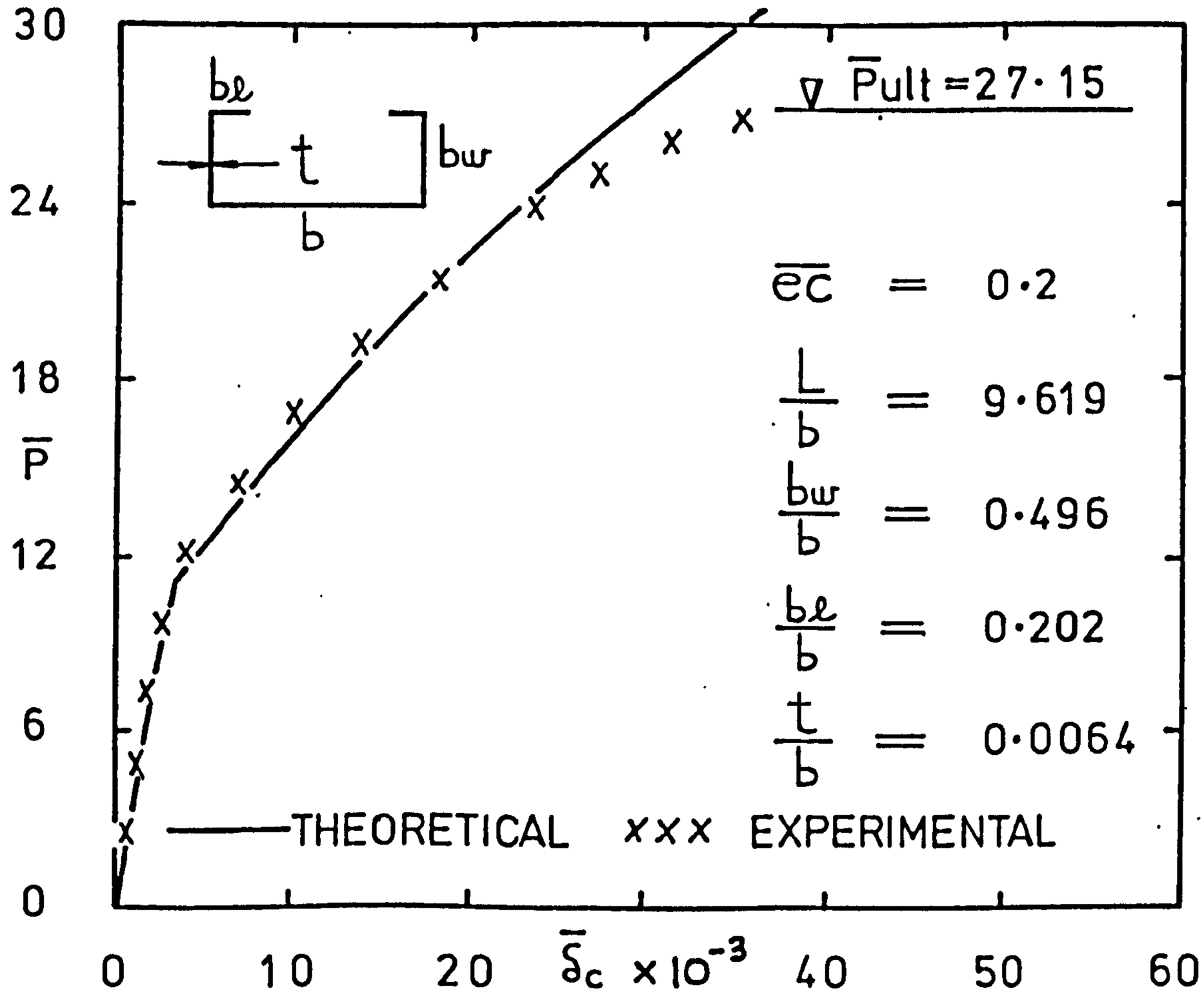

FIG. 6.2.6 LOAD-DEFLECTION COMPARISON FOR TEST COLUMN Nº 11.

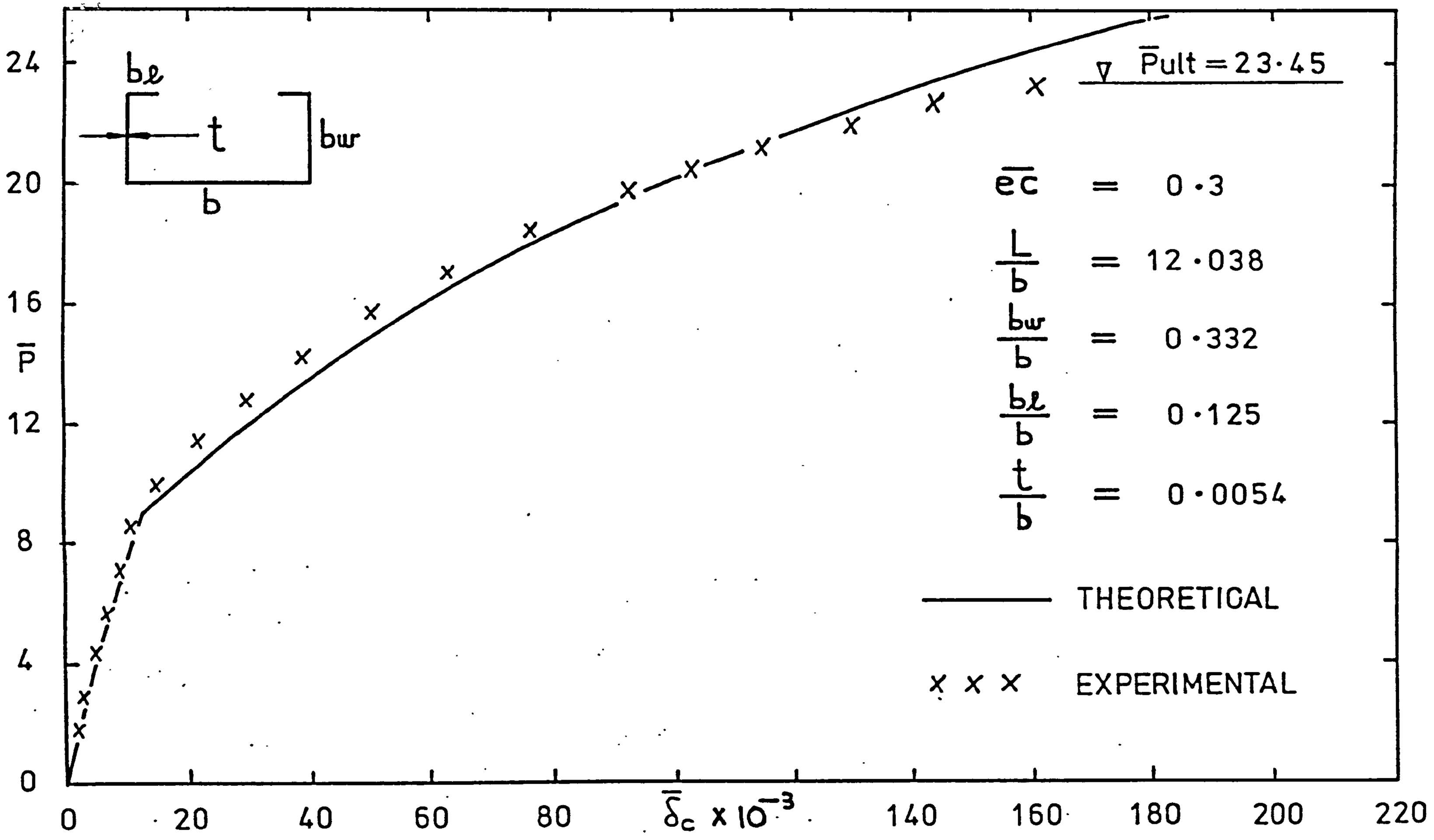

FIG. 6.2.7 LOAD-DEFLECTION COMPARISON FOR TEST COLUMN Nº 12.

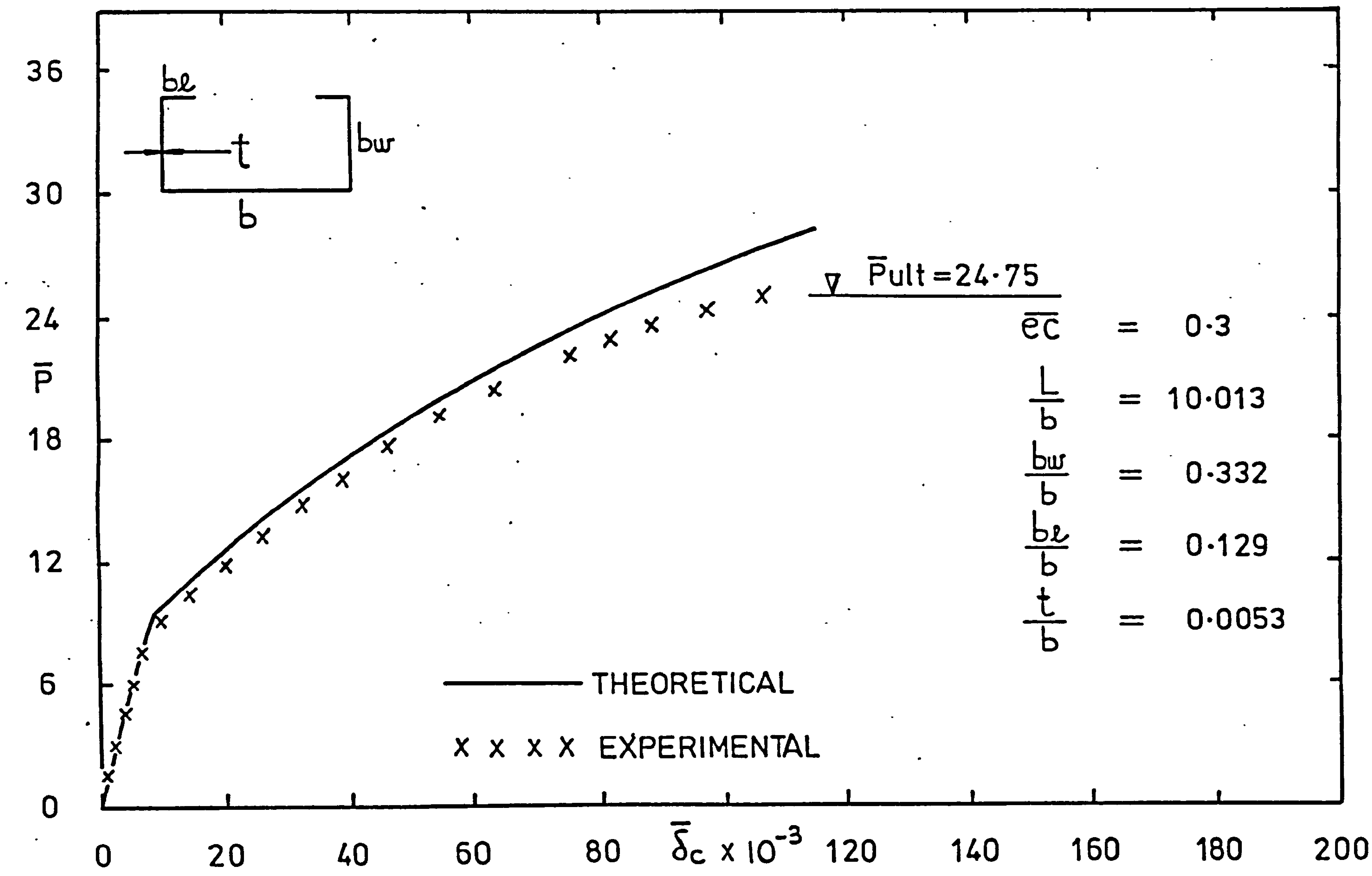

FIG. 6.2.8 LOAD-DEFLECTION COMPARISON FOR TEST COLUMN No 13.

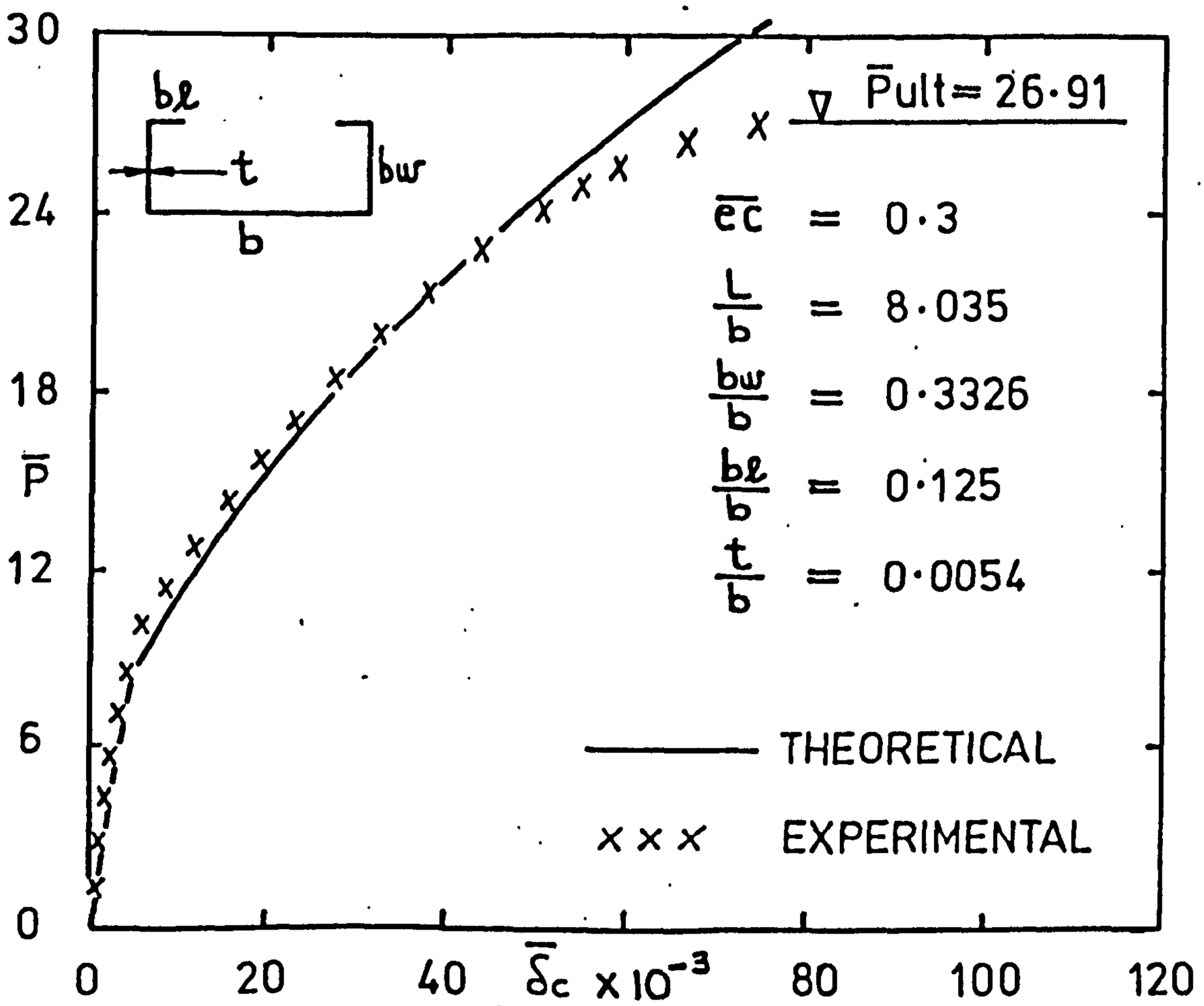

FIG. 6.2.9 LOAD-DEFLECTION COMPARISON FOR TEST COLUMN Nº 14.

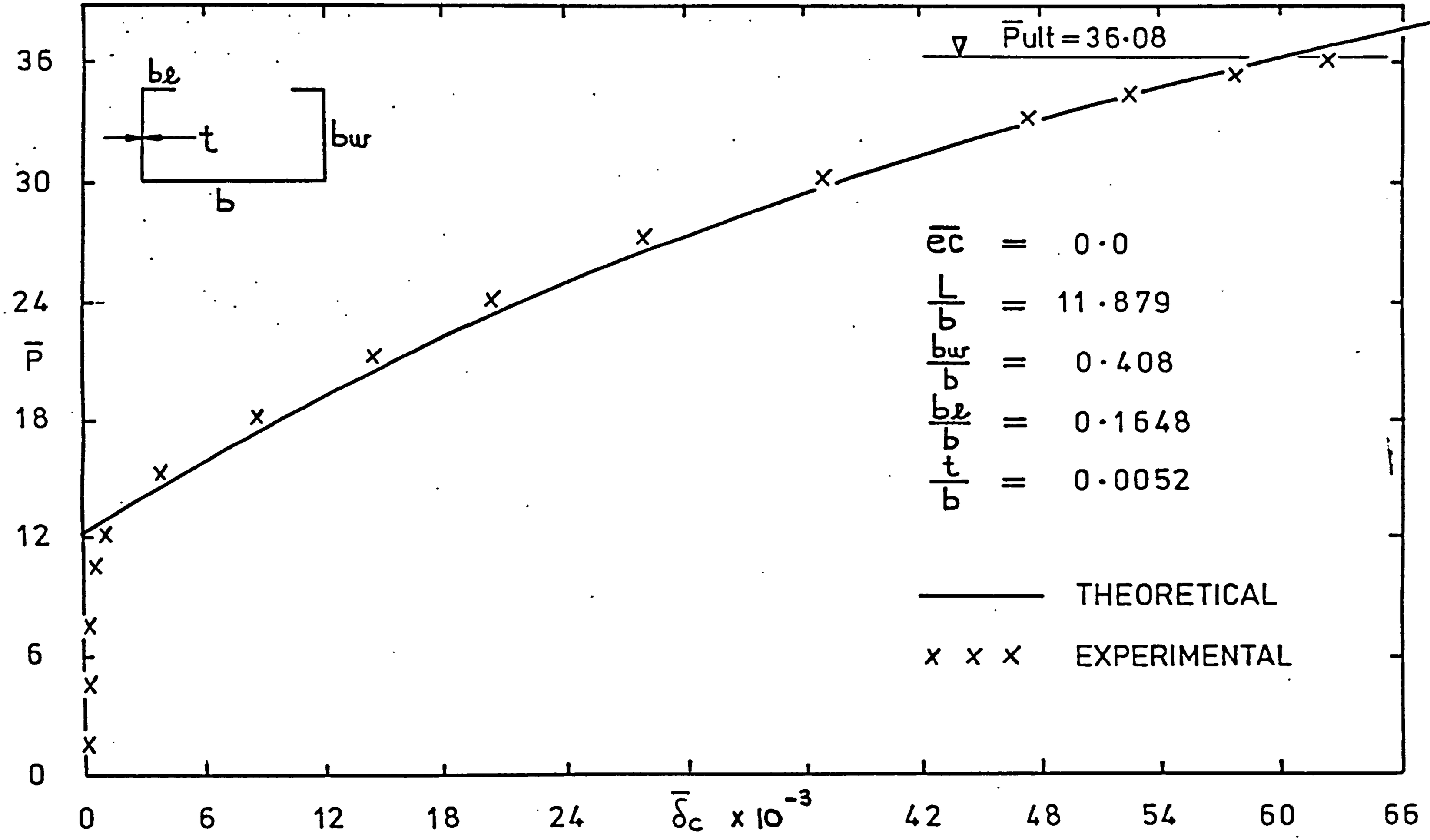

FIG. 6.2.10 LOAD-DEFLECTION COMPARISON FOR TEST COLUMN Nº 15.

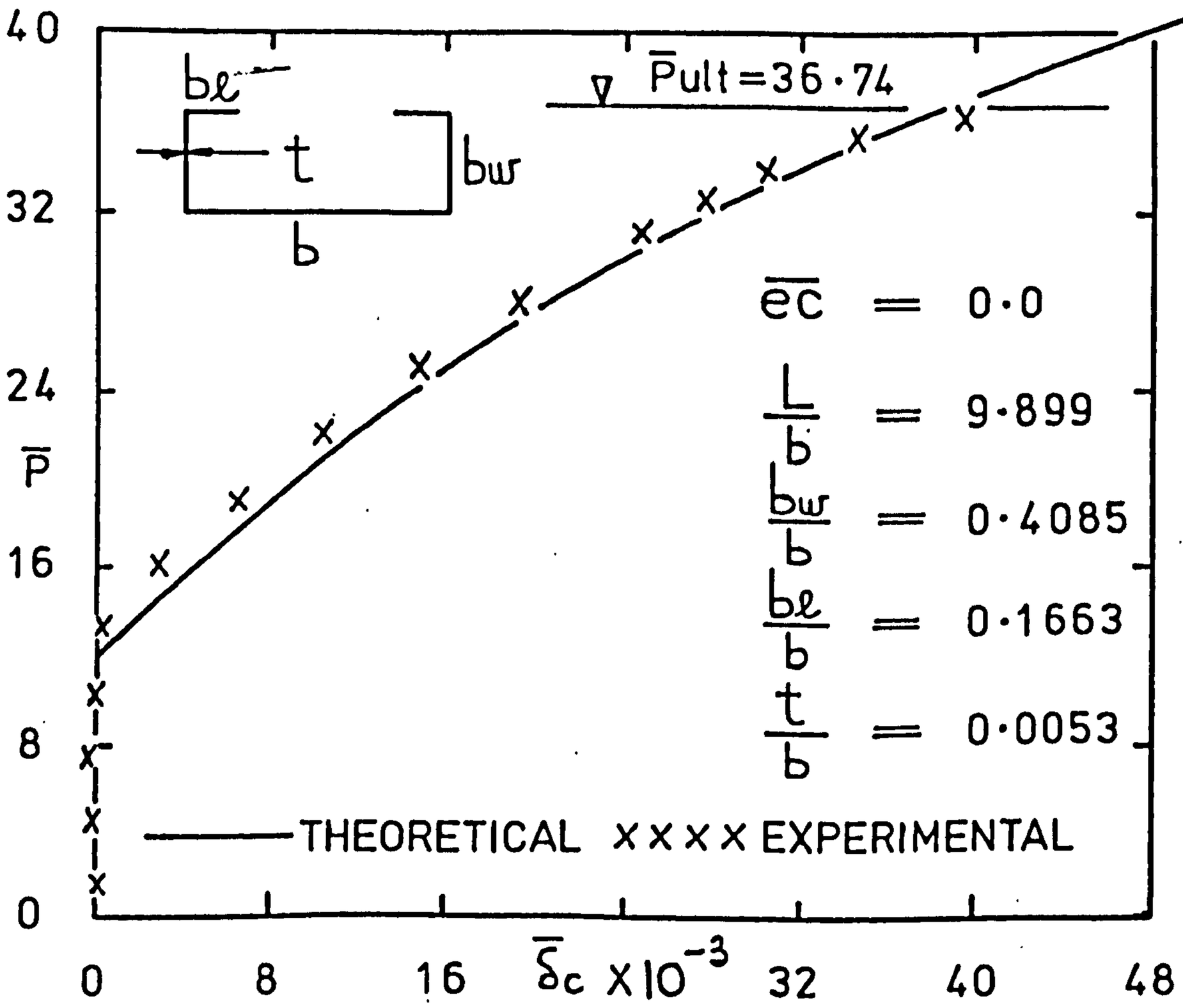

FIG. 6.2.11 LOAD-DEFLECTION COMPARISON FOR TEST COLUMN Nº 16.

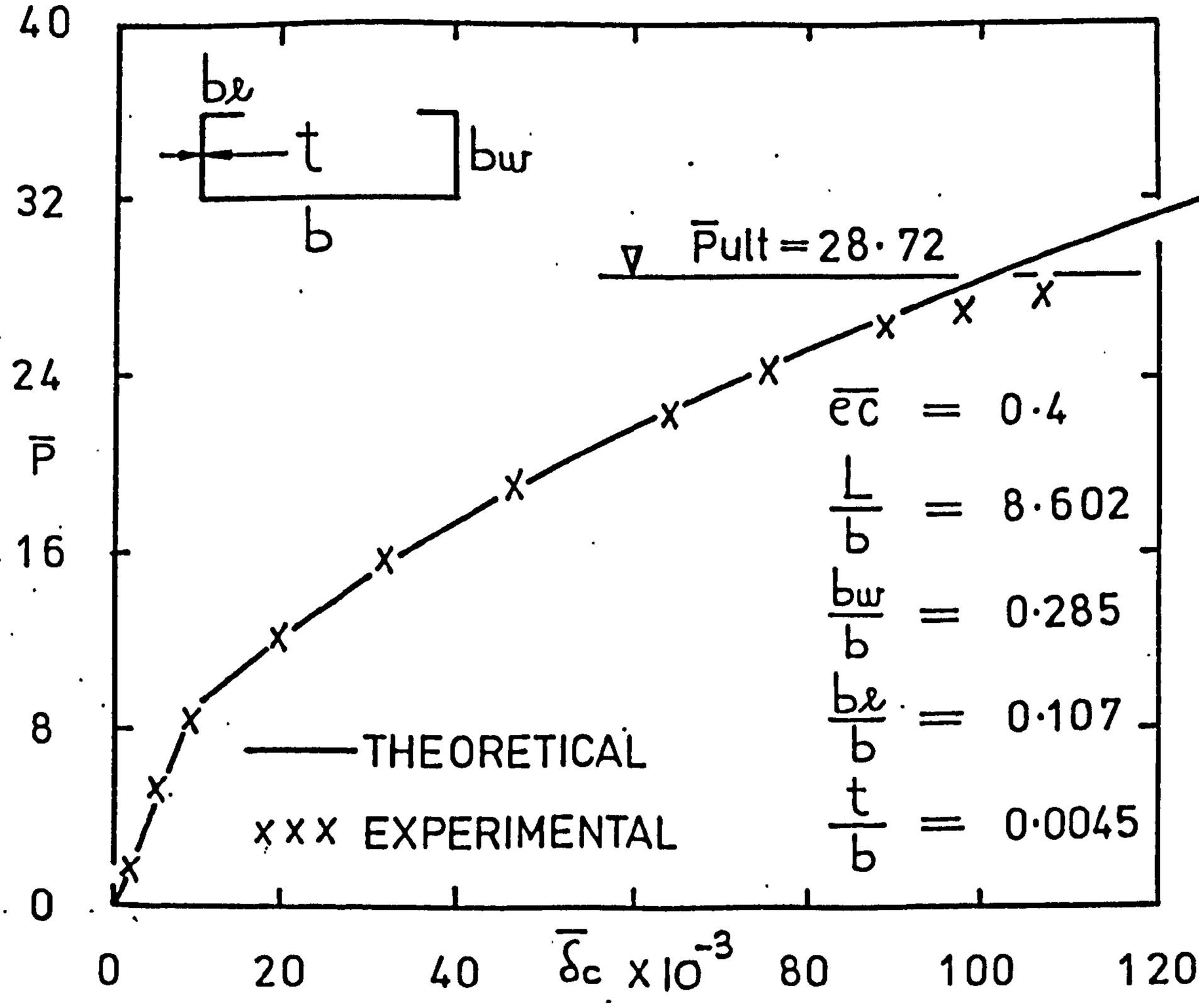

FIG. 6.2.12 LOAD-DEFLECTION COMPARISON FOR TEST COLUMN Nº 19.

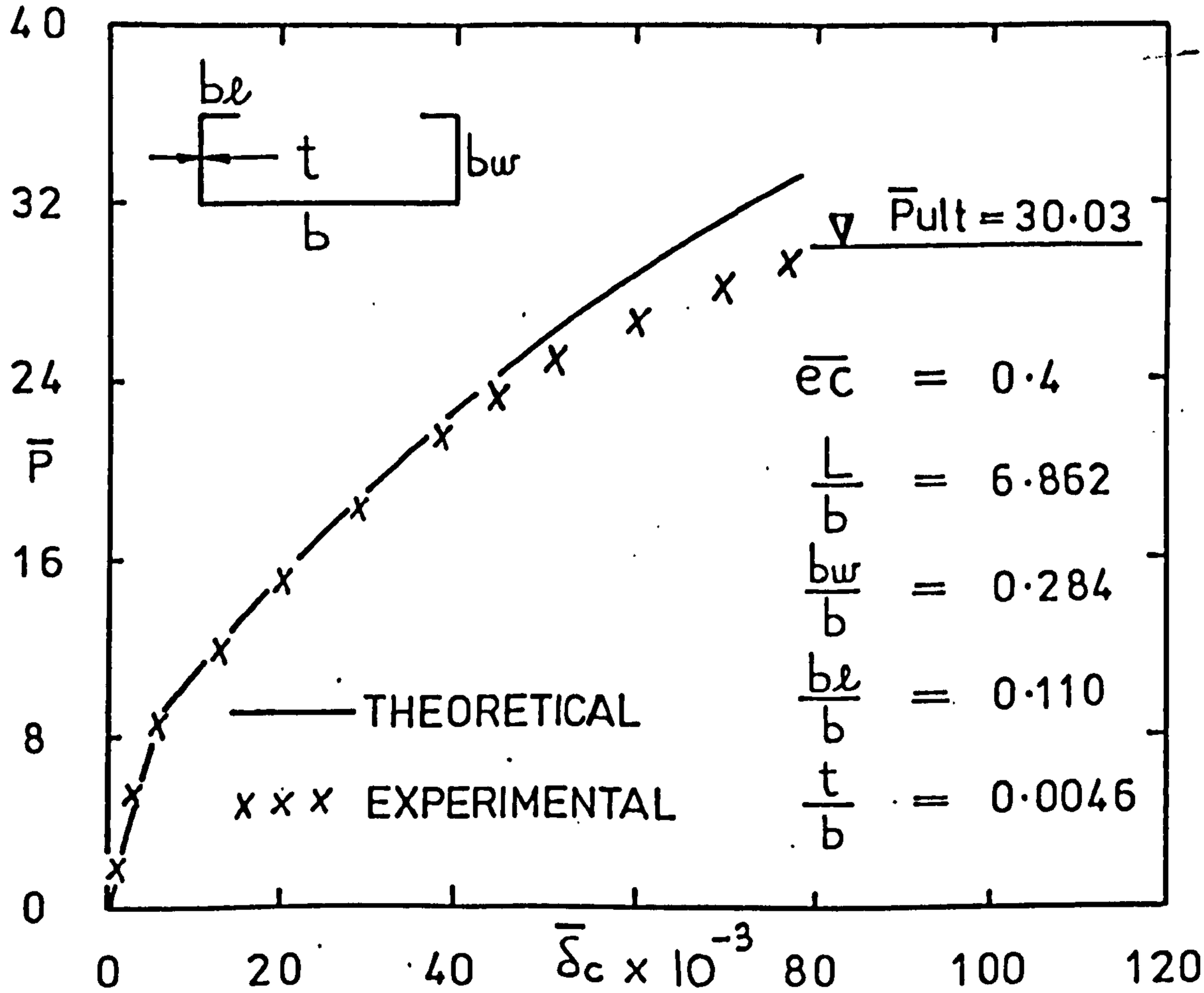

FIG. 6.2.13 LOAD DEFLECTION COMPARISON FOR TEST COLUMN N° 20.

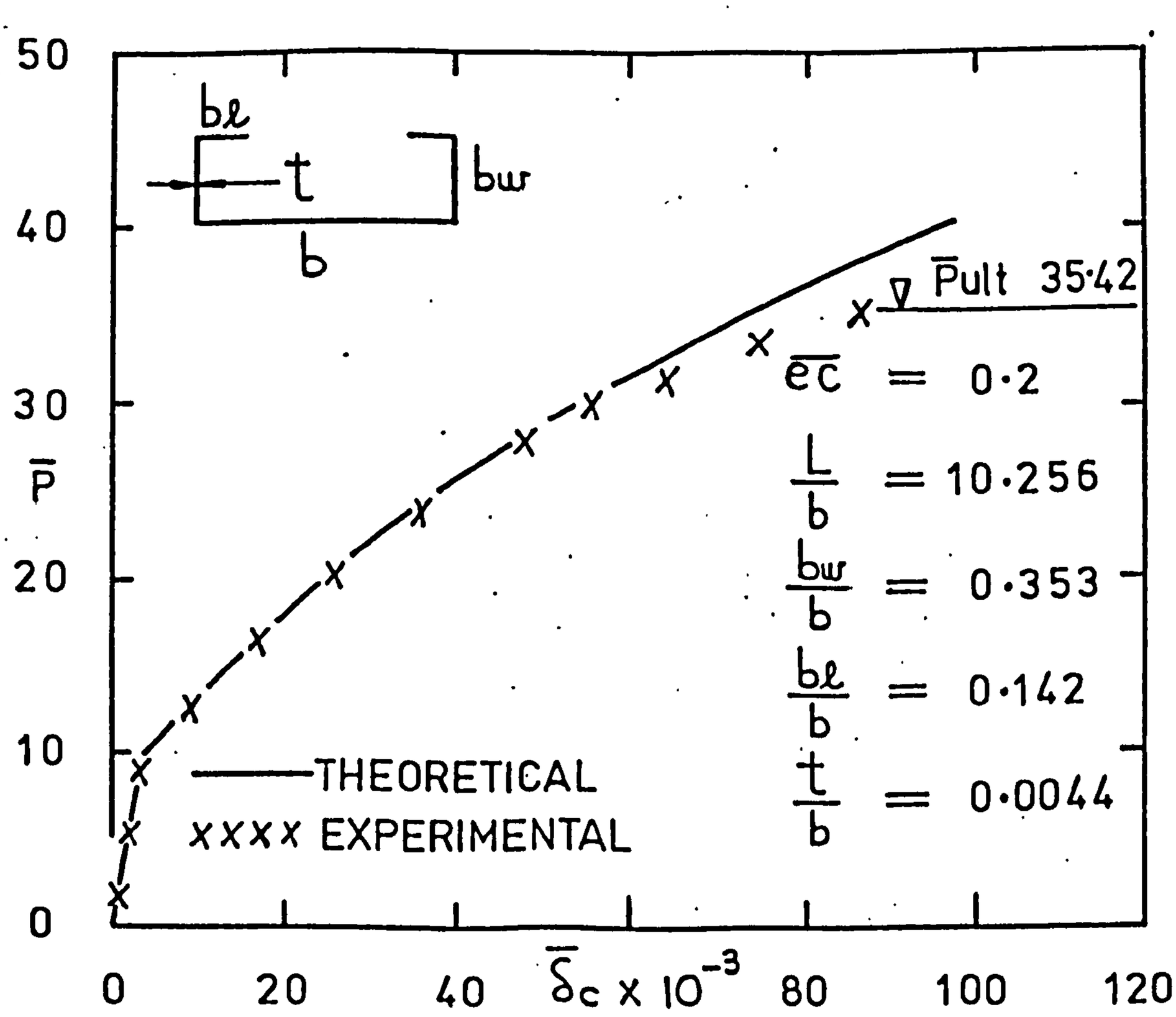

FIG. 6.2.14 LOAD DEFLECTION COMPARISON FOR TEST COLUMN N° 21.

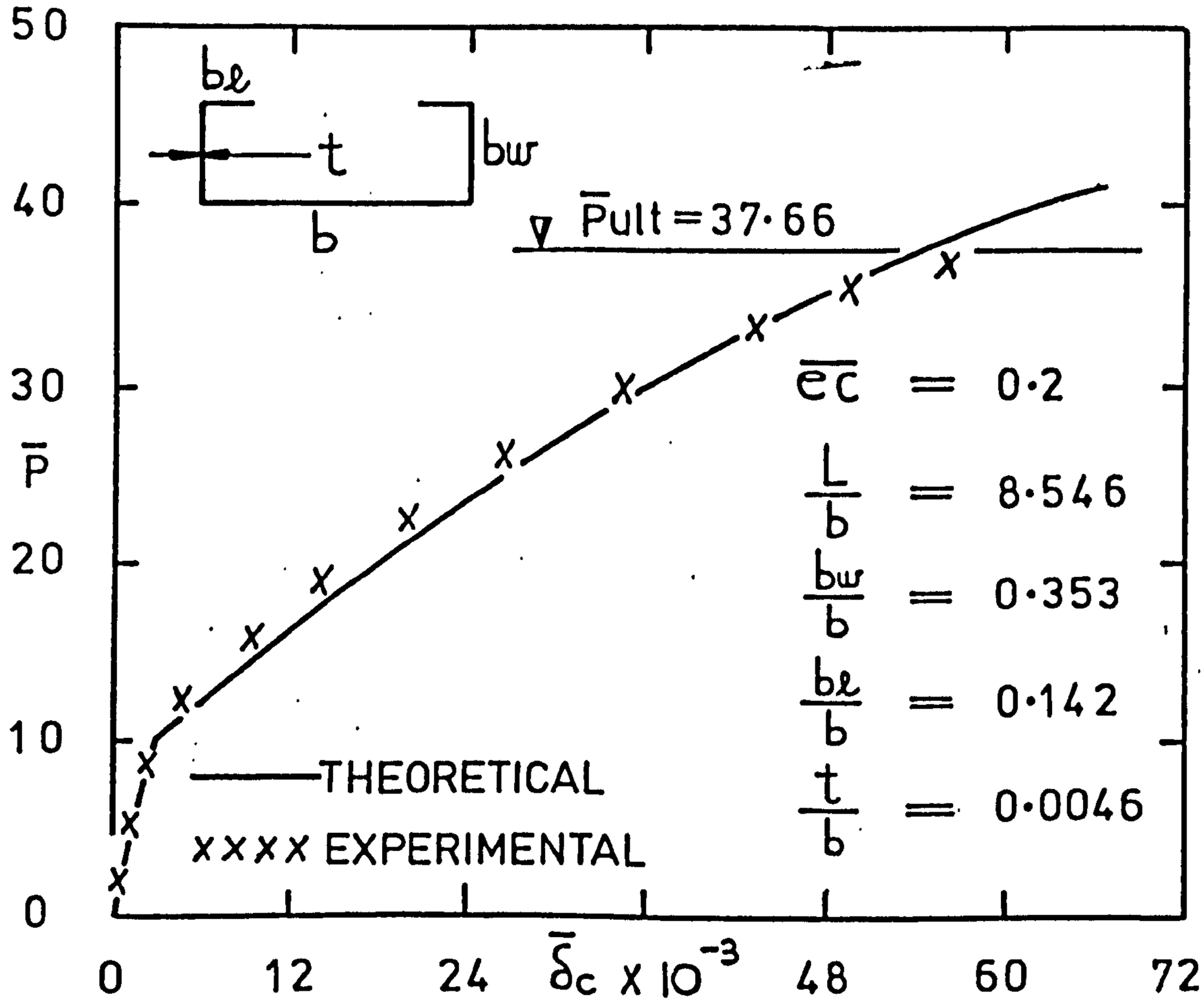

FIG. 6.2.15 LOAD DEFLECTION COMPARISON FOR TEST COLUMN N° 22.

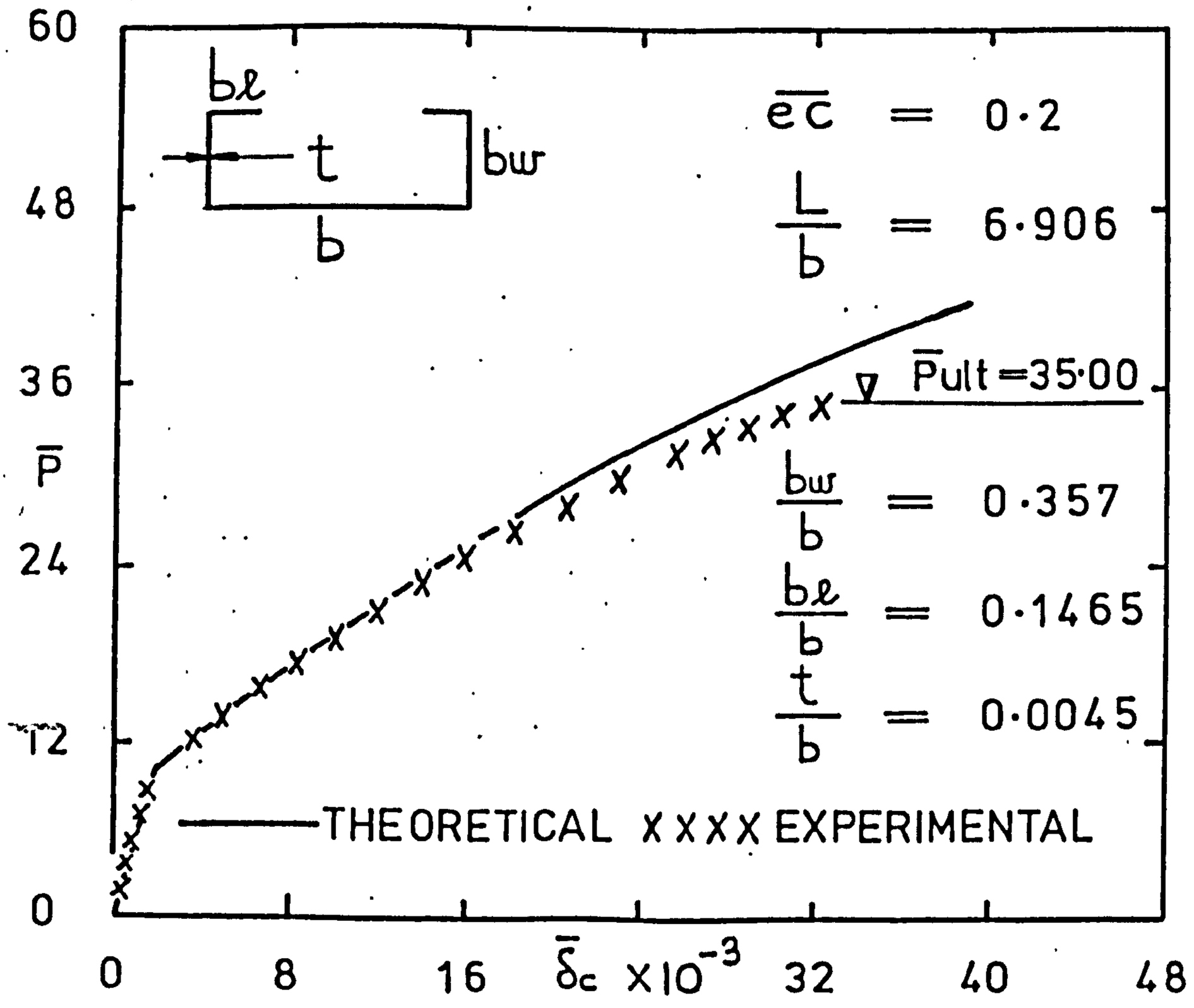

FIG. 6.2.16 LOAD DEFLECTION COMPARISON FOR TEST COLUMN N° 23.

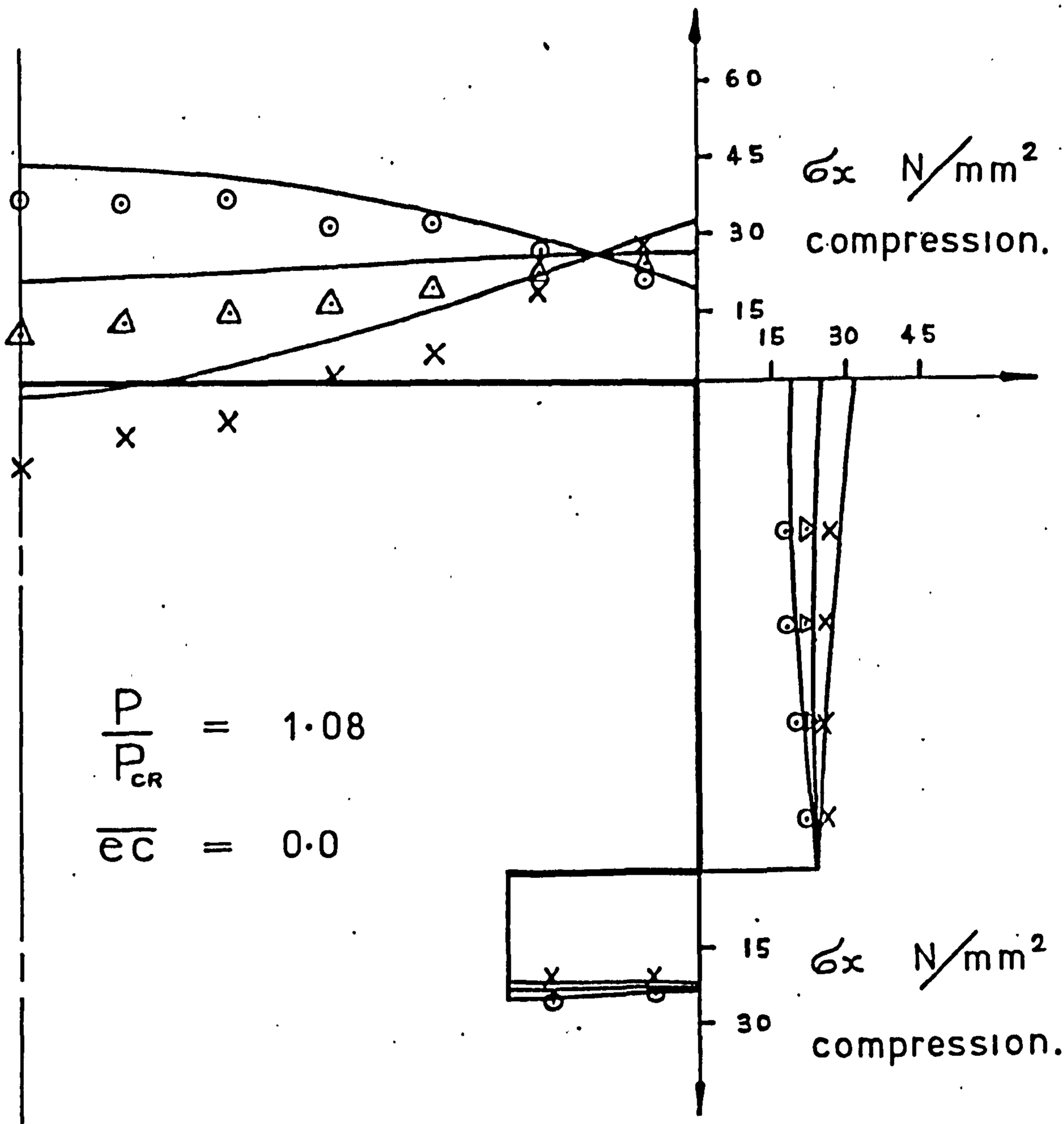

FIG. 6.3.1 LONGITUDINAL STRESS DISTRIBUTION AT LOAD P = 6·23 kN.

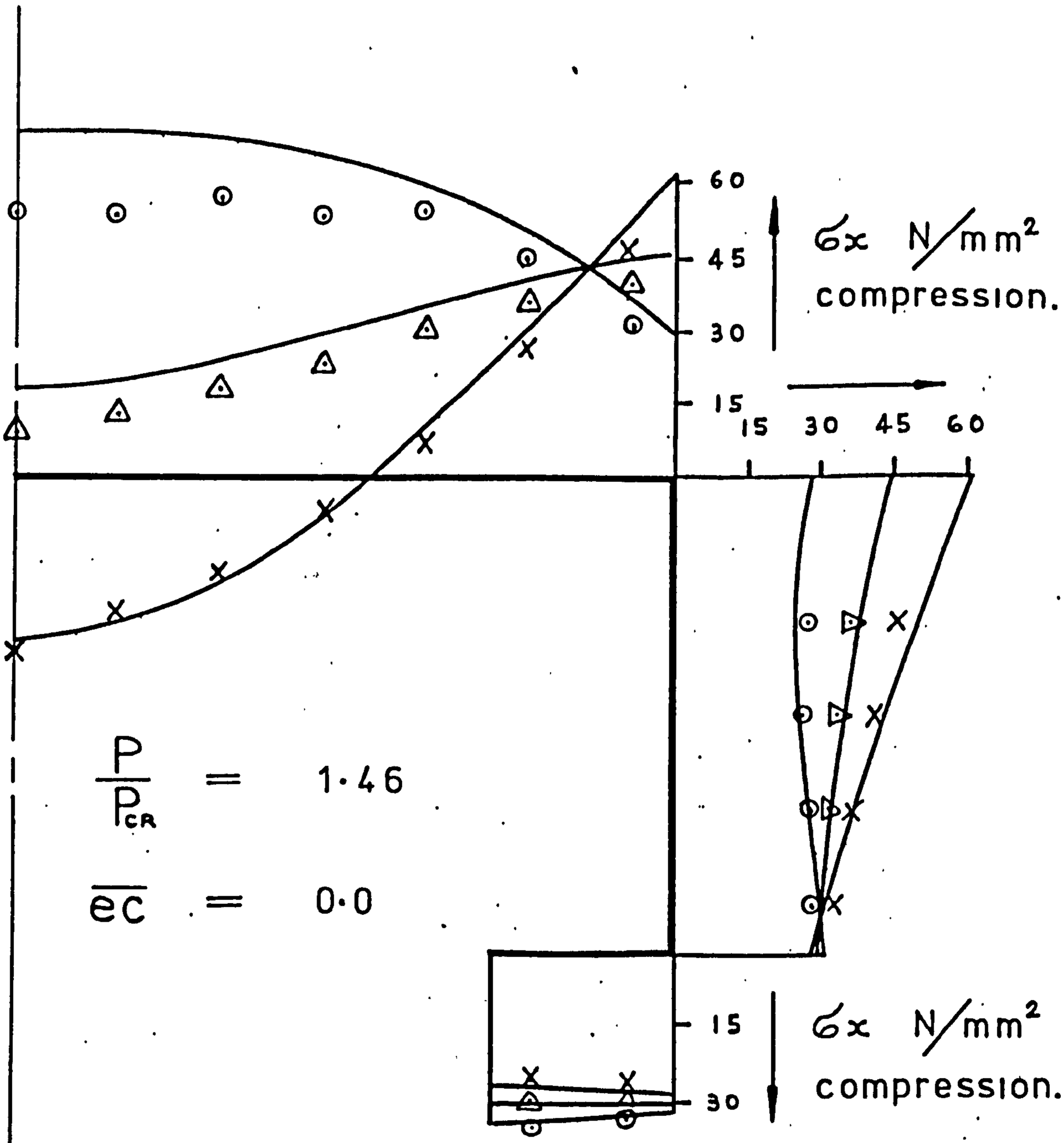

FIG. 6.3.2 LONGITUDINAL STRESS DISTRIBUTION AT LOAD P = 8·455 kN.

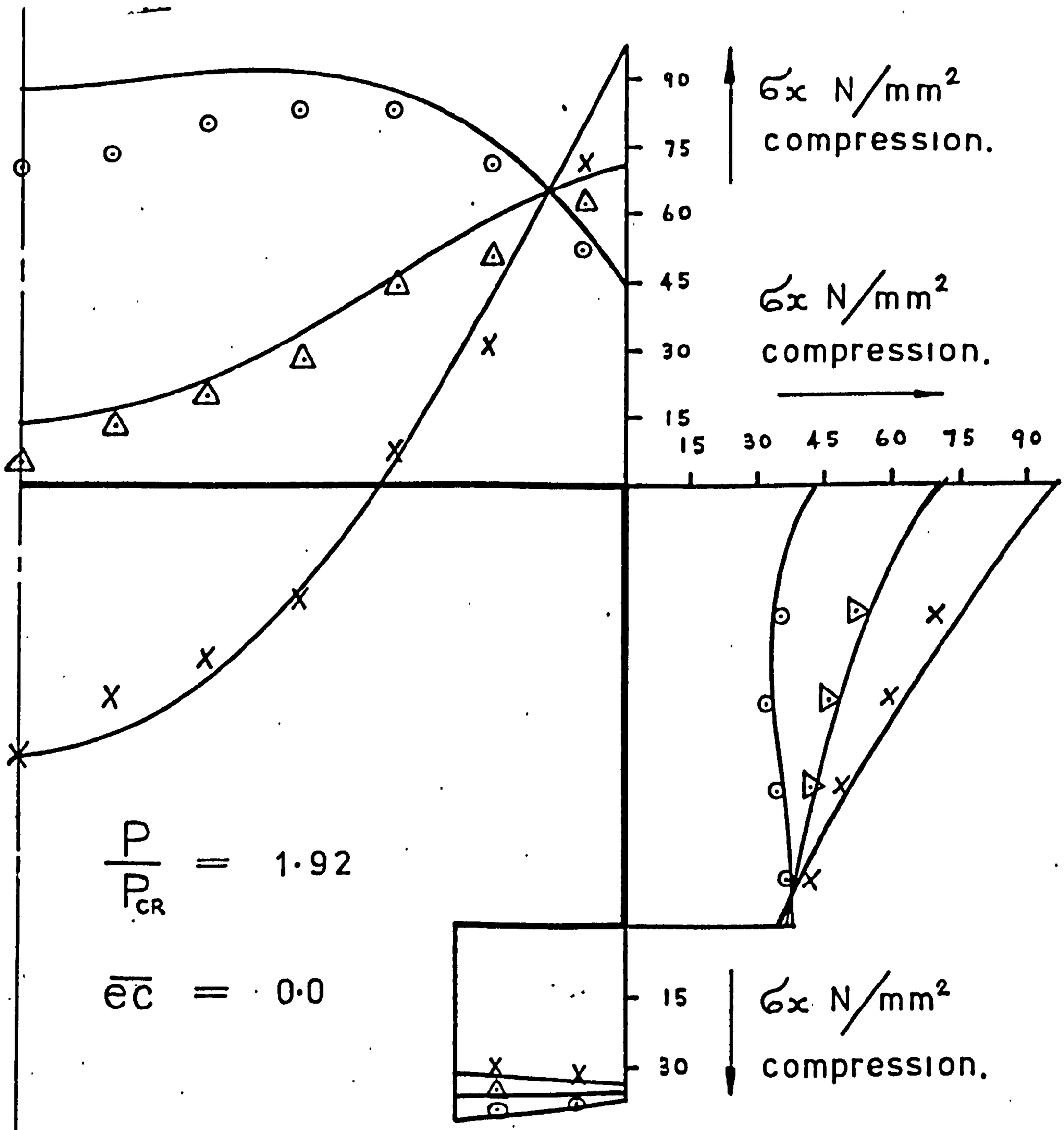

FIG. 6.3.3 LONGITUDINAL STRESS DISTRIBUTION AT LOAD P = 11·125 kN.

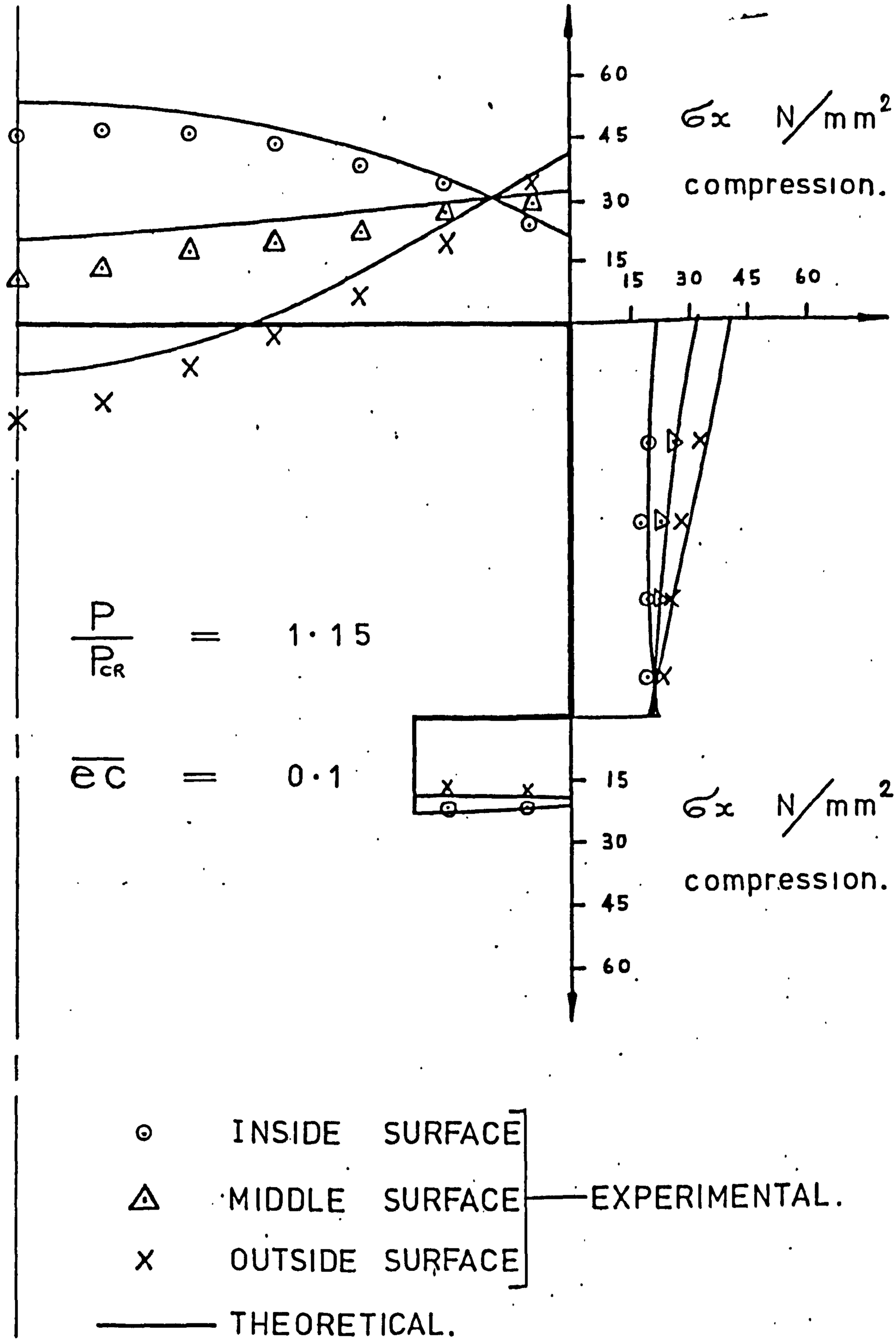

FIG. 6.3.4 LONGITUDINAL STRESS DISTRIBUTION AT LOAD P = 6·23 kN.

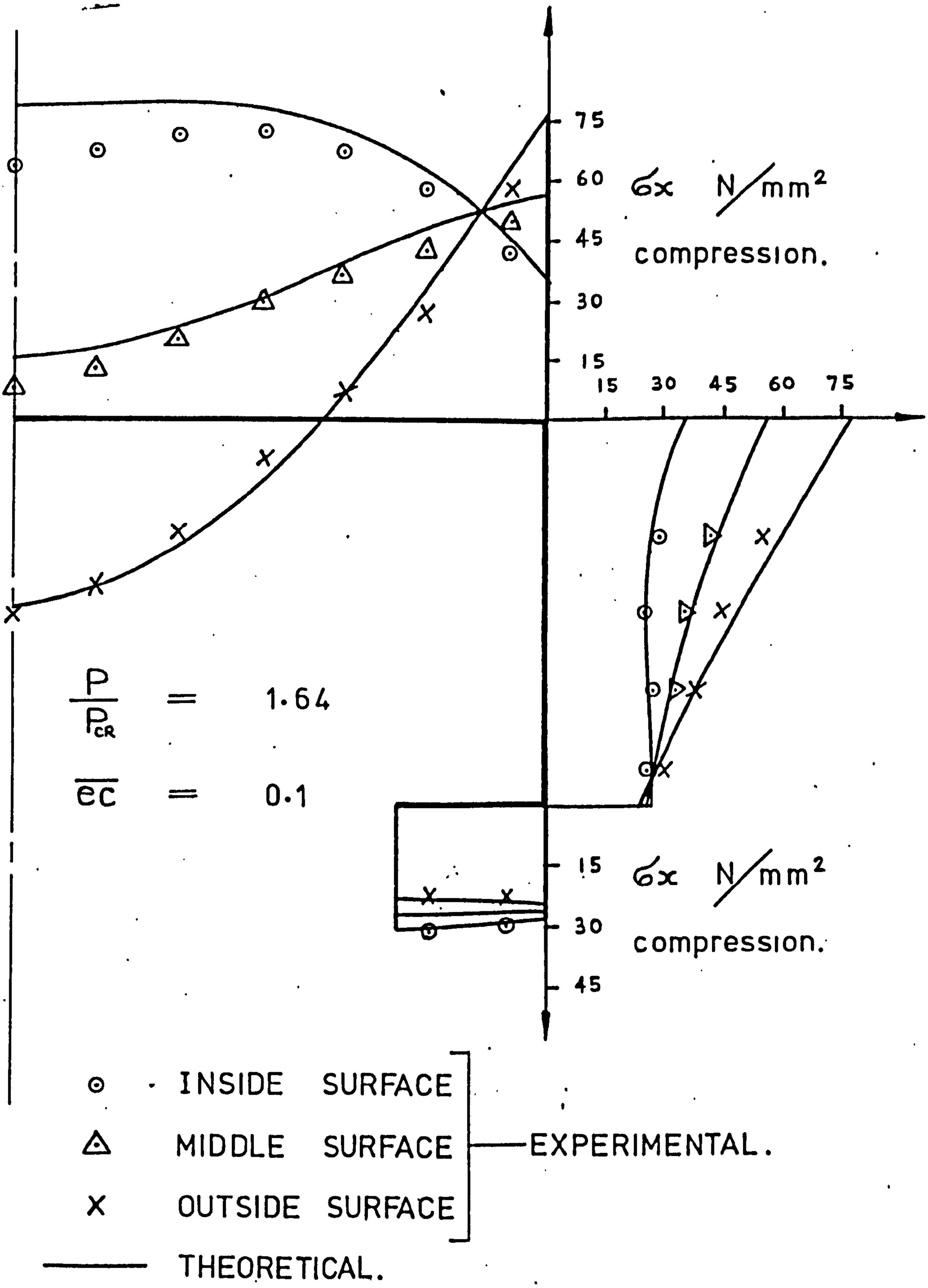

FIG. 6.3.5 LONGITUDINAL STRESS DISTRIBUTION AT LOAD P = 8·9 kN.

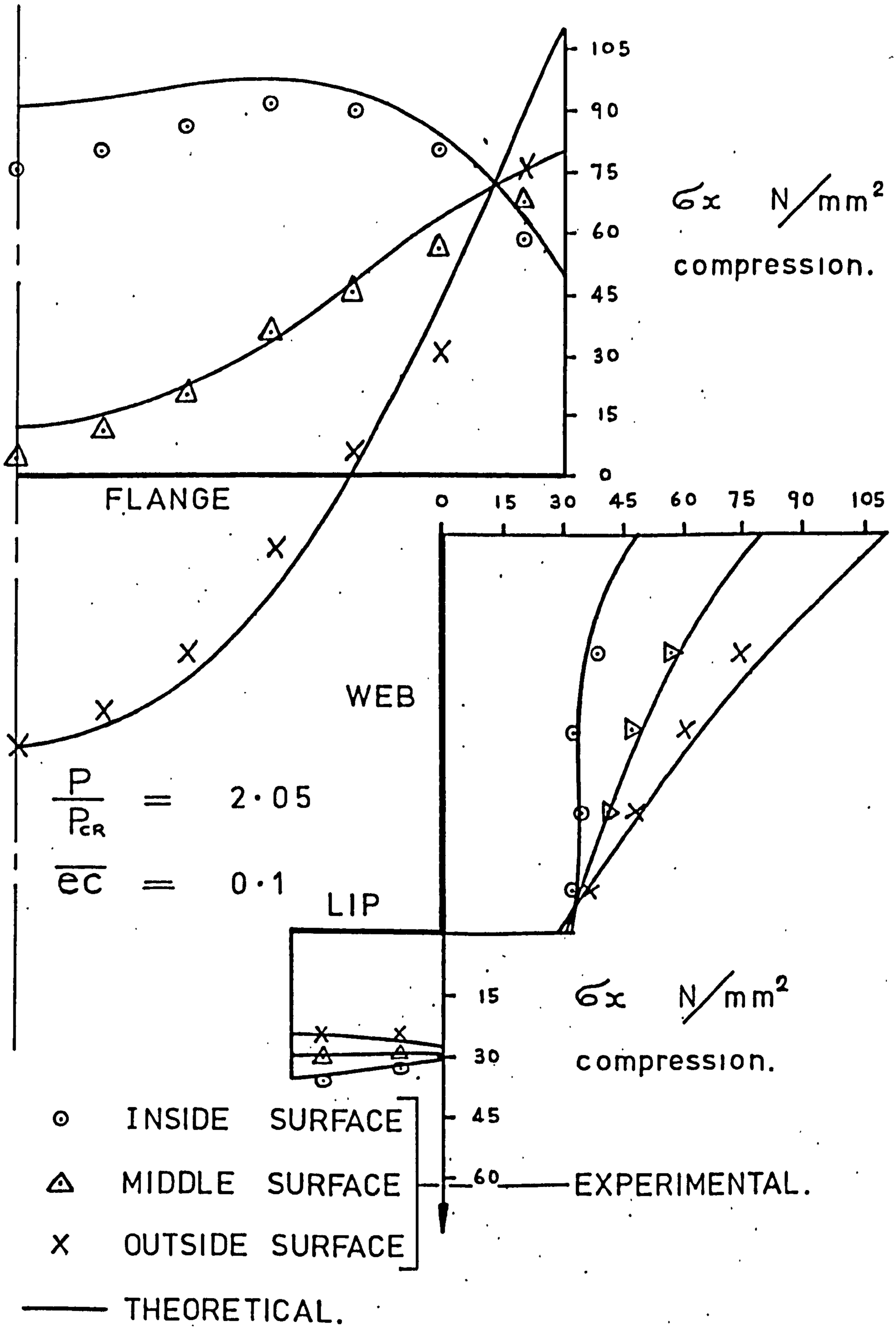

FIG. 6.3.6 LONGITUDINAL STRESS DISTRIBUTION AT LOAD P = 11·125 kN.

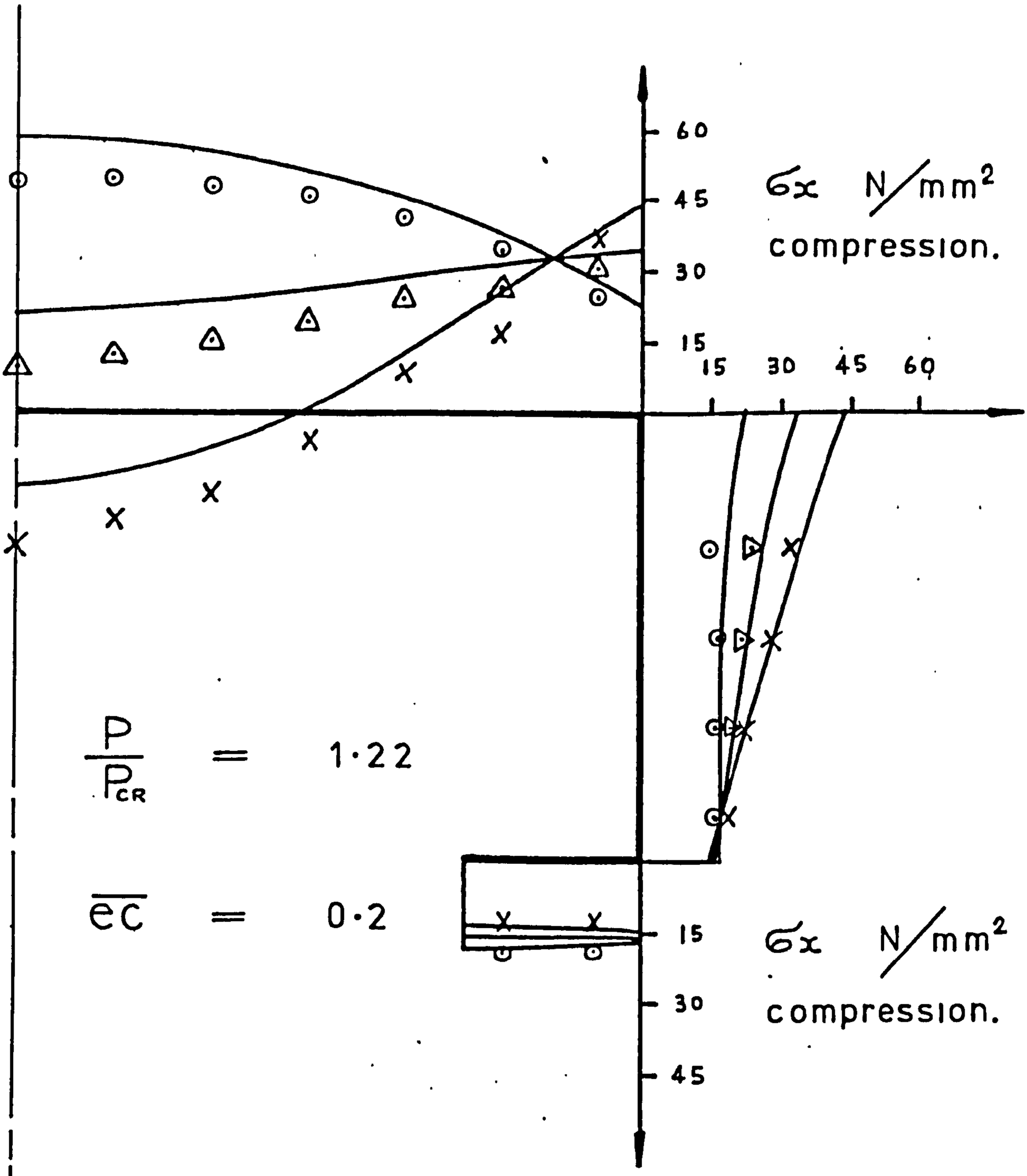

FIG. 6.3.7 LONGITUDINAL STRESS DISTRIBUTION AT LOAD P = 6·23 kN.

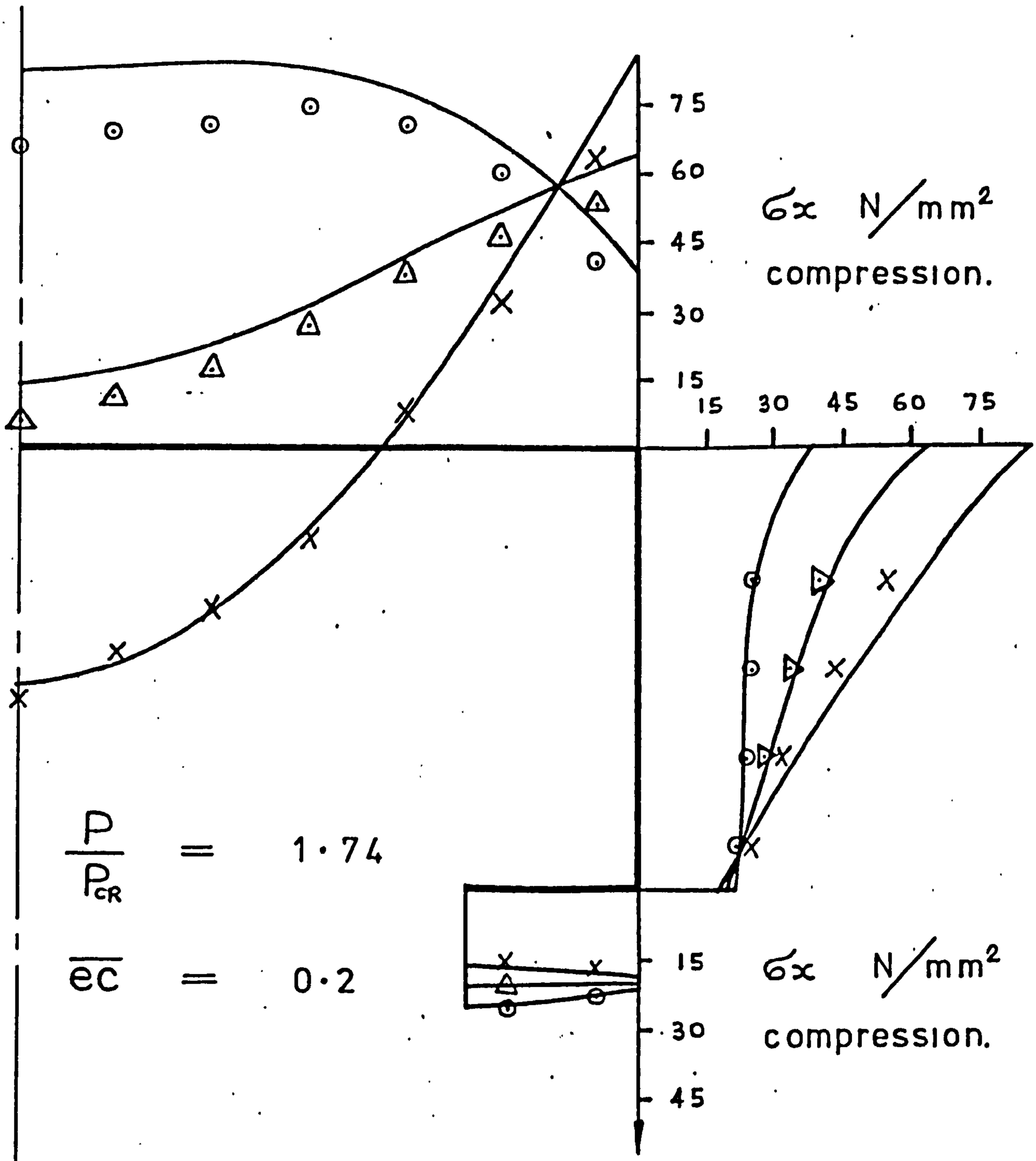

FIG.6.3.8 LONGITUDINAL STRESS DISTRIBUTION AT LOAD P = 8·9 kN.

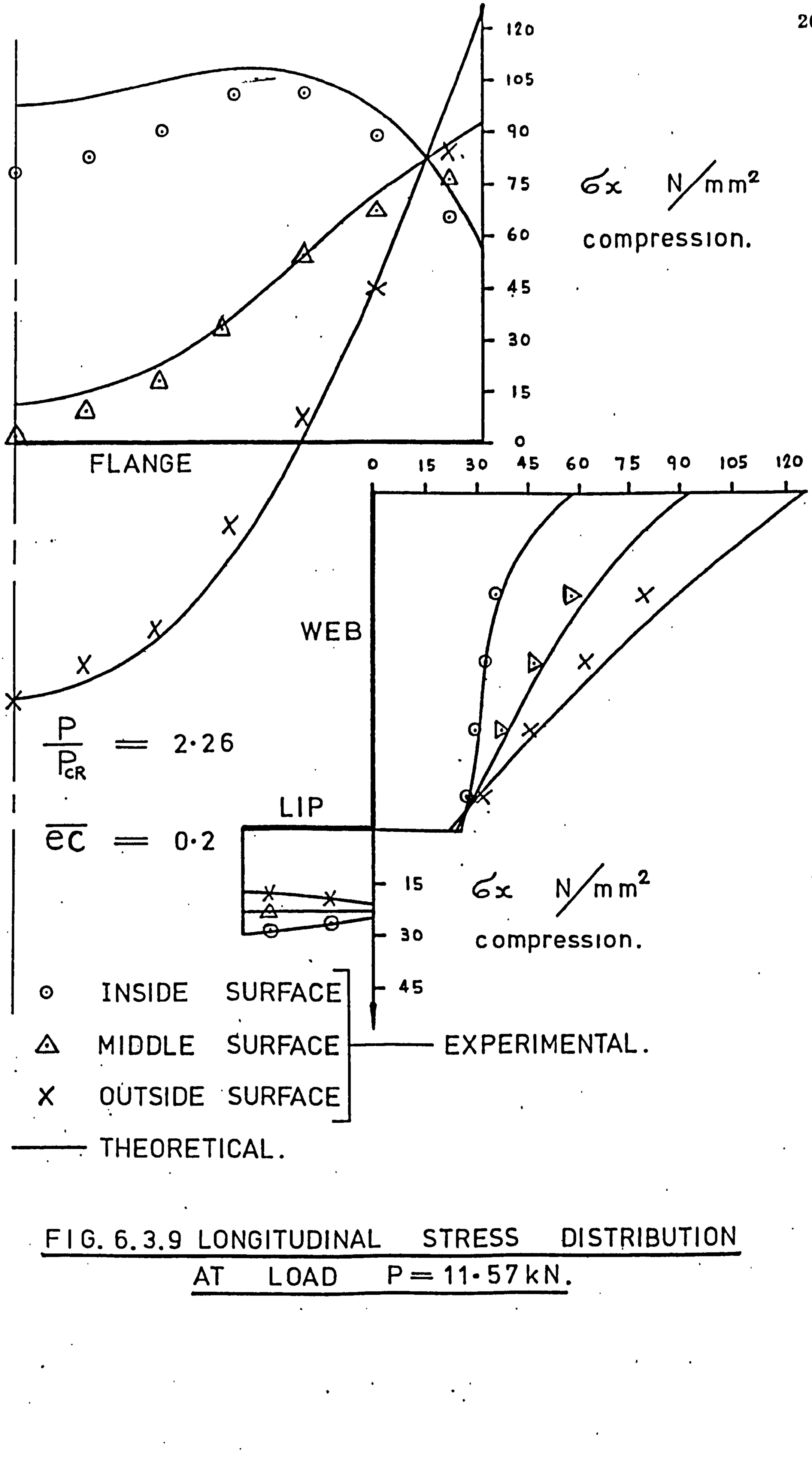

FIG. 6.3.9 LONGITUDINAL STRESS DISTRIBUTION AT LOAD P = 11·57 kN.

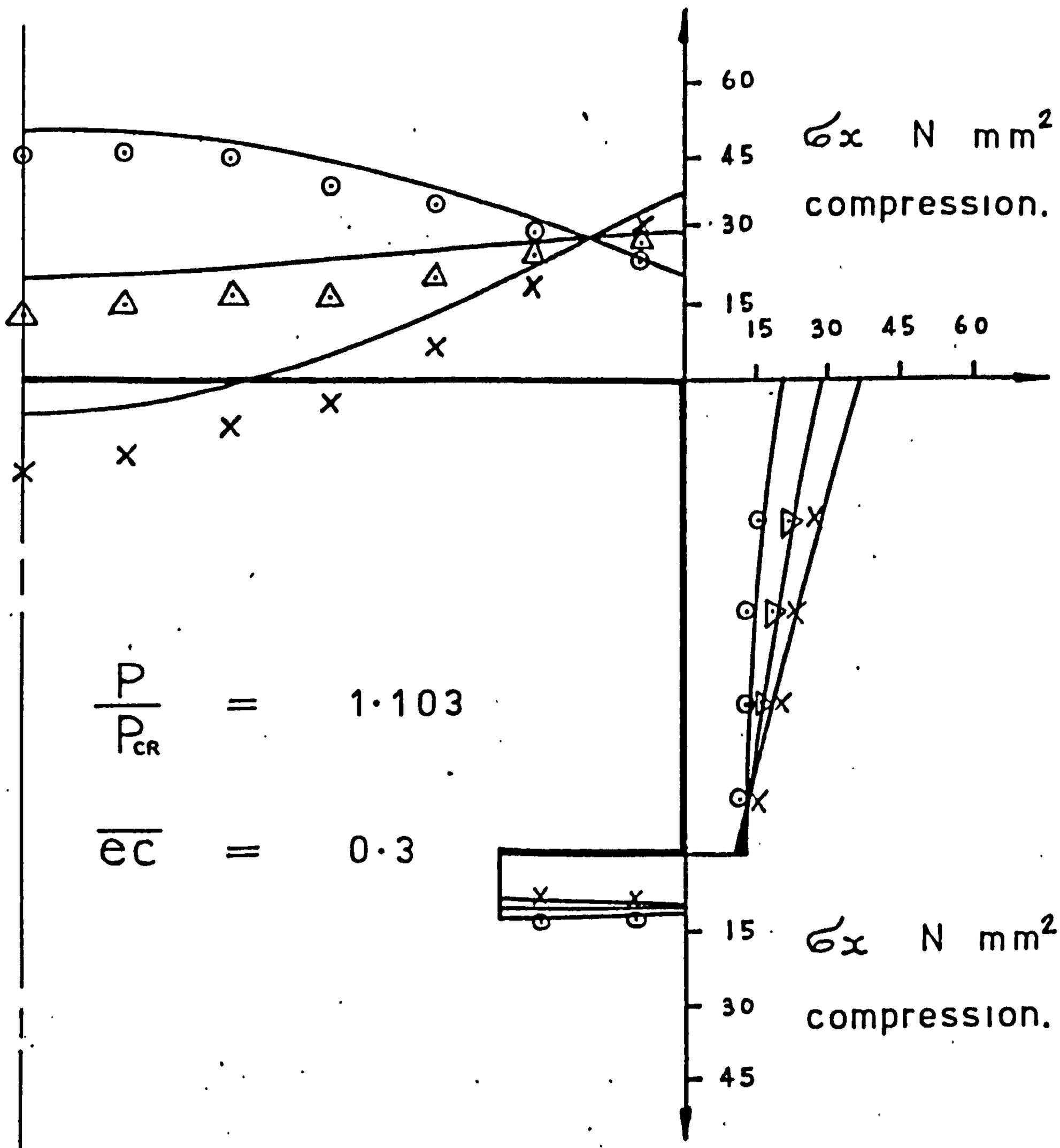

FIG. 6.3.10 LONGITUDINAL STRESS DISTRIBUTION AT LOAD P = 5·34 kN.

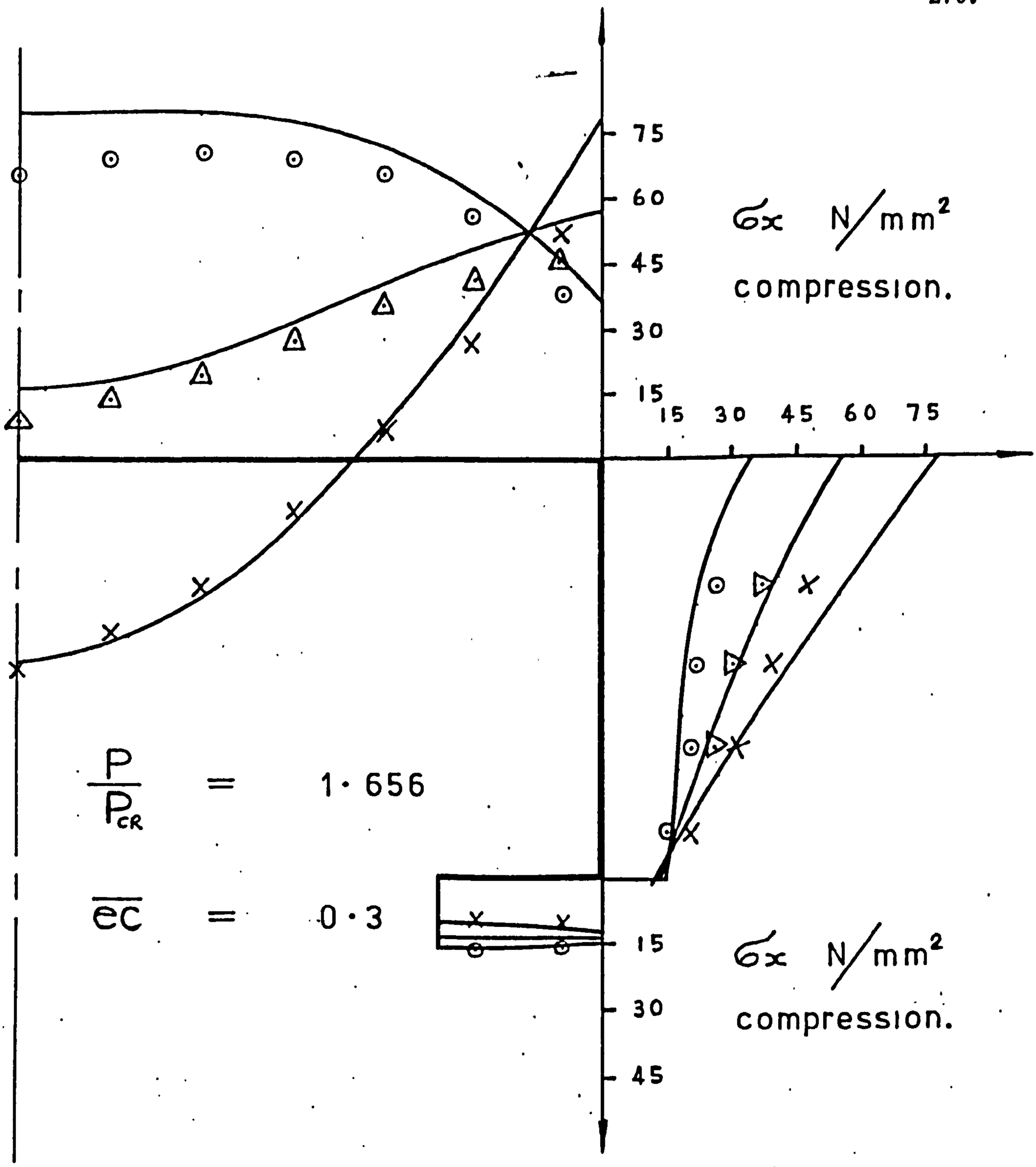

FIG. 6.3.11 LONGITUDINAL STRESS DISTRIBUTION AT LOAD P = 8·01kN.

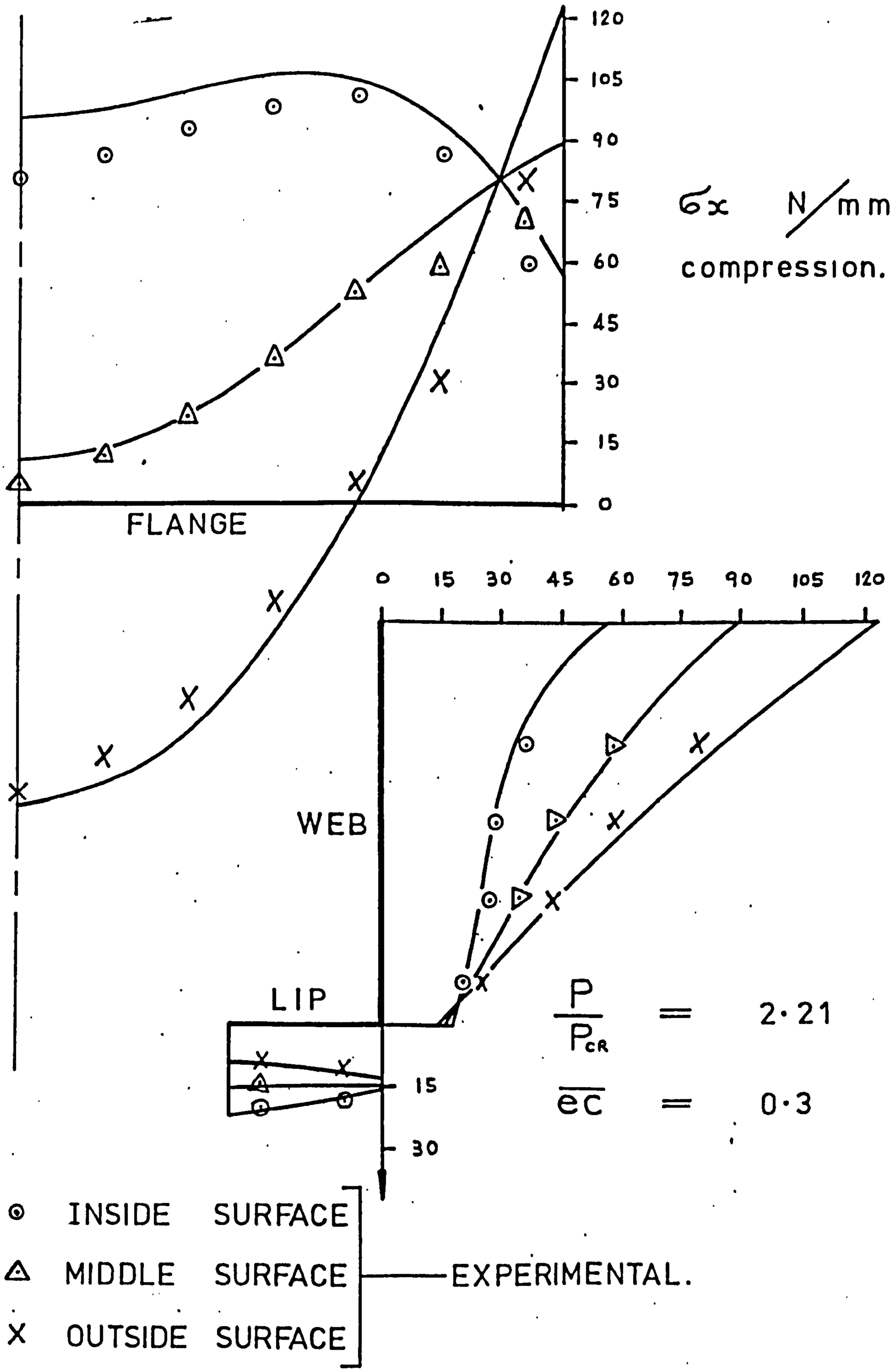

FIG.6.3.12 LONGITUDINAL STRESS DISTRIBUTION AT LOAD P = 10·68kN.

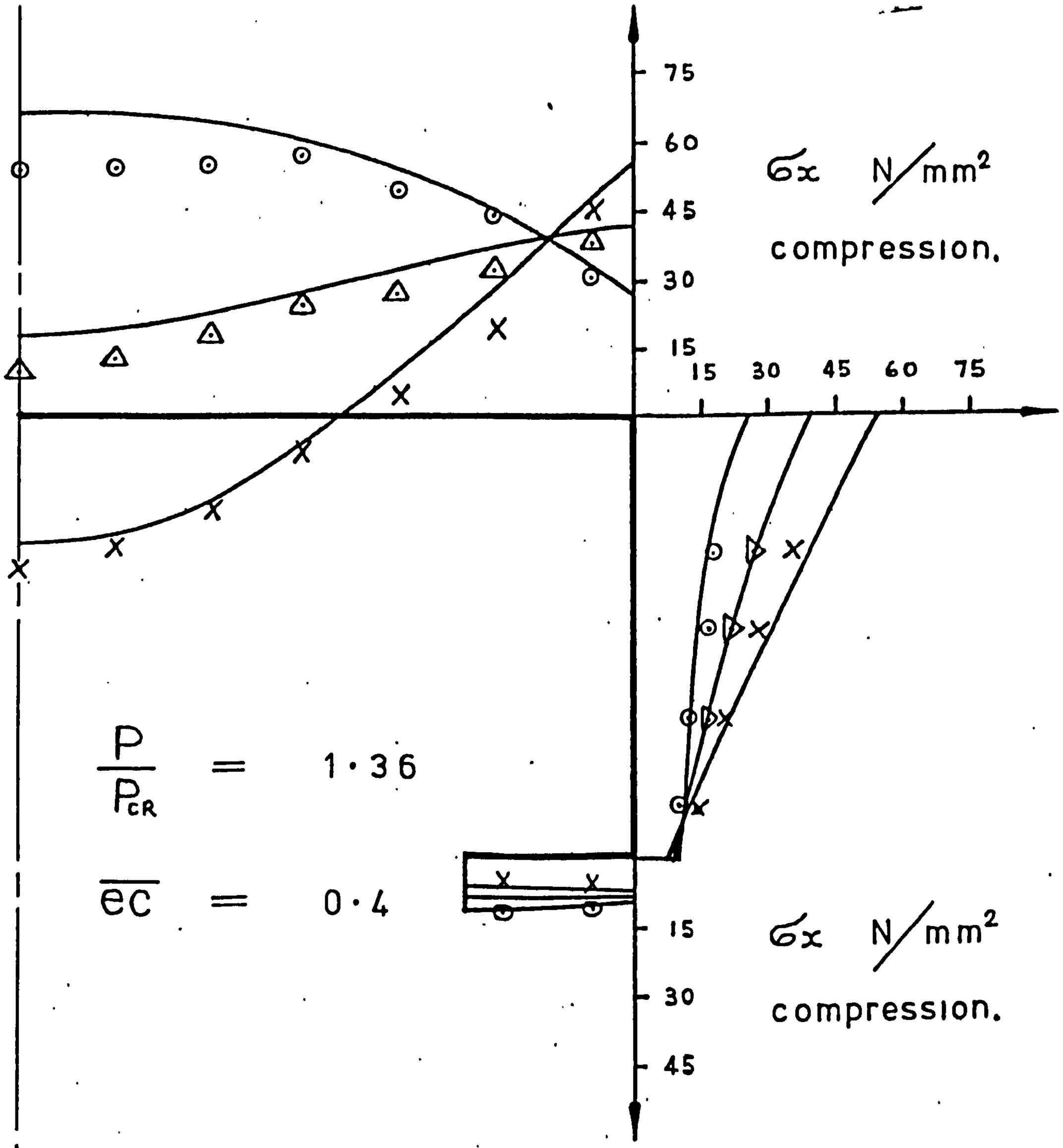

FIG. 6.3.13 LONGITUDINAL STRESS DISTRIBUTION AT LOAD P = 6·23 kN.

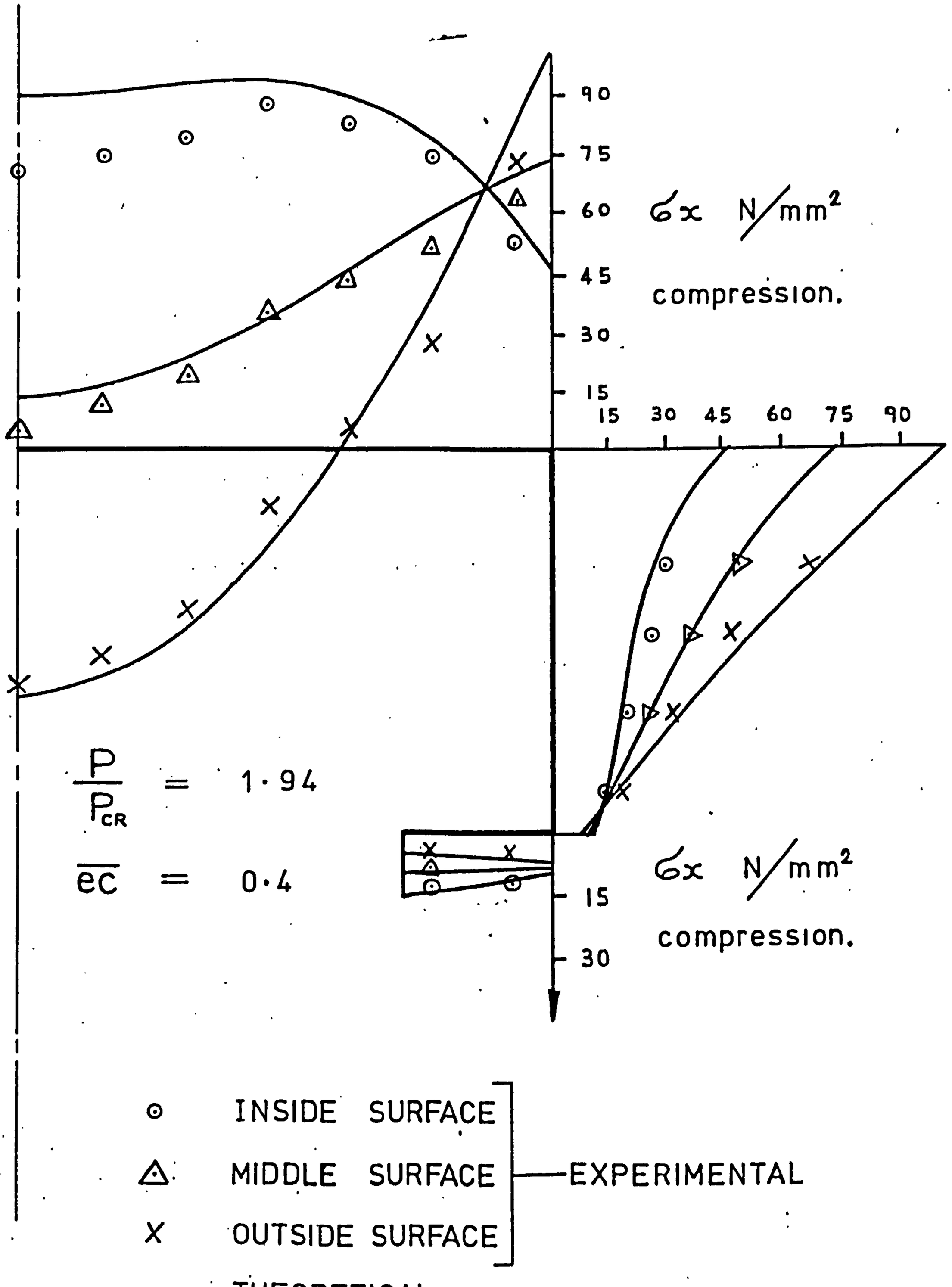

FIG. 6.3.14 LONGITUDINAL STRESS DISTRIBUTION AT LOAD P = 8·9 kN.

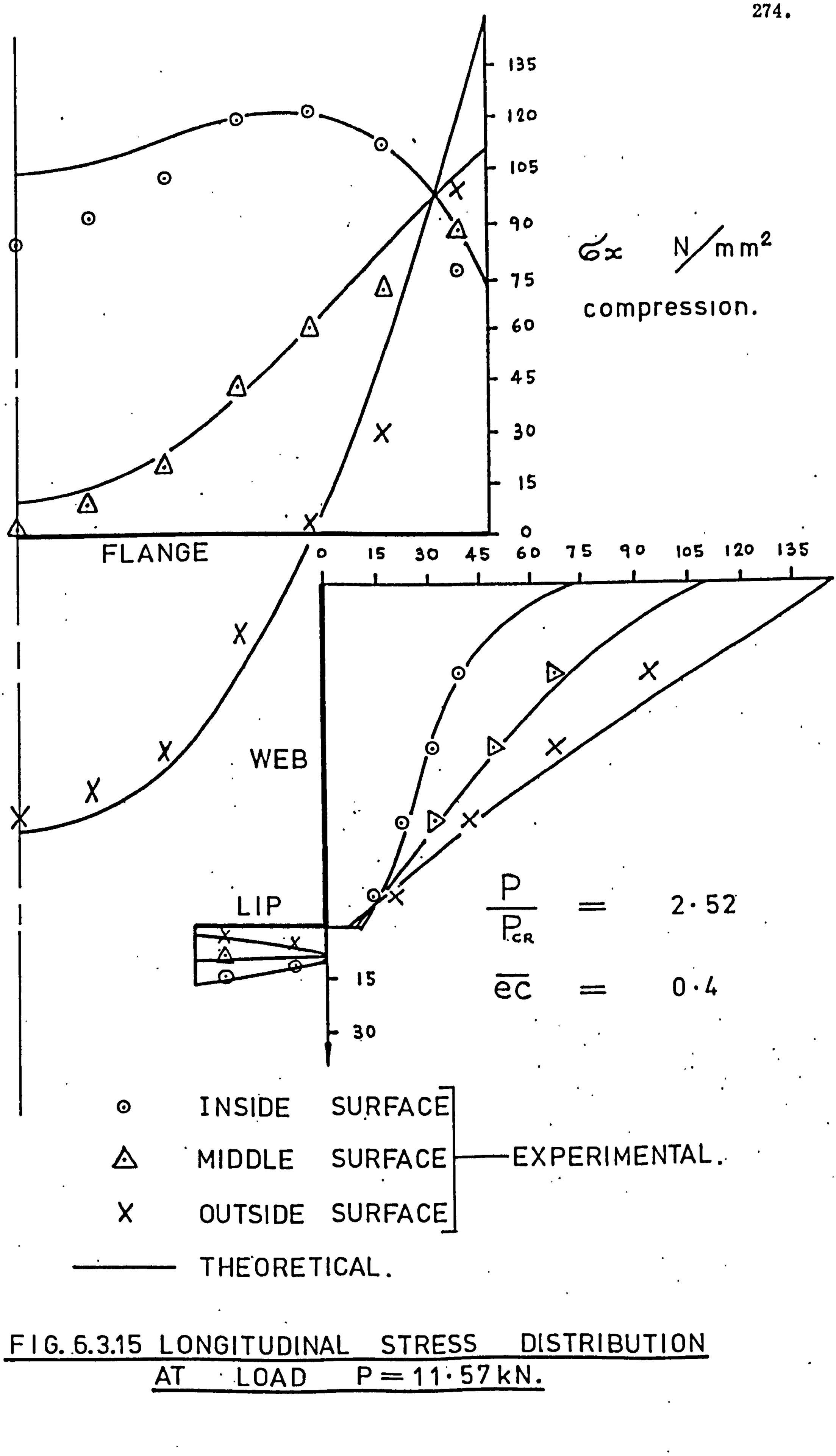

FIG. 6.3.15 LONGITUDINAL STRESS DISTRIBUTION AT LOAD P = 11·57 kN.

COLUMN Nº	$P_{ult\ exp}$ (kN)	$P_{ult\ theo}$ (kN)	$\frac{P_{ult\ theo}}{P_{ult\ exp}}$	COLUMN Nº	$P_{ult\ exp}$ (kN)	$P_{ult\ theo}$ (kN)	$\frac{P_{ult\ theo}}{P_{ult\ exp}}$	COLUMN Nº	$P_{ult\ exp}$ (kN)	$P_{ult\ theo}$ (kN)	$\frac{P_{ult\ theo}}{P_{ult\ exp}}$
1	13·9	15·60	1·12	12	14·9	16·40	1·10	23	18·44	22·10	1·20
2	16·01	17·27	1·08	13	15·7	17·89	1·14	24	65·83	66·63	1·01
3	15·66	17·05	1·09	14	17·12	19·42	1·13	25	70·95	77·36	1·09
4	16·81	18·74	1·11	15	21·8	23·97	1·10	26	72·95	80·97	1·11
5	18·24	20·19	1·11	16	23·04	25·88	1·12	27	73·84	83·99	1·14
6	16·9	17·4	1·05	17	23·62	26·20	1·11	28	51·15	54·3	1·06
7	17·66	19·35	1·10	18	13·94	15·38	1·10	29	56·27	60·91	1·08
8	19·17	21·02	1·10	19	15·08	17·09	1·13	30	60·27	64·73	1·07
9	19·3	21·28	1·10	20	16·32	18·15	1·11	31	75·39	77·86	1·03
10	20·33	22·12	1·09	21	17·19	20·24	1·14	32	75·84	81·44	1·07
11	20·68	23·24	1·12	22	19·64	21·44	1·09	33	80·29	84·34	1·05

TABLE 6.4.1 COMPARISON OF THEORETICAL AND EXPERIMENTAL COLLAPSE LOADS.

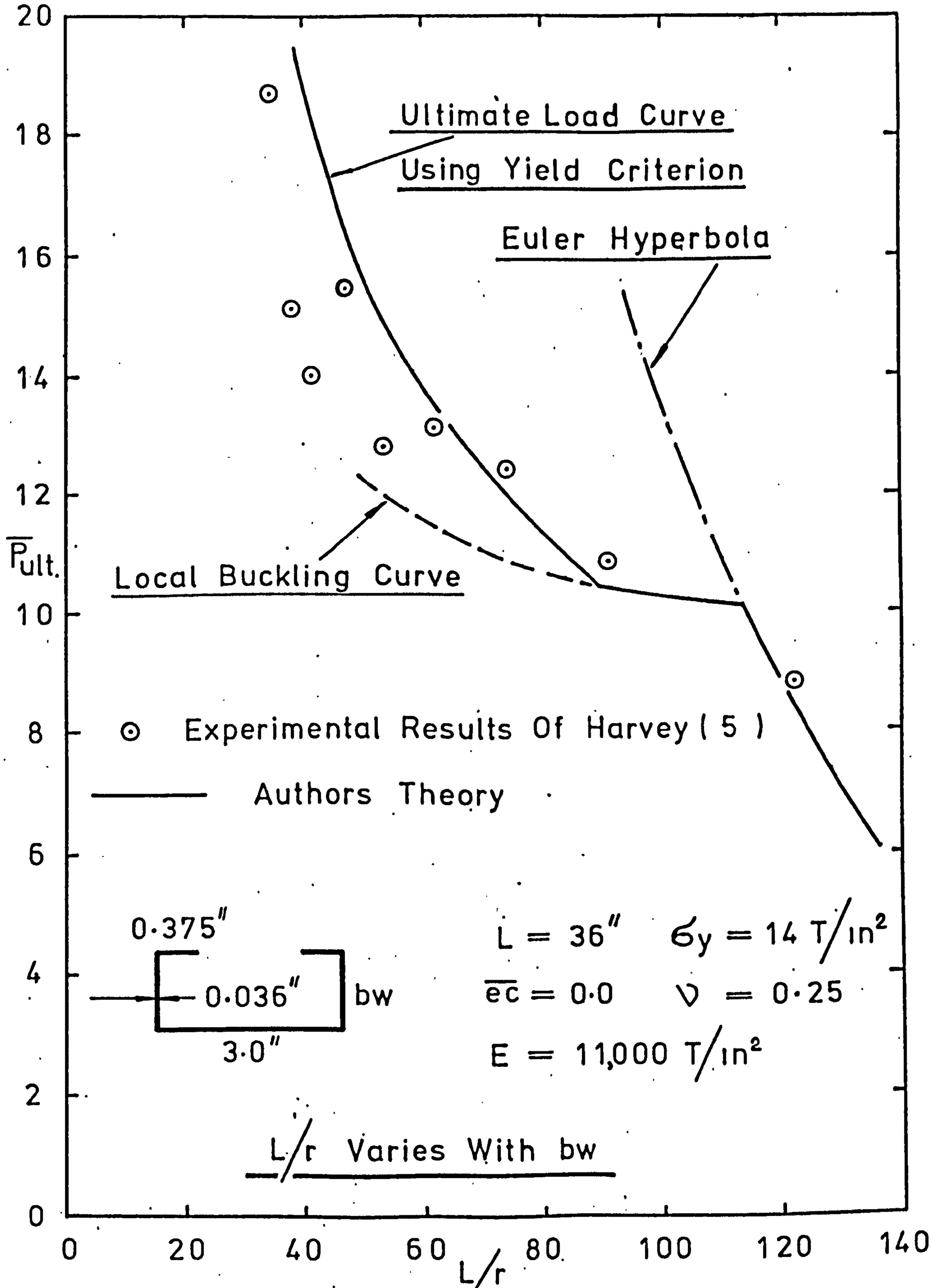

FIG. 6.4.1 COMPARISON OF THEORETICAL ULTIMATE LOADS WITH THE EXPERIMENTAL RESULTS OF HARVEY (5)

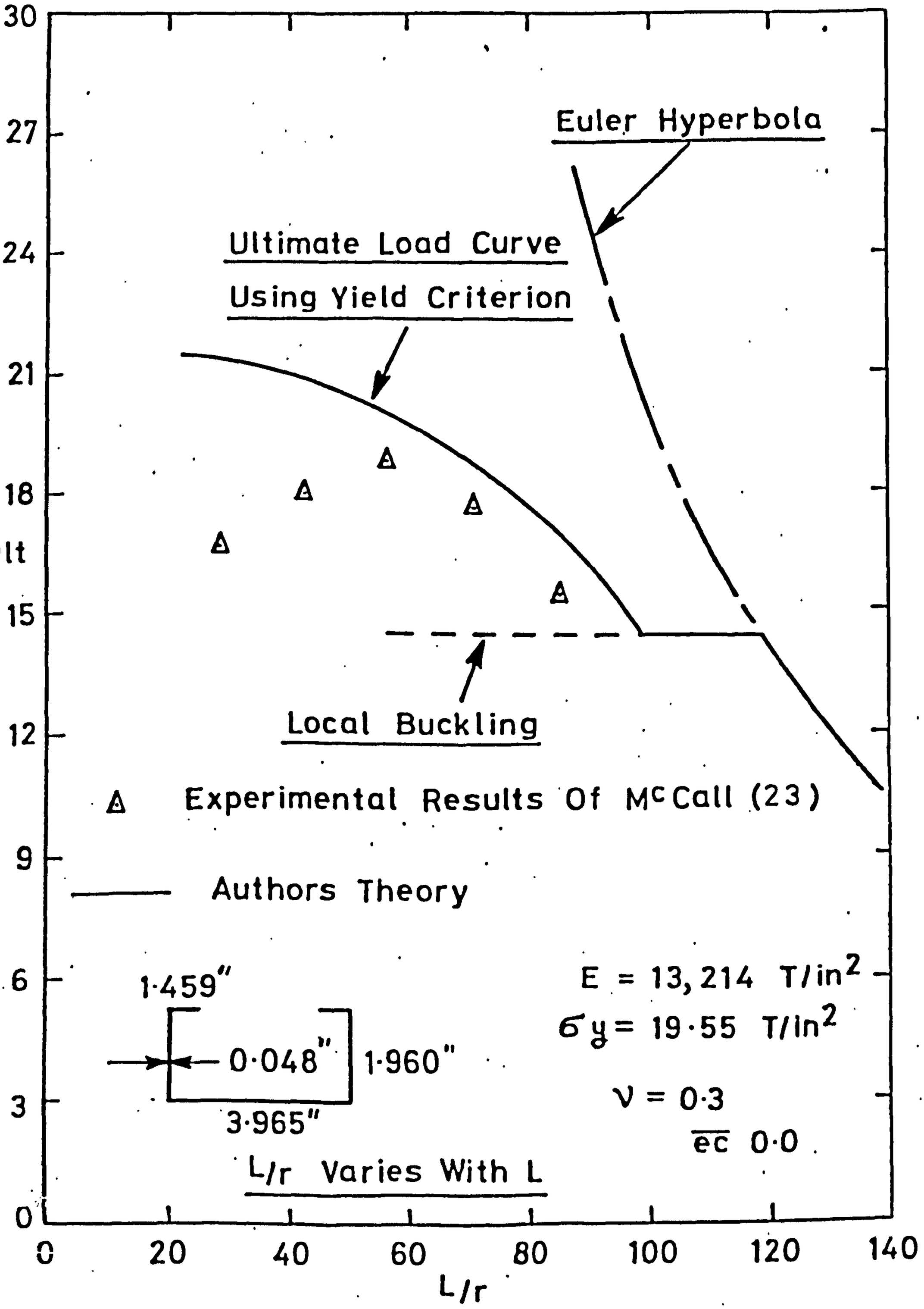

FIG. 6·4·2 COMPARISON OF THEORETICAL ULTIMATE LOADS WITH THE EXPERIMENTAL RESULTS OF Mc CALL (23)

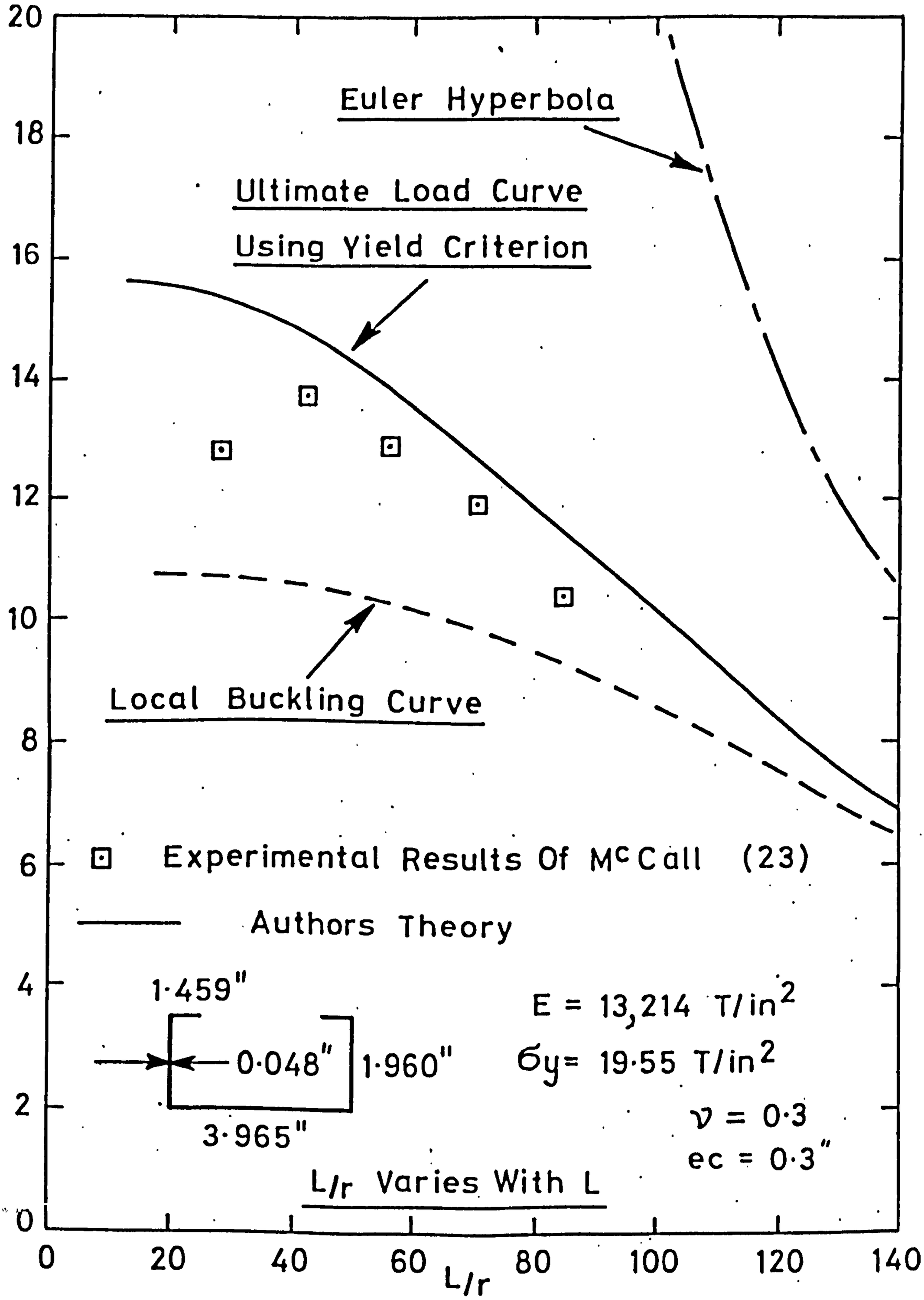

FIG. 6·4·3 COMPARISON OF THEORETICAL ULTIMATE LOADS WITH THE EXPERIMENTAL RESULTS OF McCALL (23)

CHAPTER SEVEN

SUMMARY AND CONCLUSIONS

7.0 SUMMARY AND CONCLUSIONS

7.1 GENERAL SUMMARY

A semi-energy method has been used for the analysis of column behaviour in which both local and overall deformations occur simultaneously during loading. The analysis has been carried out with reference to pin ended lipped channel columns under concentric or eccentric loading. The theoretical solution, as developed in Chapters 3 and 4, has been shown to exhibit good accuracy when compared with the behaviour of actual columns tested.

In the semi-energy approach used the facility available, of flexibility of choice in the local mode deflections, has been shown to provide a continually changing locally buckled form during loading, resulting in a continual shift in section neutral axis and a reduced Euler load for the column which constantly becomes smaller. The analysis also indicates that under completely elastic conditions all post-local buckling load-deflection paths eventually become unstable, although they may be initially stable. The theory has been shown to be capable of predicting both stable and unstable column load-deflection behaviour as associated with columns having critical loads relatively far apart and coincident, or nearly so, respectively.

From the experimental investigation it was found that both local buckling and eventually partial plasticity were instrumental in contributing to the weakening of the bending stiffness of the columns

tested although the latter was present only in the final stages of loading. The specially designed end locating units for the columns were found to be capable of transmitting the applied loading from the loading machine and of applying accurately the specified loading eccentricities relative to the minor principal axis of the section. The locating units were also found to maintain pinned conditions at the column ends. The strain investigation described in Chapter 5, although by no means comprehensive, showed clearly the effects of local buckling on the stress variations across the section at the centre of the column. The membrane-tangent method used in the experimental investigation for predicting local buckling loads has been shown to provide reasonably accurate estimates, although no consistent pattern was found to emerge.

The comparisons between theory and experiment, as illustrated and discussed in Chapter 6, have shown good agreement in relation to column load-deflection equilibrium paths and stress variations with applied loading. The simple collapse criterion of assuming failure to occur when the maximum membrane stress at the section junctions reaches the yield stress of the material, gave close estimates of the failure loads of the columns tested in the experimental program. A comparison of the theory with experimental ultimate loads from independent sources also shows good agreement.

7.2 SUGGESTIONS FOR FURTHER RESEARCH

The author realises that the work presented in this thesis by no means completes the picture of the interaction buckling behaviour of lipped channel columns. He feels, however, that a good elastic analysis is necessary to form the basic foundation for a more complete and in-depth study of the mechanics of the problem and from the results obtained in his investigation would suggest that the semi-energy method employed shows considerable expectation.

As has been shown in Chapter 1, a large proportion of the work presented on coupled mode buckling deals in the main with the effects of imperfections on the buckling behaviour of simultaneous mode designs. Many of these investigations, however, have dealt with hypothetical structural forms or simplified mathematical models of actual forms and as such the findings from them must be regarded within the context wherein they were obtained, and treated as basically illustrative of the type of behaviour associated with unstable bifurcation. On the other hand, unless material properties are such that completely elastic conditions prevail, columns whose critical loads are relatively far apart can exhibit stable post-local buckling behaviour and will eventually collapse due to the weakening effects of partial plasticity. Since a rigorous analysis of the column's behaviour when the material is undergoing plastic deformations is exceedingly difficult, and since the increase in load carried by the column between the onset of plasticity and final collapse is not very

large, work presented in the literature dealing with this type of non-linearity has used approximate methods. Among these have been the semi-empirical approach to the problem as well as that of idealising the stress-strain characteristics of the material as being elastic-perfectly plastic. Even if the stress-strain characteristics of the material could be readily represented by the assumed elastic-perfectly plastic ideal, however, the accuracy of any subsequent elasto-plastic analysis would depend to some degree on the accuracy with which the solution could describe stress variations during the completely elastic stages of loading and hence care would have to be taken to ensure that the elastic analysis was as accurate as possible.

The author feels that the time spent by him in obtaining a good elastic analysis for the lipped channel problem paves the way for an extension of his theory to include the effects of plasticity.

With regard to imperfections, the effects of Euler mode imperfections are similar to those of load eccentricity and due to this can be accounted for quite easily. The problem of local imperfections is, however, slightly more complex, due mainly to the fact that the buckled form is allowed to change during loading and this is at present under examination.

Other aspects of the work, apart from those of imperfections and plasticity, which the author suggests for further research, and feels would provide beneficial knowledge of interactive buckling

behaviour, are listed as follows:

1) The application of the semi-energy method to a wider variety of cross-sectional shapes.

2) The adaptation of the theory to predict the buckling behaviour of columns having fixed end boundary conditions.

3) A theoretical consideration of the local torsional buckling mode of the web and lip about the flange-web junction, especially for the cases of eccentric loading towards the lips and for wide webs.

4) A comprehensive experimental strain investigation, although costly, would be advantageous in obtaining knowledge of the stress variations at various sections along the length of the column as loading progresses.

5) A theoretical consideration of the variation in local deflection magnitudes along the column length. In practice it has been observed that the local buckle magnitudes decrease as the distance from the column centre increases.

6) The use of more terms in the post-buckling solution with the view to increasing the accuracy of the elastic analysis. This would involve a considerable increase in labour and

computation time with perhaps a very small increase in accuracy. Nevertheless, it would be interesting to ascertain the effect, in particular for sections whose compression flanges have exceptionally high width to thickness ratios.

7) A design approach to the coupled mode buckling problem based on the findings of the more elaborate semi-energy analysis.

The author is presently involved in some of these aspects and the findings from these works will be published on completion.

7.3 CONCLUSIONS

Based on the findings of the investigation carried out in this thesis, the author makes the following conclusions:

1) Local buckling causes reductions in the compressive and bending stiffnesses of the entire cross-section. It is the reduction of bending stiffness, however, which is responsible for the unfavourable non-linear interaction between the local and overall buckling modes of thin-walled columns having near simultaneous critical loads.

2) In the case of centroidally loaded columns designed in the near simultaneous mode region and whose local buckling load is less than its Euler value, column buckling occurs at the local buckling load and the equilibrium at bifurcation is unstable. This is in contrast to the behaviour of centroidally loaded box columns in the same area of design and is due simply to the fact that the lipped channel section has local mode deflections largely confined to one side of the cross-section. The modification in local mode shape due to the interaction at buckling with the overall bending mode has a quite different effect in this case than in the situation where the primary local mode in compression displays significant deflections on both sides of the neutral axis, in which case an initially stabilising effect will prevail.

3) The flexibility of choice in local mode deflections has shown that the asymptotic approach to a reduced Euler load based on an unchanging locally deflected form is an approximation and that the reduced Euler load constantly becomes smaller as loading progresses.

4) The theoretical analysis presented has been shown to accurately describe the load-deflection paths of lipped channel columns which have stable post-local buckling behaviour and to give stress distributions which agree well with those obtained experimentally.

5) The results of the experimental programme have shown that although the behaviour of a thin-walled column is influenced to a large extent by the effects of local buckling, the onset of plasticity further reduces the bending stiffness of the section and hence the ultimate strength of the column.

6) For columns which exhibit stable post-local buckling behaviour, failure is predicted with engineering accuracy on the assumption that when the maximum membrane stress at the section junctions reaches the yield stress, collapse ensues.

7) It has been shown that for the lower values of column slenderness, where a considerable amount of post-local buckling exists, higher values of material yield stress result in substantially increased ultimate loads. For the intermediate slenderness ratios, however, the effect of yield stress on ultimate load diminishes and in the region of near simultaneous mode designs the ultimate load is independent of the value of material yield stress, so long as the yield stress is substantially greater than the critical stress.

8) The equilibrium paths of columns loaded eccentrically towards the lips, but whose local buckling effects are most significant on the flange, may change directional sense

with the onset of local buckling, depending on column geometry.

9) The effect of load eccentricity is, in general, to reduce the local buckling capacity and the ultimate strength of a column. In cases where loading eccentricity is towards the lips, however, these may be increased if geometry is such that local buckling effects are predominant on the flange.

BIBLIOGRAPHY

1. TIMOSHENKO, S.P. and WOINOWSKY-KRIEGER, S.

"Theory of Plates and Shells". McGraw-Hill Kogakusha Limited.

2. COAN, J.M.

"Large Deflection Theory for Plates with Small Initial Curvature Loaded in Edge Compression". Transactions ASME, Vol. 73, 1951.

3. BLEICH, F.

"Buckling Strength of Metal Structures". McGraw-Hill Book Company, 1952.

4. BIJLAARD, P.P. and FISHER, G.P.

"Interaction of Column and Local Buckling in Compression Members". NACA Technical Note 2640, 1952.

5. HARVEY, J.M.

"Studies on the Interaction of Plate Components of Structural Sections under Selected Load Conditions". PhD thesis, University of Glasgow, August 1952.

6. BIJLAARD, P.P. and FISHER, G.P.

"Column Strength of H-Sections and Square Tubes in Postbuckling Range of Component Plates". NACA Technical Note 2994, 1953.

7. SEIDENFADEN, J.

"Interaction in the Post-Buckled Range for the Channel Section". Zeit.f. Flugwissenschaft, Heft 7, 1954.

8. CHERRY, S.

"The Stability of Beams with Buckled Compression Flanges". The Structural Engineer, pp 277-285, September 1960.

9. JOMBOCK, J.R. and CLARK, J.W.

"Postbuckling Behaviour of Flat Plates". Proceedings of the ASCE, Vol. 87, No. ST5, June 1961.

10. CAMPUS, F. and MASSONET, Ch.

"Comportement postcritique des plaques utilisees en construction metallique". In particular the contribution to the discussion by W.T. Koiter and M. Skaloud, pp 66-67 and p 103. Colloque international tenu ā l'Universite de Liēge, les 12 et 13 Nov. 1962. 5me sērie, tome VIII, fascicule 5.

11. KOITER, W.T.

"Elastic Stability and Post Buckling Behaviour". Proc. Symp. Nonlinear Problems, pp 257-275, University of Wisconsin Press, 1963.

12. WALKER, A.C.

"Thin Walled Structural Forms under Eccentric Compressive Load Actions". PhD thesis, University of Glasgow, June 1964.

13. BULSON, P.S.

"Local Stability and Strength of Structural Sections". Thin Walled Structures, edited by A.H. Chilver, John Wiley & Sons Inc., New York, pp 153-207, 1967.

14. GRAVES SMITH, T.R.

"The Ultimate Strength of Locally Buckled Columns of Arbitrary Length". Thin Walled Steel Constructions. Their Design and Use in Building. Symposium at University College of Swansea, 11-14 September, 1967.

15. GRAVES SMITH, T.R.

"The Ultimate Strength of Locally Buckled Columns for Various Slenderness Ratios". Local Buckling of Thin Walled Columns; CIRIA, Research Report No. 12, Part II, 1968.

16. NEUT, A. van der

"The Longitudinal Stiffness of Simply Supported Imperfect Plate Strips". Delft University of Technology, Report VTH-152, 1968.

17. NEUT, A. van der

"The Interaction of Local Buckling and Column Failure of Thin Walled Compression Members". Proceedings of the Twelfth International Congress of Applied Mechanics, Stanford University, 26-31 August, 1968. Springer-Verlag Berlin, Heidelberg, New York 1969.

18. GHOBARAH, A.A. and TSO, W.K.

"Overall and Local Buckling of Channel Columns". Proceedings of the ASCE, Vol. 95, No. EM 2, April 1969.

19. RHODES, J.

"The Non-Linear Behaviour of Thin Walled Beams Subjected to Pure Moment Loading". PhD thesis, University of Strathclyde, August 1969.

20. MEIJER, J.J. and NEUT, A. van der

"The Interaction of Local Buckling and Column Failure of Imperfect Thin-Walled Compression Members". Delft University of Technology, Department of Aeronautical Engineering, Report VTH-160, April 1970.

21. SKALOUD, M. and ZORNEROVA, M.

"Experimental Investigation into the Interaction of the Buckling of Compressed Thin-Walled Columns with the Buckling of their Plate Elements". Acta Technica Čsav, No. 4, 1970.

22. KOITER, W.T. and KUIKEN, G.D.C,

"The Interaction between Local Buckling and Overall Buckling on the Behaviour of Built-Up Columns". Delft University of Technology, Department of Mechanical Engineering, Report No. 447, May 1971.

23. McCALL, S.

"Buckling of Thin Walled Eccentrically Loaded Columns". BSc thesis, Department of Mechanics of Materials, University of Strathclyde, Glasgow, May 1971.

24. WITTRICK, W.H. and WILLIAMS, F.W.

"Initial Buckling of Channels in Compression". Proceedings of the ASCE, Vol. 97, No. EM3, June 1971.

25. GRAVES SMITH, T.R.

"The Effect of Initial Imperfections on the Strength of Thin-Walled Box Columns". J. Mech. Sci., Vol. 13, pp 911-925, 1971.

26. THOMPSON, J.M.T. and LEWIS, G.M.

"On the Optimum Design of Thin Walled Compression Members". J. Mech. Phys. Solids, Vol. 20, pp 101-109, 1972.

27. RAJASEKARAN, S. and MURRY, D.W.

"Coupled Local Buckling in Wide-Flange Beam-Columns". Proceedings of the ASCE, Vol. 99, No. ST6, pp 1003-1023, June 1973.

28. HILL, I.R.

"The Interaction of Local and Overall Buckling of Columns of Mono-Symmetric Cross-Section". MSc thesis, University of Strathclyde, September 1973.

29. WANG, S.T. and TIEN, Y.L.

"Post Local Buckling Behaviour of Thin Walled Columns". Proceedings of Second Speciality Conference on Cold Formed Steel Structures, St Louis, Missouri, pp 53-81, 1973.

30. TVERGAARD, V.

"Imperfection Sensitivity of a Wide Integrally Stiffened Panel under Compression". Int. J. Solids Structures, Vol. 9, pp 177-192, 1973.

31. NEUT, A. van der

"The Sensitivity of Thin-Walled Compression Members to Column Axis Imperfection". Int. J. Solids Structures, Vol. 9, pp 999-1011, 1973.

32. TVERGAARD, V.

"Influence of Post-Buckling Behaviour on Optimum Design of Stiffened Panels". Int. J. Solids Structures, Vol. 9, pp 1519-1534, 1973.

33. GILBERT, R.B. and CALLADINE, C.R.

"Interaction Between the Effects of Local and Overall Imperfections on the Buckling of Elastic Columns". J. Mech. Phys. Solids, Vol. 22, pp 519-540, 1974.

34. NEUT, A. van der

"Mode Interaction with Stiffened Panels". Proc. IUTAM Symp. on Buckling of Structures, Harvard University, pp 117-132, 17-21 June 1974.

35. KOITER, W.T. and PIGNATARO, M.

"An Alternative Approach to the Interaction between Local and Overall Buckling in Stiffened Panels". Proc. IUTAM Symp. on Buckling of Structures, Harvard University, pp 133-148, 17-21 June, 1974.

36. THOMPSON, J.M.T., TULK, J.D. and WALKER, A.C.

"An Experimental Study of Imperfection-Sensitivity in the Interactive Buckling of Stiffened Plates". Proc. IUTAM Symp. on Buckling of Structures, Harvard University, pp 149-159, 17-21 June, 1974.

37. TVERGAARD, V. and NEEDLEMAN, A.

"Mode Interaction in an Eccentrically Stiffened Elastic-Plastic Panel under Compression". Proc. IUTAM Symp. on Buckling of Structures, Harvard University, pp 160-171, 17-21 June, 1974.

38. MAQUOI, R. and MASSONNET, Ch.

"Interaction between Local Plate Buckling and Overall Buckling in Thin-Walled Compression Members - Theories and Experiments". Proc. IUTAM Symp. on Buckling of Structures, Harvard University, pp 365-382, 17-21 June, 1974.

39. De WOLF, J.T., PEOKOZ, T. and WINTER, G.

"Local and Overall Buckling of Cold-Formed Members". Proceedings of the ASCE, Vol. 100, No. ST 10, pp 2017-2036, October 1974.

40. WALKER, A.C.

"Interactive Buckling of Structural Components". Science Progress, Vol. 62, p 579, 1975.

41. WALKER, A.C. and DAVIES, P.

"An Elementary Study of Non-Linear Buckling Phenomena in Stiffened Plates". Proc. of Symp. on Non-Linear Behaviour and Techniques in Structural Analysis, Report 164 UC, TRRL Department of Environment, England, 1975.

42. SVENSSON, S.E. and CROLL, J.G.A.

"Interaction between Local and Overall Buckling". Int. J. Mech. Sci., Vol. 17, pp 307-321, 1975.

43. TVERGAARD, V. and NEEDLEMAN, A.

"Buckling of Eccentrically Stiffened Elastic-Plastic Panels on Two Simple Supports or Multiply Supported". Int. J. Solids Structures, Vol. 11, pp 647-663, 1975.

44. FOK, W.C., RHODES, J. and WALKER, A.C.

"Local Buckling of Outstands in Stiffened Plates". Aeronautical Quarterly, Vol. XXVII, May 1976.

45. TULK, J.D. and WALKER, A.C.

"Model Studies of the Elastic Buckling of a Stiffened Plate". Journal of Strain Analysis, Vol. 11, 1976.

46. RHODES, J. and HARVEY, J.M.

"Plain Channel Section Struts in Compression and Bending beyond the Local Buckling Load". Int. J. Mech. Sci., Vol. 8, pp 511-519, 1976.

47. KOITER, W.T. and PIGNATARO, M.

"A General Theory for the Interaction Between Local and Overall Buckling of Stiffened Panels". Delft University of Technology, Department of Mechanical Engineering, Report WTHD 83, 1976.
cf. also "Problemi attuali di meccanica teorica e applicata". Atti del Convegno Internazionale a ricordo di Modesto Panetti, 179-222, Torino 1977.

48. SKALOUD, M. and NAPRSTEK, J.

"Limit State of Compressed Thin-Walled Steel Columns with Regard to the Interaction between Column and Plate Buckling". Second International Colloquium on the Stability of Steel Structures, Liege, pp 405-414, 13-15 April, 1977.

49. REIS, A.J. and ROORDA, J.

"The Interaction between Lateral-Torsional and Local Plate Buckling in Thin Walled Beams". Second International Colloquium on the Stability of Steel Structures, Liege, pp 415-425, 13-15 April, 1977.

50. RHODES, J. and HARVEY, J.M.

"Interaction Behaviour of Plain Channel Columns under Concentric or Eccentric Loading". Second International Colloquium on the Stability of Steel Structures, Liege, pp 439-444, 13-15 April, 1977.

51. WANG, S.T. and WRIGHT, R.S.

"Torsional-Flexural Buckling of Locally Buckled Beams and Columns". Proceedings of the International Colloquium on the Stability of Structures under Static and Dynamic Loads, Washington, DC, 17-19 May, 1977.

52. NEUT, A. van der

"The Interaction of Local and Overall Buckling in Stiffened Panels". Delft University of Technology, Department of Aerospace Engineering, Report LR-255, September 1977.

53. FOK, W.C., WALKER, A.C. and RHODES, J.

"Buckling of Locally Imperfect Stiffeners in Plates". Proc. of the ASCE, Vol. 103, No. EM 5, pp 895-911, October 1977.

54. THOMASSON, P.O.

"Thin-Walled C-Shaped Panels in Axial Compression". Document DI:1978, Swedish Council for Building Research in Association with the Royal Institute of Technology, Stockholm, January 1978.

55. LOUGHLAN, J. and RHODES, J.

"Interaction Buckling of Lipped Channel Columns". Conference on Stability Problems in Engineering Structures and Components, University College, Cardiff, 12-14 September, 1978.

56. LOUGHLAN, J. and RHODES, J.

"The Interactive Buckling of Lipped Channel Columns under Concentric or Eccentric Loading". International Conference on Thin Walled Structures, University of Strathclyde, Glasgow, Scotland, 3-6April 1979.

57. KOITER, W.T. and NEUT, A. van der

"Interaction Between Local and Overall Buckling of Stiffened Compression Panels". International Conference on Thin Walled Structures, University of Strathclyde, Glasgow, Scotland. 3-6 April 1979.

58. WANG, S.T. and PAO, H.Y.

"Stability Analysis of Locally Buckled Singly Symmetric Columns". International Conference on Thin Walled Structures, University of Strathclyde, Glasgow, Scotland. 3-6 April 1979.

59. REIS, A.J. and BRANCO, F.A.

"Lateral and Local Stability of Thin Walled Sections Under Eccentric Loading". International Conference on Thin Walled Structures, University of Strathclyde, Glasgow, Scotland. 3-6 April 1979.

60. GRAVES SMITH, T.R. and SRIDHARAN, S.

"Elastic Collapse of Thin Walled Columns". International Conference on Thin Walled Structures, University of Strathclyde, Glasgow, Scotland. 3-6 April 1979.

61. KONIG, J. and THOMASSON, P.O.

"Thin-Walled C-Shaped Panels Subject to Axial Compression or to Pure Bending". International Conference on Thin Walled Structures, University of Strathclyde, Glasgow, Scotland. 3-6 April 1979.

ACKNOWLEDGEMENTS

The author wishes to thank Professor J M Harvey, Deputy Principal of the University of Strathclyde, and Head of the Department of Mechanics of Materials, for the laboratory and workshop facilities placed at his disposal.

He would like to extend special thanks to Dr J Rhodes, Senior Lecturer in the Department of Mechanics of Materials, for his continued guidance, advice, encouragement and friendship throughout this project.

Thanks are due also to the technical staff of the Department, in particular to Mr W McNab for his excellent work in manufacturing the test rig, and to Mr A Lambie for his extremely good strain gauge work.

Acknowledgement is also made of the Science Research Council and of Ward Brothers (Sherburn) Limited for their financial support throughout the project, and Ayrshire Metal Products Limited, Irvine, who supplied the columns used in the experimental investigation.

Finally the author would like to express his appreciation of the many friendships gained, from both the academic and student bodies, during his period of stay at the University.

APPENDIX I

DERIVATION AND SOLUTION OF THE DIFFERENTIAL EQUATION OF EQUILIBRIUM FOR THE LOCALLY BUCKLED COLUMN

APPENDIX I

DERIVATION AND SOLUTION OF THE DIFFERENTIAL EQUATION OF EQUILIBRIUM FOR THE LOCALLY BUCKLED COLUMN

The first step in the derivation of the differential equation of equilibrium is to consider the local buckling deflections to be described by the following expression

$$w_i = A Y_i(y_i) \cos \frac{\pi x}{s} \qquad (I.1)$$

The functions Y_i specify the shape of the local buckles across each plate while the coefficient A gives the magnitude of the deflections in all plates.

The accuracy of the solution of the differential equation is, of course, dependent on the accuracy with which the functions Y_i describe the actual deflections across each plate. It is absolutely necessary therefore, that these functions are well chosen and it is assumed at this stage that they describe extremely accurately the local deflections of each plate.

Substitution of equation (I.1) into Von Karman's Compatibility Equation (4.1.2) gives the stress function F_i in terms of the coefficient A. The parts of the stress function F_{i1} and F_{i2} of F_i being obtained from the solutions of

$$F_{i1}^{IV} = \frac{E\pi^2}{2s^2} A^2 \left[Y_i Y_i'' + (Y_i')^2 \right] \qquad (I.2)(a)$$

$$F_{i2}^{IV} - 2\left(\frac{2\pi}{s}\right)^2 F_{i2}'' + \left(\frac{2\pi}{s}\right)^4 F_{i2} = \frac{E\pi^2}{2s^2} A^2 \left[Y_i Y_i'' - (Y_i')^2 \right] \qquad (I.2)(b)$$

From equations (I.2) the following two equations are obtained

$$F_{i1}'' = \frac{E\pi^2}{4S^2} A^2 Y_i^2 + [C_1]_i y_{di} + [C_2]_i \qquad \text{(I.3)(a)}$$

$$F_{i2} = \frac{E\pi^2}{2S^2} A^2 \psi_i (y_{di}) \qquad \text{(I.3)(b)}$$

The constants $[C_1]_1$ and $[C_2]_1$, for any particular plate 1, are obtained from equations (4.4.6) and the function $\psi_1 (y_1)$ given by the solution of the following equation

$$\psi_i^{IV} - 2\left(\frac{2\pi}{S}\right)^2 \psi_i'' + \left(\frac{2\pi}{S}\right)^4 \psi_i = \left[Y_i Y_i'' - (Y_i')^2\right] \qquad \text{(I.4)}$$

The strain energy due to mid-plane stresses is now obtained by substituting equations (I.3) into equation (4.7.2) to give

$$V_M = \frac{tS}{2E} \sum_{i=1}^{i=3} \left[\left(\frac{E\pi^2}{2S^2}\right)^2 A^4 \Gamma_i + 2\left(\frac{E\pi^2}{4S^2}\right)^2 A^4 \Phi_i + \frac{E\pi^2}{S^2} A^2 \Theta_i + K_i \right] \qquad \text{(I.5)}$$

where

$$\Gamma_i = \int_0^{b_i} \left[\psi_i'' - \left(\frac{2\pi}{S}\right)^2 \psi_i\right]^2 dy_{di} \qquad \text{(I.6)(a)}$$

$$\Phi_i = \int_0^{b_i} Y_i^4 \, dy_{di} \qquad \text{(I.6.)(b)}$$

$$\Theta_i = \int_0^{b_i} \left[[C_2]_i Y_i^2 + [C_1]_i y_{di} Y_i^2\right] dy_{di} \qquad \text{(I.6.)(c)}$$

$$K_i = \int_0^{b_i} \left[2[C_1]_i^2 y_{di}^2 + 4[C_1]_i [C_2]_i y_{di} + 2[C_2]_i^2\right] dy_{di} \qquad \text{(I.6.)(d)}$$

Substituting equation (I.1) into equation (2.2.4) (Chapter 2, Section 2) gives after integration in the x direction the strain energy of bending as follows

$$V_B = \frac{SD}{2} A^2 \sum_{i=1}^{i=3} Q_i \qquad (I.7)$$

where the Q_i are obtained from

$$Q_i = \int_0^{b_i} \left[\left[Y_i'' - \frac{\pi^2}{S^2} Y_i \right]^2 + \frac{2\pi^2}{S^2}(1-\nu)\left[Y_i Y_i'' + (Y_i')^2 \right] \right] dy_i \qquad (I.8)$$

The total strain energy V_T is now given in terms of the coefficient A from the sum of equations (I.5) and (I.7).

Minimising the total strain energy with respect to A by differentiating V_T with respect to A and equating to zero gives

$$A^2 = - \frac{\sum_{i=1}^{i=3} \left[\frac{SD}{2} Q_i + \frac{\pi^2 t}{2S} \Theta_i \right]}{\sum_{i=1}^{i=3} \frac{\pi^4 E t}{8 S^3} \left[2\Gamma_i + \Phi_i \right]} \qquad (I.9)$$

Substituting equations (4.4.6) for the constants C_1 and C_2 into equation (I.6)(c) allows equation (I.9) to be written as follows

$$A^2 = \frac{\pi^2 E t}{2 a_6 S} \left[\varepsilon^* \left[a_1 + a_2 + a_3 \right] + \varepsilon^* \alpha \left[a_4 - a_2 - a_3 \right] \right] - \frac{a_5}{a_6} \qquad (I.10)$$

where ε^* is the strain value corresponding to the flange compression U* and

$$a_1 = \int_0^{bf} Y_1^2 \, dy_{d1}, \quad a_2 = \int_0^{bw} Y_2^2 \, dy_{d2}, \quad a_3 = \int_0^{b\ell} Y_3^2 \, dy_{d3},$$

$$a_4 = \int_0^{bw} \left(\frac{y_2}{bw}\right) Y_2^2 \, dy_{d2}, \qquad a_5 = \sum_{i=1}^{i=3} \frac{SD}{2} Q_i,$$

$$a_6 = \sum_{i=1}^{i=3} \frac{\pi^4 E t}{8 S^3} \left[2 \Gamma_i + \Phi_i \right] \tag{I.11}$$

The expressions for the column load P and the moment about the lips M, as given by equations (4.8.4) and (4.8.6), can now be written in terms of the coefficient A by means of substituting F_{11}" in the form of equation (I.3)(a) to give

$$P = Et\left[\varepsilon^* \left[b+2bw+2b\ell\right] - \varepsilon^*\alpha \left[bw+2b\ell\right] - \frac{\pi^2 A^2}{2S^2}\left[a_1+a_2+a_3\right]\right] \tag{I.12}$$

$$M = Et\left[\varepsilon^* bw \left[b+bw\right] - \varepsilon^*\alpha \frac{bw^2}{3} - \frac{bw\pi^2 A^2}{2S^2}\left[a_1+a_4\right]\right] = P\left[e+d+\delta c\right] \tag{I.13}$$

Substituting now equation (I.10) for A^2 into equation (I.12) gives the strain ε^* in terms of the load P and $\varepsilon^*\alpha$ in the following form

$$\varepsilon^* = \frac{P - Et\left[\frac{\pi^2}{2S^2}(a_1+a_2+a_3)\frac{a_5}{a_6} - \varepsilon^*\alpha\left[(bw+2b\ell) + \frac{\pi^4 Et}{4S^3 a_6}(a_1+a_2+a_3)(a_4-a_2-a_3)\right]\right]}{Et\left[(b+2bw+2b\ell) - \frac{\pi^4 Et}{4S^3 a_6}(a_1+a_2+a_3)^2\right]}$$

(I.14)

From the assumption that plane sections remain plane during local buckling the following equation for ε^*_α is obtained

$$\varepsilon^*_\alpha = - b_w \frac{d^2\delta}{dx^2} \qquad (I.15)$$

Substituting equation (I.10) into equation (I.13) and then substituting equation (I.14) into the result gives, after utilising equation (I.15), the differential equation of equilibrium for the lateral deflection of the locally buckled column in the form

$$\frac{d^2\delta}{dx^2} + n^2\delta = - n^2\left[e + (d-d^*) + \frac{M^*}{P}\right] \qquad (I.16)$$

where $n = \sqrt{\frac{P}{EI^*}}$ and

$$d^* = \frac{\left[b_w(b+b_w) - \frac{b_w\pi^4 Et}{4s^3a_6}(a_1+a_4)(a_1+a_2+a_3)\right]}{\left[(b+2b_w+2b_\ell) - \frac{\pi^4 Et}{4s^3a_6}(a_1+a_2+a_3)^2\right]} \qquad (I.17)(a)$$

$$I^* = b_w t\left[\left[(b_w+2b_\ell) + \frac{\pi^4 Et}{4s^3a_6}(a_1+a_2+a_3)(a_4-a_2-a_3)\right]d^* - \left[\frac{b_w^2}{3} + \frac{b_w\pi^4 Et}{4s^3a_6}(a_1+a_4)(a_4-a_2-a_3)\right]\right] \qquad (I.17)(b)$$

$$M^* = \frac{\pi^2 Et}{2s^2}(a_1+a_2+a_3)\frac{a_5}{a_6}\left[d^* - \frac{b_w(a_1+a_4)}{(a_1+a_2+a_3)}\right] \qquad (I.17)(c)$$

The general solution of equation (I.16) for the lateral deflection δ is

$$\delta = \left[e+(d-d^*)+\frac{M^*}{P}\right]\left[\sec\frac{nL}{2}\cos(nx) - 1\right] \qquad (I.18)$$

Substituting x = 0 in equation (I.18) gives the lateral deflection δ_c at the centre of the column as

$$\delta_c = \left[e+(d-d^*)+\frac{M^*}{P}\right]\left[\sec\frac{\pi}{2}\sqrt{\frac{P}{P_E^*}} - 1\right] \qquad (I.19)$$

where $P_E^* = \frac{\pi^2 E I^*}{L^2}$

As stated earlier the accuracy of equation (I.19) depends solely on the accuracy of the functions Y_i in approximating the actual local buckling deflection of the column. If the functions Y_i were of a fixed form which changed in magnitude only by means of the coefficient A, then the values of d*, I*, P_E* and M* would remain constant throughout buckling at the values obtained from the initial instability solution. In the practical case however, the buckled form changes and the values of d*, I*, P_E* and M* change continually throughout loading.

This change in form is taken into account by utilizing the functions Y_i from the two term post-buckling solution in the general form of equation (4.2.1), the specific forms being given by equations (4.2.2). These functions, having been developed through the necessary satisfaction of the relevant compatibility and equilibrium boundary conditions existing at the plate junctions of the section, automatically provide a fairly accurate representation of the local deflections occurring within the section.

Using the functions Y_i from the two term post-buckling solution results in the a_i of equations (I.11) taking the following form

$$a_1 = \sum_{n=1}^{n=N}\sum_{m=1}^{m=N} W_n W_m \int_0^{b_f} Y_{1n} Y_{1m}\, dy_{d_1} \qquad \text{(I.20)(a)}$$

$$a_2 = \sum_{n=1}^{n=N}\sum_{m=1}^{m=N} W_n W_m \int_0^{b_w} Y_{2n} Y_{2m}\, dy_{d_2} \qquad \text{(I.20)(b)}$$

$$a_3 = \sum_{n=1}^{n=N}\sum_{m=1}^{m=N} W_n W_m \int_0^{b_\ell} Y_{3n} Y_{3m}\, dy_{d_3} \qquad \text{(I.20)(c)}$$

$$a_4 = \sum_{n=1}^{n=N}\sum_{m=1}^{m=N} W_n W_m \int_0^{b_w} \left(\frac{y_{d_2}}{b_w}\right) Y_{2n} Y_{2m}\, dy_{d_2} \qquad \text{(I.20)(d)}$$

$$a_5 = \sum_{i=1}^{i=3}\sum_{n=1}^{n=N}\sum_{m=1}^{m=N} \frac{SD}{2} W_n W_m \Phi_{inm} \qquad \text{(I.20)(e)}$$

$$a_6 = \sum_{i=1}^{i=3}\sum_{n=1}^{n=N}\sum_{m=1}^{m=N}\sum_{r=1}^{r=N}\sum_{h=1}^{h=N} \frac{\pi^4 E t}{8 S^3} W_n W_m W_r W_h \left[\frac{2\Gamma_{inmrh}}{b_i^4} + \Phi_{inmrh}\right] \qquad \text{(I.20)(f)}$$

The solution of the differential equation of equilibrium for the locally buckled column is now complete, the load-deflection equilibrium path being described by equation (I.19) used in conjunction with equations (I.17) and (I.20).

APPENDIX II

PHYSICAL MEANING OF THE TERM M^*

IN THE SOLUTION OF THE DIFFERENTIAL EQUATION OF EQUILIBRIUM

APPENDIX II

PHYSICAL MEANING OF THE TERM M^* IN THE SOLUTION OF THE DIFFERENTIAL EQUATION OF EQUILIBRIUM

The term M^* was defined generally in chapter four as being an internal moment caused by the effects of local buckling. After some rather lengthy algebraic manipulation however the physical meaning of M^* can be shown more specifically to be

$$M^* = P_{CR}(d^*-d) \qquad \text{— — — — — — — — — (II.1)}$$

where P_{CR} is the critical load to cause local buckling of a uniformly compressed column, according to the current locally deflected form.

To prove equation (II.1), use is made of the equations already developed in appendix I. For the sake of expediency and to simplify the algebraic manipulations in the proof, equations (I.11) of appendix I are utilized in the following manner

$$\begin{aligned} a_1 + a_2 + a_3 &= r_1 \\ a_1 + a_4 &= r_2 \\ a_5 &= \frac{\pi^4 Et}{8S^3}.r_3 \\ a_6 &= \frac{\pi^4 Et}{8S^3}.r_4 \end{aligned} \qquad \text{— — — — — — — (II.2)}$$

where

$$r_3 = \frac{S^4 t^2}{3(1-\nu^2)\pi^4} \sum_{i=1}^{i=3} Q_i$$

$$r_4 = \sum_{i=1}^{i=3} \left[2r_i + \Phi_i \right] \qquad \text{— — — — — — — — (II.3)}$$

using equations (II.2), equations (I.10), (I.17)(a) and (I.17)(c) of appendix I take the following form

$$A^2 = \frac{4S^2}{\pi^2 r_4}\left[\varepsilon^* r_1 + \varepsilon^* \alpha (r_2 - r_1)\right] - \frac{r_3}{r_4} \qquad \text{——————(II.4)}$$

$$d^* = \frac{\left[b_w(b+b_w) - 2b_w \frac{r_1 r_2}{r_4}\right]}{\left[b+2b_w+2b_\ell - 2\frac{r_1^2}{r_4}\right]} \qquad \text{————————(II.5)}$$

$$M^* = \frac{\pi^2 E t}{2S^2} b_w \left[\frac{\frac{r_1 r_3}{r_4}\left[b+b_w - 2\frac{r_1 r_2}{r_4}\right]}{\left[b+2b_w+2b_\ell - 2\frac{r_1^2}{r_4}\right]} - \frac{r_2 r_3}{r_4}\right] \qquad \text{——(II.6)}$$

By considering equation (II.4) with A = O and α= O, the critical value of ε^* to cause local buckling for a centroidally loaded section can be obtained. This is

$$\varepsilon^*_{CR} = \frac{\pi^2}{4S^2}\ \frac{r_3}{r_1} \qquad \text{————————————(II.7)}$$

The critical load to cause local buckling is obtained from

$$P_{CR} = \varepsilon^*_{CR} \times E \times \text{cross sectional area}$$

$$\therefore \quad P_{CR} = \frac{\pi^2 E t}{4S^2} \cdot \frac{r_3}{r_1}(b + 2b_w + 2b_\ell) \qquad \text{————————(II.8)}$$

The position of the neutral axis from the section lips for a locally unbuckled section is

$$d = \frac{b_w(b + b_w)}{b + 2b_w + 2b_\ell} \qquad \text{————————(II.9)}$$

using equations (II.5), (II.8) and (II.9), the following can be written

$$P_{CR}(d^*-d) = \frac{\pi^2 Et}{4S^2}\,\frac{r_3}{r_1}(b+2b_w+2b_\ell)\left[\frac{b_w(b+b_w)-2b_w\frac{r_1r_2}{r_4}}{b+2b_w+2b_\ell-\frac{2r_1^2}{r_4}}-\frac{b_w(b+b_w)}{b+2b_w+2b_\ell}\right]$$

— — — —(II.10)

By re-arranging the parameters on the right hand side of equation (II.10) it can be shown that this is equal to that of equation (II.6) and hence equation (II.1) is true. Writing the terms in square brackets in common denominator form and taking the common parameter b_w outside the brackets gives

$$P_{CR}(d^*-d) = \frac{\pi^2 Et}{4S^2}\,b_w\,\frac{r_3}{r_1}(b+2b_w+2b_\ell)X$$

$$X\left[\frac{(b+2b_w+2b_\ell)\,(b+b_w-\frac{2r_1r_2}{r_4})-(b+2b_w+2b_\ell-\frac{2r_1^2}{r_4})\,(b+b_w)}{(b+2b_w+2b_\ell-\frac{2r_1^2}{r_4})\,(b+2b_w+2b_\ell)}\right]$$

Multiplying out the numerator of the term in square brackets and cancelling like terms allows the above equation, after some rearranging, to be written in the following form

$$P_{CR}(d^*-d) = \frac{\pi^2 Et}{2S^2}\,b_w\left[\frac{(b+b_w)\frac{r_1r_3}{r_4}-(b+2b_w+2b_\ell)\,\frac{r_2r_3}{r_4}}{(b+2b_w+2b_\ell-\frac{2r_1^2}{r_4})}\right]$$

To complete the proof use is made of a mathematical subtlety in the form of adding and subtracting the term $\frac{2r_1^2 r_2 r_3}{r_4^2}$ to the numerator of the term in square brackets as follows

$$P_{CR}(d^*-d) = \frac{\pi^2 Et}{2S^2} b_w$$

$$\frac{\frac{r_1 r_3}{r_4}(b+b_w) - \frac{2r_1^2 r_2 r_3}{r_4^2} - (b+2b_w+2b_\ell)\frac{r_2 r_3}{r_4} + \frac{2r_1^2 r_2 r_3}{r_4^2}}{(b+2b_w+2b_\ell - \frac{2r_1^2}{r_4})}$$

The terms of the numerator are then regrouped to give

$$P_{CR}(d^*-d) = \frac{\pi^2 Et}{2S^2} b_w \left[\frac{\frac{r_1 r_3}{r_4}(b+b_w - \frac{2r_1 r_2}{r_4}) - (b+2b_w+2b_\ell - \frac{2r_1^2}{r_4})\frac{r_2 r_3}{r_4}}{(b+2b_w+2b_\ell - \frac{2r_1^2}{r_4})} \right]$$

which, after some rearrangement, can be written finally as,

$$P_{CR}(d^*-d) = \frac{\pi^2 Et}{2S^2} b_w \left[\frac{\frac{r_1 r_3}{r_4}\left[b+b_w - \frac{2r_1 r_2}{r_4}\right]}{\left[b+2b_w+2b_\ell - \frac{2r_1^2}{r_4}\right]} - \frac{r_2 r_3}{r_4} \right] \text{---(II.11)}$$

Comparison of equations (II.6) and (II.11) completes the proof of equation (II.1). It should be clearly understood however, as mentioned previously, that P_{CR} is the buckling load of a centroidally loaded section, according to the current locally deflected form.

Finally, by using equation (II.1) for M^*, equations (I.19) of appendix I and (4.8.11) of chapter four, for the lateral central deflection of the column may be written

$$\delta_c = \left[e + (d - d^*)(1 - \frac{P_{CR}}{P}) \right] \left[\sec \frac{\pi}{2}\sqrt{\frac{P}{P_{E^*}}} - 1 \right] \text{—(II.12)}$$

APPENDIX III

SOLUTION OF THE ENERGY INTEGRALS

IN THE INITIAL INSTABILITY ANALYSIS.

APPENDIX III

SOLUTIONS OF THE ENERGY INTEGRALS IN THE INITIAL INSTABILITY ANALYSIS

This appendix gives the solutions of the bending strain energy integrals ψ_{nm}, ϕ_{nm}, Z_{nm} and the potential energy integrals Γ_{nm}, T_{nm}, G_{nm} in the initial instability analysis of chapter three. Knowing these, the total strain energy and potential energy integrals λ_{nm} and θ_{nm} can be set up (see equations 3.4.13, chapter three) and evaluated for any $_{nm}$, n = 1, 2, ---- N., m = 1, 2, ---- N. The λ_{nm} and θ_{nm} so obtained are then used to formulate equations 3.4.17, chapter three and the initial local instability load for the column determined by finding the lowest eigenvalue of these equations. The buckled form at instability is obtained from the corresponding eigenvector.

Flange bending strain energy integral (equation 3.4.4, chapter three)

$$\psi_{nm} = \frac{1}{b_f^3}\left[\frac{b_n(b_n-1)b_m(b_m-1)\xi_n\xi_m}{(b_n+b_m-3)} - \right.$$

$$\frac{a_m(a_m-1)b_n(b_n-1)\xi_n}{(a_m+b_n-3)} - \frac{a_n(a_n-1)b_m(b_m-1)\xi_m}{(a_n+b_m-3)}$$

$$\left. + \frac{a_n(a_n-1)a_m(a_m-1)}{(a_n+a_m-3)}\right] - \frac{\pi^2}{b_f S^2}\left[b_n\xi_n - \right.$$

$$\frac{b_n(b_n-1)\xi_n}{(a_m+b_n-1)} - b_n\xi_n\xi_m + \frac{b_n(b_n-1)\xi_n\xi_m}{(b_m+b_n-1)} -$$

$$a_n + \frac{a_n(a_n-1)}{(a_m+a_n-1)} + a_n\xi_m - \frac{a_n(a_n-1)\xi_m}{(b_m+a_n-1)} +$$

$$b_m\xi_m - \frac{b_m(b_m-1)\xi_m}{(a_n+b_m-1)} - b_m\xi_m\xi_n + \frac{b_m(b_m-1)\xi_m\xi_n}{(b_n+b_m-1)}$$

$$\left. - a_m + \frac{a_m(a_m-1)}{(a_n+a_m-1)} + a_m\xi_n - \frac{a_m(a_m-1)\xi_n}{(b_n+a_m-1)}\right]$$

$$+ \frac{\pi^4 b_f}{S^4}\left[1 - \frac{1}{(a_m+1)} - \xi_m + \frac{\xi_m}{(b_m+1)} - \frac{1}{(a_n+1)}\right.$$

$$+ \frac{1}{(a_n+a_m+1)} + \frac{\xi_m}{(a_n+1)} - \frac{\xi_m}{(a_n+b_m+1)} - \xi_n + \frac{\xi_n}{(a_m+1)}$$

$$\left. + \xi_n\xi_m - \frac{\xi_n\xi_m}{(b_m+1)} + \frac{\xi_n}{(b_n+1)} - \frac{\xi_n}{(b_n+a_m+1)} - \frac{\xi_n\xi_m}{(b_n+1)}\right.$$

$$\left. + \frac{\xi_n\xi_m}{(b_n+b_m+1)}\right] \qquad \text{---------(III.1)}$$

Flange potential energy integral (equation 3.4.5, chapter three)

$$\Gamma_{nm} = b_f\Bigg[1 - \frac{1}{(a_m+1)} - \xi_m + \frac{\xi_m}{(b_m+1)} - \frac{1}{(a_n+1)} + \frac{1}{(a_n+a_m+1)} + \frac{\xi_m}{(a_n+1)} - \frac{\xi_m}{(a_n+b_m+1)} - \xi_n + \frac{\xi_n}{(a_m+1)} + \xi_n\xi_m - \frac{\xi_n\xi_m}{(b_m+1)} + \frac{\xi_n}{(b_n+1)} - \frac{\xi_n}{(a_m+b_n+1)} - \frac{\xi_n\xi_m}{(b_n+1)} + \frac{\xi_n\xi_m}{(b_n+b_m+1)}\Bigg] \qquad \text{---------(III.2)}$$

Web bending strain energy integral (equation 3.4.7., chapter three)

$$\phi_{nm} = \frac{1}{b_w{}^3}\Bigg[\frac{\beta_n\ \beta_m\ k_n\ k_m\ (k_n-1)(k_m-1)}{(k_n+k_m-3)} - 2\gamma_m\beta_nk_n - 2\gamma_n\beta_mk_m + 4\gamma_n\gamma_m\Bigg] - \frac{\pi^2}{b_wS^2}\Bigg[\mu_m\beta_n(k_n-1) - \frac{\gamma_m\beta_nk_n(k_n-1)}{(k_n+1)} + \frac{\beta_m\beta_nk_n(k_n-1)}{(k_n+k_m-1)} - \gamma_n\mu_m + \frac{2\gamma_n\gamma_m}{3} - \frac{2\gamma_n\beta_m}{(k_m+1)}\Bigg] - \frac{\pi^2}{b_wS^2}\Bigg[\mu_n\beta_m(k_m-1) - \frac{\gamma_n\beta_mk_m(k_m-1)}{(k_m+1)} + \frac{\beta_n\beta_mk_m(k_m-1)}{(k_m+k_n-1)} - \gamma_m\mu_n + \frac{2\gamma_m\gamma_n}{3} - \frac{2\gamma_m\gamma_n}{(k_n+1)}\Bigg] + \frac{\pi^4b_w}{S^4}\Bigg[\frac{\mu_n\mu_m}{3} - \frac{\mu_n\gamma_m}{4} + \frac{\mu_n\beta_m}{(k_m+2)} - \frac{\gamma_n\mu_m}{4} + \frac{\gamma_n\gamma_m}{5} - \frac{\gamma_n\beta_m}{(k_m+3)} + \frac{\beta_n\mu_m}{(k_n+2)} - \frac{\beta_n\gamma_m}{(k_n+3)} + \frac{\beta_n\beta_m}{(k_n+k_m+1)}\Bigg] \qquad \text{---------(III.3)}$$

Web potential energy integral (equation 3.4.8, chapter three)

$$T_{nm} = b_w(1-\alpha)\left[\frac{\mu_n\mu_m}{3} - \frac{\mu_n\gamma_m}{4} + \frac{\mu_n\beta_m}{(k_m+2)} - \frac{\gamma_n\mu_m}{4} + \frac{\gamma_n\gamma_m}{5} - \frac{\gamma_n\beta_m}{(k_m+3)} + \frac{\beta_n\mu_m}{(k_n+2)} - \frac{\beta_n\gamma_m}{(k_n+3)} + \frac{\beta_n\beta_m}{(k_n+k_m+1)}\right] + b_w\alpha\left[\frac{\mu_n\mu_m}{4} - \frac{\mu_n\gamma_m}{5} + \frac{\mu_n\beta_m}{(k_m+3)} - \frac{\gamma_n\mu_m}{5} + \frac{\gamma_n\gamma_m}{6} - \frac{\gamma_n\beta_m}{(k_m+4)} + \frac{\beta_n\mu_m}{(k_n+3)} - \frac{\beta_n\gamma_m}{(k_n+4)} + \frac{\beta_n\beta_m}{(k_n+k_m+2)}\right] \quad \text{------(III.4)}$$

Lip bending strain energy integral (equation 3.4.10 chapter three)

$$Z_{nm} = \frac{1}{b_\ell^3}\left[4\Omega_n\Omega_m + 2\Omega_n\tau_m t_m + 2\Omega_m\tau_n t_n + \frac{\tau_n\tau_m t_n t_m (t_n-1)(t_m-1)}{(t_n+t_m-3)}\right] - \frac{2\nu\pi^2}{b_\ell S^2}\left[\Omega_m\rho_n + \rho_n\tau_m(t_m-1) + \frac{2\Omega_m\Omega_n}{3} + \frac{\Omega_n\tau_m t_m(t_m-1)}{(t_m+1)} + \frac{2\Omega_m\tau_n}{(t_n+1)} + \frac{\tau_n\tau_m t_m(t_m-1)}{(t_n+t_m-1)}\right] + \frac{\pi^4 b_\ell}{S^4}\left[\frac{\rho_n\rho_m}{3} + \frac{\rho_n\Omega_m}{4} + \frac{\rho_n\tau_m}{(t_m+2)} + \frac{\Omega_n\rho_m}{4} + \frac{\Omega_n\Omega_m}{5} + \frac{\Omega_n\tau_m}{(t_m+3)} + \frac{\tau_n\rho_m}{(t_n+2)} + \frac{\tau_n\Omega_m}{(t_n+3)} + \frac{\tau_n\tau_m}{(t_n+t_m+1)}\right] + \frac{2\pi^2(1-\nu)}{b_\ell S^2}\left[\rho_n\rho_m + \rho_n\Omega_m + \rho_n\tau_m + \rho_m\Omega_n + \frac{4\Omega_n\Omega_m}{3} + \frac{2\Omega_n\tau_m t_m}{(t_m+1)} + \rho_m\tau_n + \frac{2\Omega_m\tau_n t_n}{(t_n+1)} + \frac{\tau_n t_n\tau_m t_m}{(t_n+t_m-1)}\right] \text{--(III.5)}$$

Lip potential energy integral (equation 3.4.11.,chapter three)

$$G_{nm} = b_\ell(1-\alpha)\left[\frac{\rho_n\rho_m}{3} + \frac{\rho_n\Omega_m}{4} + \frac{\rho_n\tau_m}{(t_m+2)} + \frac{\Omega_n\rho_m}{4} + \frac{\Omega_n\Omega_m}{5} + \frac{\Omega_n\tau_m}{(t_m+3)} + \frac{\tau_n\rho_m}{(t_n+2)} + \frac{\tau_n\Omega_m}{(t_n+3)} + \frac{\tau_n\tau_m}{(t_n+t_m+1)}\right] \text{---(III.6)}$$

APPENDIX IV

SOLUTION OF THE ENERGY INTEGRALS IN THE POST LOCAL BUCKLING ANALYSIS.

APPENDIX IV

SOLUTION OF THE ENERGY INTEGRALS IN THE POST LOCAL BUCKLING ANALYSIS

This appendix gives the solutions of the energy integrals Γ_{inmrp}, Φ_{inmrp}, θ_{inm} and Q_{inm} as formulated in the post local buckling analysis of chapter four by equations 4.7.4 and 4.7.6. The integrals Γ_{inmrp}, Φ_{inmrp} and θ_{inm} are associated with the strain energy of mid plane forces while the integral Q_{inm} relates to the strain energy of plate bending and twisting. The solutions of the energy integrals as given in this appendix were evaluated by the computer and the results used to formulate the ε coefficients in equation 4.7.11, the quartic for Δ, for a given value of flange compression u*. Solving equation 4.7.11 for Δ, the ratio of the local deflection coefficients $\frac{W_2}{W_1}$ in the two term post buckling solution, leads, after consideration of overall equilibrium, to the elastic solution for a particular value of u*. To obtain the complete post-local-interactive equilibrium path, the solution procedure is simply repeated for a number of discrete increments of compression u* applied to the flange.

$$\Gamma_{1nmrp} = \int_0^{b_f} \left[\psi_{1nm}{}^{11} \psi_{1rp}{}^{11} - \left(\frac{2\pi}{S}\right)^2 \psi_{1nm}{}^{11} \psi_{1rp} - \left(\frac{2\pi}{S}\right)^2 \psi_{1nm} \psi_{1rp}{}^{11} + \left(\frac{2\pi}{S}\right)^4 \psi_{1nm} \psi_{1rp} \right] dy_1$$

$$= \frac{1}{b_f{}^3} \left[4d_{3nm}d_{3rp} + \frac{1}{3}(24d_{3nm}d_{5rp} + 24d_{5nm}d_{3rp}) \right.$$
$$+ \frac{1}{5}(60d_{3nm}d_{7rp} + 144d_{5nm}d_{5rp} + 60d_{7nm}d_{3rp})$$
$$+ \frac{1}{7}(112d_{3nm}d_{9rp} + 360d_{5nm}d_{7rp} + 360d_{7nm}d_{5rp}$$
$$+ 112d_{9nm}d_{3rp}) + \frac{1}{9}(180d_{3nm}d_{11rp} + 672d_{5nm}d_{9rp}$$
$$+ 900d_{7nm}d_{7rp} + 672d_{9nm}d_{5rp} + 180d_{11nm}d_{3rp})$$
$$+ \frac{1}{11}(1080d_{5nm}d_{11rp} + 1680d_{7nm}d_{9rp} + 1680d_{9nm}d_{7rp}$$
$$+ 1080d_{11nm}d_{5rp}) + \frac{1}{13}(2700d_{7nm}d_{11rp} + 3136d_{9nm}d_{9rp}$$
$$+ 2700d_{11nm}d_{7rp}) + \frac{1}{15}(5040d_{9nm}d_{11rp} + 5040d_{11nm}d_{9rp})$$
$$\left. + \frac{1}{17}(8100d_{11nm}d_{11rp}) \right] - \left(\frac{2\pi}{S}\right)^2 \frac{1}{b_f} \left[2d_{3nm}d_{1rp} \right.$$
$$+ \frac{1}{3}(2d_{3nm}d_{3rp} + 12d_{5nm}d_{1rp}) + \frac{1}{5}(2d_{3nm}d_{5rp}$$
$$+ 12d_{5nm}d_{3rp} + 30d_{7nm}d_{1rp}) + \frac{1}{7}(2d_{3nm}d_{7rp}$$
$$+ 12d_{5nm}d_{5rp} + 30d_{7nm}d_{3rp} + 56d_{9nm}d_{1rp})$$
$$+ \frac{1}{9}(2d_{3nm}d_{9rp} + 12d_{5nm}d_{7rp} + 30d_{7nm}d_{5rp}$$
$$+ 56d_{9nm}d_{3rp} + 90d_{11nm}d_{1rp}) + \frac{1}{11}(2d_{3nm}d_{11rp}$$
$$+ 12d_{5nm}d_{9rp} + 30d_{7nm}d_{7rp} + 56d_{9nm}d_{5rp}$$
$$+ 90d_{11nm}d_{3rp}) + \frac{1}{13}(12d_{5nm}d_{11rp} + 30d_{7nm}d_{9rp}$$
$$+ 56d_{9nm}d_{7rp} + 90d_{11nm}d_{5rp}) + \frac{1}{15}(30d_{7nm}d_{11rp}$$
$$+ 56d_{9nm}d_{9rp} + 90d_{11nm}d_{7rp}) + \frac{1}{17}(56d_{9nm}d_{11rp}$$
$$\left. + 90d_{11nm}d_{9rp}) + \frac{1}{19}(90d_{11nm}d_{11rp}) \right] - \left(\frac{2\pi}{S}\right)^2 \frac{1}{b_f}$$

$$\Bigg[2d_{3rp}d_{1nm} + \frac{1}{3}(2d_{3rp}d_{3nm} + 12d_{5rp}d_{1nm})$$

$$+ \frac{1}{5}(2d_{3rp}d_{5nm} + 12d_{5rp}d_{3nm} + 30d_{7rp}d_{1nm})$$

$$+ \frac{1}{7}(2d_{3rp}d_{7nm} + 12d_{5rp}d_{5nm} + 30d_{7rp}d_{3nm}$$

$$+ 56d_{9rp}d_{1nm}) + \frac{1}{9}(2d_{3rp}d_{9nm} + 12d_{5rp}d_{7nm}$$

$$+ 30d_{7rp}d_{5nm} + 56d_{9rp}d_{3nm} + 90d_{11rp}d_{1nm})$$

$$+ \frac{1}{11}(2d_{3rp}d_{11nm} + 12d_{5rp}d_{9nm} + 30d_{7rp}d_{7nm}$$

$$+ 56d_{9rp}d_{5nm} + 90d_{11rp}d_{3nm}) + \frac{1}{13}(12d_{5rp}d_{11nm}$$

$$+ 30d_{7rp}d_{9nm} + 56d_{9rp}d_{7nm} + 90d_{11rp}d_{5nm})$$

$$+ \frac{1}{15}(30d_{7rp}d_{11nm} + 56d_{9rp}d_{9nm} + 90d_{11rp}d_{7nm})$$

$$+ \frac{1}{17}(56d_{9rp}d_{11nm} + 90d_{11rp}d_{9nm}) + \frac{1}{19}(90d_{11rp}d_{11nm}) \Bigg]$$

$$+ \left(\frac{2\pi}{S}\right)^4 b_f \Bigg[d_{1nm}d_{1rp} + \frac{1}{3}(d_{1nm}d_{3rp} + d_{3nm}d_{1rp})$$

$$+ \frac{1}{5}(d_{1nm}d_{5rp} + d_{3nm}d_{3rp} + d_{5nm}d_{1rp}) + \frac{1}{7}(d_{1nm}d_{7rp}$$

$$+ d_{3nm}d_{5rp} + d_{5nm}d_{3rp} + d_{7nm}d_{1rp}) + \frac{1}{9}(d_{1nm}d_{9rp}$$

$$+ d_{3nm}d_{7rp} + d_{5nm}d_{5rp} + d_{7nm}d_{3rp} + d_{9nm}d_{1rp})$$

$$+ \frac{1}{11}(d_{1nm}d_{11rp} + d_{3nm}d_{9rp} + d_{5nm}d_{7rp} + d_{7nm}d_{5rp}$$

$$+ d_{9nm}d_{3rp} + d_{11nm}d_{1rp}) + \frac{1}{13}(d_{3nm}d_{11rp} + d_{5nm}d_{9rp}$$

$$+ d_{7nm}d_{7rp} + d_{9nm}d_{5rp} + d_{11nm}d_{3rp})$$

$$+ \frac{1}{15}(d_{5nm}d_{11rp} + d_{7nm}d_{9rp} + d_{9nm}d_{7rp} + d_{11nm}d_{5rp})$$

$$+ \frac{1}{17}(d_{7nm}d_{11rp} + d_{9nm}d_{9rp} + d_{11nm}d_{7rp})$$

$$+ \frac{1}{19}(d_{9nm}d_{11rp} + d_{11nm}d_{9rp}) + \frac{1}{21}(d_{11nm}d_{11rp}) \Bigg]$$

$$+ \left(\frac{2\pi}{S}\right) \frac{2t_{2rp}}{b_f^2} \Bigg[2d_{3nm} + 4d_{5nm} + 6d_{7nm} + 8d_{9nm}$$

$$+ 10d_{11nm} \Bigg] \times \text{COSH}\ \frac{2\pi b_f}{S} - \left(\frac{2\pi}{S}\right)^2 \frac{2t_{2rp}}{b_f}$$

$$\left[d_{1nm} + d_{3nm} + d_{5nm} + d_{7nm} + d_{9nm} + d_{11nm} \right] X$$

$$X \text{ SINH } \frac{2\pi bf}{S} + \left(\frac{2\pi}{S}\right) \frac{2t_{2nm}}{bf^2} \left[2d_{3rp} + 4d_{5rp} + 6d_{7rp} \right.$$

$$\left. + 8d_{9rp} + 10d_{11rp} \right] X \text{ COSH } \frac{2\pi bf}{S} - \left(\frac{2\pi}{S}\right)^2 \frac{2t_{2nm}}{bf}$$

$$\left[d_{1rp} + d_{3rp} + d_{5rp} + d_{7rp} + d_{9rp} + d_{11rp} \right] X$$

$$X \text{ SINH } \frac{2\pi bf}{S} + \frac{2}{bf^2} \left(\frac{2\pi}{S}\right)^2 t_{2nm} t_{2rp} \left[\frac{S}{4\pi} \text{ SINH } \frac{4\pi bf}{S} + bf \right]$$

---------(IV.1)

$$\Phi_{1nmrp} = \int_o^{bf} Y_{1n}\, Y_{1m}\, Y_{1r}\, Y_{1p}\, dy_1$$

$$= bf \left[q_{1nm}q_{1rp} + \frac{1}{3}(q_{1nm}q_{2rp} + q_{2nm}q_{1rp}) \right.$$

$$+ \frac{1}{5}(q_{1nm}q_{3rp} + q_{2nm}q_{2rp} + q_{3nm}q_{1rp}) + \frac{1}{7}(q_{1nm}q_{4rp}$$

$$+ q_{2nm}q_{3rp} + q_{3nm}q_{2rp} + q_{4nm}q_{1rp}) + \frac{1}{9}(q_{1nm}q_{5rp}$$

$$+ q_{2nm}q_{4rp} + q_{3nm}q_{3rp} + q_{4nm}q_{2rp} + q_{5nm}q_{1rp})$$

$$+ \frac{1}{11}(q_{1nm}q_{6rp} + q_{2nm}q_{5rp} + q_{3nm}q_{4rp} + q_{4nm}q_{3rp}$$

$$+ q_{5nm}q_{2rp} + q_{6nm}q_{1rp}) + \frac{1}{13}(q_{1nm}q_{7rp} + q_{2nm}q_{6rp}$$

$$+ q_{3nm}q_{5rp} + q_{4nm}q_{4rp} + q_{5nm}q_{3rp} + q_{6nm}q_{2rp}$$

$$+ q_{7nm}q_{1rp}) + \frac{1}{15}(q_{2nm}q_{7rp} + q_{3nm}q_{6rp} + q_{4nm}q_{5rp}$$

$$+ q_{5nm}q_{4rp} + q_{6nm}q_{3rp} + q_{7nm}q_{2rp}) + \frac{1}{17}(q_{3nm}q_{7rp}$$

$$+ q_{4nm}q_{6rp} + q_{5nm}q_{5rp} + q_{6nm}q_{4rp} + q_{7nm}q_{3rp})$$

$$+ \frac{1}{19}(q_{4nm}q_{7rp} + q_{5nm}q_{6rp} + q_{6nm}q_{5rp} + q_{7nm}q_{4rp})$$

$$+ \frac{1}{21}(q_{5nm}q_{7rp} + q_{6nm}q_{6rp} + q_{7nm}q_{5rp}) + \frac{1}{23}(q_{6nm}q_{7rp}$$

$$\left. + q_{7nm}q_{6rp}) + \frac{1}{25}(q_{7nm}q_{7rp}) \right]$$

---------(IV.2)

$$\theta_{inm} = \int_0^{b_f} Y_{in} Y_{im} \, d_{yi}$$

$$= b_f \left[q_{1nm} + \frac{1}{3} q_{2nm} + \frac{1}{5} q_{3nm} + \frac{1}{7} q_{4nm} + \frac{1}{9} q_{5nm} + \frac{1}{11} q_{6nm} + \frac{1}{13} q_{7nm} \right] \qquad \text{---------(IV.3)}$$

where

$$q_{1nm} = g_{n1} g_{m1}$$

$$q_{2nm} = (g_{n1} g_{m2} + g_{n2} g_{m1})$$

$$q_{3nm} = (g_{n1} g_{m3} + g_{n2} g_{m2} + g_{n3} g_{m1})$$

$$q_{4nm} = (g_{n1} g_{m4} + g_{n2} g_{m3} + g_{n3} g_{m2} + g_{n4} g_{m1})$$

$$q_{5nm} = (g_{n2} g_{m4} + g_{n3} g_{m3} + g_{n4} g_{m2})$$

$$q_{6nm} = (g_{n3} g_{m4} + g_{n4} g_{m3})$$

$$q_{7nm} = (g_{n4} g_{m4}) \qquad \text{----------(IV.4)}$$

$$Q_{inm} = b_f \left[T_{1nm} + \frac{T_{2nm}}{3} + \frac{T_{3nm}}{5} + \frac{T_{4nm}}{7} + \frac{T_{5nm}}{9} + \frac{T_{6nm}}{11} + \frac{T_{7nm}}{13} \right] \qquad \text{---------(IV.5)}$$

where

$$T_{1nm} = \left[\frac{4}{b_f^4} g_{n2} g_{m2} - \frac{2\pi^2}{S^2 b_f^2} (g_{n2} g_{m1} + g_{n1} g_{m2}) + \frac{\pi^4}{S^4} g_{n1} g_{m1} \right]$$

$$T_{2nm} = \left[\frac{24}{b_f^4} (g_{n2} g_{m3} + g_{n3} g_{m2}) - \frac{\pi^2}{S^2 b_f^2} (4 g_{n2} g_{m2} + 12 (g_{n3} g_{m1} + g_{n1} g_{m3})) + \frac{\pi^4}{S^4} (g_{n1} g_{m2} + g_{n2} g_{m1}) \right]$$

$$T_{3nm} = \left[\frac{1}{b_f^4} (60 g_{n4} g_{m2} + 144 g_{n3} g_{m3} + 60 g_{n2} g_{m4}) - \frac{\pi^2}{S^2 b_f^2} (14 (g_{n2} g_{m3} + g_{n3} g_{m2}) + 30 (g_{n4} g_{m1} + g_{n1} g_{m4})) + \frac{\pi^4}{S^4} (g_{n1} g_{m3} + g_{n2} g_{m2} + g_{n3} g_{m1}) \right]$$

$$T_{4nm} = \left[\frac{360}{b_f^4}(g_{n3}g_{m4} + g_{n4}g_{m3}) - \frac{\pi^2}{S^2 b_f^2}(32(g_{n2}g_{m4} + g_{n4}g_{m2}) + 24g_{n3}g_{m3}) + \frac{\pi^4}{S^4}(g_{n1}g_{m4} + g_{n2}g_{m3} + g_{n3}g_{m2} + g_{n4}g_{m1}) \right]$$

$$T_{5nm} = \left[\frac{900}{b_f^4} g_{n4}g_{m4} - \frac{\pi^2}{S^2 b_f^2}(42(g_{n3}g_{m4} + g_{n4}g_{m3})) + \frac{\pi^4}{S^4}(g_{n2}g_{m4} + g_{n3}g_{m3} + g_{n4}g_{m2}) \right]$$

$$T_{6nm} = \left[\frac{\pi^4}{S^4}(g_{n3}g_{m4} + g_{n4}g_{m3}) - \frac{\pi^2}{S^2 b_f^2}(60 g_{n4}g_{m4}) \right]$$

$$T_{7nm} = \frac{\pi^4}{S^4} g_{n4}g_{m4} \qquad \text{— — — — — — (IV.6)}$$

$$\Gamma_{2nmrp} = \int_0^{bw} \left[\psi_{2nm}^{11}\psi_{2rp}^{11} - \left(\frac{2\pi}{S}\right)^2 \psi_{2nm}^{11}\psi_{2rp} - \left(\frac{2\pi}{S}\right)^2 \psi_{2nm}\psi_{2rp}^{11} + \left(\frac{2\pi}{S}\right)^4 \psi_{2nm}\psi_{2rp} \right] d_{y2}$$

$$= \frac{1}{bw^3}\left[4b_{3nm}b_{3rp} + \frac{1}{2}(12b_{3nm}b_{4rp} + 12b_{4nm}b_{3rp}) + \frac{1}{3}(24b_{3nm}b_{5rp} + 36b_{4nm}b_{4rp} + 24b_{5nm}b_{3rp}) + \frac{1}{4}(40b_{3nm}b_{6rp} + 72b_{4nm}b_{5rp} + 72b_{5nm}b_{4rp} + 40b_{6nm}b_{3rp}) + \frac{1}{5}(60b_{3nm}b_{7rp} + 120b_{4nm}b_{6rp} + 144b_{5nm}b_{5rp} + 120b_{6nm}b_{4rp} + 60b_{7nm}b_{3rp}) + \frac{1}{6}(84b_{3nm}b_{8rp} + 180b_{4nm}b_{7rp} + 240b_{5nm}b_{6rp} + 240b_{6nm}b_{5rp} + 180b_{7nm}b_{4rp} + 84b_{8nm}b_{3rp}) + \frac{1}{7}(112b_{3nm}b_{9rp} + 252b_{4nm}b_{8rp} + 360b_{5nm}b_{7rp} + 400b_{6nm}b_{6rp} + 360b_{7nm}b_{5rp} + 252b_{8nm}b_{4rp} + 112b_{9nm}b_{3rp}) + \frac{1}{8}(144b_{3nm}b_{10rp} + 336b_{4nm}b_{9rp} + 504b_{5nm}b_{8rp} + 600b_{6nm}b_{7rp} + 600b_{7nm}b_{6rp} + 504b_{8nm}b_{5rp} + 336b_{9nm}b_{4rp} + 144b_{10nm}b_{3rp}) \right]$$

$$+ \frac{1}{9}(180b_{3nm}b_{11rp} + 432b_{4nm}b_{10rp} + 672b_{5nm}b_{9rp}$$

$$+ 840b_{6nm}b_{8rp} + 900b_{7nm}b_{7rp} + 840b_{8nm}b_{6rp}$$

$$+ 672b_{9nm}b_{5rp} + 432b_{10nm}b_{4rp} + 180b_{11nm}b_{3rp})$$

$$+ \frac{1}{10}(540b_{4nm}b_{11rp} + 864b_{5nm}b_{10rp} + 1120b_{6nm}b_{9rp}$$

$$+ 1260b_{7nm}b_{8rp} + 1260b_{8nm}b_{7rp} + 1120b_{9nm}b_{6rp}$$

$$+ 864b_{10nm}b_{5rp} + 540b_{11nm}b_{4rp}) + \frac{1}{11}(1080b_{5nm}b_{11rp}$$

$$+ 1440b_{6nm}b_{10rp} + 1680b_{7nm}b_{9rp} + 1764b_{8nm}b_{8rp}$$

$$+ 1680b_{9nm}b_{7rp} + 1440b_{10nm}b_{6rp} + 1080b_{11nm}b_{5rp})$$

$$+ \frac{1}{12}(1800b_{6nm}b_{11rp} + 2160b_{7nm}b_{10rp} + 2352b_{8nm}b_{9rp}$$

$$+ 2352b_{9nm}b_{8rp} + 2160b_{10nm}b_{7rp} + 1800b_{11nm}b_{6rp})$$

$$+ \frac{1}{13}(2700b_{7nm}b_{11rp} + 3024b_{8nm}b_{10rp} + 3136b_{9nm}b_{9rp}$$

$$+ 3024b_{10nm}b_{8rp} + 2700b_{11nm}b_{7rp}) + \frac{1}{14}(3780b_{8nm}b_{11rp}$$

$$+ 4032b_{9nm}b_{10rp} + 4032b_{10nm}b_{9rp} + 3780b_{11nm}b_{8rp})$$

$$+ \frac{1}{15}(5040b_{9nm}b_{11rp} + 5184b_{10nm}b_{10rp} + 5040b_{11nm}b_{9rp})$$

$$+ \frac{1}{16}(6480b_{10nm}b_{11rp} + 6480b_{11nm}b_{10rp})$$

$$+ \frac{1}{17}(8100b_{11nm}b_{11rp})\Big] - \left(\frac{2\pi}{S}\right)^2 \frac{1}{bw}\Big[2b_{1nm}b_{3rp}$$

$$+ \frac{1}{2}(6b_{1nm}b_{4rp} + 2b_{2nm}b_{3rp}) + \frac{1}{3}(12b_{1nm}b_{5rp}$$

$$+ 6b_{2nm}b_{4rp} + 2b_{3nm}b_{3rp}) + \frac{1}{4}(20b_{1nm}b_{6rp}$$

$$+ 12b_{2nm}b_{5rp} + 6b_{3nm}b_{4rp} + 2b_{4nm}b_{3rp})$$

$$+ \frac{1}{5}(30b_{1nm}b_{7rp} + 20b_{2nm}b_{6rp} + 12b_{3nm}b_{5rp}$$

$$+ 6b_{4nm}b_{4rp} + 2b_{5nm}b_{3rp}) + \frac{1}{6}(42b_{1nm}b_{8rp} + 30b_{2nm}b_{7rp}$$

$$+ 20b_{3nm}b_{6rp} + 12b_{4nm}b_{5rp} + 6b_{5nm}b_{4rp} + 2b_{6nm}b_{3rp})$$

$$+ \frac{1}{7}(56b_{1nm}b_{9rp} + 42b_{2nm}b_{8rp} + 30b_{3nm}b_{7rp}$$

$$+ 20b_{4nm}{}^{b}{}_{6rp} + 12b_{5nm}{}^{b}{}_{5rp} + 6b_{6nm}{}^{b}{}_{4rp} + 2b_{7nm}{}^{b}{}_{3rp})$$

$$+ \frac{1}{8}(72b_{1nm}{}^{b}{}_{10rp} + 56b_{2nm}{}^{b}{}_{9rp} + 42b_{3nm}{}^{b}{}_{8rp}$$

$$+ 30b_{4nm}{}^{b}{}_{7rp} + 20b_{5nm}{}^{b}{}_{6rp} + 12b_{6nm}{}^{b}{}_{5rp} + 6b_{7nm}{}^{b}{}_{4rp})$$

$$+ \frac{1}{9}(90b_{1nm}{}^{b}{}_{11rp} + 72b_{2nm}{}^{b}{}_{10rp} + 56b_{3nm}{}^{b}{}_{9rp}$$

$$+ 42b_{4nm}{}^{b}{}_{8rp} + 30b_{5nm}{}^{b}{}_{7rp} + 20b_{6nm}{}^{b}{}_{6rp} + 12b_{7nm}{}^{b}{}_{5rp}$$

$$+ 6b_{8nm}{}^{b}{}_{4rp} + 2b_{9nm}{}^{b}{}_{3rp}) + \frac{1}{10}(90b_{2nm}{}^{b}{}_{11rp}$$

$$+ 72b_{3nm}{}^{b}{}_{10rp} + 56b_{4nm}{}^{b}{}_{9rp} + 42b_{5nm}{}^{b}{}_{8rp}$$

$$+ 30b_{6nm}{}^{b}{}_{7rp} + 20b_{7nm}{}^{b}{}_{6rp} + 12b_{8nm}{}^{b}{}_{5rp} + 6b_{9nm}{}^{b}{}_{4rp}$$

$$+ 2b_{10nm}{}^{b}{}_{3rp}) + \frac{1}{11}(90b_{3nm}{}^{b}{}_{11rp} + 72b_{4nm}{}^{b}{}_{10rp}$$

$$+ 56b_{5nm}{}^{b}{}_{9rp} + 42b_{6nm}{}^{b}{}_{8rp} + 30b_{7nm}{}^{b}{}_{7rp}$$

$$+ 20b_{8nm}{}^{b}{}_{6rp} + 12b_{9nm}{}^{b}{}_{5rp} + 6b_{10nm}{}^{b}{}_{4rp}$$

$$+ 2b_{11nm}{}^{b}{}_{3rp}) + \frac{1}{12}(90b_{4nm}{}^{b}{}_{11rp} + 72b_{5nm}{}^{b}{}_{10rp}$$

$$+ 56b_{6nm}{}^{b}{}_{9rp} + 42b_{7nm}{}^{b}{}_{8rp} + 30b_{8nm}{}^{b}{}_{7rp}$$

$$+ 20b_{9nm}{}^{b}{}_{6rp} + 12b_{10nm}{}^{b}{}_{5rp} + 6b_{11nm}{}^{b}{}_{4rp})$$

$$+ \frac{1}{13}(90b_{5nm}{}^{b}{}_{11rp} + 72b_{6nm}{}^{b}{}_{10rp} + 56b_{7nm}{}^{b}{}_{9rp}$$

$$+ 42b_{8nm}{}^{b}{}_{8rp} + 30b_{9nm}{}^{b}{}_{7rp} + 20b_{10nm}{}^{b}{}_{6rp}$$

$$+ 12b_{11nm}{}^{b}{}_{5rp}) + \frac{1}{14}(90b_{6nm}{}^{b}{}_{11rp} + 72b_{7nm}{}^{b}{}_{10rp}$$

$$+ 56b_{8nm}{}^{b}{}_{9rp} + 42b_{9nm}{}^{b}{}_{8rp} + 30b_{10nm}{}^{b}{}_{7rp}$$

$$+ 20b_{11nm}{}^{b}{}_{6rp}) + \frac{1}{15}(90b_{7nm}{}^{b}{}_{11rp} + 72b_{8nm}{}^{b}{}_{10rp}$$

$$+ 56b_{9nm}{}^{b}{}_{9rp} + 42b_{10nm}{}^{b}{}_{8rp} + 30b_{11nm}{}^{b}{}_{7rp})$$

$$+ \frac{1}{16}(90b_{8nm}{}^{b}{}_{11rp} + 72b_{9nm}{}^{b}{}_{10rp} + 56b_{10nm}{}^{b}{}_{9rp}$$

$$+ 42b_{11nm}{}^{b}{}_{8rp}) + \frac{1}{17}(90b_{9nm}{}^{b}{}_{11rp} + 72b_{10nm}{}^{b}{}_{10rp}$$

$$+ 56b_{11nm}{}^{b}{}_{9rp}) + \frac{1}{18}(90b_{10nm}{}^{b}{}_{11rp} + 72b_{11nm}{}^{b}{}_{10rp})$$

$$+ \frac{1}{19}(90b_{11nm}{}^{b}{}_{11rp})\Big] - (\frac{2\pi}{S})^{2} \frac{1}{bw}\Big[2b_{3nm}{}^{b}{}_{1rp}$$

$$+ \frac{1}{2}(2b_{3nm}{}^{b}{}_{2rp} + 6b_{4nm}{}^{b}{}_{1rp}) + \frac{1}{3}(2b_{3nm}{}^{b}{}_{3rp}$$

$$+ 6b_{4nm}{}^{b}{}_{2rp} + 12b_{5nm}{}^{b}{}_{1rp}) + \frac{1}{4}(2b_{3nm}{}^{b}{}_{4rp}$$

$$+ 6b_{4nm}{}^{b}{}_{3rp} + 12b_{5nm}{}^{b}{}_{2rp} + 20b_{6nm}{}^{b}{}_{1rp})$$

$$+ \frac{1}{5}(2b_{3nm}{}^{b}{}_{5rp} + 6b_{4nm}{}^{b}{}_{4rp} + 12b_{5nm}{}^{b}{}_{3rp}$$

$$+ 20b_{6nm}{}^{b}{}_{2rp} + 30b_{7nm}{}^{b}{}_{1rp}) + \frac{1}{6}(2b_{3nm}{}^{b}{}_{6rp}$$

$$+ 6b_{4nm}{}^{b}{}_{5rp} + 12b_{5nm}{}^{b}{}_{4rp} + 20b_{6nm}{}^{b}{}_{3rp} + 30b_{7nm}{}^{b}{}_{2rp}$$

$$+ 42b_{8nm}{}^{b}{}_{1rp}) + \frac{1}{7}(2b_{3nm}{}^{b}{}_{7rp} + 6b_{4nm}{}^{b}{}_{6rp}$$

$$+ 12b_{5nm}{}^{b}{}_{5rp} + 20b_{6nm}{}^{b}{}_{4rp} + 30b_{7nm}{}^{b}{}_{3rp}$$

$$+ 42b_{8nm}{}^{b}{}_{2rp} + 56b_{9nm}{}^{b}{}_{1rp}) + \frac{1}{8}(2b_{3nm}{}^{b}{}_{8rp}$$

$$+ 6b_{4nm}{}^{b}{}_{7rp} + 12b_{5nm}{}^{b}{}_{6rp} + 20b_{6nm}{}^{b}{}_{5rp}$$

$$+ 30b_{7nm}{}^{b}{}_{4rp} + 42b_{8nm}{}^{b}{}_{3rp} + 56b_{9nm}{}^{b}{}_{2rp})$$

$$+ \frac{1}{9}(2b_{3nm}{}^{b}{}_{9rp} + 6b_{4nm}{}^{b}{}_{8rp} + 12b_{5nm}{}^{b}{}_{7rp}$$

$$+ 20b_{6nm}{}^{b}{}_{6rp} + 30b_{7nm}{}^{b}{}_{5rp} + 42b_{8nm}{}^{b}{}_{4rp}$$

$$+ 56b_{9nm}{}^{b}{}_{3rp} + 72b_{10nm}{}^{b}{}_{2rp} + 90b_{11nm}{}^{b}{}_{1rp})$$

$$+ \frac{1}{10}(2b_{3nm}{}^{b}{}_{10rp} + 6b_{4nm}{}^{b}{}_{9rp} + 12b_{5nm}{}^{b}{}_{8rp}$$

$$+ 20b_{6nm}{}^{b}{}_{7rp} + 30b_{7nm}{}^{b}{}_{6rp} + 42b_{8nm}{}^{b}{}_{5rp}$$

$$+ 56b_{9nm}{}^{b}{}_{4rp} + 72b_{10nm}{}^{b}{}_{3rp} + 90b_{11nm}{}^{b}{}_{2rp})$$

$$+ \frac{1}{11}(2b_{3nm}{}^{b}{}_{11rp} + 6b_{4nm}{}^{b}{}_{10rp} + 12b_{5nm}{}^{b}{}_{9rp}$$

$$+ 20b_{6nm}{}^{b}{}_{8rp} + 30b_{7nm}{}^{b}{}_{7rp} + 42b_{8nm}{}^{b}{}_{6rp}$$

$$+ 56b_{9nm}{}^{b}{}_{5rp} + 72b_{10nm}{}^{b}{}_{4rp} + 90b_{11nm}{}^{b}{}_{3rp})$$

$$+ \frac{1}{12}(6b_{4nm}{}^{b}{}_{11rp} + 12b_{5nm}{}^{b}{}_{10rp} + 20b_{6nm}{}^{b}{}_{9rp}$$

$$+ 30b_{7nm}{}^{b}{}_{8rp} + 42b_{8nm}{}^{b}{}_{7rp} + 56b_{9nm}{}^{b}{}_{6rp}$$

$$+ 72b_{10nm}b_{5rp} + 90b_{11nm}b_{4rp}) + \frac{1}{13}(12b_{5nm}b_{11rp}$$

$$+ 20b_{6nm}b_{10rp} + 30b_{7nm}b_{9rp} + 42b_{8nm}b_{8rp}$$

$$+ 56b_{9nm}b_{7rp} + 72b_{10nm}b_{6rp} + 90b_{11nm}b_{5rp})$$

$$+ \frac{1}{14}(20b_{6nm}b_{11rp} + 30b_{7nm}b_{10rp} + 42b_{8nm}b_{9rp}$$

$$+ 56b_{9nm}b_{8rp} + 72b_{10nm}b_{7rp} + 90b_{11nm}b_{6rp})$$

$$+ \frac{1}{15}(30b_{7nm}b_{11rp} + 42b_{8nm}b_{10rp} + 56b_{9nm}b_{9rp}$$

$$+ 72b_{10nm}b_{8rp} + 90b_{11nm}b_{7rp}) + \frac{1}{16}(42b_{8nm}b_{11rp}$$

$$+ 56b_{9nm}b_{10rp} + 72b_{10nm}b_{9rp} + 90b_{11nm}b_{8rp})$$

$$+ \frac{1}{17}(56b_{9nm}b_{11rp} + 72b_{10nm}b_{10rp} + 90b_{11nm}b_{9rp})$$

$$+ \frac{1}{18}(72b_{10nm}b_{11rp} + 90b_{11nm}b_{10rp}) + \frac{1}{19}(90b_{11nm}b_{11rp})\Big]$$

$$+ \left(\frac{2\pi}{S}\right)^4 b_w\Big[b_{1nm}b_{1rp} + \frac{1}{2}(b_{1nm}b_{2rp} + b_{2nm}b_{1rp})$$

$$+ \frac{1}{3}(b_{1nm}b_{3rp} + b_{2nm}b_{2rp} + b_{3nm}b_{1rp}) + \frac{1}{4}(b_{1nm}b_{4rp}$$

$$+ b_{2nm}b_{3rp} + b_{3nm}b_{2rp} + b_{4nm}b_{1rp}) + \frac{1}{5}(b_{1nm}b_{5rp}$$

$$+ b_{2nm}b_{4rp} + b_{3nm}b_{3rp} + b_{4nm}b_{2rp} + b_{5nm}b_{1rp})$$

$$+ \frac{1}{6}(b_{1nm}b_{6rp} + b_{2nm}b_{5rp} + b_{3nm}b_{4rp} + b_{4nm}b_{3rp}$$

$$+ b_{5nm}b_{2rp} + b_{6nm}b_{1rp}) + \frac{1}{7}(b_{1nm}b_{7rp}$$

$$+ b_{2nm}b_{6rp} + b_{3nm}b_{5rp} + b_{4nm}b_{4rp} + b_{5nm}b_{3rp}$$

$$+ b_{6nm}b_{2rp} + b_{7nm}b_{1rp}) + \frac{1}{8}(b_{1nm}b_{8rp} + b_{2nm}b_{7rp}$$

$$+ b_{3nm}b_{6rp} + b_{4nm}b_{5rp} + b_{5nm}b_{4rp} + b_{6nm}b_{3rp}$$

$$+ b_{7nm}b_{2rp} + b_{8nm}b_{1rp}) + \frac{1}{9}(b_{1nm}b_{9rp} + b_{2nm}b_{8rp}$$

$$+ b_{3nm}b_{7rp} + b_{4nm}b_{6rp} + b_{5nm}b_{5rp} + b_{6nm}b_{4rp}$$

$$+ b_{7nm}b_{3rp} + b_{8nm}b_{2rp} + b_{9nm}b_{1rp}) + \frac{1}{10}(b_{1nm}b_{10rp}$$

$$+ b_{2nm}b_{9rp} + b_{3nm}b_{8rp} + b_{4nm}b_{7rp} + b_{5nm}b_{6rp}$$

$$+ b_{6nm}b_{5rp} + b_{7nm}b_{4rp} + b_{8nm}b_{3rp} + b_{9nm}b_{2rp}$$

$$+ b_{10nm}b_{1rp}) + \frac{1}{11}(b_{1nm}b_{11rp} + b_{2nm}b_{10rp}$$

$$+ b_{3nm}b_{9rp} + b_{4nm}b_{8rp} + b_{5nm}b_{7rp} + b_{6nm}b_{6rp}$$

$$+ b_{7nm}b_{5rp} + b_{8nm}b_{4rp} + b_{9nm}b_{3rp} + b_{10nm}b_{2rp}$$

$$+ b_{11nm}b_{1rp}) + \frac{1}{12}(b_{2nm}b_{11rp} + b_{3nm}b_{10rp}$$

$$+ b_{4nm}b_{9rp} + b_{5nm}b_{8rp} + b_{6nm}b_{7rp} + b_{7nm}b_{6rp}$$

$$+ b_{8nm}b_{5rp} + b_{9nm}b_{4rp} + b_{10nm}b_{3rp} + b_{11nm}b_{2rp})$$

$$+ \frac{1}{13}(b_{3nm}b_{11rp} + b_{4nm}b_{10rp} + b_{5nm}b_{9rp} + b_{6nm}b_{8rp}$$

$$+ b_{7nm}b_{7rp} + b_{8nm}b_{6rp} + b_{9nm}b_{5rp} + b_{10nm}b_{4rp}$$

$$+ b_{11nm}b_{3rp}) + \frac{1}{14}(b_{4nm}b_{11rp} + b_{5nm}b_{10rp}$$

$$+ b_{6nm}b_{9rp} + b_{7nm}b_{8rp} + b_{8nm}b_{7rp} + b_{9nm}b_{6rp}$$

$$+ b_{10nm}b_{5rp} + b_{11nm}b_{4rp}) + \frac{1}{15}(b_{5nm}b_{11rp} + b_{6nm}b_{10rp}$$

$$+ b_{7nm}b_{9rp} + b_{8nm}b_{8rp} + b_{9nm}b_{7rp} + b_{10nm}b_{6rp}$$

$$+ b_{11nm}b_{5rp}) + \frac{1}{16}(b_{6nm}b_{11rp} + b_{7nm}b_{10rp}$$

$$+ b_{8nm}b_{9rp} + b_{9nm}b_{8rp} + b_{10nm}b_{7rp} + b_{11nm}b_{6rp})$$

$$+ \frac{1}{17}(b_{7nm}b_{11rp} + b_{8nm}b_{10rp} + b_{9nm}b_{9rp} + b_{10nm}b_{8rp}$$

$$+ b_{11nm}b_{7rp}) + \frac{1}{18}(b_{8nm}b_{11rp} + b_{9nm}b_{10rp}$$

$$+ b_{10nm}b_{9rp} + b_{11nm}b_{8rp}) + \frac{1}{19}(b_{9nm}b_{11rp}$$

$$+ b_{10nm}b_{10rp} + b_{11nm}b_{9rp}) + \frac{1}{20}(b_{10nm}b_{11rp}$$

$$+ b_{11nm}b_{10rp}) + \frac{1}{21}(b_{11nm}b_{11rp})\Big] + \left(\frac{2\pi}{S}\right)\frac{2}{bw^2}$$

$$\Big[b_{2nm} + 2b_{3nm} + 3b_{4nm} + 4b_{5nm} + 6b_{7nm} + 7b_{8nm}$$

$$+ 8b_{9nm} + 9b_{10nm} + 10b_{11nm}\Big] X \Big[C_{4rp}\ \text{COSH}\ \frac{2\pi bw}{S}$$

$$+ C_{3rp}\ \text{SINH}\ \frac{2\pi bw}{S}\Big] - \left(\frac{2\pi}{S}\right)\frac{2}{bw^2}\ b_{2nm}\ C_{4rp}$$

$$- \left(\frac{2\pi}{S}\right)^2 \frac{2}{bw}\Big[b_{1nm} + b_{2nm} + b_{3nm} + b_{4nm} + b_{5nm} + b_{6nm} + b_{7nm} + b_{8nm} + b_{9nm} + b_{10nm} + b_{11nm}\Big] X \left[C_{4rp}\ \text{SINH}\ \frac{2\pi bw}{S} + C_{3rp}\ \text{COSH}\ \frac{2\pi bw}{S}\right]$$

$$+ \left(\frac{2\pi}{S}\right)^2 \left(\frac{2}{bw}\right) b_{1nm}C_{3rp} + \left(\frac{2\pi}{S}\right) \frac{2}{bw^2}\Big[b_{2rp} + 2b_{3rp} + 3b_{4rp} + 4b_{5rp} + 5b_{6rp} + 6b_{7rp} + 7b_{8rp} + 8b_{9rp} + 9b_{10rp} + 10b_{11rp}\Big] \ x \Big[C_{4nm}\ \text{COSH}\ \frac{2\pi bw}{S} + C_{3nm}\ \text{SINH}\ \frac{2\pi bw}{S}\Big] - \left(\frac{2\pi}{S}\right) \frac{2}{bw^2} b_{2rp}C_{4nm}$$

$$- \left(\frac{2\pi}{S}\right)^2 \frac{2}{bw}\Big[b_{1rp} + b_{2rp} + b_{3rp} + b_{4rp} + b_{5rp} + b_{6rp} + b_{7rp} + b_{8rp} + b_{9rp} + b_{10rp} + b_{11rp}\Big] X \left[C_{4nm}\ \text{SINH}\ \frac{2\pi bw}{S} + C_{3nm}\ \text{COSH}\ \frac{2\pi bw}{S}\right]$$

$$+ \left(\frac{2\pi}{S}\right)^2 \left(\frac{2}{bw}\right) b_{1rp}C_{3nm} + \frac{2}{bw^2}\left(\frac{2\pi}{S}\right)^2 \Big[C_{4nm}C_{4rp}\left(\frac{S}{4\pi}\ \text{SINH}\ \frac{4\pi bw}{S} + bw\right) + C_{3nm}C_{3rp}\left(\frac{S}{4\pi}\ \text{SINH}\ \frac{4\pi bw}{S} - bw\right) + \left(C_{4nm}C_{3rp} + C_{3nm}C_{4rp}\right)\left(\frac{S}{4\pi}\right)\ \text{COSH}\ \frac{4\pi bw}{S}\Big]$$

$$- \frac{2}{bw^2}\left(\frac{2\pi}{S}\right)^2 \left(C_{4nm}C_{3rp} + C_{3nm}C_{4rp}\right)\left(\frac{S}{4\pi}\right) \qquad \text{---------(IV.7)}$$

$$\Phi_{2nmrp} = \int_0^{bw} Y_{2n}\, Y_{2m}\, Y_{2r}\, Y_{2p}\, dy_2$$

$$= bw\Big[\frac{1}{5}J_1 + \frac{1}{6}J_2 + \frac{1}{7}J_3 + \frac{1}{8}J_4 + \frac{1}{9}J_5 + \frac{1}{10}J_6 + \frac{1}{11}J_7 + \frac{1}{12}J_8 + \frac{1}{13}J_9 + \frac{1}{14}J_{10} + \frac{1}{15}J_{11} + \frac{1}{16}J_{12} + \frac{1}{17}J_{13} + \frac{1}{18}J_{14} + \frac{1}{19}J_{15} + \frac{1}{20}J_{16} + \frac{1}{21}J_{17} + \frac{1}{22}J_{18} + \frac{1}{23}J_{19} + \frac{1}{24}J_{20} + \frac{1}{25}J_{21}\Big] \qquad \text{------(IV.8)}$$

where

$$J_1 = (z_{1nm}z_{1rp})$$

$$J_2 = (z_{1nm}z_{2rp} + z_{2nm}z_{1rp})$$

$$J_3 = (z_{1nm}z_{3rp} + z_{2nm}z_{2rp} + z_{3nm}z_{1rp})$$

$$J_4 = (z_{1nm}z_{4rp} + z_{2nm}z_{3rp} + z_{3nm}z_{2rp} + z_{4nm}z_{1rp})$$

$$J_5 = (z_{1nm}z_{5rp} + z_{2nm}z_{4rp} + z_{3nm}z_{3rp} + z_{4nm}z_{2rp} + z_{5nm}z_{1rp})$$

$$J_6 = (z_{1nm}z_{6rp} + z_{2nm}z_{5rp} + z_{3nm}z_{4rp} + z_{4nm}z_{3rp} + z_{5nm}z_{2rp} + z_{6nm}z_{1rp})$$

$$J_7 = (z_{1nm}z_{7rp} + z_{2nm}z_{6rp} + z_{3nm}z_{5rp} + z_{4nm}z_{4rp} + z_{5nm}z_{3rp} + z_{6nm}z_{2rp} + z_{7nm}z_{1rp})$$

$$J_8 = (z_{1nm}z_{8rp} + z_{2nm}z_{7rp} + z_{3nm}z_{6rp} + z_{4nm}z_{5rp} + z_{5nm}z_{4rp} + z_{6nm}z_{3rp} + z_{7nm}z_{2rp} + z_{8nm}z_{1rp})$$

$$J_9 = (z_{1nm}z_{9rp} + z_{2nm}z_{8rp} + z_{3nm}z_{7rp} + z_{4nm}z_{6rp} + z_{5nm}z_{5rp} + z_{6nm}z_{4rp} + z_{7nm}z_{3rp} + z_{8nm}z_{2rp} + z_{9nm}z_{1rp})$$

$$J_{10} = (z_{1nm}z_{10rp} + z_{2nm}z_{9rp} + z_{3nm}z_{8rp} + z_{4nm}z_{7rp} + z_{5nm}z_{6rp} + z_{6nm}z_{5rp} + z_{7nm}z_{4rp} + z_{8nm}z_{3rp} + z_{9nm}z_{2rp} + z_{10nm}z_{1rp})$$

$$J_{11} = (z_{1nm}z_{11rp} + z_{2nm}z_{10rp} + z_{3nm}z_{9rp} + z_{4nm}z_{8rp} + z_{5nm}z_{7rp} + z_{6nm}z_{6rp} + z_{7nm}z_{5rp} + z_{8nm}z_{4rp} + z_{9nm}z_{3rp} + z_{10nm}z_{2rp} + z_{11nm}z_{1rp})$$

$$J_{12} = (z_{2nm}z_{11rp} + z_{3nm}z_{10rp} + z_{4nm}z_{9rp} + z_{5nm}z_{8rp} + z_{6nm}z_{7rp} + z_{7nm}z_{6rp} + z_{8nm}z_{5rp} + z_{9nm}z_{4rp} + z_{10nm}z_{3rp} + z_{11nm}z_{2rp})$$

$$J_{13} = (z_{3nm}z_{11rp} + z_{4nm}z_{10rp} + z_{5nm}z_{9rp} + z_{6nm}z_{8rp} + z_{7nm}z_{7rp} + z_{8nm}z_{6rp} + z_{9nm}z_{5rp} + z_{10nm}z_{4rp} + z_{11nm}z_{3rp})$$

$$J_{14} = (z_{4nm}z_{11rp} + z_{5nm}z_{10rp} + z_{6nm}z_{9rp} + z_{7nm}z_{8rp} + z_{8nm}z_{7rp} + z_{9nm}z_{6rp} + z_{10nm}z_{5rp} + z_{11nm}z_{4rp})$$

$$J_{15} = (z_{5nm}z_{11rp} + z_{6nm}z_{10rp} + z_{7nm}z_{9rp} + z_{8nm}z_{8rp} + z_{9nm}z_{7rp} + z_{10nm}z_{6rp} + z_{11nm}z_{5rp})$$

$$J_{16} = (z_{6nm}z_{11rp} + z_{7nm}z_{10rp} + z_{8nm}z_{9rp} + z_{9nm}z_{8rp} + z_{10nm}z_{7rp} + z_{11nm}z_{6rp})$$

$$J_{17} = (z_{7nm}z_{11rp} + z_{8nm}z_{10rp} + z_{9nm}z_{9rp} + z_{10nm}z_{8rp} + z_{11nm}z_{7rp})$$

$$J_{18} = (z_{8nm}z_{11rp} + z_{9nm}z_{10rp} + z_{10nm}z_{9rp} + z_{11nm}z_{8rp})$$

$$J_{19} = (z_{9nm}z_{11rp} + z_{10nm}z_{10rp} + z_{11nm}z_{9rp})$$

$$J_{20} = (z_{10nm}z_{11rp} + z_{11nm}z_{10rp})$$

$$J_{21} = (z_{11nm}z_{11rp}) \qquad \text{---------- (IV.9)}$$

and

$$z_{1nm} = h_{n1}h_{m1}$$

$$z_{2nm} = (h_{n1}h_{m2} + h_{n2}h_{m1})$$

$$z_{3nm} = (h_{n1}h_{m3} + h_{n2}h_{m2} + h_{n3}h_{m1})$$

$$z_{4nm} = (h_{n1}h_{m4} + h_{n2}h_{m3} + h_{n3}h_{m2} + h_{n4}h_{m1})$$

$$z_{5nm} = (h_{n1}h_{m5} + h_{n2}h_{m4} + h_{n3}h_{m3} + h_{n4}h_{m2} + h_{n5}h_{m1})$$

$$z_{6nm} = (h_{n1}h_{m6} + h_{n2}h_{m5} + h_{n3}h_{m4} + h_{n4}h_{m3} + h_{n5}h_{m2} + h_{n6}h_{m1})$$

$$z_{7nm} = (h_{n2}h_{m6} + h_{n3}h_{m5} + h_{n4}h_{m4} + h_{n5}h_{m3} + h_{n6}h_{m2})$$

$$z_{8nm} = (h_{n3}h_{m6} + h_{n4}h_{m5} + h_{n5}h_{m4} + h_{n6}h_{m3})$$

$$z_{9nm} = (h_{n4}h_{m6} + h_{n5}h_{m5} + h_{n6}h_{m4})$$

$$z_{10nm} = (h_{n5}h_{m6} + h_{n6}h_{m5})$$

$$z_{11nm} = (h_{n6}h_{m6}) \qquad \text{--------- (IV.10)}$$

$$\theta_{2nm} = (1-\alpha)\int_o^{bw} Y_{2n}Y_{2m}d_{y2} + \frac{\alpha}{bw}\int_o^{bw} y_2Y_{2n}Y_{2m}d_{y2}$$

$$= bw\left[\frac{1}{3}z_{1nm} + \frac{1}{4}z_{2nm} + \frac{1}{5}z_{3nm} + \frac{1}{6}z_{4nm} + \frac{1}{7}z_{5nm} + \frac{1}{8}z_{6nm} + \frac{1}{9}z_{7nm} + \frac{1}{10}z_{8nm} + \frac{1}{11}z_{9nm} + \frac{1}{12}z_{10nm} + \frac{1}{13}z_{11nm}\right] + \alpha bw\left[\frac{1}{4}z_{1nm} + \frac{1}{5}z_{2nm} + \frac{1}{6}z_{3nm} + \frac{1}{7}z_{4nm} + \frac{1}{8}z_{5nm} + \frac{1}{9}z_{6nm} + \frac{1}{10}z_{7nm} + \frac{1}{11}z_{8nm} + \frac{1}{12}z_{9nm} + \frac{1}{13}z_{10nm} + \frac{1}{14}z_{11nm}\right]$$

---------(IV.11)

$$Q_{2nm} = \frac{1}{bw^3}\left[L_{1nm} + \frac{1}{2}L_{2nm} + \frac{1}{3}L_{3nm} + \frac{1}{4}L_{4nm} + \frac{1}{5}L_{5nm} + \frac{1}{6}L_{6nm} + \frac{1}{7}L_{7nm} + \frac{1}{8}L_{8nm} + \frac{1}{9}L_{9nm}\right] - \frac{\pi^2}{S^2bw}\left[\frac{1}{2}(I_{1nm} + A_{1nm}) + \frac{1}{3}(I_{2nm} + A_{2nm}) + \frac{1}{4}(I_{3nm} + A_{3nm}) + \frac{1}{5}(I_{4nm} + A_{4nm}) + \frac{1}{6}(I_{5nm} + A_{5nm}) + \frac{1}{7}(I_{6nm} + A_{6nm}) + \frac{1}{8}(I_{7nm} + A_{7nm}) + \frac{1}{9}(I_{8nm} + A_{8nm}) + \frac{1}{10}(I_{9nm} + A_{9nm}) + \frac{1}{11}(I_{10nm} + A_{10nm})\right] + \frac{\pi^4 bw}{S^4}\left[\frac{1}{3}z_{1nm} + \frac{1}{4}z_{2nm} + \frac{1}{5}z_{3nm} + \frac{1}{6}z_{4nm} + \frac{1}{7}z_{5nm} + \frac{1}{8}z_{6nm} + \frac{1}{9}z_{7nm} + \frac{1}{10}z_{8nm} + \frac{1}{11}z_{9nm} + \frac{1}{12}z_{10nm} + \frac{1}{13}z_{11nm}\right]$$

---------(IV.12)

where

$$L_{1nm} = 4h_{n2}h_{m2}$$

$$L_{2nm} = (12h_{n2}h_{m3} + 12h_{n3}h_{m2})$$

$$L_{3nm} = (24h_{n2}h_{m4} + 36h_{n3}h_{m3} + 24h_{n4}h_{m2})$$

$$L_{4nm} = (40h_{n2}h_{m5} + 72h_{n3}h_{m4} + 72h_{n4}h_{m3} + 40h_{n5}h_{m2})$$

$$L_{5nm} = (60h_{n2}h_{m6} + 120h_{n3}h_{m5} + 144h_{n4}h_{m4} + 120h_{n5}h_{m3} + 60h_{n6}h_{m2})$$

$$L_{6nm} = (180h_{n3}h_{m6} + 240h_{n4}h_{m5} + 240h_{n5}h_{m4} + 180h_{n6}h_{m3})$$

$$L_{7nm} = (360h_{n4}h_{m6} + 400h_{n5}h_{m5} + 360h_{n6}h_{m4})$$

$$L_{8nm} = (600h_{n5}h_{m6} + 600h_{n6}h_{m5})$$

$$L_{9nm} = (900h_{n6}h_{m6}) \qquad \text{———————(IV.13)}$$

and

$$I_{1nm} = (2h_{m1}h_{n2})$$

$$I_{2nm} = (6h_{m1}h_{n3} + 2h_{m2}h_{n2})$$

$$I_{3nm} = (12h_{m1}h_{n4} + 6h_{m2}h_{n3} + 2h_{m3}h_{n2})$$

$$I_{4nm} = (20h_{m1}h_{n5} + 12h_{m2}h_{n4} + 6h_{m3}h_{n3} + 2h_{m4}h_{n2})$$

$$I_{5nm} = (30h_{m1}h_{n6} + 20h_{m2}h_{n5} + 12h_{m3}h_{n4} + 6h_{m4}h_{n3} + h_{m5}h_{n2})$$

$$I_{6nm} = (30h_{m2}h_{n6} + 20h_{m3}h_{n5} + 12h_{m4}h_{n4} + 6h_{m5}h_{n3} + 2h_{m6}h_{n2})$$

$$I_{7nm} = (30h_{m3}h_{n6} + 20h_{m4}h_{n5} + 12h_{m5}h_{n4} + 6h_{m6}h_{n3})$$

$$I_{8nm} = (30h_{m4}h_{n6} + 20h_{m5}h_{n5} + 12h_{m6}h_{n4})$$

$$I_{9nm} = (30h_{m5}h_{n6} + 20h_{m6}h_{n5})$$

$$I_{10nm} = (30h_{m6}h_{n6}) \qquad \text{——————(IV.14)}$$

and

$$A_{1nm} = (2h_{n1}h_{m2})$$

$$A_{2nm} = (6h_{n1}h_{m3} + 2h_{n2}h_{m2})$$

$$A_{3nm} = (12h_{n1}h_{m4} + 6h_{n2}h_{m3} + 2h_{n3}h_{m2})$$

$$A_{4nm} = (20h_{n1}h_{m5} + 12h_{n2}h_{m4} + 6h_{n3}h_{m3} + 2h_{n4}h_{m2})$$

$$A_{5nm} = (30h_{n1}h_{m6} + 20h_{n2}h_{m5} + 12h_{n3}h_{m4} + 6h_{n4}h_{m3} + 2h_{n5}h_{m2})$$

$$A_{6nm} = (30h_{n2}h_{m6} + 20h_{n3}h_{m5} + 12h_{n4}h_{m4} + 6h_{n5}h_{m3} + 2h_{n6}h_{m2})$$

$$A_{7nm} = (30h_{n3}h_{m6} + 20h_{n4}h_{m5} + 12h_{n5}h_{m4} + 6h_{n6}h_{m3})$$

$$A_{8nm} = (30h_{n4}h_{m6} + 20h_{n5}h_{m5} + 12h_{n6}h_{m4})$$

$$A_{9nm} = (30h_{n5}h_{m6} + 20h_{n6}h_{m5})$$

$$A_{10nm} = (30h_{n6}h_{m6}) \qquad \text{——————(IV.15)}$$

Γ_{3nmrp} is of exactly the same form as Γ_{2nmrp}, equation IV.7, and is evaluated in the computer simply by re-formulating Γ_{2nmrp} and replacing b_w with b_ℓ, $b_{inm}b_{jrp}$ with $M_{inm}M_{jrp}$, C_{inm} with N_{inm} and C_{jrp} with N_{jrp}. i.e.

$$\Gamma_{3nmrp} = \Gamma_{2nmrp} \text{ provided}$$

$$b_w = b_\ell$$

$$b_{inm}b_{jrp} = M_{inm}M_{jrp}$$

$$C_{inm} = N_{inm}$$

$$C_{jrp} = N_{jrp} \qquad \text{---------(IV.16)}$$

where

$$M_{11nm} = \left(\frac{S}{2\pi}\right)^4 \bar{R}_{11nm}$$

$$M_{10nm} = \left(\frac{S}{2\pi}\right)^4 \bar{R}_{10nm}$$

$$M_{9nm} = \left(\frac{S}{2\pi}\right)^4 \left[\bar{R}_{9nm} + \frac{180\ M_{11nm}}{b_\ell^2}\left(\frac{2\pi}{S}\right)^2\right]$$

$$M_{8nm} = \left(\frac{S}{2\pi}\right)^4 \left[\bar{R}_{8nm} + \frac{144\ M_{10nm}}{b_\ell^2}\left(\frac{2\pi}{S}\right)^2\right]$$

$$M_{7nm} = \left(\frac{S}{2\pi}\right)^4 \left[\bar{R}_{7nm} + \frac{112\ M_{9nm}}{b_\ell^2}\left(\frac{2\pi}{S}\right)^2 - \frac{5040\ M_{11nm}}{b_\ell^4}\right]$$

$$M_{6nm} = \left(\frac{S}{2\pi}\right)^4 \left[\bar{R}_{6nm} + \frac{84\ M_{8nm}}{b_\ell^2}\left(\frac{2\pi}{S}\right)^2 - \frac{3024\ M_{10nm}}{b_\ell^4}\right]$$

$$M_{5nm} = \left(\frac{S}{2\pi}\right)^4 \left[\bar{R}_{5nm} + \frac{60\ M_{7nm}}{b_\ell^2}\left(\frac{2\pi}{S}\right)^2 - \frac{1680\ M_{9nm}}{b_\ell^4}\right]$$

$$M_{4nm} = \left(\frac{S}{2\pi}\right)^4 \left[\bar{R}_{4nm} + \frac{40\ M_{6nm}}{b_\ell^2}\left(\frac{2\pi}{S}\right)^2 - \frac{840\ M_{8nm}}{b_\ell^4}\right]$$

$$M_{3nm} = \left(\frac{S}{2\pi}\right)^4 \left[\bar{R}_{3nm} + \frac{24\ M_{5nm}}{b_\ell^2}\left(\frac{2\pi}{S}\right)^2 - \frac{360\ M_{7nm}}{b_\ell^4}\right]$$

$$M_{2nm} = \left(\frac{S}{2\pi}\right)^4 \left[\bar{R}_{2nm} + \frac{12\ M_{4nm}}{b_\ell^2}\left(\frac{2\pi}{S}\right)^2 - \frac{120\ M_{6nm}}{b_\ell^4}\right]$$

$$M_{1nm} = \left(\frac{S}{2\pi}\right)^4 \left[\bar{R}_{1nm} + \frac{4\ M_{3nm}}{b_\ell^2}\left(\frac{2\pi}{S}\right)^2 - \frac{24\ M_{5nm}}{b_\ell^4}\right]$$

$$\text{---------(IV.17)}$$

and

$$\bar{R}_{1nm} = -\ p_{n1}p_{m1}$$

$$\bar{R}_{2nm} = -\ 2p_{n2}p_{m1}$$

$$\bar{R}_{3nm} = (3p_{n1}p_{m3} - 2p_{n2}p_{m2} - 3p_{n3}p_{m1})$$

$$\bar{R}_{4nm} = (8p_{n1}p_{m4} - 4p_{n3}p_{m2} - 4p_{n4}p_{m1})$$

$$\bar{R}_{5nm} = (15p_{n1}p_{m5} + 4p_{n2}p_{m4} - 3p_{n3}p_{m3} - 6p_{n4}p_{m2} - 5p_{n5}p_{m1})$$

$$\bar{R}_{6nm} = (24p_{n1}p_{m6} + 10p_{n2}p_{m5} - 6p_{n4}p_{m3} - 8p_{n5}p_{m2} - 6p_{n6}p_{m1})$$

$$\bar{R}_{7nm} = (18p_{n2}p_{m6} + 5p_{n3}p_{m5} - 4p_{n4}p_{m4} - 9p_{n5}p_{m3} - 10p_{n6}p_{m2})$$

$$\bar{R}_{8nm} = (12p_{n3}p_{m6} - 8p_{n5}p_{m4} - 12p_{n6}p_{m3})$$

$$\bar{R}_{9nm} = (6p_{n4}p_{m6} - 5p_{n5}p_{m5} - 12p_{n6}p_{m4})$$

$$\bar{R}_{10nm} = - 10p_{n6}p_{m5}$$

$$\bar{R}_{11nm} = - 6p_{n6}p_{m6} \qquad \text{——————(IV.18)}$$

$$\Phi_{3nmrp} = b_{\ell}\left[\frac{1}{5}E_1 + \frac{1}{6}E_2 + \frac{1}{7}E_3 + \frac{1}{8}E_4 + \frac{1}{9}E_5 + \frac{1}{10}E_6 + \frac{1}{11}E_7 + \frac{1}{12}E_8 + \frac{1}{13}E_9 + \frac{1}{14}E_{10} + \frac{1}{15}E_{11} + \frac{1}{16}E_{12} + \frac{1}{17}E_{13} + \frac{1}{18}E_{14} + \frac{1}{19}E_{15} + \frac{1}{20}E_{16} + \frac{1}{21}E_{17} + \frac{1}{22}E_{18} + \frac{1}{23}E_{19} + \frac{1}{24}E_{20} + \frac{1}{25}E_{21}\right] \qquad \text{——————(IV.19)}$$

where

$$E_1 = (Z_{1nm}Z_{1rp})$$

$$E_2 = (Z_{1nm}Z_{2rp} + Z_{2nm}Z_{1rp})$$

$$E_3 = (Z_{1nm}Z_{3rp} + Z_{2nm}Z_{2rp} + Z_{3nm}Z_{1rp})$$

$$E_4 = (Z_{1nm}Z_{4rp} + Z_{2nm}Z_{3rp} + Z_{3nm}Z_{2rp} + Z_{4nm}Z_{1rp})$$

$$E_5 = (Z_{1nm}Z_{5rp} + Z_{2nm}Z_{4rp} + Z_{3nm}Z_{3rp} + Z_{4nm}Z_{2rp} + Z_{5nm}Z_{1rp})$$

$$E_6 = (Z_{1nm}Z_{6rp} + Z_{2nm}Z_{5rp} + Z_{3nm}Z_{4rp} + Z_{4nm}Z_{3rp} + Z_{5nm}Z_{2rp} + Z_{6nm}Z_{1rp})$$

$$E_7 = (Z_{1nm}Z_{7rp} + Z_{2nm}Z_{6rp} + Z_{3nm}Z_{5rp} + Z_{4nm}Z_{4rp} + Z_{5nm}Z_{3rp} + Z_{6nm}Z_{2rp} + Z_{7nm}Z_{1rp})$$

$$E_8 = (Z_{1nm}Z_{8rp} + Z_{2nm}Z_{7rp} + Z_{3nm}Z_{6rp} + Z_{4nm}Z_{5rp} + Z_{5nm}Z_{4rp} + Z_{6nm}Z_{3rp} + Z_{7nm}Z_{2rp} + Z_{8nm}Z_{1rp})$$

$$E_9 = (Z_{1nm}Z_{9rp} + Z_{2nm}Z_{8rp} + Z_{3nm}Z_{7rp} + Z_{4nm}Z_{6rp} + Z_{5nm}Z_{5rp} + Z_{6nm}Z_{4rp} + Z_{7nm}Z_{3rp} + Z_{8nm}Z_{2rp} + Z_{9nm}Z_{1rp})$$

$$E_{10} = (Z_{1nm}Z_{10rp} + Z_{2nm}Z_{9rp} + Z_{3nm}Z_{8rp} + Z_{4nm}Z_{7rp} + Z_{5nm}Z_{6rp} + Z_{6nm}Z_{5rp} + Z_{7nm}Z_{4rp} + Z_{8nm}Z_{3rp} + Z_{9nm}Z_{2rp} + Z_{10nm}Z_{1rp})$$

$$E_{11} = (Z_{1nm}Z_{11rp} + Z_{2nm}Z_{10rp} + Z_{3nm}Z_{9rp} + Z_{4nm}Z_{8rp} + Z_{5nm}Z_{7rp} + Z_{6nm}Z_{6rp} + Z_{7nm}Z_{5rp} + Z_{8nm}Z_{4rp} + Z_{9nm}Z_{3rp} + Z_{10nm}Z_{2rp} + Z_{11nm}Z_{1rp})$$

$$E_{12} = (Z_{2nm}Z_{11rp} + Z_{3nm}Z_{10rp} + Z_{4nm}Z_{9rp} + Z_{5nm}Z_{8rp} + Z_{6nm}Z_{7rp} + Z_{7nm}Z_{6rp} + Z_{8nm}Z_{5rp} + Z_{9nm}Z_{4rp} + Z_{10nm}Z_{3rp} + Z_{11nm}Z_{2rp})$$

$$E_{13} = (Z_{3nm}Z_{11rp} + Z_{4nm}Z_{10rp} + Z_{5nm}Z_{9rp} + Z_{6nm}Z_{8rp} + Z_{7nm}Z_{7rp} + Z_{8nm}Z_{6rp} + Z_{9nm}Z_{5rp} + Z_{10nm}Z_{4rp} + Z_{11nm}Z_{3rp})$$

$$E_{14} = (Z_{4nm}Z_{11rp} + Z_{5nm}Z_{10rp} + Z_{6nm}Z_{9rp} + Z_{7nm}Z_{8rp} + Z_{8nm}Z_{7rp} + Z_{9nm}Z_{6rp} + Z_{10nm}Z_{5rp} + Z_{11nm}Z_{4rp})$$

$$E_{15} = (Z_{5nm}Z_{11rp} + Z_{6nm}Z_{10rp} + Z_{7nm}Z_{9rp} + Z_{8nm}Z_{8rp} + Z_{9nm}Z_{7rp} + Z_{10nm}Z_{6rp} + Z_{11nm}Z_{5rp})$$

$$E_{16} = (Z_{6nm}Z_{11rp} + Z_{7nm}Z_{10rp} + Z_{8nm}Z_{9rp} + Z_{9nm}Z_{8rp} + Z_{10nm}Z_{7rp} + Z_{11nm}Z_{6rp})$$

$$E_{17} = (Z_{7nm}Z_{11rp} + Z_{8nm}Z_{10rp} + Z_{9nm}Z_{9rp} + Z_{10nm}Z_{8rp} + Z_{11nm}Z_{7rp})$$

$$E_{18} = (Z_{8nm}Z_{11rp} + Z_{9nm}Z_{10rp} + Z_{10nm}Z_{9rp} + Z_{11nm}Z_{8rp})$$

$$E_{19} = (Z_{9nm}Z_{11rp} + Z_{10nm}Z_{10rp} + Z_{11nm}Z_{9rp})$$

$$E_{20} = (Z_{10nm}Z_{11rp} + Z_{11nm}Z_{10rp})$$

$$E_{21} = (Z_{11nm}Z_{11rp}) \qquad \text{-------(IV.20)}$$

and

$$Z_{1nm} = P_{n1}P_{m1}$$

$$Z_{2nm} = (P_{n1}P_{m2} + P_{n2}P_{m1})$$

$$Z_{3nm} = (P_{n1}P_{m3} + P_{n2}P_{m2} + P_{n3}P_{m1})$$

$$Z_{4nm} = (P_{n1}P_{m4} + P_{n2}P_{m3} + P_{n3}P_{m2} + P_{n4}P_{m1})$$

$$Z_{5nm} = (P_{n1}P_{m5} + P_{n2}P_{m4} + P_{n3}P_{m3} + P_{n4}P_{m2} + P_{n5}P_{m1})$$

$$Z_{6nm} = (P_{n1}P_{m6} + P_{n2}P_{m5} + P_{n3}P_{m4} + P_{n4}P_{m3} + P_{n5}P_{m2} + P_{n6}P_{m1})$$

$$Z_{7nm} = (P_{n2}P_{m6} + P_{n3}P_{m5} + P_{n4}P_{m4} + P_{n5}P_{m3} + P_{n6}P_{m2})$$

$$z_{8nm} = (p_{n3}p_{m6} + p_{n4}p_{m5} + p_{n5}p_{m4} + p_{n6}p_{m3})$$

$$z_{9nm} = (p_{n4}p_{m6} + p_{n5}p_{m5} + p_{n6}p_{m4})$$

$$z_{10nm} = (p_{n5}p_{m6} + p_{n6}p_{m5})$$

$$z_{11nm} = (p_{n6}p_{m6}) \qquad \text{——————(IV.21)}$$

$$\theta'_{3nm} = (1-\alpha)b_{\ell}\left[\frac{1}{3}z_{1nm} + \frac{1}{4}z_{2nm} + \frac{1}{5}z_{3nm} + \frac{1}{6}z_{4nm} + \frac{1}{7}z_{5nm} + \frac{1}{8}z_{6nm} + \frac{1}{9}z_{7nm} + \frac{1}{10}z_{8nm} + \frac{1}{11}z_{9nm} + \frac{1}{12}z_{10nm} + \frac{1}{13}z_{11nm}\right] \qquad \text{————————(IV.22)}$$

$$Q_{3nm} = \left\{\frac{1}{b_{\ell}^3}\left[\beta_{1nm} + \frac{1}{2}\beta_{2nm} + \frac{1}{3}\beta_{3nm} + \frac{1}{4}\beta_{4nm} + \frac{1}{5}\beta_{5nm} + \frac{1}{6}\beta_{6nm} + \frac{1}{7}\beta_{7nm} + \frac{1}{8}\beta_{8nm} + \frac{1}{9}\beta_{9nm}\right] - \frac{\pi^2}{S^2 b_{\ell}}\left[\frac{1}{2}\rho_{1nm} + \frac{1}{3}\rho_{2nm} + \frac{1}{4}\rho_{3nm} + \frac{1}{5}\rho_{4nm} + \frac{1}{6}\rho_{5nm} + \frac{1}{7}\rho_{6nm} + \frac{1}{8}\rho_{7nm} + \frac{1}{9}\rho_{8nm} + \frac{1}{10}\rho_{9nm} + \frac{1}{11}\rho_{10nm}\right] + \frac{\pi^4 b_{\ell}}{S^4}\left[\frac{1}{3}z_{1nm} + \frac{1}{4}z_{2nm} + \frac{1}{5}z_{3nm} + \frac{1}{6}z_{4nm} + \frac{1}{7}z_{5nm} + \frac{1}{8}z_{6nm} + \frac{1}{9}z_{7nm} + \frac{1}{10}z_{8nm} + \frac{1}{11}z_{9nm} + \frac{1}{12}z_{10nm} + \frac{1}{13}z_{11nm}\right] + \frac{2\pi^2}{S^2}(1-\nu)\tau_{3nm}\right\} \qquad \text{————————(IV.23)}$$

where

$$\beta_{1nm} = 4p_{n2}p_{m2}$$

$$\beta_{2nm} = (12p_{n2}p_{m3} + 12p_{n3}p_{m2})$$

$$\beta_{3nm} = (24p_{n2}p_{m4} + 36p_{n3}p_{m3} + 24p_{n4}p_{m2})$$

$$\beta_{4nm} = (40p_{n2}p_{m5} + 72p_{n3}p_{m4} + 72p_{n4}p_{m3} + 40p_{n5}p_{m2})$$

$$\beta_{5nm} = (60p_{n2}p_{m6} + 120p_{n3}p_{m5} + 144p_{n4}p_{m4} + 120p_{n5}p_{m3} + 60p_{n6}p_{m2})$$

$$\beta_{6nm} = (180p_{n3}p_{m6} + 240p_{n4}p_{m5} + 240p_{n5}p_{m4} + 180p_{n6}p_{m3})$$

$$\beta_{7nm} = (360p_{n4}p_{m6} + 400p_{n5}p_{m5} + 360p_{n6}p_{m4})$$

$$\beta_{8nm} = (600p_{n5}p_{m6} + 600p_{n6}p_{m5})$$

$$\beta_{9nm} = (900p_{n6}p_{m6}) \qquad \text{---------(IV.24)}$$

and

$$\rho_{1nm} = (2p_{m1}p_{n2} + 2p_{n1}p_{m2})$$

$$\rho_{2nm} = (6p_{n1}p_{m3} + 2p_{n2}p_{m2} + 6p_{m1}p_{n3} + 2p_{m2}p_{n2})$$

$$\rho_{3nm} = (12p_{n1}p_{m4} + 6p_{n2}p_{m3} + 2p_{n3}p_{m2} + 12p_{m1}p_{n4} + 6p_{m2}p_{n3} + 2p_{m3}p_{n2})$$

$$\rho_{4nm} = (20p_{n1}p_{m5} + 12p_{n2}p_{m4} + 6p_{n3}p_{m3} + 2p_{n4}p_{m2} + 20p_{m1}p_{n5} + 12p_{m2}p_{n4} + 6p_{m3}p_{n3} + 2p_{m4}p_{n2})$$

$$\rho_{5nm} = (30p_{n1}p_{m6} + 20p_{n2}p_{m5} + 12p_{n3}p_{m4} + 6p_{n4}p_{m3} + 2p_{n5}p_{m2} + 30p_{m1}p_{n6} + 20p_{m2}p_{n5} + 12p_{m3}p_{n4} + 6p_{m4}p_{n3} + 2p_{m5}p_{n2})$$

$$\rho_{6nm} = (30p_{n2}p_{m6} + 20p_{n3}p_{m5} + 12p_{n4}p_{m4} + 6p_{n5}p_{m3} + 2p_{n6}p_{m2} + 30p_{m2}p_{n6} + 20p_{m3}p_{n5} + 12p_{m4}p_{n4} + 6p_{m5}p_{n3} + 2p_{m6}p_{n2})$$

$$\rho_{7nm} = (30p_{n3}p_{m6} + 20p_{n4}p_{m5} + 12p_{n5}p_{m4} + 6p_{n6}p_{m3} + 30p_{m3}p_{n6} + 20p_{m4}p_{n5} + 12p_{m5}p_{n4} + 6p_{m6}p_{n3})$$

$$\rho_{8nm} = (30p_{n4}p_{m6} + 20p_{n5}p_{m5} + 12p_{n6}p_{m4} + 30p_{m4}p_{n6} + 20p_{m5}p_{n5} + 12p_{m6}p_{n4})$$

$$\rho_{9nm} = (30p_{n5}p_{m6} + 20p_{n6}p_{m5} + 30p_{m5}p_{n6} + 20p_{m6}p_{n5})$$

$$\rho_{10nm} = (30p_{n6}p_{m6} + 30p_{m6}p_{n6}) \qquad \text{——————(IV.25)}$$

$$\begin{aligned}\tau_{3nm} = \frac{1}{b_\ell}\Big[& p_{n1}p_{m1} + (2p_{n1}p_{m2} + p_{n2}p_{m1}) + (3p_{n1}p_{m3} \\ & + 2p_{n2}p_{m2} + p_{n3}p_{m1}) + (4p_{n1}p_{m4} + 3p_{n2}p_{m3} \\ & + 2p_{n3}p_{m2} + p_{n4}p_{m1}) + (5p_{n1}p_{m5} + 4p_{n2}p_{m4} \\ & + 3p_{n3}p_{m3} + 2p_{n4}p_{m2} + p_{n5}p_{m1}) + (6p_{n1}p_{m6} \\ & + 5p_{n2}p_{m5} + 4p_{n3}p_{m4} + 3p_{n4}p_{m3} + 2p_{n5}p_{m2} + p_{n6}p_{m1}) \\ & + (6p_{n2}p_{m6} + 5p_{n3}p_{m5} + 4p_{n4}p_{m4} + 3p_{n5}p_{m3} \\ & + 2p_{n6}p_{m2}) + (6p_{n3}p_{m6} + 5p_{n4}p_{m5} + 4p_{n5}p_{m4} \\ & + 3p_{n6}p_{m3}) + (6p_{n4}p_{m6} + 5p_{n5}p_{m5} + 4p_{n6}p_{m4}) \\ & + (6p_{n5}p_{m6} + 5p_{n6}p_{m5}) + (6p_{n6}p_{m6})\Big]\end{aligned}$$

$$\text{———(IV.26)}$$

APPENDIX V

FLOW DIAGRAM OF COMPUTER SOLUTION

APPENDIX V

FLOW DIAGRAM OF COMPUTER SOLUTION

As will be realised, the buckling and post buckling interaction analyses involved the writing and development of a rather lengthy computer program and because of its length the program has not been reproduced in the thesis. The steps taken in the computer solution, however, are shown in the flow diagram of Figure V.1, which indicates clearly the logic paths contained within the program and, hopefully, enables the reader to understand more easily the incremental solution process of the analysis.

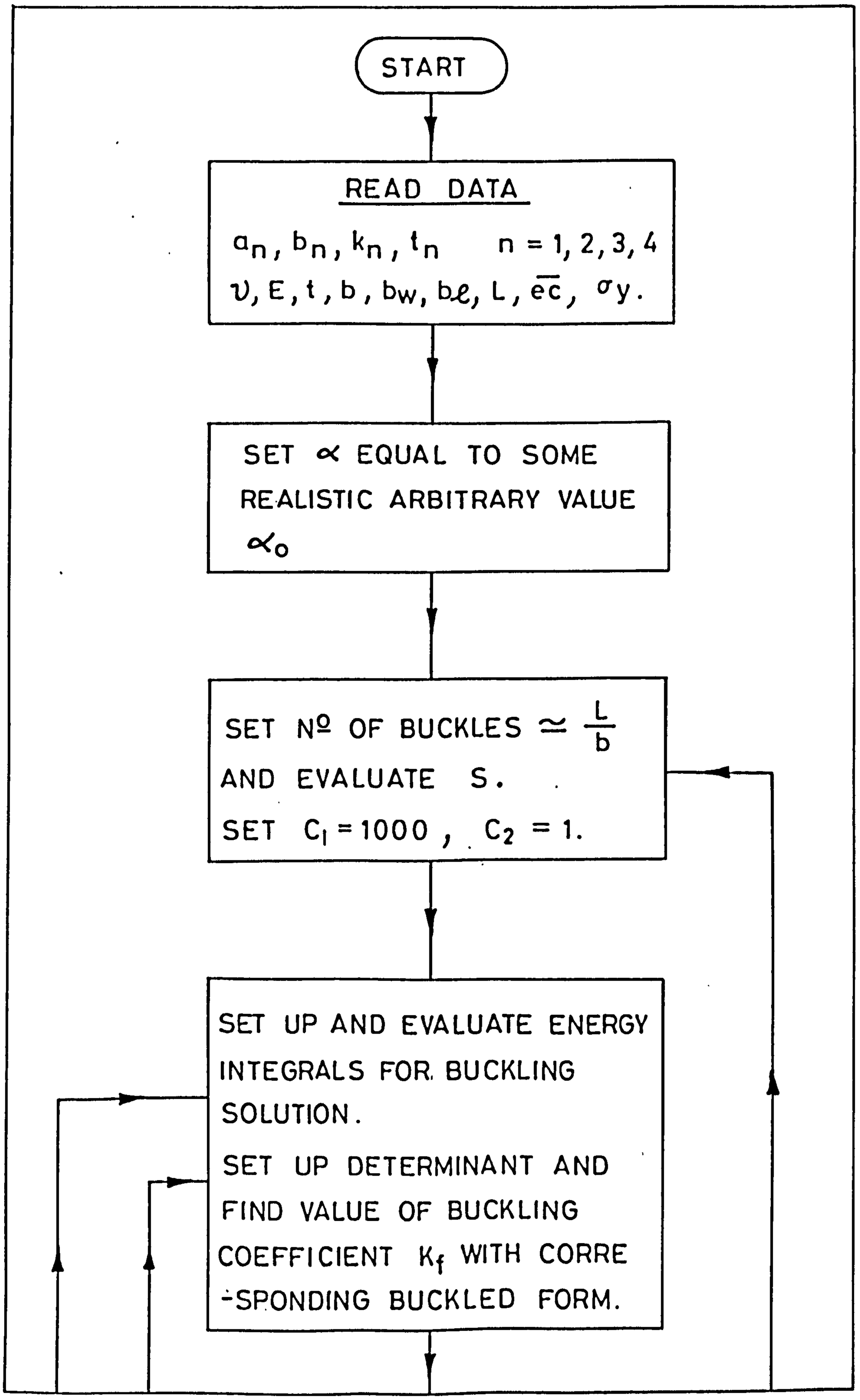

FIG. V.1 FLOW DIAGRAM OF COMPUTER SOLUTION.

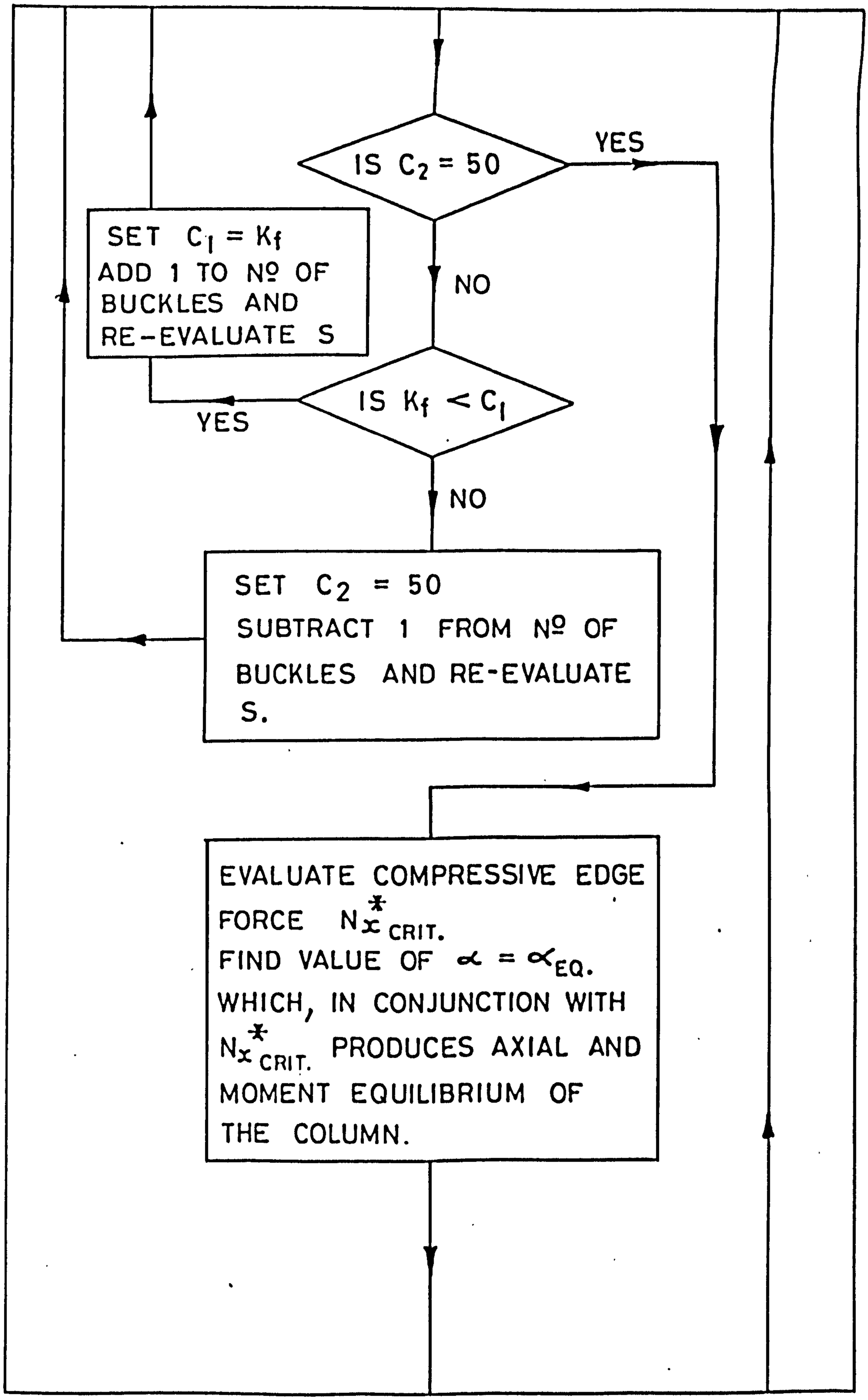
IS $C_2 = 50$
YES
NO
SET $C_1 = K_f$
ADD 1 TO Nº OF BUCKLES AND RE-EVALUATE S
IS $K_f < C_1$
YES
NO
SET $C_2 = 50$
SUBTRACT 1 FROM Nº OF BUCKLES AND RE-EVALUATE S.
EVALUATE COMPRESSIVE EDGE FORCE $N^*_{x\,CRIT.}$
FIND VALUE OF $\alpha = \alpha_{EQ.}$
WHICH, IN CONJUNCTION WITH $N^*_{x\,CRIT.}$ PRODUCES AXIAL AND MOMENT EQUILIBRIUM OF THE COLUMN.

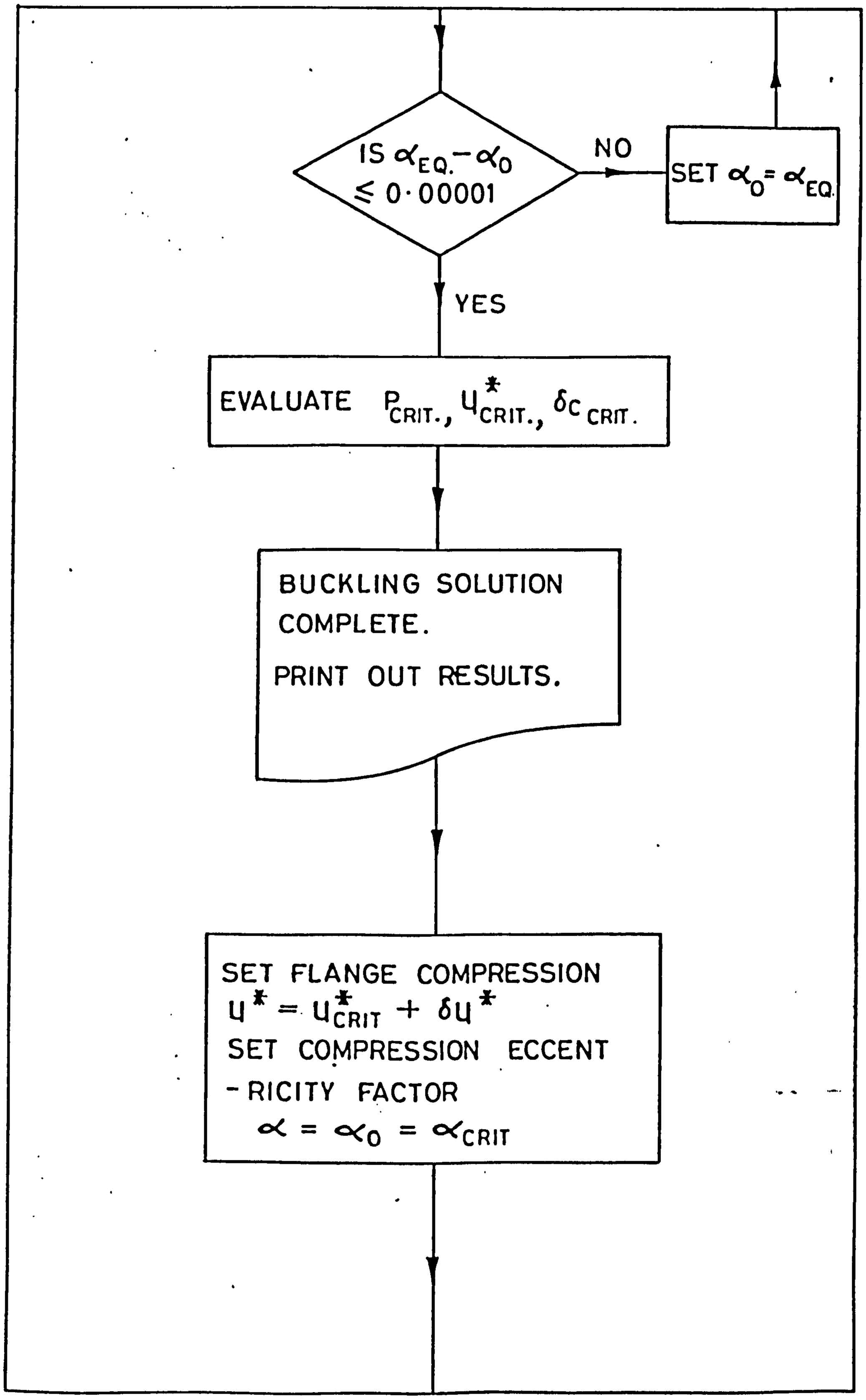
IS $\alpha_{EQ.} - \alpha_0 \leq 0 \cdot 00001$
NO
SET $\alpha_0 = \alpha_{EQ.}$
YES
EVALUATE $P_{CRIT.}$, $U^*_{CRIT.}$, $\delta c_{CRIT.}$
BUCKLING SOLUTION COMPLETE.
PRINT OUT RESULTS.
SET FLANGE COMPRESSION
$U^* = U^*_{CRIT} + \delta U^*$
SET COMPRESSION ECCENT
-RICITY FACTOR
$\alpha = \alpha_0 = \alpha_{CRIT}$

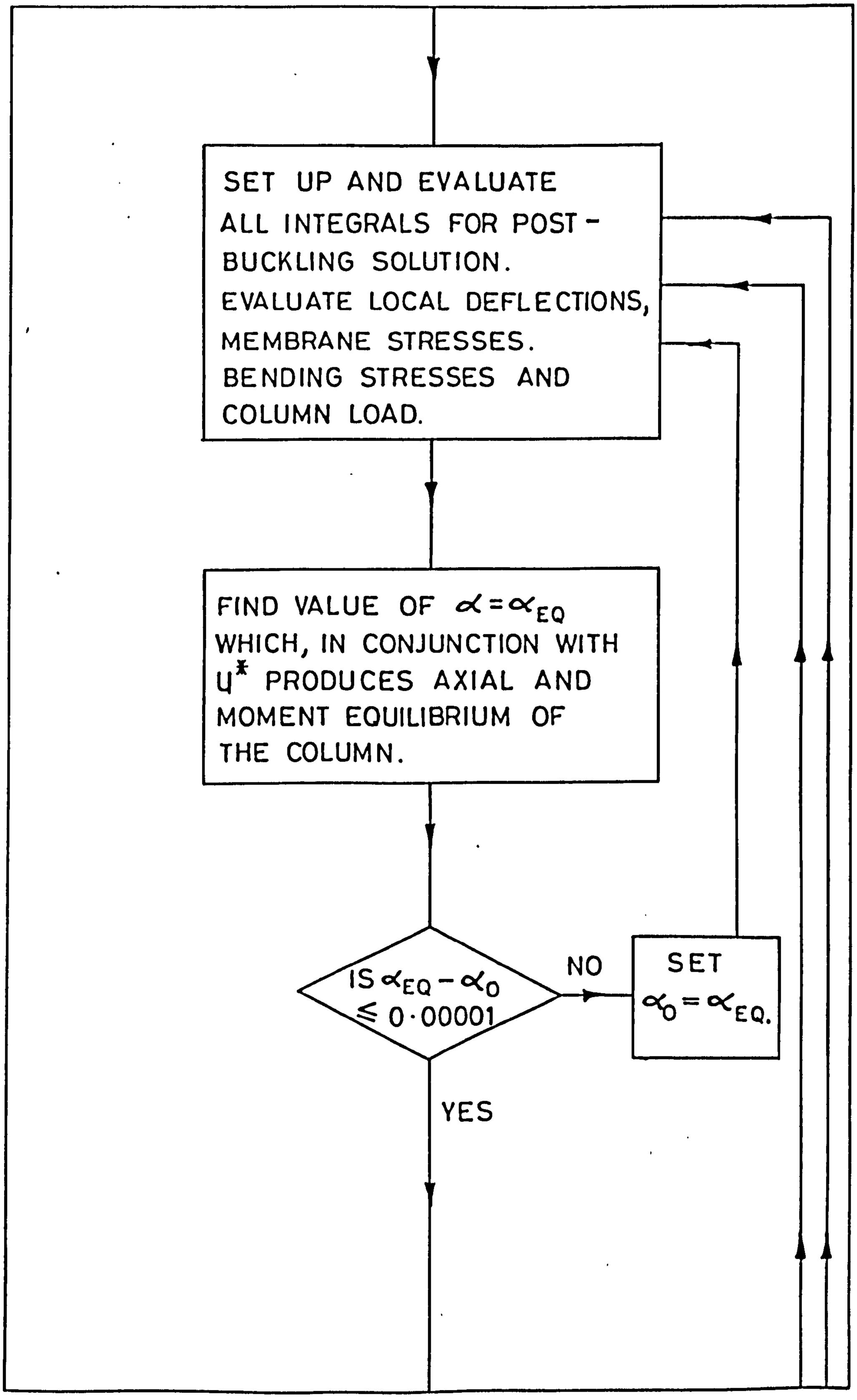
SET UP AND EVALUATE ALL INTEGRALS FOR POST-BUCKLING SOLUTION.
EVALUATE LOCAL DEFLECTIONS, MEMBRANE STRESSES. BENDING STRESSES AND COLUMN LOAD.
FIND VALUE OF $\alpha = \alpha_{EQ}$ WHICH, IN CONJUNCTION WITH U^* PRODUCES AXIAL AND MOMENT EQUILIBRIUM OF THE COLUMN.
IS $\alpha_{EQ} - \alpha_0 \leq 0 \cdot 00001$
NO
SET $\alpha_0 = \alpha_{EQ}$.
YES

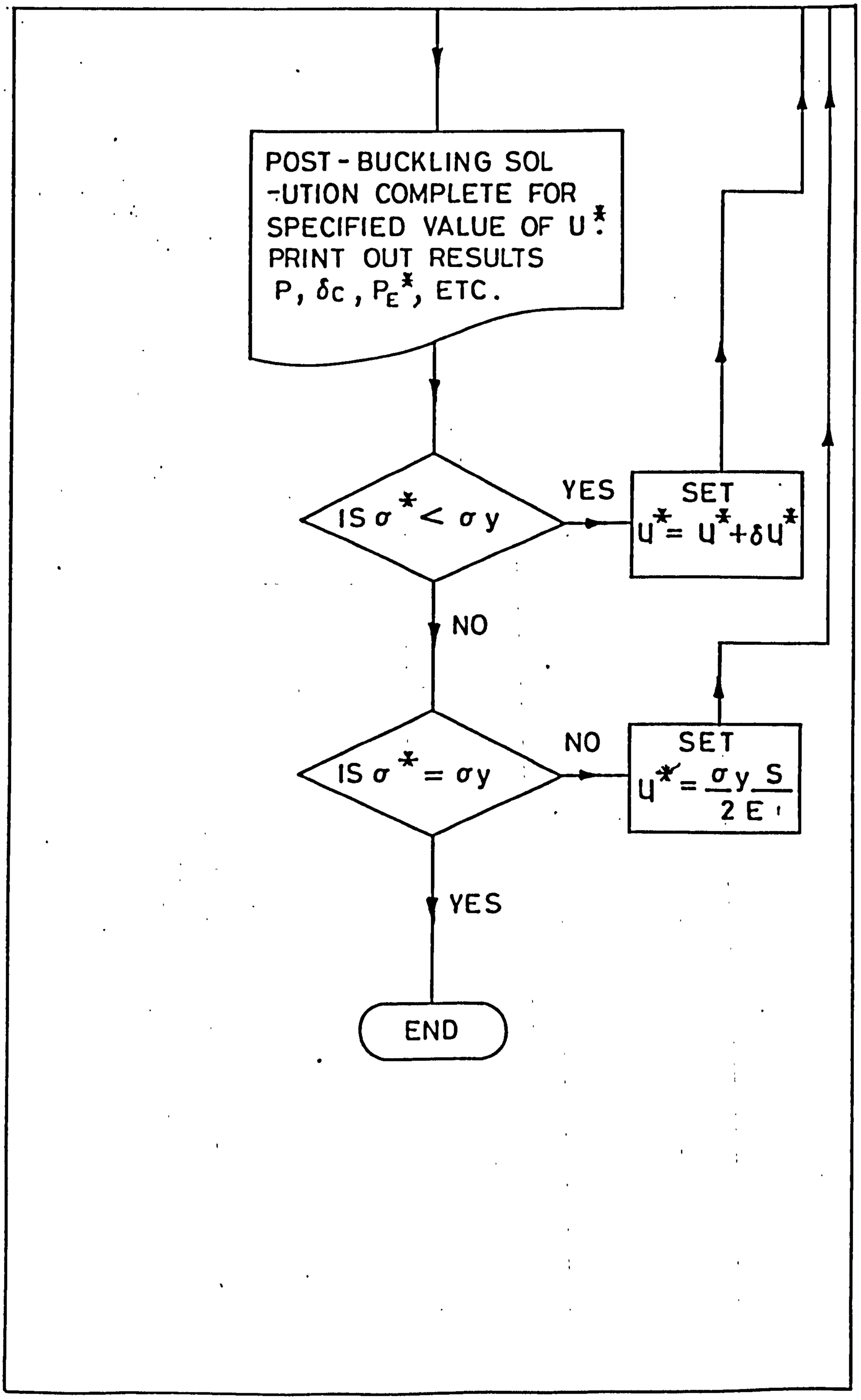
POST - BUCKLING SOL -UTION COMPLETE FOR SPECIFIED VALUE OF U*. PRINT OUT RESULTS P, δc , PE*, ETC.
IS σ* < σy
YES
SET U* = U* + δU*
NO
IS σ* = σy
NO
SET U* = σy S / 2 E'
YES
END

APPENDIX VI

LIST OF TEST COLUMNS, DIMENSIONS AND LOADING ECCENTRICITIES

APPENDIX VI

LIST OF TEST COLUMNS, DIMENSIONS AND LOADING ECCENTRICITIES

In this appendix the dimensions and loading eccentricities of the 33 columns tested in the experimental program are given. The cross-sectional dimensions shown in Table VI.1 are the average centre line values obtained from outside dimensions of the flange, web and lip measured at 12 different cross-sections along the length of each column. The values shown in the table are those used in the computer solution to determine the behaviour of each column theoretically.

TEST COLUMN DIMENSIONS AND LOADING ECCENTRICITY

COLUMN NΩ	$\overline{ec}$	b (mm)	b_w (mm)	b_ℓ (mm)	t (mm)	L (mm)
1	0·4	101·55	50·57	18·85	0·81	1828·80
2	0·4	101·12	50·50	19·24	0·79	1219·20
3	0·4	102·74	62·77	25·44	0·79	1828·80
4	0·4	101·98	62·79	25·40	0·81	1524·00
5	0·4	101·63	62·99	25·74	0·79	1219·20
6	0·1	127·86	50·60	18·68	0·79	1828·80
7	0·1	126·39	50·47	18·86	0·79	1524·00
8	0·1	126·47	50·55	19·14	0·80	1219·20
9	0·2	127·79	62·71	25·42	0·80	1828·80
10	0·2	127·36	63·02	25·50	0·80	1524·00
11	0·2	126·75	62·92	25·58	0·81	1219·20
12	0·3	151·92	50·75	18·95	0·81	1828·80
13	0·3	152·20	50·60	19·66	0·81	1524·00
14	0·3	151·74	50·47	19·02	0·81	1219·20
15	0·0	153·95	62·79	25·37	0·80	1828·80
16	0·0	153·95	62·89	25·60	0·81	1524·00
17	0·0	152·02	62·97	25·57	0·80	1219·20
18	0·4	178·03	50·17	18·86	0·80	1828·80
19	0·4	177·17	50·47	18·94	0·80	1524·00
20	0·4	177·67	50·50	19·58	0·81	1219·20

TABLE VI.1

TEST COLUMN DIMENSIONS AND LOADING ECCENTRICITY

COLUMN Nº	$\overline{ec}$	b (mm)	b_w (mm)	b_ℓ (mm)	t (mm)	L (mm)
21	0·2	178·31	62·94	25·23	0·79	1828·80
22	0·2	178·33	62·97	25·32	0·80	1524·00
23	0·2	176·53	63·02	25·85	0·80	1219·20
24	0·0	152·30	49·28	17·74	1·64	1828·80
25	0·1	152·25	61·72	24·58	1·66	1828·80
26	0·1	152·04	61·67	24·74	1·68	1524·00
27	0·1	151·38	61·82	24·86	1·66	1219·20
28	0·2	178·05	49·25	17·99	1·64	1828·80
29	0·2	177·75	49·38	17·97	1·65	1524·00
30	0·2	176·10	49·10	18·10	1·65	1219·20
31	0·0	178·23	61·85	24·62	1·63	1828·80
32	0·0	177·93	61·62	24·77	1·64	1524·00
33	0·0	176·73	61·98	25·71	1·64	1219·20